université PARIS-SACLAY

AgroParisTech
INSTITUT DES SCIENCES ET INDUSTRIES DU VIVANT ET DE L'ENVIRONNEMENT
PARIS INSTITUTE OF TECHNOLOGY FOR LIFE, FOOD AND ENVIRONMENTAL SCIENCES

NNT: 2019SACLA020

Rational design of plastic packaging for alcoholic beverages

Thèse de doctorat de l'Université Paris-Saclay
préparée à AgroParisTech, Institut des sciences et industries du vivant et de l'environnement

École doctorale n°581 agriculture, alimentation, biologie, environnement et santé (ABIES)
Spécialité de doctorat : Génie des Procédés

Thèse présentée et soutenue à Massy, le 17 Juillet 2019, par

Yan ZHU

Composition du Jury :

Martine ESTEBAN-DECLOUX Professeur, AgroParisTech – UMR 1145	Président
Eric FAVRE Professeur, UMR 7274, ENSIC, Université de Lorraine	Rapporteur
Thomas KARBOWIAK Professeur, AgroSup Dijon, UMR PAM, Université de Bourgogne	Rapporteur
Catherine JOLY Maître de Conférences, EMA 3733 Université Lyon 1	Examinateur
Bruno GUILLEMAT Ingénieur de recherche, Pernod Ricard	Examinateur
Olivier VITRAC Chargé de recherches, INRA – UMR 1145	Directeur de thèse

Thèse de doctorat

Rational design of plastic packaging for alcoholic beverages

Yan Zhu, Ingénieur ENSIC

With 89 Illustrations and 31 Tables

Acknowledgments

Firstly, I would like to thank sincerely to my academic supervisor Dr. Olivier Vitrac for his continuous and practical support during my Ph.D. study and related industrial projects, and for his guidance along my entire time of research and writing thesis manuscript. I also would like to express my gratitude to my industrial supervisor of the group Pernod Ricard, Mr. Bruno Guillemat for his patience, motivation, and continuous support and suggestion along with my Ph.D. study and internal industrial projects. Besides, I thank gratefully to Dr. Violette Ducruet as my former academic supervisor before her retirement, for her encouragement, guidance, and immense knowledge to help me in the first year and a half of my Ph.D. study.

Besides my supervisors, I would like to thank the rest members of my thesis committee. I thank Dr. Frank Welle (Fraunhofer IVV, Freising, Germany) and his group for the warm welcome at IVV in July 2017, and also for the fruitful exchange of ideas and data on the diffusion of homologous solute series in various polymers above or near T_g. I also thank Dr. Nicolas Delpouve (UMR 6634 GPM, University of Rouen Normandy, France), for his insightful and useful suggestions and encouragement. Both of their meaningful questions helped me to widen and deepen my research from various perspectives.

My sincere thanks also go to Dr. Phuong-Mai Nguyen, Dr. Maxime Touffet, Ph.D. student Benjamin Le Delliou, master student Denia Osmani for their experimental guidance, support, and encouragement, especially at Synchrotron Soleil. I want to express also my friendship to Ph.D. student Hajar Faraj for her technique information and encouragement.

I thank all my rest fellows in the group of Interactions Matériaux et Milieux au Contact (I2MC, UMR GENIAL 1145) for their technical and laboratory support and guidance. My laboratory work would not have been done well without the technical support of Mr. Cedric Plessis and Mr. Flavien Lecourtier.

I thank Association Nationale de la Recherche et de la Technologie (ANRT) and Pernod Ricard for the financial funding (N° 2015/1059) along with the three-year thesis study.

Finally, I would like to thank my family: my parents and my boyfriend for supporting me, spiritually throughout my thesis study and manuscript writing.

Foreword

"The mere formulation of a problem is far more often essential than its solution, which may be merely a matter of mathematical or experimental skill. To raise new questions, new possibilities, to regard old problems from a new angle requires creative imagination and marks real advances in science."

—Albert Einstein

I was a graduated master on chemical engineering and ambitious to have a rational plastic packaging design for various products in the fields of food, pharmaceuticals and cosmetics based on my educational background, initially. As broadening my knowledge and widening my horizons in multidisciplinary progressively, I realized scientific knowledge could not have solved rational design without a clarification and integration of the problems. A rational design of plastic packaging should insist mainly three predominant issues: the environmental impact (plastic wastes, marine litters, global warming, etc.), the social impact (food consumption and food wastes, human health, circular economic, etc.) and industrial effects (benefits and responsibilities, etc.). After integration of the constraints, I found the complicated problems for rational design might not be solved by studying merely the mass transfer and thermodynamics. Therefore, I would like to imagine and build a general engineering approach: [E]valuation, [D]ecision, and [S]olving, so-called [E][D][S] approach. According to the linked [D]ecisions as the integration of constraints, a simple model with ideal hypothesis will be established, simulated, and optimized to have a fast prototype design. [E]valuation could be considered as the further and more profound investigation of the transport and thermodynamic mechanisms on derived problems, such as safety, shelf-life, and packaging weight. [S]olving the problems should encompass the calculation, optimization, and reverse engineering upon on the [E]valuation and the [D]ecision.

This thesis is in cooperation with the group of Pernod Ricard, and the objective is to build a rational design of plastic packaging for alcoholic beverages, which could validate and improve my general [E][D][S] approach for safe-by-design. I may not be an expert in one of the domains, such as food, polymer, computer science, and the environment. However, I think it's of importance to focus on how to design rationally within a complex problem system in an interdisciplinary filed considering the organization of knowledge, engineering and engineering management. I hope this thesis could deliver some ideas, acquired knowledge, and methodologies to further related research topics and projects.

Table of Contents

CHAPTER I. INTRODUCTION **2**

I.1. CONTEXT 2

I.2. RATIONAL DESIGN 4

I.3. ORGANIZATION OF THE MANUSCRIPT 5

CHAPTER II. LITERATURE REVIEW **8**

II.1. BEYOND ENGINEERING: COMPUTER-AIDED DECISION MAKING 10

II.1.1. Problems which can be solved today with a computer *11*

II.1.2. Decision-based on utility theory *12*

II.1.3. Problem-solving methods in engineering *12*

II.1.4. Multicriteria optimization *17*

II.1.5. Ecodesign concepts and tools *22*

II.2. EVALUATION OF THE MIGRATION FROM PACKAGING MATERIALS 29

II.2.1. Preamble and scope *29*

II.2.2. Principles of tiered migration modeling for risk assessment *30*

II.2.3. Common assumptions used in migration modeling *32*

II.2.4. Diffusion properties in polymers *60*

II.2.5. Sorption properties and partition coefficients *70*

II.2.6. Probabilistic modeling of the migration *79*

II.2.7. Generalized migration modeling and holistic approaches *91*

II.3. EVALUATION OF THE ENVIRONMENT IMPACTS OF FOOD PACKAGING 95

II.3.1. A short history *95*

II.3.2. Sustainability and the difficult transition to sustainable food supply chain *96*

II.3.3. From legal frameworks to packaging wastes *97*

II.3.4. Life cycle assessment (LCA) *98*

II.3.5. Applications of LCA to beverage packaging *102*

II.4. ADDITIONAL INDICES TO CONSIDER IN FOOD PACKAGING DESIGN 107

II.4.1. Food shelf-life *107*

II.4.2. Mechanical resistance of PET bottles *112*

II.4.3. Sustainable and green chemistry *113*

II.5. CONCLUSIONS OF THE LITERATURE REVIEW 116

CHAPTER III. GOALS AND APPROACHES **120**

III.1. PREAMBLE 120

III.2. GENERAL GOAL AND CASE-STUDY 121

III.2.1. Towards holistic food-packaging engineering *121*

III.2.2. Epistemology of mathematical-computational instruments *122*

III.2.3. Case-study at tier zero *122*

III.3. SPECIFIC OBJECTIVES AND APPROACHES 129

CHAPTER IV. MATERIALS AND METHODS 134

IV.1. MATERIALS 134

IV.1.1. Studied PET materials 134

IV.1.2. Studied solutes 137

IV.1.3. Reference data and properties 137

IV.2. EXPERIMENTAL METHODS 144

IV.2.1. Mutual permeation of water and ethanol in real bottles 144

IV.2.2. Gravimetric measurements of water and ethanol sorption and diffusion (F1-F5, M) 146

IV.3. COMPUTATIONAL METHODS 149

IV.3.1. Mass transfer modeling of water and ethanol at tiers 1 and 2 149

IV.3.2. Mechanical constraints: risk of overpressure and collapse in the headspace 151

IV.3.3. Packaging design and optimization: case-study 155

CHAPTER V. RESULTS AND DISCUSSION 158

V.1. SCOPE OF TIERED MODELING 158

V.2. OPTIMIZATION OF THE DESIGN OF PET BOTTLES AT TIERS 1-2 159

V.2.1. Overview of the [E][D][S] implementation and choices 159

V.2.2. Dual bottle geometry models 161

V.2.3. Driving forces controlling primary shelf-life of liquors 164

V.2.4. Comparison of simulated and measured water-ethanol mass transfer across bottles M .. 168

V.2.5. Optimal design of packaging systems for liquors: bottles X as a case study 174

V.2.6. Main directions and limits of the optimization of PET bottles with fixed shelf-life 177

V.3. TERNARY ISOTHERMS OF WATER AND ETHANOL IN PET AT TIERS 2,3 178

V.3.1. Why is it difficult to estimate $\{C_{i,eq}^{T,Tg}\}_{i=w,e}$ in PET at glassy state? 180

V.3.2. Interpretation of swelling in ternary isotherms of PET 187

V.3.3. Ternary Flory-Huggins model with temperature and composition effects 188

V.3.4. Parameterization of binary parameters: χ_{w+P}^{T} and χ_{e+P}^{T} 191

V.3.5. Experimental validation of ternary isotherms 196

V.3.6. Ternary FH3 isotherms from 20°C to 50°C 198

V.4. A BLOB-FREE-VOLUME MODEL OF SOLUTE DIFFUSION COEFFICIENTS IN POLYMERS AT TIERS 3-4 . 200

V.4.1. Ambition and assumptions 200

V.4.2. Derivation of the blob free-volume theory 202

V.4.3. Experimental validation for linear probes 212

V.4.4. $P^{(T,T_g)}$ and reliable estimates of K_α and K_β 225

V.4.5. Prediction of diffusion coefficients 231

V.4.6. Main findings 240

V.5. GENERAL DISCUSSION ON TIERED PACKAGING DESIGN 242

V.5.1. Critical interactions between PET and solutes 242

V.5.2. The rule of the maximum driving force *245*
V.5.3. Estimation of the uncertainty in diffusivities *251*
V.5.4. Probabilistic estimation of shelf-life *253*

CHAPTER VI. CONCLUSIONS AND PERSPECTIVES 258

VI.1. CONCLUSIONS 258
VI.2. PERSPECTIVES 261

CHAPTER VII. RESUME DU TRAVAIL DE THESE EN FRANÇAIS 266

VII.1. CONTEXTE DU PROJET DE THESE 266
VII.2. PRINCIPAUX RESULTATS 271
VII.2.1. Exemple d'optimisation non supervisée aux paliers 1 et 2 ..... *271*
VII.2.2. Cosorption non linéaire dans le polyéthylène téréphtalate (PET) *273*
VII.2.3. Prédiction des coefficients de diffusion à partir d'une généralisation de la théorie des volumes libres *275*
VII.3. DISCUSSION, CONCLUSIONS ET PERSPECTIVES 278

CHAPTER VIII. REFERENCES 284

List of Publications

Articles

Zhu, Y., Guillemat, B., and Vitrac, O. (2019). Rational Design of Packaging: Toward Safer and Ecodesigned Food Packaging Systems. Frontiers in Chemistry Vol. 7. Article 349. https://doi.org/10.3389/fchem.2019.00349.

Zhu, Y., Welle, F., Vitrac, O. (2019). A blob model to parameterize polymer free-volumes and solute diffusion. submitted for Soft Matter.

Book chapter

Zhu, Y., Nguyen, P.M., Vitrac, O. 2019. Risk assessment of migration from packaging materials into food. In "Reference Module in Food Science". Volume *In Press*. Elsevier. Amsterdam. https://doi.org/10.1016/B978-0-08-100596-5.22501-8. 64p.

List of Figures

Figure II-1. Interplaying factors in engineering design: example of food-packaging design (modified from Figure 3.2 of Alexiou et al., 2010). 9

Figure II-2. (a-b,d) Illustrations of nonconvex goals; (c) convexification by adding boundaries $xL \leq x \leq xR$; (d) nonconvex problem combining a convex problem with Gaussian white noise ($infxf*$ and $supxf*$ are the bounds of the domain where the minimum can occur); (e) composition of two convex goals. The green triangle represents the initial guess and the red square the final solution of a randomized steepest descent algorithm. The intermediate positions are depicted with connected orange circles. In non-convex problems, the final solution may dependent on the initial guess (see (a) and (b)). 18

Figure II-3. Geometric interpretation of multidimensional optimization problem: (a) convex function; (b) nonconvex function; (c) the epigraph of a convex function is convex set; (d) polygonal convex set; (e-f) nonconvex sets; (g) convex hull of discrete points; (h) conic hull of (g); (i) convex hull of (e); (j) conic hull of (e); (k) intersection between a linear goal and a conic hull; (i) nonlinear feasible region associated to a convex goal; (j) idem under integer constraints. 21

Figure II-4. How environmental impact is created along the decision chain supporting product development (after Lewis et al., 2001). 23

Figure II-5. Aspects to consider in ecodesign of food packaging: (a) hierarchy of packaging waste management, (b) An example of a design guideline for source reduction of horizontal pouches used in the Korean food industry. “Acceptable” and “Optimum” refer to the dimensional allowable ranges (mm) in the design process (after Han, 2014). 25

Figure II-6. Overview of the bestiary of eco-design and design process tools from Ramani et al. (2010) 26

Figure II-7. Principle of the tiered approach to demonstrate compliance for food contact materials. Compliance is demonstrated as soon as the estimated concentration is greater than the threshold of concern. Tier 1 is usually associated with total migration (see Eq. (II.4)).... 31

Figure II-8. One-dimensional description of solute diffusion (e.g., additive, monomer) from the packaging wall (position: $0 \leq x/l_p \leq 1$, individual solutes identified as ×) to the contacting phase (individual solutes identified as ■) via the food boundary layer (individual solutes identified as ●): (a) random distribution of solutes and corresponding concentration profile at $Fo = 0.1$ and (b) after contact times up to $Fo = 2$. The percentages in the top part represent the residual amount in each compartment. 35

Figure II-9. Dimensionless desorption kinetics $\overline{v}^*\left(Fo\right) = \dfrac{C_F\left(Fo\right)}{C_F^{eq}}$ for various values of $L_{P/F}$, $K_{F/P}$ and Bi with $C_F^{eq} = \dfrac{C_P^0}{1/L_{P/F} + 1/K_{F/P}}$. Approximations [1] and [2] are given by Eqs. (II.17) and (II.18), respectively. 42

Figure II-10. Indexing rule of a material including m layers (total thickness l_P) in contact with a food indexed 0. The left and right external boundaries are considered impervious (no mass loss). The concepts of “functional barrier” and “reservoir” assume that layer j is the source (with non-zero initial concentration). It is used in §II.2.3.5.5. and §II.2.3.5.6. 44

Figure II-11. Concentration profiles (top) and migration kinetics (bottom) for the bilayer structure and scenarios detailed in **Table II-9**. 46

Figure II-12. Illustration of the additivity of the sources (see Eq. (II.26)) for a trilayer structure ABC associated with the case study detailed in **Table II-10**: concentration profiles (top), kinetics (bottom). The case “sources ABC” is obtained by simulating the whole structure.

The result A+B+C corresponds to the mathematical addition of the contributions of the three sources. 49

Figure II-13. Illustration of the conservative scenario of **Table II-10** based on the overestimation of the contribution of each source. The reference corresponds to the initial case-study configuration also depicted in **Figure II-12**.....50

Figure II-14. Principles of the simplification of a m -layer problem (here $m = 3$) into a problem with a lower number of layers and, therefore, easier parameterization. The represented distributions in the packaging correspond to initial conditions at various tiers. 51

Figure II-15. Illustration of the redistribution of the migrants from UV-cured printing ink and their subsequent migration in food for long shelf life products. The depicted cases cover hot-filled or aseptically filled products (e.g., soups, pasteurized juices, sterilized dairy products), and dry or ready-to-eat products stored in cardboard boxes. 52

Figure II-16. Illustration of the composition rules (a) for distances and (b) for the migration from a monolayer material, and of their invariance with the order of the steps (see Eqs. (II.28) and (II.35)).....54

Figure II-17. Scaling of diffusion coefficients between rigid and connected blocks with molar mass and van der Waals volume in a thermoplastic polymer (groups A and B refer to substances defined in **Figure II-18**). 64

Figure II-18. Scaling of diffusion coefficients of 49 substances (n-alkanes, two groups of molecules A and B with similar $\boldsymbol{DP}$ values) in LDPE at 23°C with molar mass, M, and the van der Waals volume.....66

Figure II-19. Diffusivities of various substances at 25°C in glassy and rubber polymers: (a) raw values, (b) normalized data to remove polymer effects (standardized to $\boldsymbol{Tg}$ value of 0°C corresponding to atactic polypropylene PP). Filled symbols correspond to n-alkanes (scaling laws $\boldsymbol{Dp \propto M - \alpha}$ as dashed lines) and empty symbols to various solutes including gases and plastic additives (scaling laws $\boldsymbol{Dp \propto M - \alpha}$ as continuous lines). Data from Schwope et al. (1990).....68

Figure II-20. Arrhenius plot of diffusivities of n-alkanes in polyethylene terephthalate. Data from Ewender and Welle (2014, 2016, 2018a). 69

Figure II-21. Ratio of fugacities between pure solid and amorphous states for 11 model migrants (data fromFornasiero et al., 2002) and its continuous approximation proposed in Figure S1 of the Supporting Information of Nguyen et al. (2017). 72

Figure II-22. Variation of the binary Flory-Huggins coefficient in water-ethanol mixtures. Data from Gillet et al. (2010). “abv” values represent the equivalent alcohol strength (alcohol-by-volume at 20°C and atmospheric pressure). Simulant C: 10% ethanol for alcoholic foodstuffs; simulant D1: 50% ethanol for high alcoholic and milk. 76

Figure II-23. Illustration of safety margins (SM), overestimation factors (Q) and uncertainty according to the method of calculation: real, likely and very conservative..... 81

Figure II-24. Probabilistic modeling of the contamination from a monolayer material via Eqs. (II.13) and (II.63): (a) point distribution for $\overline{Fo} = 0.5$; (b) corresponding 10th and 90th percentile curves. The likeliest migration curve corresponding to the maximum probability (mode) of the Fo distribution appears in bold.....89

Figure II-25. (a) Effect of Bi on the dimensionless migration kinetics. (b) Effect for $Bi \to \infty$ (the percentiles are represented as equivalent kinetics; distributions of $\overline{v}^*$ for $\overline{Fo}$ =0.5, 1,2, 3 and 4. 90

Figure II-26. Evolution of the scope of migration modeling during the last decades..... 91

Figure II-27. Sustainability defined at the joint intersection of society, economy and environment spheres: (a) original concept from concept of Remmen et al. (2007); (b) interpretation for food packaging. 96

Figure II-28. Interpretation of the ISO standards applicable for food production and food packaging management. 98

Figure II-29. Life cycle thinking applied to PET bottles for beverages adapted from Remmen et al. (2007) and by integrating the study of Almeida et al. (2010) 99

Figure II-30. Principles of multiobjective optimization with extensive indices (after Nielsen and Bastianoni, 2007). 102

Figure II-31. Review of LCA studies of plastics bottles per country, issuing organization and year 105

Figure II-32. Overview of conditions affecting the shelf-life of packaged food products: (a) main industrial steps (after Figure 1.1 of Rahman, 2007); (b) mass transfer and reactions (after Figure 2.2 of Singh et al., 2017). 108

Figure II-33. Principle of shelf-life calculations for a dry food product (initial water activity 0.15) stored in a humid atmosphere (75% RH) within a packaging slowing down water permeation: (a) water sorption isotherm and variation of glass transition temperature (Tg) with water content; (b) variation of texture induced by water uptake. Shelf-life is determined by the tolerance on the shift of Tg before (primary shelf-life) or after opening (secondary shelf-life). 110

Figure II-34. Simulated CO_2 depletion in a PET bottle containing a carbonated beverage (Carrieri et al., 2012): (a) simulated 2D wall profile along its axis of revolution; (b) details of the mesh (Lagrange quadratic); (c) diffusion coefficients of CO_2 in PET (Dp for preforms W_1 and W_2), in the headspace (Dh) and in water (Dw); (d) 2D CO_2 concentration profiles in bottles (W_1) quiver plot showing molar flux superimposed to concentration profiles; (e) evolution of Co_2 concentration in the bottle in variable temperature conditions. 112

Figure II-35. Relationship between bottle geometry, wall thickness distribution and mechanical resistance of PET bottles: (a) typical preform and temperature distribution during blowing; (b) relationship between yield strength and crystallinity; (c) vertical distribution of PET material after blowing for two preforms (40 and 37 g); distribution of buckling stress (compression tests a-c); (e) distribution of stresses in a petaloid shape bottle for carbonated bottles; (f) details of the distribution of stresses at the petaloid bottom (red = maximum stress at the center) 113

Figure II-36. (a) green chemistry pocket guide of the American Chemical Society; (b) schematic definition of sustainable and green chemistry 114

Figure II-37. The role of chemical thermodynamics in the objective evaluation of the performance of engineered systems (after Figure 1.5 of Valsaraj and Melvin, 2018). 117

Figure III-1. Initial designs ($D1..D4$) considered in the global optimization problem. The height b of $D1$ and $D2$ is fixed to 15 cm. The black circle on top represents the opening (cap not shown) 124

Figure III-2. Principle of the iterative resolution of the ecodesign problems using the [E][D][S] framework 125

Figure III-3. Typical sphericity values for convex regular polyhedrons. 126

Figure III-4. Weights of the bottle (counted as 100% waste) versus shelf-life for the designs $D1..D4$ calculated according to Eq. (III.3) for bottle capacities $V_F^{t=0}$ ranging from 0.05 L to 0.75 L. 128

Figure III-5. Main capabilities (this work) and foreseen evolutions (considered by construction) in the considered [E][D][S] framework 131

Figure IV-1. *Bottle geometry: (a) radius profile (the arrows indicate the top and bottom position of the sleeve and the vertical line indicate the level of liquid for pure water); (b) 3D-representation assuming a revolution geometry; (c) thickness profile (the shadow indicates the variation range of measurements among 10 bottles); (d) filled and sealed bottle; (e) bottle equipped with a shrink sleeve label.* 136

Figure IV-2.*Example of initial bottle design to be optimized*..... 136

Figure IV-3*. List of studied solutes*..... 143

Figure IV-4*. Example of calculations to estimate the risk of exceeding the lower flammability limit (LFL) in large scale experiments.* 144

Figure IV-5*. Principle of the cosorption microbalance (denoted B in* ***Table IV-8****): (a) overview of the gas circuit involving two saturators; (b) the entire microbalance and the anti-vibration platform are placed in the oven. SOS: sensor of sound speed.* 147

Figure V-1. Overview of four tiers considered for packaging optimization with the proposed [E][D][S] framework..... 158

Figure V-2. Dual representation of the geometry of bottle ***Figure IV-1*** in 3D and curvilinear coordinates. The equivalent geometry of the bottles as seven independent sections in contact with the same liquid is shown in d as histograms. 162

Figure V-3. Comparison between (a) an unwrapped hollow 3D geometry and (b) its approximation with uniform thickness. The arrow represents the normal mass flux crossing each geometry. The values of indicated thicknesses are indicative; in real bottles, the thinnest regions exhibit the largest surface area of transfer (see distribution in **Figure V-2**d)..... 163

Figure V-4. Binary properties of water-ethanol mixtures: (a) activities, (b) partial pressures, (c) total pressure in vacuum, (d) liquid density. The symbols depict the tested beverages and storage conditions. Horizontal lines in (a) show the variation of RH when the air temperature is increased from 20°C up to 70°C..... 166

Figure V-5. Calculated iso-headspace pressures (P_{head}) and iso-headspace volume (V_{head}) at equilibrium in the bottle depicted in **Figure IV-1** according to the headspace volume (V_{head}^{0}) and temperature (T_0) at filling time. The results are presented for two storage temperature 50°C (a,b,c) and 35°C (d,e,f) three abv values (0,15, 0.4, 0.7). 167

Figure V-6. Comparison of experimental (exp) and simulated (sim) mass loss and abv variations. The dashed lines plot the thresholds used to calculate shelf-life (see text). Empty symbols (triangles) represent the theoretical variation of abv when concentration effects due to water permeation are corrected..... 170

Figure V-7. Reconstruction of mass losses by sorption and permeation for (a,b) water and (c,d) ethanol..... 171

Figure V-8. Modifications of mass transfer when a sleeve is added to the bottles containing the beverage B3 and B4 after several months of storage: mass loss during condition S3 (dash lines, one line per considered bottle) and S4 (continuous lines, one line per considered bottle). 173

Figure V-9. Space of geometries explored and optimized for a 160 mL bottle (capacity 150 mL) containing a vodka-type beverage: (a) shapes corresponding to a 30×30 combination of W and D, (b) 5×5 combination, (c) weights of bottles optimized to fulfill a shelf-life of 180 days at 25°C. 175

Figure V-10. (a) iso-weight and (b) iso-thickness contours of optimized bottles (minimum shelf-life of 180 days) shown in **Figure V-9**. The filled symbols locate the sampled Pareto front. A selection of designs sampled along the Pareto front (from left to right) is presented in (c). 176

Figure V-11. Schematic representation (a) of the state of the polymer and (b) the corresponding mechanism of diffusion during a sorption experiment. *Deb* stands for the Deborah number. (modified fromVrentas et al., 1975). 179

Figure V-12. Interpretation of water sorption kinetics in 280 µm thick PET of Dubelley et al. (2017a): (a) $1/\beta$-isocontours in days (continuous lines; β>0: positive effect of relaxation on uptake, i.e. swelling; β<0: negative effect of relaxation on uptake, i.e. densification); (b) corresponding iso-Deborah numbers (continuous lines; same sign as β). Dashed lines represent iso-*pw* in kPa of the corresponding water vapor. 183

Figure V-13. Cycle of sorption-desorption of water in 12 µm think PET films (reference F1) involving 16 steps from 50% to 99% RH (steps 1-6) and from 99% down to 0% RH (steps 7-16) at 50°C. Continuous lines are fitted models from Eq. (V.4). Corresponding values of $1/\beta$ and ϕ are plotted in the lower and upper insets. $Mdry$ = sample dry mass 185

Figure V-14. Cycle of sorption-desorption of water in 12 µm think PET films (reference F1) involving seven steps from 45% to 95% RH (steps 1-4) and from 95% down to 45% RH (steps 5-7) at 50°C. Continuous lines are fitted models from Eq. (V.4). Corresponding values of $1/\beta$ and ϕ are plotted in the lower and upper insets. $Mdry$ = sample dry mass 186

Figure V-15. Water sorption/desorption kinetics of the PET walls (thickness 629±33 µm) at 50°C for four stepwise variations of relative humidity (RH steps are indicated in legend): (a) mass uptake relative to dry mass $Mdry$; (b) mass uptake normalized by its final value. Continuous lines are fitted models from Eq. (V.4). 187

Figure V-16. Fitted binary Flory-Huggins isotherms for (a) water, (b) ethanol and (c) methanol at temperatures ranging from 20°C to 100°C. 192

Figure V-17. Effect of temperature on $\chi i + PT$ values. Data sources are shown in **Figure V-16**. The models for subcooled PET are shown in continuous lines (smoothed cubic spline). The model for densified PET materials are shown as dashed lines (smoothed quintic spline). 193

Figure V-18. Long-term sorption behavior of 12 µm thick PET films after exposure (a) to 97.5% RH and (b) 99% ethanol. Two repetitions are shown in (a) (denoted r_1 and r_2); five repetitions are combined in (b). The inset is showing the same kinetics during the first month. The continuous lines describe a sorption model similar to Eq (V.4) (a) with double relaxation (one positive for swelling and one negative to describe densification) and (b) with a single relaxation. 195

Figure V-19. Typical diffusion behaviors in glassy polymers with penetrant concentration and Deborah numbers for differential step-change sorption experiments. (modified from (modified from Vrentas and Vrentas, 2001), the dimensionless sorption curves are calculated from Eq. (V.4) for $\phi = 0.7$). 196

Figure V-20. Theoretical iso-mass uptake of water and ethanol in PET at 35°C at equilibrium with a water or ethanol gas mixture (below the liquidus curve), with a hydroalcoholic solution (on the liquidus curve) and at high pressure (above the liquidus curve): (a) $meaw, ae$ (b) $mwaw, ae$ and (c) $mwaw, ae + meaw, ae$). The liquidus curve calculated from **Figure V-4**a is plotted as a continuous line. The symbols depict the conditions tested experimentally. 197

Figure V-21. Comparison of mass uptakes for conditions depicted in **Figure V-20** with continuous predictions from ternary isotherms (to be used for equilibriums with hydroalcoholic solutions) and ternary isotherms (to be used for equilibriums with saturated salt solutions). 198

Figure V-22. Ternary FH3 isotherm of water and ethanol in PET at 20°C and 50°C. 199

Figure V-23. Inheritance between FV contributions (a) and (b) definitions of free-volumes. The horizontal arrows define the direction of the extensions. αg and αc are the thermal expansion coefficients at glassy state and at the critical temperature. 201

Figure V-24. Illustration of the procedure to calculate arbitrary diffusion coefficients from the proposed blob-FV model a) solute blob model; b) free volume parameterization and *D* model; c) example of water diffusion prediction in PET 202

Figure V-25. Scaling of diffusion coefficients, D_{lin} or D_a, of n-alkanes (n-A), 1-alcohols (1-O) and alkyl-acetates (a-A) with the molecular mass of the alkyl chain, M in: (a) PET, (b) PA6, (c) PS and (d) PVAc. Continuous and dotted lines correspond to the regression lines for regular solutes (n-alkanes) and their generalization to anchored ones (1-alcohols and alkyl acetates) via Eq. (V.39), respectively. $\langle M_{blob} \rangle$ was estimated the common intersection of all regression lines of $\ln D_{lin}$ vs $\ln M$ (see its interpretation in Eqs.(V.19) and (V.30)). 215

Figure V-26. Apparent activation energies $\langle E_a \rangle$ of linear solutes in function of the alkyl chain mass, M, in: (a) PET, (b) PA6, (c) PS and (d) PVAc. Data sets were split according to the considered families of molecular probes (n-A: n-alkanes, 1-O: 1-alchols and a-A: alkyl acetates) and according to the temperature ranges used for the determination of $\langle E_a \rangle$. The linear regressions $\langle E_a \rangle$ vs $\ln M$ are plotted as continuous lines (see Eqs. (V.29) and (V.31)). 220

Figure V-27. Normalized activation energies (see Eq. (V.29)) when free volume effects are normalized by the dimensionless temperature $\langle I \rangle$ defined in Eq.(V.28). All values are expressed in excess to a theoretical hexyl chain (C_6H_{13}). Regression lines with $\ln M$ are plotted as continuous and dashed lines, for probes with low and high anchor effects, respectively.222

Figure V-28. Variation of $\alpha_{lin}(T)$ with $T - T_g$ when it is estimated from regular linear probes (blob model) and equivalent anchored solutes. Symbols correspond to determinations according to method 1 (scaling of D_{lin} or D_a with M; see **Figure V-25** and Eq.(V.19)) or according to method 2 (regression of $\langle E_a \rangle$ with $\ln M$; see **Figure V-26** and Eq.(V.29)). The continuous model ((V.22)) is plotted as continuous lines for different estimates of K_α, K_β and r for both regular solutes and anchored ones (see text for values). 224

Figure V-29. Polymer function $P(T, T_g)$ versus $T - T_g$ predicted by Eq. (V.20)(continuous lines) and by Eq.(V.15) using either specific (dashed lines) or generic (dotted lines) WLF constants. The corresponding FV parameters are listed in **Table V-2**. All models are plotted for three typical r values at glassy state (0.5, 0.25 and 0.1) leading to three branches when $T - T_g$ <0. As constant thermal expansion is assumed at rubber and glassy states, the diagrams are limited by the inequalities: $T - T_g > \frac{1}{r}\left(\frac{K_\alpha}{\alpha(T, T_g) - 1} - K_\beta \right)$ and $\alpha_{lin}(T, T_g) \geq 1$. The square and round symbols depict the $P(T, T_g)$ values corresponding to $\alpha_{lin} = 4$ and $\alpha_{lin} = 9$, respectively. 230

Figure V-30. Experimental (symbols) and predicted (lines) diffusion coefficients via Eq. (V.30)and parameters listed in **Table V-2** for n-alkanes in PVAc (bold continuous lines), PA6 (continuous lines), PET (dashed-dotted lines), PS (dashed lines) and PEN (dotted lines). The dashed vertical line represents the T_g value of the polymer for the corresponding set of data. The predictions assume the inequality: $T - T_g > \frac{1}{r}\left(\frac{K_\alpha}{\alpha_{(T, T_g)^{-1}}} - K_\beta \right)$. T_g values of PVAc and PA6 are out of bounds. 232

Figure V-31. Experimental (symbols) and predicted (lines) diffusion coefficients via Eqs.(V.30) and (V.39) along with parameters in **Table IV-5** for (a) 1-alcohols and (b) alkyl acetates in PVAc (bold continuous lines), PA6 (continuous lines), PS (dashed lines) and PEN (dotted lines). The dashed vertical line represents the T_g value of the polymer for the corresponding set of data; the corresponding. T_g values of PVAc and PA6 are out of bounds. 233

Figure V-32. Comparison of experimental diffusion coefficients, ("exp", filled symbols), and simulated ones by molecular dynamics ("sim", open symbols) with values predicted from Eq. (V.25) and parameters reported in **Table V-3** for (a) water and (b) toluene in amorphous PET at infinite dilution of not mentioned otherwise. All calculations are performed with a theoretical T_g of 349 K (continuous lines). Swollen PET due to a contact with a liquid or measurements at high solute activities is identified as "swollen" and is associated to an indicative T_g of 333 K, value from Langevin et al. (1994) for PET fully swollen with water; corresponding values are plotted as dashed lines. 238

Figure V-33. Comparison of predicted and experimental diffusion coefficients of toluene at infinite dilution in various polymers. 240

Figure V-34. Microscopic observations in phase contrast of the cross sections of 12µm-thick PET film F1. (a) neat film; (b) film immersed in water at 50°C for 10 hours; (c) film immersed in ethanol at 50°C for 10 hours. 243

Figure V-35. Comparison of the apparent activation energies of diffusion of ethanol (gravimetric measurement after liquid contact with 99% ethanol, five repetitions for each condition). The inset shows the distribution of apparent activation energies based on 1000 bootstrap samples. 244

Figure V-36. Sorption kinetics of ethanol and toluene in 12 µm thick PET films (F_1) at 50°C at high activities. The fitted model is a delayed version of Eq. (V.4). 245

Figure V-37. Theoretical and experimental mass losses (water and ethanol) in 12 µm thick PET film (F1) at 50°C: (a) theoretical residual ethanol content; (b) theoretical residual water content; (c) cumulated amount of water and ethanol; (d) comparison between experimental and theoretical value along the routes ABEDF and ABCDF. 247

Figure V-38. Independent simulation of the mass transfer of water and ethanol associated with a negative step of water activity of 0.51 down to 0.40 and a positive step of ethanol activity to 0.38 at 50°C. Concentration profiles (100 times) are shown for the whole period and are distributed as the square root of time. 248

Figure V-39. Comparison between simulated mass uptake and experimental determinations for 680 µm thick bottle walls at 50°C using the cosorption microbalance (experimental conditions and simulated results are shown in **Figure V-38** with fitted values for water and ethanol listed in **Table V-4**). 249

Figure V-40. Analysis of the fluctuations of mass uptake vs the fluctuations of relative humidity (period 240 s) in 12 µm thick PET bottle (M) at 50°C: (a) raw results, (b) correlation between fluctuations when the average delay between has been removed. 250

Figure V-41. Sorption/desorption cycles of 12 µm thick PET films at 25°C from an initial state at 50±10% RH. Cases leading to significant desorption are plotted in dashed lines. 251

Figure V-42. Principles of the probabilistic determination of shelf-life based on a double criterion on weight loss and *abv* variation. The input temperature distributions are shown in upper inset. The corresponding transportation, storage and combined distributions are shown horizontally. The distribution of weight loss and abv variations on the left and right, respectively. The tolerances are shown as dashed lines. The filled areas represent the probability to exceed tolerances. 255

***Figure VII-1**. Designs simplifiés de bouteilles (D1..D4) utilisés pour illustrer la démarche d'optimisation géométrique sous contraintes du matériau et du produit emballé. La hauteur b of D1 and D2 est fixée à 15 cm. Le disque noir (Ø 2 cm) représente l'ouverture de la bouteille (le bouchon n'est pas visible).* 268

Figure VII-2. Représentation géométrique des équations *(VII.1)* et *(VII.3)-(VII.4)* pour une bouteille de 0.25 L. Les isocontours représentent les valeurs du rapport $\frac{M_P\left(V_F^{t=0}=0.25\,L\right)}{M_P\left(V_F^{t=0}=1\,L\right)}$ 269

***Figure VII-3**. Principe du prototypage rapide de bouteilles pour les boissons alcoolisées via l'approche itérative à trois Etapes [E]valuation, [D]écision et ré[S]olution proposée.* 270

Figure VII-4. Optimisation de la géométrie d'une mignonnette (capacité 150 mL et un volume d'espace de tête de 10 mL) utilisée pour le transport aérien avec une durée de vie de 180 jours à 25°C pour une boisson de type vodka. 272

Figure VII-5. Principe de l'étude des propriétés de sorption dans le PET (a-b) et isotherme ternaire eau-éthanol déterminée à 50°C (c-f). La courbe en gras représente le « liquidus » et les symboles les conditions utilisées pour la validation présentée dans la **Figure V-21**. 273

Figure VII-6. Comparaison entre les prédictions de l'isotherme ternaire eau-éthanol dans le PET à 35°C avec les sorptions expérimentales. 275

Figure VII-7. Relations en lois d'échelle, théorie des volumes libres et coefficients de diffusion : (a) comparaison des lois d'échelle avec la masse moléculaire pour des solutés linéaires et encombrés ; (b) filiation de la théorie des volumes libres ; (c) lois d'échelle dans le polyéthylène basse densité à 23°C ; (d) principe du paramétrage de la théorie des volumes libres à partir des coefficients de diffusion de molécules sondes linéaires. L'équation de Piringer utilisée pour démontrer la conformité des matériaux d'emballages alimentaires est représentée en pointillés sur la figure (a) ; elle correspond à un surestimateur empirique qui sous-estime la dépendance réelle à la masse moléculaire *M*. 276

Figure VII-8. Paramétrisation et prédictions des coefficients de diffusion de l'eau et de l'éthanol dans le PET à l'état caoutchoutique et vitreux : (a) lois d'échelle à l'état caoutchoutique et vitreux pour des molécules sondes linéaires ; (b) modèle générique de coefficients de diffusion et paramétrage du modèle pour l'eau et le toluène ; (c) validation pour l'eau sur la base d'une identification de *r* à partir des données de Launay et al. (1999) ; (d) validation pour le toluène dans cinq polymères ; (e) dépendance des coefficients de diffusion du toluène à la température ; (f) cinétiques de sorption à 50°C mettant en évidence la relaxation du polymère. 277

Figure VII-9. Analyse des fluctuations du flux de matière en fonction de la fluctuation périodique (période de 240 s) de la pression partielle en vapeur d'eau à 50°C pour un échantillon de 630 µm d'épaisseur. 279

Figure VII-10. Distribution de la perte de poids (droite) et de la variation du titre alcoolique (gauche) en fonction des distributions combinées des températures au cours du transport et du stockage (encart). La figure centrale montre la variation déterministe de la perte de poids et du titre alcoolique (abv) en avec un temps de séjour équivalent à 25°C. 280

List of Tables

Table II-1. Overview of problem-solving methodologies. 14

Table II-2. Comparison between the complexity level defined by Genrich Altshuller and the TRL. 16

Table II-3. Typology of optimization problems 18

Table II-4. List of relevant monographies to tackle complex optimization problems (convex or not) met in engineering and related fields. 22

Table II-5. Classification of ecodesign tools and methodologies and associated problem-solving method (see **Table II-1**). 27

Table II-6. Prerequisites and indicative tiers to be used for compliance testing (R1=most severe, R3=most refined) 32

Fo and Bi correspond to dimensionless time and ratio internal-to-external mass transfer resistance, which are both defined in **Table II-7**. 35

Table II-8. Key dimensionless quantities of the migration from monomaterials. Contact is assumed to be initiated at $t = 0$ 36

Table II-9. Illustration of the main behaviors associated with multilayer structures. The concepts of functional barrier and reservoir are illustrated in **Figure II-11**. 45

Table II-10. Parameters used to construct realistic and conservative migration scenarios depicted in **Figure II-12** and **Figure II-13**. Quantities are expressed respectively to the likely values[+] for the first layer (the three layers ABC are indexed 1,2,3). They are scalar when the contribution of each layer as a source is considered in combination with others (the three sources are considered at once). The contributions of individual sources are indicated by 3×1 vectors mentioning the properties of all layers considered as a source or not. 48

Table II-11. Expressions of practical partial pressures and saturation concentrations in relationship with the reference state of the substance in the conditions where its migration its studied 71

Table II-12. Density (kg·m^{-3}) of water-ethanol mixture and corresponding volume fraction of ethanol ($\phi_{ethanol}$) between 10 and 60°C. Volume fractions are calculated from partial molar volumes. 76

Table II-13. Recommended distributions for probabilistic modeling of the migration from monolayer materials. The distributions of $\overline{v}^*$ and $\sqrt{Fo^*}$ are posterior distributions. 85

Table II-14. Main steps in LCA analysis 100

Table II-15. Overview of typical packaging materials for beverages (after Marsh and Bugusu, 2007;Welle,2011;Ramos et al.,2015) 103

Table II-16. Comparative environmental impacts of PET containers vs alternative materials from a selection of studies. Containers are bottles except if mentioned differently. The selection is based on peer-reviewed studies except if indicated otherwise. Considered impacts include the production of containers, transport, disposal of solid waste resulting from packaging and recycling. 106

Table II-17. Main factors affecting food shelf-life or safe life (after Table 2.1 of Singh et al., 2017). 109

Table II-18. Examples of sustainable and green chemistry applicable to food packaging ..115

Table III-1. Specific goals to be extended and the corresponding approach followed in this work 129

Table III-2. List of the considered tiers in the nested formulation $\left[E_{T_i}^{tier} \left[D \right] \left[S \right] \right]$ 132

Table IV-1. *Studied PET films and bottles* 135

The solutes incorporated in the contacting phase (gas, liquid, solution) are listed in ***Table IV-2.*** Water and ethanol, alone or in mixtures were the main solutes. The composition of hydroalcoholic mixtures were denoted by their alcohol-by-volume (abv), defined as the number of liter (L) of pure ethanol present in 1 L of solution at 20 °C (pure ethanol: $abv = 1$). Other aromatic solutes were surrogate molecules chosen with double purposes: comparison with literature data on similar PET materials and naturally fluorescent molecules consisting of linearly repeated jumping units. Toluene was preferred to benzene (single jumping unit) due to its high toxicity. 142

Table IV-3. *Thermodynamic and transport properties of water and ethanol in PET* 139

Table IV-4. *Consolidated data t D_e o develop and validate high-tier modeling in PET* 139

Table IV-5. *Overview of the database for binary diffusion coefficients in PET and in additional polymers used for validation* 142

Table IV-6. *Hydroalcoholic solutions simulating real alcoholic beverages* 145

Table IV-7. Studied long-term storage conditions 146

Table IV-8. Overview of sorption measurement strategies 147

Table V-1. Comparison of shelf-lives extrapolated from experiments and calculated from simulations 172

Table V-2. Main parameters used to predict diffusion coefficients, and free volume effects plotted in Figures 5-7. 228

Table V-3. Main parameters used to predict diffusion coefficients of water and toluene in Figures 8 and 9. 236

Table V-4. Comparison of diffusion coefficients determined at different tiers and using different methods 252

NOMENCLATURE

The symbols are listed in alphabetic order and grouped by similarities. Redundant definitions are given on independent lines. When the definitions may be ambiguous, reference equations are indicated. All units are in SI.

Roman symbols

$\%A,\%B$	volume fractions of saturated gas on the co-sorption microbalance (-)
abv	alcohol-by-volume (volume of ethanol at 20°C, number of mL of pure ethanol in 1 mL of mixture)
a_i	activity of solute i (-)
a_{lin}	constant equal to 0.24 in the extended FVT (Eq. V.17)
A	surface area of contact or exposed (m^2)
A'_p	preexponential factor in the Piringer's Equation (Eq. II.44)
$B(\epsilon)$	Boltzmann factor (Eq. II.57)
$Bi = \frac{hl_p}{D_{i,p}}$	dimensionless mass Biot or Sherwood number (-)
c	crystallinity = volume fraction of crystalline phase (-), celerity of the sound ($m \cdot s^{-1}$)
C, $C_{i,k}$, $\underline{\boldsymbol{C}}$	volume concentration ($mol \cdot m^{-3}$ or $kg \cdot m^{-3}$), concentration of substance i in the phase/layer k, concentration field after discretization
C_p^i	heat capacity of pure substance i ($J \cdot kg^{-1} \cdot K^{-1}$)
C_{12},C_{22}	universal WLF constants (17.44 and 51.6 K, respectively)
D	bottle depth (m)
D,D_j ,$D_{i,k}$	diffusion coefficient ($m^2 \cdot s^{-1}$), diffusion coefficient in layer j, diffusion coefficient of substance i in the phase/layer k
D_0	preexponential coefficient in the FVT of Vrentas and Duda ($m^2 \cdot s^{-1}$)
D_{lin}, D_a	diffusion coefficients of homologous solutes with repeated patterns without and with anchors ($m^2 \cdot s^{-1}$)
D_{blob}, D_{anchor}	diffusion coefficients associated to the isolated blob and anchor ($m^2 \cdot s^{-1}$)
$Deb = \frac{D_{i,p}}{\beta l_p^2}$	Deborah number or dimensionless relaxation time (-)
E^*, E^*_{blob}, E^*_{anchor}	specific solute-polymer interaction energy in the FVT of Vrentas and Duda ($J \cdot mol^{-1}$), its generalizations for an individual blob and anchor, respectively
E_a,$\langle E_a \rangle$	activation energy ($J \cdot mol^{-1}$), apparent activation energy
f	frequency (Hz) or arbitrary function, generalized driving force $f = -\frac{\partial \mu}{\partial x}$
$f_{i,j}$	fugacity of substance i in layer/material j
$Fo = \frac{D_{i,p}t}{l_p^2}$	Fourier number or dimensionless time (-)
g_{CM}	mean-square displacement
G,$G^{\ddagger}$,G_k	molar free energy ($J \cdot mol^{-1}$), value at transition state, value for component k
$\Delta G_{i,j}^{solvation}$	molar solvation free energy of substance i in phase or layer j ($J \cdot mol^{-1}$)

h,h_i mass transfer coefficient through liquid boundary layer (m·s^{-1}), equivalent conductance for substance i

$\langle h_{A+B} \rangle_T$ ensemble-averaged enthalpy of mixing (J·mol^{-1})

H bottle height (m)

$\Delta H_{F_1+F_2}^{molar}$ molar enthalpy of the mixing of liquids F_1 and F_2 (J·mol^{-1})

$\langle \mathrm{I} \rangle$ dimensionless temperature defined in Eq. V.27 (-)

j,J mass flux density (mol·m^{-2}·s^{-1} or kg·m^{-2}·s^{-1}), index of layer/material with the food indexed $j = 0$

j_{ref} reference layer maximizing $\frac{l_j D_j}{k_j}$ (-)

k, k_j Henry coefficient (Pa·m^3·mol^{-1} or Pa·m^3·kg^{-1}), Henry coefficient of layer j

K_{12},K_{22} constants in the FVT of Vrentas and Duda related to WLF constants (Eqs V.10 and V.11)

K_α, K_β polymer specific constants in the FVT extended to flexible solutes (K)

$K_{i,j_1/j_2} = \frac{C_{i,j_1}}{C_{i,j_2}} = \frac{\gamma_{i,j_2}}{\gamma_{i,j_1}}$ partition coefficient of substance i between the phases/layers j_1 and j_2 (-)

l, l_j,l_{wall} distance or thickness (m), thickness of layer j, thickness of walls

ℓ visited distance (m)

$\ell_F = \frac{K_{F/p}}{L_{P/F}}$ dimensionless equivalent length of the contacting phase (-)

L_j accumulated distance or thickness up to layer j

$L_{P/F}$ material-to-food volume or mass ratio (-)

m number of layers (-)

m_i,m_F, $\%\Delta m_F$, m_p residual mass of compound i, mass of the food (kg), relative weight variation tolerance (-), mass of the empty packaging unit (kg)

M, M_i, M_j molecular mass (kg·mol^{-3}), molecular mass of substance i, amount transferred from layer/material j

M_{anchor},M_{blob},ΔM_{eq}^a molecular masses of the terminal rigid units (different of the repeated blob) and the repeated pattern (kg·mol^{-3}), equivalent molecular associated to the anchor to reach the same diffusion coefficient as in a regular linear solute

M_p accumulated mass of the packaging units corresponding to a consumption rate (kg)

n exponent associated to the system of coordinates ($n = 0$: Cartesian, $n = 1$: cylindrical, $n = 2$: spherical)

n_i^g,n_a number of molecules i in the gas phase (Eq. IV.13), initial number of molecules of dry air in the headspace (Eq. IV.14)

n_{nodes},n_{steps} number of nodes in the discretization scheme, number of steps in the migration scenario

$n_{\substack{rigid \\ blocks}}$, n_{blobs} or N number of rigid jumping units or blobs

N,N_0 number of substances

p, p_i,$\boldsymbol{p}$ partial pressure (Pa), partial pressure of solute i, parameter vector

$P(T, T_g)$ polymer function in the extended FVT (Eqs. V.15, V.20)

$q = \frac{x}{l_p}$, q_n dimensionless position (-), zeros of the transcendental equation $\tan q_n = -\ell_F q_n$ (Eq. II.19)

Q_A,Q_B total volume flow rates of ways A and B of the co-sorption microbalance (m^3·s^{-1})

r radius (m)

$r = \frac{\alpha_g}{\alpha_c}$	subcooling ratio (-)
$\boldsymbol{r}$	position vector
$r_{i,k} \approx \frac{\bar{V}_k}{\bar{V}_i}$	number of molecules of phase k displaced by the insertion of solute i
$\Re$	overall mass transfer resistance (s·m^{-1})
R	ideal gas constant (8.314 J·K^{-1}·mol^{-1})
RH	relative humidity (%)
S_n	summation term in Eq. II.17
t	time (s)
$t_{consumption}$	time to consume the content of the packaging (s)
t_{shelf}	shelf-life (s)
T, T_g, $T_{i,m}$	temperature (K), glass transition temperature, melting temperature of pure compound i
u,v	parameters in the FVT of Vrentas and Duda so that $\tilde{V}_2^* = u + vT_g$
$u = \frac{C_{(x,t)}}{C_{ref}}$	dimensionless concentration (-), usually with C_{ref} the averaged initial concentration
$\bar{v}^* = \frac{C_F}{C_F^{eq}}$	normalized concentration representing the distance to equilibrium (-)
$\tilde{V}_1^*$, $\tilde{V}_{1\,lin}^*$	critical volume of the solute jumping unit or of its largest rigid unit (m^3), value for linear solutes
$V_{consumption}$	volume of food consumed during a prescribed amount of time (m^3)
V_F, $V_F^{t=0}$,$V_{beverage}$,V_{head}	food volume (m^3), initial food volume, packaging capacity, volume of the headspace
$\hat{V}_2^*$	specific hole free volume of the equilibrium liquid polymer in the FVT of Vrentas and Duda (m^3)
$\tilde{V}_2^*$	critical volume of the polymer jumping unit (m^3, Eq. V.13)
$\bar{V}_i$	molar volume (m^3·mol^{-1})
$V_{\substack{rigid \\ block}}^{vdW}$	volume of the rigid unit (m^3)
W	bottle width (m)
$\boldsymbol{x}$ or $\boldsymbol{y}$, $\boldsymbol{x^L}$, $\boldsymbol{x^U}$	input vectors, lower bounds of $\boldsymbol{x}$, upper bounds of $\boldsymbol{x}$
x	position (m)
x_i	molar fraction in compound i
z	number of neighbors in the off-lattice FH formulation (-)

Greek symbols

α, α_{lin},α_a	scaling exponents of diffusion coefficients with their molecular mass at infinite dilution (-), idem for linear solutes, idem for solutes with anchors
α_g,α_c	thermal expansion coefficients at glassy state and at the critical temperature $T = T_g$ (-)
α_2^g,α_2	as above with the original notations of Vrentas and Duda (-)
β	polymer relaxation rate (s^{-1})
β_{lin}	scaling exponents of self-diffusion coefficients of linear solutes (-)
γ	overlap factor in the FVT of Vrentas and Duda (Eq. V.8)
$\gamma_{i,k}^v$	activity coefficient of solute i in phase k relative to volume fraction $\phi_{i,k}$ (-)

$\Gamma = 1 + \frac{\partial \ln \gamma^v}{\partial ln\phi}$ thermodynamic factor associated to mutual diffusion coefficients (-)

$\Delta a_w, \Delta a_e$ tolerances of the co-sorption microbalance on the variation of activities of water and ethanol (-)

Δj fluctuation of mass flux (kg·s^{-1})

Δp difference of partial pressure responsible of permeation (Pa), fluctuation of partial pressure

ϵ, ϵ_{A+B} small variation or porosity, pair contact energy (J or J·mol^{-1}), pair contact energy between A and B

ζ,ζ_{trace},ζ_{mutual} friction coefficient (J·s·mol^{-1}· m^{-2}), at infinite dilution and higher concentration, respectively

κ preexponential factor in Eq. II.6 (Hz)

λ arbitrary weight in Eq. II.3, parameter related to the thermal expansion of the polymer in the FVT of Vrentas and Duda (Eq. V.12)

μ, $\mu_{i,k}$ chemical potential (J·mol^{-1}), chemical potential of solute i in phase k

$\xi = \frac{\widetilde{V}_1^*}{\widetilde{V}_2^*(T_g)}$, ξ_M ratio of the critical volume of the solute jumping unit to the critical volume of the polymer jumping unit in the FVT of Vrentas and Duda (-), value of ξ associated with molecular mass M

ρ, ρ_k molar density (mol·m^{-3}) or probability density (m^{-3}), density of phase k (kg·m^{-3})

τ dimensionless excess activation energy in the Piringer's equation (Eq. II.44)

τ_0 longest polymer relaxation time (s)

$\phi_{i,k}$ volume fraction of solute i in phase k (-)

$\chi_{i,k}$ or χ_{i+k} binary Flory-Huggins coefficient between the components i and k (-)

$\Psi = \frac{\pi^{\frac{1}{3}}(6V_F^{t=0})^{\frac{2}{3}}}{A}$ sphericity of the packaging with a capacity $V_F^{t=0}$ and an exposed surface area A

ω_i weights (-)

Mathematical operators

Ω_{int} internal volume

$\partial\Omega_{int}$ internal surfaces in contact with the liquid or its vapors

$argmin(f) = x_{min}$ argument of the minimum (*i.e.* $f(x_{min})$ is minimum)

Δ difference operator

$f_{i,P}^T(a_i) = w_i, {f_{i,P}^T}^{-1}(w_i) = a_i$ sorption isotherm, its inverse

$f_k(\boldsymbol{x})$,$g(\boldsymbol{x})$,$h(\boldsymbol{x})$ k^{th} goal function of $\boldsymbol{x}$, lower constraints, upper constraints

$f_v^T(\ldots)$,$g_v^T(\ldots)$ FVT model for rigid solutes and anchors (Figure V.24)

$f_X(x) = pr(X = x)$ probability that the random variable X takes the value x (probabilistic description)

$F_X(x) = pr(X \leq x)$ cumulated density function of the random variable X (probabilistic description)

$Gamma(a_\Gamma, b_\Gamma)$ gamma distribution of parameters a_Γ and b_Γ

$\boldsymbol{J}$ Jacobian

$\underline{\underline{\boldsymbol{M}}}$ diffusion operator matching boundary conditions so that the mass diffusion problem is discretized as $\frac{\partial \boldsymbol{C}}{\partial t} = \underline{\underline{\boldsymbol{MC}}}$.

$Norm\left(1, s_{C_0}\right)$ normal distribution with an unitary expectation and a standard deviation s_{C_0}

Q_X overestimation factor of X

s_X shape factor associated to the distribution of X^* (probabilistic description)

$\bar{X}$ likely value of X (probabilistic description)

$\tilde{X}$ sample of X (probabilistic description)

X^* dimensionless random contribution of X so that $X = \bar{X}X^*$ (probabilistic description)

$\langle X \rangle$ arithmetic average of X

$\langle X \rangle_T$ ensemble average of X at temperature T

$\lfloor X \rfloor$ lower limit of X (floor)

$\lceil X \rceil$ upper limit of X (ceiling)

$X_i = h_i^{-1}(Y_1, Y_2, \ldots, Y_n)$ back-transformation of random variables Y_1, Y_2,…,Y_n when it exists

$Y_i = h_i(X_1, X_2, \ldots, X_n)$ multivariate transformation of random variables X_1, X_2,…,X_n

$Weib(0, s_t) = s_t x^{s_t - 1} e^{-x^{s_t}}$ for $x \geq 0$ and 0 otherwise: Weibull distribution of parameters 1 and s_t

Subscripts

0	initial
1	solute in Flory notations
2	polymer in Flory notations
α, β, δ	arbitrary phases α, β, δ
a	dry air
$A+B$	A and B in mixture (random contacts)
$A \rightarrow B$	transition from A to B
(AB)	copolymer AB
$beverage$	beverage
$bottle$	bottle
BL	boundary layer
e	ethanol
eq	at equilibrium
F	food or liquid food simulant
$head$	in the headspace
i	solute index
int	internal domain
j	material or layer index
k	component, variable or dimension index
lin	linear solutes
$mutual$	mutual (high concentration)
$pure$	pure compound
P	polymer
$rigid\ block$	rigid units (blob)
sat	saturation
$total$	accumulated (e.g. total partial pressures)
$trace$	trace (infinite dilution)
w	water
$wall$	walls

Superscripts

$*$	dimensionless
‡	transition state
0, $t=0$	initial
CM	center-of-mass
eq	at thermodynamical equilibrium

g	in the gas phase
$likely$	likely value (probabilistic description)
L	liquid state
$mutual$	mutual (high concentration)
ref	reference value used for normalization
sat	saturation
S	solid state
t	at time t
$theoretical$	theoretical value
$tier\ i$	evaluation at tier i
$trace$	trace (infinite dilution)
T	at temperature T
v	relative to volume fraction
vdW	van-der-Waals
x,y,z,t	function of spatial coordinates x, y, z and time t

ABBREVIATIONS

[E][D][S]	Evaluation, Decision, Solving
BC	boundary condition
cdf	cumulated density function
CFD	computational fluid dynamics
CFDA	Chinese Food and Drug Administration
CFR	Code of Federal Regulations
CM	center-of-mass
D4S	Design for Sustainability
DDBST	Dortmund Data Bank Software + Separation Technology
DfE	Design for Environment
DVS	dynamic vapor sorption
EC	European Communities
EFSA	European Food Safety Authority
ENR	Event Notification Reports
EU	European Union
EUROVOC	multilingual, multidisciplinary thesaurus covering the activities of the EU
FDA	US Food and Drug Administration
FDCA	2,5-furandicarboxylic acid
FH2	Flory-Huggins theory for binary mixtures
FH3	Flory-Huggins theory for ternary mixtures
FMECA	Failure Mode Effects and Criticality Analysis
FV	free volume
FVT	free volume theory
h-FV	hole Free-Volume
IC	Initial Condition
ISO	International Organization for Standardization
LCA	life cycle assessment
LDPE	low-density polyethylene
LFL	lower flammable limit
MB	mass balance
NASA	National Aeronautics and Space Administration

NFPA	National Fire Protection Association
NIST	National Institute of Standards and Technology
NRC	Event Notification Reports
OECD	Organization for Economic Co-operation and Development
OIML	International Organization of Legal Metrology
OML	overall migration limit
PA6	Polyamide 6
PDE	partial differential equation
pdf	probability density function
PEF	polyethylene furanoate
PEN	polyethylene naphthalate
PET	polyethylene terephthalate
PMMA	poly (methyl methacrylate)
PP	polypropylene
PS	polystyrene
PVAc	polyvinyl acetate
PVC	polyvinyl chloride
QM	maximum amount
RASFF	Rapid Alert System for Food and Feed
RH	relative humidity
SM	safety margin
SML	specific migration limit
TE	transport equation
TRIZ	theory of inventive problem solving
UN	United Nations
UNEP	United Nations Environment Programme
UNIFAC	UNIQUAC Functional-group Activity Coefficients
US	United States of America
WLF	William-Landel-Ferry
WOS	Web of Science

Chapter I. INTRODUCTION

Chapter I. Introduction

I.1. Context

- *Global challenges for food packaging*

During the last decade, two opposite views on the benefits of food packaging have emerged. The world population is projected to reach 9.8 billion in 2050 from 7.6 billion today (UN, 2017), with 68% living in urban areas (UN, 2018). According to the dominant point of view, food packaging provides the solution of delivering food to urban and aging populations, living distantly from production areas, and wishing read-to-eat meals, consumer convenience, and experience. In this perspective, food packaging contributes to reducing food waste (Williams and Wikström, 2011;Williams *et al.*, 2012). All choices need to be sustainable and efficient: first on the market, cost competitive, enhancing consumer experience, and minimizing environmental impacts (Coles and Kirwan, 2011). Food safety issues are envisioned as a trade-off between the food protection and hygiene brought by the packaging and the risk of contamination associated with their use.

Alternative opinions on food packaging have evolved progressively from beneficial to significantly negative (Hamaide *et al.*, 2014). They have been sucessively associated with potential sources of harmful substances, wastes, greenhouse gases, etc. During the last meeting of the Food Packaging Forum (Stieger, 2018), experts concluded that materials in contact with food (plastics, elastomers, varnishes, adhesives, printing inks, paper, and board) are likely to be the main source of chemical contaminants in food. Among them, plastic materials have the largest market share for food contact applications (Geueke *et al.*, 2018). They are responsible for 80-85% of the total marine litter affecting all the world's oceans (Bergmann *et al.*, 2017), including the deep seafloor (Pierdomenico *et al.*, 2019). The use of plastics in multimaterial-multilayer systems possibly printed and coated complicate the identification, collect and recycling of these materials (PlasticsEurope, 2018), with a growing contribution of ready-to-eat foods (Silberbauer and Schmid, 2017). Additionally, new raising concerns are brought by plastic debris (Pierdomenico *et al.*, 2019), microplastics (Lusher *et al.*, 2017), and nanoplastics (EFSA, 2016) with possible impacts on the wildlife and the whole food chain.

- *Food packaging design should obey to a large corpus of rules in the EU*

Among developed countries, the EU is equipped with the strictest arsenal of rules on both environmental and safety issues (Rijk and Veraart, 2010). The reduction of the environmental impact of packaging and its wastes has been enforced since twenty-five years ago in EU with the Directive 94/62/EC (EEC, 1994) and its successive amendments (EC, 2004a, 2005, 2015). Its annex II imposes that any "packaging shall be so manufactured that the packaging volume and weight be limited to the minimum adequate amount to maintain the necessary level of safety, hygiene, and acceptance for the packed product and for the consumer". Since foods are not explicitly mentioned, no association has been made between barrier properties, shelf-life, and amount of plastic materials and finally wastes. The draft of EU directive 2018/0172(COD) (EC, 2018) will enforce a series of measures for single-use plastic items, including beverage containers and bottles, their caps, and lids. The actions will comprise stricter product design requirements, extended producer responsibility, collection objectives, and awareness-raising measures. The directive suggests explicitly changes in packaging design and switch to more sustainable raw materials. Stakeholder and public consultations showed support to legislative requirements to better design as one of the most effective approaches, in particular, for drink bottles and tethered caps, followed by reduction targets.

EU framework regulation 1935/2004/EC (2004c) makes a risk assessment and risk management compulsory for the introduction of any new substance, material or industrial practice (active/intelligent packaging system, recycling) regardless the material is in plastics or not. While not mentioning design, EU regulation 2023/2006/EC (2006) encourages the developments of good manufacturing practices and quality assurance systems at all stages of the production and handling for each of the seventeen groups materials and their combinations accepted for food contact.

- *Relationship between food packaging design and food wastes*

The environmental impacts of packaging are relatively small compared with the foods they contain. Ten million tons of food is wasted in France annually with 14% during distribution and 33% during consumption stage (Matamoros, 2019); it represents 173 kg food waste per person each year in the EU (Schweitzer and Janssens, 2018). Current EU regulations manage exclusively plastic wastes. Designing fit-for-purpose packaging can, however, both i) reduce environmental impacts by eliminating or light-weighting packaging components and ii) minimize the risk of packaging failure and product damage in transport and handling. The Australian industry (Verghese *et al.*, 2013) recommends barrier, and mechanical performances need to be distributed through the three levels of the packaging: primary in contact with food (portion), secondary (e.g., bag, box, plastic crate) and tertiary food packaging used for transit (e.g., pallets, large boxes, sacks). Consumers are, hence, increasingly looking for

convenience and ready-to-eat foods, while processors and retailers are looking to extend product shelf life. The challenge is to balance product waste, shelf-life, and packaging design. The study of Williams *et al.* (2012) reports three technical reasons associated with the packaging and responsible for food waste: an oversized packaging, a packaging difficult to empty and a too short "best before date". Pre-prepared or pre-packed food products offer a solution to the first problem. This solution increases the demand for packaging disposal and recycling at the household level, but this negative impact is offset by food preparation waste shifted from the home or food service establishments to the manufacturing sector, where they can be more easily recovered. The LiquiGlide surface treatment developed by the Massachusetts Institute of Technology in the United States is an example of a solution to the second problem for thixotropic and viscoplastic products. It enables sauces and other liquid products (e.g., mayonnaise, ketchup, yogurt) to be completely dispensed from a bottle or jar (Yirka, 2015).

When shelf-life is dominated by mass transfer (water vapor or oxygen) across packaging walls, a Zeno paradox is usually reached: shelf-life cannot be extended without increasing food packaging waste. Several alternative exists, however, as reviewed in Robertson (2009a): adapting finely the packaging size, its shape to the mass transfer mechanism, redistributing the plastic material between rigidity and barrier regions, combining several materials, changing distribution and storage conditions, using a modified atmosphere (Zhang *et al.*, 2016) or adding some active components (Ozdemir and Floros, 2004).

I.2. Rational design

Continuing innovation in packaging materials and packaging design can contribute to tackling global challenges posed by food packaging, the transformation, and distribution of food. A systematic methodology is nevertheless required to meet on the short and long term environmental and safety goals. Rational design is usually a word applied in biology to describe the modifications at the molecular level of cells, genes, peptides, proteins, and other macromolecules to reach therapeutic or technological effects. These orientations led to new engineering approaches, including structure drug design or discovery, computational drug design. In this thesis, the concept of "*rational design*" with the same intent: supporting the discovery and the exploration of packaging concepts with lower impacts for the environment and human health. Because the design aspects of food packaging are poorly analyzed in the open literature (Azzi *et al.*, 2012), the concepts of rational design for food packaging remains highly immature. Little works have been carried out to develop a systematic problem-solving methodology to tackle through designs global challenges. Some premises have been introduced as corrective actions in the packaging design process (Grönman *et al.*, 2013) and via the Best Worst Method (Rezaei *et al.*, 2019). They remain quantitative, and they do integrate complex

criteria such as shelf-life or safety. The most cited papers address the prediction of equilibrium modified atmospheres (Jacxsens *et al.*, 2002), but not their optimization to reach a particular shelf-life (Belay *et al.*, 2016;Giannoulis *et al.*, 2017;Jalali *et al.*, 2017). Non-technical factors related to design, including aesthetics, functionality, and emotional factors, are usually omitted, whereas they shape the expectations and color the attitude of the consumers (Lockwood, 2009). As an example of the interactions between senses, some results suggest that the shape of the packaging can be associated to the taste of the food it contains (Becker *et al.*, 2011;Velasco *et al.*, 2014). Design thinking, engineering systems thinking, conceptualization, and prototyping should also be included in the proposed "*rational design*" framework along with tailored calculations of barrier and mechanical performances.

Virtualizing time-consuming steps of packaging design such as conceptualization, prototyping, packaging optimization, and shelf-life validation can accelerate exploration of many alternative solutions while offering some chances of fruitful feedbacks. Coding complex technical details in mechanistic models or artificial intelligence can change even the entire paradigm of food packaging design. The designer is free from the complex engineering and can connect his work seamlessly to engineering, manufacturing, and processing steps. As a result, most of the design effort can be redirected to consumer expectations and impact reduction rather than on production parameters. The approach is revisable and augmentable to integrate future evolutions of regulations, food supply chain, and new materials. Similar ambitions have been applied successfully to safe-by-design approaches for food contact materials (Nguyen *et al.*, 2013;Zhu *et al.*, 2019a). It is proposed to derive the foundation of "*rational design*" concepts from the safe-by-design methodology. The expected outcome is to reach a unique computational framework capable of integrating both environmental and safety issues separately or within the same global minimization problem. Alcoholic beverages are proposed in this work as an application study of these developments.

I.3. Organization of the manuscript

The manuscript is organized into five sections. Section two reviews the methodologies supporting computer-aided decision making and how they have been transposed to the concepts of safe-by-design. Contrarily to safety issues managed by international standards and organizations, the evaluation of environmental impacts remains essentially retrospective and somewhat subjective. The concept of shelf-life is presented in a very simplified manner as a mass transfer problem. It is acceptable for beverages, but it is not sufficient when microbiological safety must also be considered. The "*rational design*" framework combines two major ingredients: i) tiered modeling and ii) an iterative [E]validation, [D]ecision and [S]olving algorithm. Its formulation is illustrated on an oversimplified case-study in Section 3. This

"ecodesign" problem at tier 0 and its solutions are used to justify the goals and approaches followed in this work. Additionally, they demonstrate that even a coarse model can stimulate and orient packaging design to more effective solutions. The studied conditions and the numerical developments followed in this work are detailed in the fourth section, "*Materials and Methods*". The results and discussion are presented in the next section with a progressive modeling complexity. The whole packaging design problem is firstly presented for liquors when the physics of mass transfer is essentially linear (tiers 1 and 2) and without restrictions on the shape of the packaging, the conditions of storage and alcoholic strength. Non-linear and more complex physics of glassy polymers are progressively introduced at higher tiers (tiers 3 and 4). The main findings and perspectives are summarized in the last section.

Chapter II. LITERATURE REVIEW

Chapter II. Literature review

> This is the whole point of technology. It creates an appetite for immortality on the one hand. It threatens universal extinction on the other. Technology is lust removed from nature.
>
> —Don DeLillo, *White Noise*

The thesis adopts **three vantage points**, which are justified and detailed from a critical review of the scientific and legal literature. **One** is that common engineering techniques are not sufficient to tackle the main challenges of the 21st century: global warming, environmental degradation, life-long exposure to chemicals, etc. The old-fashioned engineering was in some ways responsible for the current problems, to meet the demand of consumers without considering the consequences. Contrarily to the dominant opinions in the Engineering Ethics literature, the current problems are, however, not associated with wrongdoing and the solution is not its avoidance and its prevention (Pritchard, 2001). With the economy and challenges becoming more global, corporates and industry are facing continuously increasing complexity, which cannot be resolved anymore with conventional engineering (Alexiou *et al.*, 2010). An overview of the interplaying factors in food packaging design are summarized in **Figure II-1**. The complications arise from the spanning of technical problems and societal constraints over several disciplines (material, food, toxicology and environmental sciences), roles (designers, engineers, users, and authorities), processes, length and time scales and the entanglement with many legal and sometimes contradictory requirements. As an example of the heavy legal framework, 6165 legislation, preparatory documents, international agreements, communications on case law are associated with foodstuffs in EU according to the EUROVOC classification(Eur-lex, 2019a). The same classification comprises 3092 documents for “food plastic environment” (Eur-lex, 2019b).

The **second viewpoint** is that computers and automatic algorithms could help to support the burden for managing complexity met in food packaging design. Three-dimensional geometry and design optimization can be currently carried out with simple laptops (Zuo and Xie, 2015), using a push-pull approach (Zou and Feng, 2019) and without strong expertise in materials science (Khosravani *et al.*, 2019). Combined with augmented reality and rapid prototyping (Liu and Ma, 2016), new concepts of food packaging could rapidly emerge and being adapted to the consumer, the supply chain and the considered food.

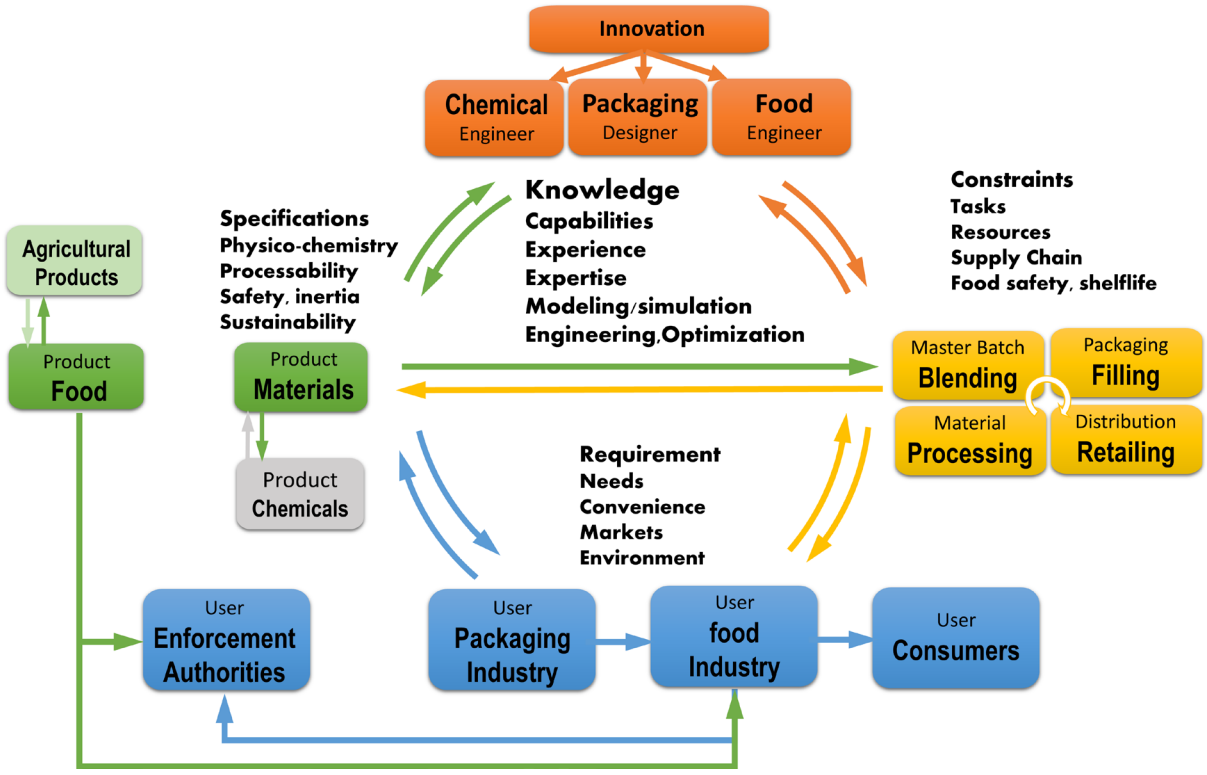

***Figure II-1**. Interplaying factors in engineering design: example of food-packaging design (modified from Figure 3.2 of Alexiou et al., 2010).*

The **two first viewpoints** are central to this ideal of post-industrial civilization where creative technologists would be replacing progressively engineers specialized only in some fields. The technical constraints (manufacturability, suitability, flexibility) would be considered with the help of automatic tools used partial or without supervision. The feasibility of the principles of augmented engineering for food packaging design is reviewed in the **first section** within a mathematical perspective emphasizing optimal decision making. The prevalence of computers in decision making implies that the impact of human activities can be evaluated with cardinal numbers. Reusing such numbers retroactively in algorithms to explore alternative packaging designs could appear even more controversial. What if predictors were biased, misguided or simply wrong? Optimizing design presupposes that the new solution is objectively better than the original one.

The **third vantage point** is epistemic and almost philosophical; the evaluation (assessment) should be neutral and separated from the decision process (management) to keep its rationality. This principle was central in the white paper on the EU "*White Paper on Food and Feed*" (EC, 1999) encouraging the creation of the European Food Safety Authority, and in the US doctrine to manage technological risks at federal level (NRC, 1983). Following the same logic, **section two** describes how hierarchical modeling of mass transfer can be used to

evaluate the risk of migration of packaging substances into foodstuffs under uncertainty. The general methodology to derive deterministic numbers (overestimates) or probabilities from a mechanistic model is proposed as a template for more general estimates, which could be transposed in methods targeting environmental impacts associated with food and packaging. Though environmental impacts mirror food safety indices; their definitions remain comparatively more subjective. Associated indices do not represent a natural tendency of an impact to occur, but the measures of how strongly one believes they will occur. The corresponding probabilities and therefore any measure of uncertainty cannot be seen as evidential, but as propensities (Belnap, 2007) instead. From a strictly mathematical point of view, there is a peril in using relative probabilities (or propensities) to describe systems out-of-equilibrium in the long term (Runde, 1996). In the absence of some stationary trends in the environment, there is no guarantee that any improved solution in the present time will be optimal in the future. The capacity to integrate environment indices in semi-supervised design optimization is discussed in the last section from a critical review of environment impacts.

II.1. Beyond engineering: computer-aided decision making

The Merriam-Webster dictionary defines engineering as “the application of science and mathematics by which the properties of matter and the sources of energy in nature are made useful to people”. As an illustration, the first Ph.D. degree in engineering was awarded in the US to Williard Gibbs at Yale College in 1863 after his work "On the Form of the Teeth of Wheels in Spur Gearing". His subsequent contribution to the foundation of statistical mechanics was immense. In his contribution as in the work of many framers of modern engineering, there was no clear mention of the necessity to protect human health, well-being and the environment. Simplifications are indeed very common in engineering. The mother nature was thought simultaneously as an infinite reservoir of resources and as a perfect sink with an infinite capacity to dilute and dissolve wastes. In this perfect thermodynamic cycle, the environment was thought falsely at equilibrium with no entropy change. A recent application of statistical mechanics revealed that the approximation was abusive; there is an entropy change (Mahbub *et al.*, 2017). Simplifications are inherent to the art of the engineer, they are required to solve the problem, but they should not be excessive and misrepresent the impacts of the final assessment or decision. In this section on the extensions of engineering, we agree with the point of view from Kleingeld M. (2010) “*Engineers need to guard against focusing solely on the technical content of their work*”. Some sorts of simplifications could be even beneficial to apprehend holistically the consequences of linked decisions at the largest scale. The computer and proper mathematical algorithms could support innovation while addressing the immense challenges of the 21st century of sustainability.

II.1.1. Problems which can be solved today with a computer

The computer overpasses humans for brute-force calculations and has been used extensively in many engineering fields. Using supported decisions made unsupervised or partly supervised is a logical step for our societies facing global challenges. By removing the need for strong technical expertise, the evolution could aid large groups in the industry to make quantitative choices in a near real-time in one sitting. Such developments look very appealing to resolve complex linked decisions delaying the innovation process and access to the market. The thesis addresses three kinds of global constraints, which could be summarized as follows.

- Technical constraints inherent to packaging and beverage specifications (shelf-life, mechanical constraints)
- Environmental constraints (e.g., amount of non-recycled material)
- Food safety constraints associated with the mass of recycled material.

With our current knowledge, no solution or optimization could be employed as a *deus ex machina*. A solution is only a compromise between alternatives and not "the best of all possible worlds" as expressed by the Pangloss's optimistic philosophy, criticized by Voltaire in his famous book Candid. Global issues, such as sea littering, microplastics, chemicals in food, occur not because "God" created the world and humans, but the other way around, because humans created plastic containers. The obviousness of the conclusion lies in the separation of causes and effects. Any enlighten algorithm, such as trivial truth (trivial falsity) and backtracking optimization algorithms, will reach a similar conclusion: by removing the source, we remove and solve the problem. In this thesis, we propose to orient the exploration of creative alternatives by adding a large number of constraints and rules so that the solutions may:

- have acceptable tradeoffs (successful solution)
- meet constraints (successful solution)
- be acceptable to users (successful solution)
- exhibit good cost/benefit ratio (efficient solution)
- be practical (efficient solution)
- be reliable (efficient solution)
- be new or original (innovative solution)
- be different from the ordinary belief/surprising (innovative solution)
- be seminal or universal (innovative solution)
- be unified (coherent solution for many problems)
- be esthetic or refined (coherent and innovative solution).

II.1.2. Decision-based on utility theory

The art of solving complex global problems has been extensively discussed in the literature by decision scientists since the seventies with variable success. Quoting Keeney and Raiffa (1993), "*Decision analysis is widely recognized as sound prescriptive theory*". The usual approach for Decision making in the presence of conflicting objectives is initiated after suitable modeling has been done (Evaluation step) and it involves two distinctive features: uncertainty analysis and preference (or value or utility) analysis. Quoting the same authors "*Imagine that the problem is so complicated that a computer-based simulation model is designed such that for each policy choice under review, a scenario can be generated that indicates how the future might unfold in time. Now suppose that the analyst effectively summarizes the relative desirability of any future scenario not by a single number but, let us say, by a dozen well-chosen numbers: some reflecting costs, others reflecting benefits. Since these output performance numbers may simultaneously deal with economic, environmental, social and health concerns, these summarizing indices will, in general, be in incommensurable units. To complicate matters, suppose that stochastic elements are involved in the simulation so that, for a single policy choice being investigated, repeated simulation runs result in different sets of summary performance measures. The joint probability distribution of these performance measures as made manifest through repeated realizations of the simulation will, in general, indicate that these 12 measures are probabilistically dependent. Now assume you are a harassed decision maker sitting in front of an output display device deluged with a mountain of conflicting information. You are confused. What should you do*?"

A variant of the utility theory has been developed by Nguyen *et al.* (2013) in their approaches of safe-by-design of packaging. The authors used the adapted the methodology of Failure Mode Effects and Criticality Analysis (FMECA) to mass transfer problems to avoid human biases: favoring authority opinions, false causality bias, certainty effect causing aversion for losses (Kahneman and Tversky, 1979). Even if the tool FMECAengine (Vitrac, 2018) includes a powerful inference engine to derive new properties from existing packaging designs, the whole approach of Nguyen *et al.* (2013) remains essentially retrospective and forensic. The proposed local indices, so-called severities, and cumulative indices, so-called criticalities, help only the analyst to choose among a set of alternatives which should preexist. For example, the approach cannot automatically propose a new design, a new formulation or a new supply chain to resolve the problem of migration or contamination.

II.1.3. Problem-solving methods in engineering

Quoting Akeel and Bell (2013), "*Systems engineering is unique in being characterized by its methods rather than its artefacts. Consequently, the scope of systems engineering is*

difficult to define. While some systems engineers contend that systems engineering is capable of addressing socio-technical problems, including climate change and terrorism, others argue that it is strictly a technical field". We can dispute the arguments, but it may be difficult for engineers to be judge and defendant of the same cause: justifying they can continue to do business as usual. We review in this section the engineering tools available in the industry to stimulate creativity and innovation. Common approaches such as brainstorming, and trial and error become useless when they reach contradictions and when they involve linked decisions and complex scenarios which cannot be explored in real time.

II.1.3.1. Overview of methods

Problem-solving methods gather several empirical strategies aiming at stimulating the search of solutions while fluidifying creativity. The approaches tend to be generic and rational, but they can include some subjectivity in their premises (Mair *et al.*, 2009). Common implicit assumptions include: the sum collective and cooperative human intelligence is greater than individual ones, stimulation of thoughts does not require the subjects to be aware of the procedural methodology followed (synectic); human can learn from analogies and comparisons (imitation); solutions are usually thought within the space of current knowledge (futurology is an exception); the problems present some invariance so that the same type of solution can be applied to several problems (principle of self-similarities or case-based reasoning) (Engel, 2013). Recent studies in behavioral sciences showed that innovation and problem solving obeyed to the same cognitive dynamics (abstraction, searching, learning, inference, decision making) and should not be separated (Griffin and Guez, 2014). The main methodologies and corresponding strategies are reviewed in **Table II-1** according to an early classification proposed by Wang and Chiew (2010). The five main categories correspond to:

- a procedural evaluation of facts and beliefs (analysis);
- a collective evaluation and sharing experience (group solving);
- exploration of solutions according to some sets of prescribed (heuristic);
- prospective exploration (thought experiments);
- theory of problem-solving developed by Genrikh Saulovich Altshulle, a Soviet scientist and engineer, based on its own experience as a clerk in patent office.

***Table II-1**. Overview of problem-solving methodologies.*

↓ Examples / Strategies→		Abstraction	Analogy	Brainstorming	Divide and conquer	Hypothesis testing	Lateral thinking	Means-ends analysis	Methods of focal objects	Morphological analysis	Proof	Reduction	Research	Root cause analysis	Trial-and-error	REFERENCES
Analysis	Issue trees (Ishikawa diagram, issue map, A3 problem solving), why-because analysis (Five whys, Five/Six Ws, GROW)		×			×						×		×		a
	Criticism			×	×	×	×				×				×	
	Decision analysis (operation research, risk analysis, decision, tree, decision support system)		×	×		×	×							×	×	b
	Impacts (environmental, risk, technology), quality, standards	×				×					×	×	×	×	×	
	Inductive reasoning (generalization, inductive fallacies, inference)	×	×	×		×	×	×	×	×	×		×			
	Knowledge representation (assumption, inductive, deductive, automated)	×		×		×	×	×	×	×	×		×	×		
	System analysis (feedback, optimization, structure, fault, optimization…)	×	×	×	×	×	×					×	×	×	×	
	Finance validation	×	×									×		×		
Group Solving methods	635 Brainwriting method		×	×			×	×	×							c
	Brainstorming			×			×	×	×							
	Crowdsolving, a community of practice			×				×	×							
	Disney method, six thinking hats		×	×			×		×							
	General group thinking			×				×								
	Nominal group technique			×			×	×	×							
	Organization workshop			×			×	×								
	Socratic debate		×	×			×	×								
Heuristics	Forensics	×	×	×							×	×	×	×		d
	Metaheuristics (nature inspired: stochastic diffusion search, ant colony optimization, particle swarm, boids, evolutionary algorithms, artificial immune systems)		×		×			×	×	×		×	×			e
	Razors principles (parsimony)		×									×		×		
	Rules of thumb (adages, expert opinions)		×	×							×				×	
Thought Experiments	Futurology, prevention, computational study, technology assessment, transhumanism, resource and impact evaluation, life extension	×	×			×							×	×		
	Artificial intelligence, fuzzy logic theory	×				×	×	×	×	×	×	×	×	×		f
	Paradoxes in utility theory (Allais, Ellsberg, Proebsting, value)	×	×			×	×					×	×			
Theory of Inventive Problem	Original TRIZ		×		×			×				×				g
	40 principles of invention 39 characteristics of a technical system 39×39 TRIZ contradiction matrix Lean TRIZ, Lean Process TRIZ		×					×								h
	AIDA (Advanced Innovation Design Approach)		×		×		×	×	×		×	×	×			
	Laws of technical systems evolution		×		×			×			×	×	×	×		

Five or six Ws: Who, What, Where, When, Why, How; GROW = Good Reality Obstacles Way Forward; 635 Brainwriting = 6 participants writing down 3 ideas within 5 minutes; six thinking hats= six distinct directions of critical thinking when exposed to novelty and with assigned colors: Managing Blue, Information White, Emotions Red, Discernments Black, Optimistic response Yellow, Creativity Green; General group thinking = identifications of antecedents, tendencies, symptoms, defects and outcome; Nominal group technique=introduction, silent generation of ideas, sharing ideas, groups of discussion, voting and ranking.

References: a. Pressman (2018); b. Masys (2015); c. Robertson (2016b); d. Matlack and Dicks (2015); e. Pearl (1984);Salhi (2017); f. Nilsson (1971);Kowalski (1979);Pearl (1984);Ofitserov and German (1995);Luger and Stubblefield (1998);Liu *et al.* (2006); g. Savransky (2000); h. Cavallucci (2017);Harrington (2017).

Contrarily to intuition and according to literature, digital technologies look to play a minor role in the act of inventing itself. In its theory of diffusion and innovations, Rogers (see p. 11 of Rogers, 2003) defines innovation as "*an idea, practice, or object that is perceived as new by an individual or other unit of adoption. It matters little, so far as human behavior is concerned, whether or not an idea is 'objectively' new as measured by the lapse of time since its first use or discovery*". Five stages are indeed required to transform an idea into a recognized innovation (knowledge, persuasion, decision, implementation and confirmation) and computers participate mainly to one: implementation. Their role is, however, increasingly dominant in some strategies of problem-solving, as acknowledged by the conferences SocPros "Soft Computing for Problem Solving" (Bansal *et al.*, 2018), which address under the umbrella "soft computing": fuzzy logic, neural networks, evolutionary algorithms, swarm intelligence algorithms. Despite a broad variability between methods, combinatory algorithms are the common denominator (Jain, 2016;Bansal *et al.*, 2018).

II.1.3.2. The TRIZ methodology

- *Short history*

In its preface to Lean Triz (Harrington, 2017), Thoreau noted that Quality management procedures such as Six Sigma, Lean, supply chain, error proofing are considered best practices today. In 1910 without any computer and customer relationship management system, Henry Ford Sr. developed a cycle of production of a car in seven days from iron ore to the completed car, the car was delivered to the dealer within the next seven days, the payment was sent back to Ford's industries 10 days before they had to pay the part-suppliers. Ford had one single motto "Simplify, simplify, simplify". The different evolutions of the TRIZ "*theory of the resolution of invention-related tasks*" (Savransky, 2000), as systematic inventive thinking (Goldenberg *et al.*, 2001), is the methodology of choice for many organizations to conduct all phases of product and process design and redesign. Comparatively to other techniques such as evolutionary design, the superiority of the TRIZ approach initiated in 1946 relies upon its capacity to bring rapidly improvements and to offset contradictions embedded in the proposed design.

- *The analogy between the complexity invention level and TRL scale*

Genrich Altshuller based upon his study of over 200,000 patents and technological systems, he identified five levels of invention, which can be compared to the maturation index of technology, coined as Technology Readiness Level and initially proposed by NASA with seven or nine levels (Héder, 2017). The scales as reverse and both can be initiated starting from any level up to the state "ready to flight". At the scale of the society, most of the discovery and research effort is applied where the complexity is maximum (low TRL), where the risk of losing effort is maximum. The TRIZ methodology has been devised to target levels 1-3 (*i.e.*, from TRL 3-9), which correspond to the main needs of companies.

Table II-2. *Comparison between the complexity level defined by Genrich Altshuller and the TRL.*

complexity invention level	Interpretation of	TRL scale	Civil interpretation in the EU Horizon 2020 program
5	**Discovery**: inventions represent a rare scientific discovery or the pioneering of a new industry altogether	1	**Basic principles** observed
4	**New paradigms**: inventions entail the development of an entirely new operating principle and represent radical changes	2	**Technology concept** formulated
3	**Major improvements**: inventions include fundamental improvements to a system involving methods known outside of the domain. This involves applying an idea to the domain that has never been used in the domain previously.	3	**Experimental proof** of the concept
		4	**Technology validated** in laboratory
2	**Minor improvements**: inventions constitute minor nonobvious improvements to a system, using methods known within the domain of discourse but applied in a new way.	5	**Technology validated** in a relevant environment (industrially relevant environment in the case of key enabling technologies)
		6	**Technology demonstrated** in a relevant environment (industrially relevant environment in the case of key enabling technologies)
1	**Apparent solutions**: inventions are obvious and apparent solutions involving well-known methods and knowledge requiring no new invention of any consequence	7	**System prototype** demonstration in an operational environment
		8	**System complete** and qualified
	n.d.	9	**Actual system is proven** in an operational environment (competitive manufacturing in the case of key enabling technologies or in space)

- *Anticipating the evolution of technical systems*

The TRIZ methodology proposes a holistic decomposition of any technological system into three main laws and principles (Cavallucci, 2017). They are sketched with the case of food packaging in mind.

1) Static laws describing the viability of the solution

a. Completeness of the parts of the system (e.g., the packaging should protect all aspects of food shelf-life, contribute to the transport, retailing and preparation of food, etc.);

b. Conservation law (e.g., no mass loss);
c. Harmony law (e.g., inertia of the packaging: low food-contact interactions, plasticizing, off-flavors);

2) Kinematic laws

a. Increasing the system ideality (e.g., preventing harmful effects on health and the environment);
b. Uneven developments of parts may lead to technical and physical contradictions (e.g., replacement of some parts of the packaging may affect barrier properties);
c. Transition to a super system (e.g. introducing secondary and ternary packaging);

3) Dynamic laws

a. The transition from macro to the micro level (e.g., modifying polymers and additives may bring new possibilities and innovations);
b. Increasing the Substance field involvement (e.g., increasing or decreasing fluxes).

II.1.4. Multicriteria optimization

Previous techniques rely on preexisting inventories of recipes and solutions. They require strong human expertise and cannot be performed automatically. Operational research developed several techniques of multi-objective optimization, also known as multi-objective programming, vector optimization, multicriteria optimization, multiattribute optimization or Pareto optimization. They have extensively used in chemical engineering (Rangaiah, 2009).

II.1.4.1. Overview

Research in optimization started once significant advances in linear programming, and its subclasses became a mature technology. The general problem multicriteria optimization obeys to:

$$\begin{aligned} &\text{minimize } f_1(\mathbf{x}), \text{minimize } f_2(\mathbf{x}), \ldots \text{with respect to } \mathbf{x} \\ &\mathbf{x}^L \le \mathbf{x} \le \mathbf{x}^U \\ &\text{subject to } \quad h(\mathbf{x}) = 0 \\ &g(\mathbf{x}) \le 0 \end{aligned} \tag{II.1}$$

where $\{f_k(\mathbf{x})\}_{k=1..m}$ are the objective or goals function of the decision variables $\mathbf{x} = [x_1, x_2, \ldots x_n]^T$ bounded by the values $\mathbf{x}^L$ and $\mathbf{x}^U$ and subject to equality and/or inequality constraints.

***Table II-3**. Typology of optimization problems*

Goals: $\{f_k(\boldsymbol{x})\}_{k=1..n}$		**Constraints** $h(\boldsymbol{x}), g(\boldsymbol{x})$		**Type of problem**
Linearity with $\boldsymbol{x}$	convexity	Linearity with $\boldsymbol{x}$	convexity	
linear	convex	linear	convex	linear programming
nonlinear	-	linear	convex	nonlinear programming
linear	convex	nonlinear	-	nonlinear programming
-	convex	-	convex	convex optimization
-	nonconvex	-	convex	nonconvex optimization
-	convex	-	nonconvex	nonconvex optimization
-	nonconvex		nonconvex	nonconvex optimization

The classification of optimization problems depend on the linearity and convexity of the functions $\{f_k(\mathbf{x})\}_{k=1..m}$, $h(\mathbf{x})$ and $g(\mathbf{x})$, as summarized in **Table II-3**.

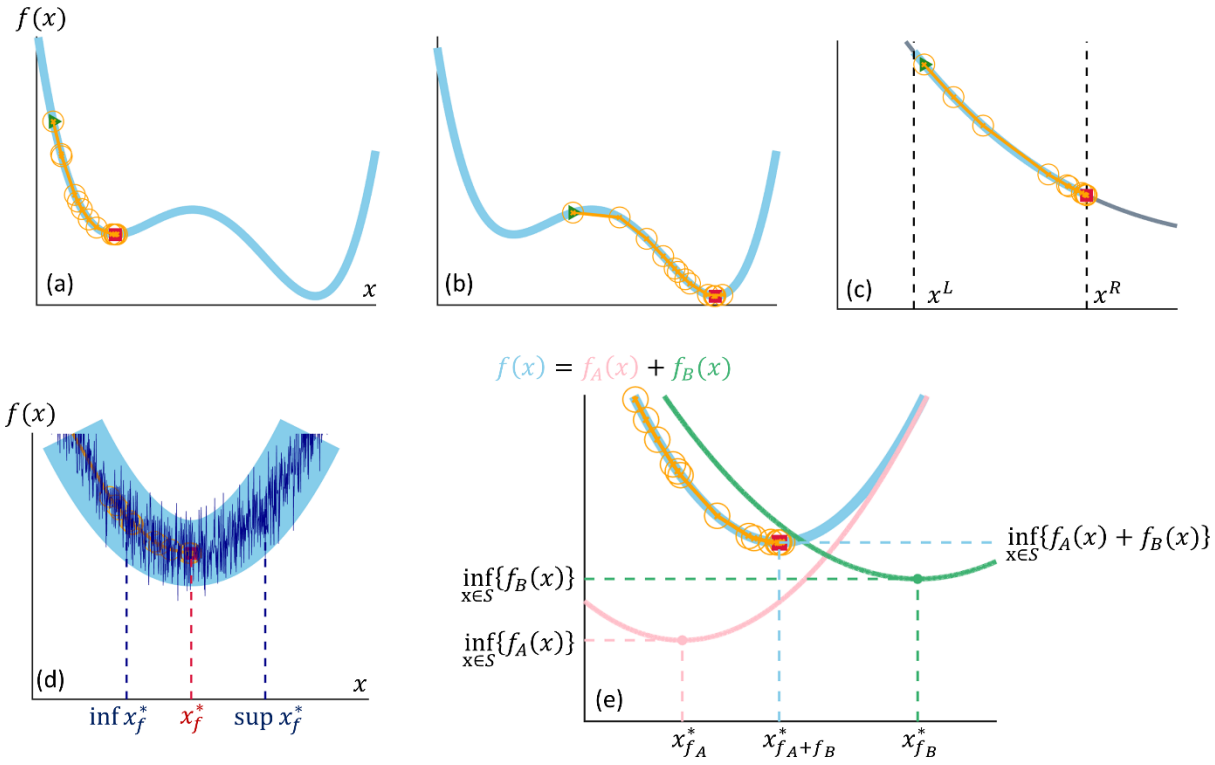

***Figure II-2**. (a-b,d) Illustrations of nonconvex goals; (c) convexification by adding boundaries $x^L \leq x \leq x^R$; (d) nonconvex problem combining a convex problem with Gaussian white noise (inf x_f^* and sup x_f^* are the bounds of the domain where the minimum can occur); (e) composition of two convex goals. The green triangle represents the initial guess and the red square the final solution of a randomized steepest descent algorithm. The intermediate positions are depicted with connected orange circles. In non-convex problems, the final solution may dependent on the initial guess (see (a) and (b)).*

Nonconvex and nonlinear problems are the most general, as shown in **Figure II-2**. They are the most complex to solve as they may be associated with no-minimum or more than one minimum. Optimization problems without any particular structure are less amenable to

analysis and computational study. Some basic classes have attracted more attention than others and benefit greater developments. **Figure II-2**d-e exemplifies some useful properties:

- the true minimum of a convex functional subjected to white noise (uncorrelated and unbiased errors) is bounded statistically by the positions of the first and last occurrence values (**Figure II-2**d);
- the minimum of a sum of two or more functionals is bounded by the positions of the minima of each functional (**Figure II-2**e).

II.1.4.2. From linear problems to nonconvex structures

All linear problems and more generally problem with strictly monotonic goals subjected to convex constraints are convex. The minimum lies exclusively at an extreme point (vertex) or a boundary (edge). In linear programming, the solution - when it exists - is obtained by the intersection of the goal function with the convex polytope (feasible region). The algorithm of resolution using successive pivots was popularized by George B. Dantzig (1998), who developed the simplex method. For single goal functions, the numerical strategy of exploring extreme vertices and walking along edges always terminate in finite time.

As an application of the principle of maximum entropy, impacts intended to be minimized are likely to be monotonic functions. The canonical problem reads:

$$\begin{aligned} &\text{minimize } f_1(\mathbf{x}), \text{minimize } f_2(\mathbf{x}), \ldots \text{with respect to } \mathbf{x} \\ &\text{subject to } \begin{matrix} g(\mathbf{x}) \le \mathbf{x} \le h(\mathbf{x}) \\ \{x_j \ge 0\}_{j=1..n} \end{matrix} \end{aligned} \tag{II.2}$$

It is easily demonstrated that if $\mathcal{F}$ denotes the family of increasing impacts on $\mathbb{R}_n^+$ ($f_1(\boldsymbol{x}), f_2(\boldsymbol{x}), \ldots \in \mathcal{F}$), $min\{f_1(\boldsymbol{x}), f_2(\boldsymbol{x}), \ldots\} \in \mathcal{F}$ belong also to the family of increasing impacts, so that the minimization of impacts can be obtained iteratively from a nested optimization strategy. Similarly the linear combination of impacts $\sum_{i=1}^{m} \omega_i f_i(\mathbf{x})$, with positive weights $\{\omega_i \ge 0\}_{i=1..m}$ is also an impact function and justify evaluations such as Life Cycle Assessment (LCA, see §II.3.4.). Similar considerations have been expressed for utility functions in mathematics economics under the assumptions that all goods are useful, that is when they are associated to nonnegative coefficients (see chapter 11 of Tuy,2016).

The problem loses triviality on non-convex polytopes end/or when the feasible domain is disjoint. One useful strategy is to enclose the solution in an extended feasible and convex set. To avoid a too large sensitivity to noise and uncertainty, the solution should be sought in a neighborhood (ϵ-optimal solution, see **Figure II-2**e), within a tolerance on the criterion (η-optimal solution, see **Figure II-2**d), on by combining both (ϵ,η-optimal solution).

II.1.4.3. Convexity and convexification

Convex analysis is an emerging calculus of inequalities while *convex optimization* is its application. Analysis is inherently the domain of a mathematician while optimization belongs to the engineer. Because many non-convex goals and convex sets can be "convexified" by adding a cost function, splitting the feasible region into small convex ones or by extending the feasibility region, the study of convex problems is of general interest for resolving engineering problems under constraints. The properties of convexity and the strategies to extend them to non-convex problems or sets are illustrated in **Figure II-3** based on geometrical interpretation of the optimization problem.

A convex optimization problem is conventionally regarded as minimization of a convex objective function subject to an artificial convex domain imposed upon it by the problem constraints. The constraints comprise equalities and inequalities of convex functions whose simultaneous solution set generally constitutes the imposed convex domain: called feasible set.

- *Definitions*

A function $f(x)$ is called convex if it verifies the following inequality for all $\boldsymbol{x}, \boldsymbol{y} \in \mathbb{R}^n$ respectively to any weight $0 \leq \lambda \leq 1$:

$$f\left(\lambda \mathbf{x}+\left(1-\lambda\right)\mathbf{y}\right) \leq \lambda f\left(\mathbf{x}\right)+\left(1-\lambda\right) f\left(\mathbf{y}\right) \tag{II.3}$$

Eq. (II.3) generalizes the restrictive concept of linear functions for some particular affine sets. The equality $f\left(\lambda \mathbf{x}+\left(1-\lambda\right)\mathbf{y}\right)=\lambda f\left(\mathbf{x}\right)+\left(1-\lambda\right) f\left(\mathbf{y}\right)$ verified for any linear function is replaced by the concept of membership to the epigraph of the curve. Any barycenter between two points of the curve (*i.e.*, the affine or manifold set) should lie above the curve (see **Figure II-3**a-c) over the entire considered interval. It is verified only for continuous functions with finite and left and right derivatives over the entire interval (see chapter 2 of Tuy,2016).

A set is said convex if it contains any line segment joining two edges or two points belonging to the contour. The kidney shape shown in **Figure II-3**e is not convex. Convexity can be recovered either by adding an external vertex (**Figure II-3**j) or by closing the hole (*i.e.*, convex hull, **Figure II-3**i). At this stage, it is worth noticing that the roles of constraints and goals tend to have symmetric roles as the feasible solutions lie at their intersections. According to the type of problem, either the goals or the constraints can be more expensive to calculate. For monotonic goals and in the absence of an optimal solution, an acceptable solution can be proposed as a compromise between many constraints.

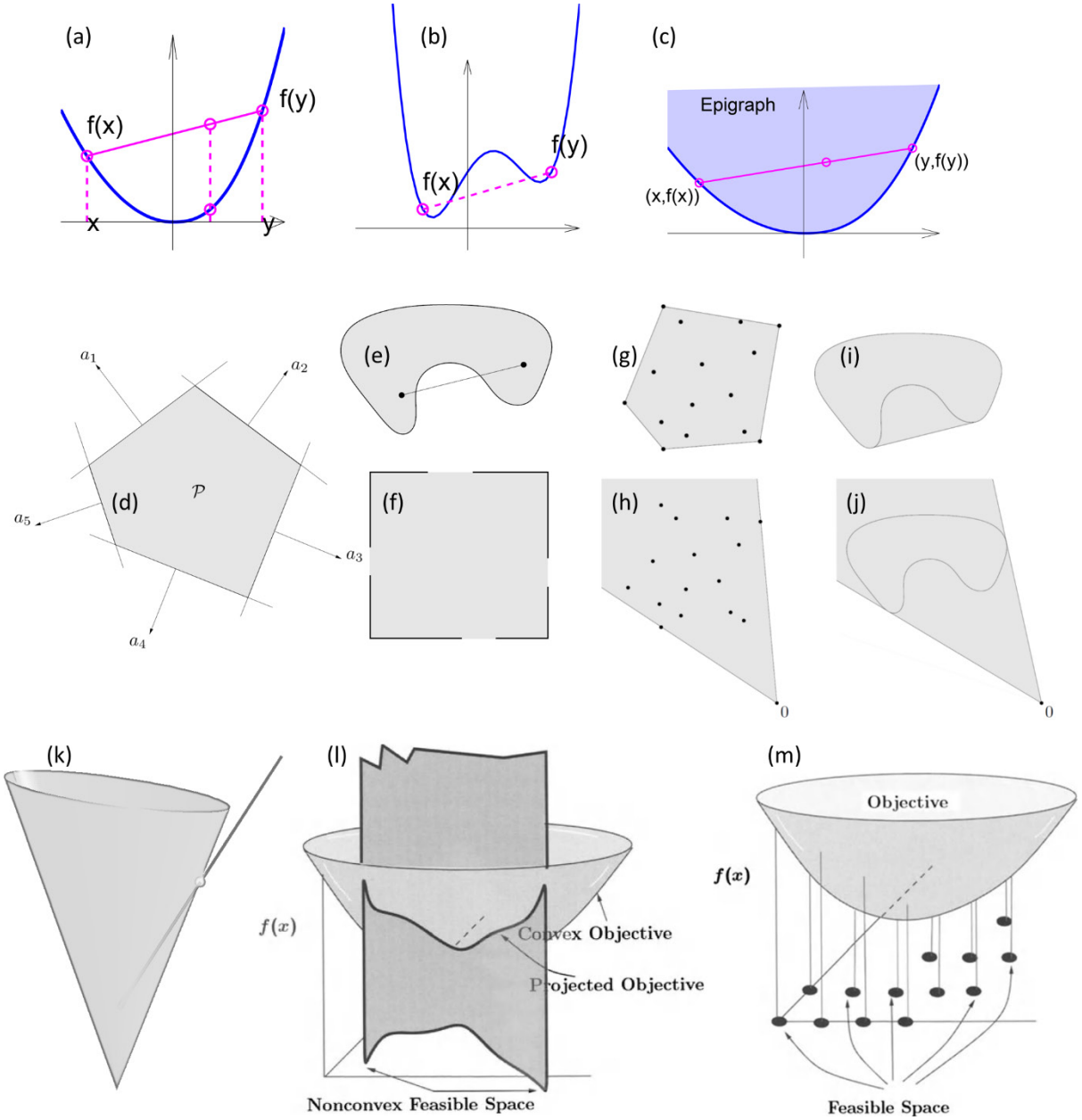

***Figure II-3**. Geometric interpretation of multidimensional optimization problem: (a) convex function; (b) nonconvex function; (c) the epigraph of a convex function is convex set; (d) polygonal convex set; (e-f) nonconvex sets; (g) convex hull of discrete points; (h) conic hull of (g); (i) convex hull of (e); (j) conic hull of (e); (k) intersection between a linear goal and a conic hull; (l) nonlinear feasible region associated to a convex goal; (j) idem under integer constraints.*

- *Decomposition by projections*

Complex combinations of convex and non-convex goals and constraints can be simplified by projecting the goal on the convex hull (**Figure II-3**k) or by projecting the space of constraints of the convex objective (**Figure II-3**l,m). Projections combined with polyhedral annexation (**Figure II-3**i), outer approximation (**Figure II-3**h,j) and optimization on separable domains offers a global strategy to resolve complex and high dimensional problems in

almost polynomial-time. Reference monographies on the techniques are presented in **Table II-4**.

***Table II-4**. List of relevant monographies to tackle complex optimization problems (convex or not) met in engineering and related fields.*

Topic	Public	References
Fundamentals of convex analysis	advanced	a
Convex optimization and convex geometry	intermediate	b
Convex optimization	intermediate	c
Linear and nonlinear programming	intermediate	d
Convex analysis and global optimization	intermediate	e
Convexification and global optimization	advanced	f
Illustrations of multiobjective optimization in chemical engineering	intermediate	g

a. Hiriart-Urruty and Lemaréchal (2004); b. Dattorro (2005); c. Boyd et al. (2004); d. Luenberger and Ye (2008); e.Tuy (2016); f. Tawarmalani and Sahinidis (2013); g. Rangaiah (2009).

II.1.5. Ecodesign concepts and tools

The concepts of green technology or clean technology and green chemistry are not standardized, but they strive to meet consumer and citizen expectations through sustainable technology. The presumption is that industrial design applied in the 19th century and a significant part of the 20th century damaged the quality of air, created marine litters, increased the number of chemicals to which we are exposed. Ecodesign targets new products and technologies which are intended to mitigate or reverse the effects of human activities. The orientation is complementary to the life cycle initiative (see §II.3.) and eco-labeling efforts. The definition of the technical report ISO/TR 14062 (ISO, 2002) is more general and includes not only products but also processes all along the entire life cycle of the product. As shown in **Figure II-4**, most of the impacts are created at early stages in the design and development of new products, by an inappropriate choice of raw materials or performances for the finished product. Ecodesign aims at reducing these impacts without prescribing all technical details. The EU directive 2009/125/EC (2009), so-called "*Ecodesign Directive*" established a framework for the setting of eco-design requirements for all "energy-related products" in the EU, where "'*energy-related product', (a 'product'), means any good that has an impact on energy consumption during use which is placed on the market and/or put into service*". Though the directive targets the reduction of energy use, it includes additional considerations such as water use, polluting emissions, and waste and recyclability issues. The working plan is ongoing, it mentions packaging but not food production, and does not set a minimum of ecological requirements.

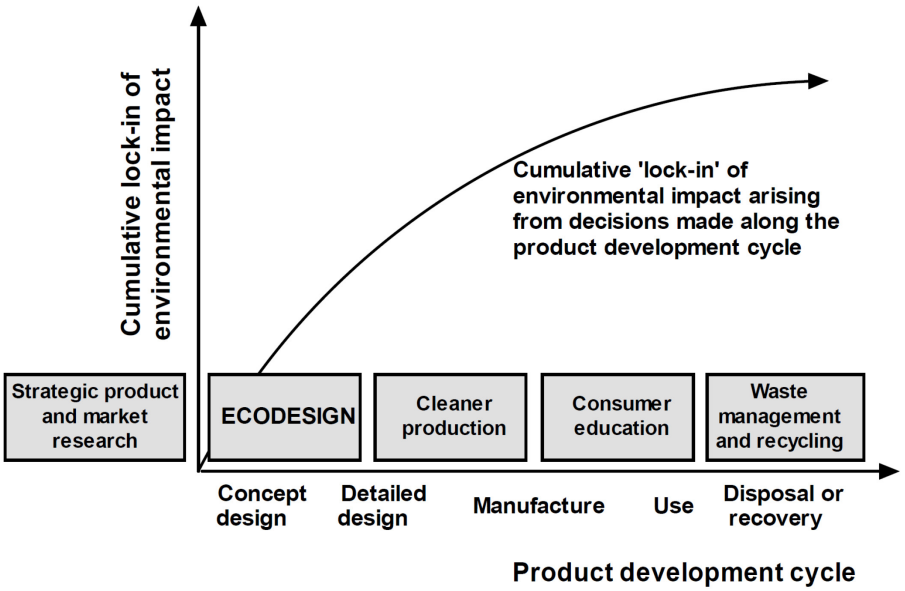

***Figure II-4**. How environmental impact is created along the decision chain supporting product development (after Lewis et al., 2001).*

II.1.5.1. Overview

The "ecodesign" or "eco-design" literature is relatively recent and rapidly growing to reach 972 peer-reviewed articles published during the last decade (WOS). This number may look large, but it covers all applications of ecodesign. The first review on ecodesign was published in 1994 (Roy, 1994). The first similar work on food packaging was proposed by Gordon Robertson (2009b) fifteen years later as a chapter in the "Handbook of waste management and co-product recovery in food processing – Volume 2".

All publications on ecodesign are contemporary of the groundbreaking manual "*Ecodesign: A Promising Approach to Sustainable Production and Consumption*" published in 1997 by the United Nations Environment Programme (Brezet and Van Hemel, 1997). It was built upon the work carried out mainly at the Dutch Delft University of Technology. As quoted from the 2009 report (Crul *et al.*, 2009) of UNEP "*Design for sustainability: a step-by-step approach*": "The concept of product re-design has since then spread as seen in the number of manuals and sector-specific supporting materials now produced in many languages. As a result, and based on experience gained, ecodesign has evolved through Design for Environment (DfE) to the broader concept of D4S– which encompasses issues such the social component of sustainability and the need to develop new ways to meet consumer needs in a less resource intensive way. D4S goes beyond how to make a 'green' product – and now strives to meet consumer needs through sustainability in a systematic and systemic way".

II.1.5.2. Definitions and example

Various environment-related terms and definitions have been used to highlight the importance of sustainable development in the packaging field, such as eco, green, environmentally sustainable, friendly, conscious, and extra, all of which reflect a desire to "protect our environment for the future." (see chapter 12 of Han,2014). The standardization committee ISO/TC 207/SC 1 (ISO, 1993), created in 1993 to work on Environmental management systems, introduced the concepts of ecodesign in the standard ISO 14006 (2011) with the following definitions:

- **design and development**: "set of processes that transforms requirements into specified characteristics or the specification of a product, process or system";
- **ecodesign**: "integration of environmental aspects into product design and development, to reduce adverse environmental impacts throughout a product's life cycle";
- **products**: "any good or service".

Additionally, it is stated that "*Ecodesign can be understood as a process integrated within the design and development that aims to reduce environmental impacts and continually to improve the environmental performance of the products, throughout their life cycle from raw material extraction to end of life. In order to be of benefit to the organization and to ensure that the organization achieves its environmental objectives, it is intended that ecodesign be carried out as an integral part of the business operations of the organization. Ecodesign might have implications for all functions of an organization.*" According to Karlsson and Luttropp (2006), engineering and design should be reinvented with EcoDesign as foundation with a significant place given to environmental sciences in engineering cursus. An example of the aspects covered by ecodesign is shown in **Figure II-5**. They include packaging waste management and the definition of an optimal shape to meet technical requirements (e.g., sealing) without impacting the functionality of the packaging.

a)

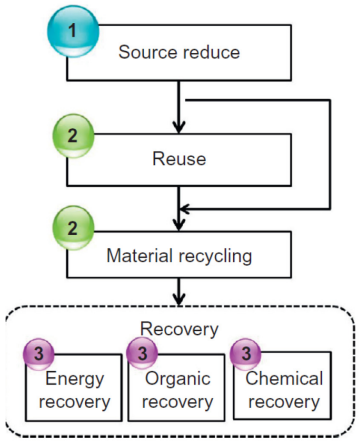

b)

Horizontal form/fill/seal pouch			Acceptable	Optimum
Seal width	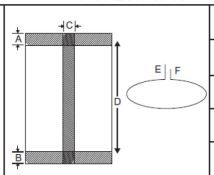	A : End seal width	12 mm	7 mm
		B : End seal width	12 mm	7 mm
		C : Fin seal width		
		D : Pouch length between seal		
		E+F : Total fin seal width	25 mm	20 mm
Pouch length (cut)	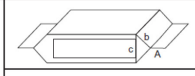	b : Allowance for sealing	5 mm or $c \div \sqrt{2}$	
		c : Product height		
	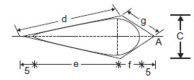	d : Allowance for sealing	$\sqrt{(e+5)^2+(c/2)^2}$	
		c : Product height		
		g : Allowance for sealing	$\sqrt{(f+5)^2+(c/2)^2}$	
Pouch width	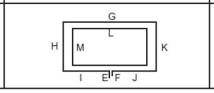	Product circumference: (L+M) x 2	Product circumference +6+E+F	Product circumference +4+E+F

***Figure II-5**. Aspects to consider in ecodesign of food packaging: (a) hierarchy of packaging waste management, (b) An example of a design guideline for source reduction of horizontal pouches used in the Korean food industry. "Acceptable" and "Optimum" refer to the dimensional allowable ranges (mm) in the design process (after Han, 2014).*

II.1.5.3. Ecodesign methodologies: a critical review

The methodologies of ecodesign are evolving with the appropriation of the concepts by the different branches of the industry. They mutate progressively from TRIZ-derived and ranking approaches suggested by pioneers to new hybrid methods including computational engineering. Despite the forest of methods, they can be classified by their degree of quantification and their ability to be prospective and to be integrated into the design process. An overview of the trends is shown in Figure II-6. It is notable that the tools and approaches follow an evolution different from the one followed with engineering and detailed design approaches. The lack of integration is apparent, and the software in ecodesign and life cycle analysis start to generate their own ecosystem with their own logic, vocabulary, and concepts.

The pro and con of the different methodologies have been significantly discussed in the literature, with the notable references (Karlsson and Luttropp, 2006;Sakao, 2007;Ramani *et al.*, 2010;Bovea and Pérez-Belis, 2012;Dufrene *et al.*, 2013;Vallet *et al.*, 2013;Rossi *et al.*, 2016;Brones *et al.*, 2017;Buchert *et al.*, 2017). The analysis from the open literature has; however, inherent limits, it does not enable to establish which method is effectively used in the industry. The main barriers that limit their implementations are rarely reported, but they include the need of specific knowledge, time-consuming efforts and personnel efforts, the large number of tools and the over-formalization (Rossi *et al.*, 2016).

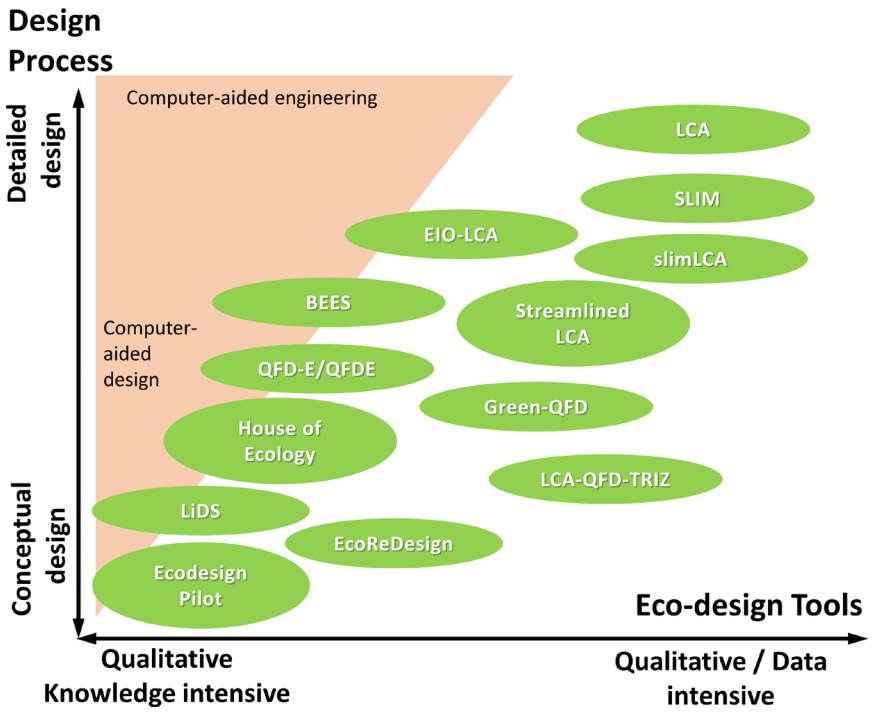

Figure II-6. Overview of the bestiary of eco-design and design process tools from Ramani et al. (2010).

BEES=Building for Environmental and Economic Sustainability; EIO-LCA = The Economic Input-Output Life Cycle Assessment; LCA = Life Cycle Assessment, LiDS = Lifecycle Design Strategy; QFD=SLIM=Sustainable and Life Cycle Information-based Manufacturing; QFD = quality Function Deployment; QFDE = quality Function Deployment for Environment; TRIZ= theory of the resolution of invention-related tasks.

A non-inclusive classification of main methodologies is proposed in **Table II-5** with an intent of showing that they can be understood as a special case of solving problem strategies listed in **Table II-1**. The classification of ecodesign tools is derived from a prior categorization by Baumann *et al.* (2002) and subsequently discussed by Buchert *et al.* (2017). Ecodesign methods were initially split into five first categories "frameworks, checklists and guidelines, rating and ranking tools, analytical tools, software, and expert systems, and organizing tools" to which computer-aided design approaches, not available at the time, need to be appended.

The whole framework for ecodesign tools remains immature without common standards and interoperability. No significant collaborative and interdisciplinary project organize the numeric implementation of eco-concepts. The applicability of presented tools to hybrid systems such as food and packaging remains challenging and without specific guidance.

Table II-5. *Classification of ecodesign tools and methodologies and associated problem-solving method (see* ***Table II-1****).*

Problem-solving method →	Analysis									Heuristics	Thought experiments			TRIZ	
Ecodesign tools and methods ↓	Check list, case-based study	Quality Function deployment (QFD)	Failure mode and Effect Analysis (MEA)	Value analysis	Life Cycle Assessment (LCA)	Life Cycle Cost analysis (LCC)	Social Life Cycle Assessment (SLCA)	Diagrams and matrix-based tools	Decision analysis (multicriteria)	Heuristics: multicriteria optimization	Thought Experiments (Simulations)	Artificial intelligence, fuzzy logics	Artificial intelligence, axiomatic	Theory of inventive problem	Typical references
FRAMEWORKS															
Design for Sustainability (D4S)					×			×						×	a
Sustainable Product Development (SPD)		×			×	×		×			×				b
Life Cycle Planning (LCP)					×	×					×			×	c
Redesign framework (RF)					×				×		×				d
Life Cycle Sustainability Assessment (LCSA)					×	×		×							e
CHECK LIST AND GUIDELINES															
Many guidelines (Fast Five, Black, Whide and Grey list, Ten Golden Rules, Ecodesign pilot…)	×														f
Consumer integration in suistainable product development	×														g
RATING AND RANKING TOOLS															
Cost estimation for environmentally conscious product development		×	×	×								×			h
SEEbalance (Socio-Ecoefficiency analysis)					×	×	×								i
Axiomatic design	×			×									×		j
Product Sustainability Index (ProSi)	×		×		×										k
ANALYTICAL TOOLS (see software)															
SOFTWARE AND EXPERT SYSTEMS (examples)															
Multicriteria optimization					×	×		×			×	×		×	l
COMPLIMENT: LCA, environment indicators and multicriteria optimization					×				×						m
Platform G.ENE.SI	×				×	×	×								n
Commercial software: GABI	×				×										o
Commercial software: Simpro					×										p
Commercial database: Ecoinvent					×										q
Opensource software: openLCA	×				×										r
ORGANIZING TOOLS (example)															
Integrated ecodesign decision making	×	×			×										s
CAD INTEGRATED TOOLS AND METHODOLOGIES (examples)															
Ecologic CAD	×	×			×			×						×	t
EcoCAD (design for disassembly)	×	×			×									×	u
Design for remanufacture	×	×			×			×						×	v

References: a. Crul and Diehl (2006); b. Buchert et al. (2017);Charter and Tischner (2017); c. Kobayashi (2006); d. Yu et al. (2017); e. Finkbeiner et al. (2010); f. Lewis et al. (2001);Luttropp and Lagerstedt (2006); g. Hoffmann (2007); h. Dong et al. (2003); i. Kolsch et al. (2008); j. Morrison et al. (2013): k. Shuaib et al. (2014); l. Thurston and Srinivasan (2003);Khan et al. (2004); m. Hermann et al. (2007); n. Dufrene et al. (2013); o. thinkstep (2019); p. (simapro, 2019); q. (ecoinvent, 2019): r. (GreenDelta, 2019); s. Romli et al. (2015); t. Leibrecht (2005); u. Cappelli et al. (2007); v. Hatcher et al. (2011).

Key points of II.1. Beyond engineering: computer-aided decision making

Facing numerous challenges which could affect the survivability of mankind on our planet, all industries should turn their practices to more environment-friendly approaches. No industry can avoid the effort, either the food or the packaging industries. They face together simultaneous challenges including food security, food safety, and environmental challenges. **Decisions need to be made by anticipation and integrated at the early stages of the development of products**. The methodologies to take objective decisions in the presence of contradictory goals (e.g., profit, sustainability, performance, etc.) exist as well as the methods to find Pareto optimums.

Ecodesign initiated a special branch of approaches merging engineering methodologies and environmental design. **The nascent formalization of ecodesign** methodologies is similar to the situation met by innovators before the industrialization era. Each master and country created a school of thoughts but **without granting that both safety and environmental principles are mastered at all stages**. As an example, the role of the supply chain for food packaging is not documented. On the one hand, smaller packaged food portions contribute to reducing food wastes, but they increase packaging wastes. On the other hand, exporting small portions with large surface areas to distant markets increase the dependence on high barrier materials.

The next sections will discuss how chemical and environmental risks can be **evaluated** independently the way they are managed along the value chain.

II.2. Evaluation of the migration from packaging materials

II.2.1. Preamble and scope

The evaluation of the migration has been subjected to an extensive review as a chapter in curated reference collection in Food Science of Elsevier. (Zhu *et al.*, 2019b) The chapter has been designed to serve as in depth and comprehensive compendium of the methods available to assess the risk of migration. **Migration** is a generic term belonging to the jargon used by several communities dealing with packaging, food, medical, pharmaceutical and biotechnological applications. In the context of food packaging, it encompasses all mass transfer phenomena associated to the chemical contamination of food by any material (thermoplastics, elastomer, timber, printing ink, glue, varnish, etc.) intended to be in contact (primary packaging) without excluding contaminations by secondary and ternary packaging. The underlying phenomena include diffusion, sorption and desorption from or to a condensed phase (liquid or solid) and from/to a gas phase. Migration problems present several similarities with outgassing phenomena met in ultra-vacuum and spatial applications (NASA, 2018). In porous media, outgassing is usually associated to the release of trapped gas and the evaporation of water. In dense thermoplastics and thermosets subjected to strong temperature variations, outgassing phenomena cover the desorption of any chemical substance and usually its condensation on another material or a colder surface. In closed automobiles and rooms, outgassing is responsible for the smell of the air inside.

The **risk of migration** is one important step in the **risk assessment** methodology aiming at evaluating the exposure of consumers (by ingestion) to substances originating from food contact materials. In simpler words, the methodology assesses whether the mass transfer of a given substance in one or several modalities is tolerable regarding some thresholds: maximum concentration in food, maximum amount transferable to food, maximum concentration acceptable in the original material, tolerable daily intake, threshold of concern based on toxicological considerations. In **quantitative risk analysis**, the concept of risk is associated with the probability to have a given threshold value to be exceeded. **The final decision to accept or reject the risk is based on the value of this probability and not on the extent of the mass transfer**. The final probability includes both the **variability of the results** (which could be measured but not reduced) and the **uncertainty in the knowledge** of the phenomena (which could not be measured but which could be reduced with additional expertise).

This section reproduces the aspects of the chapter related to the description of mass transfer between a thermoplastic and a liquid food from molecular to macroscopic scales. The

concepts enabling to generalize results obtained in constant conditions to variable ones (e.g. temperatures) are presented as well as the mathematical framework required to evaluable objective probabilities associated to these mass transfer. Many results have been specifically developed for the needs of risk assessment, but they can be seen as fundamental for any mass transfer involving molecular diffusion, monotonic operators (contamination is evaluated as a cumulant).

The full content of this section is available in:

Zhu, Y., Nguyen, P.M., Vitrac, O. 2019. Risk assessment of migration from packaging materials into food. In "Reference Module in Food Science". Volume *In Press*. Elsevier. Amsterdam. https://doi.org/10.1016/B978-0-08-100596-5.22501-8. 64p.

II.2.2. Principles of tiered migration modeling for risk assessment

II.2.2.1. Verifiable and auditable modeling to support decisions about safety

Migration modeling has been developed to enable a rapid demonstration of the compliance of materials in contact with food. It follows good practices in modeling stated by Marc Spiegelman (2019): (i) work on right decision problem, (ii) specify your objectives, (iii) create imaginative alternatives, (iv) understand the consequences, (v) grapple with tradeoffs, (vi) clarify your uncertainties, (vii) think hard about risk tolerance, (viii) Consider linked decisions. In the field of risk assessment, the following rule should be added: modeling should be verifiable and auditable as modeling is to take decision with legal consequences.

Tiered modeling is a methodology enabling to create a confidence in modeling among stakeholders. Sophisticated modeling with complex reasoning and computational power should be limited to situations, where simple conservative scenarios cannot demonstrate the safety of considered application. As a result, tiered modeling is not seen as one single step simulation, but as iterative process with enriched hypotheses and mechanisms at each step.

II.2.2.2. Principles of tiered modeling

- *Overview*

From an epistemological point of view, the exact value of the contamination of the food is never achievable because the conditions of contact are variable (time, temperature) between comparable products and because knowledge of molecular mechanisms is not perfect. The concept of successive approximations is shown in **Figure II-7**. At the first tier, the estimation is very coarse and connected with the highest overestimation factor. If the determined concentration at tier n is higher than the threshold of concern, the next tier is triggered by introducing substantial refinements and details, and so on. The process stops when no additional

information can be introduced (experiments need to be preferred) or when the calculated concentration is lower than the threshold of concern. The lowest tier within the threshold of concern defines the proper level of knowledge required to demonstrate compliance or to guarantee the safe use of a material, substance, or process. There is no systematic procedure to identify the minimum tier to reach the goal, and only the needed information can be listed. In Europe, the Joint Research Centre (Ispra, Italy) of the European Commission updated regularly a guide exemplifying the principles of tier modeling and application under "Plastics" regulation 10/2011/EC (2011a). It is thought that the compliance of ca. two thirds of all food contact in materials on plastics is verified by modeling.

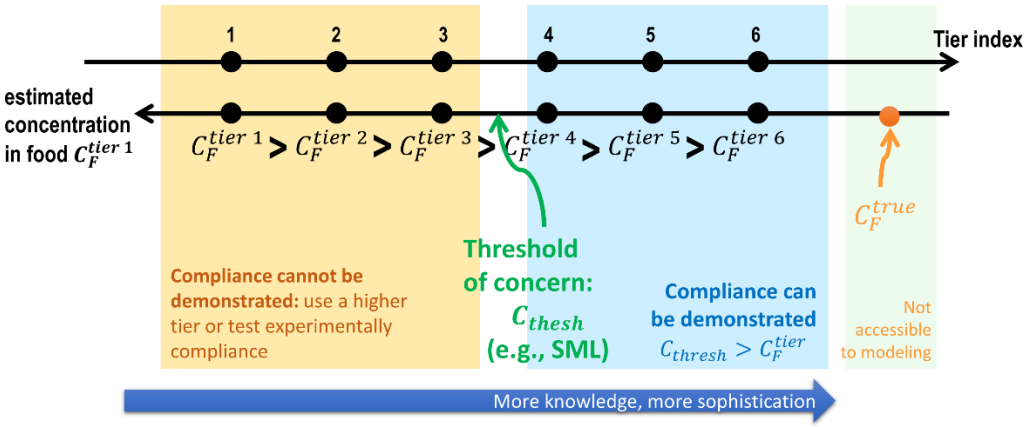

***Figure II-7**. Principle of the tiered approach to demonstrate compliance for food contact materials. Compliance is demonstrated as soon as the estimated concentration is greater than the threshold of concern. Tier 1 is usually associated with total migration (see Eq. (II.4)).*

- *First tier model*

The possibilities and prerequisites for using migration modeling in compliance testing are reviewed in Table 3 of Zhu *et al.* (2019b), which reproduced succinctly in **Table II-6**. The first tier is usually coined "total migration" and corresponds to the total transfer of substances into food. The corresponding concentration in food, $C_F^{tier\,1}$, is determined by a "dilution" model:

$$C_F^{tier\,1} = L_{P/F} C_P^0 \tag{II.4}$$

where C_P^0 is the initial concentration in the material (regardless of its distribution) expressed in mass per volume (preferred in this work) or in mass per mass (industrial practice). $L_{P/F}$ is the material-to-food volume or mass ratio. When one-dimensional representations are used, $L_{P/F}$ is also the ratio between the thickness of packaging walls, denoted l_p, and the characteristic dimension of the food, denoted $l_F = \frac{V_F}{A}$, where A is the effective surface area in

contact, counting usually the total surface area in contact with the food and the headspace. By contrast, the food volume V_F is restricted to the condensed part of the food (solid or liquid).

Table II-6.*Prerequisites and indicative tiers to be used for compliance testing (R1=most severe, R3=most refined)*

Prerequisites	Type of estimate	tier
Migration modeling or related calculations	• Guidance documents • Reference text books	R1 R2
Identity of material	• technical specification • recycling code • measurement	R1 R2 R3
Characteristics of the polymer	• density • glass transition temperature • crystallinity	R1 R2 R3
Identity of the substance	• real substance (disclosed by supplier) • chemical structure (spectroscopic technique) • chemical descriptors (analogous substance)	R1 R2 R3
Packaging geometry	• 1 kg packed in 6 dm^2 • 1D approximation of real geometry • 3D real geometry	R2 R2 R3
Contact conditions (time, temperature, phase in contact…)	• standard test conditions • accelerated conditions • real conditions	R1 R2
Initial concentration	• overestimates (guidance) • real values (technical sheet) • estimates from brute force deformulation	R1 R2 R3
Diffusion coefficients Partition coefficients Sorption isotherms	• overestimates • real values • molecular theory (e.g. Flory-Huggins, free-volume) • molecular modeling (e.g. atomistic calculations)	R1 R2 R3 R3
Mass transfer resistance in the contacting phase	• no resistance • boundary layer approximation • explicit transport in the food (solid and semi-solid food) • full Graetz problem with flow	R1 R2 R2 R3
Acceptable thresholds	• maximum amount in the raw material QM • specific migration limit: SML • threshold of regulation • toxicological threshold of concern: TTC	R1 R2 R3 R3

II.2.3. Common assumptions used in migration modeling

II.2.3.1. Underlying microscopic assumptions

Substances non-covalently bound to the polymer are subjected to thermal agitation, which causes in return a random translation of their center-of-mass. Each additive, monomer, or residue jumps or walks randomly in the polymer matrix from one accessible void to the next. The substances eventually reach the interface with the food, where the same hopping process is repeated, usually at a higher pace. When volatile substances meet a gas phase, their skew trajectories are governed by the collision with gas molecules. In all cases, random walks occur in three-dimensions, but a concentration gradient develops only at leaching interfaces, in a

perpendicular direction. As the walls of the packaging are thin compared to the characteristic food dimension, migration can be approximated as a one-dimensional mass transfer problem as shown in **Figure II-8**. The migrating substances are depicted either as individual molecules or solutes (i.e., scales are not respected) showing microscopic concentration fluctuations or as smooth macroscopic concentration profiles (continuous lines). Different symbols are used depending on whether the solutes are in the polymer (position $0 \le x/l_p < 1$); in a small boundary layer in the food and of thickness x_{BL}, where a concentration gradient exists (position $1 < x/l_p \le 1 + x_{BL}/l_p$); or in the food bulk ($x/l_p > 1 + x_{BL}/l_p$) without any significant concentration gradient (e.g., assumption of a perfectly mixed medium). Choosing x_{BL}/l_p as a free parameter enables covering almost all contacting phases (gas, liquid food or simulant, solid and semi-solid food) with reasonable complexity.

Figure II-8 plots simulation results using the concepts of statistical physics (i.e., the molecules jump randomly vertically and horizontally without "knowing" where the interface is located) and by using the concept of continuum mechanics (i.e., balance on populations and macroscopic fluxes on elementary volumes). The stochastic and deterministic point of views are equivalent and highlight that the observed macroscopic gradients are the consequence of the evolution of the distributions of solutes with time and not its cause. In the upward direction, the random displacements are compensated by the same and opposite microscopic flux in the downward direction. The net balance is zero, and no concentration gradient can develop. The substances translate at the same frequency in the horizontal direction (i.e., isotropic diffusion), but since no solute comes to compensate the flux from left to right at the beginning of the contact, a net flux develops from left to right, resulting in the spreading of a concentration gradient from the source (the polymer: P) to the food (the food: F). Statistical physics and continuum mechanics counts molecules in a very similar fashion, via the concepts of probability density, $\rho = \frac{N}{N_0 V}$ and of volume concentration $C = \rho N_0$, respectively. N_0 is the total number of migrating substances in the whole system and N the number of molecules in an elemental volume V . The concentration at the interface between F and P (denoted P-F) requires specific treatment and analysis. Since the principle zero of thermodynamics does not hold for mass transfer, both density and concentration are discontinuous at the P-F interface. If no reaction occurs at the interface, the mass balance is kept across the interface (i.e., no substance is lost). Additionally, the principle of microscopic reversibility entails that the amount of substances crossing the interface per time unit from left to right (denoted P→F) is exactly matched by the amount of substances crossing the interface in the opposite direction

(denoted F→P). In other words, any substance located exactly at the interface $x = l_p$ has the same probability to go in P and F, irrespective of its origin. This principle of microscopic mass balance reads:

$$\rho_F f_{P\to F} = \rho_P f_{F\to P} \tag{II.5}$$

where $f_{A\to B}$ is the frequency of translating from the compartment A to the compartment B. The concept of local chemical equilibrium developed among others by Henry Eyring provides a robust framework to express the frequencies of passage from one state to another without justifying the details on how the change in conformations and local velocities affect the passage from A to B. The frequency of passage is written as:

$$f_{A\to B} = \kappa \exp\left(-\frac{G^{\ddagger} - G_A}{RT}\right) \tag{II.6}$$

with $G^{\ddagger}$ the free energy associated with the transition state and G_A the free energy of sorption of the solute in A. The preexponential factor κ is independent of temperature; its expression depends on the statistical ensemble used to express probabilities. By combining Eqs (II.5) and (II.6), the molecules distribute across the interface with a ratio of probabilities equal to:

$$K_{F/P} = \frac{\rho_F}{\rho_P} = \frac{C\left(x = l_P + \epsilon, t\right)}{C\left(x = l_P - \epsilon, t\right)} = \exp\left(-\frac{G_P - G_F}{RT}\right) \text{ with } \epsilon \to 0 \text{ and } t > 0 \tag{II.7}$$

where x and t indicate the position and time; the food-packaging interface is located at $x = l_P$.

The concentration profiles are, therefore, continuous across the P-F interface only when the free sorption energies are similar in both compartments. In the general case, the concentration profile is discontinuous across the interface. **Figure II-8** plots cases for an apparent partition coefficient $K_{F/P}$ of 0.5. In other words, the substance has double the chemical affinity for P than for F, as expected for plastic additives and monomers. For conservative migration modeling, values of $K_{F/P}$ higher than unity are preferred to maximize the gradient and consequently the amount transferred to the food. When the release of a substance does not modify the properties of the polymer (e.g. polymer densification, or a shift in the glass transition temperature T_g), the ratio of concentrations is likely to be constant at the interface.

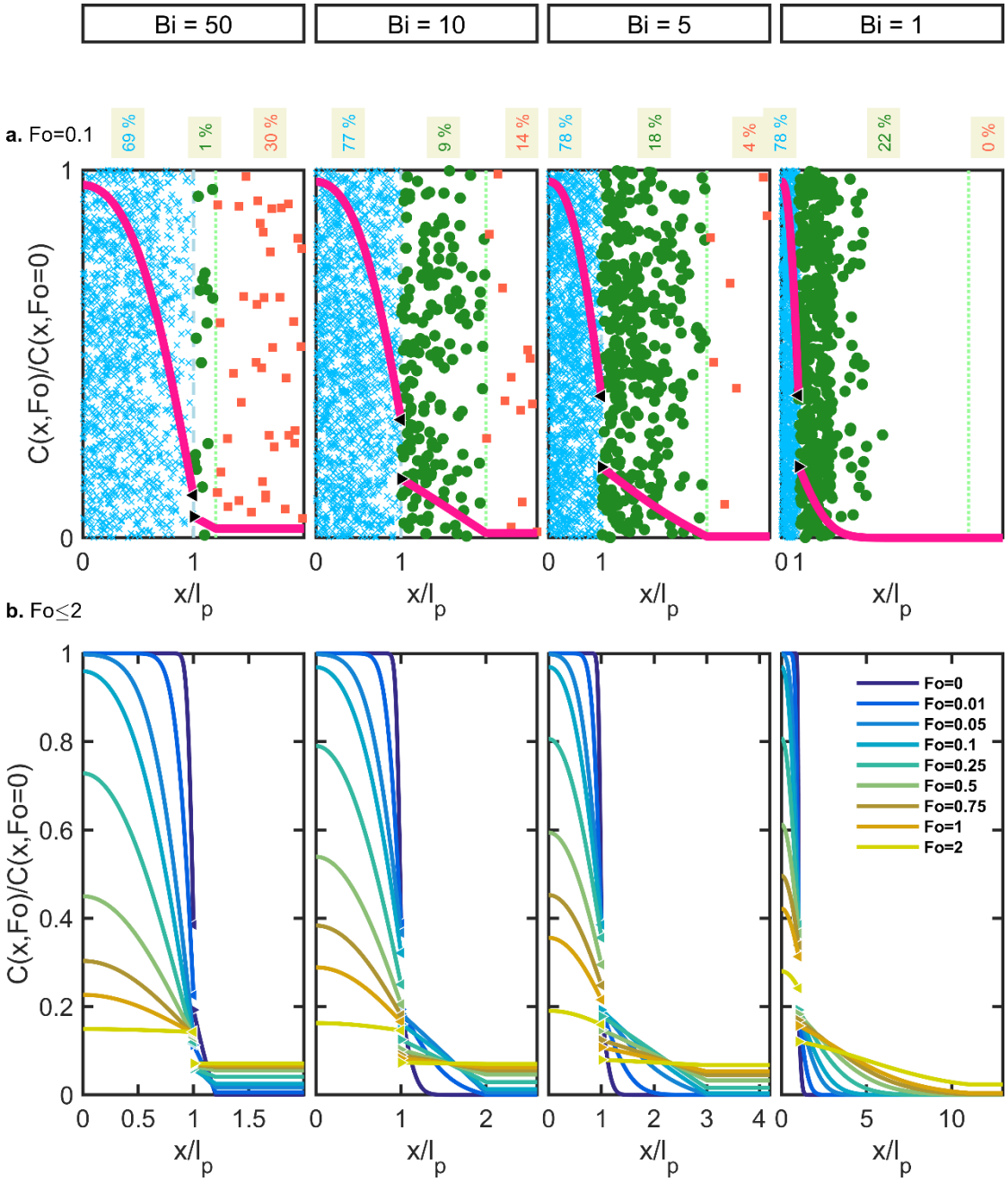

***Figure II-8**. One-dimensional description of solute diffusion (e.g., additive, monomer) from the packaging wall (position: $0 \le x/l_p \le 1$, individual solutes identified as ×) to the contacting phase (individual solutes identified as ■) via the food boundary layer (individual solutes identified as ●): (a) random distribution of solutes and corresponding concentration profile at $Fo = 0.1$ and (b) after contact times up to $Fo = 2$. The percentages in the top part represent the residual amount in each compartment.*

*Fo and Bi correspond to dimensionless time and ratio internal-to-external mass transfer resistance, which are both defined in **Table II-7**.*

II.2.3.2. Migration modeling and similitude properties

Under the assumption of uniform and constant transport and thermodynamic properties in each compartment (polymer: P, boundary layer: BL, bulk contacting phase or food: F), the mass transfer problem is similar according to a small number of dimensionless parameters

or ratios. According to the principle of similitude, a real problem can be compared to a theoretical case without dimensions if all independent dimensionless quantities are similar. The key dimensionless quantities are reviewed in **Table II-8**.

Table II-8*. Key dimensionless quantities of the migration from monomaterials. Contact is assumed to be initiated at* $t = 0$.

Dimensionless quantity	Meaning	Justification
$u(x,t) = \frac{C(x,t)}{C_{ref}}$	Dimensionless concentration	C_{ref} is a reference concentration, usually the initial concentration in the polymer $C_P^{t=0}$.
$K_{F/P}$ it is defined from Eq.(II.7).	Partition coefficient	At macroscopic equilibrium, it is also defined as $K_{F/P} = \frac{C_F(t \to \infty)}{C_P(t \to \infty)}$ with $C_F(t)$ and $C_P(t)$ the volume-averaged concentrations in F and P, respectively.
$q = \frac{x}{l_p}$	Dimensionless position	l_P is characteristic food dimension, usually the thickness or the ratio $\frac{V_P}{A}$ if the geometry is complex, with V_P the volume of the material and A the surface area in contact with F . It is recommended to maximize A by also including the headspace in the calculations of A .
$Fo = \frac{D_P t}{l_p^2} = \int_0^t \frac{D_p(t)\,dt}{l_p^2}$	Dimensionless time	D_P is the diffusion coefficient in the polymer at the temperature of contact. The integral form is preferred if the diffusion coefficient is variable with time (temperature change)
Bi or Sh $= \frac{D_F}{D_P}\frac{l_p}{x_{BL}} = \frac{hl_p}{D_P}$	mass Biot or Sherwood number	where x_{BL} is the thickness of the boundary layer and D_F the diffusion coefficient in F, such that $h = \frac{D_F}{x_{BL}}$ is the effective mass transfer coefficient across the boundary.
$L_{P/F} = \frac{l_p}{l_F} = \frac{V_P / A}{V_F / A}$	Dilution ratio	This number is defined as the ratio of characteristic lengths and controls how the substances are diluted in the food, usually much larger than the packaging.

II.2.3.3. Explicit vs implicit food representation

It would be logical that migration models describe explicitly how the migrants distribute in the food. Solid foods, such as a chicken or a pizza, are not expected to have all parts contaminated similarly. For risk assessment, all the parts that are intended to be ingested, including the most contaminated sauce in contact with the packaging are considered. As a result, only a global estimate of the food contamination is required, as measured with a liquid simulating the entire food. Replacing a solid by a liquid or vice-versa has a consequence on the rates of mass transfer. This section discusses the differences between explicit and implicit representations of the food and the risk of underestimating the real migration.

Figure II-8 represents explicitly mass transfer in the food, that is the concentration profiles in the food are also calculated. The depicted cases correspond to a characteristic food

length $l_F = \frac{V_F}{A}$ of $12 l_p$ (i.e., thin food to make the boundary layer visible). The total domain has a length of $13 l_p$. When the food is represented explicitly, the amount transferred to the food is defined as:

$$C_F(t) = \frac{1}{l_F} \int_{x=l_P}^{x=l_p+l_F} C(x,t)\, dx \tag{II.8}$$

Eq. (II.8) accumulates substances in the boundary layer (round symbols) and in the food bulk (square symbols). Implicit food representation will describe mass transfer only in the packaging and apply a proper boundary condition between the food and the packaging at the position $x = l_p$. With the help of Eq.(II.7), the flux at the interface, denoted j, can be expressed only with concentrations taken inside the packaging or in the food far from the interface, $C(x \to \infty, t)$.This assumption opens the way for an implicit representation of the food via a boundary condition relating the diffusion at the packaging-food interface with the flux entering into the food:

$$\begin{aligned} j(t) &= -D_P \left.\frac{\partial C}{\partial x}\right|_{x=lp-\epsilon,t} = h\left(C(x+\epsilon,t) - C(x\to\infty,t)\right) \\ &= h\left(K_{F/P} C(x-\epsilon,t) - C(x\to\infty,t)\right) \end{aligned} \quad \text{with } \epsilon \to 0 \text{ and } t > 0 \tag{II.9}$$

Eq. (II.9) offers a good approximation of the explicit representation when the contact time is sufficient to reach a fully developed concentration profile (linear, so-called Prandtl approximation) inside the boundary layer. The critical Fourier number is given by $Fo_{critical} = \left(x_{BL}/l_p\right)^2 \Big/ \left(6\, D_F/D_P\right) = \left(x_{BL}/l_p\right) \Big/ \left(6Bi\right)$. The profile plotted in **Figure II-8**a for $Bi = 1$ and $Fo = 0.1$ deviates from the assumption above. The critical Fourier number is 1.67 and the value of $C(x \to \infty, t)$ is close to zero, whereas the food is already contaminated via its boundary layer.

Implicit food representation approximates the concentration in the food, $C_F(t)$, by its concentration far from the interface. By noting that the flux $j(t)$ is taken after the boundary layer, one gets:

$$C_F(t) = C(x\to\infty,t) \approx C_F(t=0) + \int_0^t j(t)\, dt \text{ for } t > Fo_{critical} \frac{l_p^2}{D_P} \tag{II.10}$$

For $Bi > 50$ and if the threshold of concern is not too low, the amount present in the boundary layer can be neglected (less than 1% in **Figure II-8**a when $Bi = 50$) and an implicit

representation can be used. Its main advantage is the dramatic reduction in the problem complexity and the computational time. In very thin or low barrier films and in solid foods, the implicit food representation may severely underestimate the contamination of the food. The amounts in the boundary layer reported in **Figure II-8**a reach 9%, 18% and 22% for Bi = 10,5,1 respectively. When an implicit representation is used, calculating the concentration in the food from the mass balance in the packaging between $t = 0$ and t does not solve the issue as the closure equalities are enforced at any time:

$$\frac{d}{dt}\left(\int_0^{l_p} C(x,t)\,dx\right) = j(t) = \frac{dC_F}{dt} = \frac{dC(x \to \infty, t)}{dt} \text{ for } t > 0 \qquad \text{(II.11)}$$

The amount present in the boundary layer is always neglected in migration representing the food implicitly. Only by choosing artificially $Bi \to \infty$ as a worst-case scenario makes this amount negligible at the price of migration much faster than that expected in the real conditions.

- *Other assumptions*

In this section the constitutive equations to describe mass transfer from monolayer and multilayer materials, when the food is represented implicitly via the boundary condition (II.9) and the food mass balance (II.11) are presented. The total packaging thickness is denoted $l_p = \sum_{i=1}^{m} l_i$ for a packaging (e.g. laminate) consisting of m layers. At the position $x = 0$ (usually the surface exposed to the ambient environment), an impervious boundary layer is assumed so that the amount transferred to the food is maximized. All substances are assumed to be well dispersed where they have been incorporated (e.g., no blooming effect) and below their concentration at saturation (i.e., no supersaturation).

II.2.3.4. Governing equations for monolayer materials

II.2.3.4.1. Overview

The full set of equations for monolayer materials including the initial condition (IC), the transport equation (TE), the boundary conditions (BC) and the mass balance on the food compartment (MB) are:

$$\begin{cases} IC: C_{(x,t=0)} = C_P^{t=0} \text{ for } 0 \le x \le l_p \\ TE: \dfrac{\partial C_{(x,t)}}{\partial t} = \dfrac{1}{x^n}\dfrac{\partial}{\partial x}\left(D_P\left(C_{(x,t)}\right) x^n \dfrac{\partial C_{(x,t)}}{\partial x} \right) \text{for } 0 \le x \le l_p, t > 0 \\ BC: j(t) = -\left(D_P \dfrac{\partial C}{\partial x} \right)\Big|_{x=l_p-\epsilon,t} = h\left[K_{F/P} C_{(x=l_p-\epsilon,t)} - C_F(t) \right]; \\ \left.\dfrac{\partial C}{\partial x}\right|_{x=0,t} = 0 \text{ for } t > 0 \text{ and } \epsilon \to 0 \\ MB: C_F(t) = C_F(t=0) + \dfrac{A}{V_F}\int_0^t j(\tau)\, d\tau \text{ for t} \ge 0 \end{cases} \qquad \text{(II.12)}$$

where n is an exponent controlling the system of coordinates ($n = 0$: Cartesian, $n = 1$: cylindrical; $n = 2$: spherical); $D_P\left(C_{(x,t)}\right)$ is the diffusion coefficient that possibly varies with concentration (e.g., in the case of plasticizers used at high concentrations).

When the diffusion coefficient in the packaging is considered constant along with $C_F(t=0) = 0$,**Table II-8** and system (II.12) yield the following dimensionless formulation for Cartesian coordinates:

$$\begin{cases} IC: u_{(q,Fo=0)} = 1 \text{ for } 0 \le q \le 1 \\ TE: \dfrac{\partial u_{(q,Fo)}}{\partial Fo} = \dfrac{\partial^2 u_{(q,Fo)}}{\partial q^2} \text{ for } 0 \le q \le 1, Fo > 0 \\ BC: j^*(Fo) = -\left.\dfrac{\partial u_{(q,Fo)}}{\partial q}\right|_{q=1-\epsilon} = Bi\left[K_{F/P} u_{(q=1-\epsilon,Fo)} - \dfrac{C_F(t)}{C_P^{t=0}} \right]; \\ \left.\dfrac{\partial u_{(q,Fo)}}{\partial q}\right|_{q=0} = 0 \text{ for } t > 0 \text{ and } \epsilon \to 0 \\ MB: \dfrac{C_F(t)}{C_P^{t=0}} = L_{P/F}\int_0^{Fo} j^*(\tau)\, d\tau \text{ for t} \ge 0 \end{cases} \qquad \text{(II.13)}$$

When $Bi \to \infty$, the third type boundary condition at $q = 1$ (Robin boundary condition) can be replaced by a simple coupling with the mass balance. Differentiating BM with respect to Fo, yields:

$$j^*(Fo) = -\left.\frac{\partial u_{(q,Fo)}}{\partial q}\right|_{q=1-\epsilon} = \frac{1}{L_{P/F} C_P^{t=0}} \frac{dC_F(t)}{dFo} = \frac{K_{F/P}}{L_{P/F}} \frac{\partial u_{(q=1,Fo)}}{\partial Fo} \qquad \text{(II.14)}$$

The worst-case scenario when $Bi \to \infty$ and $K_{F/P} \to \infty$ corresponds to the Dirichlet boundary condition $u_{(q=1,Fo)} = 0$.

II.2.3.4.2. Concentration in the contact phase at thermodynamic equilibrium

According to Eq. (II.13), the maximum concentration in food is obtained at thermodynamic equilibrium ($j^* \to 0$):

$$\frac{C_F^{eq}}{C_P^{t=0}} = \frac{C_F\left(Fo \to \infty\right)}{C_P^{t=0}} = \frac{1}{1/L_{P/F} + 1/K_{F/P}} \tag{II.15}$$

In practice it is convenient to express the kinetics of desorption in food as a function of the fraction of the equilibrium value:

$$\begin{aligned} C_F\left(Fo, Bi, K_{F/P}, L_{P/F}\right) &= \frac{C_P^{t=0}}{1/L_{P/F} + 1/K_{F/P}} \overline{v}^*\left(Fo, Bi, K_{F/P}, L_{P/F}\right) \\ &= C_F^{eq} \overline{v}^*\left(Fo, Bi, K_{F/P}, L_{P/F}\right) \end{aligned} \tag{II.16}$$

II.2.3.4.3. Dimensionless migration kinetics and their analytical approximations

The dimensionless migration kinetics $\overline{v}^*\left(Fo, Bi, K_{F/P}, L_{P/F}\right)$ are plotted in **Figure II-9**. The analytical solution associated with the Dirichlet condition $C\left(x = l_p, t\right) = 0$ is given by Eq. 4.18 in Crank's book (1975) and reads:

$$\overline{v}^*\left(Fo\right) = \frac{C_F\left(Fo\right)}{C_F^{eq}} = 1 - \frac{8}{\pi^2} \lim_{n \to \infty} S_n\left(Fo\right) \text{ with } S_n\left(Fo\right) = \sum_{i=0}^{n} \frac{\exp\left(-\frac{\pi^2}{4}\left(2i+1\right)^2 Fo\right)}{\left(2i+1\right)^2} \tag{II.17}$$

For small Fo values, the approximation (II.17) requires n to be very large (10^3 or 10^4) and a more efficient approximation can be obtained by combining an approximation of Eq 4.20 in Crank's book (1975) with Eq. (II.17) for $i = 0$ as:

$$\overline{v}^*\left(Fo\right) = \min\left[\frac{2\sqrt{Fo}}{\pi}, 1 - \frac{2}{\pi^2}\exp\left(-\frac{\pi^2}{4} Fo\right)\right] \le \min\left[\frac{2\sqrt{Fo}}{\sqrt{\pi}}, 1\right] \tag{II.18}$$

Approximations (II.17) and (II.18) are plotted along with the results of numerical simulations in **Figure II-9**. The common assumption of the linearity of $\overline{v}^*$ with $\sqrt{Fo}$ is well verified while $Fo \le 0.8$ and when the equivalent length of the contacting phase $\ell_F = K_{F/P}/L_{P/F}$ and Bi are large. At intermediate Bi values, the Dirichlet condition offers a conservative approximation (i.e., $\overline{v}^*$ is overestimated) and Eq. (II.18) can be used safely for compliance testing. However, when $\ell_F \ll 100$ (e.g., small food volume, low chemical affinity

for the food), Eq. (II.18) must be avoided due to a significant risk of underestimation of low Fo values. The equilibrium is, indeed, reached much faster due to a much smaller amount to transfer and because the concentration at the F-P interface never vanishes. An accurate estimation of migration requires ad-hoc numerical solutions or special analytical solutions. In mathematical terms, finite volume effects cause the propagation of shockwaves between the polymer and the contacting phase: the addition of substances to F modifies instantaneously the capacity of P to transfer additional substances, and so on for the next substances creating positive and destructive interference across the mass transfer boundary layer when it exists. One practical consequence is that analytical solutions are without closed-forms and therefore more complex than Eq. (II.18).

For $Bi \to \infty$ and $L_{P/F} < 1$, the analytical solution verifying finite volume effects and boundary condition **Figure II-9** is given by Eq. 4. 37 in Crank's book (1975) and is very accurate at a reasonable cost for $Fo > 10^{-4}$.

For arbitrary Bi and ℓ_F values, new solutions verifying the general boundary condition **Figure II-9** (Sagiv, 2001, 2002;Vitrac and Hayert, 2006;Goujot and Vitrac, 2013). Short-time and long-time solutions were optimized for efficiency and to integrate more complex physics such as non-linear sorption isotherms or for boundary conditions variable in time.

The general solutions are not detailed here as their expressions exceed the scope of the work. When $Bi \to \infty$, the Eq. 4. 37 in Crank's book (1975) reads:

$$\overline{v}^*\left(Fo\right) = 1 - \sum_{n=1}^{\infty} 2\frac{\ell_F\left(1+\ell_F\right)}{1+\ell_F+\ell_F^2 q_n^2}\exp\left(-q_n^2 Fo\right) \text{ where } q_n \text{ are zeros of } \tan q_n = -\ell_F q_n \qquad \text{(II.19)}$$

The zeros of the transcendental equation, q_n, increase with n and also when ℓ_F decreases. This behavior demonstrates that $\overline{v}^*\left(Fo\right)$ converges exponentially and more rapidly to equilibrium when ℓ_F values are low. The linearization with $\sqrt{Fo}$ ceases to be correct earlier and is associated to slopes varying with ℓ_F. As the values of q_n are usually not tabulated beyond $n = 6$ in reference text books (see Table 4.1, p. 379 in Crank, 1975), it is recommended to restrict the use of Eq. (II.19) to $Fo > 10^{-4}$.

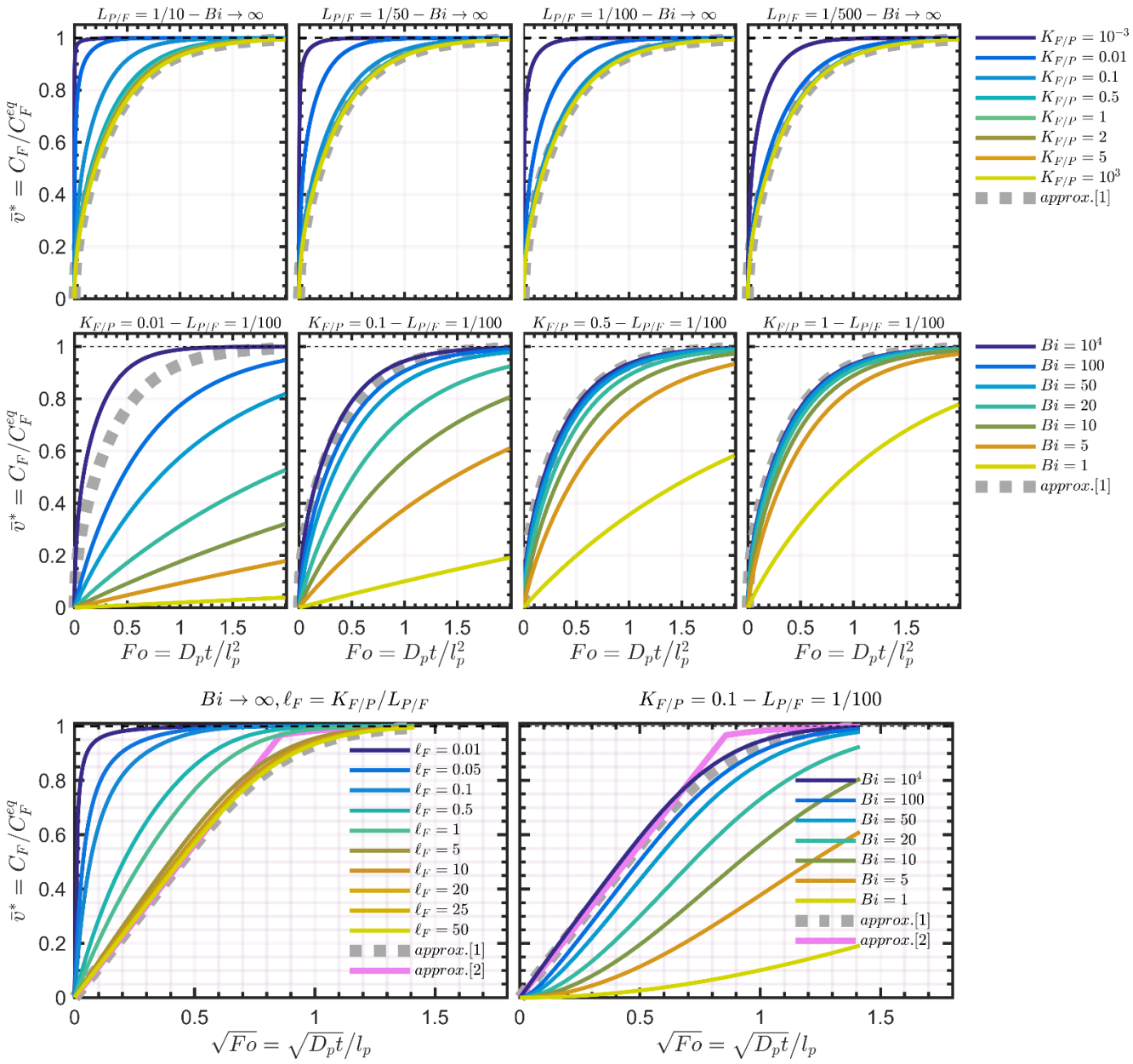

***Figure II-9**. Dimensionless desorption kinetics* $\bar{v}^*\left(Fo\right) = \dfrac{C_F\left(Fo\right)}{C_F^{eq}}$ *for various values of* $L_{P/F}$, $K_{F/P}$ *and* Bi *with* $C_F^{eq} = \dfrac{C_P^0}{1/L_{P/F} + 1/K_{F/P}}$. *Approximations [1] and [2] are given by Eqs. (II.17) and (II.18), respectively.*

II.2.3.5. Governing equations for multilayers

II.2.3.5.1. Thermodynamic assumptions

The case of materials consisting of m materials or layers ($m > 1$) can be seen as a generalization of the monolayer case ($m = 1$) at the expense of a few additional assumptions and conventions. Because monolayer systems were dominating in the 20th century, the reasoning supporting US and EU regulations was, therefore, devised based on an assumption of migration without delay and obeying a scaling proportional to the square root of time. The conventional condition of ten days at 40°C was thus thought to be equivalent to a test of one hundred days with a factor comprised between unity (equilibrium) and $\sqrt{\frac{100\ \text{days}}{10\ \text{days}}} \approx 3.16$ ($Fo \ll 1$). Moving the substances away from the P-F interface delays substantially the mass transfer to the contacting phase. This behavior is central to the concept of functional barrier (Feigenbaum *et al.*, 2005); it was initially explored to promote the incorporation of recycled material – possibly contaminated due to post-consumer misuse or mixing with non-food grade materials – in co-extrudates. The recycled polymer is sandwiched within two layers of virgin polymers. Similar problems can be resolved only by adapting the initial condition $C(x, t=0)$ in the equation system (II.12) to the need instead of using a uniform distribution.

When the materials are different in nature, a contact condition similar to Eq. (II.7) needs to be considered. The proposed description relies on an assumption of a linear and reversible sorption of substances in each layer so that a linear sorption isotherm is assumed in any layer, including in the food. By denoting $p(x,t)$ the partial pressure of the migrating substance, the isotherm associated with the Henry constant $\{k_j\}_{j=0..m}$ for each layer is:

$$p(x,t) = k_j C(x,t) \text{ for } 0 \le L_{j-1} \le x < L_j \text{ and } t > 0 \text{ ; with } L_j = \sum_{i=1}^{j} l_i \text{ and } 0 \le j \le m \quad \text{(II.20)}$$

For the sake of generalization, the layers including the food are indexed from $j = 0$ (food: F) to $j = m$ (layer the most distant to F), with $j = 1$ being the contact layer, as shown in **Figure II-10**. The residual concentration in each layer is $C_j(x,t) = \frac{1}{l_j} \int_{L_{j-1}}^{L_j} C(x,t)\,dt$ for $1 \le j \le m$ and $C_0(t) = C_F(t)$.

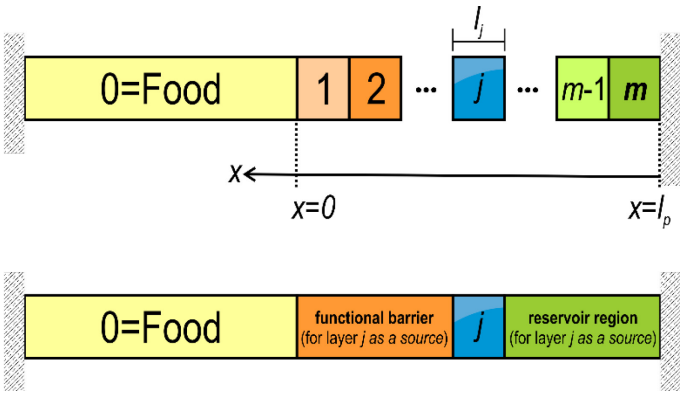

***Figure II-10**. Indexing rule of a material including m layers (total thickness l_P) in contact with a food indexed 0. The left and right external boundaries are considered impervious (no mass loss). The concepts of "functional barrier" and "reservoir" assume that layer j is the source (with non-zero initial concentration). It is used in §II.2.3.5.5. and §II.2.3.5.6. .*

II.2.3.5.2. Concentration in the contact phase at thermodynamic equilibrium

The Henry sorption isotherm defined in Eq. (II.20) offers a robust but simplified thermodynamic representation of the variation of the chemical potential with the local composition in the system. The validity of the model and its generalization are discussed in §II.2.5.2. Partial pressure $p(x,t)$ is a continuous potential, and thermodynamic equilibrium is achieved when its value is uniform across the structure. By neglecting mass losses, Eq. (II.20) and the mass balance between $t=0$ and $t\to\infty$ $\sum_{j=0}^{m} C_j^{t\to\infty} l_j = \sum_{j=0}^{m} C_j^{t=0} l_j$ enables generalization of Eq. (II.15):

$$C_F^{eq} = C_0^{t\to\infty} = \frac{\sum_{j=0}^{m} \frac{l_j}{l_0} C_j^{t=0}}{1+\sum_{j=1}^{m} \frac{k_0}{k_J}\frac{l_j}{l_0}} \qquad \text{(II.21)}$$

where $k_0/k_j = C_j^{t\to\infty}/C_0^{t\to\infty}$ is the partition coefficient between the layer j and the food.

II.2.3.5.3. Transport equations

Transport equations are unchanged and are defined as:

$$\frac{\partial C(x,t)}{\partial t} = D_j \frac{\partial^2 C(x,t)}{\partial x^2} \text{ for } 0 \le L_{j-1} \le x < L_j \text{ and } 1 \le j \le m \qquad \text{(II.22)}$$

and connected at internal interfaces via the double conditions of mass conservation and local thermodynamic equilibrium:

$$\begin{aligned} &D_j \left.\frac{\partial C(x,t)}{\partial x}\right|_{x=L_j-\epsilon} = D_{j+1} \left.\frac{\partial C(x,t)}{\partial x}\right|_{x=L_j+\epsilon} \quad \text{for } 1 \le j < m \\ &k_j C\left(x = L_j - \epsilon, t\right) = k_{j+1} C\left(x = L_j - \epsilon, t\right) \quad \text{for } 0 \le j < m \end{aligned} \quad \text{and } \epsilon \to 0 \text{ , } t > 0 \qquad \text{(II.23)}$$

II.2.3.5.4. Limiting mass transfer resistance

A dimensionless formulation of Eqs (II.9), (II.22) and (II.23) is achievable at the expense of choosing a reference layer, $1 \le j_{ref} \le m$, and setting the reference time scale as $\frac{l_{j_{ref}}^2}{D_{j_{ref}}}$.

In numerical algorithms, where stability and convergence are very stringent, it is convenient to choose as a reference layer, the layer associated with the highest mass transfer resistance (lowest permeability) is the best choice:

$$j_{ref} \text{ such that } \frac{l_{j_{ref}} k_{j_{ref}}}{D_{j_{ref}}} = \max\left[\left\{\frac{l_j k_j}{D_j}\right\}_{j=1..m}\right] \qquad \text{(II.24)}$$

If several conditions need to be compared, a natural choice is to choose the contact layer as the reference layer ($j_{ref} = 1$).

II.2.3.5.5. Typologies of migration behaviors

The main behaviors, which can be observed with multilayers, are illustrated in simple configurations corresponding to a bilayer structure (each layer has a thickness $l_p/2$) in contact with a liquid phase with a characteristic thickness $50 l_p$ and associated with $k_0 = 1$. The five considered cases are summarized in **Table II-9** and were associated with a similar initial amount and comparable final concentration in the contacting phase *ca.* $2.0 \cdot 10^{-2} \cdot \left(C_1 + C_2\right)/2$.

The other parameters were $Bi \to \infty$, $l_1 = l_2 = \frac{l_p}{2}$, $D_1 = D_2$ and the time scale $\frac{l_p^2}{4D_1}$. The calculated profiles and kinetics corresponding to the five scenarios are plotted in **Figure II-11**.

Table II-9. *Illustration of the main behaviors associated with multilayer structures. The concepts of functional barrier and reservoir are illustrated in* ***Figure II-11***.

C_j^0		k_j		interpretation	code
$j=1$	$j=2$	$j=1$	$j=2$		
1	1	1	1	uniform distribution (equivalent to a monolayer)	[1,1]×[1,1]
0	2	1	1	functional barrier (barrier to diffusion only)	[0,2]×[1,1]
2	0	1	1	reservoir layer (same capacity)	[2,0]×[1,1]
0	2	2	1	functional barrier (barrier to diffusion and of solubility)	[0,2]×[2,1]
2	0	1	2	reservoir layer (with reduced capacity by half)	[2,0]×[1,2]

Monolayers and functional barriers lead to uniformly decreasing concentration profiles. The corresponding desorption kinetics in F are respectively proportional to the square-

root of time and proportional to time after some lag time equal to $\frac{l_1^2}{6D_1}$. For the same initial amount in the structure and after the lag time, the functional barrier ceases to operate and leads to a migration proportional to $\frac{D_1}{k_1 l_1}$. Only a functional barrier combining a diffusion barrier ($\frac{D_1}{l_1} \ll \frac{D_2}{l_2}$) and a solubility one ($\frac{k_1}{k_0} \gg \frac{k_2}{k_0}$) can slow down the desorption durably. Reservoirs behave very differently; they are associated with non-monotonous concentration profiles, accelerated desorption kinetics while converging to a very similar concentration at equilibrium. For the same initial content and when the barrier on the right is higher than the barrier on the left $\frac{k_2 l_2}{D_2} \gg \frac{k_0}{Bi}$, the "reservoir" configuration overestimates the migration kinetics associated with all other configurations.

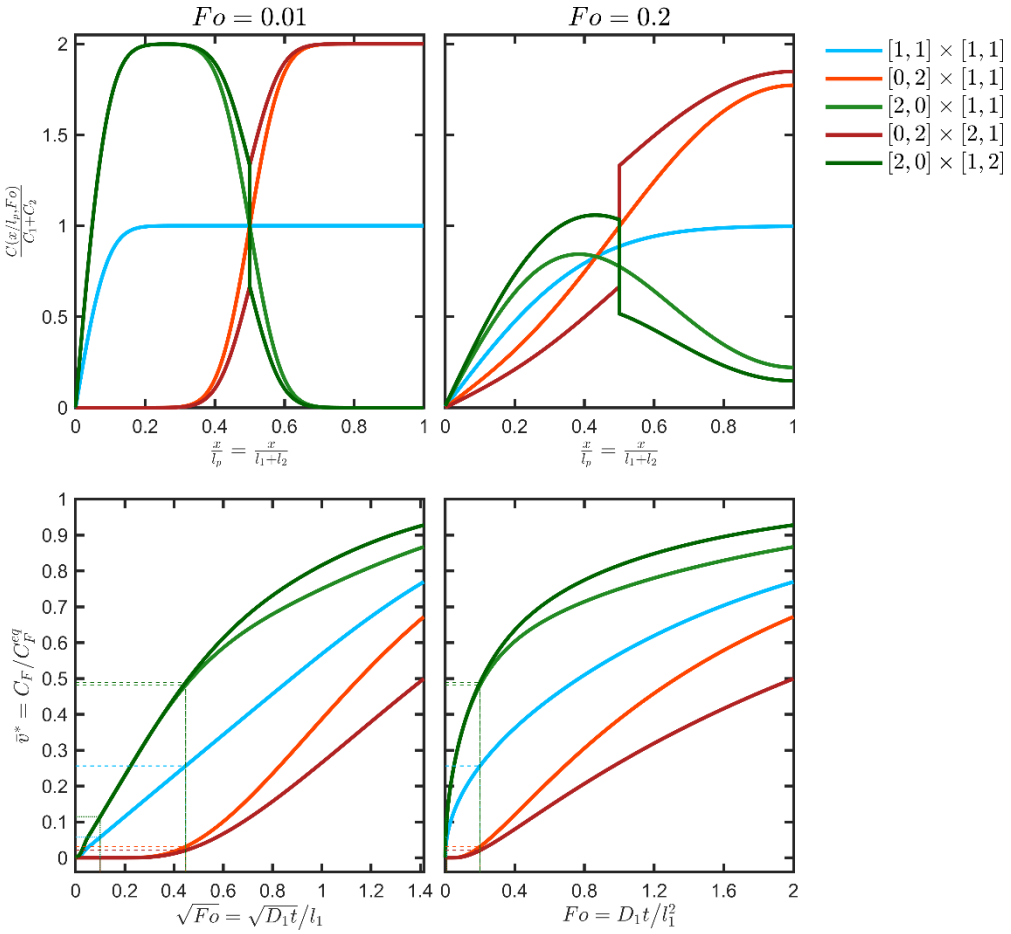

***Figure II-11**. Concentration profiles (top) and migration kinetics (bottom) for the bilayer structure and scenarios detailed in **Table II-9**.*

II.2.3.5.6. Superposition principles and conservative scenarios for multilayer and multicomponent systems

- *Mathematical principles*

Multilayer structures offer a broad range of behaviors. In the simplest cases, as shown in **Figure II-11**, desorption kinetics are monotonous with time. It may not be the case if the functional barrier and reservoir effects are combined. The calculations for complex multilayers are complicated by the difficulty to associate the uncertainty in diffusion $\left\{D_j\right\}_{j=1..m}$ and sorption properties $\left\{k_j\right\}_{j=1..m}$ with the concentration in food. For monolayer materials, a conservative scenario is achieved by overestimating simultaneously D_1 , $\frac{k_0}{k_1}$ and Bi. For multilayer materials, no similar rule holds. Intuitively based on the illustrated configurations in **Figure II-11**, it can be stated that for the capacity of the layer j to transfer its content, $M_j(t)$ (amount transferred to F at the time t), is maximized (denoted $\lceil M_j \rceil(t)$) if the following properties are fulfilled:

$$\begin{aligned} &D_i \text{ is replaced by } \lceil D_i \rceil > D_i \text{ for } 1 \le i \le j \text{ and } k_i \text{ is replaced by } \lfloor k_i \rfloor < k_i \text{ for } 0 \le i \le j \\ &D_i \text{ is replaced by } \lfloor D_i \rfloor < D_i \text{ and } k_i \text{ is replaced by } \lceil k_i \rceil > k_i \text{ for } j < i \le m \end{aligned}$$

(II.25)

Conditions (II.25) have a mathematical justification in the linear properties of the equations (II.22)-(II.23). The solution of any linear decomposition of the initial concentration profile is equal to the sum of the individual solutions:

$$C(t=0,x) = \sum_{j=1}^{p} C_j(t=0,x) \text{ where } p \ge 1 \text{ is the number of profiles, } 0 \le x \le l_p$$

$$\begin{aligned} C_F\left(t, C(t=0,x)\right) &= \frac{M\left(t, C(t=0,x)\right)}{V_F} = \frac{\sum_{j=1}^{p} M_j\left(t, C_j(t=0,x)\right)}{V_F} \\ &\le \frac{\sum_{j=1}^{p} \lceil M_j \rceil\left(t, C_j(t=0,x)\right)}{V_F} = \lceil C_F \rceil\left(t, C(t=0,x)\right) \end{aligned}$$

(II.26)

- *Example for a trilayer material ABC*

Eq. (II.26) is particularly significant as it is valid for any partitioning of the source terms in the material, irrespective of the positions of the layers. An application of the additivity

of M_j values (concentration profiles and kinetics) is shown in **Figure II-12** for a trilayer structure ABC detailed in **Table II-10**.

Table II-10. *Parameters used to construct realistic and conservative migration scenarios depicted in* ***Figure II-12*** *and* ***Figure II-13***. *Quantities are expressed respectively to the likely values† for the first layer (the three layers ABC are indexed 1,2,3). They are scalar when the contribution of each layer as a source is considered in combination with others (the three sources are considered at once). The contributions of individual sources are indicated by 3×1 vectors mentioning the properties of all layers considered as a source or not.*

property	**case-study (likely)** contribution of the jth layer			**conservative scenario (high tier)** contribution of the jth layer			**worst-case scenario (low tier)** contribution of the jth layer		
	$j=1$	$j=2$	$j=3$	$j=1$	$j=2$	$j=3$	$j=1$	$j=2$	$j=3$
$\frac{l_j}{l_1^{likely}+l_2^{likely}+l_3^{likely}}$	0.2	0.5	0.3	0.2	0.5	0.3	0.2	0.5	none
$C_j^0 \big/ C_1^{0,likely}$	1	1	1	[1,0,0]	[0,1,0]	[0,0,1]	3.5	0.6	none
$D_j \big/ D_1^{likely}$	1	1	1	[1,10^{-3},10^{-3}]	[1,1,10^{-3}]	[1,10,10]	1	1	none
$k_j \big/ k_0^{likely}$	0.3	0.8	2.0	[10,10,10]	[1,10,10]	[1,1,10]	10	10	none

†Likely value = true value or close to the true value in the considered scenario.

The simulation of each layer individually underlines the different mechanisms controlling the contribution of each layer: reservoir effect for source A (scaling of desorption kinetics with the square root of time) and functional barriers for B and C (desorption kinetics linear with time after significant lag-times). The depicted profiles are assumed to the "likely" or "true" ones. They are considered inaccessible to simulation and should be approximated at some tier in a way that the concentration in F is always overestimated (see **Figure II-14**).

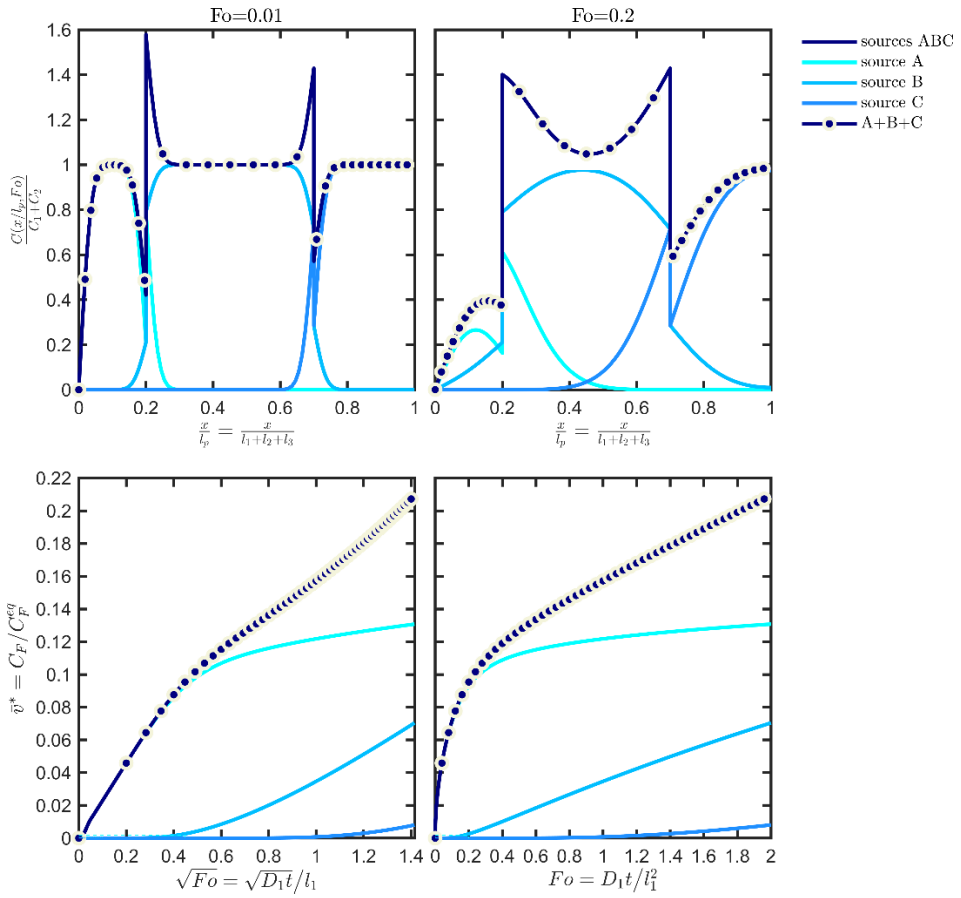

***Figure II-12**. Illustration of the additivity of the sources (see Eq.* (II.26)*) for a trilayer structure ABC associated with the case study detailed in **Table II-10**: concentration profiles (top), kinetics (bottom). The case "sources ABC" is obtained by simulating the whole structure. The result A+B+C corresponds to the mathematical addition of the contributions of the three sources.*

Eq. (II.25) provides a numerical procedure to devise conservative scenarios for multi-layer structures. A similar procedure has been detailed in section 4.2 of the European guidance document (Hoekstra *et al.*, 2015). Here the procedure for the sole overestimation of the chemical affinity effects is repeated by keeping the diffusion coefficients to their "likely" values. The core idea is to prevent or hinder the diffusion of the substances in the jth layer to the right (by assuming that the food is on the left) and to facilitate their desorption to the left, to bring the contaminants closer to the food. The "conservative scenario" of **Table II-10** applies a factor ten to the Henry-like coefficient(s) k_j of the source and behind. The likely k_j and D_j values are kept for the layers between the food and the jth layer. To prevent back diffusion in the reservoir layers the diffusion coefficients were divided arbitrarily by a factor 10^3. The corresponding kinetics are shown in **Figure II-13**, with their parameters listed in the section "conservative scenario" of **Table II-10**. The diffusion coefficients towards the food are overestimated by a factor of 10. At intermediate Fourier numbers below 0.4, the kinetics is not significantly overestimated, but a significant conservatism is achieved at larger Fourier numbers when the overall migration is controlled by the second and third layers as sources. This case study

demonstrates how migration scenarios can be finely tuned to decrease the uncertainty related to the behavior of internal layers. The contact layer as a source can always be considered as a single monolayer.

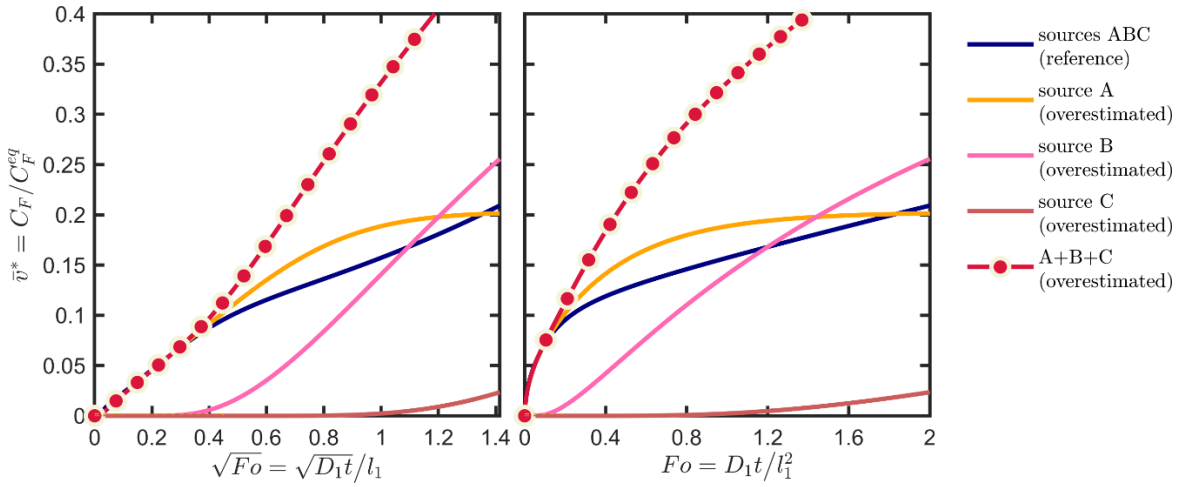

***Figure II-13**. Illustration of the conservative scenario of **Table II-10** based on the overestimation of the contribution of each source. The reference corresponds to the initial case-study configuration also depicted in **Figure II-12**.*

In practice, any uncertainty on the internal partitioning between layers can be converted into a conservative scenario by forcing mass transfer to the food and by relocating "artificially" the content from layer j to layer $j-1$. The iterative procedure is illustrated in **Figure II-14** and can be applied to decrease a m-layer problem into a $m-1$, $m-2$, etc. layer problem, until reaching tier 1 (total migration). The first iteration applied to the case-study is denoted "worst-case" scenario in **Table II-10**. The procedure may overestimate dramatically the real migration, but it keeps the applicability of conservative calculations to demonstrate safety at low cost. For risk assessment, the procedure may be applied with caution as it may lead to unrealistic consumer exposure.

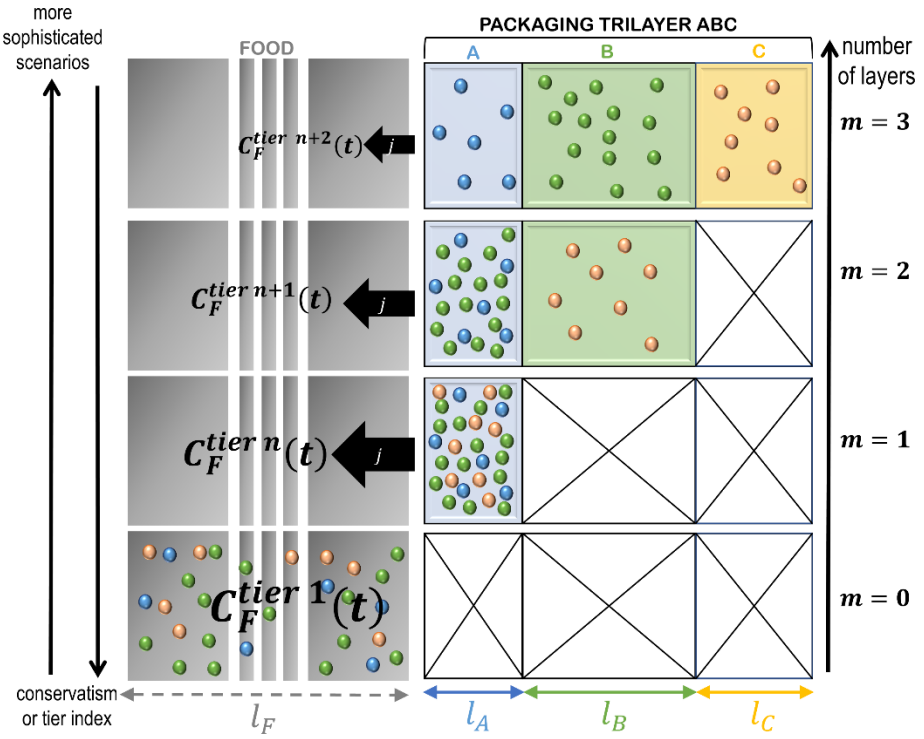

Figure II-14. *Principles of the simplification of a m-layer problem (here $m = 3$) into a problem with a lower number of layers and, therefore, easier parameterization. The represented distributions in the packaging correspond to initial conditions at various tiers.*

II.2.3.6. Strategies and equations to simulate multiple steps and conditions

This part discusses the invariance of migration estimates, namely $C_F(t)$, with the order of contact and the thermodynamic conditions met by the components of the packaging before and during food contact.

II.2.3.6.1. Problem formulation

Mass transfer between components and materials occur insidiously along the supply chain. **Figure II-15** illustrates conditions triggering or altering migration from printed materials. Many uncontrolled factors may affect the extent of mass transfer: i) variable contact or exposure times, ii) random combinations of storage and transportation steps for intermediate, finished packaging materials and packaged foods, iii) changes in temperature and relative humidity (e.g., seasonal, diurnal, international transportation), iv) modifications of boundary conditions during any stage of materials lifetime and product shelf life. The redistribution of migrants between materials, layers, and components deserve special attention as it usually remains ignored by end-users. In practice, cross-contamination occurrences can also be considered indirectly (i.e., without causailty) as impurities and non-intentionally added substances. Without being exhaustive, cross-contamination is highly likely from cured adhesives and printing inks, recycled materials and any material with rich volatile organic compounds. Packaging and materials stored in stacks and reels ease cross contaminations by contacting

internal and external layers, regardless of the presence of a functional barrier (absolute such as a metallic layer or relative such as a barrier polymer) in the structure. Due to periodic conditions, the inner layer can act as a reservoir of contaminants before the food is put in contact.

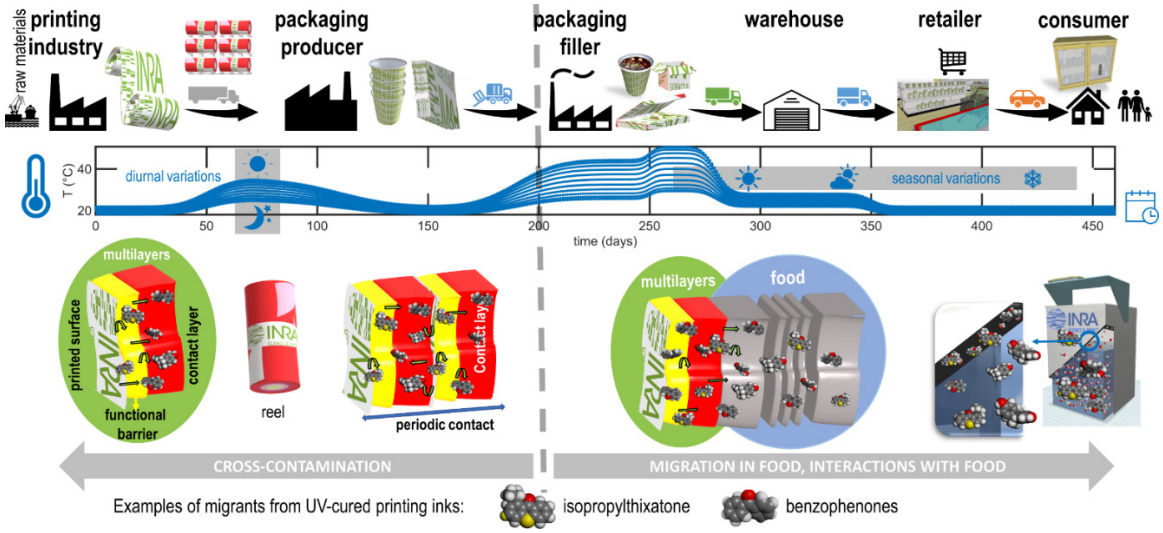

Figure II-15. *Illustration of the redistribution of the migrants from UV-cured printing ink and their subsequent migration in food for long shelf life products. The depicted cases cover hot-filled or aseptically filled products (e.g., soups, pasteurized juices, sterilized dairy products), and dry or ready-to-eat products stored in cardboard boxes.*

From a mathematical viewpoint, the succession of steps and temperature variations can be seen as a sequence of constant conditions occurring in variable order. In the presence of n_{steps} conditions occurring at time $t = 0, t_1, t_2, ..., t_{n_{steps}}$, the composite solution is obtained by integrating the coupled system (II.12) via the Chasles' relation:

$$C\left(x,t_{n_{steps}}\right) = \int_0^{t_{nsteps}} \frac{\partial}{\partial t} C(x,t)\Big|_{C(x,t=0)} dt = \sum_{i=0}^{n_{steps}} \int_{t_i}^{t_{i+1}} \frac{\partial}{\partial t} C(x,t)\Big|_{C(x,t=t_i)} dt$$

$$C_F\left(t_{n_{steps}}, C_P^{t=0}, C_F^{t=0}\right) = \int_0^{t_{nsteps}} \frac{dC_F\left(t,C(x,t)\right)}{dt}\Big|_{C_P^{t=0},C_F^{t=0}} dt = \sum_{i=0}^{n_{steps}} \int_{t_i}^{t_{i+1}} \frac{dC_F\left(t,C\left(x,t\right)\right)}{dt}\Big|_{C_P^{t=t_i},C_F^{t=t_i}} dt$$

(II.27)

Determining the duration of each step $\{\Delta t_i\}_{i=t_{i+1}-t_i}$ and their corresponding temperatures are critical. Representing all diurnal and seasonal temperature variations shown on the timeline of **Figure II-15** would require 2×450=900 successive simulations (one every 12 hours). On the one hand, a rigorous approach suggests that the congruence of all the steps should be strictly preserved to get reliable conclusions. In this case, how to identify the worst-case combination of conditions or steps? If the temperature variations are uncontrolled, how to build a

conservative sequence? On the other hand, a naïve approach would suggest that the times series in Eq. (II.27) could be built from mutually independent steps assembled as the sum of a series of standard and well-controlled steps (*e.g.*, cold, moderate and warm days), and one series with stochastic contributions, representing an extra safety margin.

II.2.3.6.2. A first intuitive approach

The variations of C_F between steps are not factorizable but the dimensionless times are. Their effects are additive and commutative $C_F\left(\Delta Fo_1+\Delta Fo_2\right)=C_F\left(\Delta Fo_2+\Delta Fo_1\right)$ (see Eq. (II.13) for the demonstration). If the diffusion coefficient is the only quantity varying with temperature and the plasticizer content (*i.e.,* no change in the partitioning, and the packaging dimensions), the effects of n_{steps} is captured via the generalized Fourier number:

$$Fo\left(t_{nsteps}\right)=\frac{\int_0^{t_{nsteps}} D_{j_{ref}}\left(T\left(t\right),\text{plasticizer}\left(t\right)\right)dt}{l_{j_{ref}}^2} \qquad \text{(II.28)}$$

where $D_{j_{ref}}$ is the diffusion coefficient of the most limiting material, component or layer, and $l_{j_{ref}}$ the one-dimensional equivalent thickness (see Eq. (II.24) to identify j_{ref}).

Eq. (II.28) is equivalent to the low of the composition of velocities along a curvilinear coordinate system tangent to the trajectory going from A ($\overline{v}^*\left(t=0\right)=0$) to B ($\overline{v}^*\left(t\to\infty\right)=1$). The analogy between spatial translation along a winding road and the translation along the curve $\overline{v}^*$ vs. Fo is illustrated in **Figure II-16** by comparing the travel via three modes of transport (each of duration $\left\{\Delta t_i\right\}_{i=1,2,3}$ at a speed: $\left\{v_i\right\}_{i=1,2,3}$) with the cumulative contamination after three steps (of duration $\left\{\Delta t_i\right\}_{i=1,2,3}$ at temperature $\left\{T_i\right\}_{i=1,2,3}$. The total distance is $v_1\Delta t_1+v_2\Delta t_2+v_3\Delta t_3$, and the cumulative migration is $\overline{v}^*\left(\left(D\left(T_1\right)\Delta t_1+D\left(T_1\right)\Delta t_2+D\left(T_3\right)\Delta t_3\right)/l^2\right)$ independent of the order of the steps. Replacing the physical time by cumulatively measuring the total arc-length of the curve or the road makes it possible to use endpoint estimates (one simulation) instead of chained simulations (n_{steps} simulations). In this new space, the residence times – represented by the density of markers on the curves – are not uniform. They are distributed more densely at departure and destination, but more sparsely in the middle region where the studied system follows different routes.

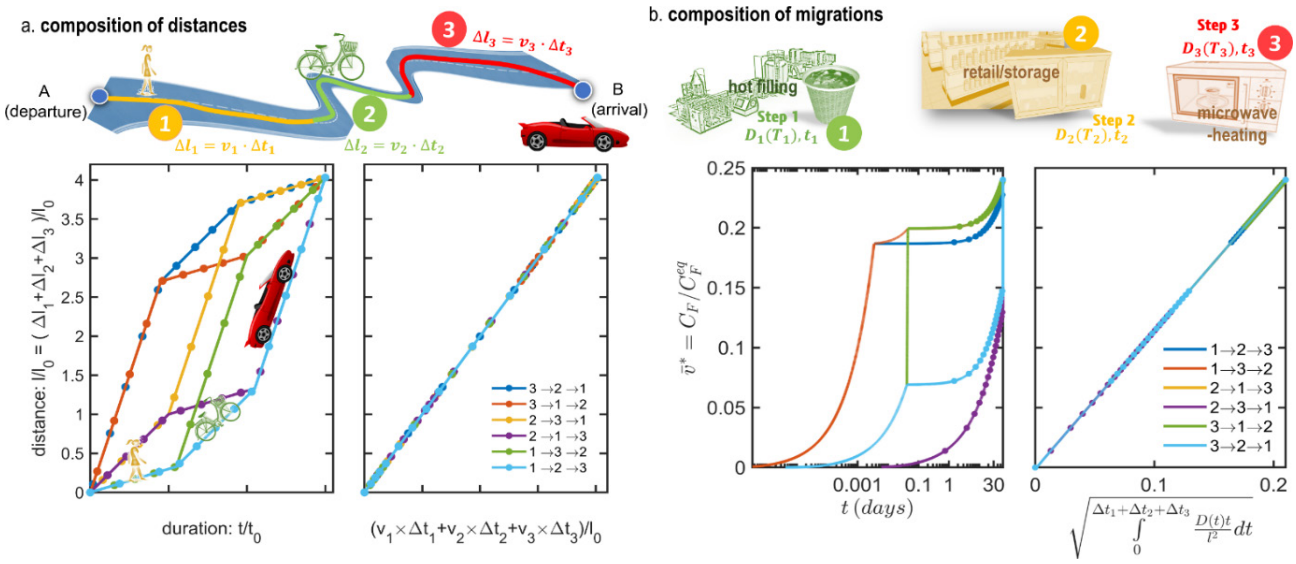

***Figure II-16**. Illustration of the composition rules (a) for distances and (b) for the migration from a monolayer material, and of their invariance with the order of the steps (see Eqs. (II.28) and (II.35)).*

Eq. (II.28) suffers, however, from a lack of generality as it applies only to the limiting mass transfer resistance and not to all layers. As a rule of thumb, it offers an acceptable solution if the function $\bar{v}*$ is monotone with Fo (i.e., $\bar{v}^*\left(Fo_1\right) \le \bar{v}^*\left(Fo_2\right)$ when $Fo_1 \le Fo_2$. A simple counterexample can be, however, constructed by noting that the concentration at equilibrium C_F^{eq} depends only on the initial and final states, but not on intermediate steps.

The conditions of exchangeability of steps (which is more generic than Eq. (II.28)) is discussed hereafter in more general terms. Two conditions are analyzed: i) when the effect of the mass transfer resistance is considered (explicit representation) and the number of molecules does not change, and ii) when an implicit food representation is used (i.e., Eqs. (II.12), (II.13) and (II.23)). The distinction between explicit and implicit food representation is relevant, as the boundary layer delays the effects of perturbations and may contain a significant amount of contaminants, which are ignored at low Bi values in implicit representations (see §II.2.3.3.).

II.2.3.6.3. Strict conditions of exchangeability with explicit food models

- *Microscopic description of the random walk of molecules between P and F*

The visited distance by a deterministic system is $\ell = \Delta\ell_1 + \Delta\ell_2 + \Delta\ell_3 + \cdots$ and is invariant with the order of the visits. At a microscopic scale (*i.e.*, at a scale where they can be separated), the trajectories of migrants in materials and the food verify this property (distances are additives), but with a different relationship with time (displacements are proportional with time). The random displacements of additives and residues shares, instead, notable features with random walks and continuous stochastic paths. In a loose sense, substances jump randomly at discrete times (random walks) or as continuous events (stochastic paths). Their skewed trajectories are nowhere differentiable, and velocities cannot be defined in a classical sense. Under a hypothesis of stationarity of the microscopic random process (the quantity $X(t)$ has the same statistics as $X(t+\epsilon)$ for any ϵ), a law of composition can be justified for the mean-square-distances, denoted $\langle \ell^2 \rangle$, visited by the molecules: $\langle \ell^2 \rangle = D_1\Delta t_1 + D_2\Delta t_2 + D_3\Delta t_3 + \cdots$. $\langle \ell^2 \rangle$ is mathematically defined as $\langle x^2(t) \rangle - \langle x(t) \rangle^2$, where $\langle x(t) \rangle$ is the average distance (first moment) and $\langle x^2(t) \rangle$ the square distance to the food-packaging interface located at $x = 0$:

$$\begin{aligned} \langle x(t) \rangle &= \int_{-\infty}^{+\infty} x\rho(x,t)dx \\ \langle x^2(t) \rangle &= \int_{-\infty}^{+\infty} x^2\rho(x,t)dx \end{aligned} \qquad \text{(II.29)}$$

The one-dimensional space approximation with explicit food representation is defined on the domain $-l_F \le x \le l_p$ so that the probability density $\rho(x,t)$ verifies: $\int_{-l_F}^{l_p} \rho(x,t)\,dx = 1$ and $\rho(x,t) = 0$ for $x < -l_F$ or $x > l_p$. A differential form of the growth of $\langle x^2(t) \rangle$ with time is inferred from a special case of the Fokker-Planck equation $\frac{\partial \rho(x,t)}{\partial t} = D\frac{\partial^2 \rho(x,t)}{\partial x^2}$ (similar to Eq. (II.12)). By multiplying both sides by x^2 and by integrating over the entire domain, gives:

$$\int_{-\infty}^{+\infty} x^2 \frac{\partial \rho(x,t)}{\partial t} dx = \int_{-\infty}^{+\infty} x^2 D \frac{\partial^2 \rho(x,t)}{\partial x^2} dx \quad \text{with } D = D_p \text{ when } x \ge 0 \text{ and } D = D_F \text{ otherwise}$$

(II.30)

with D_p and D_F being the diffusion coefficients in P and F, respectively. The left-hand side is equivalent to $\frac{\partial}{\partial t}\left\langle x^2(t)\right\rangle$. The right-hand side requires two successive integration by parts along with the impervious boundary conditions at $x=-l_F$ and $x=l_P$, and the conservation of the flux at $x=0$. The simplifications associated with the compact support of $\rho(x,t)$ leads to:

$$\begin{aligned}
&\frac{\partial}{\partial t}\left\langle x^2(t)\right\rangle = \int_{-\infty}^{+\infty} Dx^2 \frac{\partial^2\rho(x,t)}{\partial x^2}dx = \left[D_F x^2 \frac{\partial\rho(x,t)}{\partial x}\right]_{-\infty}^{0} + \left[D_p x^2 \frac{\partial\rho(x,t)}{\partial x}\right]_{0}^{+\infty} \\
&-2D_F \int_{-\infty}^{0} x\frac{\partial\rho(x,t)}{\partial x}dx - 2D_P \int_{0}^{+\infty} x\frac{\partial\rho(x,t)}{\partial x}dx \\
&= 0+0-2D_F\left(0-\int_{-\infty}^{0}\rho(x,t)dx\right) - 2D_P\left(0-\int_{0}^{+\infty}\rho(x,t)dx\right) \qquad \text{(II.31)} \\
&= 2D_F\int_{-l_F}^{0}\rho(x,t)dx + 2D_P\int_{0}^{+l_p}\rho(x,t)dx = 2D_P + 2\left(D_F-D_P\right)\int_{-l_F}^{0}\rho(x,t)dx \\
&= 2D_{eff}(t)
\end{aligned}$$

For any initial distribution of substances $\rho(x,t=0)$ (single molecule or a collection of molecules), Eq. (II.31) describes the evolution of the mean-square distance $\left\langle x^2(t)\right\rangle$ to the FP interface. Since equations do not include any thermodynamic consideration, Eq. (II.7) was not enforced, Eq. (II.31) is valid while $\left\langle x^2(t)\right\rangle < \left(\frac{l_p+l_f}{2}\right)^2$ (beyond this length scale, finite size effects dominate and $D_{eff}(t)\to 0$). It shows that $\left\langle x^2(t)\right\rangle$ increases as $2D_p t$, when the concentration in F ($C_F = \frac{l_p}{l_F}C_P^0\int_{-l_F}^{0}\rho(x,t)dx$) is low. When the amount of substances in F becomes larger and because the molecules diffuse faster in F than in P, $\left\langle x^2(t)\right\rangle$ increases more rapidly. $D_{eff}(t)$ is the effective diffusion coefficient between P and F when both materials are replaced by an equivalent medium. A version similar to Eq. (II.31) for a homogeneous medium and known as the Einstein equation is presented in §II.2.4.1.1. (see (II.38)).

- *Condition of invariance of the dispersion of solutes with the properties of the contacting phase*

Eq. (II.31) shows that the composition $\left\langle x^2(t)\right\rangle$ is independent of D_F and of the amount already transferred to the food only if the inequality $\int_{-\infty}^{0}\rho(x,t)dx \ll \frac{D_P}{D_F}\int_{0}^{+\infty}\rho(x,t)dx$ is verified. The dispersion of contaminants is, hence, independent of the order of variations of D_P with time when:

$$C_F(t) \ll \frac{l_p}{l_F}\frac{D_P}{D_P+D_F}C_P^0 = \frac{D_P}{D_P+D_F}L_{P/F}C_P^0 \approx \frac{D_P}{D_F}L_{P/F}C_P^0 \qquad \text{(II.32)}$$

By noting that $L_{P/F}C_P^0$ is the total migration (see Eq. (II.4)) and that the diffusion in polymers is 1:100 or less lower than in the food , it can be seen that the invariance with the order of the steps hold only at the beginning of the migration process or when the chemical affinity for the food is very low. Eq. (II.32) could be justified with the example of a large food volume submitted to a cold condition during Δt_0, denoted $(\Delta t_0, T_1)$ followed by a warm condition during the same time, denoted (t_0, T_2) with $T_2 > T_1$. The normal order $(\Delta t_0, T_1)\times(\Delta t_0, T_2)$ would lead to a small mass transfer during $(\Delta t_0, T_1)$ and a very strong one during $(\Delta t_0, T_2)$. Performing the transfer in the reverse order $(\Delta t_0, T_2)\times(\Delta t_0, T_1)$ will cause an even higher mass transfer during the first step. If the food is large, the extra number of molecules transferred to the food during the first step $(\Delta t_0, T_2)$ will not have enough time to be transferred back to the packaging. As the food-packaging contact is not symmetrical $D_F \gg D_P$ and $l_F \gg l_p$, the two orders might not lead to similar irreversible behaviors: the food is contaminated in both cases but not to the same extent.

- *Discussion on the limits introduced by implicit models*

The fundamental results exposed here rely on an explicit representation of the food, where molecules displace at a finite velocity. This subtle detail is not reproduced in implicit representations, which assume a perfect mixing outside the mass transfer boundary layer (the velocity of molecules). Only a delay is considered in the boundary assuming a linear profile instead of a parabolic one (see the distribution of molecules depicted by green symbols in **Figure II-8**). The next paragraph reviews the conditions of commutativity of implicit models under variable conditions. The condition of commutativity is less severe as the back flux from the contacted phase is immediately compensated in the numerical scheme. But as shown here, the condition of commutativity is expected to be verified in real life, only when condition

(II.32) is met. The equivalence between time and temperature is acceptable only far from the equilibrium ($\overline{v}^* \to 0$), but it is unacceptable closer to equilibrium ($\overline{v}^* \to 1$), where the effective mass transfer is governed by an effective partition coefficient across the P-F interface. From Eq. (II.7), partitioning coefficients are independent of the temperature only if the difference of free sorption energies between P and F are kept constant ($G_P = G_F$) when the temperature is raised.

II.2.3.6.4. Conditions of exchangeability in food implicit models

- *Overview of implicit numerical models and their solutions*

Food implicit models are by far the most used. They are more flexible to accommodate variable conditions and chained conditions. They have been implemented with various numerical models using different spatial discretization schemes. The finite difference method is the dominant approach in one-dimension problems, but it loses accuracy at interfaces when large jumps in concentrations and diffusion coefficients occur. The finite element method is the standard in the industry as it enables integration of any partial differential equation system on arbitrary geometrical domains, using a grid approximation (consisting of triangles, quadrangles, and curvilinear polygons). The finite volume method is in essence similar (values are calculated on a meshed geometry), but the equations are integrated on small, but not infinitesimal, volumes. By positioning the interface between volumes at the exact location where thermodynamic constraints such as Eq. (II.7) need to be strictly verified, the method enables maintenance of the exact mass balances and the continuity of chemical potentials between materials. The pros and cons of each method are discussed in Nguyen *et al.* (2013). The three methods can be put in a matrix form, with coding for a system of ordinary differential equation:

$$\frac{\partial \underline{\mathbf{C}}(t)}{\partial t} = \underline{\underline{\mathbf{M}}}\underline{\mathbf{C}}(t) \tag{II.33}$$

The common practice is to include the concentration in P discretized n_{nodes} and the concentration in F in $\underline{\mathbf{C}}(t)$. Since the food is represented implicitly, one node is sufficient for the food and $\underline{\mathbf{C}}(t)$ is a $(n_{nodes}+1)\times 1$ vector mapping its continuous version $C(x,t)$. $\underline{\underline{\mathbf{M}}}$ is a triband matrix $(n_{nodes}+1)\times(n_{nodes}+1)$ for a discretization scheme at order 1 and pentaband matrix for quadratic finite elements techniques.

When the transport and thermodynamic properties are constant, the solution of Eq. (II.33) with respect to the initial condition $\underline{\mathbf{C}}(t)=0$ is $\exp\left(-\underline{\underline{\mathbf{M}}}t\right)\underline{\mathbf{C}}(t=0)$, with $\exp\left(-\underline{\underline{\mathbf{M}}}t\right)=\sum_{k=0}^{\infty}\frac{(-t)^k}{k!}\underline{\underline{\mathbf{M}}}^k$.

- *Composition rules when chained simulations are used (example with three steps)*

The solution of the mass transfer associated with three conditions: $\left(\underline{\underline{\mathbf{M}}}_1,\Delta t_1\right)\times\left(\underline{\underline{\mathbf{M}}}_2,\Delta t_2\right)\times\left(\underline{\underline{\mathbf{M}}}_3,\Delta t_3\right)$, with $\left\{\underline{\underline{\mathbf{M}}}_i\right\}_{i=1..3}$ the stiffness matrix for the ith step (e.g., coding the effect of temperature on diffusion and partition coefficients) is:

$$\underline{\mathbf{C}}\left(\Delta t_1+\Delta t_2+\Delta t_3\right)=\exp\left(-\underline{\underline{\mathbf{M}}}_3\Delta t_3\right)\exp\left(-\underline{\underline{\mathbf{M}}}_2\Delta t_2\right)\exp\left(-\underline{\underline{\mathbf{M}}}_1\Delta t_1\right)\underline{\mathbf{C}}(t=0) \qquad \text{(II.34)}$$

The steps are exchangeable if the equality (II.34) satisfies also:

$$\underline{\mathbf{C}}\left(\Delta t_1+\Delta t_2+\Delta t_3\right)=\exp\left(-\underline{\underline{\mathbf{M}}}_1\Delta t_1-\underline{\underline{\mathbf{M}}}_2\Delta t_2-\underline{\underline{\mathbf{M}}}_3\Delta t_3\right)\underline{\mathbf{C}}(t=0) \qquad \text{(II.35)}$$

which is verified only if $\left\{\underline{\underline{\mathbf{M}}}_i\right\}_{i=1..3,i\neq j}$ and $\left\{\underline{\underline{\mathbf{M}}}_j\right\}_{j=1..3,i\neq j}$ commutes (meaning that $\underline{\underline{\mathbf{M}}}_i\underline{\underline{\mathbf{M}}}_j=\underline{\underline{\mathbf{M}}}_j\underline{\underline{\mathbf{M}}}_i$ for $i\neq j$).

- *Conditions of exchangeability imposed by the physical chemistry*

Nguyen *et al.* (2013) demonstrated that a necessary and sufficient condition to have solution (II.35) applicable is that the ratios of the Henry coefficients $\left\{\frac{k_u(t)}{k_v(t)}\right\}_{u,v=0...m,u\neq v}$ (see their definitions in Eq. (II.20)) remain constant with time between all considered steps. As a result, adding or removing a material/layer/food (*i.e.*, changing k_u from ∞ to 0 or the reverse) breaks the condition of exchangeability of steps. The condition of exchangeability is also likely to be lost for polar solutes dispersed between polar and apolar phases. As shown in §II.2.5.2.2. (see (II.50) at infinite dilution when $\phi_i\to 0$), the excess enthalpies of mixing are negative for the firsts and positive for the lasts. In this particular case, the apparent activation energy of the partition coefficient between u and v is maximal, and the effect of temperature needs to be simulated by respecting the order of the temperature variations (i.e., by using Eq. (II.34) of Eq. (II.35)). For apolar solutes, the activation of k_u is, conversely, almost compensated by a symmetrical variation of k_v, when the temperature is changed.

II.2.4. Diffusion properties in polymers

II.2.4.1. Definitions of diffusion coefficients

Diffusion coefficients in the polymer, D_P , are essential properties to calculate migration according to Eqs. (II.12) and (II.22). Reference textbooks (see chapter 11 of Crank, 1975;Vrentas and Vrentas,2013) have proposed several definitions of diffusion coefficients including overestimations (Piringer and Baner, 2008). In this section the definitions which are relevant in macroscopic migration models and which can incorporate the effects of the molecular structure of the migrants and the polymer are reviewed.

II.2.4.1.1. Self- and trace-diffusion coefficients

As a starting point, it is worth noticing that the random walk of migrants (without gradient) does not occur in an empty space but among other molecules (polymer segments and other solutes, such as plasticizers). By reusing the illustrations of **Figure II-8**, the net flux density perpendicular to a cross section located at a position x is proportional to the difference of the net velocities between the solutes (*i.e.,* molecules of the migrant of interest), $u(x,t)$ and the Stokesian velocity of the surrounding molecules $u_0(x,t)$:

$$J(x,t) = C(x,t)\left[u(x,t) - u_0(x,t)\right] = -D_P \left.\frac{\partial C(x,t)}{\partial x}\right|_x \qquad \text{(II.36)}$$

In the limiting case where the migrant is of the same nature as the surrounding molecules (e.g., pure liquid plasticizers, pure solvents), $u(x,t) = u_0(x,t)$, there is no net flux ($J(x,t) = 0$) and no macroscopic gradient $\left.\frac{\partial C(x,t)}{\partial x}\right|_x = 0$. The diffusion coefficient is still defined and is called the self-diffusion coefficient but is not correlated to any macroscopic gradients.

The opposite limiting case corresponding to infinite dilution ($C(x,t) \to 0$) and a solid behavior ($u_0(x,t) \to 0$) also leads to an extremely low net flux ($J(x,t) \to 0$), but with a concentration gradient. The corresponding diffusion coefficient is called the trace diffusion coefficient. Experimentally, the velocity $u(x,t)$ can be determined from the lag-time, t_{lag} , associated with the migration across a functional barrier of thickness l_{fb} . Noting that $t_{lag} = \frac{l_{fb}^2}{6D_P}$ (see §II.2.3.5.5.) leads to:

$$u\left(x=0, t=t_{lag}\right) = \frac{J\left(x=0, t=t_{lag}\right)}{C\left(x=0, t=t_{lag}\right)} = \frac{l_{fb}}{t_{lag}} = 6\frac{l_{fb}}{l_{fb}^2} D_P = 6\frac{D_P}{l_{fb}} \qquad \text{(II.37)}$$

Eq. (II.37) is correct but suffers from a lack of generality for an arbitrary initial distribution of solutes. The approach presented in §II.2.3.6.3. is more general. Eq (II.31) associated to $D_F = D_P$ shows that:

$$D_P = \frac{1}{6N_{migrants}} \lim_{t\to\infty} \frac{d}{dt} \left\langle \sum_{i=1}^{N_{migrants}} \left\| \mathbf{r}_i^{CM}(t) - \mathbf{r}_i^{CM}(0) \right\|^2 \right\rangle = \frac{1}{6} \lim_{t\to\infty} \frac{d}{dt} g_{CM}(t) \approx \frac{g_{CM}(t)}{6t} \quad \text{(II.38)}$$

Factor 6 appears in Eqs. (II.37)-(II.38) instead of factor 2 shown in Eq (II.31), because the random walks are considered in three dimensions and not anymore in one dimension. The mean-square-displacement $g_{CM}(t) = \left\langle \sum_{i=1}^{N_{migrants}} \left\| \mathbf{r}_i^{CM}(t) - \mathbf{r}_i^{CM}(t=0) \right\|^2 \right\rangle \Big/ N_{migrants}$ is calculated accordingly from the 3D positions of the center-of-mass of all migrants, $\left\{ \mathbf{r}_i^{CM}(t) \right\}_{i=1..N_{migrants}}$ and averaged over all possible initial positions $\left\{ \mathbf{r}_i^{CM}(t=0) \right\}_{i=1..N_{migrants}}$. The definition (II.38) is used to calculate diffusion coefficients by molecular dynamics simulations in polymers (Vitrac and Hayert, 2007b;Durand *et al.*, 2010). In practice and to remove any uncontrolled drift (*i.e.,* $|u_0| > 0$) due to the displacement of surrounding molecules, the positions are not absolute but taken respectively to the center-of-mass of the whole system.

II.2.4.1.2. Mutual diffusion coefficients

Section II.2.4.1.1. describes diffusion either in a stream or when there is only one diffusing species. Diffusion in a medium with variable composition generates fluctuations in u_0 (see Eq. (II.36)) and changes the nature of the interactions with the surrounding molecules. The picture is complete if consideration is given to the point of view of the surrounding molecules whose diffusion is also affected. An example could be the diffusion of an antioxidant (or any large molecule) in a heterogeneously plasticized polymer (Courgneau *et al.*, 2013), where the local mobility of the antioxidant is strongly enhanced by the local amount of plasticizer in the ternary system (migrant+plasticizer+polymer). Similarly, the diffusion of the plasticizer increases the mobility of polymer segments. Strictly speaking, all these effects cannot be described by the sole shift of the glass transition temperature and the increase of free volumes presented in §II.2.4.3. (see also discussion in chapters 5 and 6 of the reference textbook Vrentas and Vrentas, 2013). As the diffusion of one species affects the diffusion of all other species and reciprocally, self- and trace diffusion coefficients cannot be used. The correct description requires the use of Onsager's theory and generalized forces. The entire system (polymer+solutes) reorganizes to minimize its total free energy. A cationic surfactant will, for example, accumulate at the surface of the material to minimize its interaction with the polymer.

A poorly soluble colorant or pigment will do the same at high concentration. The resulting concentration profiles therefore evolve spontaneously from an initial uniform distribution after processing to a highly heterogeneous one. Such evolutions with matter moving from low to high concentrated regions cannot be predicted with concentration gradients as effective driving forces. The gradients of chemical potentials need to be used as an effective driving force. For the sake of simplicity and to avoid a tensor definition of the diffusion coefficient, only the effect of the chemical potential of the migrant, denoted $\mu(x,t)$, as the driving force is considered. Rigorously, a linear relationship should be considered between the flux of the migrating substance and the driving forces associated with all species in the mixture. The generalized driving force, f, induced by the local variation of the chemical potential of the migrant in the mixture is:

$$f = -\left.\frac{\partial \mu(x,t)}{\partial x}\right|_t = \zeta_{mutual}\left[u(x,t) - u_0(x,t)\right] = \zeta_{mutual}\frac{J(x,t)}{C(x,t)} \tag{II.39}$$

where ζ_0 is a friction coefficient; and $\mu(x,t) = \mu_0 + RT\ln\left(\gamma^v\phi\right)$ is the chemical potential of the migrant defined respectively to its volume fraction ϕ and activity coefficient γ^v. The relationship between the gradient of chemical potential and the concentration gradient is given by:

$$\begin{aligned}\left.\frac{\partial \mu(x,t)}{\partial x}\right|_t &= \left.\frac{\partial \mu(x,t)}{\partial \phi}\right|_t \left.\frac{\partial \phi(x,t)}{\partial x}\right|_t = RT\left.\frac{\partial \ln\left(\gamma^v\phi(x,t)\right)}{\partial \phi}\right|_t \left.\frac{\partial \phi(x,t)}{\partial x}\right|_t \\ &= \frac{RT}{C(x,t)}\left[\left.\frac{\partial \ln\left(\gamma^v\right)}{\partial \ln\left(\phi(x,t)\right)}\right|_t + 1\right]\left.\frac{\partial C(x,t)}{\partial x}\right|_t = \Gamma\frac{RT}{C(x,t)}\left.\frac{\partial C(x,t)}{\partial x}\right|_t\end{aligned} \tag{II.40}$$

with $\Gamma(\phi) = 1 + \left.\frac{\partial \ln\left(\gamma^v\right)}{\partial \ln\left(\phi(x,t)\right)}\right|_t$ being the thermodynamic factor depending on the composition, whose dependence with concentration can be determined from the expression of the sorption isotherm see §II.2.5.2.). An effective diffusion coefficient, D_P^{mutual}, related to the flux $J(x,t) = -D_P^{mutual}\left.\frac{\partial C(x,t)}{\partial x}\right|_t$ is identified from Eqs. (II.39) and (II.40) as:

$$D_P^{mutual}(\phi) = \Gamma(\phi)\frac{RT}{\zeta_{mutual}(\phi)} = \Gamma(\phi)\frac{\zeta_{trace}}{\zeta_{mutual}(\phi)}D_P^{trace} \tag{II.41}$$

where subscripts *trace* and *mutual* refer to the value of the property at infinite dilution and in mixture, respectively. For binary solvent-polymer mixtures, Vrentas and Vrentas (1993) proposed the following evolution of the friction coefficient:

$$\frac{\zeta_{mutual}(\phi)}{\zeta_{trace}} = \alpha\phi^2 + (1-\phi)(1+2\phi) \quad \text{(II.42)}$$

with $\alpha = \frac{\overline{V}_{\substack{pure \\ solvent}}}{\overline{V}_{\substack{dissolved \\ polymer}}} \frac{D^{self}_{solvent}}{D^{\substack{trace \\ dissolved \\ polymer}}}$ and $\overline{V}_X$ the molar volume of X. Eq. (II.42) is not thought to be general for non-solvent or not plasticizing molecules such as hindered phenols or aromatic amines. The fundamental reason is that such migrants are crystalline (solids) at high concentration.

It is worth noting that D_P^{trace} can contain additional concentration dependence due to the extra free volumes brought by the solute itself and the possible shift in the glass transition temperature. For most applications and in the absence of a unified theory, the equation of Fujita can be applied to describe the concentration dependence:

$$\ln \frac{D_P^{mutual}(C)}{D_P^{mutual}(C_{ref})} = -\beta\left(1 - \frac{C}{C_{ref}}\right) \quad \text{(II.43)}$$

with β a concentration to be determined experimentally.

II.2.4.2. Effect of the geometry of migrants on D_p values

Migrants from polymers are not gas molecules such as water, oxygen, and carbon dioxide, but heavy molecules larger than voids in the polymer. The smallest additives are monomer residues and solvents commensurable to one or several monomers. At the concentration of use of most of additives and residues (*i.e.*, except plasticizers which are used at concentration ranges from 10 w% to 50 w%), the many pair contacts between the segments of the polymer and the migrant control the rate of the translation of the most mobile species (the migrant). This configuration is very different from the situation in food or liquid food simulants, where the food constituents (water, oil, ethanol, etc.) are much smaller than the polymer chains and are usually packed less densely. The correct picture is to consider that the trace diffusion of the migrant in the polymer is smaller than the self-diffusion of food constituents (typically 10^{-9}-10^{-10} $m^2 \cdot s^{-1}$), but much larger than the self-diffusion of the polymer itself (<10^{-22} $m^2 \cdot s^{-1}$).

The exact mechanism of translation of molecules larger than voids in solid polymers has not been fully elucidated yet. They have been investigated independently by two communities: the community of free-volume-theory was interested in the mutual-diffusion of polymer solvents whereas the food packaging community was focused on the development of practical overestimate models for compliance testing. Due to the different nature of the considered substances and the type of considered diffusion coefficients (mutual diffusion measured in ^1H spin-echo nuclear magnetic resonance and trace diffusion coefficients measured via desorption kinetics), the interactions between the two communities have been limited. Based

on the works of Fang et *al.* (2013) and Fang and Vitrac (2017), a unified approach has been sketched and is summarized in **Figure II-17**. Early works (Vitrac *et al.*, 2006;Ewender and Welle, 2013;Welle, 2013;Ewender and Welle, 2014, 2018a) suggested that the volume of the entire molecule or its rough estimate the molecular mass (see the discussion in Zhao *et al.*, 2003) offered a proper scaling parameter of diffusivities, at least, at the first tier. The use of the entire mass or volume of the migrant is misleading as it covers very different realities for rigid and flexible solutes. Flexible migrants, possibly with large masses, can benefit from the translation of smaller rigid units; whereas a large rigid migrant rarely requires free volumes matching the shape and size of a larger rigid block. Without paying attention, both the effects of block sizes and their numbers combine, giving an apparent correlation of the logarithm of D_P with the logarithm of the molecular mass M (concerted displacements of rigid units or blocks) and with the total volume of the migrant $n_{\substack{rigid\\block}} \cdot V^{vdW}_{\substack{rigid\\block}}$. In this description, short *n*-alkanes are partly rigid since the constraints of torsion prevent blocks from translating independently.

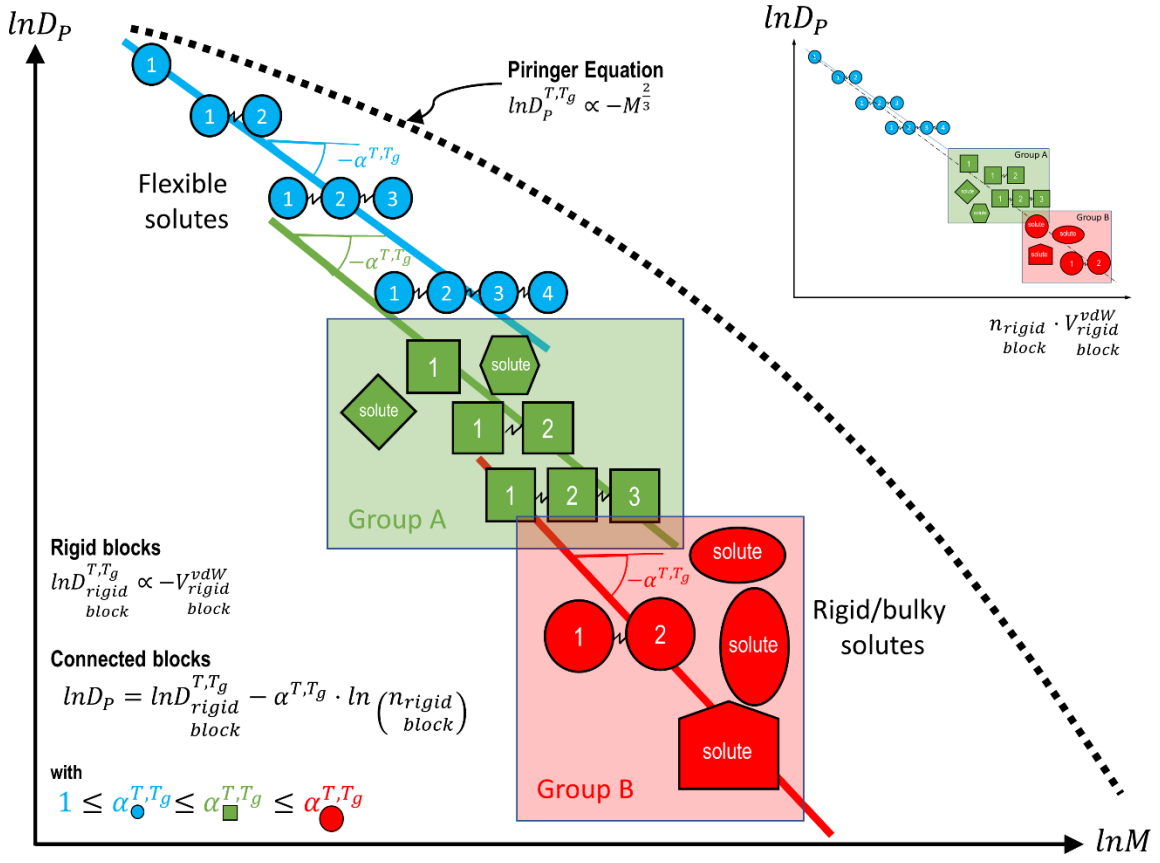

***Figure II-17**. Scaling of diffusion coefficients between rigid and connected blocks with molar mass and van der Waals volume in a thermoplastic polymer (groups A and B refer to substances defined in **Figure II-18**).*

Figure II-18 presents the diffusion coefficients of 49 substances (105 D_P values) in low-density polyethylene (LDPE) at 23°C collected by the National Institute of Standards (NIST, 2019) and the European Commission (EC) (Hinrichs and Piringer, 2002) from the literature. The data were selected to reproduce the main features of **Figure II-17**: the decrease of D_P values with the number of rigid blocks and the almost invariance of D_P with the exact shape and flexibility of the solute. The concept of invariance considers here that there is no visible effect if the induced variation is lower than the uncertainty associated with the measurement of D_P. As an illustration, Vitrac *et al.* (2006) showed that the group of substances denoted A and B presented differences in diffusivities which could not be explained by the differences between molecules. Three parameters were considered: the van der Waals volume (V_{vdW} in Å^3), the gyration radius and the shape factor. Linear alkanes scaled as a power law with the molecular mass M, $D_p \propto M^{-\alpha}$ with α of 1.58 (range: 1.09-1.68) for [1] NIST data and 1.84 (range: 0.75-2.01) for [2] EC data. For bulky solutes, the large uncertainty in the experimental D_P values suggests that diffusivities can be considered significantly different only if the V_{vdW} differences between molecules are larger than 35 Å^3. The correlation with volume is consistent with the free-volume theory of diffusion (Fang and Vitrac, 2017), and as V_{vdW} is also correlated with the number of heavy atoms (see **Figure II-18**e, the correlation depends on the type of substances), a reasonable upper envelope of D_P values has been proposed to overestimate diffusivities (Fang *et al.*, 2013). The equation is coined the Equation of Piringer:

$$\ln D = A'_P - 0.1351 M^{2/3} + 0.003 M - \frac{\tau + 10454}{RT} \qquad \text{(II.44)}$$

with the key parameters $A'_P = 11.5$ and $\tau = 0$ for LDPE. The values for other polymers are reported in the EU report (Hoekstra *et al.*, 2015). The model of Piringer provides only a variable overestimation ranging from a factor 0.63 (underestimation) to 100 (see the inset **Figure II-18**a).

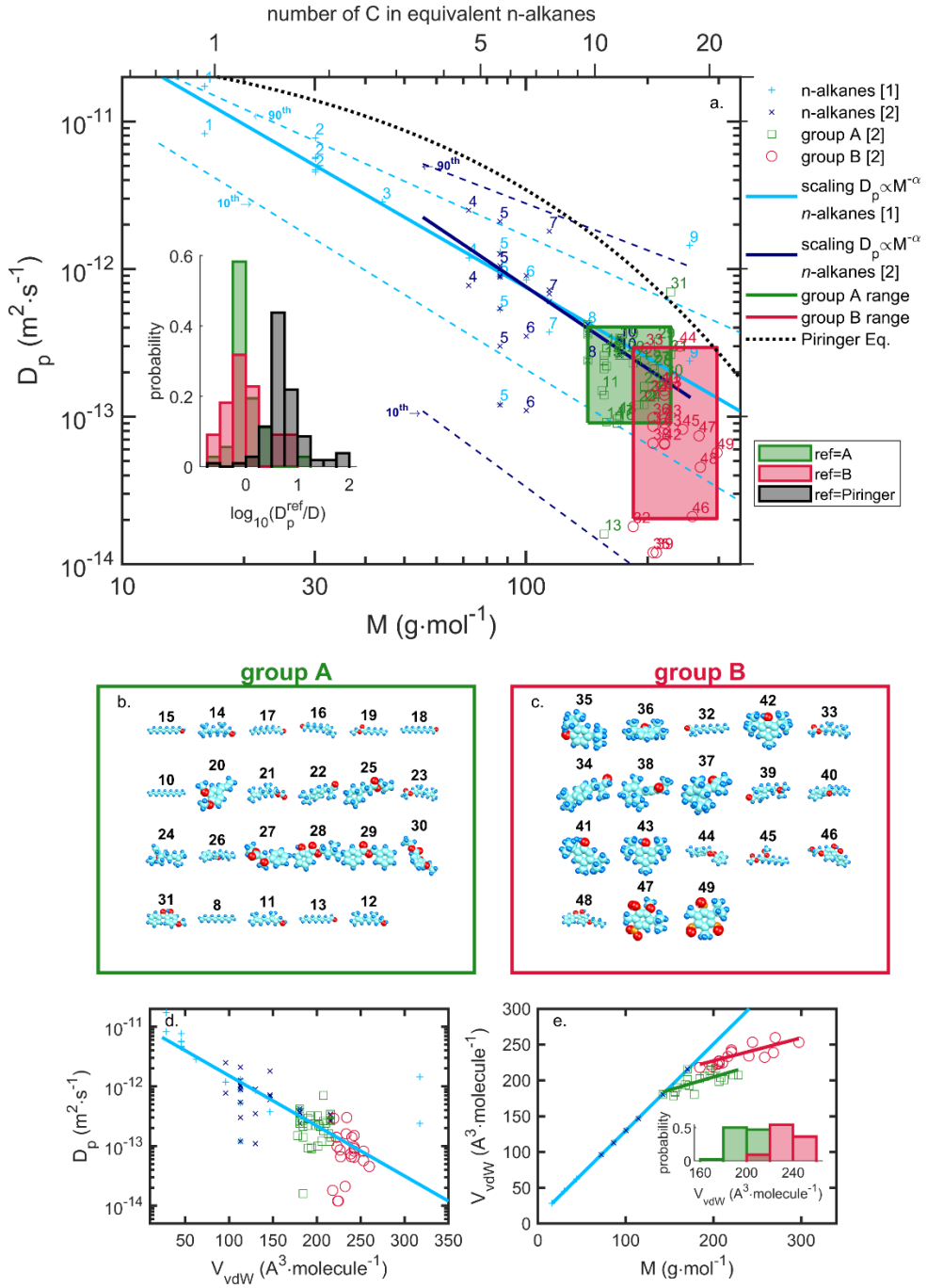

Figure II-18. *Scaling of diffusion coefficients of 49 substances (n-alkanes, two groups of molecules A and B with similar D_P values) in LDPE at 23°C with molar mass, M, and the van der Waals volume.*

Data from: [1] Flynn (1982), [2] Hinrichs and Piringer (2002);NIST (2019).

1: methane [1]; 2: ethane [1]; 3: propane [1]; 4: n-pentane [1,2]; 5: n-hexane [1,2]; 6: n-heptane [1,2]; 7: n-octane [1,2]; 8: n-decane [1,2,A]; 9: n-octadecane [1]; 10: n-dodecane [2,A]; 11: 2-trans-3,7-dimethyl-2,6-octadien-8-ole (geraniol) [A]; 12: 3,7-dimethyl-6-octen-1-ol (citronellol) [A]; 13: n-decylaldehyde or n-decanal (aldehyd c10) [A]; 14: 3,7-dimethyl-1-octanol [A]; 15: decylalcohol or 1-decanol [A]; 16: cis-undecen-8-al (aldehyd c11 inter) [A]; 17: n-undecen-2-al (aldehyd c11) (2-undecenal) [A]; 18: n-undecylaldehyde (aldehyde c11) [A]; 19: ethyloctanoate [A]; 20: 2-methoxy-4-propenylanisol (methylisoeugenol) [A]; 21: citronellyl formate or 6-octen-1-ol, 3,7-dimethyl-, formate [A]; 22: 2-methyl-3-(4-isopropyl)phenylpropanal (cyclamen aldehyde) [A]; 23: 2,6-octadien-1-ol, 3,7-dimethyl-, acetate, (2e)- (geranyl acetate) [A]; 24: 3,7-dimethyl-1,6-octadien-3-ylacetate (linalylacetate) [A]; 25: allyl-3-cyclohexylpropionate [A]; 26: amylcinnamicaldehyde or 2-phenylmethylene-heptanal [A]; 27: 3-methyl-3-phenylglycidate (aldehyde c16) [A]; 28: iso-amylsalicilate [A]; 29: benzylbenzoate [A]; 30: diethylphthalate (dep) [A]; 31: 2-hydroxy-4-methoxybenzophenone (chimassorb 90) [A]; 32: 2-methyl-undecanal (aldehyde c12 mna) [B]; 33: 3,7-dimethyl-6-octen-1-ylacetate [B]; 34: 3-[4-tert,-buthylphenyl]-2-methylpropanale (lilial) [B]; 35: 2,4-di-t-butylphenol [B]; 36: 2,6-di-t-

butylphenol [B]; 37: 4-(2,6,6-trimethyl-2-cyclohexen-1-yle)-3-methyl-3-buten-2-one (methylionone-gamma) [B]; 38: 5-(2,6,6-trimethyl-2-cyclohexen-1-yle)-3-methyl-3-buten-2-one (methylionone-alpha) [B]; 39: 4-[4-methyl-4-hydroxyamyl]-3-cyclohexen-carboxaldehyde (lyral) [B]; 40: 2-hexyl-3-phenyl-2-propenal [B]; 41: 2,5-tertbutyl-4-hydroxy-toluene [B]; 42: 2,6-di-tert-butyl-4-methylphenol [B]; 43: 2,6-di-tert-butyl-4-methylphenol (ionol or BHT) [B]; 44: phenylethylphenylacetate [B]; 45: nonane-1,3-dioldiacetate (jasmelia) [B]; 46: 2-hydroxy-4-ethanediolbenzophenone [B]; 47: 2,6-dinitro-1-methyl-3-methoxy-4-tert,-butylbenzole (moschus ambrette) [B]; 48: 2-hydroxy-4-butoxybenzophenone [B]; 49: 2,4,6-trinitro-1,3-dimethyl-5-tert,-butylbenzene (moschus xylol) [B]

II.2.4.3. Effect of the polymer

The effects of the polymer on the diffusion of migrants are twofold: i) the relaxation of polymer segments affects the renewal of free volumes around the solute and ii) specific interactions between rigid blocks and the polymer may increase the release time of rigid blocks. In the original free-volume theory of Vrentras and Duda (1996;1998), the translation of rigid blocks is assumed to be associated with the local reorganization of special free-volumes, so-called hole free-volume (hFV), whose redistribution is not activated by temperature. As an approximation of the thermal expansion of polymers, the amount of hFV available for the diffusion of migrants is proportional to $T - T_g + K_\beta$, where T_g is the glass transition temperature and K_β a constant possibly dependent on the polymer and the shape of the translating block. This interpretation is illustrated in the diffusion of various migrants in rubber ($T \geq T_g$) and glassy ($T < T_g$) polymers in **Figure II-19**. The apparent scaling exponent $\alpha\left(T, T_g\right)$ decreases rapidly with $T - T_g$; for linear solutes, Fang et *al.* (2013) demonstrated that its general expression was:

$$\alpha\left(T - T_g\right) = 1 + \frac{K_\alpha}{T - T_g + K_\beta} \text{ with } T > T_g + K_\beta \qquad \text{(II.45)}$$

with K_α essentially a polymer-dependent constant and K_β a positive constant for rigid blocks smaller than the cross-section of polymer segments and otherwise negative.

Eq. (II.45) and **Figure II-19**a demonstrate that mass dependence increases rapidly when T approaches or goes below T_g . In elastomers and rubbers (with very low T_g) as well as in polymer melts, the mass dependence for linear migrants approaches unity. This theoretical value corresponds to the independent displacements of jumping units. Due to the dependence of K_β with the type of rigid blocks, Eq. (II.45) describes different mass dependence (see the three series of linear molecules in **Figure II-17**) for different molecules. Although approximate, the technique can be used to extrapolate the results of $\ln D_P$ from one polymer to a new

polymer (denoted R) via the correction $\frac{\alpha\left(T,T_g^R\right)}{\alpha\left(T,T_g\right)}\ln M$. The principles are illustrated in **Figure II-19**b by showing that almost any of the presented polymers (except rubbers) can be used to predict the diffusion coefficients of the same substances in polypropylene only by setting the T_g of the source and destination polymer. The same correction can be used to predict diffusivities in plasticized polymers from their values in non-plasticized ones.

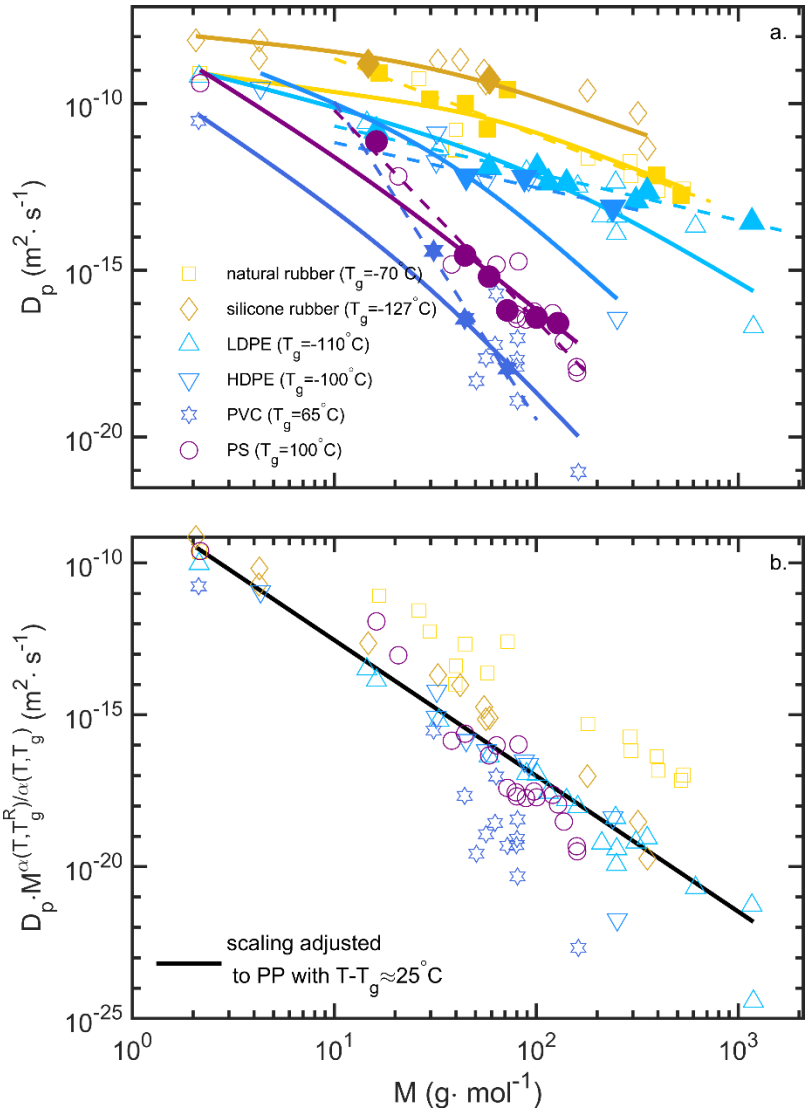

***Figure II-19**. Diffusivities of various substances at 25°C in glassy and rubber polymers: (a) raw values, (b) normalized data to remove polymer effects (standardized to T_g value of 0°C corresponding to atactic polypropylene PP). Filled symbols correspond to n-alkanes (scaling laws $D_p \propto M^{-\alpha}$ as dashed lines) and empty symbols to various solutes including gases and plastic additives (scaling laws $D_p \propto M^{-\alpha}$ as continuous lines). Data from Schwope et al. (1990).*

II.2.4.4. Activation of diffusion by temperature

Increasing temperature affects firstly the structure of the polymer, which, in return, facilitates the translation of the migrants. Temperature activation is consequently higher in polymers with high thermal expansion coefficients (higher in rubber state than in glassy state, higher in plasticized than in non-plasticized polymer, higher in thermoplastics than in thermosets). Below or near T_g, apparent activation energies $Ea = RT^2 \frac{\partial \ln D_p}{\partial T}$ are dominated by free-volume effects and are higher than at higher temperatures. The effects of temperature for linear solutes near T_g are shown in **Figure II-20**. If the behavior was strictly Arrhenian, the dependence of $\ln D_p$ would be linear with $1/T$, which is not obviously the case for large diffusants near T_g. Apparent activation energies increase with the size of diffusants as $E_a \propto \ln M$. The interested reader will find a consistent review of free-volume and specific-migrant activation in Fang and Vitrac (2017). In any case, it is not recommended to extrapolate D_p values from low temperatures to high temperatures for polymer recycling, as it would overestimate diffusivities and consequently the rate of decontamination of the polymer.

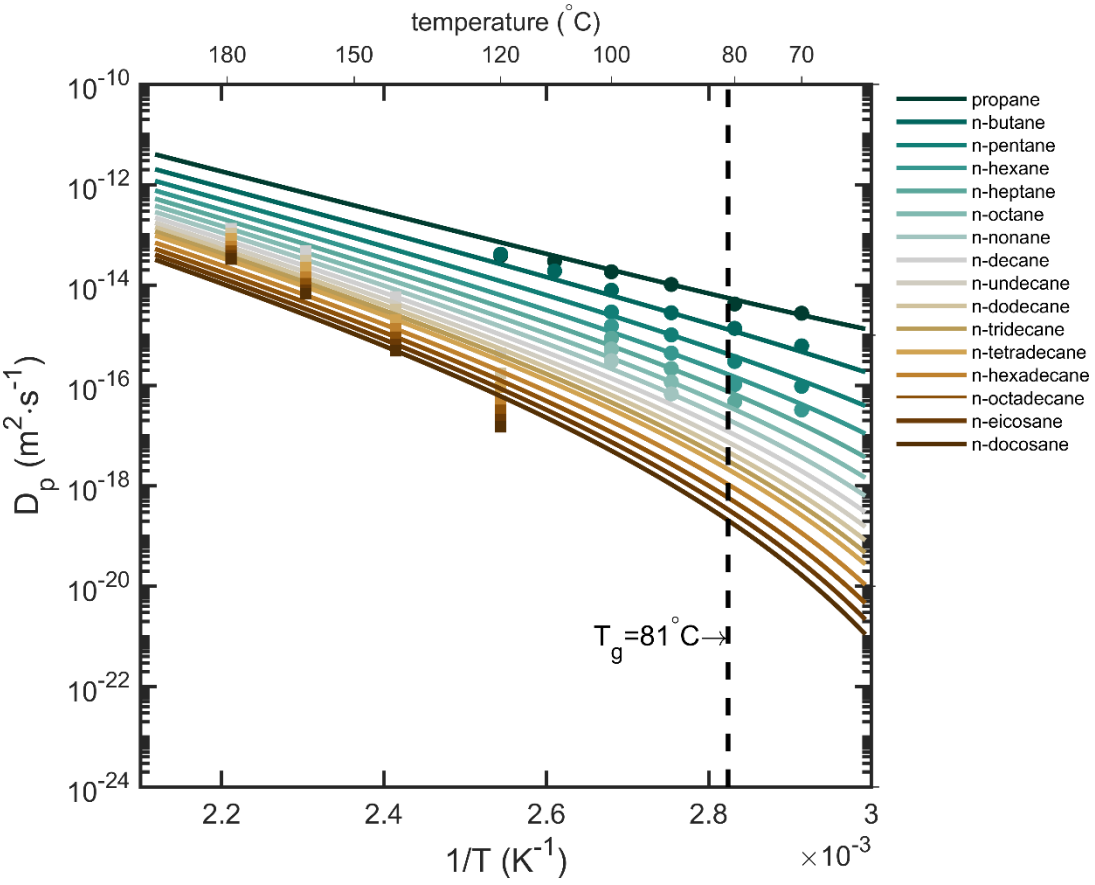

***Figure II-20**. Arrhenius plot of diffusivities of n-alkanes in polyethylene terephthalate. Data from Ewender and Welle (2014, 2016, 2018a).*

II.2.5. Sorption properties and partition coefficients

As shown in §II.2.3.1. and §II.2.4.1.2. , sorption properties and partitioning between materials, food and polymer affect both the kinetics of migration and the distribution of migrants at thermodynamic equilibrium. Previous descriptions were essentially counting the number of substances in a representative elementary volume or a compartment (material, food). The present description will show explicitly the role of pair interactions between the migrant indexed i and all other constituents (P for the polymer, F for the contact phase, e for ethanol, w for water). Generic phases in equilibrium (in contact or not) are denoted α, β and δ regardless of whether they are a solid (polymer or solid food), a liquid contact phase or a gas (headspace, storage environment).

II.2.5.1. Some definitions

II.2.5.1.1. Chemical potentials, fugacities, and activities

Two phases, α and β, are said to be at thermodynamic equilibrium if they are at the same temperature T, pressure P and the same chemical potential for any migrant i: $\mu_{i,\alpha}(T,P) = \mu_{i,\beta}(T,P)$. The concept of thermodynamic potential was proposed by G. N. Lewis, with initially in mind pure ideal gases, verifying that $\left.\frac{\partial \mu_{i,\alpha}}{\partial P}\right|_T = \overline{V}_i$, where $\overline{V}_i = \frac{RT}{P}$ is the molar volume of the gas i. After integration at a constant temperature, the change in chemical potential from pressure P^{ref} to P is $RT \ln \frac{P}{P^{ref}}$ for a pure ideal gas. Lewis generalized to phase mixtures (ideal or not) by replacing pressure by a function f_i, called fugacity and assessing the capacity of a substance literally to flee:

$$\mu_{i,\alpha} - \mu_{i,\alpha}^{ref} = RT \ln \frac{f_{i,\alpha}}{f_{i,\alpha}^{ref}} \qquad \text{(II.46)}$$

Reference values at the temperature T $\mu_{i,\alpha}^{ref}$ and $f_{i,\alpha}^{ref}$ are physically related, but the choice of the reference chemical potential or the reference fugacity is arbitrary. The ratio $a_{i,\alpha} = \frac{f_{i,\alpha}}{f_{i,\alpha}^{ref}}$ defines the activity of the solute i in the phase α; it provides a measure of the difference of the substance(s) chemical potential in α with its reference state. To describe mass transfer between the phases α and β (*i.e.*, with $f_{i,\alpha}^{eq} = f_{\beta,\alpha}^{eq}$) at equilibrium, it is convenient to choose the same reference state $\mu_{i,\alpha}^{ref} = \mu_{i,\beta}^{ref}$ in both phases. Following the intuition of

Lewis, equivalent partial pressures in an ideal gas offer an almost universal potential to estimate the potential of transfer of any substance (e.g., a volatile organic compound, a liquid plasticizer, a crystalline pigment or a poorly soluble additive or mineral oil residues). The reference fugacity needs to be adapted accordingly as shown in **Table II-11**.

Table II-11. *Expressions of practical partial pressures and saturation concentrations in relationship with the reference state of the substance in the conditions where its migration its studied.*

Application	Choice for the fugacity: f_i	Choice for the reference fugacity: f_i^{ref}	Relationship with the concentration of substance i in the phase α : $C_{i,\alpha}$ (SI unit is mol·m^{-3})
Volatile substance in a gas phase (α =gas phase)	partial pressure: p_i	total pressure: P	$p_i = RTC_{i,\alpha}$
Dissolved substance in a condensed phase (polymer, liquid) with a liquid reference state (α =P or F)	partial pressure (equivalent partial pressure in the theoretical gas phase δ in equilibrium with α): p_i	saturation pressure of the pure substance at the same temperature: $p_{i,sat}(T)$	$\frac{p_i}{p_{i,sat}} = \gamma_{i,\alpha}^{v}\phi_{i,\alpha} = \gamma_{i,\alpha}^{v}\bar{V}_i C_{i,\alpha}$ with $\gamma_{i,\alpha}^{v}$ the activity coefficient of the substance i in the phase α relatively to its volume fraction $\phi_{i,\alpha}$. At saturation, one gets: $C_{i,\alpha}^{sat} = \frac{1}{\gamma_{i,\alpha}^{v}\bar{V}_i}$
As above but with a solid reference state	partial pressure (equivalent partial pressure in the theoretical gas phase δ in equilibrium with α): p_i	Partial pressure at the surface of the crystal expressed as: $\left(\frac{f_{i,pure}^{S}}{f_{i,pure}^{L}}\right)_{(T)} p_{i,sat}(T)$ with $\left(\frac{f_{i,pure}^{S}}{f_{i,pure}^{L}}\right)_{(T)}$ being the ratios of fugacities of the pure solute between solid (pure crystalline) and molten (pure amorphous) state.	$\frac{p_i}{\left(\frac{f_{i,pure}^{S}}{f_{i,pure}^{L}}\right)_{(T)} p_{i,sat}} = \gamma_{i,\alpha}^{v}\phi_{i,\alpha} = \gamma_{i,\alpha}^{v}\bar{V}_i C_{i,\alpha}$

Migrants with a reference solid state in the conditions of migration are very common in plastics and thermosets. They encompass almost all antioxidants, colorants and pigments. They are liquid in conditions of processing of the polymer (e.g., above 160°C), but solid in the conditions of service of the finished material (at T and P). The partial pressures are lower in this case but non-zero. The variation of fugacities between a pure crystal and its pure amorphous state depends on the temperature difference between T and its melting temperature, $T_{i,m}$ as shown in **Figure II-21**.

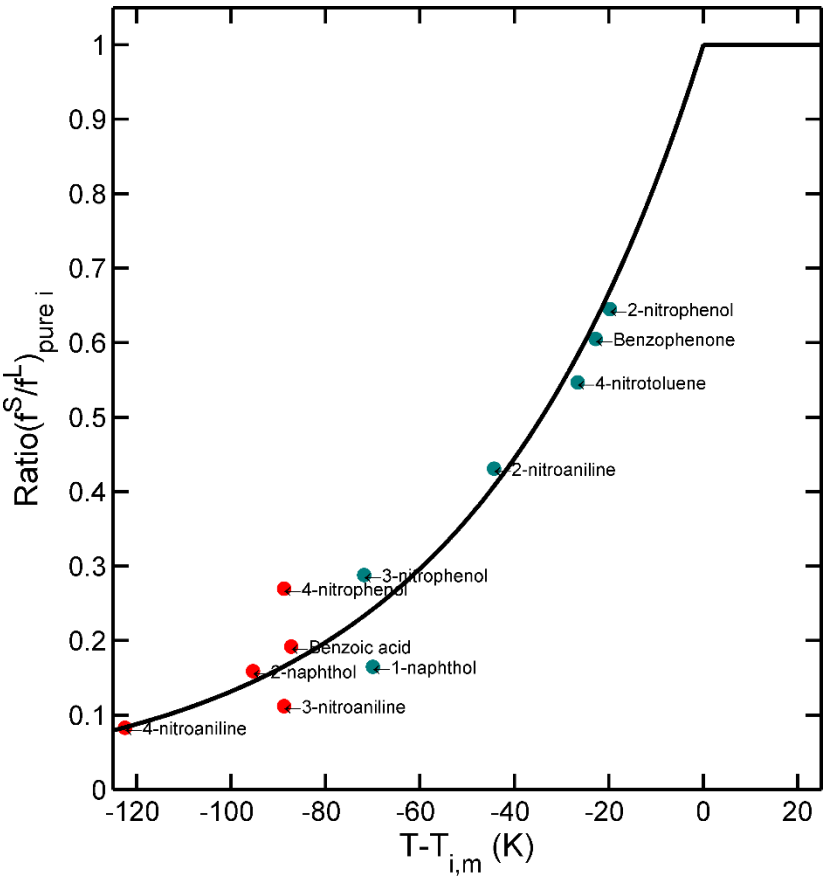

***Figure II-21**. Ratio of fugacities between pure solid and amorphous states for 11 model migrants (data fromFornasiero et al., 2002) and its continuous approximation proposed in Figure S1 of the Supporting Information of Nguyen et al. (2017).*

It is worth noting that thermodynamic models and simulation calculations may use different reference states (e.g., amorphous reference states even if the reference one is solid). The choices presented here are consistent with the definition of the molar solvation energy:

$$\begin{aligned}\Delta G_{i,solvated\ in\ \alpha}^{solvatation} &= \mu_{i,\alpha} - \mu_{i,\delta}^{\delta=ideal\ gas} = RT\ln\left(\frac{p_{i,sat}(T)\overline{V}_i}{RT}\frac{\gamma_{i,\alpha i}^{v}\phi_{i,\alpha}}{C_{i,\delta}}\right) \\ &= RT\ln\left(\frac{p_{i,sat}(T)\overline{V}_i}{RT}K_{i,\alpha/\delta}\right)\end{aligned} \quad \text{(II.47)}$$

with $K_{i,\alpha/\delta}$ being the effective partition coefficient between the condensed phase α and the theoretical ideal gas phase δ. With respect to mass transfer, the use of partition coefficients should be preferred to solvation energies. Free energies need to be preferred to analyze and interpret quantitatively the nature of the interactions (van der Waals, electrostatic, hydrogen bonding) in the phase α. Thermodynamic integration at molecular scale offers direct access to $\Delta G_{i,solvated\ in\ \alpha}^{solvatation}$ without requiring a theoretical separation of enthalpic and entropic effects.

II.2.5.1.2. Effective partition coefficients between P and F

From relationships presented in **Table II-11**, effective partition coefficients between a material P and the contacting phase is given by the ratio of activity coefficients. For semi-crystalline polymers, it is well accepted that crystallites and crystalline phases are impenetrable to migrants. By assuming that no migrating substance has been trapped during processing in the crystalline phase, the effective partition coefficient reads:

$$K_{i,F/P} = \frac{1}{(1-c)(1-\epsilon)} \frac{\overline{V}_i \phi_{i,F}^{eq}}{\overline{V}_i \phi_{i,P}^{eq}} = \frac{1}{(1-c)(1-\epsilon)} \frac{\gamma_{i,P}^{v}}{\gamma_{i,F}^{v}} \tag{II.48}$$

where $\phi_{i,P}^{eq}$ refers to the volume fraction in the amorphous phase of the material (possibly porous and semi-crystalline); c and ϵ are the volume crystallinity and porosity of the material. Thermoplastics are not porous materials and $\epsilon = 1$.

For very porous materials such as papers, it is preferable not to homogenize concentration between all phases (solid crystalline, solid amorphous and gas) and to choose the fibers as P and to adapt the exchange surface area to the shape of the fibers. The characteristic dimension of the material should be chosen accordingly and be commensurable to the half-diameter of fibers.

II.2.5.2. Sorption isotherms

Sorption isotherms are experimental or theoretical curves, which relate the amounts absorbed by a condensed phase in relationship to an applied activity at constant temperature. Their use is more general than partition coefficients, when the values of $\left\{\gamma_{i,k}^{v}\right\}_{k=P,F}$ depend on concentrations. In this section, we call isotherm a curve relating the activity coefficient or the excess chemical potential (*i.e.*, in excess respectively to the ideal contribution $RT \ln \phi_i$) with the composition in the mixture.

II.2.5.2.1. Linear isotherms

For most applications at infinite dilution, activity coefficients can be assumed independent of composition. The relationship between mass uptake and partial pressure is linear and governed by a Henry isotherm (see Eq.(II.20)). The relationship between the Henry constant $\left\{k_{i,k}\right\}_{k=P,F}$ and $\left\{\gamma_{i,k}^{v}\right\}_{k=P,F}$ is given by:

$$k_{i,k} = p_{i,sat}(T) \overline{V}_i \gamma_{i,k}^{v} \text{ for } k = P, F \tag{II.49}$$

It is worth noting that if the condition of infinite dilution is well verified in foods regardless of the considered substance (migrations are expected to be low), it may not be verified in the material for substances used close to saturation (e.g., pigments) and for plasticizing substances (e.g. used at weight fractions up to 50%). The proposed description assumes that

the substances are well mixed and exclude, by definition, surfactants and substances causing blooming.

II.2.5.2.2. Binary Flory isotherms

- *General formulation*

The Flory-Huggins theory offers a robust framework to account for concentration effects. The theory extends the regular solution theory for liquid mixtures to mixtures with molecules with dissimilar sizes such as solutes mixed with segments of polymers or large additives dispersed in a food simulant. Enthalpic and entropic interactions are calculated on a lattice assuming that the mixture is incompressible and that molecules fill space commensurably to their molar volumes. For binary mixtures, $i+P$ or $i+F$, the activity coefficient is given by:

$$\ln \gamma_{i,k}\left(\phi_{i,k},T\right)=\left(1-\left(\frac{1}{r_{i,k}}-n_{k\ around\ i}^{compressible}\right)\right)\left(1-\phi_{i,k}\right)+\chi_{i,k}^{(T)}\left(1-\phi_{i,k}\right)^2 \qquad \text{(II.50)}$$

where $r_{i,k}$ is the size of the host molecule with respect to the size of the solute i . In a polymer, the chain is considered infinitely long $r_{i,P}\to\infty$. In foods and a liquid simulating food, $r_{i,F}^{-1}$ represents the number of molecules of F displaced by the insertion of the substance i in F. For most of the migrants, $r_{i,F}^{-1}$ is expected to be larger than unity in water and ethanol and lower than unity in oil. $r_{i,F}$ can be approximated as $\frac{\overline{V}_F}{\overline{V}_i}$ with $n_{k\ around\ i}^{compressible}$ accounting for the partial compressibility of the molecules of i and F . Rigorously, partial molar volumes should be used instead of molar volumes.

- *Approximation at infinite dilution*

At infinite dilution and pending estimations of the Flory-Huggins coefficients $\left\{\chi_{i,k}\right\}_{k=P,F}$, Eq. (II.50) provides an estimator of activity and partition coefficients in amorphous regions:

$$\begin{aligned}\left(1-c\right)\left(1-\epsilon\right)K_{i,F/P}^{(T)}=\frac{\gamma_{i,P}^{v}}{\gamma_{i,F}^{v}}&\approx\frac{\exp\left(1+\chi_{i,P}^{(T)}\right)}{\exp\left(1-r_{i,F}+\chi_{i,F}^{(T)}+\text{compressible correction}\right)}\\&=\exp\left(\chi_{i,P}^{(T)}-\chi_{i,F}^{(T)}+r_{i,F}-\text{compressible correction}\right)\end{aligned} \qquad \text{(II.51)}$$

- *Effect of temperature on partitioning*

According to Eq. (II.51), the variation of $K_{i,F/P}$ with temperature depends on the variation of the difference $\chi_{i,P}^{(T)} - \chi_{i,F}^{(T)}$ with T. When $\chi_{i,P}^{(T)}$ and $\chi_{i,F}^{(T)}$ have the same sign, their variations with T are similar and compensate each other. When $\chi_{i,P}^{(T)} \cdot \chi_{i,F}^{(T)} < 0$, there is no compensation and the effect of temperature is maximal (case of polar solute distributed between a polar and an apolar phase). In both cases, the absolute values of $\left\{\chi_{i,k}\right\}_{k=P,F}$ tend to decrease with temperature, so each mixture becomes progressively ideal (*i.e.,* with no enthalpy of mixing). The temperature dependence is predicted via Eqs. (II.55)-(II.57).

II.2.5.2.3. Ternary Flory isotherms

Eq. (II.50) can be generalized to ternary mixtures with two practical applications: i) the estimation of activity coefficients in polar polymers which contain some amount of water, and ii) the estimation of activity coefficients in water-ethanol mixtures.

The activity coefficient in a wet polymer associated with a volume fraction of water ϕ_w, depends on the three pairs of Flory-Huggins coefficients, $\chi_{i,P}$, $\chi_{w,P}$ (water in dry P), $\chi_{i,w}$ (solute in water), as (see Eq.9a in Fornasiero *et al.*, 2002):

$$\ln\gamma_{i,P_{wet}} = (1-\phi_i) - \phi_w\frac{\overline{V}_i}{\overline{V}_w} - (1-\phi_i-\phi_w)\frac{1}{r_{i,P}} + \left(\chi_{w,i}\frac{\overline{V}_i}{\overline{V}_w}\phi_j + \chi_{i,P}(1-\phi_i-\phi_w)\right)(1-\phi_i) - \chi_{w,P}\frac{\overline{V}_i}{\overline{V}_w}\phi_w(1-\phi_i-\phi_w) \tag{II.52}$$

The activity coefficient in water-ethanol mixtures or in any mixture of two miscible liquids F_1 and F_2 can be estimated similarly (Gillet *et al.*, 2010):

$$\begin{aligned}\ln\gamma_{i,F_1+F_2}^{v} = {} & (1-\phi_i) - r_{i,F_1}^{-1}\phi_{F_1} - r_{i,F_2}^{-1}\phi_{F_2} + \left[\left(\chi_{i,F_1}\phi_{F_1} + \chi_{i,F_2}\phi_{F_2}\right)\left(\phi_{F_1}+\phi_{F_2}\right)\right] \\ & - \chi_{F_1,F_2}\left(\frac{V_i^{vdw}}{V_{F_2}^{P}}\right)\phi_{F_1}\phi_{F_2} - \phi_i\phi_{F_2}\phi_{F_2}\left(\frac{d\chi_{i,F_2}}{d\phi_{F_2}}\right) - \phi_i\phi_{F_1}\phi_{F_2}\left(\frac{\partial\chi_{i,F_1}}{\partial\phi_{F_2}}\right) \\ & - \phi_i\phi_{F_1}^2\left(\frac{\partial\chi_{i,F_1}}{\partial\phi_{F_2}}\right) - \phi_i\phi_{F_1}^2\left(\frac{\partial\chi_{i,F_1}}{\partial\phi_{F_1}}\right) - \left(\frac{V_i^{vdw}}{V_{F_2}^{P}}\right)\phi_{F_1}\phi_{F_2}^2\left(\frac{\partial\chi_{F_1,F_2}}{\partial\phi_{F_2}}\right) \\ & - \left(\frac{V_i^{vdw}}{V_{F_2}^{P}}\right)\phi_{F_1}\phi_{F_2}^2\left(\frac{\partial\chi_{F_1,F_2}}{\partial\phi_{F_1}}\right) - \phi_i\phi_{F_1}\phi_{F_2}^2\left(\frac{\partial\chi_{i,F_1,F_2}}{\partial\phi_{F_1}}\right) - \phi_i\phi_{F_1}^2\phi_{F_2}\left(\frac{\partial\chi_{i,F_1,F_2}}{\partial\phi_{F_2}}\right) \\ & - \chi_{i,F_1,F_2}\phi_{F_1}\phi_{F_2}(1-2\phi_i)\end{aligned} \tag{II.53}$$

with χ_{i,F_1,F_2} being a ternary Flory-Huggins coefficient whose contribution can be neglected in the absence of a specific ternary complex in the solution. The binary Flory-Huggins coefficient

between water (F1) and ethanol (F2) is obtained from the molar heat of mixing of the mixture, $\Delta H^{molar}_{F_1+F_2}$, as $\chi_{F_1,F_2} = y_{F_2}(1-\phi_2)\frac{\Delta H^{molar}_{F_1+F_2}}{RT}$, using the polynomial approximation proposed for water-ethanol mixtures in Boyne and Williamson (1967). **Figure II-22** reports the value of $\chi_{water,ethanol}$ with the volume fraction in ethanol as well as the values for common food simulants expressed in alcohol-by-volume (abv) instead of volume fraction. The volume fractions ethanol and water in the mixture are tabulated from their partial molar volumes between 10°C and 60°C in **Table II-12**.

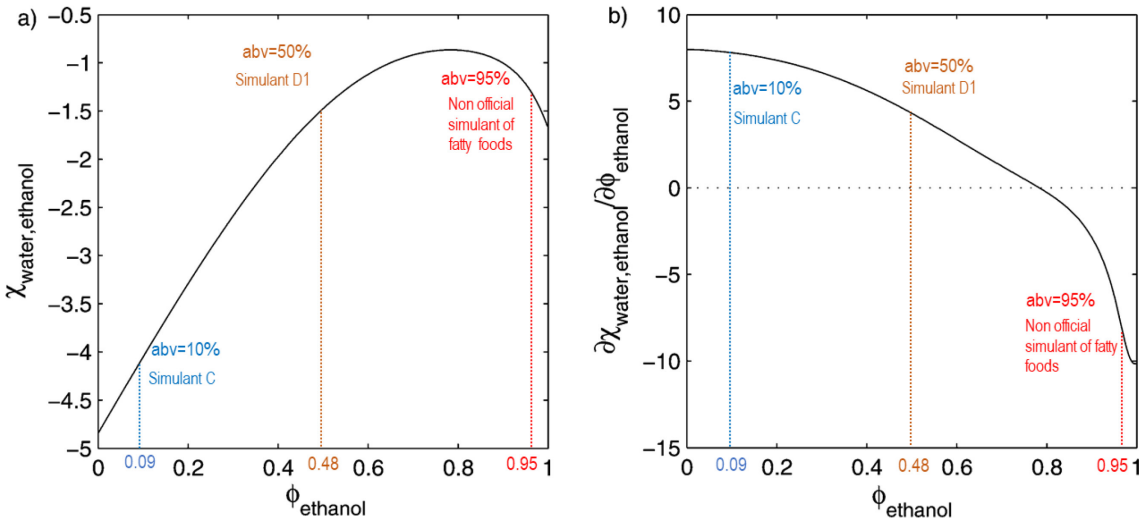

***Figure II-22**. Variation of the binary Flory-Huggins coefficient in water-ethanol mixtures. Data from Gillet et al. (2010). "abv" values represent the equivalent alcohol strength (alcohol-by-volume at 20°C and atmospheric pressure). Simulant C: 10% ethanol for alcoholic foodstuffs; simulant D1: 50% ethanol for high alcoholic and milk.*

***Table II-12**. Density (kg·m⁻³) of water-ethanol mixture and corresponding volume fraction of ethanol ($\phi_{ethanol}$) between 10 and 60°C. Volume fractions are calculated from partial molar volumes.*

abv (%)	10°C		20°C		30°C		40°C		60°C	
	$\rho_{mixture}$ ($kg \cdot m^{-3}$)	$\phi_{ethanol}$	$\rho_{mixture}$ ($kg \cdot m^{-3}$)	$\phi_{ethanol}$	$\rho_{mixture}$ ($kg \cdot m^{-3}$)	$\phi_{ethanol}$	$\rho_{mixture}$ ($kg \cdot m^{-3}$)	$\phi_{ethanol}$	$\rho_{mixture}$ ($kg \cdot m^{-3}$)	$\phi_{ethanol}$
5	992.6087	0.0463	991.0594	0.0465	988.4199	0.0466	984.8805	0.0467	975.3125	0.0473
7	990.0815	0.0640	988.4460	0.0643	985.7365	0.0646	982.1110	0.0650	972.3164	0.0660
10	986.5772	0.0903	984.7554	0.0912	981.8636	0.0920	978.0521	0.0928	967.9100	0.0938
12	984.3969	0.1080	982.3832	0.1092	979.3060	0.1103	975.3416	0.1113	965.0044	0.1125
15	981.3355	0.1339	978.9701	0.1356	975.5866	0.1372	971.3450	0.1386	960.6287	0.1407
20	976.6829	0.1773	973.5916	0.1800	969.5825	0.1826	964.7720	0.1847	953.2020	0.1883
30	967.1218	0.2695	962.2368	0.2739	956.6964	0.2775	950.5944	0.2807	937.1834	0.2857
40	954.5007	0.3722	948.0405	0.3755	941.2003	0.3789	933.9794	0.3816	918.9400	0.3863
50	937.5325	0.4773	930.1519	0.4795	922.4957	0.4816	914.5695	0.4837	898.2414	0.4877
60	917.0055	0.5812	909.1314	0.5828	901.0173	0.5844	892.6443	0.5859	875.3261	0.5894
70	893.7478	0.6847	885.5598	0.6858	877.1417	0.6869	868.4696	0.6883	850.5234	0.6908
80	867.6778	0.7889	859.2628	0.7896	850.6228	0.7906	841.7478	0.7915	823.5828	0.7929
90	837.7669	0.8940	829.2000	0.8946	820.4500	0.8950	811.4700	0.8954	792.9257	0.8971
95	819.9502	0.9478	811.3845	0.9479	802.6589	0.9481	793.7375	0.9482	774.9002	0.9491
99	802.7596	0.9900	794.2436	0.9900	785.6217	0.9901	776.8538	0.9901	758.1182	0.9900

II.2.5.2.4. Binary Flory-Huggins coefficients in a copolymer AB

Based on calculations at the molecular scale, Nguyen *et al.* (2017) demonstrated that Eq. (12) in Fornasiero *et al.* (2002) was acceptable for copolymers consisting of repeated blocks shorter than the persistence length of polymer segments. Beyond its persistence length, the polymer losses memory of its configuration and a block polymer can be treated as a polymer blend. The corresponding Flory-Huggins interaction coefficient in a copolymer AB, $\chi_{i,(AB)}$, reads:

$$\chi_{i,(AB)} = \chi_{i,A}\phi_A + \chi_{i,B}\phi_B - \chi_{AB}\phi_A\phi_B \quad \text{(II.54)}$$

Eq. (II.54) is based on an averaging of all possible contacts between $i-A$ and $i-B$, where the term $\chi_{AB}\phi_A\phi_B$ represents the additional cohesion energy brought about by the interactions between A and B. It can be generalized to more complex copolymers while the contacts can be assumed perfectly random (*i.e.*, no macro- or microphase separation).

II.2.5.3. High throughput calculations of Flory-Huggins coefficients at atomistic scale

II.2.5.3.1. Justification and limitations

Molecular modeling offers a good alternative to time-consuming and complex experiments to estimate Flory-Huggins coefficients for various substances: monomers, oligomers, solvent, additives, residues, breakdown products, and non-intentionally added substances. The results can be tabulated in advance and used directly with Eqs. (II.50)-(II.54) for a broad range of applications. In this respect, they are more intrinsic than partition coefficients. In detail, molecular modeling can be seen as an alternative to earlier group contribution methods relying on estimating Flory-Huggins coefficients from solubility parameters (Hansen, 2007;van Krevelen and te Nijenhuis, 2009). The limits of the approach have been discussed in Gillet *et al.* (2009) and compared with calculations at the atomistic scale. In short, group contribution methods provide only an average picture of the interactions. The real conformation of molecules and the distance between interacting chemical groups are, in particular, not preserved. The principles of calculation of $\chi_{i,P}^{(T)}$ and $\chi_{i,F}^{(T)}$ have been reviewed (Gillet *et al.*, 2009;Gillet *et al.*, 2010;Vitrac and Gillet, 2010;Nguyen *et al.*, 2016;Nguyen *et al.*, 2017). They apply to any homo- and copolymer as well as almost any solute while no net charge is present on the polymer, on the food simulant or the solute. The main limitations are intrinsic to the Flory approximation itself: no energetic barrier should exist in the host system (P and F) so that all states are accessible. It is not true in glassy polymers where hysteresis is frequent.

The contribution of the subcooling and accumulated elastic energy can be introduced *a posteriori* by combining Flory and free-volume theories (Krüger and Sadowski, 2005;Kadam *et al.*, 2014). These extensions are beyond the scope of this work.

II.2.5.3.2. Principles

The Flory-Higgins coefficient $\left\{\chi_{i,k}\right\}_{k=P,F}$ is defined as the dimensionless mixing energy (enthalpy) in excess relative to pure compounds:

$$\chi_{i,k}^{(n_k,T)} = \frac{\left\langle h_{i+k}^{n_k}\right\rangle_T + \left\langle h_{k+i}^{n_k}\right\rangle_T - \left\langle h_{k+k}^{n_k}\right\rangle_T - \left\langle h_{i+i}\right\rangle_T}{2RT} \text{ for } k = P, F \tag{II.55}$$

where $\left\langle X\right\rangle_T$ represents an ensemble-average of X, n_P is the length used in the approximation of the polymer and $n_F = 1$. In agreement with the original Flory approximation, enthalpies $\left\langle h_{A+B}\right\rangle_T$ are estimated by summing energies of contact ϵ_{AB} when B is contacting the seed molecule A. $\left\langle h_{B+A}\right\rangle_T$ represents the same energy when B is used as a seed molecule. In practice, ϵ_{AB} is calculated by choosing an orientation randomly for the contact molecule and by translating it along a random line until at least one point of contact is established between the van der Waals surfaces of the contact and seed molecules. The process is repeated for all conformers and stereoisomers considered. Finally, h_{A+B} is estimated as the product of contact energies and the number of neighbors z_{AB} (number of B molecules surrounding A):

$$\left\langle h_{A+B}\right\rangle_T = \left\langle n_{cooperative} z_{AB}\varepsilon_{AB}\right\rangle_T \approx n_{cooperative}\left\langle z_{AB}\right\rangle\left\langle \varepsilon_{AB}\right\rangle_T \tag{II.56}$$

Eq. (II.56) assumes that ϵ_{AB} and z_{AB} are statically independent (zero covariance). For polymers, the property of independence is achieved from a sufficiently large n_P value so that the surface of contact of the polymer is independent of the length of the considered polymer. The main advantage of the whole approach is that there is no need to represent entanglements in the polymer and free-volume. The shape of the backbone of an infinitely long chain with shorter oligomers prevents head and tail atoms from coming in contact with any van der Waal surface. Cooperative hydrogen bonding is accounted for by using a value of $n_{cooperative}$ greater than one. The latent heat of vaporization of water can be correctly approximated by $\left\langle h_{water+water}\right\rangle_T$ using a value of $n_{cooperative}$ different to unity. This value depends on the type of forcefield used to simulate water. As an example, the rigid water model governed by the TIP4P forcefield gives an acceptable value with $n_{cooperative} = 1$ whereas $n_{cooperative} = 4$ is required with the same forcefield but using three-point charges (forcefield TIP3P). The number 4 reinforces

in this case that any water molecule is on average involved in 4 hydrogen bonds of similar strength.

Contact energies are calculated irrespective of any temperature consideration. The effect of temperature is recovered by weighting the distribution of contact energies with the Boltzmann factor $B(\epsilon)$:

$$\left\langle \varepsilon_{AB} \right\rangle_T = \frac{\int_{-\infty}^{+\infty} pr(\varepsilon) B(\varepsilon) \varepsilon d\varepsilon}{\int_{-\infty}^{+\infty} pr(\varepsilon) B(\varepsilon) d\varepsilon} \text{ with } \mathrm{B}(\varepsilon) = \exp\left(-\varepsilon / (RT)\right) \tag{II.57}$$

At the price of calculating two integrals, Eq. (II.57) can be used to estimate $\chi_{i,k}^{(n_k,T)}$ at several temperatures. Conformers need to be generated in a way that they are representative of their conformations (radial distribution, constraints of torsion) in the corresponding condensed phase. In practice, they are sampled from molecular dynamics simulations of the equivalent condensed phase.

II.2.6. Probabilistic modeling of the migration

II.2.6.1. Beyond intuition

Any risk assessment procedure needs to account for the possible variabilities in the considered scenario (e.g. variable temperature, contact time) and the numerous sources of uncertainties inherent in the limitations of our knowledge and oversimplifications. Variability and uncertainty can be easily recognized and separated by noticing that only uncertainty can be reduced by bringing additional knowledge or refinement. By contrast, variability represents multiple values of several instances (lots, compositions, final use), storage conditions, etc. For compliance testing, conservative assumptions are mandatory, but the relationship between the maximization of parameters (or their minimization depending on the case) and the maximization of the amount transferred is straightforward only in simple configurations: one material or one single layer, one step, and no variable conditions.

The intuitive approach is illustrated in **Figure II-9** for a single component and monolayer packaging in contact with food. When the whole food-packaging system is perfectly impervious (no loss to the outside), the cumulative amount leaving the packaging-food interface is a monotonic function of the time, the initial concentration, the diffusion coefficient in the polymer, the chemical affinity for food, the temperature, etc. As a result, choosing a conservative or upper bound for all inputs guarantees an overestimation of the food contamination. In the presence of multiple materials or steps, the property of monotonicity between parameters and inputs is not mathematically verified anymore. In particular, food contamination can be

maximal before reaching equilibrium. For example, overestimating all diffusion coefficients or partition coefficients in laminates will spread migrants everywhere instead of bringing them faster to the contacting phase. For laminates, methods described in §II.2.3.5.6. and theorized in Vitrac and Hayert (2007a) can be used to recover conservative estimates. The calculation procedure consists of splitting the contribution of n components/materials into $m \leq n$ independent simulations and in accumulating the concentration in food: $\left\{C_{i,F}^{k}\right\}_{k=1..m}$. The algorithm is sketched for a substance i present simultaneously in the walls (bilayer AB, B is contact) and the cap of the bottle (C). The problem comprises $n=3$ materials and requires $n=2$ simulations:

- One-dimension mass transfer simulation from B to the food (without A and C) to calculate $C_{i,F}^{B}$
- One-dimension mass transfer simulation from C to food (without A and B, *i.e.* no walls).

It is worthwhile noting that the scenario described is also conservative if it is assumed that the substance has been distributed between A and B before being put in contact with the food. It also covers the case when i is initially located in A and not in B (see **Figure II-11**), but with a higher safety margin.

II.2.6.2. Epistemic uncertainty

In systems engineering, reliability and safety are quantified with respect to some safety margins, defined as the differences between reference values accepted by the regulating body and calculated values. A system is considered safe when the differences calculated for a set of postulated scenarios verify a minimum distance or when the probability of the distance being zero or negative is lower than some prescribed value. Introducing conservatism randomly by mixing worst-case bounds may propagate uncertainty and lead to uncontrolled overestimation of the amount transferred to the food. At the beginning of the supply chain, the chemical industry and compounders face mainly variability with the different applications of their chemicals and raw materials. On the opposite side of the supply chain, the packaging filler and the retailers face a more different situation with strong uncertainties on the nature of the materials, their thicknesses, and their composition. In 2009 and despite the possibilities offered by EU directive 2002/72/EC (2002), migration modeling was evaluated to see if it could be helpful to demonstrate compliance in finished products; it was only in less than 5% of cases (Gillet *et al.*, 2009). The chief reason was the loss of compositional information along the supply chain. Calculations could be done on part supplies and compounds to produce certificates of food contact compliance, but not on the full system assembled in the intended conditions of use of the packaging. Compositional information is currently better shared in the EU and new

deformulation techniques provide grounds for spreading calculation practices from the chemical industry to the food industry (Nguyen *et al.*, 2015).

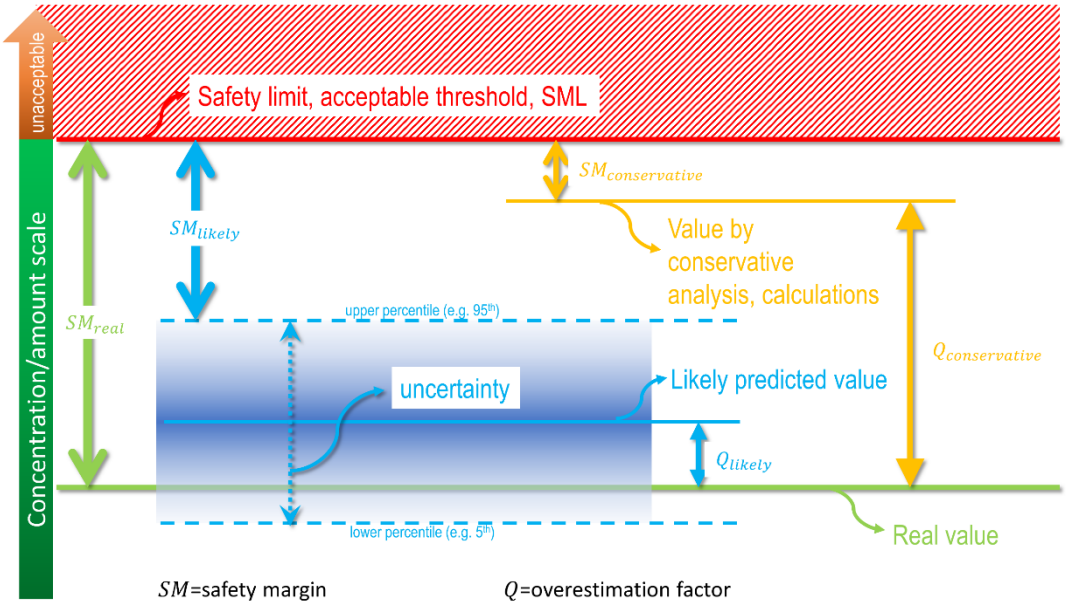

***Figure II-23**. Illustration of safety margins (SM), overestimation factors (Q) and uncertainty according to the method of calculation: real, likely and very conservative.*

The best practice for industry relies on sharing minimal information so that a significant safety margin remains for the end-user and keeping the utility of migration modeling. As an illustration, **Figure II-23** compares the safety margins when over-conservative estimates and realistic overestimates are used. It is worth noting that the location of the "real" value is not usually known so that the overestimation factor cannot be guessed *a priori*. Only the safety margin is directly accessible to calculations. The definition of the safety margin and its use in various technical guides and supporting risk assessment documents can be inconsistent and confusing. In particular, the concept of safety margin is frequently confused with the concept of overestimation. The definition of safety margin used here is applied in medicine to evaluate drugs, in structural engineering, and in nuclear engineering, The concept of overestimation applied to some factors including diffusion (D_P) and partition coefficients ($K_{F/P}$)can be misleading. Indeed, their overestimation by a factor Q_X causes an overestimation of the concentration in the medium in contact which is not proportional. For the layer in contact, it varies from $\sqrt{Q_{D_P}}$ (short contact times) down to 0 (equilibrium) for diffusion ($X = D_P$) . For $X = K_{F/P}$, it increases from 0 to a value which depends on the volume of the food.

By evaluating the uncertainty associated with realistic estimates, probabilistic modeling offers a robust methodology to assess the effects of the combined sources of uncertainties and finally to have no safety margin at all. The example depicted shows that the upper limit of

likely overestimates including uncertainty (95th percentile) offers a higher safety margin than the very conservative overestimate. The distinction between overestimations and realistic conservative estimates can be exemplified by considering a long contact at a variable temperature (e.g. due to transportation). A conservative estimate will calculate migration at the highest temperature, whereas a realistic conservative value will be provided by replacing time with its integral dimensionless version, Fourier number, $Fo = \int_{t_1}^{t_2} \frac{D(T(t))dt}{l^2}$. The proposed approximation does not introduce any significant approximation and can be carried out at the same cost as standard simulations (see §II.2.3.6. and Eq. (II.28)).

II.2.6.3. Sensitivity analysis of migration models

II.2.6.3.1. Local sensitivity analysis

Deterministic modeling and simulation yield the same output (concentration in food, concentration profile in the packaging material) for the same set of inputs. The analysis of the sensitivity to input parameters entails evaluating the effect of a modification of each parameter $\{p_k\}_{k=1..N}$ (initial concentration, diffusion coefficient, partition coefficient, etc.) on the safety margin, SM. Since the parameters have different units, it is convenient to calculate the derivatives of SM with respect to the logarithm of each parameter:

$$\begin{aligned}\mathbf{J}(\mathbf{p}) = \mathbf{J}\left(\left[p_1 \cdots p_N\right]^T\right) &= \left[\left.\frac{\partial SM}{\partial p_1}\right|_{p_2..p_N} p_1 \cdots \left.\frac{\partial SM}{\partial p_N}\right|_{p_1..p_{N-11}} p_N\right] \\ &= \left[\left.\frac{\partial SM}{\partial \ln p_1}\right|_{p_2..p_N} \cdots \left.\frac{\partial SM}{\partial \ln p_N}\right|_{p_1..p_{N-11}}\right]\end{aligned} \quad \text{(II.58)}$$

$\mathbf{J}(\mathbf{p})$ is the Jacobian matrix of the migration model and it can be used to evaluate a linear approximation of the safety margin when inputs are changed from $\mathbf{p_0}$ to $\mathbf{p}$:

$$SM(\mathbf{p}) \approx SM(\mathbf{p}_0) + \mathbf{J}(\mathbf{p}_0)(\ln \mathbf{p} - \ln \mathbf{p_0}) \quad \text{(II.59)}$$

Eq. (II.59) provides analytical solutions only in simple configurations, but its application is very general. Additionally, implementing the difference $\ln p_k - \ln p_{k,0}$ as $\ln \frac{p_k}{p_{k,0}}$ prevents the problem of step size known as subtractive cancellation. Its usage is shown for a variant of the realistic but conservative model for monolayer materials presented in §II.2.3.4. (see Eq. (II.18)):

$$\lceil C_F \rceil_{(Fo,K_{F/P},C_p^0)} \approx \frac{C_p^0}{\frac{1}{K_{F/P}}+\frac{1}{L_{P/F}}} \lceil \overline{v}^* \rceil_{(Fo)} \le \frac{2}{\sqrt{\pi}} \frac{C_p^0}{\frac{1}{K_{F/P}}+\frac{1}{L_{P/F}}} \min\left(\frac{\sqrt{\pi}}{2}, \sqrt{Fo}\right) \quad \text{(II.60)}$$

When the input values are changed to $\left[Fo=\frac{D_P t}{l_P^2}, K_{F/P}, C_p^0\right]$ from an initial set $\left[\overline{Fo}=\frac{\overline{D_P}t}{l_P^2}, \overline{K_{F/P}}, \overline{C_p^0}\right]$, the safety margin $SM_{\left(Fo,K_{F/P},C_p^0\right)} \approx SML - \lceil C_F \rceil_{\left(Fo,K_{F/P},C_p^0\right)}$ becomes:

$$\begin{aligned} \frac{SM_{\left(Fo,K_{F/P},C_p^0\right)} - SM_{\left(\overline{Fo},\overline{K_{F/P}},\overline{C_p^0}\right)}}{\overline{\lceil C_F \rceil}} &\approx 1 - \frac{\lceil C_F \rceil}{\overline{\lceil C_F \rceil}} \\ &= -\left[\frac{1}{\overline{K_{F/P}}} \frac{1}{\frac{1}{\overline{K_{F/P}}}+\frac{1}{L_{P/F}}} \ln\left(\frac{K_{F/P}}{\overline{K_{F/P}}}\right) + \ln\left(\frac{C_P^0}{\overline{C_P^0}}\right) + \frac{1}{2}\ln\left(\frac{\min\left(\frac{\sqrt{\pi}}{2}, \sqrt{\mathrm{Fo}}\right)}{\min\left(\frac{\sqrt{\pi}}{2}, \sqrt{\overline{\mathrm{Fo}}}\right)}\right)\right] \end{aligned} \quad \text{(II.61)}$$

with Fo $\overline{\lceil C_F \rceil} = \frac{2\overline{C_P^0}}{\sqrt{\pi}} \frac{\min\left(\frac{\sqrt{\pi}}{2}, \sqrt{\overline{\mathrm{Fo}}}\right)}{\left(\frac{1}{\overline{K_{F/P}}}+\frac{1}{L_{P/F}}\right)}$.

Besides showing the interactions and additivity of the different sources of uncertainty, it offers a rapid methodology to identify the main influencing parameters without requiring any simulation or software. Eq. (II.58) also applies to numerical simulations, but it requires $N+1$ simulations (the reference one and N variations). When the number of inputs increases, it is preferable to reduce the computational effort by using similitude principles and dimensionless numbers. In the detailed example, the use of a dimensionless time $Fo=\frac{D_P t}{l_P^2}$ enables simultaneous testing of the effects of t, D_P and l_p. Eq. (II.58) is a first order approximation and, despite the use of a logarithm scale, it looses accuracy as soon as parameters are tested beyond several factors.

II.2.6.3.2. Global sensitivity analysis via stochastic simulation

When the number of variables becomes large as well as the intervals to be explored, the statistical sampling of inputs is preferable. Statistical analysis of the outputs can be used to extract the influence of each variable and the probability to have the prescribed threshold exceeded. Each component of the vector $\mathbf{p}$ needs to be sampled randomly and uniformly over its interval of interest. The technique is the so-called Monte-Carlo trials and its numerical implementation stochastic simulation. By denoting $\left\{\tilde{\mathbf{p}}_{k,i}\right\}_{i=1..M}$ M samples chosen around the

likely vector $\overline{\mathbf{p}}$ so that only the parameter $\{p_k\}_{k=1..N}$ is modified at a time, and by denoting $\left\{SM\left(\tilde{\mathbf{p}}_{k,i}\right)\right\}_{i=1..M}$ the corresponding safety margins, the sample covariance is given by:

$$\mathbf{V_{SM}} = \frac{1}{M-1}\sum_{i=1}^{M}\left(SM\left(\tilde{\mathbf{p}}_{k,i}\right)-\left\langle SM\left(\tilde{\mathbf{p}}_{k,i}\right)\right\rangle\right)\left(SM\left(\tilde{\mathbf{p}}_{k,i}\right)-\left\langle SM\left(\tilde{\mathbf{p}}_{k,i}\right)\right\rangle\right)^{T} \quad \text{(II.62)}$$

where $\left\langle SM\left(\tilde{\mathbf{p}}_{k,i}\right)\right\rangle = \frac{1}{M}\sum_{i=1}^{M} SM\left(\tilde{\mathbf{p}}_{k,i}\right)$ is the average safety margin, which does not coincide with $SM\left(\overline{\mathbf{p}}\right)$ in the general case. $SM\left(\overline{\mathbf{p}}\right)$ represents the prediction associated with the 50th percentile.

Eq. (II.62) generalizes the local sensitivity analysis performed in Eq. (II.58), based on small variations and partial derivatives. The concept of covariance enables screening of the whole input spectrum to identify the interaction and dependency structure on all parameters including the analysis. If the geometry, temperature and contact time are introduced, the design and conditions of use can also be explored.

A probabilistic interpretation is achievable but, as means and covariances provide only the first and second moments, a likely distribution of the safety margin or the concentration in food is required. If the concentration in food is normally distributed, the problem is fully determined with the first and second moments. This assumption is valid only in the presence of a low range of variabilities and uncertainties. Indeed, the Gaussian distribution is unbounded, and it implies, even with very low probabilities, that the concentration in food could also be negative and the amount transferred could be higher than the amount in the material. The next section removes these limitations for risk assessment and the evaluation of consumer exposure.

II.2.6.4. Principles of the probabilistic interpretation of mass transfer

Global sensitivity analysis presented in II.2.6.3.2. introduces the first interpretation of mass transfer with a marginal distribution on each input variable, which is assumed to be uniform. The combination of these variables and its interpretation is known as a copula in probability theory and statistics. Copulas describe well the dependence between inputs on the output(s) of a model, but they fail to describe the joint distribution of contamination in realistic situations. The diffusion and partition coefficients, as well as the initial concentration in food, are not distributed uniformly. The industry is not applying randomly any concentration value or the molecules do not have random properties. It is because of limited knowledge and the variability of practices that spread the inputs around a likely value. In short, the sensitivity analysis is a perfect tool to optimize the geometry, formulation, etc. but it is not appropriate to get a reliable estimate of the probability to have a concentration threshold exceeded.

The principles of probabilistic modeling of migration have been described in Vitrac and Hayert (2005) and applied to various cases (Vitrac *et al.*, 2007a;Vitrac and Leblanc, 2007). The central idea is to combine a dimensionless formulation (with a reduced number of input variables) along with random numbers. For the same reason as invoked for the local decomposition in §II.2.6.3.1. , each quantity X is written as the product of a scaling value (with units), denoted $\overline{X}$ (usually the likeliest value), and a random dimensionless number X^* distributed around unity. As an illustration, the dimensionless time reads:

$$Fo = \frac{\left(\bar{D}D^*\right)\left(\bar{t}t^*\right)}{\left(\bar{l}l^*\right)^2} = \frac{\bar{D}\bar{t}}{\bar{l}^2}\frac{D^*t^*}{l^{*2}} = \overline{Fo}Fo^* \qquad \text{(II.63)}$$

II.2.6.4.1. Input distributions

The distributions of X^* can be chosen either from experimental measurements or from prior guesses or beliefs. In this second alternative, distributions which have a shape factor and are non-negative, denoted $f_X\left(1, s_X\right)$, should be preferred (beta, Erlang, exponentially modified Gaussian, exponential, gamma, inverse-gamma, inverse-Gaussian, lognormal, Weibull, etc.). For some quantities, such as concentrations or thicknesses, symmetric distributions are more realistic; truncated normal distributions can be used for this purpose. A non-exhaustive list of practical distributions is given in **Table II-13**.

Table II-13*. Recommended distributions for probabilistic modeling of the migration from monolayer materials. The distributions of* $\bar{v}^*$ *and* $\sqrt{Fo^*}$ *are posterior distributions.*

random contribution		distribution	recommendations	
			rubber polymers	glassy polymers
diffusion coefficient	$\log_{10} D_P^*$	$Norm\left(O, s_D\right)$	$s_D = 0.1$	$s_D = 0.5$
contact time	t^*	$Weib\left(1, s_t\right)$†	s_t to be determined	
initial concentration	C_P^{0*}	$Norm\left(1, s_{C_0}\right)$ truncated†	$1 \le s_{C_0} \le 5$	
thickness	l^*	$Norm\left(1, s_l\right)$	s_l to be determined	
mass Biot number	$\log_{10} Bi^*$	$Norm\left(O, s_{Bi}\right)$	$s_{Bi} \to 0$	$s_{Bi} \to 0$
partition coefficient	$\log_{10} K_{F/P}^*$	$Norm\left(O, s_K\right)$	< 0.2	< 0.2
Fourier number	$Fo^{*\frac{1}{2}}$	$Gamma\left(a_\Gamma, b_\Gamma\right)$	a_Γ, b_Γ : to be calculated	
concentration in food	$\bar{v}^*$	$Beta\left(a_\beta, b_\beta\right)$	a_β, b_β : to be calculated	

† *to be normalized to get a unitary expectation.*

II.2.6.4.2. Estimation of probabilities via Monte-Carlo sampling

Probabilistic modeling aims at determining the cumulative density function (cdf), which can be written for monolayer materials as the probability to get a value of C_F lower than an arbitrary number x :

$$pr\left(C_F \le x\right) = F\left(\overline{Fo}, \overline{Bi}, \overline{K_{F/P}}, \overline{C_P^0}, a_\Gamma, b_\Gamma, s_{K,} s_{Bi}, s_C\right) \tag{II.64}$$

For the sake of efficiency, Fo (see Eq. (II.63)) was used instead of $\left(\bar{t}, \overline{D_P}, \overline{l_P}, s_t, s_D, s_l\right)$. Indeed using Eq. (II.13), it can be shown that the distribution *a posteriori* of $\sqrt{Fo^*}$ converges in law to a Gamma distribution with parameters $\left(a_\Gamma, b_\Gamma\right)$. Nguyen *et al.* (2015) tabulates their values with s_t , s_D and s_l.

The cumulated probability $pr\left(C_F \le x\right)$ (or its complement $pr\left(C_F > x\right)$) can be estimated by repeating the simulations for different values of input parameters and by counting the number of occurrences for which the inequality $C_F \le x$ (or $C_F > x$) is verified. If the intent is to demonstrate that $pr\left(C_F > x\right)$ is low for a sufficiently large x, it might be thought that it suffices to apply some worst-case scenarios (bounds of intervals) and to demonstrate that the value x is never exceeded. This approach is correct only if $pr\left(C_F > x\right) = 0$, that is for a value of x larger than the one corresponding to a total extraction. In the general case, the intervals of all parameters need to be sampled with each value chosen according to its theoretical prescribed distribution. This technique of randomly picking input values and launching the corresponding simulation is known as Monte-Carlo simulation.

In practice, for each input quantity X, a random number g is chosen uniformly between 0 and 1 (function rand() in many programming languages). The specific value to be included in the considered simulation vector will be $F_X^{-1}\left(g\right)$, with $F_X\left(x\right) = pr\left(X \le x\right)$ being the cdf of the variable X. Depending on the size of the intervals, 10^3 to 10^5 simulations are required. For multilayer materials, the sampling effort can be even higher. The total cost of simulations can be reduced dramatically by tabulating the results in advance for a significant range of dimensionless numbers and by subsequently interpolating the values of interest. These concepts are now justified mathematically. They make the cost of probabilistic modeling close to the cost of deterministic modeling.

II.2.6.4.3. Estimation of joint probabilities via the composition theorem

The calculation of probability density functions (pdf) associated with a combination of variables $X_1,\cdots,X_n$ *(e.g., Eq.* (II.*63)) or with the resolution of partial differential equations is particularly expensive computationally and requires a specific treatment of the joint density* $f_{X_1,\cdots,X_n}\left(x_1,\cdots,x_n\right)=pr\left(X_1=x_1,\cdots,X_n=x_n\right)$. The composition theorem offers a very efficient computational approach for invertible and differentiable transformations:

$$\begin{aligned} Y_i &= h_i\left(X_1,\ldots,X_n\right);\ i=1,\ldots,n \\ X_i &= h_i^{-1}\left(Y_1,\ldots,Y_n\right);\ i=1,\ldots,n \end{aligned} \tag{II.65}$$

Mathematical functions $\left\{h_i\right\}_{i=1..n}$ represent either a variable transformation (e.g., Eq. (II.63)) or the full mass transfer model. The joint density of $Y_1,\cdots,Y_n$ is given by the determinant of the Jacobian matrix $\partial h_i / \partial x_i\big|_{x_{j\neq i}}$, denoted J_g:

$$\begin{aligned} &f_{Y_1,\cdots,Y_n}\left(y_1,\cdots,y_n\right)= \\ &f_{X_1,\cdots,X_n}\left(h_1^{-1}\left(y_1,\cdots,y_n\right),\cdots,h_n^{-1}\left(y_1,\cdots,y_n\right)\right)\cdot\left|J_g\left(h_1^{-1}\left(y_1,\cdots,y_n\right),\cdots,h_n^{-1}\left(y_1,\cdots,y_n\right)\right)\right|^{-1} \end{aligned}$$

(II.66)

Eq. (II.66) can be generalized to non-monotonic functions by splitting the transformation into intervals which are locally monotone. For example, in the special case where the dimensionless concentration in food $\overline{v}^*$ is not a continuous function of Fo (some multilayer or multicomponent configurations), the pdf of $\overline{v}^*=h\left(Fo\right)$ is obtained by the accumulation of the p transformations over p contiguous intervals:

$$f_{\overline{v}^*}\left(v\right)=\sum_{k=1}^{p} f_{Fo}\left(\overline{v}^{*-1}\Big|_{Fo\in Y_k}\left(v\right)\right)\left|\frac{d}{dv}\overline{v}^{*-1}\Big|_{Fo\in Y_k}\left(v\right)\right|^{-1} \tag{II.67}$$

with $\left\{Y_k\right\}_{k=1..p}$ the partitions of Fo where $\overline{v}^*=h\left(Fo\right)$ is piecewise monotonic.

II.2.6.5. Some illustrations

Probabilistic modeling must be envisioned as the generalization of deterministic modeling, but its clear definition depends on how the normalization of X^* is performed, how deterministic inputs are set (likeliest values or averaged ones) and how the transformation stretches or contracts the probability space. Deterministic modeling provides the unique solution of the initial-value problem. Probabilistic modeling generates the distributions of outputs (e.g., C_F) for any combination of input parameters and initial conditions. The use of

dimensionless numbers such as a cumulated Fourier number including temperature variations $\int_0^t \frac{D_p\left(T\left(t\right)\right)}{l_p^2}dt$ or the ones associated with homologous solutes $\frac{\left\{D_{i,p}\right\}_{i\in\underset{\text{solutes}}{\text{homologuous}}}t}{l_p^2}$, offers an even broader interpretation by including random variations of temperature or uncertainty of diffusion coefficients (Vitrac et al.,2006). In the context of risk assessment, the scaling quantities $\overline{Fo}$, $\overline{Bi}$ and $\overline{K_{F/P}}$ as acceptable conservative estimates and the effects of uncontrolled variations and uncertainties can be captured with the distributions of Fo^* , Bi^* and $K_{F/P}^*$ or by choosing them equal to unity.

II.2.6.5.1. Typical probabilistic migration kinetics

Without loss of generality for estimating multivariate distributions of concentrations, the principles of composition are illustrated in **Figure II-24** for the dimensionless migration kinetics from monolayer materials (see. §II.2.3.4.). In this example, Fo^* is the only random variable and all other parameters remain fixed (not distributed). The distribution of the dimensionless concentration $\overline{v}^*$ is inferred from Eq (II.67) with $p=1$ (strictly monotonic curve). It can be viewed as the projection of the support of $Fo=\overline{Fo}Fo^*$ onto the curve $\overline{v}^*=f\left(Fo^*\right)$. When the transformation is repeated for different values for $\overline{Fo}$, the upper and lower percentiles of the migration kinetics can be interpolated continuously with Fo. Such curves are not accessible to the direct simulation and are not parallel to the deterministic or 50th percentile. The vertical distance between the extreme percentiles represent the resulting uncertainty in the amount transferred according to the original dispersion in Fo values. It is worthwhile noting that dispersion increases with time but that its effect on $\overline{v}^*$ is decreasing after $Fo>\frac{\sqrt{\pi}}{2}$. Close to equilibrium, Fo ceases to have a significant effect.

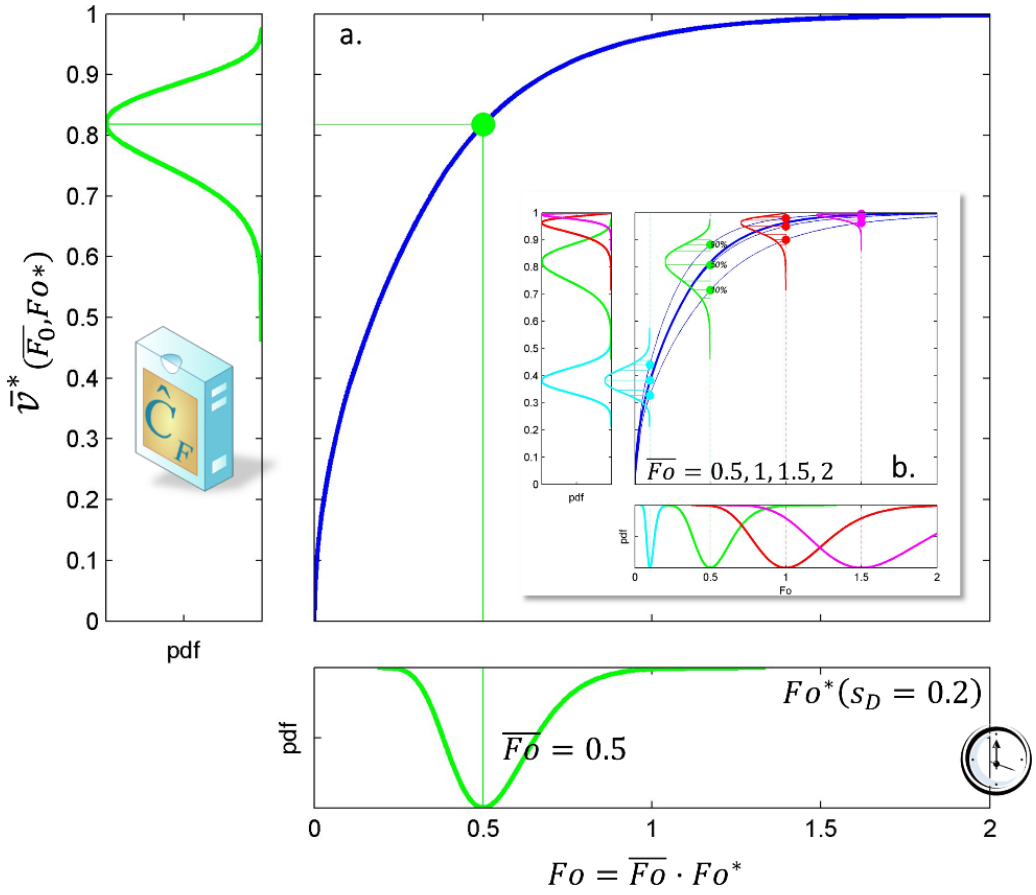

Figure II-24. *Probabilistic modeling of the contamination from a monolayer material via Eqs. (II.13) and (II.63): (a) point distribution for* $\overline{Fo} = 0.5$ *; (b) corresponding 10th and 90th percentile curves. The likeliest migration curve corresponding to the maximum probability (mode) of the Fo distribution appears in bold.*

II.2.6.5.2. Effect of Bi and S_D

The overall mass transfer resistance, $\Re$, of any compartment (either the food or the packaging layer) is evaluated as $\frac{kl}{D}$ or $\frac{l}{D}$, whether the chemical affinity of the substance is considered or not. For monolayer materials, the packaging-to-food mass transfer resistance ratio is given by $K_{F/P}Bi^{-1}$ and Bi^{-1}, respectively. Bi values are expected to be large above 10^3 with well-mixed and low viscous liquids in contact with thick or barrier polymers. Low values ranging between 5 and 10^3 were observed only in polyolefins in contact with liquids (Vitrac *et al.*, 2007b). In semi-solids, solids and dry foods in contact with polyolefins and plasticized polymers, migration kinetics linearize with time (Till *et al.*, 1987) and Bi approaches unity.

The effects of Bi and s_D are illustrated in **Figure II-25**. Increasing the mass transfer resistance on the food side (*i.e.* decreasing Bi) affects non-linearly the dispersion. As justified

by Eq. (II.67) and because the contamination is strictly increasing, the dispersion of the contamination is weighted by the term $\left|\frac{d}{dv}\bar{v}^{*-1}(v)\right|^{-1} = \frac{d\bar{v}^*}{dFo}(Fo)$. As low Bi values and large Fo ones lead to low slopes of $\bar{v}^*$ vs Fo , the dispersion of concentration values are, as expected, maximal for intermediate concentration values far from the initial and equilibrium states. Increasing s_D modifies strongly the shape of the median kinetics, the upper limits and the overall distribution in food. The depicted example demonstrates that the migration can be overestimated reliably by considering a likely value for $\overline{D_p}$ and by taking for example the 95th percentile of $\bar{v}^*$ along with a proper value of s_D. Doing the reverse, calculating $\bar{v}^*$ from the 95th percentile of values does not guarantee that the value of the contamination is overestimated in 95% of cases. It is not verified in the case when the slope of $\bar{v}^*$ changes rapidly with Fo. This is true only when $Bi \to 1$, as shown in **Figure II-25**a.

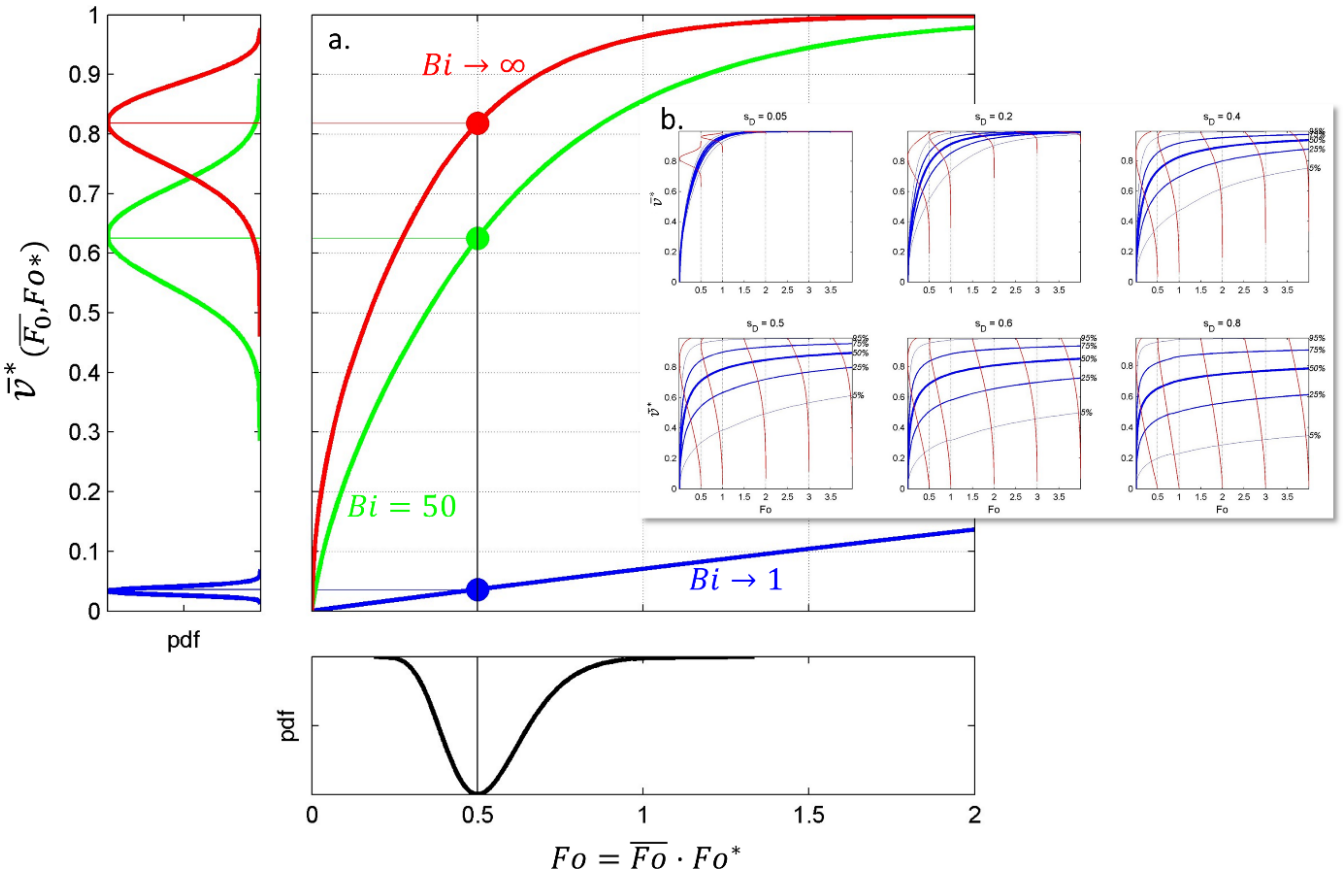

***Figure II-25**. (a) Effect of Bi on the dimensionless migration kinetics. (b) Effect for $Bi \to \infty$ (the percentiles are represented as equivalent kinetics; distributions of $\bar{v}^*$ for $\overline{Fo}$ =0.5, 1,2, 3 and 4.*

II.2.7. Generalized migration modeling and holistic approaches

II.2.7.1. Achievements

During the last decades, the scope of migration expanded to cover emerging risks, more complex conditions representative industrial practices until to consider closed recycling loops. The evolution of the state of the art is illustrated in **Figure II-26**. The capability of considering contamination scenarios from materials more distant to the food and occurring at early stages of the supply chain enabled a general review of causalities and critical industrial practices. Cross-contaminations between materials contributing to the redistribution of migrants between materials at all stages of the value chain are better understood. Many new contamination pathways, which does not require any direct contact, have been identified. A global science started to emerge beyond common mistaken beliefs: migration can be avoided, biosourced materials are safer, biodegradable and recycled materials can be used without a safety assessment. Migration modeling becomes an essential tool for high throughput evaluation of consumer exposure (Vitrac and Leblanc, 2007;Ernstoff *et al.*, 2017).

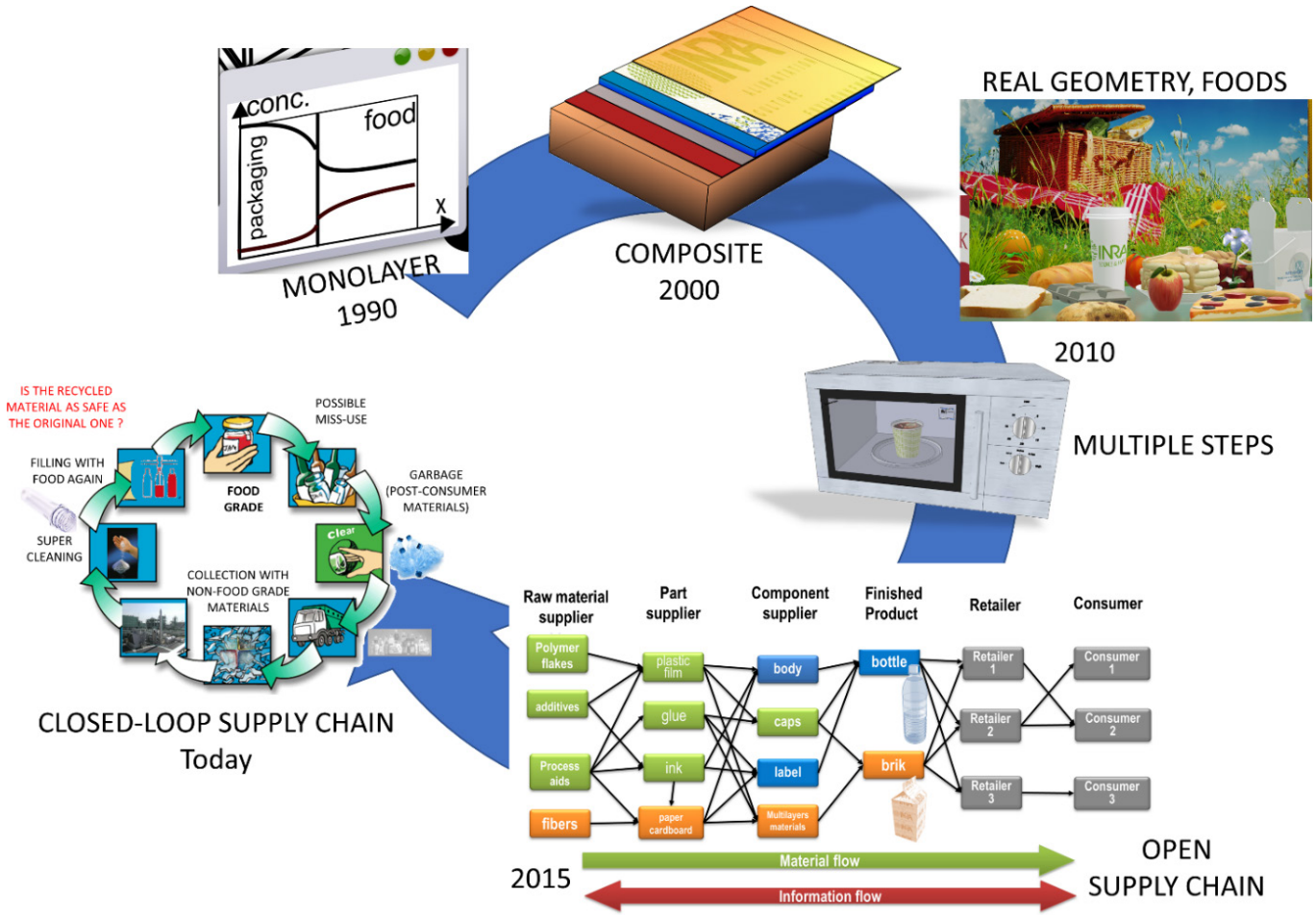

***Figure II-26**. Evolution of the scope of migration modeling during the last decades*

II.2.7.2. Acceptation of migration modeling and restrictions setup by authorities

A robust validation of the macroscopic equations of mass transfer (transport equations and boundary conditions) has been central to the development of the US legal system authorizing migration modeling in the nineties (Schwope *et al.*, 1990). The European system (Hoekstra *et al.*, 2015) focused during the two past decades on diffusion coefficients with much smaller attention on partition coefficients. In the US and EU cases, migration modeling is accepted for compliance testing, only for thermoplastics, as stated in EU regulation 10/2011/EC (2011a). Its application to thermosets, elastomers, paper and board is comparatively supported by a much small number of scientific and technical publications. Recently, Chinese regulation (GB, 2008) adopted migration modeling and equivalent calculations without material restriction. This move is a logical step after the substitution of negative lists by positive ones and the adoption of specific migration limits for a broad range of applications. The non-compliance cannot be determined by modeling and only direct measurements can be used by authorities to trigger a product recall.

II.2.7.3. The promises of multiscale migration modeling

The validations of functional barriers and recycled materials are the success-stories of migration modeling. Migration modeling, including multiscale modeling, offers the only viable solution to evaluate complex problems met by the food industry and the food packaging supply chain:

a. NIAS: non-intentionally added substances (no need for standards or analytical methods; hypothetical molecules can be accepted);
b. cross-contamination between materials at any stage of the supply chain (all configurations can be included);
c. post-consumer contaminations, including misuse
d. optimization of decontamination steps in mechanical recycling processes
e. materials and articles with repeated use (no need for long experiments)
f. materials and devices used with flows (no need for any setup)
g. materials subjected to aging and long-term storage.

NIAS include hypothetical and unknown substances (e.g., breakdown products), but also known impurities and substances intentionally present or added to third-party materials (printing inks, adhesives, lacquers, overpackaging, secondary packaging). All the cases can be evaluated by combining molecular and migration modeling. The same approaches can be used to optimize decontamination conditions (solvent choice, temperature, duration) in recycling processes.

II.2.7.4. Linking risk assessment and LCA

For construction materials, revised LCA methodologies have been proposed to include chronic effects on health (Csiszar *et al.*, 2016;Huang *et al.*, 2018b). This initiative could be extended to food packaging either by integrating some migration modeling into LCA or, in the other way around, by integration some LCA flavors along with migration modeling. Such extensions will have mutual benefits for all applications where the release of chemicals by materials is of concern.

Key points of II.2. Evaluation of the migration from packaging materials

Migration modeling is a mature subject authorized by law in the US, EU and more recently in China. It benefited the accumulation of data and numeric methods over several decades. Hierarchical modeling in a deterministic or stochastic manner is the best achievement. The nested approach remains transposable to many applications governed by mass transfer and thermodynamic problems. The current implementation remains, however, perfectible: (1) Free-volume theory of diffusion in polymers is originally a predictive theory for rigid solutes translating as a simple jumping unit. Extensions hold only for the same rigid units linearly repeated and in rubber polymers. A new parameterization is required for any new polymers. Several families such as polyesters, polyamides, polyvinyls are poorly or not documented. (2) Current diffusion models, while integrating plasticizing effects in some ways, neglect the interactions between solutes. (3) Mass transfer models are 1D and do not fulfill requirements for models with distributed thicknesses.

Migration modeling is objective and can be introduced in an automatic and semi-supervised decision-making process but at the cost of accepting significant safety margins. The concept of safety-margin is intrinsic to the philosophy of risk assessment. Combining several safety-margins can be carried out through interval algebra or using probabilistic description. In both cases, the inherent adverse risk to discard a safe solution falsely will exist along the risk to miss hazardous situations. Risk-based reasoning with objective or subjective probabilities could handle both situations. By stating that migration modeling cannot demonstrate that a packaging is neither safe nor compliant, the EU regulation 10/12011/EC introduces an epistemic logic. How to choose between two alternatives in a formal framework? The issue arises due to simplifications applied in the mass transfer model (e.g., constant diffusion coefficient, overestimated chemical affinity), which are made to maximize the amount transferred to the food and not represents its amount with fidelity. The difficulty can be circumvented by applying the tiered approach as a non-monotonic logic: the algorithm generates successive solutions with improved safety (e.g., design) defeasibly when it reserves the possibility to retract some sequences in the light of further information (better description of mass transfer). The tree exploration of solutions can be applied to discrete and continuous variables.

II.3. Evaluation of the environment impacts of food packaging

II.3.1. A short history

Contrary to risk assessment and engineering methods rooting in the nineteenth century, the assessment of environmental impacts flourished recently with specific journals such as Environmental Impact Assessment Review, Environmental Monitoring, and Assessment, Integrated Environmental Assessment and Management, Science of the Total Environment, Journal of Environmental Assessment Policy and Management. Before being one the great popular causes of our time, ecology was an unfamiliar word among engineers and industrialists. In the middle of the space race, the universally acclaimed book Silent Spring of Rachel Carson, firstly published in 1962, brought the issue of pesticides centerstage, with mass scale poisoning and with thousands of farmers committing suicide (Carson *et al.*, 2002). "*FOR THE FIRST TIME in the history of the world, every human being is now subjected to contact with dangerous chemicals, from the moment of conception until death. In the less than two decades of their use, the synthetic pesticides have been so thoroughly distributed throughout the animate and inanimate world that they occur virtually everywhere.*" As a direct result of the message in Silent Spring, President Kennedy asked his Science Advisory Committee to study specifically the problem of pesticides. In the following years, the book motivated the first environmental legislation. In 1970, President Nixon consolidated many environmental responsibilities of the federal government under one agency, a new Environmental Protection Agency (EPA). One of the first measures of EPA was to secure a phase-out of dichlorodiphenyltrichloroethane (DDT), an insecticide formalized as a persistent organic pollutant with endocrine-disrupting and potentially carcinogenic effects. Comparatively, the European Environment Agency has been created twenty years later in Copenhagen but with an employee figure (200), which remains far behind the figure of EPA (>14000). National and international agencies maintain and enforce standards, but also supports a wide range of voluntary prevention and energy conservation efforts. In 1972, the United Nations Conference on the Human Environment held in Stockholm created the UN Environment Programme, which oversees with a staff of 300 all environmental problems among United Nations agencies. Additionally, many non-governmental environmental organizations contribute to raise environmental issues to public knowledge and to influence both the private and public sectors. The most visible association is Greenpeace and was founded in 1971 to protest against underground nuclear tests.

II.3.2. Sustainability and the difficult transition to sustainable food supply chain

The move of policies towards more sustainability predates energy crises of 1979 and originates from the U.S. National Environmental Policy Act of 1969 (NEPA), which formulated "*create and maintain conditions, under which humans and nature can exist in productive harmony, that permit fulfilling the social, economic, and other requirements of present and future generations.*" Sustainability relies on three intersecting pillars creating ten priorities presented in Figure II-27, which have been extended to seventeen goals (UN, 2015) by the United Nations. Similar principles can be to transposed to any industrial products (Crul *et al.*, 2009) as sketched in Figure II-27b. Sustainable engineering has been proposed accordingly, as a systems-based approach that seeks to understand the interactions which exist among environmental, social, and economic pillars to better understand the consequences of human actions (Vallero and Brasier, 2008). Though Sustainable solutions seek to protect the environment, should ideally also strengthen communities and fosters prosperity.

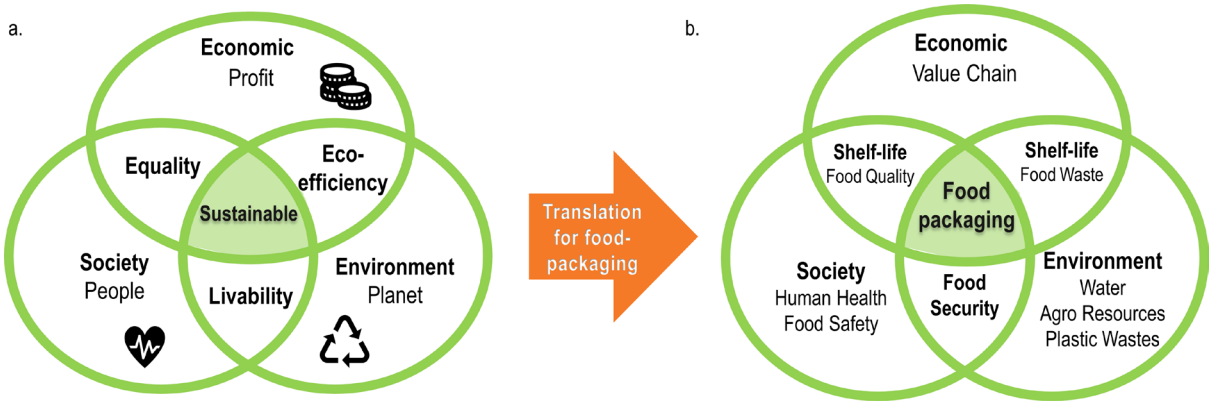

Figure II-27. Sustainability defined at the joint intersection of society, economy and environment spheres: (a) original concept from concept of Remmen et al. (2007); (b) interpretation for food packaging.

Feeding the world requires spanning food distribution chains far beyond production places and require therefore packaging. When food is stabilized (dried, fried, sterilized), packaging extends passively shelf-life without additional energy cost. When food is not stabilized (chilled and frozen), shelf-life is extended actively with the help of packaging and modified atmosphere. Because of food production, its transformation, stabilization and distribution, food consumption is a significant stressor of the environment. The apparent paradox between environment impacts and consumption has been identified by Brower and Leon (2009) and quantified as follows:

$$impact = population \cdot consumption\ rate \cdot \frac{impact\ resource\ use}{unit} \qquad \text{(II.68)}$$

The paradox of Eq. (II.68) can be removed by noting that sustainability implies from Figure II-27 feeding the planet safely while minimizing environmental impacts. Sustainability is consequently a complex equation of indexes to fulfill (constraints) and goal indices to achieve. Deciding which index is a constraint or a goal belongs to political choices of the societies.

II.3.3. From legal frameworks to packaging wastes

As shown in §II.2. , the safety of food contact materials is managed through a broad spectrum of laws and good manufacturing practices, which have been progressively built and spread out worldwide during the last three decades. The corresponding research field is still active and aims at minimizing either the exposure to contaminants or their hazards by banning or avoiding some of them. By contrast, the science related to the management of environmental impacts is more recent. The corresponding laws in developed countries are mainly coercive on sustainability practices and do emphasize cooperation (Gunningham, 2011;Earnhart and Glicksman, 2015). In the EU, the Polluter Pays Principle based on the extended producer responsibility concept is set out in the Treaty on the Functioning of the European Union (EU, 2008) and Directive 2004/35/EC (2004b) of the European Parliament and of the Council of 21 April 2004.

The industry adapted to the regulatory pressure by encouraging standard integration. The ISO standards applicable to food production and food packaging gained during the last decades a maturity into which environmental and safety concepts can be developed and audited. They are summarized in Figure II-28 with standard ISO 14006(2011) as cornerstone. This standard equipped with the unified methodology of life cycle assessment (LCA) defined in ISO 14040 (2006a) and ISO 14044(2006b) offers the most comprehensive principle and guidance for setting an environmental management system in the industry. The three aspects of product development and production are covered: design, management systems and environment. The triple quality in design, production, and environment can be certified according to standards ISO 9001 (2015a), 9002 (2016) and 14001 (2015b), respectively. The certification of designs for the environment exists for some electric and electronic products according to European standard IEC 62430 (2009), but they can be thought for more general products according to the ISO technical report ISO/TR 14062 (2002). For food and packaging applications, the previous ecosystem is compatible with food safety management systems (ISO 22000:2018), good manufacturing practices for food contact materials (2023/2006/EC, 2006) and the preventive methodologies of risk assessment Hazard Analysis and Control Critical Point (HACCP) and Failure Mode Effect and Criticality Analysis (FMECA). Environment

issues including "environmental responsibility" (2004/35/EC, 2004b) and EU waste management laws (2008/98/EC, 2008b) and (2015/720/EC, 2015) are fully enforceable in the described ecosystem.

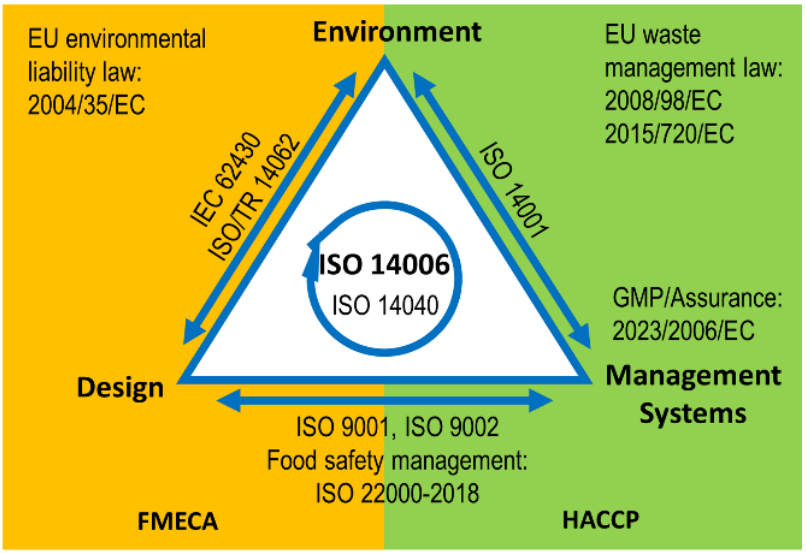

Figure II-28. Interpretation of the ISO standards applicable for food production and food packaging management.

II.3.4. Life cycle assessment (LCA)

II.3.4.1. Life cycle thinking

Environmental impact assessment (EIA) is mandatory or recommended in developed countries and aims to identify the impact of specific human activities before their development will occur. It is mainly a tool for decision making and is rooted in the US National Environmental Policy Act (NEPA) enacted in 1969. Life-cycle assessment, also known as life-cycle analysis, ecobalance and cradle-to-grave analysis, is part of the industry-specific methods to evaluate the impact of new products (Daniel *et al.*, 2004). The main goal is to participate to sustainable development by reducing a product's resource use and emissions to the environment as well as improve its socio-economic performance throughout its life cycle (Remmen *et al.*, 2007). As it is directed beyond the traditional focus on the production site and manufacturing processes to include the environmental, social, and economic impact of a product over its entire life cycle, it offers a broader scope than conventional engineering approaches. Additionally, Extended Producer Responsibility and Integrated Product Policies mean that the producers can be held responsible for their products from the cradle to the grave and therefore, should develop products, which have improved performance in all stages of the product life cycle. The methodology is intended to facilitate cooperation within organizations, along a supply chain including the recycling loop and more generally throughout is value chain.

An example of life cycle thinking for polyethylene terephthalate (PET) bottles used for retailed beverages is shown in **Figure II-29**. The bottles are produced from preforms, which are usually designed from a broad range of applications. The same preform (i.e., the same weight of PET, same necks) can be used to produce bottles of different formats by adapting the thickness profile.

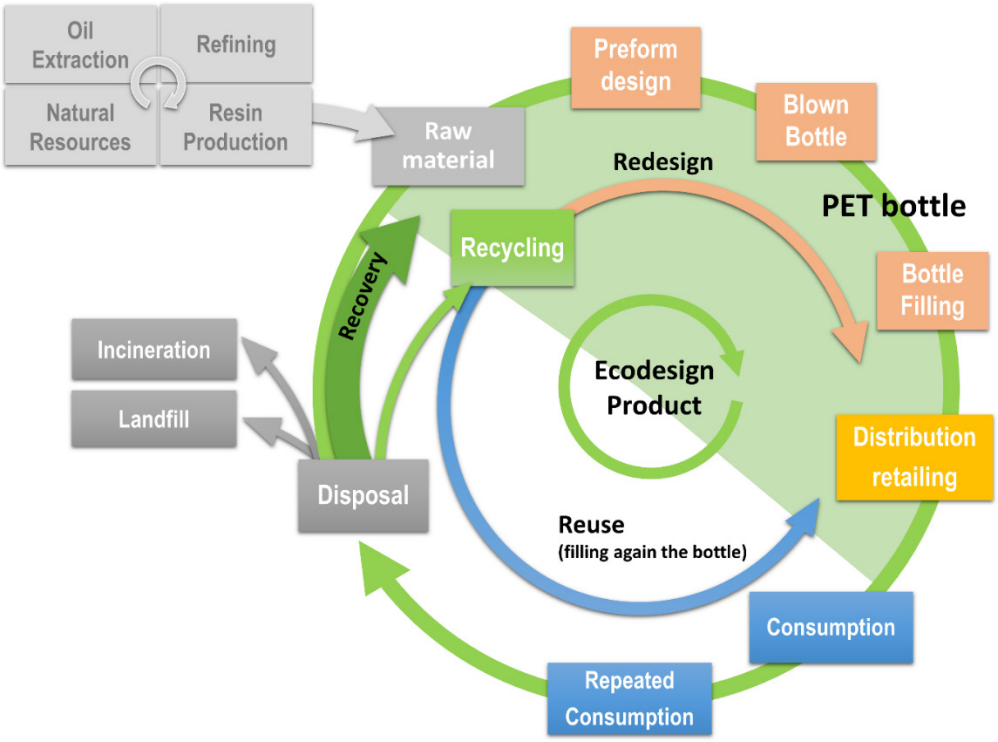

***Figure II-29**. Life cycle thinking applied to PET bottles for beverages adapted from Remmen et al. (2007) and by integrating the study of Almeida et al. (2010).*

The final bottle is usually produced by blowing the perform at 85°C, above the glass transition of PET, filled, sealed, distributed and retailed until reaching the final consumer. The bottle itself enables multiple consumptions over several days. After disposal, several options are applicable: solution 1) direct reuse (cleaning and refilling) (Uehara and Ynacay-Nye, 2018), solution 2) mechanical recycling for food contact, solution 3) chemical recycling (see chapters 4-7 edited by Thomas *et al.*, 2019) for food contact, solution 4) recycling for non-food applications such as textile (see chapter 9 edited by Thomas *et al.*, 2019) or construction applications (Mansour and Ali, 2015) and solution 5) finally incineration. Solutions 1) and 2) scored equivalently in the study conducted by the independent research organization (Delft and CE, 2004). The rules for authorizing recycled plastics for food contact has been laid down in regulation 282/2008/EC (2008a). Any recycling process must be evaluated, registered and authorized. The origin and the quality of the material should be characterized. The environment impact of PET is significantly reduced when a significant amount of recycled PET is introduced in the

primary loop (food contact) or in the secondary loop (other recycling) (see chapter 8 edited by Thomas *et al.*, 2019).

II.3.4.2. Steps in LCA

Though the ecodesign standard (see §II.1.5.) does not refer explicitly to life cycle assessment (LCA), LCA is the most frequently used tool for determining the environmental profile of mass-manufactured products. Aspects such as socioeconomic considerations are specific to ecodesign. To encourage the reduction of environmental consumption and pollution, the LCA methodology guides the end-user on how to perform a balance of environmental impacts along the entire life-cycle depicted in Figure II.9: from the cradle to the grave. For packaging systems with plastic components, all effects assignable to substances (monomers, polymers, additives…), industrial steps (raw material extraction or production, polymerization, processing, distribution, use, collect, recycling, cleaning, elimination) and consumer practices should be considered (Muthu, 2015). According to the ISO 14040: 2006, LCA framework contains four stages summarized in Table II-14. In thermodynamic terms, LCA is like a mass balance on consumed resources and produced emissions and wastes, applied on the environment at the interface with all operations required to produce, use and eliminate the packaging. All impacts accounted negatively. The impacts are expressed for a functional unit, which can be for food packaging respectively to the mass of food (Simon *et al.*, 2016) or to the mass of waste (see a review in Table 8.2 of Marathe *et al.*, 2019).

Table II-14. Main steps in LCA analysis

Step	Goal
1. Goal and scope definition	Describing the most important (often subjective) choices are described, such as the reason for executing the LCA, a precise definition of the product and its life cycle, and a description of the system boundaries.
2. Inventory analysis (LCI)	Listing environmental inputs and outputs associated with a product or service, such as the use of raw materials and energy, the emission of pollutants and the waste stream.
3. Impact assessment (LCIA)	Evaluating and ranking environmental impacts (objectively/subjectively and relatively to the desired targets) and translating them into environmental themes such as global warming or human health.
4. Interpretation	Checking the substantiation of conclusions: check tests, sensitivity analysis, alternative scenarios.

II.3.4.3. Known limitations

LCA suffers important limitations. As any study using system modeling, LCA thoroughness and accuracy depends on the availability of data. Other limitations are more systemic and require specific attention. Classic LCA is not holistic and does not incorporate a seek procedure to identify the most impacting (critical) product, process, or technology. Environmental, technical and social metrics need to be combined independently with LCA for comprehensive sustainability analysis. Unlike traditional risk assessment, LCA does not

necessarily attempt to quantify any specific actual impacts. While seeking to establish a linkage between a system and potential impacts, LCA models are suitable for relative comparisons but may be not enough for absolute predictions of risks.

Even for relatively small systems, LCA is a comprehensive task that requires interdisciplinary knowledge in the technical and economic areas. Hence, LCA projects are typically assigned to teams of experts (with accreditations when possible) and can rarely be performed by a single person with enough accuracy. Its incorporation in automatic algorithms is debatable with the current state of the art. The conclusions of the US EPA guidance are very specific: "*This valuable information provides a way to account for the full impacts of decisions, especially those that occur outside of the site that are directly influenced by the selection of a product or process. Remember, LCA is a tool to better inform decision-makers and should be included with other decision criteria, such as cost and performance, to make a well-balanced decision.*" (see p.60 of SAIC, 2006).

II.3.4.4. Complementary thinking to LCA

It could be tempting to associate LCA with comparable approaches analyzing material and energy flows of industrial production. The thermodynamical concept of exergy and the newer concept of emergy, proposed early by H. T. Odum (1996), offer indices, which mirror environmental impacts. Exergy and emergy are energetic concepts, which measure the efficiency of fluxes (energy or material) and the energetic cost of a structure, respectively. They cannot replace, however, LCA, because:

i) they are centered on current production and not on the environment, whose resources need to be protected for the next generations;
ii) they focus on management (reducing costs) and not on an independent assessment of impacts;
iii) there is no guarantee that a production system, which reduces its entropy (dissipations), also minimizes its environment impact.

Aggregated thermodynamic indices keep a general interest because they are extensive quantities equipped with additivity, factorizability and commutativity properties. They can be easily implemented in global optimization strategy via simple matrix representation of production systems (Nielsen and Bastianoni, 2007). The possibility to introduce a feedback loop to control how impacts are generated at any time is sketched in **Figure II-30**. None of the environmental impacts (land and water use, solid waste, natural resources, global warming, photochemical oxidation, eutrophication) offer similar flexibility and can be used as universal "currency" to compare alternative scenarios and to track root causes. This example proves, nevertheless, that environmental considerations can stimulate innovation in engineering and

bridges production systems and ecosystems. Only indicators of social developments as desired during the Rio Conference of 1992 do not fit within the proposed accounting. An energy unit for impacts is sound for a chemical engineer, but it may lack clarity for food and packaging systems.

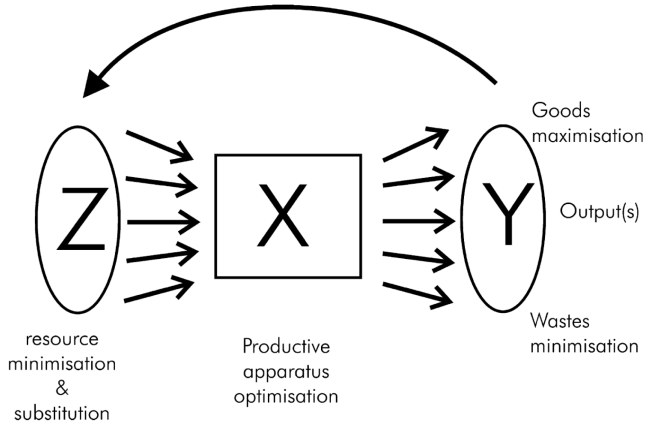

***Figure II-30**. Principles of multiobjective optimization with extensive indices (after Nielsen and Bastianoni, 2007).*

II.3.5. Applications of LCA to beverage packaging

Beverages are essential components of the diet for human beings. Since the earliest times, containers and packaging prevent the contamination and to transport water and fermented beverages. In his seminal book on Food Packaging, Robertson (2016a) separates packaging systems to pack liquid beverages (water, soft drinks, juices, beer, wine and liquors, milk) from those used to pack their dried content (tee, coffee, chocolate, milk…). This section reviews the impacts of the primary materials used to pack liquids for several weeks, months or years. Although big bags or tanks enable to pack several cubic meters of liquids, the comparison focus on small formats adapted to the individual consumption and adapted to aseptic treatments applied to beverages (filtration, pasteurization, sterilization, fermentation, distillation). Despite this simplification, the choice of a unique functional unit is not possible. The rate of consumption depends indeed on the considered beverage (the consumption of vinegar is less than milk), and the weight of the packaging depends on the format of the beverage (see the discussion in chapter 1 edited by Vignali, 2016). The biases are minimum by focusing on bottled water: daily consumption spread over the entire population.

II.3.5.1. A short review of packaging used for long shelf-life liquid beverages

- *Overview of materials compatible for long shelf-life liquid beverages*

Packaging systems for liquid beverages received many optimizations over the twenty century to meet both industrial, retailing and consumer demand. Technical constraints include filling at high temperature or in aseptic conditions, accepting thermal treatments such

as pasteurization or high-pressure treatments such as pascalization, tolerating high internal gas pressures, easy cleaning and poring, recyclable materials, lightness, mechanical resistance, chemical resistance to alcohols and acids. Due to these constraints, all categories of materials are used for liquid beverages: glass, metals, paperboard, plastics, hybrid systems with plasma treatments or complex, active systems, etc. The different applications of these materials have been reviewed in Coles and Kirwan (2011) and are summarized in **Table II-15**. The technical benefits of each material category are compared with their negative impacts on the environment or food safety.

Table II-15. *Overview of typical packaging materials for beverages (after Marsh and Bugusu, 2007;Welle,2011;Ramos et al.,2015)*

Material type (example)	Main beverages	Technical benefits (environmental benefits in **bold**)	Negative impacts (environment impacts in **bold**)
Glass (bottles)	fruit drinks, sparkling water, carbonated beverages, beer, wine, liquors…	**Refillable** **Fully recyclable** (in the same color) **Reusable** and good insulation Odorless, chemically inert Absolute barrier to gases and vapors Accept heat sterilization rigid, transparent, various colors and shapes High resistance to internal pressure.	**High weight** **High recycling energy** **Fragile, sensitive to thermal shock** **Color** cannot be removed during recycling (colored glasses should be kept for the usage) Minor risks of contamination by heavy metals Closure systems (metallic or cork) are sources of contaminants.
Metal: steel (cans) Metal: aluminum (cans)	soft drinks, soda, water, lemonade beverages, beer, fruit drinks …	**Fully recyclable** and easily separable from non-magnetic metals Absolute barrier to gases, water vapor, light and odors Strong mechanical resistance **Fully recyclable** Light weight and flexible Absolute barrier to gases, water vapor, light and odors Highly resistant to corrosion	Requires an internal varnish or coating: source of contaminants **Difficulty in sorting and separating aluminum materials** from other metals (may preclude economically feasible recycling) **High cost** compared to other metals Inability to be welded Requires an internal varnish or coating: source of contaminants
Paper, paperboard (aseptic carton, gable top)	Milk, soft drinks, …	**Recyclable only for disposable packaging** (glass, cup) Lightweight, good strength to weight characteristics Economical compared to other packaging systems, efficient, low-cost protection	Not recyclable when combined with other materials (plastics, aluminum) Migration of mineral oils and printink ink constituents, adhesives.
Plastics (PET bottles)	soft drinks, mineral water, energy drinks, ice-tea, juice, beer, wine…	**Recyclable** for non-food contact (textile fibers) and food contact (after mechanical or chemical recycling). Easy processing from preforms final bottles. Light weight and shatter resistance Good barrier to water vapor, oxygen, CO_2 Semi-crystalline PET has good strength, ductility, stiffness, and hardness Transparent and high clarity material Functional uses (thermosealable, microwavable, optical properties and unlimited size and shape)	**Degradation of PET during recycling** Risk of plasticizing by ethanol, water, CO_2 Rapid loss of barrier properties with high temperature during storage and transportation Migration of acetaldehyde, terephthalic acid, and other degradation products of PET, as well as migration from post-consumer contaminants. Poor reputation, regarded as a potential source of endocrine disrupting substances

- *Polyesters compatible with long shelf-life beverages*

Polyethylene terephthalate (PET) is one of the most worldwide used semi-crystalline thermoplastic on food packaging, covering ca. 30% of food contact applications. PET bottles are used for near 70% of all packaging applications for water and soft drinks worldwide (Welle, 2015). Each year, plastic drinking bottles (almost all in PET) are in the top 10 litters in the Mediterranean Sea (12% of collected objects in 2016 according to Hanke (2016). There is no industrial alternative to PET for long shelf-life and carbonated beverages (Mangaraj *et al.*, 2019). Coca-Cola made this statement: "*Plastic has lots of benefits: it's light, easy to use on the go, uses less material than glass and doesn't break easily. One of the biggest advantages is that as long as it's disposed of properly, it can be recycled and turned into new bottles again and again.*" The Coca-Cola Company (2019) PlantBottle® packaging is a division of Coca-Cola converting sugarcane into ethylene glycol (EG) and replacing synthetic EG in the polymerization process of PET. As purified terephthalic acid (PTA) is still from synthetic origin, the final PET contains ca. 30% of plant-based material. Using biobased 2,5-furandicarboxylic acid (FDCA) in place of PTA opens the way to 100% plant-based polymers, such as polyethylene furanoate (PEF). As aromatic polyesters from EG, that are chemical analogs of PET and polyethylene naphthalate (PEN) (Bomgardner, 2017). To capture the full value of furanic polymers produced from different pathways, bottles and other packaging systems will, however, need to be redesigned, and strategies for identification and recycling will require to be revisited. The monomers and the criteria of purity of initial substances (Rosenboom *et al.*, 2018) must be additionally approved by the European Food Safety Authority before being used for food contact.

Before the substitution of PET by alternative polyester is occurring, the global demand of PET is still increasing with at a pace of 4-8% each year (Gouissem *et al.*, 2014) and rises to 81.5% by weight for beverages across 2016-2017 (Pira, 2016). PET bottle wastes in EU arise to 1.88 Mt with a concomitant increase of the collection rate to 59% in 2016 and 129Kt more in 2014 (PETCORE EUROPE., 2017).

II.3.5.2. Comparison of environmental performances of PET bottles with alternative materials

- *Compilation of studies*

During the last two decades, the environmental impacts of PET bottles for beverages have been discussed in thirty-eight scientific publications, which have been reviewed recently by Gomes et al. (2019). Earlier studies targeted alternatives to landfill disposal (energy production, fiber valorization), whereas most recent studies seek replacement of PET by recycled PET, glass, aluminum, other polyesters such as poly(lactic acid) or PEF, other plastics such as polystyrene).

- *PET impacts vs. those of alternative materials*

The first reported LCA study was performed by the Coca-Cola Company in 1969 and concluded that plastic bottles have a less environmental impact than their glass equivalents (Gomes *et al.*, 2019). LCA results are not expressed on an absolute scale independent of the geographic area and the period covered. The results of different LCA studies cannot, consequently, be compared together in different contexts. A global image of the environmental performances of PET was reconstructed indirectly from the pair comparisons of PET with alternative materials. An overview of the forty-four comparative studies considered in the analysis is shown in **Figure II-31**. To increase the statistical significance, reports and theses publicly available were also included. One-third of the studies were carried out in the USA and on behalf of the industry. In Europe, most of the studies were available in academic reports or publications.

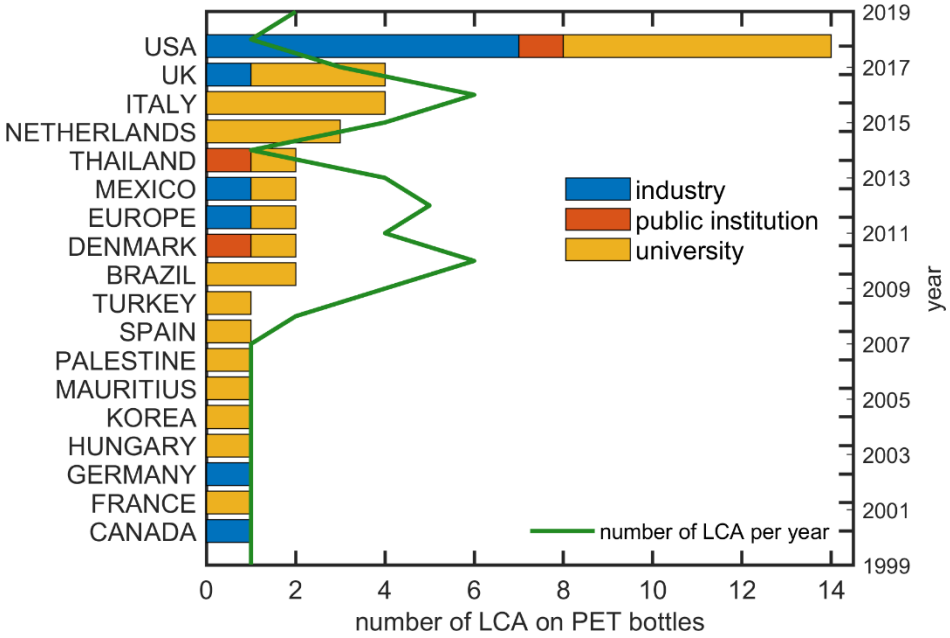

***Figure II-31**. Review of LCA studies of plastics bottles per country, issuing organization and year.*

Referenced studies: (Song *et al.*, 1999;Franklin Associates, 2007;Dogan, 2008;Foolmaun and Ramjeawon, 2008;Franklin Associates, 2009b, a;Romero-Hernández *et al.*, 2009;Almeida *et al.*, 2010;Chilton *et al.*, 2010;Fry *et al.*, 2010;PE-Americas and Five International., 2010;Shen *et al.*, 2010;von Falkenstein *et al.*, 2010;Belley, 2011;Franklin Associates, 2011;Gironi and Piemonte, 2011;Kuczenski and Geyer, 2011;Amienyo, 2012;Eerhart *et al.*, 2012;Komly *et al.*, 2012;Nessi *et al.*, 2012;PE International Inc., 2012;Shen *et al.*, 2012;Amienyo *et al.*, 2013;Flanigan *et al.*, 2013;Nogueda, 2013;Toniolo *et al.*, 2013;Papong *et al.*, 2014;Accorsi *et al.*, 2015;ECO Paper Loop, 2015;Flanagan *et al.*, 2015;Kang, 2015;Chen *et al.*, 2016;Garfí *et al.*, 2016;Saleh, 2016;Simon *et al.*, 2016;Almeida *et al.*, 2017;Kang *et al.*, 2017;Lorite *et al.*, 2017;Horowitz *et al.*, 2018;Valentina *et al.*, 2018;Boesen *et al.*, 2019)

The main conclusions of the pair-wise comparison of environmental impacts between materials are shown in **Table II-16**. The studies outscore the good performances of PET against almost any considered material, inorganic as glass or even biosourced as poly(lactic acid), as soon as PET is recycled in open (textile fibers) or closed (food contact) loop. Two recent studies (Ashurst, 2016;Ashurst *et al.*, 2017) confirmed that PET bottles have globally similar or fewer

impacts than other options for carbonated beverages. Substantial mitigation of environmental impacts by choosing PET bottles have been uniformly highlighted in all LCA studies of the past decade. Best sustainable strategies comprise increasing recycling rates and the amount of recycling material in PET bottles, minimizing the weight of PET bottles, and shortening the distances of one-way bottled water, preferring bottles with capacities ranging from 0.5 to 2 L. It is noticeable that only beverage cartons outpace PET bottles for climate change, cumulative energy, fossil resource consumption and acidification impacts (von Falkenstein *et al.*, 2010).

***Table II-16**. Comparative environmental impacts of PET containers vs alternative materials from a selection of studies. Containers are bottles except if mentioned differently. The selection is based on peer-reviewed studies except if indicated otherwise. Considered impacts include the production of containers, transport, disposal of solid waste resulting from packaging and recycling.*

PET vs (application)	LCA study	in favor of PET	In disfavor of PET
glass (extra-virgin olive oil)	a	Recycled PET is much better than glass even when recycled due to a lower energy consumption of the recycling process.	Glass is less impactful if recycled at a rate larger than 40%.
glass (mineral water)	b	Light weight packaging with fewer impacts than glass.	Higher impacts for global warming and photochemical oxidation potentials.
carton box (juice and milk)	c	Higher recycling rate (open and close loops) and light weight.	Carton has the lowest impact of greenhouse gas emissions, lowest fossil energy consumption and lower acidification potential.
recycled / bio-based PET	d	Fossil-based PET has less impact on acidification, terrestrial eutrophication potential, ecotoxicity, and ozone depletion.	Recycled and bio-based PET has the lowest consumption of non-renewable energy use and greenhouse gas emissions.
poly(lactic) acid (PLA) (mineral water)	e	PET has lower eutrophication and acidification potentials, as well as lower greenhouse gas emission	PLA has a lower total greenhouse gas emission and fossil energy demand.
Polyethylene furandicarboxylate (PEF)	f	Technologies for PET are much well developed.	PET has a high consumption of non-renewable energy use and greenhouse gas emissions.
Polystyrene (PS) (boxes)	g	PET has a low global warming potential as PS.	Lowest cost.
high-density polyethylene (HDPE)	h	Less energy to recycle PET	More solid wastes and greenhouse gas emission to recycle PET than HDPE

References: a. Accorsi *et al.* (2015); b. Garfí *et al.* (2016); c. von Falkenstein *et al.* (2010); d. Shen *et al.* (2012) Chen *et al.* (2016); e. Papong *et al.* (2014); f. Nicoli (2012); g. Madival *et al.* (2009);Leejarkpai *et al.* (2016); h. Franklin Associates (2011).

Key points of II.3. Evaluation of the environment impacts of food packaging

Because the Life-Cycle Initiative focuses on the environment in interactions with the object of concern and not on the object itself, the approach is essentially retrospective and simplified. The details of the design are lost, but it entails such as in the calculation of consumer exposure global reasoning. The format of the packaging, the rate of consumption, the frequency of purchase, the shelf-life of the product become key factors.

The pairwise comparisons of existing materials showed that PET remains the best choice for long shelf-life beverages. It outperforms biobased materials for its good inertia with all beverages and its capacity to be recycled in open or closed loop up to 100%. No plastics or glass reach similar performances. The absence of collection of PET bottles and their caps is responsible for marine litters, but not the bottle itself.

II.4. Additional indices to consider in food packaging design

Environmental impacts of food packaging do not enable to establish an honest presentation of the benefits of food packaging. The role of the primary package is to be in contact with food, to contain it and to protect by being a mechanical, physical, chemical, biological and microbiological barrier. It corresponds either to the retailing or consumption unit. The additional functions of the packaging, convenience and symbolic representation of food, are minor comparatively to the primitive functions of containment and protection. This section addresses three levels of performances affecting the first role of packaging: food shelf-life, mechanical resistance and green chemistry. The corresponding colloquial benefits are a reduction of food waste, logistical efficiency safer and more biodegradable raw materials, and additives. In their review, Molina-Besch *et al.* (2019) refers such benefits as indirect environmental impacts, that is as the consequences of packaging design on the food product's life cycle.

II.4.1. Food shelf-life

II.4.1.1. An attempt of definition

Packaging and food shelf-life are closely related. A product with a long shelf-life will require a higher barrier than a product with a shorter one. Due to the diversity of foodstuffs, the modalities of food transformation and stabilization, shelf-life is not defined by a unique criterion. The EU regulation 1169/2011/EC (2011b) on "food information to consumers" states defines the 'date of minimum durability of a food' as the date until which the food retains its

specific properties when properly stored. Given the variety of definitions including those proposed by the Institute of Food Technologists in the US and in the UK, Robertson (see chapter 12 in Robertson, 2009a) suggested the following definition: *"For the majority of foods and beverages in which quality decreases with time, it follows that there will be a finite length of time before the product becomes unacceptable. This time from production to unacceptability is referred to as shelf life."*

II.4.1.2. Methodology to estimate food shelf-life

- *Principles*

Estimating shelf-life is critical as it is related to food safety, nutritional value, appearance, texture, flavor. The task is mainly for new products or new packaging systems when no similar food product or food packaging has been tested before. As a rule of thumb, food shelf-life is directly or indirectly affected by mass transfer phenomena occurring across packaging walls and reactions in food as sketched in **Figure II-32**. The main mechanisms of quality loss coupled with mass transfer, chemical and biological reactions are reported in **Table II-17**.

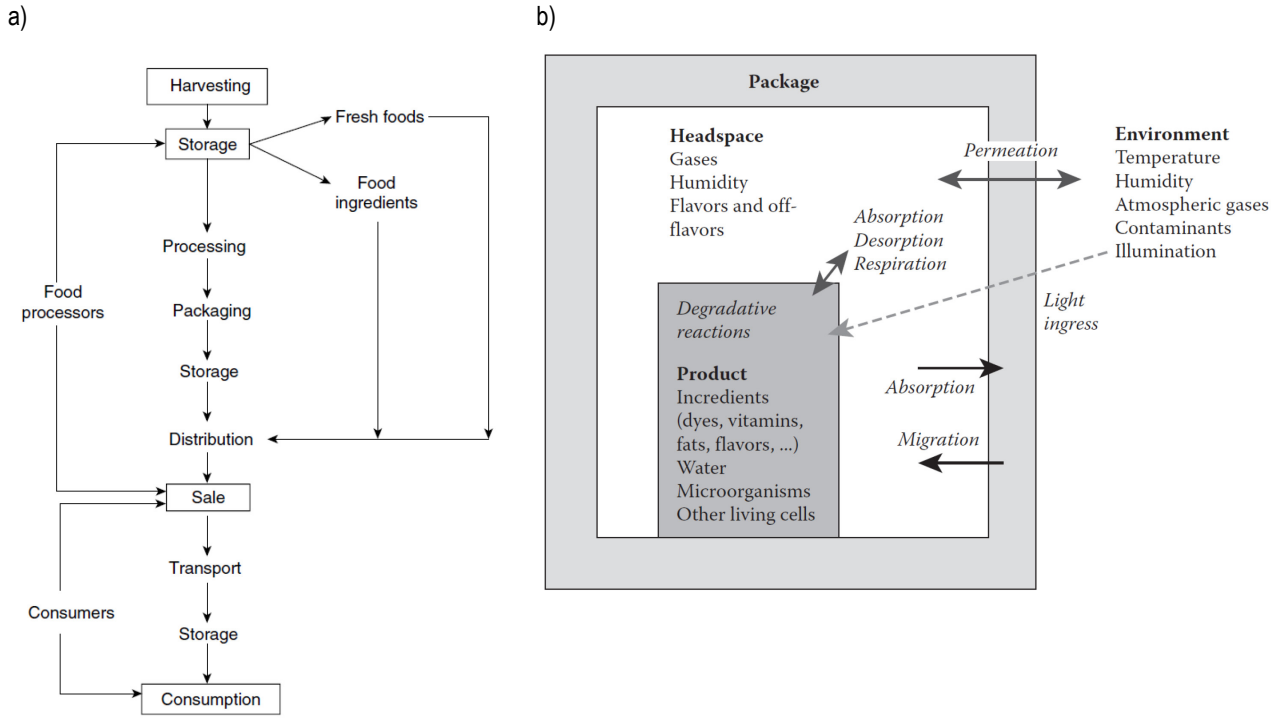

***Figure II-32**. Overview of conditions affecting the shelf-life of packaged food products: (a) main industrial steps (after Figure 1.1 of Rahman, 2007); (b) mass transfer and reactions (after Figure 2.2 of Singh et al., 2017).*

Shelf-life determinations such as "pack date" and "best-before" have been conventionally determined by measuring the rate of change of a given quality attribute (Rahman, 2007). The nonlinearity between quality loss and storage time does not facilitate the extrapolation of

shelf-life. The high sensitivity to the type of food, composition, formulation and storage conditions and packaging prevents the creation of tabulated kinetics (Singh and Singh, 2013). At the first tier, modeling is the feasible viable solution to adjust rapidly food packaging properties (surface area, wall thickness, material) to the desired shelf-life. The details of the calculations are rarely shared in the scientific literature and most incorporated mainly in in-house and commercial software.

***Table II-17**. Main factors affecting food shelf-life or safe life (after Table 2.1 of Singh et al., 2017).*

	Mechanisms	coupled with the following transfer	activation	overall influence of packaging (**risk**)
CHEMICAL MECHANISMS	autooxidation of lipids	permeation of oxygen, dissolution of oxygen from headspace	temperature + UV light transmission	high **(food quality)**
	secondary oxidation (induced by the decomposition of hydroperoxides) color changes of meat, dairy products, beer			
	Decay of compounds with nutritional value (vitamins, antioxidants)			high (**shelf-life**)
PHYSICAL MECHANISMS	water-related texture changes (from glassy to rubber behavior or in the reverse order)	permeation of water	relative-humidity temperature	high **(food quality)**
	water-mediated texture change (induced crystallization, physical aging of emulsions and foams)	heat transfer	temperature variations	
	aroma scalping (sorption, permeation)	plasticizing of the packaging material, permeation/sorption of water, alcohols for polar materials	temperature	
	permeation of off-flavors			
	Global water loss (reduction of volume or weights in beverages, dairy products, vegetables, meat, etc.)		relative-humidity temperature	medium, low (**shelf-life**)
BIOTIC MECHANISMS	Growth of spoilage microorganisms	accumulation co_2 (bacteriostatic, metabolism inhibitor), permeation of oxygen	oxygen temperature relative humidity	medium **(food quality)**
	Growth of pathogens, production of toxins			medium **(food safety)**
	Loss of metabolic activities in fresh products due to senescence, softening and staining (fruits, vegetables, mushrooms)	gas transfer water transfer		medium **(food quality)**

- *Relating food quality attributes with mass transfer*

The principles linking a quality attribute (texture) and water transfer is illustrated in **Figure II-33** for a dry product (biscuit, chips) based on case-studies discussed by Robertson in Chapter 12 "Shelf-Life of Foods" of Robertson (2016a) and in Chapter 2 "Food Quality and Indices of Failure" of Robertson (2009a). The concept of secondary shelf-life justified by Cappuccio *et al.* (2001) represents the minimum durable time after the opening of the package

during which the coffee maintains acceptable quality. The depicted case represents the evolution of the glass transition temperature due to a water uptake consecutive to an increase of the humidity in the headspace (see a similar case in Nicoli, 2012). The key assumptions are:

- water mass transfer across packaging walls are much slower than the equilibration time between the headspace and the product;
- the evolution of texture is well correlated with the glass transition temperature (T_g) of the product;
- the sorption isotherm of water in food and the variation of T_g with water content;
- a mass transfer model across packaging combined with a global mass balance can be devised.

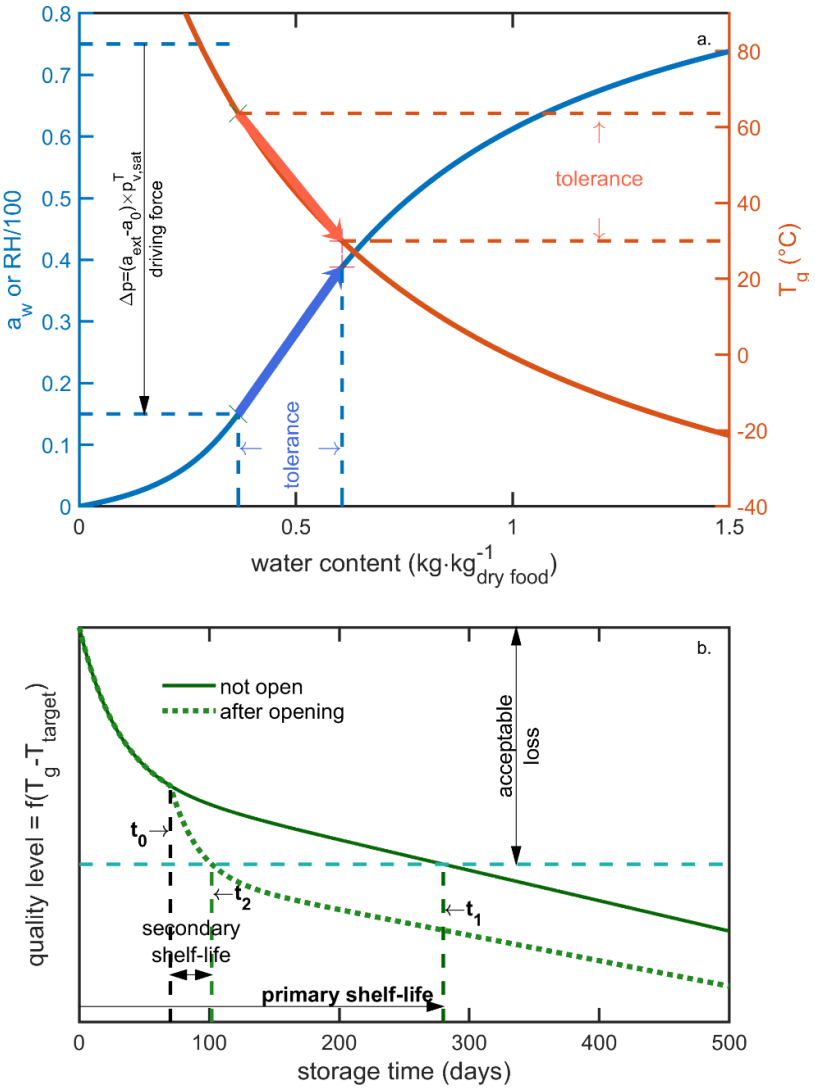

***Figure II-33**. Principle of shelf-life calculations for a dry food product (initial water activity 0.15) stored in a humid atmosphere (75% RH) within a packaging slowing down water permeation: (a) water sorption isotherm and variation of glass transition temperature (T_g) with water content; (b) variation of texture induced by water uptake. Shelf-life is determined by the tolerance on the shift of T_g before (primary shelf-life) or after opening (secondary shelf-life).*

Considering secondary shelf-life with a technological point of view is a quite new field of investigation (Nicoli and Calligaris, 2018). The turn follows a dual motive of reducing food loss and waste at a global scale, and of improving the role of the packaging in the shelf-life extension after opening. Secondary shelf-life of liquid food exceeds one week only in rare cases: oil, mayonnaise, syrups, liquors and the main risk are evaporation and oxidation.

II.4.1.3. A 2D revolution simulation to estimate the shelf-life of carbonated beverages in PET bottles

The feasibility to calculate shelf-life from computational fluid dynamics (CFD) has been discussed by Carrieri *et al.* (2012) for carbonated beverages. The methodology and main findings associated with CO2 depletion during long-term storage in constant and variable temperature conditions are shown in **Figure II-34**. The CFD model was diffusive and described explicitly mass transfer in the food and the bottle walls with 5800 triangular elements. Three compartments are considered: the beverage, the headspace, and the walls. The diffusion coefficients in the wall were assumed isotropic, uniform and dependent only on temperature (no effect of plasticizing, aging). The modeling part includes two limitations:

1. Local thermodynamical equilibria between the headspace and the liquid, between the liquid and the walls, and between the headspace and the walls are not enforced;
2. The quality of the mesh is insufficient to describe mass transfer across the walls during transient regimes (initial time, change of state).

Despite these limitations, the work offers the first insights on the relationships between design, bottle format, initial composition, storage conditions and some aspects of shelf-life. Methodology to include explicitly thermodynamics is shown in **Figure II-33**.

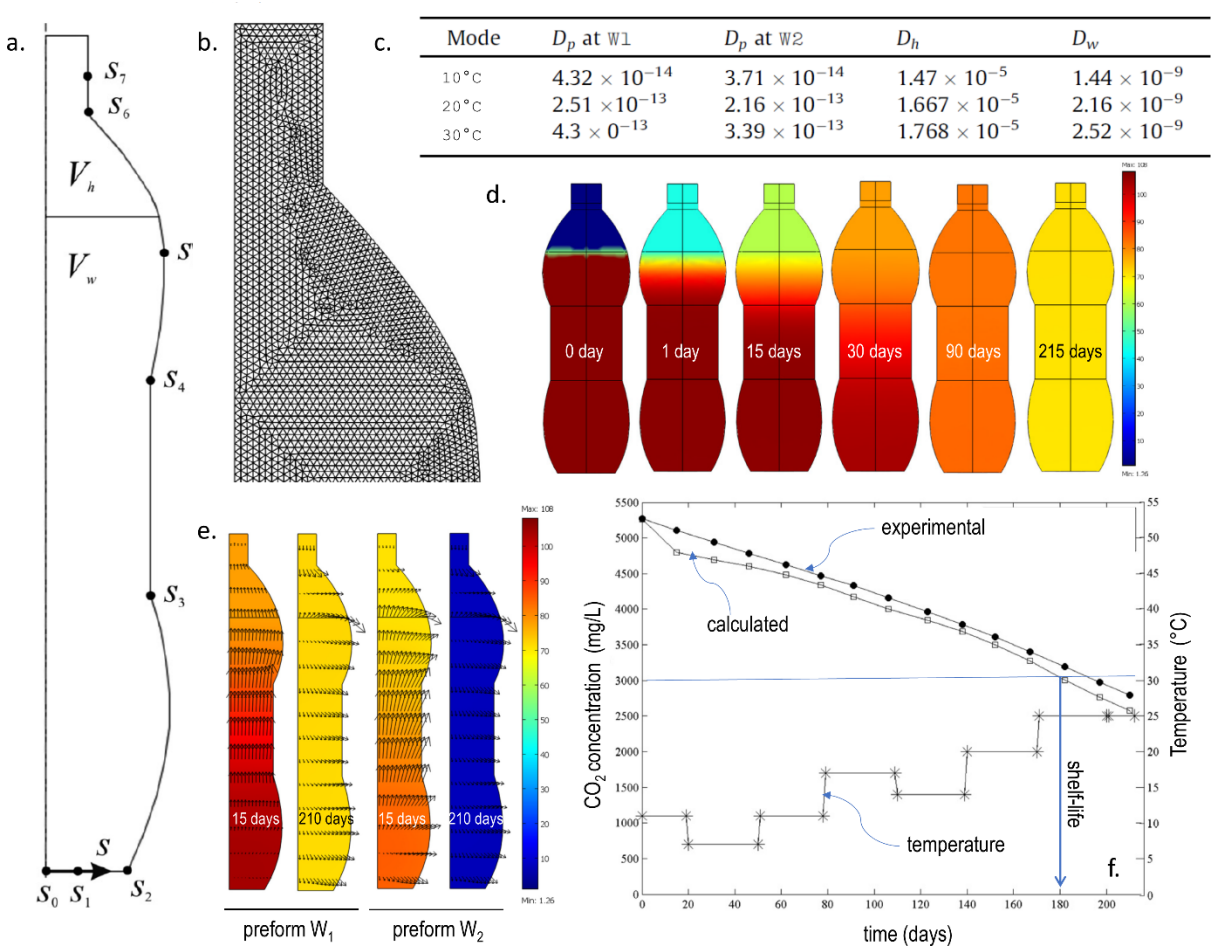

Mode	D_p at W1	D_p at W2	D_h	D_w
10°C	4.32×10^{-14}	3.71×10^{-14}	1.47×10^{-5}	1.44×10^{-9}
20°C	2.51×10^{-13}	2.16×10^{-13}	1.667×10^{-5}	2.16×10^{-9}
30°C	4.3×0^{-13}	3.39×10^{-13}	1.768×10^{-5}	2.52×10^{-9}

***Figure II-34**. Simulated CO_2 depletion in a PET bottle containing a carbonated beverage (Carrieri et al., 2012): (a) simulated 2D wall profile along its axis of revolution; (b) details of the mesh (Lagrange quadratic); (c) diffusion coefficients of CO_2 in PET (D_p for preforms W_1 and W_2), in the headspace (D_h) and in water (D_w); (d) 2D CO_2 concentration profiles in bottles (W_1) quiver plot showing molar flux superimposed to concentration profiles; (e) evolution of Co_2 concentration in the bottle in variable temperature conditions.*

II.4.2. Mechanical resistance of PET bottles

The shape of the PET bottles and the thickness of the wall must be adapted to the stacking of bottles during transportation and storage in pallets. The resistance to vertical compression by axial load is essential. The observed rigidity in a closed bottle is associated with cylindrical symmetry of bottle sidewalls. According to shell stability theory, the loss of symmetry modifies the equilibrium position of vertical walls and causes a loss of carrying capacity (Hu *et al.*, 2012). The maximum capacity, so-called buckling load, is affected by the structure and the distribution of the mass in the final blown bottle. All these phenomena can be studied by finite element techniques with an intent of minimizing both the weight of preform and the thickness of all walls. Typical simulation results are shown in **Figure II-35** for non-petaloid and petaloid bottles. Similar results are available for large fountain bottles (Masood and KeshavaMurthy, 2005) or bottles with handles (Huang *et al.*, 2018a).

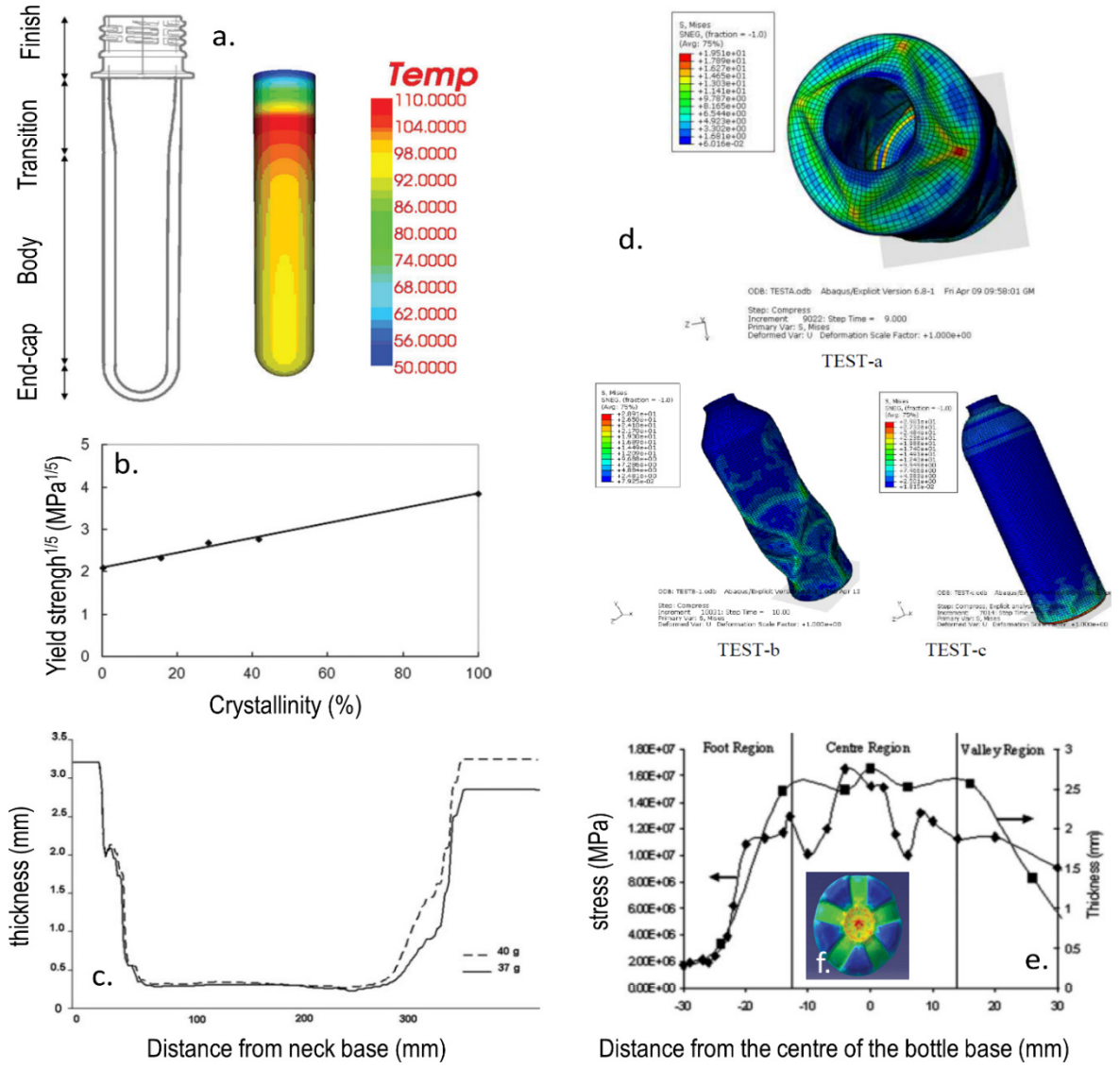

Figure II-35. *Relationship between bottle geometry, wall thickness distribution and mechanical resistance of PET bottles: (a) typical preform and temperature distribution during blowing; (b) relationship between yield strength and crystallinity; (c) vertical distribution of PET material after blowing for two preforms (40 and 37 g); distribution of buckling stress (compression tests a-c); (e) distribution of stresses in a petaloid shape bottle for carbonated bottles; (f) details of the distribution of stresses at the petaloid bottom (red = maximum stress at the center)*

(a-c) from Daver et al. (2012) (d) Hu et al. (2012); (e-f) from Demirel and Daver (2009);

It is significant that none of the simulations consider explicitly the beverage, the resistance induced by the headspace pressure and consequently its loss caused by weight loss due to permeation.

II.4.3. Sustainable and green chemistry

The safety and ecodesign of food packaging should benefit from the growing paradigm of sustainable and green chemistry. The paradigm could be a game changer by offering a systematic substitution of the most impacting polymers and substances.

II.4.3.1. Motivation

The Organization for Economic Co-operation and Development (OECD) defines "*Sustainable chemistry as a scientific concept that seeks to improve the efficiency with which natural resources are used to meet human needs for chemical products and services. Sustainable chemistry encompasses the design, manufacture, and use of efficient, effective, safe and more environmentally benign chemical products and processes*" (OECD, 2017). The twelve concepts of green chemistry formulated twenty-five years ago (Anastas and Warner, 2000) are shown in **Figure II-36**a . Sustainable and green chemistry has been subjected to a recent special issue in Chemical Reviews (Horváth, 2018) "*general, sustainable chemistry should use resources, including energy, at a rate at which they can be replaced naturally, and the generation of waste cannot be faster than the rate of their remediation. It should be noted that not all sustainable chemicals or reactions or processes could be green. Therefore, the selection of chemicals, reactions, and processes, which are sustainable and green at the same time, should be preferred or the target of design and innovation.*" The philosophy is summarized in **Figure II-36**b.

a)



b)

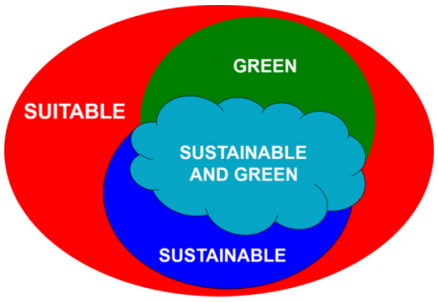

***Figure II-36**. (a) green chemistry pocket guide of the American Chemical Society; (b) schematic definition of sustainable and green chemistry*

II.4.3.2. Meaningful examples

Sustainable and green chemistry is not yet rocket science, but alternative solutions can be learned and inspired by examples. Some of them are envisioned for food packaging from the thirty meaningful examples detailed by Matlack and Dicks (2015) from his own experience of teaching environmental and industrial chemistry using problem-based learning. Three strategies dominate: elimination, substitution and better control. They are summarized in **Table II-18**.

***Table II-18**. Examples of sustainable and green chemistry applicable to food packaging*

Domain	Examples	Application for food packaging
Toxicity and chemical wastes	Biologically safer chemicals through retrometabolic design	reengineer all substances with endocrine disruption potential
Longer service life	Controlled wear and breakage, durable materials	refillable, reusable packaging
Chemistry of waste management and recycling	Recycling materials free of contaminants Separating the streams of synthetic and biodegradable polymers in the waste stream	controlling the flux of paper, board, plastics, avoiding multimaterials, recycling polyester at dry state to prevent hydrolysis reorienting biodegradable polymers to food applications with short shelf-life and finally compost them together.
Energy and the environment	Use microwave in the processing of plastics	possibility to process by-products of the food industry to produce polymer blends
Environmental economics **The greening of the society**	Green accounting: include the value of natural support in consideration of profit and loss Example of a problem addressed to undergraduate students: They are looking for a new name for the company, for example, "Sustainability Unlimited," or perhaps "Innovation Plus." They are considering slogans that will market the new image, for example, "The future is now. Make more money with Innovation Plus." Your job is to make the announced policy come true. How can you possibly do this?	Uniform application to all materials intended to be in contact with food or not. be imaginative

Key points of II.4. Additional indices to consider in food packaging design

Shelf-life and mechanical constraints are additional goals or constraints, which need to be considered in packaging design along with safety and environmental ones. The choice to consider them as targets to maximize or as minimal constraints to fulfill depends on the emphasis put on environmental impacts and safety. As a rule of thumb, it could be suggested that the constraint on shelf-life and mechanical resistance can be relaxed if the distribution and retailing chains are adapted accordingly. As finite-element analysis requires computer intensive calculations, it is logical to imagine the integration of shelf-life, safety and some environmental aspected into a single computer-aided framework. The immediate adding value will be a global minimum instead of disconnected local minima. The level of coupling will determine the computational cost of the entire approach. A tiered approach can, again, help to manage uncertainties in non-critical (low coupling) and critical (high coupling) situations straightforwardly.

II.5. Conclusions of the literature review

This chapter reviewed the strategies to evaluate and mitigate negative impacts of food packaging. The initial intent was to show that [S]olving the global challenge could be thought as a minimization problem that engineering and mathematical concepts could handle. The review does not elaborate on the merit or on the negative side of technology; objectivity is shown to be one of the founding principles of any independent [E]valuation supporting the [D]ecision-making process. The final [D]ecision based on the [E]valuation conclusions or not will impact in any case both humans and the environment. Semi-supervised and automatic reasoning can help to produce a discrete or continuous list of Pareto optima. According to the context (food product, market, availability of technology, social environment), one solution or another close to the Pareto front could be preferable. This final decision will always belong to humans. A corollary is that the exploration of the Pareto front may benefit the more general concept of sustainability and may support product and service innovation.

Theoretically, one solution identified by following an optimization methodology could strive to meet several challenges linked to social expectations, safety and well-being, planet and equitable profit along the global value chain. This description appears, however, too idyllic by several aspects. The first limitation is how to identify the direction of progress. At the expense of overestimations and worst-case scenarios, it has been shown that semi-supervised decisions were possible. Increasing safety margins such as excess of precaution principles can eliminate some alternative solutions, but it should not preclude innovative packaging design and formulation. By comparison, environmental impacts do not fit within the scheme. The contours of any LCA or equivalent study result from specific choices and no specific guidance has been proposed for food packaging. LCA is to the environment what the first law of thermodynamics is to chemical engineering. Raw resources are converted into effluents and gas emissions, but we are interested in the secondary consequences of these primary impacts and how they the future viability of the planet. The underlying process runs only in one sense and it is not reversible energy flows. Due to entropy production and because ecosystems are continually changing, the concept of “balance of nature” is not enough robust and accurate to support detailed industrial decisions. The margin of uncertainty can be too high. In its attempt to link thermodynamics and ecological considerations (Jorgensen and Johnsen, 1989), more general concepts such as disruption of the natural control and homeostasis of the biosphere should be considered instead. This approach would require sophistication and knowledges, which are not accessible even today. More realistically, Valsaraj and Melvin (2018) suggested that thermodynamics should be still applied to engineered and designed systems with an environmental balance focused on quantities chosen to be extensive, verifiable and auditable. As a result,

a feedback on industrial practices can be proposed with a logic of evaluation, optimization and control as shown in **Figure II-37**.

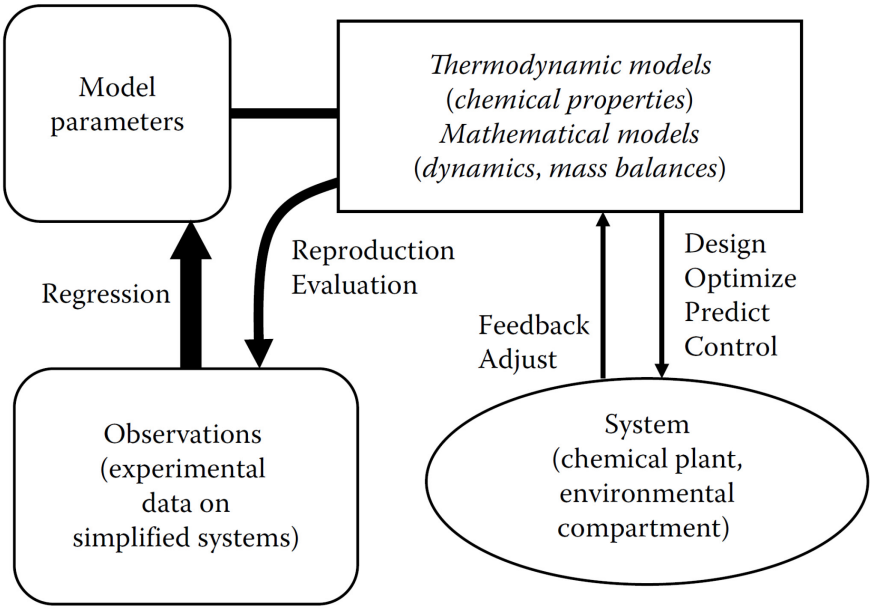

***Figure II-37**. The role of chemical thermodynamics in the objective evaluation of the performance of engineered systems (after Figure 1.5 of Valsaraj and Melvin, 2018).*

Figure II-37. does not apply, however, directly to food packaging. Food packaging is a special case of product with only a temporary value, during the time it is in contact with food. After this period, it is losing any value and it will become exclusively a waste when it is not recycled. Introducing the food in the equation change the perspective, the packaging should protect the food the time needed to process, distribute, retail and consume food. For beverages, one of the best choices remain PET bottles, which can be partly biosourced and are fully recyclable. The technology is mature and relaxing mechanical and shelf-life constraints could offer new opportunities to reduce its impact. The generalized replacement of glass by recycled PET bottles open additionally new challenges: safety of the closed loop, interactions between bottle walls and its content, validation of the shelf-life, shifting consumer experience. Not all the approaches are available to make computer-aided ecodesign available to food companies wishing to explore rapidly all alternatives to glass.

this page is left blank intentionally

Chapter III. GOALS AND APPROACHES

Chapter III. Goals and Approaches

III.1. Preamble

Chapter II. reviewed some methodological arguments to suggest how the food, the packaging and the chemical industry could tackle the incommensurable challenges that mankind is facing in the 21st century. The solution with zero packaging is currently not viable as the food needs to be protected from its production or transformation place to its consumption place. The human population became mainly urban, partly disconnected from nature but it should protect it. The solution for now should be a GLOBAL MINIMIZATION problem: less material, less effects of materials on human, less impacts, less food loss. Due to the many linked decisions and the broad range of expertise required to adapt each packaging to each food, to each distribution chain, to each market or consumer, the task looks immense and non-economically viable. Decision making assisted with proper computer calculations could accelerate the process of exploration and validation of alternative solutions. Only the substitution of mass market applications of food packaging will have a significant benefit on human health and the environment. The chief difficulty is the validation of any massive substitution more than its implementation (*i.e.* design, marketing, upscaling production): how to guarantee that the new solution is objectively better than the previous one, adapted to existing recovery loops and regulations, without adverse effects not thought at the first place. Even if the replacement process is assisted by computers, it should be inspired by the state of the art in decision-making and problem-solving. The conclusions of Chapter II. emphasized the letters E, D and S for [E]valuation, [D]ecision and [S]olving, respectively. They correspond to the three individual steps, which should be carried-out during the exploration and validation of any solution:

- **Step [E]** guarantees a neutral (mechanistic) evaluation of well-known phenomena independent of any social, economic, legal acceptation rule;
- **Step [D]** introduces "human" rules supporting the acceptation or rejection of any choice or alternative;
- **Step [S]** is a mathematical process enabling to explore in a neutral manner contradictory goals under uncertainty.

III.2. General goal and case-study

The general goal of the thesis is to devise, implement and evaluate the feasibility of the [E][D][S] approach for the rapid prototyping of new food packaging systems for alcoholic beverages. The entire approach is intended to be generic, incrementable and support the rationale design of any safe and environment-friendly food packaging or related systems. The food, the packaging, the materials, the substances and the supply chain are parts of the equation.

III.2.1. Towards holistic food-packaging engineering

Comparatively to previous works aiming at reducing environmental impacts, the thesis does not study the solution (new polymer, new use, new recycling etc.), but the cognitive process which will create new solutions optimal in some sense according to the market demand, food requirements, etc. Even the best polymer, the best bottle, the best supply chain and the best recovery/recycling loop needs to be optimized together to get a global solution for each pair of food and packaging, each market segment, etc. By updating regularly packaging to market needs rather than expecting a Holy Grail packaging, impacts could be minimized in an ongoing process following the evolution of food supply chains and its governance. **Additionally, linked decisions such as food safety could be managed with the same approach and without additional cost.**

Premises of holistic engineering already exist in chemical engineering, which, as a meta-discipline, links physical understanding, mathematical modeling and technical skills. The best example is process design and development. The application to food and packaging is at this stage very primitive. The priority research directions are not well established. The ecodesign strategy proposed initially by Brezet and Van Hemel (1997) is taken consequently as a template. The authors split the problem of "ecodesign" into seven *subproblems*, denoted in this work from *P1* to *P7*. They can be addressed with the proposed scheme [E][D][S] as:

- **[E]valuating the impact** of materials (common to subproblem*s P1 to P7*)
- **Preferring materials** with lower impacts (**[D]ecision**) (subproblem *P1*)
- **[S]olving the problems P2 to P7**: reduction of material use (subproblem P*2*), optimization of production techniques (*P3*), optimization distribution system (subproblem *P4*), reduction of impact during use (*P5*), optimization of product lifetime or shelf-life (subproblem P*6*), optimization of the end of life systems (subproblem *P7*).

A translation the *seven subproblems* to food packaging is proposed as follows. The impact could be mass of waste or the mass of the depletion created by the packaging itself, that is the mass of non-recycled or non-recyclable material for the same purpose (food contact). The subproblem*s P2 to P7* could correspond hence to: the minimization of the mass (*P2*), the optimization of the shape (*P3*), the optimization transportation and retailing conditions (*P4*), updating to the volume consumed (*P5*), the optimization of the food shelf-life (*P6*), optimization its collect and recycling (*P7*).

III.2.2. Epistemology of mathematical-computational instruments

Epistemology is not part of the [E][D][S] framework, but it encourages the development of a critical view of all optimization and automatic decision methods. A thoughtful example is proposed here to illustrate how being uncertain can have dramatic consequences and may lead to cognitive biases.

By using a non or semi-supervised decision algorithm, an important question is raised: *Is there enough rationality to put our faith or thrust in an algorithm, which could not be verified by a human expert or by an independent experiment*? A common example chosen in epistemology to separate knowledge and belief is to suppose that a person thinks (or use the result of a computer algorithm) that a particular bridge is safe, and attempts to cross it; unfortunately, the bridge collapses under her weight. One might say that she believed that the bridge was safe (she believed in the algorithm), but that her belief (the algorithm) was mistaken. Alternatively, if the bridge had supported her weight, we would have said that she knew that the bridge was safe (the algorithm was predictive). In fact, this example teaches us that only the experience of crossing the bridge brings us the proof. In the same vein, our predecessors did not believe that our industrial practices could damage permanently our planet, only the next generations could observe that it was not true.

III.2.3. Case-study at tier zero

A tier (pronounced TEE-er) is coming from the medieval French *tire* and meant the rank in a line of soldiers. By extension, it is the row or layer in a series of similarly arranged objects. A four-tier approach is proposed for the design of food packaging. Tier zero is proposed as conceptual engineering to serve to identify the principles and feasibility of more sophisticated approaches at higher tiers.

III.2.3.1. Justification

As early discussed by Dufrene *et al.* (2013), ecodesign tends to be idiographic, case-centric, without easy generalization and without standards. The thesis proposes to resolve automatically or in a semi-supervised manner the subproblems *P2 to P6* with an evidence-based approach. The feasibility and difficulty are illustrated on a toy model offering a parallel with real cost and objective functions. The subproblems *P1* and *P7* are excluded because they are assumed to be resolved independently using, for example, life-cycle assessment tools: glass vs plastics, biodegradable vs recyclable materials, reusable vs recyclable systems…

At this point, it is worth noting that goals corresponding to *P2 to P6* are essentially monotonic and mutually correlated, for example: more materials (subproblem *P2*) is needed to reach a longer shelf-life (subproblem *P6*). Without a loss of generality, the case-study is simplified to reach a global optimization problem solvable with linear programming, with many fundamental results rooting from the pioneer work of Joseph Fourier. Important results will be, however, demonstrated, such as the possibility to eliminate some subproblems or constraints (inequalities) to check whether the whole problem (S2-S5) accepts a feasible solution. When several solutions are possible, enumeration or iso-impact contours can be used to find the best solution or to meet some Pareto optimality (Pareto front or Pareto set). When there is no feasible solution due to either too restrictive or contradictory constraints, a least infeasible solution will be sought.

III.2.3.2. Description of the case study

- *Formulation of the problems Q1, Q2, Q3*

A vodka-type beverage (40% alcohol-by-volume) is packed in containers with simple geometries, shown in **Figure III-1** : a regular parallelepiped shape (design D_1) with an edge a and of height b; a cylinder of diameter a and height b (design D_2); a cube with an edge a (design D_3); a sphere of diameter a (design D_4). Each design is equipped with an opening of two centimeters width. The walls are assumed to be in plastics (for example in PET). The ecodesign problem can be translated in different questions:

- **Q1 (concurrent design alternative)**: What is the shape minimizing the amount of waste if a minimum shelf-life of two years is enforced at ambient temperature for a capacity of $V_F^{t=0} = 0.25$ L .
- **Q2 (optimal design and supply chain)**: What is the best shape and capacity (between 0.05 L and 0.75 L) minimizing impacts for average consumer with a consumption rate of one glass per week and adapted to low consumer with a consumption rate of one glass per month? The shelf-life is not imposed and can be adjusted.

Though the spherical shapes exhibit the lowest surface-to-volume ratio, the proposed solutions should include innovative alternative with performances similar to D_4 with a shelf-life of two years.

- **Q3 (innovative design solution)**: Where is the pareto front corresponding to the evolutive geometry linking continuously designs from D_1 to D_4. What would be the alternative geometries with a resemblance to D_2 and with performances close to the ones of D_4 ?

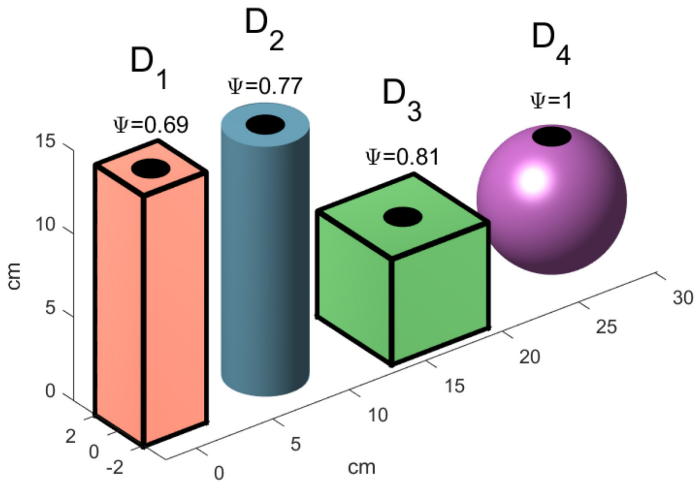

***Figure III-1**. Initial designs (D_1..D_4) considered in the global optimization problem. The height b of D_1 and D_2 is fixed to 15 cm. The black circle on top represents the opening (cap not shown).*

- *Assumptions and simplifications*

To keep the problem feasible with simple reasoning, vodka will be assumed to be pure water with density ρ_F and molecular mass M (ethanol content is neglected in this case-study). The shelf-life will be assumed to be governed only by the loss of water. The thickness of the walls is assumed to be uniform and equal to l_p (weight of the bottle: $m_p = \rho_p A l_p$, with A the surface area of contact and ρ_p the density). The transport properties are also uniform and governed by constant diffusion coefficient D_p and Henry coefficient k_p. The partial pressure across the walls Δp is assumed to be constant and controlling the mass leak. The mass absorbed in the walls is neglected as the contribution of the headspace. The parameter b is fixed to 0.15 m and only the parameter a is adjustable for all designs. Design D_1 is chosen as reference and is subjected to the presented optimization problem.

III.2.3.3. [E][D][S] resolution procedure

The framework [E][D][S] to solve problems Q1, Q2 and Q3 is shown in **Figure III-2**. with notations detailed hereafter. The remaining mass of the food is defined as $m_F^t = \rho_F V_V^t$ and the shelf-life is defined relatively to tolerable weigh loss $\%\Delta m_F$.

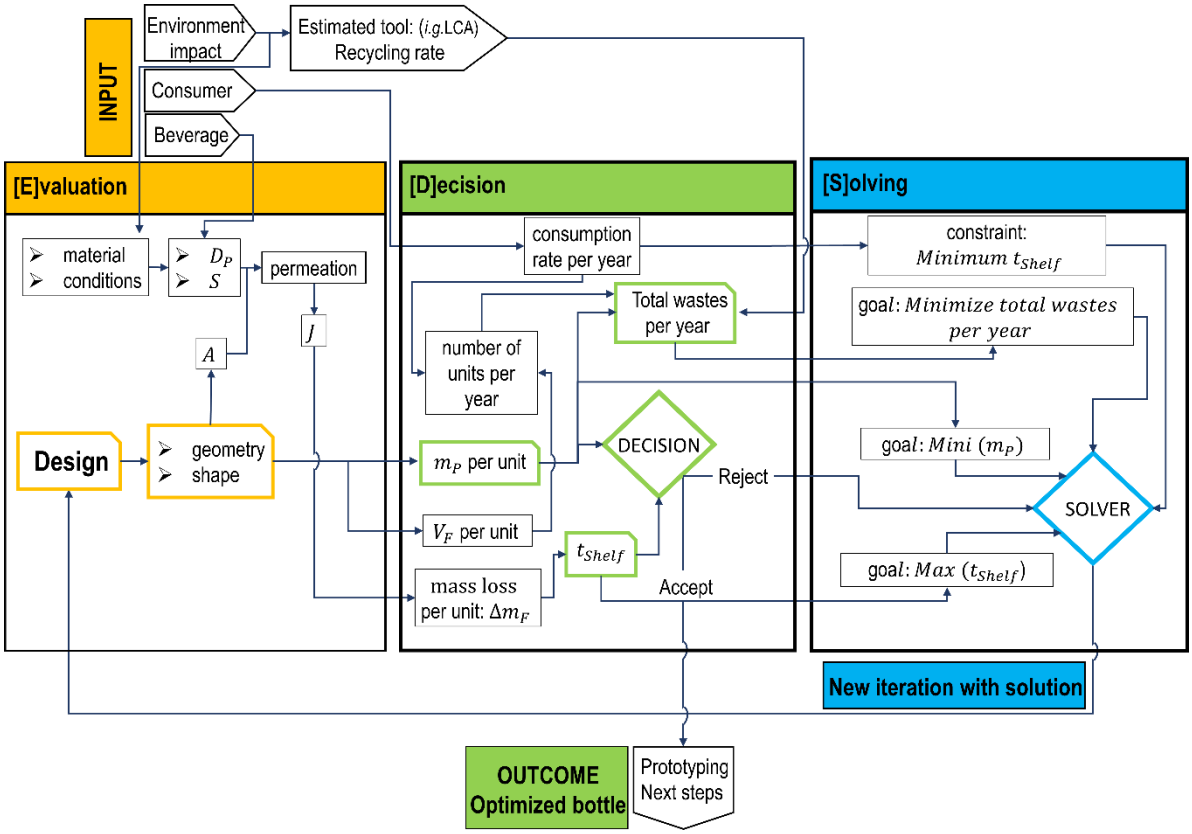

***Figure III-2**. Principle of the iterative resolution of the ecodesign problems using the [E][D][S] framework*

- *Mass transfer model of used in [E]valuation step*

By assuming a mass loss by permeation at steady state, the mass flux reads:

$$J = -\frac{dm_F}{dt} = A \cdot M \cdot \frac{D_p}{k_p} \cdot \frac{\Delta p}{l_p} \qquad \text{(III.1)}$$

- *Conditions and assumptions added to the [D]ecision step*

The simple mass transfer model (III.1) incorporates all the details of the design. Its integration with time enables to construct an estimator of shelf-life:

$$t_{shelf} = \frac{\%\Delta m_F}{J} m_F^{t=0} = \%\Delta m_F \frac{\rho_F V_F^{t=0}}{A \cdot M \cdot \Delta p} \frac{k_p}{D_p} l_p = \%\Delta m_F \frac{\rho_F V_F^{t=0}}{A^2 \cdot M \cdot \Delta p} \frac{k_p}{D_p} \frac{m_p}{\rho_p} \qquad \text{(III.2)}$$

or of the packaging weight:

$$m_P = A\rho_p l_p = \frac{\rho_p}{\rho_F}\frac{D_p}{k_p}\frac{A}{V_F^{t=0}}\cdot A\frac{M\Delta p}{\%\Delta m_F}t_{shelf} \qquad \text{(III.3)}$$

- *Goals and constraints considered in the [S]olving step*

Eq. (III.3) demonstrates that the best shape must have the lowest $A/V_F^{t=0}$ ratio, which is obtained for a sphere. Arbitrary shapes can be interpolated or extrapolated from designs D_1 to D_4 by using the concept of sphericity (Wadell, 1935) defined as $\Psi = \pi^{\frac{1}{3}}\left(6V_F^{t=0}\right)^{\frac{2}{3}}/A$ and varying from a value significantly lower than 1 for an aspherical design to unity for a perfect sphere. Typical values of Ψ for regular polyhedrons are presented in **Figure III-3** and values for designs D_1.. D_4 shown in **Figure III-2**.

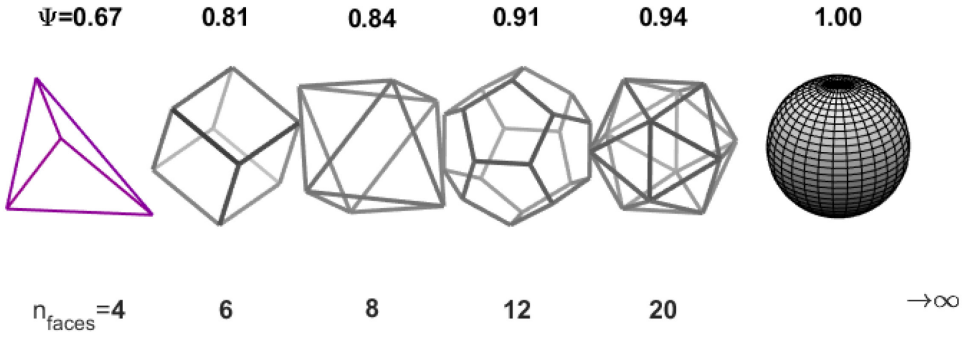

***Figure III-3**. Typical sphericity values for convex regular polyhedrons.*

In first approximation, the impact of the packaging, denoted M_p, is proportional to the number of units to reach an average consumption $\langle V_{consumption} \rangle$:

$$M_P = \frac{\langle V_{consumption} \rangle}{V_F^{t=0}} m_P = \left(\frac{36\pi}{V_F^{t=0}}\right)^{\frac{2}{3}} \frac{\rho_p}{\rho_F}\frac{D_p}{k_p}\frac{1}{\Psi^2}\frac{M\Delta p}{\%\Delta m_F}t_{shelf}\langle V_{consumption} \rangle \qquad \text{(III.4)}$$

Eq. (III.4) does not consider the obsolescence (concept of secondary shelf-life shown in II.4.1.), when the primary shelf-life is too short. The number of bottle units to meet $\langle V_{consumption} \rangle$ must account also for the time needed to finish the bottle, $t_{consumption}$.

$$M_P\left(V_F^{t=0}\right) = \max\left(\frac{\langle V_{consumption} \rangle}{V_F^{t=0}}, \frac{t_{consumption}}{t_{shelf}}\right) m_P \qquad \text{(III.5)}$$

The impact results are respectively to a bottle of 1 L with a shelf-life of one year chosen to be outside the explored domain. Finally, the polytope encompassing all feasible solutions obeys to the following convex set of constraints:

$$
\begin{aligned}
&(a)\ t_{\text{chain}}^{\text{supply}} + t_{\text{consumption}}^{\text{low-profile}} \le t_{shelf} \le 2 \text{ years} \\
&(b)\ m_p^{sphere} \le m_p \le m_p^{D_1, V_F^{t=0}} \\
&(c)\ 0.25 \text{ L} \le V_F^{t=0} \le 0.75 \text{ L}
\end{aligned}
\tag{III.6}
$$

Shelf-life inequalities (a) in Eq. (III.6) integrate distribution time ($t_{\text{chain}}^{\text{supply}}$, chosen to be equal to 3 months) and the time of consumption ($t_{\text{consumption}}^{\text{low-profile}}$) for a low consumer (one glass per month). Inequalities are enforced by the physics: the best design is D_4 and the worst D_1.

III.2.3.4. Solutions

The feasible solutions matching the constraints (III.6) are shown in **Figure III-4**. The possible solutions for problem **Q1** (maximum shelf-life) are denoted A-D for the designs D_1.. D_4. The opposite points (minimum shelf-life) are identified by the vertical segment $A'D'$. When the bottle capacity is imposed, all solutions lie between $A'D'DA$. Contrary to intuition, the weight of packaging increases slowly with the capacity of the bottle when the shelf-life is fixed. Due to their larger specific area, walls are indeed thicker in small bottles. Due to the longer time to drink the content of a large bottle, the viability domain is consequently reduced with large bottles. In all cases, D_4 bottles are more than twice lighter than D_1 ones.

Relaxing the shelf-life constraint enables to generate solutions for problem **Q2,** which are as efficient as point D (same weight) but at the expense of a reduced shelf-life. They are denoted α , β, γ , respectively to designs D_1, D_2 and D_3. As an illustration for a 0.25 L bottle, substituting solution A by solution B reduces weight by 19% whereas substituting by solution β offers a weight gain of -55%, for a shelf-life loss of -42%. Such optimizations are viable for bottles with capacities equal or smaller than 0.5 L. Beyond 0.5 L, low consumers waste beverages. Problem **Q2** accepts a variant formulation with a prescribed weight (e.g. 20 g), the solutions are a, b and c. Imposing a too low weight is acceptable only for small bottles offering the best compromise between weight and enough consumption time.

Problems **Q1** and **Q2** seek solutions with the bottle as a functional unit. Choosing a yearly intake instead changes the perspective. Parameterizing the bottle shape with a single scalar Ψ enables to shift continuously from one shape to another one. The functional $M_p\left(V_F^{t=0}, t_{shelf}, \Psi\right)$ offers a continuous strategy to resolve **Q3**. The impacts of the largest bottle (0.75 L) is one magnitude order smaller than with the smallest one (0.05 L). This effect is mainly related to the larger number of bottles to reach the same consumption. According to Eq. (III.4), M_p decreases as Ψ^{-2} suggesting that ellipsoidal shapes (large and small radii set to b and a, respectively) could improve slightly the results by approaching the sphere as soon

as $b \approx a$. Since the impact for a same consumption is independent of shelf-life for a same consumption rate, the problems of shelf-life and weight of packaging appears decoupled (horizontal iso-M_p values). One important consequence is that in presence of various consumers, the optimal solution should propose various formats adapted to the consumption: one large format for high consumers and much smaller ones for low consumers.

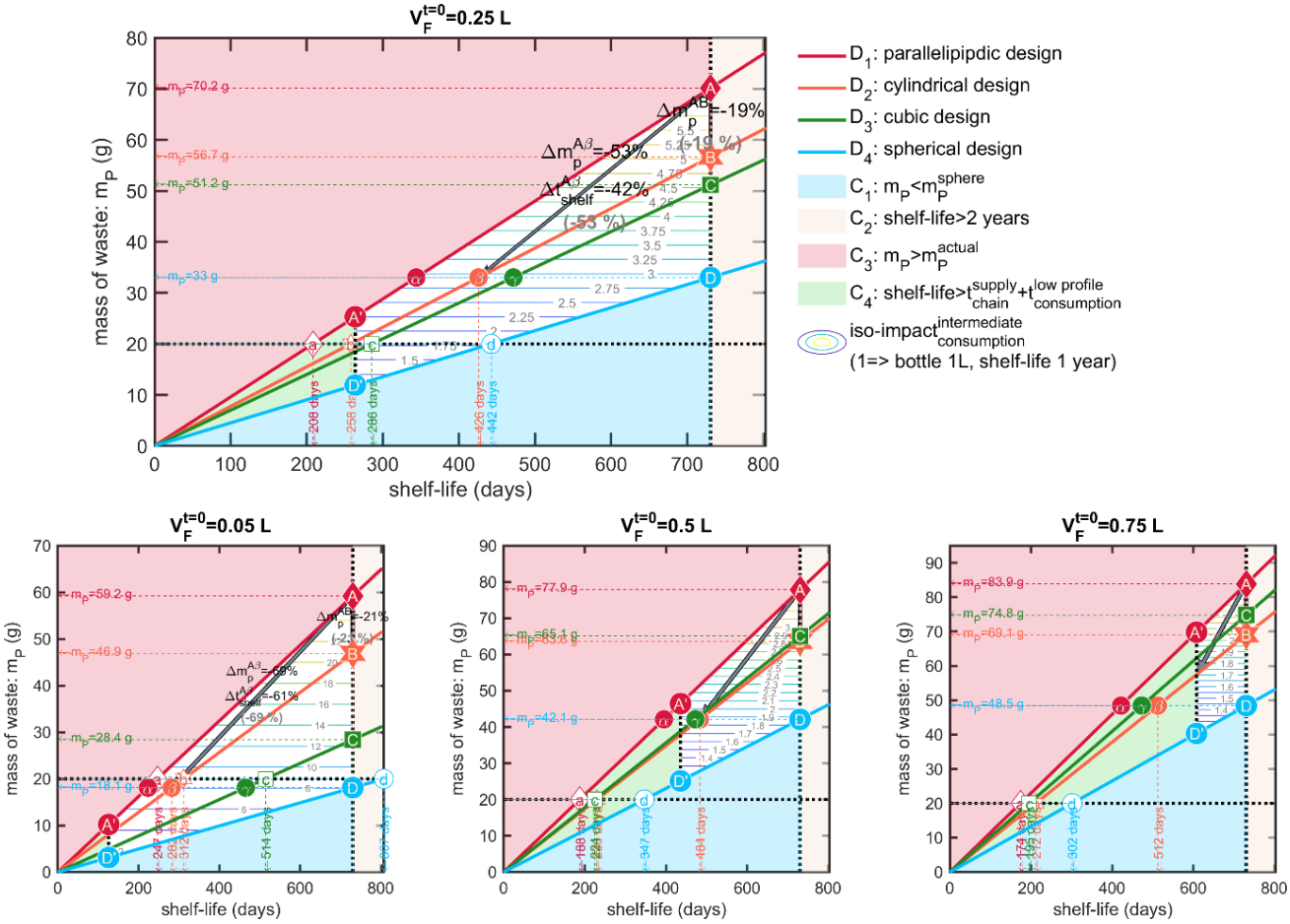

Figure III-4. *Weights of the bottle (counted as 100% waste) versus shelf-life for the designs* D_1.. D_4 *calculated according to Eq.* (III.3) *for bottle capacities* $V_F^{t=0}$ *ranging from 0.05 L to 0.75 L.*

The design offer (format, shape) should be enough flexible to adapt the demand to minimize environmental impacts and not only the consumer convenience. Packaging formats and shapes need to be revised regularly to adapt to the evolution of the supply chain and consumer practices. The generalization of these calculations for real beverages and packaging is at the core of the proposed research work.

III.3. Specific objectives and approaches

- *List of specific objectives:* $O_1 \dots O_{11}$

The [E][D][S] framework is enough generic to resolve many types of mass transfer problems and their consequences on packaging design. Its development and consolidation beyond the presented case-study focused on the linked technological problems listed in **Table III-1.** Each optimization goal was translated into eleven scientific questions or specific objectives ($O_1 \dots O_{11}$), which could be resolved with the tools of research. **Alcoholic beverages** were chosen as a template of optimization problems involving packaging materials in contact with interacting liquids facilitating mass transfer from the food to the surrounding (mass loss, change in composition) and from the packaging to the food (migration). **Polyethylene terephthalate (PET)** was chosen as reference model material. The modular structure of the framework enabled to build and extend progressively the number of goals considered in the global multicriteria optimization problem. The approach involves theory, modeling, simulation, coding and different validation experiments to guarantee the robustness of the choices for alcoholic beverages in contact with PET. Without a loss of generality, water-ethanol mixtures were used as food simulants instead of real beverages.

Table III-1*. Specific goals to be extended and the corresponding approach followed in this work*

Goals to reach "optimal Design"	Step(s) to be refined†	Scientific objectives $O_1 \dots O_{11}$	Approaches followed in this work
Shelf-life maximization	[E] *(filling cognitive gaps)*	O1/ **Thermodynamics** of the beverage O2/ **Mutual diffusion and sorption** (water-ethanol) in the polymer O3/ **Activation of diffusion and sorption** by temperature and plasticizing	O1-O3/ **Theoretical approach** (UNIFAC for water-ethanol mixtures, free-volume for diffusion, ternary Flory isotherms) O2-O3/ **Experimental approach** to assess the validity limits of models and uncertainties associated to them **on materials with uniform thicknesses (PET films)**.
Packaging weight minimization	[E][D][S] (extending tools and validation)	O4/ **Water and ethanol sorption and permeation through a "complex" geometry with a thickness profile.** O5/ **Risk of plasticizing and aging** of the structure with a thickness profile.	O4/ **3D simulation scheme** with **implicit food model** and **section refactorization**. O4/ **Real challenge test on real bottles** filled with model hydroalcoholic solutions in controlled conditions. O5/ **Identification of polymer relaxations after exposure to water**, ethanol on thin and thick films. Microstructure determinations via intrinsic fluorescence, Raman and FTIR-ATR microspectroscopy (results not shown)

Packaging shape optimization (evolutive geometry)	[E][S] (sophisticated geometry models)	O6/ **Parametric geometry models** of arbitrary bottle shapes (with cylindrical symmetry or not) defined by a set of constraints (shape, capacity, opening, neck length, additional constraints such as shape feasibility)	O6/ **Parametric geometry coding** (solid of revolution, projection of arbitrary surface), volume discretization (curvilinear, triangular, quadrangle). O6/ **Geometry solver to verify design constraints** and **specifications** (internal volume integration, regularized splines, etc.)
Minimization the risk of mechanical constraints (overpressure and collapse)	[E][D] (implicit model)	O7/ **Mass transfer balance on the headspace**	O7/ **compressible mass transfer model** integrating the thermal expansion of gases and liquids. Oxygen and nitrogen will be assumed insoluble in the beverage.
Minimization of the migration	[E] (molecular model)	O8/ **General model of diffusion coefficients** (other properties such as activity coefficients are expected to be calculated at atomistic scale using the methods detailed in §V.4.)	O8/ **parameterization of the general coarse-grained model** of diffusion in arbitrary polymers (above and below T_g)
Maximization of the amount of recycled materials	[D][S] (linking design)	O9/ **Risk formulation integrating design** in alcoholic beverages (see §V.2.)	O9/ **Optimization scheme** accounting for the bottle capacity and shape, maximum ethanol consumption, ethanol-strength
Integration of all goals together	[S] software integration and robustness analysis	O10/ Looping evaluation, decision and solving steps into a **seamless formulation** with prioritization of assumptions and scenarios. O11/ Sensitivity analysis and risk assessment	O10-O11/ **Integration within an expandable toolbox** written in mainly in Matlab language and object-oriented. **The mutiobjective optimization problem** is an ill-posed problem without clear meaning when all goals cannot be achieved simultaneously. The sequential optimization enables to introduce interactions and to combine several methods (active set method, goal achievement).

†comparatively to the case-study presented in §III.2.3.

- *Overview of targeted capabilities and extensions of the [E][D][S] framework*

The [E][D][S] framework is enough flexible to accommodate future evolutions and extensions. They are reviewed in **Figure III-5**. All the tools and concepts have been thought with the extensions in mind, even if they are not implemented yet or are available from external modules already developed by the hosting laboratory. The contribution of the thesis is to prepare the "ecosystem" of these new tools by removing the main scientific obstacles. Though the packaging parameterization focused on PET bottles, other materials and kind of packaging could be implemented. Closure systems (sealants, caps) were not considered in this version, as it was admitted that the reproducible mass loss was due to the permeation through the bottle walls. Leaks from closures were by contrast responsible for random and accidental mass losses. PET films and bottles differ due to their biaxially and uniaxially orientation. In first

approximation, thin PET films were thought to offer a good prototype of materials with uniform and thin thicknesses to study in a reasonable amount of time diffusion and sorption properties. The validity and limits of these choices are discussed in §V.3.

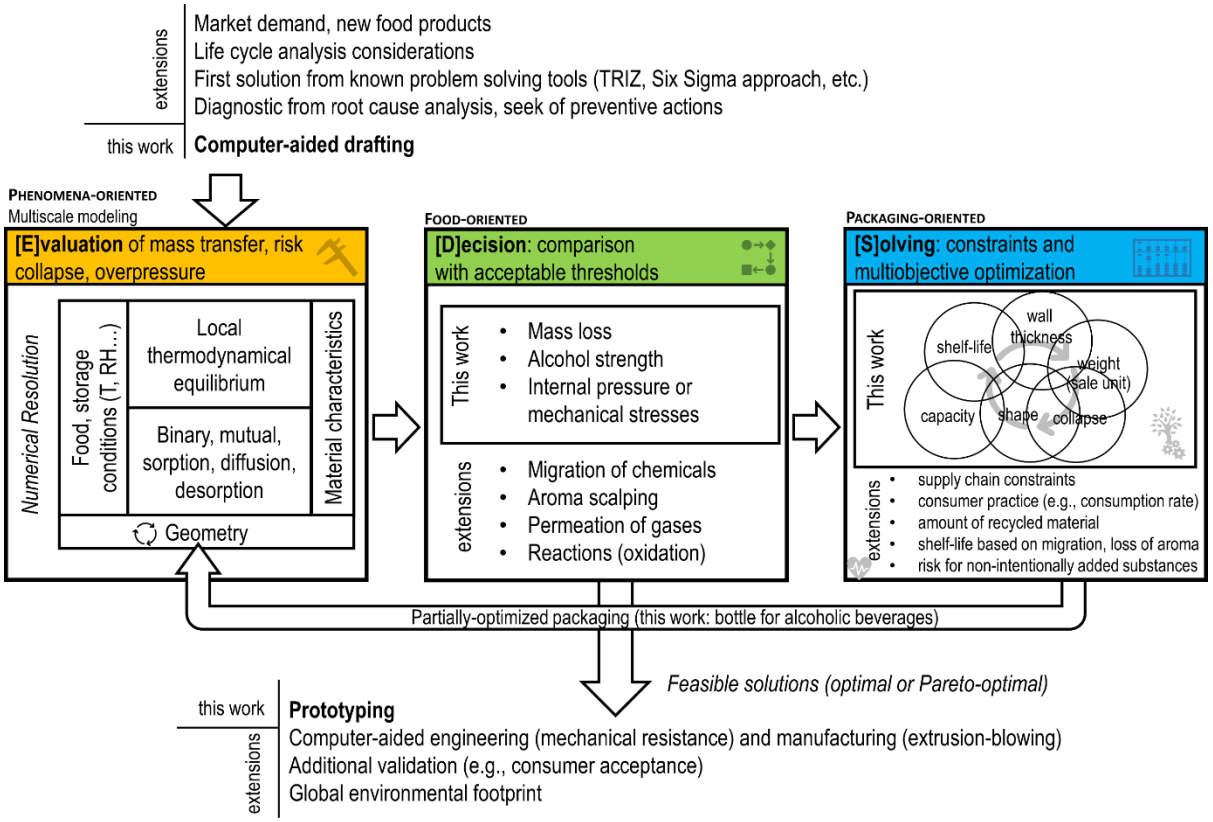

***Figure III-5**. Main capabilities (this work) and foreseen evolutions (considered by construction) in the considered [E][D][S] framework*

- *A multi-resolution [E][D][S] framework*

The framework as the superposition of independent steps [E], [D] and [S]. In the general case, the [E]valuation step, involving the resolution of coupled non-linear partial differential equations, is the most computationally intensive task, far before the [D]ecision and the iterative [S]olving steps. The [E]valuation step itself was constructed by reusing an earlier nested modeling library developed by INRA, enabling to couple many simulation steps together (see §II.2.3.6.), as well as deterministic and probabilistic modeling (see §II.2.6.). Following the same strategy and by reusing the tier approach shown in §II.2.2. , the steps [D] and [S] were nested into the [E]valuation one and calculated as a sequence: $\left[E_{T1}^{tier}[D][S]\right] \rightarrow \left[E_{T2}^{tier}[D][S]\right] \rightarrow \left[E_{T3}^{tier}[D][S]\right] \rightarrow$ ... For example, parameterizing a 3D geometry to fit a given capacity and bottle shape, followed by the generation of a valid mesh, is a very fast step and can

be repeated as necessary within the $\left[E_{T_i}^{tier}[D][S]\right]$ step. Conversely, the resolution with full coupling over the entire beverage shelf-life (several months) needs to be restricted to feasible solutions or even better to the solutions belonging to the Pareto front.

Coarse but consistent simulations are sufficient to explore a large domain, whereas detailed simulations combined with proper sensitivity analysis are required only for validation purposes. As a result, the optimization problem was formulated as a multiresolution (different tiers) and multiscale (molecular scale for transport and thermodynamic properties, mass transfer at the scale of walls, shelf-life scale) simulation problem. Since there is no general rule to define *a priori* the proper levels of details required to describe the considered mass diffusion problems, a systematic comparison with the results obtained with the next tier or experiments were considered. Up to five tiers were included as shown in **Table III-2**.

***Table III-2**. List of the considered tiers in the nested formulation* $\left[E_{T_i}^{tier}[D][S]\right]$

tier T_i	Macroscopic description	Transport properties and other phenomena	Strategy to evaluate the refinement needs
T_1	Decoupled fluxes in the walls, no coupling with the mass balance in the liquid	Constant and uniform (tabulated data, free-volume theory and Flory-Huggins at infinite dilution)	comparison with T2
T_2	as T1 with coupling in the liquid	Food thermodynamic model	Comparison with experiments and T3
T_3	as T2 with plasticizing effects (and polymer relaxation)	as T1 and T2 with concentration or volume fraction as parameter	Comparison with experiments associated to long-term contact and thin films.
T_4	as T3 with coupling between fluxes	Phenomena to be identified firstly.	Hysteresis

Chapter IV. MATERIALS AND METHODS

Chapter IV. Materials and Methods

This chapter summarizes the main materials and methods used in this study. The work was both experimental and theoretical using modeling and simulations. The framework [E]valuation, [D]ecision and [S]olving is generic and it has been developed to be applicable theoretically to any packaged food product and related systems with proper extensions (see the scope in **Figure III-5**. Main capabilities (this work) and foreseen evolutions (considered by construction) in the considered [E][D][S] framework). Though its design was general, it was developed with a primarily focus on alcoholic beverages.

IV.1. Materials

Polyethylene terephthalate (PET) in contact with hydroalcoholic solutions was chosen as reference material to support assumptions and validation of the [E][D][S] framework. The extensions to other materials and to the mass transfer of other solutes were considered by assembling databases of transport and thermodynamic properties from literature and obtained partly from a collaboration with Fraunhofer Institut für Verfahrenstechnik und Verpackung (Freising, Germany).

IV.1.1. Studied PET materials

- *Overview*

Experimental approaches on PET provided reference values (e.g. kinetics, equilibrium curves) for estimating specific properties and for validating assumptions and predictions. The different PET materials are reviewed in ***Table IV-1***.

Two kinds of PET materials were considered:

1. **Twelve micrometers thick** biaxially oriented PET films with uniform thickness and good thermal stability due to biorientation
2. **PET bottles** with heterogeneous orientation, crystallinity and thickness (from hundreds of micrometers to several millimeters).

The microstructures of the two PET materials were not identical and the transposition of the results from one to the other required proper assessment. Thin films were preferred for all thermodynamical and mass transport characterization. Bottles were used for validation and

deformulation. It is thought, nevertheless, that the structure rigidity of bottles blocks lateral thermal expansion and swelling as in biaxially oriented PET films with thermal expansion lower than 1% between ambient and 100°C. As a result, transport and thermodynamic obtained on bottles and films were thought to be *a priori* exchangeable at the first tiers.

Table IV-1. *Studied PET films and bottles*

format	code	type	reference (supplier)	goals
thin film 12 µm	F1	biaxially-oriented monolayer PET film crystallinity:31 ± 1 %†, T_g=77±1°C‡	Lumirror 60.01 (Toray, France)	reference transport and thermodynamic measurements
	F2	biaxially-oriented coextruded PET film	Lumirror 10.21 (Toray, France)	
	F3	biaxially-oriented	FLEXPET F-PAP (Amcor, Canada)	
	F4	biaxially-oriented PET film	commercial film (Solvay, Belgium)	
23 µm	F5	biaxially-oriented PET film	commercial film (Solvay, Belgium)	
bottles	M	miniature PET bottles (capacity 55 mL, weight of 10.4 ± 0.2 g wall thickness: 0.42 mm – 2.3 mm) crystallinity: 32 ± 1.2%†, T_g=82±1°C‡	Miniature PET bottle 55mL (Pernod Ricard, France)	validation of shelf-life prediction
	X	PET bottle of 150 mL to be designed as an alternative of bottle M for aerial transport	the bottle exists only virtually	case study

†value estimated by differential scanning calorimetry (DSC, model DSC 3, Mettler Toledo, Switzerland) on three samples with an enthalpy of fusion of 140.1 J·g^{-1} (Wunderlich, 2005); ‡value was inferred from DSC measurements (model DSC Q100, TA Instruments, USA) with a heating rate of 10 °C·min^{-1}.

- *Miniature bottles (M)*

PET miniatures play a significant role as they were used for validating the capacity to predict shelf-life in variable storage conditions. The geometry model determined over 10 bottles is shown in **Figure IV-1**. Thicknesses were measured by dissection and with the help of a magnetic wall thickness gauge (model MiniTest 7200 FH with probe FH10, ElektroPhysik GmbH, Germany). As the miniatures are produced directly by injection-blowing (no preform), the distribution of the PET matter is not uniform radially. As a result, the variation of thickness presented in **Figure IV-1**c (based on more than 2,000 measurements) is mainly associated to internal variations within the same bottles.

During permeation tests, miniature bottles were sealed with 21.5 mm diameter pre-cut foils (aluminum-polyester lid, supplier Embatherm, France) as shown in ***Figure IV-1***d. A lab-scale pneumatic-controlled heat sealer (model TIME 160, Embatherm, France) was used with a set temperature of 180°C and a set pressure of 200 kPa. The capacity to extend shelf-life was investigating by adding a sleeve (thermo-shrinking PET film, reference PET sleeve label, Fuji Seal France SAS, France) to some bottles after a prescribed storage time. It is worth noticing that the sleeve and studied films in ***Table IV-1*** are different. Sleeves are strongly subcooled PET, which crystallize during heating whereas PET films F1-F3 include biaxially oriented crystallites blocking thermal expansion.

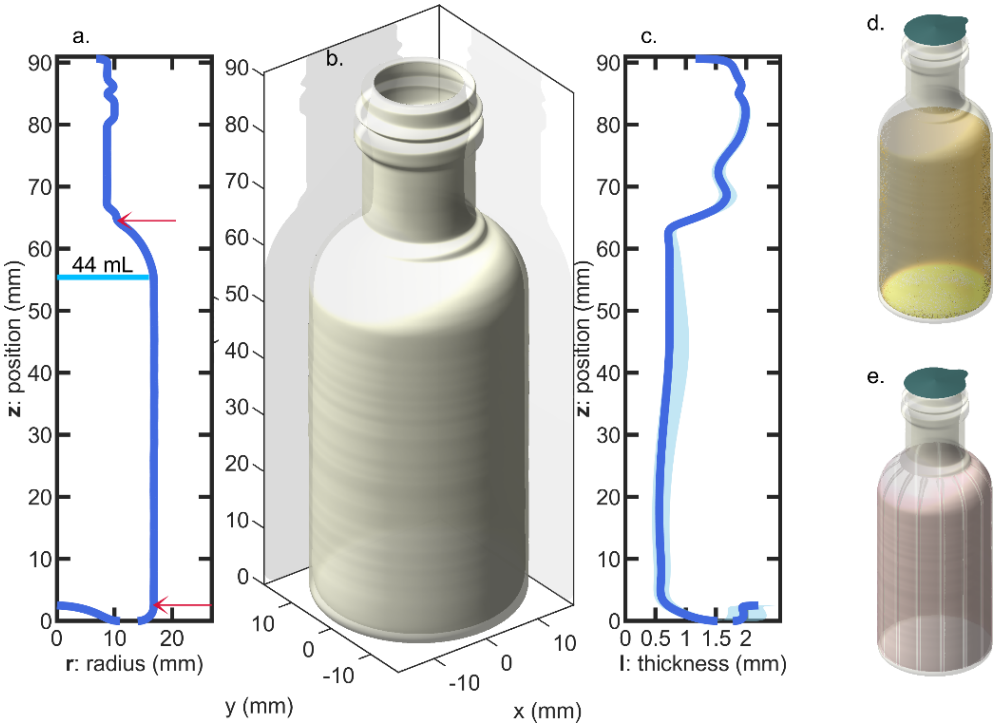

Figure IV-1. *Bottle geometry: (a) radius profile (the arrows indicate the top and bottom position of the sleeve and the vertical line indicate the level of liquid for pure water); (b) 3D-representation assuming a revolution geometry; (c) thickness profile (the shadow indicates the variation range of measurements among 10 bottles); (d) filled and sealed bottle; (e) bottle equipped with a shrink sleeve label.*

- *New project of PET miniature bottle (X)*

Shape optimization was illustrated on bottles homothetic to the 3D shape presented in ***Figure IV-2*** (non-optimized). For all generated bottles, the geometry was calculated so that the internal volume matched 160 mL for a nominal capacity of $V_{beverage} = 150$ mL and a shelf-life of at least 180 days at 25°C for a vodka-type beverage.

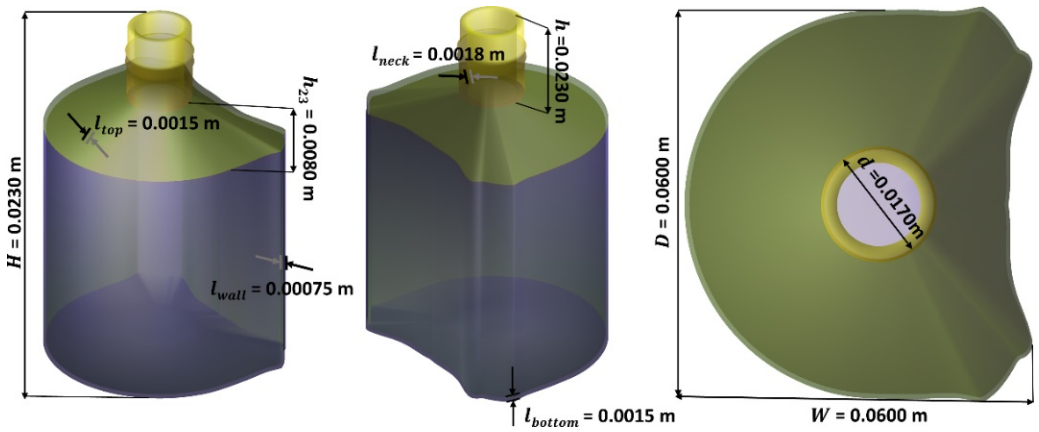

Figure IV-2.*Example of initial bottle design to be optimized*

IV.1.2. Reference data and properties

The [E]valuation step relies on a tiered approach. The "tiers" used in this work are essentially mass transfer models that progress in complexity and data requirements, intended to produce gradually more robust estimations of the mass transfer contributions: sorption, desorption and diffusion. The comparison between the current and refined scenarios was used to estimate the uncertainty associated to the considered idealization. This approach is expected to bring more insights than the direct comparison with macroscopic experiments, which spread the uncertainty over all considered phenomena. Since the iterative process was stopped when no further refinement was obtained, computational resources and algorithmic complexity was focused on essential phenomena, whose identifications were also part of the ambition of this work.

At the first tier (see **Table III-2**), diffusion and solubilities are assumed constant and to depend only on temperature. These assumptions were formulated for water and ethanol in PET, but they were enough general for other polymers and conditions of mutual diffusion (see §II.2.4.). More general descriptions at higher tiers were devised by collecting reference data to parameterize general ternary Flory-Huggins isotherms of water and ethanol in PET at arbitrary temperatures and an extended free-volume blob-model for trace diffusion in arbitrary polymers.

IV.1.2.1. Properties of water-ethanol mixtures

The thermodynamical properties of water, ethanol pure or in mixtures are required to parameterize the driven forces applied at the boundaries of the packaging walls. Alcohol-by-volume denoted *abv*, was chosen as intensive value was chosen as intensive value to describe the composition of hydroalcoholic solutions. It is legally defined in EU as "the ratio of the volume of pure alcohol present in the product in question at 20°C to the total volume of that product at the same temperature" (see Annex I of EU Regulation 110/2008/EC).

- *Vapor saturation pressures*

Saturation pressures of water and ethanol were approximated with a good accuracy via the modified Goff and Gratch equation (see Eq.(III.7) in Goff, 1946;1957) and with the Antoine equation (see Eq.(III.8) in DDBST, 2018) for water and ethanol, respectively.

With pressures in Pa and temperatures in K, $p_{w,sat}^{(T)}$ reads:

$$\log_{10} p_{w,sat}^{(T)} = -7.90298\left(\frac{T_{w,sat}}{T}-1\right)+5.02808\log_{10}\frac{T_{w,sat}}{T} -1.3816\cdot10^{-7}\left(10^{11.344\left(1-\frac{T}{T_{w,sat}}\right)}-1\right)+8.1328\cdot10^{-3}\left(10^{3.49149*\left(1-\frac{T_{w,sat}}{T}\right)}-1\right)+\log_{10} P_{\text{std}} \quad \text{(IV.1)}$$

with all temperatures in Kelvin and the water saturation temperature $T_{w,sat} = 373.15\ K$ chosen at the standard pressure P_{std} =101324.6 Pa.

Similarly, $p_{e,sat}^{(T)}$ reads:

$$\log_{10} p_{e,sat}^{(T)} = 2.12490 + A - \frac{B}{C+T} \quad \text{(IV.2)}$$

with $A = 8.20417$, $B = 1642.89$, $C = 230.3$ for $-57 \le T \le 80°C$.

- *Densities of mixtures between 10°C and 60°C*

The procedure of calculation overpressure in headspace requires accurate determinations of $\rho_{w+e}^{(T,abv)}$. Values in vacuum have been initially tabulated by OIML (1975) ranging from -20°C up to 40°C, with factual errors discussed in Chanson (2015) to include the revised formula proposed by Bettin and Spieweck (1990). The upper limit of 40°C was imposed by the decrease of the boiling point of ethanol at low pressures. In this study, an extensive database was compiled by assembling the OIML data and by extending them with the predictions of the commercial software AlcoDens (version 3.3, Katmar Software, USA) above 40°C. The slight compressibility of the mixture at atmospheric pressure was based on the compressibility values was corrected from the values reported by the US National Bureau of Standards in Table 6 of CFR (2006) originated from Osborne *et al.* (1913).

- *Activity coefficients in hydroalcoholic solutions*

Vapor-liquid equilibria of hydroalcoholic mixtures were calculated from the UNIFAC contribution method (Wittig *et al.*, 2003).

IV.1.2.2. Reference diffusion and Henry coefficients of water and ethanol in PET at tiers 1,2

At the first tier, diffusion and sorption in PET are assumed to be independent of crystallinity, orientation, subcooling effects, aging and to remain constant with time and concentration. These assumptions are acceptable for diffusivity of water but look restrictive for ethanol. The corresponding properties at tiers 1 and 2 are reported in ***Table IV-3***.

Table IV-2. *Thermodynamic and transport properties of water and ethanol in PET*

Diffusivities	Values	Tier	Deborah number[i]	
			l=12 µm	l=628 µm
$D_w^{T=35°C}$	[a]1.5 × 10⁻¹² m²·s⁻¹	1,2	5180	1.89
$D_w^{T=50°C}$	[b]2.6 × 10⁻¹² m²·s⁻¹	1,2	7637	2.79
$D_e^{T=35°C}$ when abv = 0.15	[c]5.5 × 10⁻¹⁶ m²·s⁻¹	1	1.90	6.9 10⁻⁴
$D_e^{T=35°C}$ when abv = 0.4	[c]6.3 × 10⁻¹⁶ m²·s⁻¹	2	2.18	7.9 10⁻⁴
$D_e^{T=35°C}$ when abv = 0.7	[c]8.9 × 10⁻¹⁶ m²·s⁻¹	2	3.07	1.1 10⁻³
$D_e^{T=50°C}$ when abv = 0.7	[d]2.4 × 10⁻¹⁵ m²·s⁻¹	2	0.70	2.6 10⁻⁴
Saturation concentrations	**Values**	**Tier**		
$C_{w,sat}^{T=35°C}$	[e]0.0118 kg· kg⁻¹ dry PET	1	-	-
$C_{w,sat}^{T=50°C}$	[f]0.0107 kg· kg⁻¹ dry PET	1	-	-
$C_{e,sat}^{T=35°C}$	[g]0.0208 kg· kg⁻¹ dry PET	1	-	-
$C_{e,sat}^{T=50°C}$	[h]0.0224 kg· kg⁻¹ dry PET	1	-	-

[a]from the Supplemental Information of Burgess *et al.* (2014a); [b]by assuming an activation energy of 49 ± 5 kJ/mol extracted from table 1 between 23°C and 50°C, and averaged over the range of RH between 10% and 90% of Dubelley *et al.* (2017a); [c]from figures 6 and 12 with the conversion between abv and p/po from figure 2 of Chandra and Koros (2009b); [d]from (35 °C, abv = 0.7) calculated with Arrhenius activation by T an apparent activation energy 54 kJ/mol; [e]from figure 3 of Burgess *et al.* (2014b); [f]from table I of Launay *et al.* (1999); [g]from table 3 of Chandra and Koros (2009b); [h]from inhouse vapor sorption experiments with the help of a gravimetric microbalance (model: DVS Resolution, Surface Measurement Systems Ltd.). [i]Deborah number $Deb = 10^{12}\frac{D_i}{l^2}\exp\left(-\frac{17.74(T-T_g)}{51.6+T-T_g}\right)$ calculated for a characteristic thickness l according to Billovits and Durning (1988).

IV.1.2.3. Reference mutual sorption properties of water and ethanol in PET at higher tiers

At higher tiers, concentration effects and possible effects of physical and chemical ageing need to be accounted. The sophistications capable to describe hysteresis are important but the number of supporting data is limited. ***Table IV-4*** collects reference data used in this work to test and parameterize the different level of refinements.

Table IV-3. *Consolidated data t D_e o develop and validate high-tier modeling in PET*

Sophistication	Solute	Material code or Reference	Activity range (a_e *or* a_w)	Temperature range (°C)
Effects of concentration in binary diffusion	water	F1,F2,F3,F4,F5,M References see **Figure V-16a**	0-1	20,23,25,35,50,60, 70,80,90,100
	ethanol	F1,F2,F3,M References see **Figure V-16a**	0-1	4,25,35,40,50,57
	methanol	Chandra and Koros (2009b)	0-0.95	35
Effects of concentration in ternary isotherm	water, ethanol	F1,M	-	40,50
Effects of physical aging (polymer plasticization, relaxation, densification)	water	Dubelley *et al.*, 2017a	0-0.9	23,40,50,60,70
Hysteresis	water	F1,M	0-0.95	25,50
Solute-specific relaxation	water, ethanol, toluene	F1,M	1	50

IV.1.2.4. Database of trace diffusion coefficients of rigid, linear and anchored solutes in seven polymers

Trace diffusion coefficients (D) are essential properties to [E]valuate shelf-life and migration. They are scarce in many polymers relevant for food applications polyesters, polyvinyls and polyamides. These barrier polymers are glassy at room temperature and D values are particularly difficult to estimate. In this work, a general model of diffusion involving rigid blobs connected or not, with similar shape or not, with similar size or not is intended to be developed and extended from rubber to glassy state. Its design and validation require large data sets of D values on homologous solutes collected at different temperatures on the same material and with the same methodology of measurement. A database of 433 D values in seven polymers with various chemical structures and polarities was assembled. As the blobs of the solute need to be discussed according to their resemblance with the blobs of the polymers, three polymer families were considered.

- *aliphatic polymers*: low-density polyethylene (PE), polystyrene (PS); polyvinyl acetate (PVAc); poly (methyl methacrylate) (PMMA), polyamide 6 (PA6);
- *semi-aromatic* polymers: poly (ethylene terephthalate) (PET); poly(ethylene naphthalate) (PEN);
- *aromatic polymer*: polystyrene (PS).

The content of the database is summarized in **Table IV-5** with the selection procedure detailed in table footnotes. Concentration ranges, polymer plasticization and additional parameters such as polymer crystallinity were common criteria to decide whether D values were introduced or not. The broad temperature range covers $-70\ \mathrm{K} \le T - T_g \le 160\ \mathrm{K}$, where T is the absolute temperature and T_g the glass transition temperature. Original Free Volume Theory (FVT, see §II.2.4.) has been parameterized on mutual diffusivities of small solutes (usually solvents) in amorphous polymers with values typically above 10^{-13} $m^2 \cdot s^{-1}$. Diffusivities listed in **Table IV-5** originated conversely uniquely from larger solutes (e.g. *n*-alkanes, 1-alcohols) and were collected at infinite dilution and on industrial-thin films at both glassy and rubber states. The molecular mass of the repeated unit is denoted M_{blob} whereas the molecular mass of pattern larger than M_{blob} is called anchor with a molecular mass denoted M_{anchor}. The definitions of anchors and blobs were not unique, and they corresponded to the somewhat arbitrary definitions of the rigid jumping units in the solute. The power laws associated to the scaling of D were, nevertheless, shown to be invariant with the replacement of M_{blob} by $k \cdot M_{blob}$, with k a

small integer greater than unity. Additionally, the list of polymers included polymers with parameterized FV parameters (PE, PS, PVAc, PMMA) and others without any FV parameterization (PET, PEN, PA6).

The 422 already published values were combined with 11 internal *D* values in PET from Fraunhofer (IVV, Freising, Germany) in an attempt to fill the most critical gaps: comparison of the behavior of n-alkanes with 1-alcohols, completion of the alkylbenzene series. Diffusion coefficients above T_g were inferred from the lag-times in permeation experiments. (Ewender and Welle, 2014) Values below T_g were measured using an automatic gravimetric microbalance (see §IV.2.2.) on film F1.

Table IV-4. *Overview of the database for binary diffusion coefficients in PET and in additional polymers used for validation*

	linear probes including an alkyl chains of mass M	range of M (g·mol^{-1})	M_{anchor}‡ (g·mol^{-1})	M_{blob}‡ (g·mol^{-1})	polymer	T_g (K)	experimental T range (K)	number of D values	Method of determination	References
Regular solutes	***n*-alkanes**	44 -198	0	28	PET	354	343- 373	35	(a)	(Ewender and Welle, 2014)
		170-310	0	28	PET	354	393 - 452	24	(b)	(Ewender and Welle, 2013, 2018)
		72 - 198	0	28	PA6	342	353 - 373	39	(a)	(Ewender and Welle, 2016)
		114-226	0	28	PS	367	348 - 418	24	(c)	(Bernardo, 2012)
		86 - 128	0	28	PVAc	305	363 - 383	12	(d)	(Arnould and Laurence, 1992)
		16 - 170	0	28	PEN	397	383 - 413	66	(a)	(Ewender and Welle, 2019)
Non-regular solutes	**1-alchohols**	43 - 113	17	28	PET	354	373	6	(a)	Fraunhofer Institute†
		43 - 113		28	PA6	342	343-373	21	(a)	(Ewender and Welle, 2016)
		15 - 225		28	PS	367	328-418	32	(c)	(Bernardo, 2013)
		43 - 113		28	PEN	397	383 - 413	30	(a)	(Ewender and Welle, 2019)
		15		14	PMMA	393	362 - 444	12	(e)	(Pawlisch *et al.*, 1988)
	alkyl-acetates	15 - 71	59	28	PVAc	305	333 - 383	25	(e)	(Arnould and Laurence, 1992)
		15	59	14	PMMA	393	398 - 434	4	(e)	(Pawlisch *et al.*, 1988)
	alkyl-benzenes	15 - 225	77	14	PS	373	383 - 413	21	(e)	(Pawlisch *et al.*, 1988)
		1 - 57		14	PET	354	373	5	(a)	Fraunhofer Institute †
	methacrylate	15	85	14	PMMA	393	408 - 434	3	(e)	(Pawlisch *et al.*, 1988)
Validation solutes	**water**	-	-	-	PET	349	292 - 463	48	(c,d,f,g)	(Kloppers *et al.*, 1993;Launay *et al.*, 1999;Sammon *et al.*, 2000;Shigetomi *et al.*, 2000;Eslami and Müller-Plathe, 2009;Dubelley *et al.*, 2017a)
	toluene	-	-	-	PMMA	354	403 - 433	3	(d)	(Zielinski and Duda, 1992)
					PS	373	383 - 451	5	(e,i)	(Zielinski and Duda, 1992;Vrentas and Vrentas, 1994b)
					PET	349[a] 333[b]	313 - 453	14	(a,b,d,h)	(Ewender and Welle, 2013, 2018) (Pennarun *et al.*, 2004;Franz and Welle, 2008)
					PVAc	305	313 - 383	3	(d)	(Zielinski and Duda, 1992)
					LDPE	153	343	1	(d)	(Lutzow *et al.*, 1999)
Total		**-**	**-**	**-**	**7 polymers**	**-**	**-**	**433 values**	**-**	**21 refs.**

† Welle (2016); [a]dry state and [b]swollen state of PET. Experimental method: (a) permeation experiments, (b) desorption (migration) experiments into a liquid, (c) gravimetric sorption after immersion in a liquid, (d) gravimetric sorption in the gas phase, (e) capillary column inverse gas chromatography, (f) FTIR-ATR method, (g) values calculated from molecular dynamics simulation, (h) from concentration profiles using solid-solid contact, (i) pulsed-gradient spin-echo NMR technique.

‡ M_{blob} is the molar mass of the rigid repeated unit: –CH_2-CH_2- or -CH_2-;‡ M_{anchor} is the molar mass of functional group as anchor in non-regulated solutes: -OH, -CH_3COO^-., C_6H_5- and $CH_3(CH_2)CCOO^-$.

IV.1.3. Studied solutes

- *Overview*

The solutes incorporated in the contacting phase (gas, liquid, solution) are listed in ***Table IV-5.*** Water and ethanol, alone or in mixtures were the main solutes. The composition of hydroalcoholic mixtures were denoted by their alcohol-by-volume (abv), defined as the number of liter (L) of pure ethanol present in 1 L of solution at 20 °C (pure ethanol: $abv = 1$).

Other aromatic solutes were surrogate molecules chosen with double purposes: comparison with literature data on similar PET materials and naturally fluorescent molecules consisting of linearly repeated jumping units. Toluene was preferred to benzene (single jumping unit) due to its high toxicity.

***Figure IV-3**. List of studied solutes*

Solute	Chemical structure	Phase contacting PET (alcohol-by-volume value)	Purpose
deionized water (0.01 meq/mL)		pure liquid or vapor *(0)*	sorption, permeation kinetics
ethanol (purity 99 v%)		liquid or vapor *(1)*	
hydroalcoholic solutions†	mixtures	liquid *(0.08,0.15,0.32,0.40,0.70,0.82,0.96)*	
water – ethanol		gas mixtures *(not defined)*	
toluene		vapor or in hexadecane solution (2 g·L^{-1})	sorption kinetics, concentration profiles
biphenyl	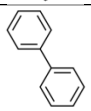	in 80:20 (v/v) dichloromethane-ethanol solution (10 g·L^{-1})	sorption profiles
p-terphenyl	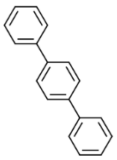	in 80:20 (v/v) dichloromethane-ethanol solution (~2 g·L^{-1})	sorption profiles

† prepared by mixing at 20°C±1°C a volume of ethanol matching the desired abv value with a *quantum satis* amount of water.

- *Safety considerations on the manipulation of large volume of water-ethanol mixtures in closed oven*

The manipulation of large amounts of ethanol above its flash point (13, 21, 26, 36°C for pure ethanol, 0.7, 0.4 and 0.2 *abv*, respectively) in soaking (films soaked in hydroalcoholic solutions) and permeation (bottles filled with hydroalcoholic solutions) experiments required specific precautions to reduce flammability hazards and the exposure of operators. Hazard analysis and risk assessment via modeling were systematically applied to assess whether the lower flammable limit (*LFL*) of ethanol (ca. 3.3%)(NFPA, 1994) could be exceeded. An example of risk calculations for miniature bottles stored in a closed oven for several weeks is shown in ***Figure IV-4***. The Monte-Carlo analysis considered an accumulation of ethanol due to permeation across the walls of the bottles and to a fraction of leaking bottles. The decrease of the number of bottles was considered. The time to reach *LFL* in the absence of air renewal gave the maximum duration the experiment could be ran without proceeding to an introduction of fresh air. For mixtures with 70% *abv* stored at 50°C, this duration was as low as 3 days; air was therefore renewed therefore three times per week at least.

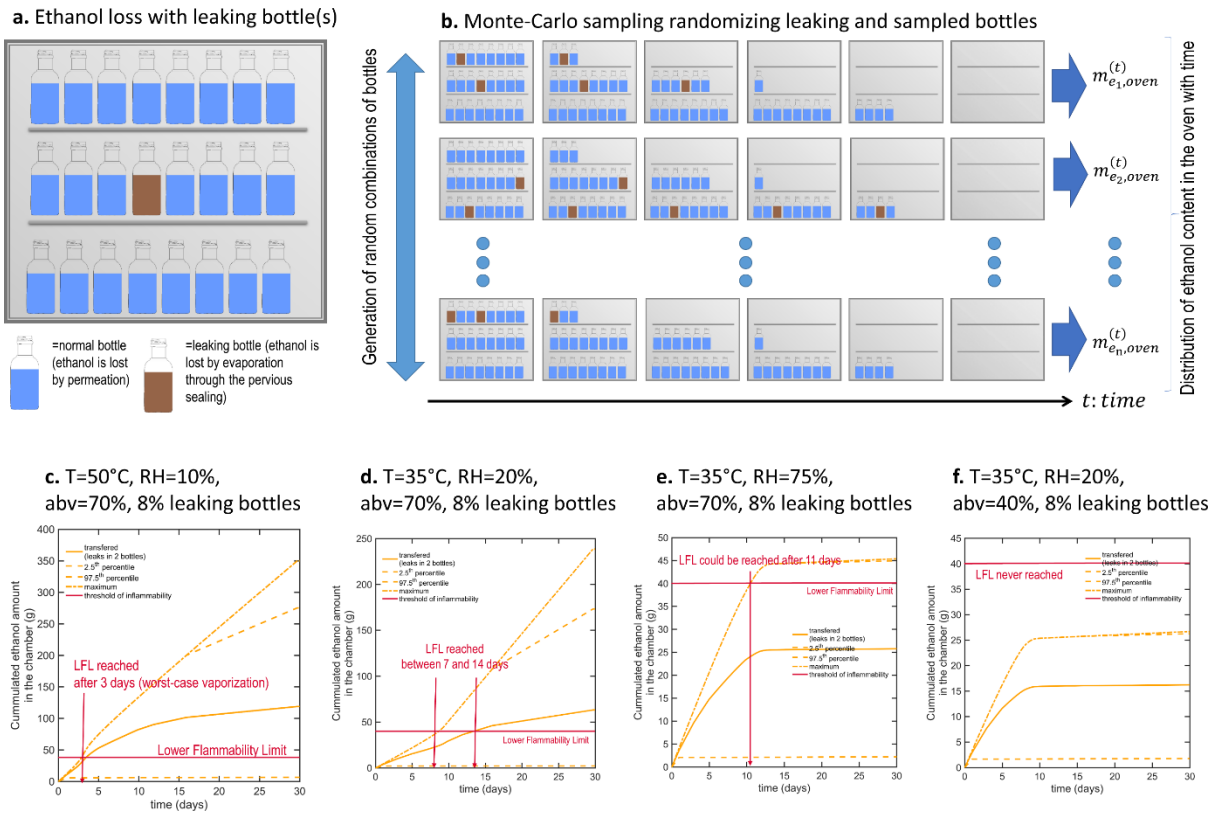

***Figure IV-4**. Example of calculations to estimate the risk of exceeding the lower flammability limit (LFL) in large scale experiments.*

IV.2. Experimental methods

Experiments fell in three categories: validation experiments of predictions at first tiers (1 or 2), identification of non-linear binary and ternary sorption and diffusion properties (tiers 3 and 4) and identification of chemical or structural modifications in PET at molecular level (tier 5). Additional experiments were carried out to identify the common migrants of PET from a significant sample of PET bottles used worldwide by the group Pernod-Ricard.

IV.2.1. Mutual permeation of water and ethanol in real bottles

IV.2.1.1. Principles

Mutual permeation was assessed indirectly from non-destructive measurement of mass loss of sealed bottles; and from the destructive determination of *abv* variations. The measurements were repeated for a large set of bottles to achieve a uniform sampling over a period up to 7 months. To minimize disturbances in the storage rooms and to bring consistent determinations, a full random design was applied (ten non-destructive measurements and three destructive ones per week) and updated regularly to account for leaking bottles.

IV.2.1.2. Tested conditions

A challenge test with 425 flasks was carried out on four model beverages (*abv*=0, 0.2, 0.4, 0.7) stored in bottles M stored in three conditions summarized in ***Table IV-6*** and in **Table IV-7**.

Table IV-6. *Hydroalcoholic solutions simulating real alcoholic beverages*

Beverage code	abv_{target} (-)	$abv_{measured}$ (-)	Comment	Number of bottles and measurements in each storage condition†:			
				S1	S2	S3	S4
B1	0.7	$0.7004 \pm 9\times10^{-4}$	simulant of absinthe type	a. 84 b. 44 c. 247 d. 45	a. 82 b. 57 c. 265 d. 44	a. 77 b. 64 c. 318 d. 59	a. 10 b. 0 c. 9 d. 0
B2	0.4	$0.4029 \pm 6\times10^{-4}$	simulant of vodka type	n.c.	n.c.	a. 85 b. 66 c. 338 d. 66	n.c.
B3	0.15	$0.1515 \pm 5\times10^{-4}$	simulant of wine type	n.c.	n.c.	a. 85 b. 77 c. 393 d. 72	n.c.
B4	0	0	deionized water	a. 10 b. 0 c. 57 d. 0	a. 10 b. 0 c. 62 d. 0	a. 30 b. 0 c. 209 d. 0	a. 10 b. 0 c. 180 d. 0

†see the storage condition code in **Table IV-7**.
a. total tested bottle; b. non-leaking bottles; c. mass loss measurement; d. abv measurement. n.c.: not considered.

Mass transfer was monitored regularly by weighing the whole bottles (bottle, content and sealing) with an electronic precision balance (±0.001g, PE160, Mettler Toledo, USA). At regular times, some bottles were sacrificed (opened) randomly to enable ethanol content determinations. The contents of the tested bottles were transferred to glass measurement tubes. Alcohol strength by volume of each sample was subsequently determined at three different depths in the tube using an automatic densimeter (model DMA 5000, Anton Paar GmbH, Austria; accuracy of 10-5 % with pure water-ethanol mixtures) equipped with an accurate temperature controller and an autosampler. Ultrapure water was used as reference.

Table IV-7. Studied long-term storage conditions

Storage condition	T (°C)	RH_{target} (%)	$RH_{measured}$ (%) †	Indicative equivalent storage/ transportation conditions
S0	20	50	55 ± 3	initial condition for filling and sealing
S1	50	10	7 ± 3	e.g. deep-sea container shipping
S2	35	75	80 ± 3	e.g. storage tropical region
S3	35	20	12 ± 3	e.g., transport condition corresponding to the air 50% RH at 20°C and heating up to 35°C
S4	35	20	12 ± 3	following S3 with a sleeve around the bottle shown in the **Figure IV-1**e

† RH average value measured during the experiment.

IV.2.1.3. Extension of the test with sleeve

The capacity to predict the effect of the PET thickness was tested by adding a sleeve surrounding the flask main body for condition RH=20% at 35°C. The initial test was prolonged for beverages B3 and B4 stored in condition S4 shown in **Table IV-7** by adding a 60 µm thick shrinkable PET sleeve label on remaining bottles as illustrated in **Figure IV-1**e.

IV.2.2. Gravimetric measurements of water and ethanol sorption and diffusion (F1-F5, M)

- *Overview*

Binary and ternary sorption/desorption properties of PET were assessed using gravimetric measurements at 4°C, 25°C, 40°C, 50°C, 57°C and 60°C. The measurements themselves did not provide any absolute determination of the absorbed amounts and any separation of the amounts of water and ethanol absorbed. The concentrations in PET should be reconstructed from proper mass balances (e.g. from dry state or from any known initial state) or from an *ad hoc* theory of multicomponent sorption. Extracting diffusivities from sorption kinetics exhibited the same difficulty and was possible only when the fluxes could be normalized with the maximum amounts absorbed or desorbed (see Eq.(II.15) in §II.2.3.) were known.

Two distinct strategies were considered for binary (PET+water or PET+ethanol) and ternary sorption (PET+water+ethanol) and are summarized in **Table IV-8**. Binary measurements were carried out using water vapor (using saturated salts or an automatic microbalance A or B) or ethanol vapor (via an automatic microbalance B). Ternary measurements were performed using either liquid or gas water-ethanol mixtures. Soaking films in pure water, in ethanol 96% and 99% were extreme cases of ternary measurements. The cosorption microbalance (B) enabled to explore isothermally (typically at 50°C) the domain below the co-existence curve of water and ethanol at liquid state (so-called in this work “liquidus”).

Table IV-8. Overview of sorption measurement strategies

type	Strategies	Initial storage	Temperature	Range of activities (abv)	Material code	Extracted properties
Binary: water in PET	saturated salts (75%: NaCl; 90%: KNO_3)	desiccator at 40°C	40°C	0	F1	isotherms
	soaking	ambience	25,57,60°C	0	F1	kinetics isotherm
	automatic microbalance (A)	ambience (sorption) / equilibrium with an hydroalcoholic solution (desorption)	50°C	0	F1, M	kinetics isotherm
Binary: ethanol in PET	automatic microbalance (B)	ambience (sorption) / equilibrium with an hydroalcoholic solution	25,50°C	0	F1, F2, F3	kinetics isotherm
	soaking	ambience	4, 25, 57°C	0.96, 0.99	F1, F2, F3	kinetics isotherm activation energy
Ternary: mixture of water and ethanol in PET	soaking	ambience	40°C	0.08, 0.32, 0.82	F1	isotherms
	automatic microbalance (B)	ambience (sorption) / equilibrium with an hydroalcoholic solution	50°C	0-0.6	F1, M, C	kinetics isotherm

†ambience = 25°C, 50±5 % RH
A. Sorption/desorption microbalance model DVS Intrinsic (Surface Measurement System, UK; accuracy ±0.2 µg) at atmospheric pressure equipped with a capacitive detector (RH 0-98%) and operating at 298 K with nitrogen as gas carrier (gas flow rate up 200 mL·min^{-1}); B. Co-sorption/desorption microbralance model DVS Resolution at atmospheric pressure equipped with two saturators (water and organic solute, two organic solutes, operating temperature 25°C-85°C), a reference cell and two ultrasonic sensors measuring the gas composition at the outlet of each saturator (Surface Measurement System, UK; ; accuracy ±0.1 µg).

- *Principle of the cosorption microbalance* (B)

The cosorption microbalance (B) associated in parallel two saturators fed with dry nitrogen to generate ternary gas mixtures (nitrogen as a gas carrier, water and ethanol) as shown in ***Figure IV-5***.

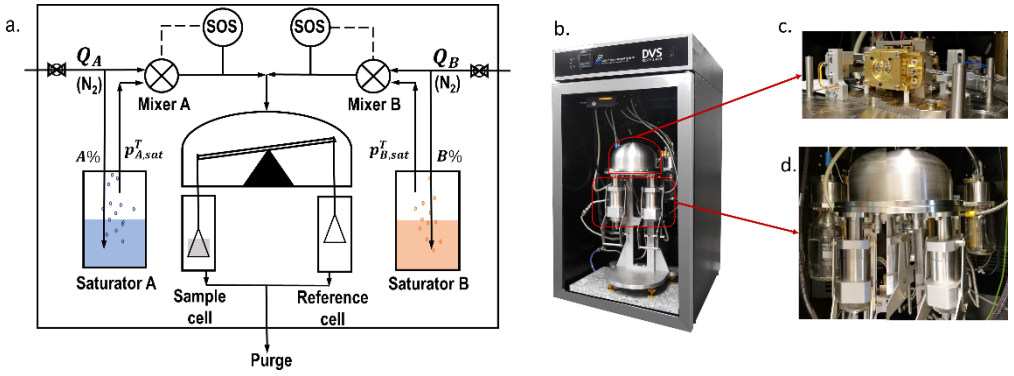

Figure IV-5*. Principle of the cosorption microbalance (denoted B in* ***Table IV-8****): (a) overview of the gas circuit involving two saturators; (b) the entire microbalance and the anti-vibration platform are placed in the oven. SOS: sensor of sound speed.*

As in conventional microbalances at atmospheric pressures, the activity measured by the sensor (ultrasonic on ways A and B) is given by the fraction of flowrate of saturated or wet

gas, denoted $\%A$ and $\%B$, respectively. As both gas lines A and B are mixed together, the activity is subsequently reduced before reaching the sample cell. The values of %A and %B should be adjusted to reach the desired activity values temperature T , $\left\{a_i^T\right\}_{i=w,e}$. By assuming that water ($i=w$) is located in way A and that ethanol ($i=e$) is in B, one gets the following dilution rules:

$$\begin{aligned}\%A &= \frac{Q_A+Q_B}{Q_A}\frac{1}{1-\Delta a_w}a_w^T \le 1\\ \%B &= \frac{Q_A+Q_B}{Q_B}\frac{1}{1-\Delta a_e}a_e^T \le 1\end{aligned} \qquad \text{(IV.3)}$$

where Q_A and Q_B are the total flow rates on ways A and B, respectively. Δa_w and Δa_e are deviations to idealities to consider because the saturators are not perfect (the residence time in the saturator is finite) and because the ethanol at 99% is not pure.

Since $\%A$ and $\%B$ are necessary lower than unity, not all activities are achievable when both water and ethanol were combined together. Increasing Q_A and Q_B improved the hydrodynamic conditions around the sample but provoked also higher evaporation rates. The corresponding evaporation rates reads:

$$\begin{aligned}q_w &= \left(1-\Delta a_w\right)M_w\frac{p_{w,sat}^T}{RT}\%AQ_A = \frac{p_{w,sat}^T}{RT}M_w\left(Q_A+Q_B\right)a_w^T\\ q_e &= \left(1-\Delta a_e\right)M_e\frac{p_{e,sat}^T}{RT}\%BQ_B = \frac{p_{e,sat}^T}{RT}M_e\left(Q_A+Q_B\right)a_e^T\end{aligned} \qquad \text{(IV.4)}$$

- *Principle of concentration measurements in a gas phase with ultrasonic sensors*

The speed of sound in an ideal gas depends only on its temperature and composition. From the Newton-Laplace equation, the square speed of the sound, c^2 , is given by the ratio of the gas bulk elasticity and of its density. Ultrasonic sensors use the relationships between c^2 and the ratio of adiabatic heat capacities as well as the molecular densities of gas components to reach an estimate of the gas composition before the sample cell. The non-linear relationship between c^2 and the molar fraction of solute x_i reads:

$$c^2 = \frac{RT}{M_{N_2}\left(1-x_i\right)+M_i\left(1-x_i\right)}\frac{C_p^{N_2}M_{N_2}\left(1-x_i\right)+C_p^iM_i\left(1-x_i\right)}{C_v^{N_2}M_{N_2}\left(1-x_i\right)+C_v^iM_i\left(1-x_i\right)} \qquad \text{(IV.5)}$$

with R the ideal gas constant, T the absolute temperature, $\{M_k\}_{k=N_2,i}$ the molecular mass of N2 and of solute i. $\{C_p^k\}_{k=N_2,i}$ and $\{C_v^k\}_{k=N_2,i}$ are corresponding the heat capacities of pure gases at constant pressure and volume, respectively.

- *Control loop during long-term experiments*

The sensor could be used in a control loop to estimate a regular times Δa_w and Δa_e, or to introduce a periodic variation with controlled amplitude. This strategy was used to anticipate the delays when the organic composition of gases was changed.

IV.3. Computational methods

Computer aided approach is significant for [E][D][S] framework with the complexity issues and linked decisions as shown in case-study in §III.2. . In this section, the importance of computational methods mainly focuses on [E]valuation of mechanism on thermodynamic and transport properties applicable to the packaging design and optimization in this thesis.

IV.3.1. Mass transfer modeling of water and ethanol at tiers 1 and 2

At first tiers, mass transfer across the walls of the container are described in simplified but not oversimplified calculations. No assumption of steady state is required. Only the modifications of the polymer induced caused by the sorption of water and ethanol are neglected. In the case of PET, polymer relaxation effects are triggered by critical temperatures and relative humidities (see the pseudo state diagram 5 in Dubelley *et al.*, 2017a), but they do not modify the diffusion coefficients of water in PET significantly (see Figure 14 in Burgess *et al.*, 2014a).

IV.3.1.1. Transport equations at bottle walls

The internal side of the container (e.g., bottle) is exposed to the vapors of the water-ethanol mixture, denoted with subscripts w and e, whereas the external side is exposed only to the relative humidity of the storage place or room at the same temperature. In this description, the beverage is assumed to be macroscopically at thermal equilibrium with the surroundings and that the storage place does not accumulate ethanol (i.e., good ventilation and extraction).

Without distinguishing whether the mass transfer was initiated in the liquid or in the headspace compartment (they are both at thermodynamical equilibrium), the diffusive fluxes at the interfaces in contact with polymer walls are described satisfactorily within the thin film approximation. On the internal side, denoted $\partial\Omega_{\text{int}}$ and its normal vector $\mathbf{n}_{\partial\Omega_{\text{int}}}$, an effective

mass transfer resistance can be considered to account for the vaporization-condensation process associated with the sorption of water and ethanol. By denoting $\left\{C_i^{x,y,z,t}\right\}_{i=e,w}$ the solute concentration (SI units in kg·m^{-3}) in the walls at a position (x,y,z) at the time t and $\left\{f_{i,P}^{T}\right\}_{i=e,w}$ the binary sorption isotherms in the walls, the mass flux densities at the internal boundary condition reads

$$\begin{bmatrix} j_e^{(T,abv)}\big|_{\partial\Omega_{\text{int}}} \\ j_w^{(T,abv)}\big|_{\partial\Omega_{\text{int}}} \end{bmatrix} = \begin{bmatrix} -D_e^{(T)}\,\nabla C_e^{x,y,z,t}\big|_{\partial\Omega_{\text{int}}}\cdot\mathbf{n}_{\partial\Omega_{\text{int}}} \\ -D_w^{(T)}\,\nabla C_w^{x,y,z,t}\big|_{\partial\Omega_{\text{int}}}\cdot\mathbf{n}_{\partial\Omega_{\text{int}}} \end{bmatrix} = \begin{bmatrix} h_e\dfrac{p_{e,sat}^{(T)}}{M_e RT}\left(x_e\gamma_e^{(T,abv)} - f_{e,P}^{T\ -1}\left(C_e^{x,y,z,t}\big|_{\partial\Omega_{\text{int}}}\right)\right) \\ h_w\dfrac{p_{w,sat}^{(T)}}{M_w RT}\left((1-x_e)\gamma_w^{(T,abv)} - f_{w,P}^{T\ -1}\left(C_w^{x,y,z,t}\big|_{\partial\Omega_{\text{int}}}\right)\right) \end{bmatrix} \tag{IV.6}$$

where $\left\{f_{i,P}^{T\ -1}\right\}_{i=e,w}$ is the inverse function of the function $\left\{f_{i,P}^{T}\right\}_{i=e,w}$ giving the amount of solute i absorbed in the walls according to its activity at temperature T; $\{h_i\}_{i=e,w}$ is the equivalent mass transfer conductance across the boundary layer (SI units in m·s^{-1}). The molar fraction of ethanol in the mixture x_e is derived from its weight fraction $\dfrac{m_e^{(t)}}{m_e^{(t)}+m_w^{(t)}}$ (see Eq. (IV.12)) and the global mass balance in water and ethanol over all internal interfaces of the packing. For a bottle of height H and cylindrical symmetry, the rates of variation of the mass in water and ethanol, denoted $m_w^{(t)}$ and $m_e^{(t)}$, reads:

$$\frac{d}{dt}\begin{bmatrix} m_e^{(t)} \\ m_w^{(t)} \end{bmatrix} = \oiint_{\partial\Omega_{\text{int}}} \begin{bmatrix} j_e^{(T,abv,x,y,z)}\big|_{\partial\Omega_{\text{int}}} \\ j_w^{(T,abv,x,y,z)}\big|_{\partial\Omega_{\text{int}}} \end{bmatrix} dA = \int_{z=0}^{H} \begin{bmatrix} j_e^{(T,abv,z)} \\ j_w^{(T,abv,z)} \end{bmatrix} 2\pi r(z)\,dz \tag{IV.7}$$

where $r(z)$ is the radial profile of the bottle along the vertical coordinate z.

IV.3.1.2. Transport equations within bottle walls

Since the thickness of bottle walls is several magnitude orders smaller than the height of the bottle, mass transfer through bottle walls can be therefore assumed one-dimensional without a significant loss of accuracy. By neglecting the contribution of the polymer relaxation as driving force, the mutual diffusion of water and ethanol in polymer walls reads:

$$\frac{\partial}{\partial t}\begin{bmatrix} C_e^{(r,z,t)} \\ C_w^{(r,z,t)} \end{bmatrix} = \frac{1}{r}\frac{\partial}{\partial r}\left(r \begin{bmatrix} D_e^{(T,[C_e,C_w]',z)} & 0 \\ 0 & D_w^{(T,[C_e,C_w]',z)} \end{bmatrix} \frac{\partial}{\partial r}\begin{bmatrix} C_e^{(r,z,t)} \\ C_w^{(r,z,t)} \end{bmatrix} \right) \tag{IV.8}$$

where $\left\{ D_i^{(T,C_i,z)} \right\}_{i=w,e}$ is the diffusion coefficient in the normal direction of the walls. The dependence with the vertical position z and with the local solute concentration accounts for non-uniform drawing and plasticizing effects.

Eq. (IV.8) can be solved efficiently for any arbitrary initial solution $\left[C_e^{(r,z,t=0)}, C_w^{(r,z,t=0)} \right]'$ along with boundary condition (IV.6) by decomposing the bottle into vertical sections with similar thickness and transport properties. In other words, mass transfer across container walls can be factorized into $n \geq 1$ boundary conditions between the beverage and n equivalent sections coupled via mass balance Eq. (IV.7). By assuming that container walls are at equilibrium with the storage atmosphere at a relative humidity RH_0 and a temperature T_0, and which is not contaminated by ethanol vapors, the corresponding initial condition is:

$$\begin{bmatrix} C_e^{(r,z,t=0)} \\ C_w^{(r,z,t=0)} \end{bmatrix} = \begin{bmatrix} 0 \\ f_{w,P}^{T_0}\left(RH_0\right) \end{bmatrix} \tag{IV.9}$$

Equations (IV.6)-(IV.9) have been implemented by following the finite-volume formulation of Nguyen *et al.* (2013) and the opensource project FMECAengine (Vitrac, 2018).

IV.3.2. Mechanical constraints: risk of overpressure and collapse in the headspace

Water and ethanol mass transfer are controlled by two driving forces: partial pressure gradients across walls and the difference of total pressure on both sides of the closure system. By neglecting internal mass transfer in the beverage and the heat transfer required for the vaporization or the condensation of water and ethanol at the liquid-gas interface, the driving potentials on the beverage side are set by the total pressure and the partial pressures in the headspace.

IV.3.2.1. Practical approximations of partial pressures: $\left\{p_i^{(T)}\right\}_{i=e,w}$

In this study, the state of pure components is chosen as reference state of water and ethanol. As a result, the partial pressures, $\left\{p_i^{(T,abv)}\right\}_{i=e,w}$ in the headspace, can be inferred from the binary activity coefficients, $\left\{\gamma_i^{(T,abv)}\right\}_{i=e,w}$, relative to the molar fraction of water or of ethanol in the beverage, $\left\{x_i\right\}_{i=e,w}$ and from their pure vapor saturation pressures $\left\{p_{i,sat}^{(T)}\right\}_{i=e,w}$:

$$p_i^{(T,abv)} = x_i \gamma_i^{(T,abv)} p_{i,sat}^{(T)} \text{ for } i = e,w \tag{IV.10}$$

with T the absolute temperature in Kelvin but expressed in °C in the description of storage conditions.

Eq. (IV.10) is exact when the interactions between water (and also ethanol in a less extent) and the other beverage constituents (pectins, proteins, aroma…) can be neglected. When the real alcoholic beverage is replaced by an equivalent hydroalcoholic solution, one gets:

$$x_e = 1 - x_w \text{ for } i = e,w \tag{IV.11}$$

By noticing that abv is defined at 20°C, molar fractions are related to the density of the mixture with the same composition at the same temperature, denoted $\rho_{w+e}^{(20°C,abv)}$:

$$x_e = \frac{w_e/M_e}{w_e/M_e + (1-w_e)/M_w} = \frac{\frac{1}{M_e}\left(\frac{\rho_e^{20°C}}{\rho_{w+e}^{(20°C,abv)}} abv\right)}{\frac{1}{M_e}\left(\frac{\rho_e^{20°C}}{\rho_{w+e}^{(20°C,abv)}} abv\right) + \frac{1}{M_w}\left(1 - \frac{\rho_e^{20°C}}{\rho_{w+e}^{(20°C,abv)}} abv\right)} \tag{IV.12}$$

with $w_e = \frac{\rho_e^{20°C}}{\rho_{w+e}^{(20°C,abv)}} abv$ being the weight fraction in ethanol, $\{M_i\}_{i=e,w}$ the molecular weights and $\{\rho_i^{20°C}\}_{i=e,w}$ the densities of pure components at 20°C.

IV.3.2.2. Practical approximation of the total pressure in the headspace in equilibrium with the beverage.

The total pressure in the headspace P_{head} results from several equilibria: i) the chemical equilibrium between the liquid and the headspace, ii) the thermal equilibrium with the gas and liquid phase and iii) the balance of forces on the sides of the wall. All equilibria are connected, changing temperature or changing the volume of the headspace affect both the total pressure and the composition of the headspace (and corollary the composition of the liquid). The presence of air or an inert gas affect these equilibria. An efficient procedure to calculate

the final total pressure and composition of the headspace has been devised. It takes into account the internal volume of the bottle V_{bottle}, the initial temperature T_0, the initial total pressure P_0, the initial composition of the beverage abv_0 and the initial headspace volume $V_{head}^{t=0}$. Without a loss of generality, some simplifications are introduced. The deformations of the wall are not considered (the total volume of the gas and liquid is constant), the leaks and mass transfer across the walls are discarded (the equilibration is faster than permeation), the headspace behaves as an ideal gas, air or inert gas cannot dissolve in the liquid and is incondensable.

At any time t, the number of solutes $i = w, e$ in the gas phase, $\left\{n_i^g\right\}_{i=w,e}$, is derived by combining Eq. (IV.10) and the ideal gas law as:

$$n_i^g = p_i \frac{V_{head}}{RT} = \gamma_i^{(T,abv)} x_i \frac{P_{i,sat}^{(T)} V_{head}}{RT} \tag{IV.13}$$

where V_{head} is the volume of headspace and R is the ideal gas constant.

Since air (or the inert gas) is assumed to be incondensable, insoluble and initially dry (no water inside), the number of air molecules, n_a, is given by the initial amount of air in the headspace:

$$n_a = \frac{P_0 V_{head}^{t=0}}{RT_0} \tag{IV.14}$$

Eq. (IV.14) and subsequent mass balance on air assumes that nitrogen and oxygen are not exchanged between the beverage and the headspace. The assumption is reasonable with nitrogen (low solubility), but questionable for oxygen. At atmospheric conditions, the solubility of oxygen in water is very low, about eight parts of oxygen per million at 25°C (Truesdale and Downing, 1954). Its solubility increases slightly with ethanol content to reach a value of 3.5% higher than in pure water for $abv = 0.15$ (see Table 1 and Figure 1 of Kutsche *et al.*, 1984). The total desorption or sorption of oxygen in a headspace representing 1:15 of the volume beverage will cause a variation of the total pressure lower than ±0.02 %. Comparatively to the risk associated with ethanol and water, the contribution of oxygen on the risk of collapse was therefore neglected. In the absence of an inert gas, the beverage is additionally assumed to be already at or close to the equilibrium with the earth atmosphere, so that significant desorption or sorption of oxygen is unlikely.

By assuming that the headspace does not contain ethanol initially before the bottle is filled, the total number of ethanol molecules in the bottle is hence given by:

$$n_e^{t=0} = \frac{\rho_e^{20°C}}{M_e}\left(V_{bottle} - V_{head}^{t=0}\right) abv_0 \tag{IV.15}$$

For water, the number of water molecules in the bottle is derived from the density of the initial water-ethanol mixture, $\rho_{w+e}^{(T_0,abv_0)}$:

$$n_w^{t=0} = \frac{\rho_{w+e}^{(T_0,abv_0)}\left(V_{bottle} - V_{head}^{t=0}\right) - n_e^{t=0}M_e}{M_w} \tag{IV.16}$$

For a given volume of the headspace V_{head}, the theoretical density of the liquid mixture, $\rho_{w+e}^{theoretical}\left(V_{head}\right)$, is given:

$$\rho_{w+e}^{theoretical}\left(V_{head}\right) = \frac{\left(n_e^{t=0} - n_e^g\right)M_e + \left(n_w^{t=0} - n_w^g\right)M_w}{V_{bottle} - V_{head}} \tag{IV.17}$$

Equilibrium is reached when the density of the mixture matches the equilibrium density of hydroalcoholic mixture as reported in handbooks and denoted $\rho_{w+e}^{(T,abv)}$. Finding V_{head} is equivalent to solve the equality:

$$\rho_{w+e}^{theoretical}\left(V_{head}\right) = \rho_{w+e}^{T}\left(x_e\left(V_{head}\right)\right) \tag{IV.18}$$

with:

$$x_e\left(V_{head}\right) = \frac{n_e^{t=0} - n_e^g\left(V_{head}\right)}{n_e^{t=0} + n_w^{t=0} - n_e^g\left(V_{head}\right) - n_w^g\left(V_{head}\right)} \tag{IV.19}$$

Finally, the total pressure in the headspace at equilibrium is given by:

$$P_{head} = \frac{n_a + n_w^g + n_e^g}{V_{head}}RT \tag{IV.20}$$

The full procedure reads:

$1:$ calculate $n_a\left(Eq.IV.14\right), n_e^{t=0}\left(Eq.IV.15\right), n_w^{t=0}\left(Eq.IV.16\right)$

$2:$ initialization $V_{head} \leftarrow V_{head}^{t=0}$ at T_0

$3:$ initialization $x_e \leftarrow x_e^{t=0}$

$4: x_e^{old} \leftarrow x_e^{t=0}$, calculate $\left\{n_i^g\right\}_{i=w,e}\left(Eq.IV.15\right)$ with the previous guess of $x_e, 1-x_e$

$5:$ (fix point iteration) : update $x_e\left(Eq.IV.21\right)$

$6:$ go to step 4 until $\left|x_e - x_e^{old}\right| \le \epsilon$

$7:$ find abv from $x_e\left(Eq.IV.12\right)$ and read $\rho_{w+e}^{(T,abv)}$

$8:$ calculate $\rho_{w+e}^{theoretical}\left(V_{head}\right)\left(Eq.IV.19\right)$

$9:$ calculate $\Delta\rho = \left|\rho_{w+e}^{(T,abv)} - \rho_{w+e}^{theoretical}\left(V_{head}\right)\right|$

$10:$ update V_{head} according to the Gold section search method

$11:$go to step 3 until $\Delta\rho$ is minimized

$12:$calculate $P_{head}\left(Eq.IV.6\right)$

(IV.21)

IV.3.3. Packaging design and optimization: case-study

Packaging design and optimization refers to the design and optimization of the bottle shapes and geometry. The simulation-optimization strategy implemented in this work is illustrated in **Figure III-5**.

Nonlinear and non-convex problems such as shelf-life and weight optimization problems remain intrinsically more difficult to [S]olve. The optimal solution may be not unique, it may occur at an interior point of the feasible region, at its boundary or at one the extreme points of the feasible region. Integrating uncertainty inherent to any [E]valuation step complicates the definition of a robust termination condition. The best solution lies within a tolerance from the last best optimum and at an acceptable distance of critical constraints to be considered "safe" or "compliant" ([Decision step]). In this work, the internal domain is mapped with a regular grid to offer to enable a sensitivity analysis close to constraints. An instance of the [S]olving step is detailed for a packaging design problem with a prescribed capacity (150 mL). The shape of the bottle is based on the geometry parameters defined in ***Figure IV-2***, the weight optimization problem was split into a two-step optimization process: i) setting macroscopic dimensions H, W, D, d, h to match the prescribed internal volume and ii) optimizing $l_{wall}, l_{bottom}, l_{top}, l_{neck}$ to adjust the barrier properties of the bottle. Without a loss of generality, the general problem is solved using a multiresolution method (Amaran *et al.*, 2014) for a review of applicable algorithms). At the lowest level, all parameters in the group are frozen except one. The elementary problem with shelf-life and capacity constraints reads hence:

$$l_{wall}(X) = \arg\min \begin{bmatrix} mass_{bottle}(X, l_{wall}) \\ \text{with } shelf\text{-}life\left(l_{wall}, X, abv_0, V_{beverage}, T\right) \geq 180 \text{ days} \end{bmatrix} \quad \text{(IV.22)}$$

$$\text{where } X = \left[V_{bottle}, W, D, d, h, l_{top}, l_{bottom}, l_{neck}\right]' \text{ and } V_{head} = V_{bottle} - V_{beverage} \geq 0$$

where the shelf-life function is defined as:

$$shelf\text{-}life\left(l_{wall}, X, abv_0, V_{beverage}, T\right) = \min \begin{bmatrix} \arg\min\left(\left|abv\left(t, l_{wall}, X, abv_0, V_{beverage}, T\right)\right| \geq 0.003\right), \\ \arg\min\left(m_{beverage}\left(t, l_{wall}, X, abv_0, V_{beverage}, T\right) \geq 1.5\%\right) \end{bmatrix} \quad \text{(IV.23)}$$

and where the height of the bottle is found by adding the complementary constraint:

$$H\left(V_{beverage}, l_{wall}\right) = \arg\min\left[\left|V_{\text{internal}}\left(H, l_{wall}, V_{bottle}\right) - V_{beverage}\right|\right] \quad \text{(IV.24)}$$

As a result, the internal loop manages implicitly design and product constraints in a conventional simulation framework. All input parameters are set conventionally except H

and l_{wall}, which are optimized by resolving successively the capacity and the shelf-life problem via a golden-section search method (see section 10.1 in Press, 1992). Additional degrees of freedom controlling the shape of the bottle are introduced at a higher tier by resolving again the elementary problem. The current implementation is sufficiently efficient to screen hundreds or thousands of geometries/designs under constraints. The global optimization when W and D are released has been explored on a 30×30 grid (*i.e.* 900 hundred bottle geometries were optimized).

Chapter V. RESULTS AND DISCUSSION

Chapter V. Results and Discussion

V.1. Scope of tiered modeling

The sale proposed framework [E]valuation, [D]ecision, and [S]olving has been implemented in a multitiered approach comprising four major tiers as illustrated in **Figure V-1**. The decomposition in tiers is somewhat arbitrary and correspond to a progressive strategy to develop and to use simulation. The first tier incorporates all important features to evaluate mass transfer on real geometries, with dynamic storage conditions and unlimited diffusion-dissolution mass transport equations in single or multilayer structures. The limitations are, however, important:

- non-linear coupling is accepted for water-ethanol and at the boundary with the beverage;
- fluxes within the packaging are not coupled and obey strictly to binary diffusion; all sorption isotherms are linear;
- all properties are uniform.

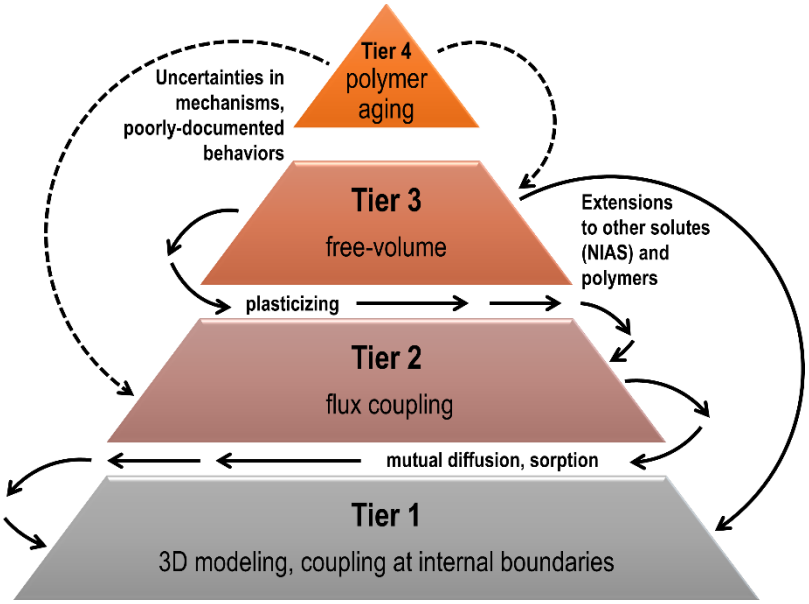

***Figure V-1**. Overview of four tiers considered for packaging optimization with the proposed [E][D][S] framework.*

The description at the first tier is based on common assumptions, which can always be considered as approximations of more complex scenarios. Additionally, as the [E]valuation step is called iteratively (see **Figure III-5**), there is significant computational gain in accepting

simplified descriptions to explore a large space of geometry parameters. Estimations at high tiers are important only to identify biases, to refine optimized solutions, to generalize to different situations (polymers, migrations, aroma scalping, etc.). In this work, high tiers are considered to justify sophistications and to analyze the best strategy to implement them. Flux coupling and free-volume effects are discussed in §V.3. and §V.4.

V.2. Optimization of the design of PET bottles at tiers 1-2

Polyethylene terephthalate (PET) is the dominant material used to produce bottles for water and carbonated beverages (see §II.3.5.1.). Fruit juices can also be packed in PET bottles, but the temperature of filling cannot exceed 62°C to prevent deformation of the bottles, and its mechanical resistance needs to be adapted to accommodate the strong risk of collapse during cooling. The filling temperature limit makes PET bottles acceptable in the EU for storage at room temperature only for low-acid fruit juices (e.g., orange juice). For other fruit juices in the EU and all fruit juices in the US, the risk of spoilage should be prevented by keeping the bottles at chilled temperature or by using aseptic packaging such as carton packages (bricks, pouches) or glass containers. PET bottles are attractive containers for other beverages such as liquors; they are light, more cost-effective and environment-friendly that glass (see discussion in §II.3.5.1.), they can be used to bring a broad variety of shapes, aspects, and colors. They can be, for example, assembled in refillable or recyclable cartridges and incorporated in semi-automatic cocktail or delivery machines (Pernod Ricard, 2015). The presence of ethanol reduces dramatically the risk of microbiological spoilage, and hot filling is not required. The containers need, however, to fulfill severe requirements to guarantee a shelf-life for the consumer.

This section reports the principles of optimization of such packaging containers for liquors similarly as the problem Q1 discussed in §III.3. The developed method is very generic and can also solve problems Q2 and Q3, but at the expense of a wider exploration of geometry parameters. The optimization focused on the design of miniature bottles consumed in airplanes. The design denoted "*M*" in ***Table IV-1*** already exists and was used as a reference for validation. Optimization targeted shelf-life extension and minimization of the fire hazard associated with ethanol loss, both critical features for aerial transportation. A case study is proposed for larger bottles with a more original shape, denoted "*X*".

V.2.1. Overview of the [E][D][S] implementation and choices

Shelf-life plays a significant role as it an essential constraint to verify (minimum shelf-life) or goal to maximize. The geometry of bottles brings additional constraints (capacity, shape) or goals to achieve (weight), but also the degree of freedoms to get substantial gains on

weight and shelf-life. The first challenge test was to demonstrate that such a tool could [E]valuate equivalent shelf-life of hydroalcoholic solutions stored in real bottles in controlled conditions. [S]olving ecodesign principles for such bottles was subsequently explored with the intent of introducing new original shapes and capacities.

V.2.1.1. The legal definition of shelf-life for liquors

Packaging for long shelf-life products is designed to offer significant barrier properties to gases from the ambiance (water vapor, oxygen) and to food constituents. Aside from oxidation issues in oxygen-sensitive products, the reduction of shelf-life of beverages is primarily caused by mass loss (usually water content) and by the loss of both aroma and sapid compounds. Weight loss occurs as the balance of all mass transfer across container walls and the closure system. As an example, water bottles stored in a dry place are losing weight due to a net permeation rate of water from the inside to the outside. The loss of aroma is usually slower and associated to reversible sorption in the walls, coined "scalping" process (Ducruet *et al.*, 2007;Dombre *et al.*, 2015); and which dominates over the mass loss by permeation. Predicting the rates of each mass transfer requires a proper characterization of diffusion and sorption properties in the considered polymer, usually a polyester material such as polyethylene terephthalate (PET), at the different stages of transportation, retailing, storage and final consumption. In this study, the non-linear behavior of water-ethanol mixtures stored in PET bottles is thought to represent the properties of real alcoholic beverages such as ciders, beer, wines, and spirits realistically. Since only water and ethanol are considered, the type of beverage is defined by its alcoholic strength by volume, denoted *abv*. It is legally defined in EU as "*the ratio of the volume of pure alcohol present in the product in question at 20°C to the total volume of that product at the same temperature*" (see Annex I of EU Regulation 110/2008; EC). The case of bottled water is a special case corresponding to abv=0. Tolerances setting the shelf-life of alcoholic beverages are also relative to the variation of abv during storage and transportation, denoted $\left|\Delta abv\right|$. EU regulation 1169/2011/EC (2011b) sets out a stringent tolerance of ± 0.3% for non-beer related beverages with abv values larger than 1.2%. Finally, the EU applies a tolerable negative error of 1.5% for the weight of prepackaged liquids, Δw , with volumes equal or larger than 1 L (see Annex I of Directive 76/211/EEC; 1976). In the context of plastic containers, it should be interpreted as the maximum allowable variation from the weight labeled on the package according to unavoidable variations in weighing, measuring and mass transfer across packaging walls.

In this work, only concepts of primary shelf-life (see §II.4.1.) consecutive to regular mass transfer through bottle walls have been implemented. Any mass transfer through the opening and the closure system is not considered. In future versions, the capacity to change

headspace dynamically and capacity volumes could be used to mimic bottle opening and to introduce secondary shelf-life concepts.

V.2.2. Dual bottle geometry models

Increasing shelf-life based on bottle geometry parameters or minimizing weight at constant shelf-life for one or several beverages requires to generate virtually a large number of bottle prototypes (from thousands to millions) and to evaluate all of them in a sequence (e.g., grid variation, downhill simplex method or other direct search techniques). The geometry models require to be exact to enable a [D]ecision based on packaging weight. They can be updated in almost in real time for any condition. [E]valuating mass transfer on each bottle requires conversely much more computational power. A dual geometry model was introduced to symmetrize the costs of the two steps: a detailed 3D geometry model using field evaluations to assess weight, verify the capacity of the bottle, and an equivalent geometry in curvilinear coordinates to simulate mass transfer.

V.2.2.1. Example: dual geometry of bottle M

The principles of the transformation are shown in **Figure V-2** for the bottle *M* with symmetry of revolution. In the case of the depicted bottle X, the curvilinear coordinate follows the parting line, where the mold halves have been open after injection molding. Since the radial information is not required in food implicit model, the bottle can be idealized as a wrapped shell where thickness, defined as the normal distance between internal and external walls (*i.e.,* perpendicular to the curvilinear coordinate). Since sections with similar thicknesses are expected to offer similar barrier properties, the geometry information along the curvilinear coordinate can be replaced by the distribution of the thickness over the entire surface area of the bottle (**Figure V-2**c). In this work, this distribution was subsequently discretized into a smaller number of representative sections (seven sections are shown in **Figure V-2**d) where transport equations could be efficiently resolved in almost one-dimension along the direction normal to the surface. All sections are considered independent (no flux exchange) and conservative of the total surface area. Coupling occurred only the boundary as they were in contact with the same liquid.

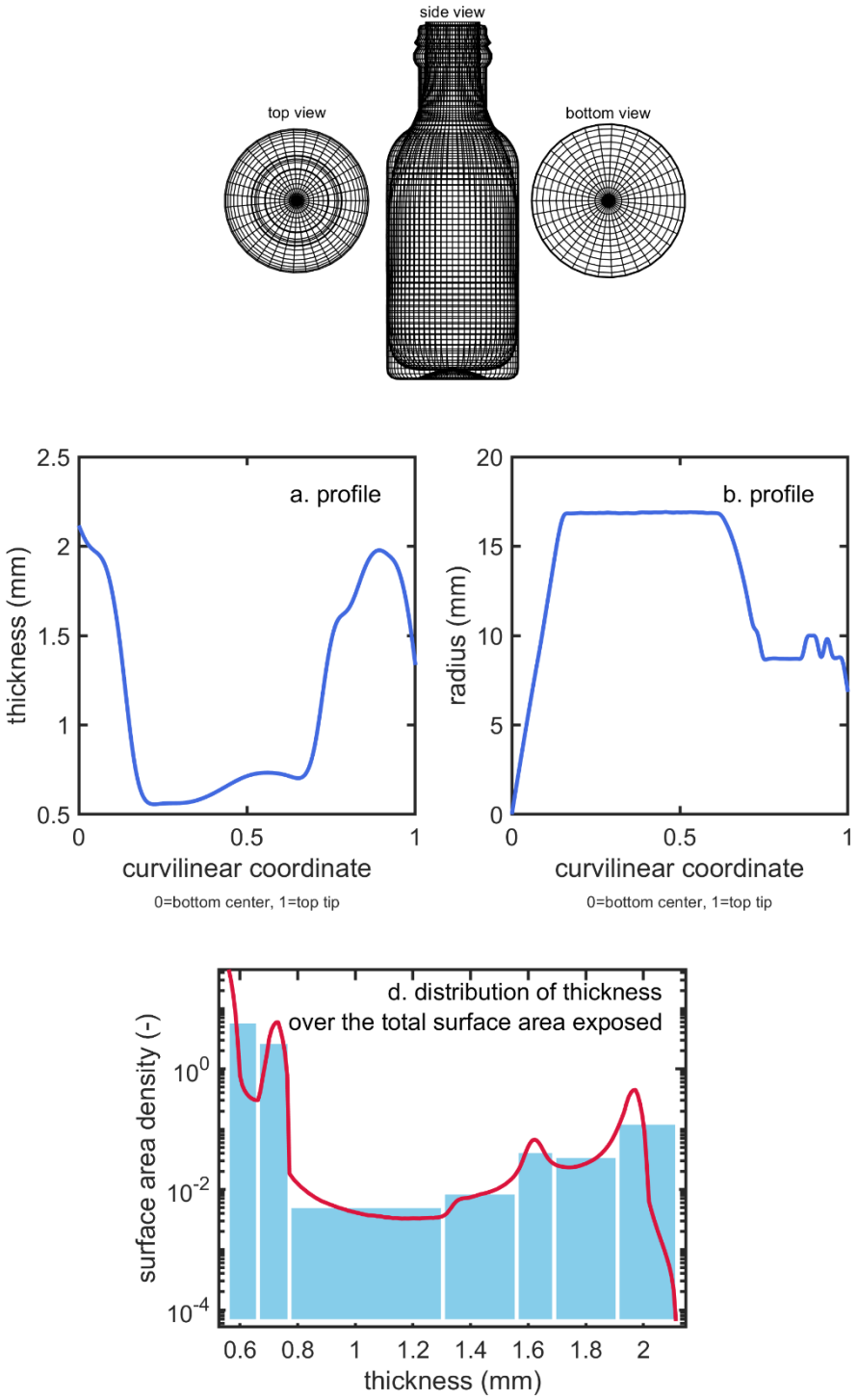

Figure V-2. Dual representation of the geometry of bottle ***Figure IV-1*** in 3D and curvilinear coordinates. The equivalent geometry of the bottles as seven independent sections in contact with the same liquid is shown in d as histograms.

The dual geometry involves three ingredients: i) smooth 3D parameterized manifolds, ii) a description of mass transfer in curvilinear coordinates (one or several) and iii) a factorization of sections in curvilinear coordinates to reduces the total cost. The whole scheme is

freely inspired from higher order of grid convergence methods, which have been designed to provide higher resolution than the classical second-order accuracy implemented in most industrial grade codes. For the bottle *M*, mass transfer equations are 2D with the cost of resolution of 1D systems. This approach is computationally more efficient that the one described in (Carrieri *et al.*, 2012) and shown in **Figure II-34**. The discretization is, indeed, much more accurate along thickness with hundreds of finite-volume elements were used against few finite elements in the original work. Its implementation in FMECAengine (Vitrac, 2018) enables additional sophistications such as nanometric barrier layers brought by plasma treatments and multilayer structures of arbitrary complexity.

Non-axisymmetric designs such as bottle *X* are implemented similarly by adding partitions on different curvilinear coordinates. In all cases, the discretization should be chosen to preserve exactly the total surface area of the primary 3D model. A loss information is known to occur only in the corners where impervious boundary conditions are applied. As the overall calculation cost is linear with the number of sections, there is a partial decoupling between the complexity of the original 3D design and the complexity of mass transfer calculations.

V.2.2.2. Discussion on the possibility to extends additional simplifications

It is straightforward to demonstrate that introducing additional simplifications lead to more harm than any substantial gain. Replacing the different cross-sections shown in **Figure V-2**d by single one is physically exact but only at steady state (see principles in **Figure V-3**). Indeed, diffusional transport is scaled with the square visited distance in semi-infinite geometries (see dispersion law in §II.2.3.6.3.), whereas the fluxes are scale with the thickness at steady state (see Eq. (III.1)).

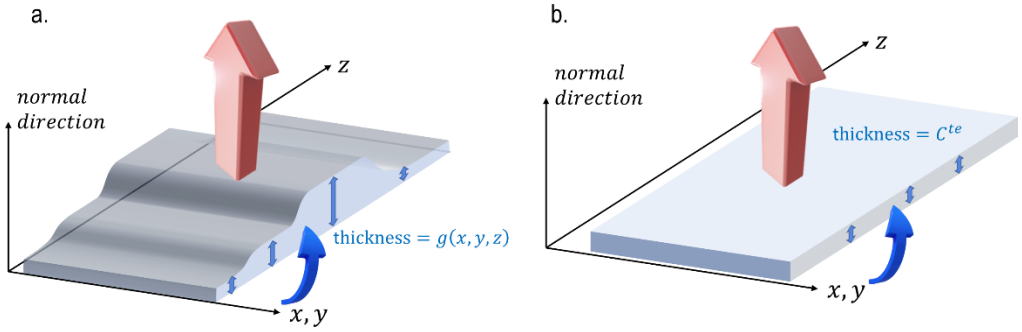

***Figure V-3**. Comparison between (a) an unwrapped hollow 3D geometry and (b) its approximation with uniform thickness. The arrow represents the normal mass flux crossing each geometry. The values of indicated thicknesses are indicative; in real bottles, the thinnest regions exhibit the largest surface area of transfer (see distribution in **Figure V-2**d)*

Additionally, such simplification does not authorize a coupling of fluxes and non-linear behaviors. As a rule of thumb, it was shown that water permeation on a period longer than several days could be described at steady state, but it was not the case for ethanol. Such

simplifications already used in the case-study presented in §III.2. were not used in the remaining part of the work. The considered thicknesses were obtained from a geometry decomposition, which converged in distribution to the real distribution of thicknesses. The term distribution was interpreted as the joint distribution along all wall normal vectors. This description in curvilinear coordinates is physically very acceptable as:

- it is more general and accurate than cartesian or cylindrical coordinates for the 1D approximation of mass transfer (gyration radii need not to be too large);
- there is no need on the composition of mass transfer resistances (in series or in parallel);
- there is no need to decide which surface is in contact with the liquid
- thickness variability or safety margins can be easily added on distributions;
- the overall cost of calculations can be easily adjusted by increasing or reducing the number of sections.

V.2.3. Driving forces controlling primary shelf-life of liquors

As reviewed in Herstein and Gregory (1935), liquors are produced by distillation and reach therefore high abv values, generally ranged between 0.35 and 0.9 (denoted 35-90% in volume on commercial products). The origin of the process of distillation itself, in the fifteenth century, is rooted in the production of brandy (*abv*: 0.36-0.), obtained by distilling wine. The most renowned brandies are Armagnac and Cognac. Other distilled beverages made from fruit other than grapes are called eaux-de-vie. Liquors obtained by distillation of grains or vegetables or herbs, which have already gone through alcoholic fermentation, are popular and include: whisky (from fermented grain mash with *abv*: 0.4-0.55), vodka (from cereal grains or potatoes , *abv*: 0.38-0.40), gin (from juniper berries, *abv*: 0.38-0.55), rum (from sugarcane juice or its byproducts, *abv*: 0.38-0.55), tequila and mezcal (from blue agave plant, *abv*>0.4), shaojiu or baijiu (from rice, *abv*: 0.4-0.55) and absinthe (from anise, *abv*: 0.45-0.74). Reported alcohol strengths were from Buglass *et al.* (2011);and Mudgil and Barak (2018) and mainly products in the market. EU regulation 1576/89/EEC has a broader definition of liquors and includes any alcoholic liquid with *abv* values above 0.15 "*produced directly by the distillation, with or without added flavourings, of natural fermented products, and/or by the maceration of vegetable substances… or by the mixture of a spirit drink with one or more other spirit drinks, ethyl alcohol of agricultural origin, distillate of agricultural origin or spirit, one or more alcoholic drinks, one or more drinks*".

This sub-section analyzes the relationships between the alcohol-strength, the ratio headspace volume-to-beverage volume, temperature (filling and storage), partial and total pressures.

V.2.3.1. Partial pressures

By noting that PET is not a porous material, water and ethanol mass transfer across bottle walls occur prior dissolution in the polymer and obey to the general sorption-diffusion-desorption model. The main driving forces are the partial pressure differences between the beverage and the surrounding. The variations of binary properties of water-ethanol mixtures with abv between 10°C and 70°C: mixture density $\rho_{w+e}^{(T,abv)}$, activities $\left\{a_i^{(T,abv)}\right\}_{i=e,w}$, partial pressures $\left\{p_i^{(T,abv)}\right\}_{i=e,w}$ and the theoretical pressure of the headspace at constant volume (no air) $p_{total}^{theoretical} = p_w^{(T,abv)} + p_e^{(T,abv)}$ in equilibrium with the mixture are presented in **Figure V-4**.

By neglecting the amounts transferred to the headspace, binary equilibrium data offer a first approximation of the driving forces based on the alcohol strength (abv) of the considered beverages and the conditions of storage. Activities of water and ethanol do not evolve significantly with temperature. Water activities at 35°C of typically alcoholic beverages correspond to 0.977 ($abv = 0.08$), 0.960 ($abv = 0.15$), 0.911 ($abv = 0.4$) and 0.819 ($abv = 0.7$) as lower limits for beer, wine, vodka, rum, respectively. In non-tropical regions (for RH<0.8), alcoholic beverages stored in plastic bottles lose water and therefore weight. Ethanol activities are comparatively much lower 0.153 ($abv = 0.08$), 0.243 ($abv = 0.15$), 0.408 (abv=0.4) and 0.541 ($abv = 0.7$). The effective driving forces $a_w^{(abv)} - \frac{RH(T)}{100}$ and $a_e^{(T,abv)} - 0$ across bottle walls tend to be of the same magnitude order in dry conditions. Temperature affects differently the partial pressure of water and ethanol. Increasing the temperature in a closed storage room will cause a dramatic decrease in $RH(T)$ and therefore of water transfer. In our experiments, condition S1 is the most extreme and corresponds to conditions met in container transport. The cumulated pressures $p_{total}^{theoretical}$ offer a lower bound for the total pressure reached in the headspace under vacuum (no air). It can reach up to 25 kPa for liquors at 50°C (point B1 (abv=0.7, $p_{total}^{theoretical}$=25 kPa) in **Figure V-4**b).

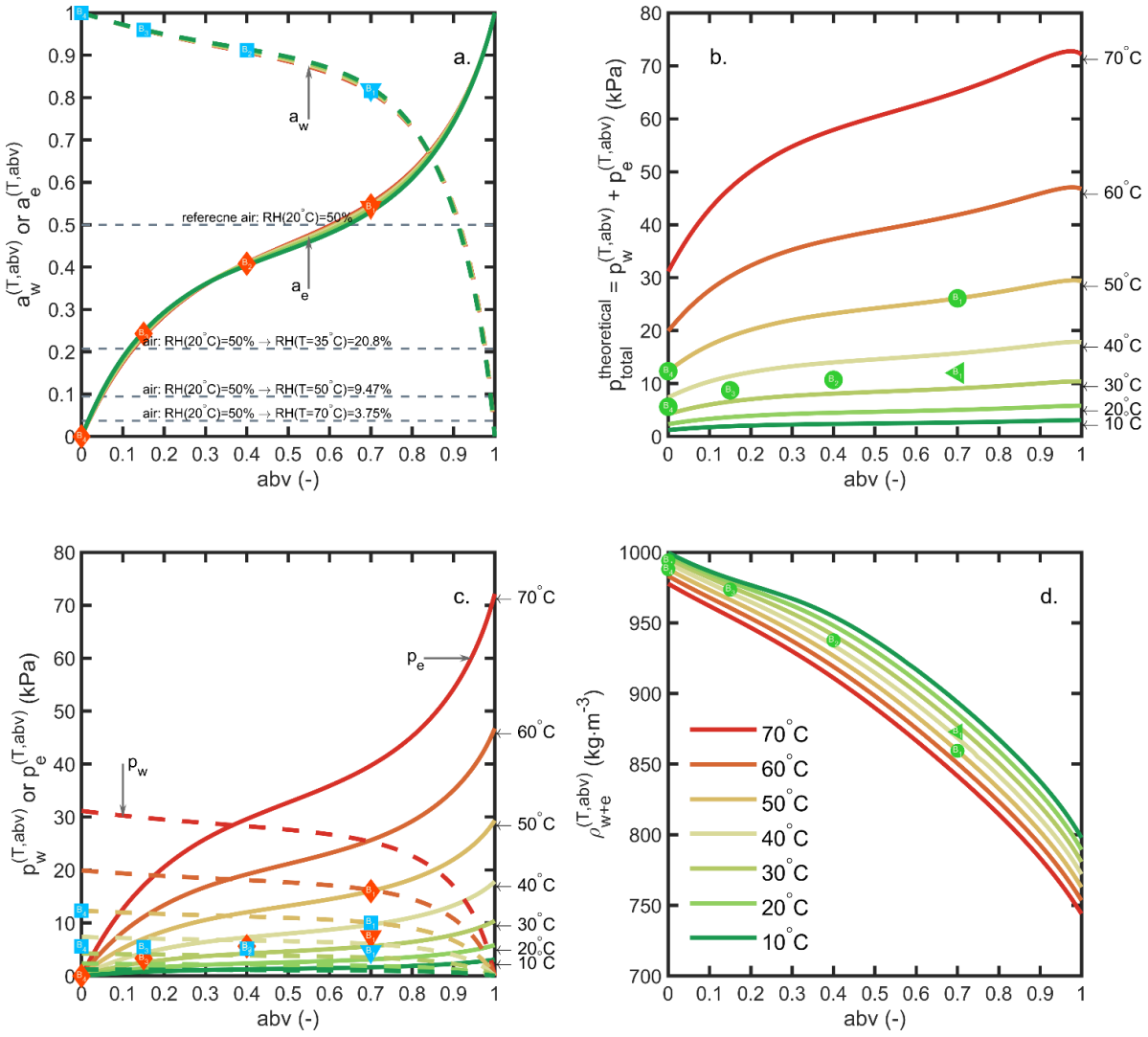

Figure V-4. *Binary properties of water-ethanol mixtures: (a) activities, (b) partial pressures, (c) total pressure in vacuum, (d) liquid density. The symbols depict the tested beverages and storage conditions. Horizontal lines in (a) show the variation of RH when the air temperature is increased from 20°C up to 70°C.*

V.2.3.2. Total pressure in bottles M

- *Overview*

Bottles are commonly filled with air at atmospheric pressure and a temperature lower than the storage temperature. These conditions provoke significant evaporation of ethanol and in a less extent of water, as well as thermal expansion of the mixture (see **Figure V-4**b and 4c). According to the volume of headspace, V_{head} , the pressure difference between the headspace, P_{head} , and the surrounding, P_{atm} =100 kPa, can be much higher than $p_{total}^{theoretical}$. Total Pressures were calculated in bottles M with a total capacity of 55 mL by varying the headspace volume from 0.5 mL to 35 mL, and by assuming that the walls of the bottle are rigid. The

results for different filling temperatures T_0 and initial headspace volumes V_{head}^0 are summarized as iso-pressure contours in **Figure V-5** for $abv = 0.15, 0.4, 0.7$ shown in **Figure V-4**. When the filling temperature is equal to the storage temperature T, the internal overpressure, $P_{head} - P_{atm}$, is commensurable to $p_{total}^{theoretical}$ and independent of V_{head}.

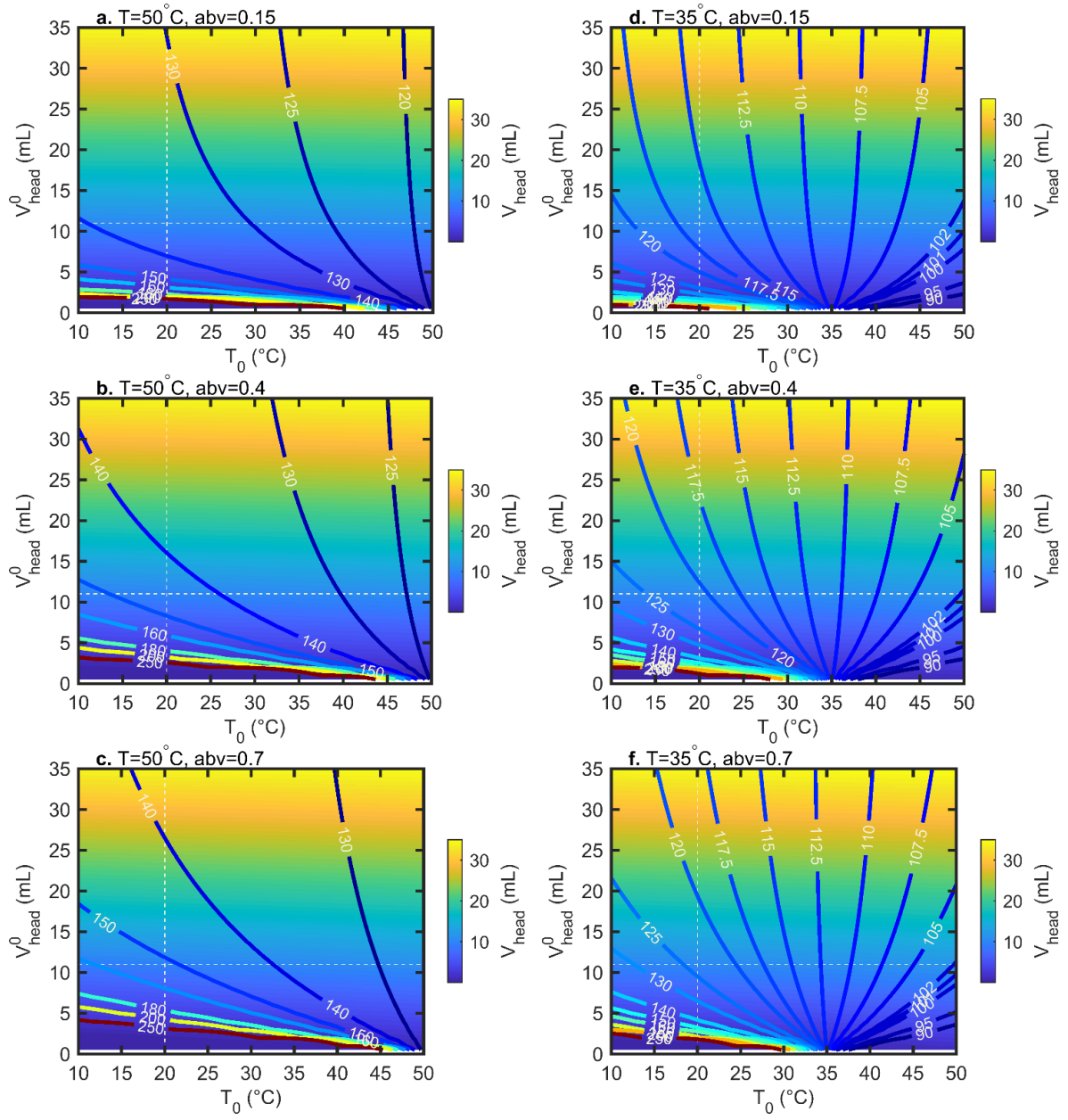

Figure V-5. *Calculated iso-headspace pressures (P_{head}) and iso-headspace volume (V_{head}) at equilibrium in the bottle depicted in* ***Figure* IV-1** *according to the headspace volume (V_{head}^0) and temperature (T_0) at filling time. The results are presented for two storage temperature 50°C (a,b,c) and 35°C (d,e,f) three abv values (0,15, 0.4, 0.7).*

Temperatures greater than T_0 provoke strong overpressures heavily dependent on V_{head} and on abv values. Small headspace volumes more than temperature contrast can lead to strong overpressures up to 300 kPa or more. They can be responsible for additional mass transfer (leaks) across the closure system. Such mass transfer driven by total pressure difference instead of partial pressure gradients across bottle walls were not considered in the modeling part. As a result, bottles expected to have leaked during the tests were discarded from the comparison with simulation. Collapse is known to occur as the consequence of mass transfer, but calculations demonstrated that thermal contraction after hot filling could also cause collapse. Its maximum intensity was of a few kPa, that is slightly above the natural variation of the atmospheric pressure but lower than the variation of pressure with elevation. Finally, it is worth noticing that the effect of the headspace pressure on activity coefficients in the beverage was not considered.

- *Theoretical overpressures in our experimental conditions*

In our experimental conditions, $V_{head} \approx 11$ mL and $T_0 = 20°C$, P_{head} reaches 135, 145, 152 kPa at $T = 50°C$ and 116, 121, 123 kPa at $T = 35°C$ for $abv = 0.15, 0.4, 0.7$ shown in **Figure V-4**, respectively. V_{head} decreases from 11 mL down to 10.43, 9.99, 9.67 mL at $T = 50°C$ and 10.76, 10.51, 10.36 mL at $T = 35°C$ for $abv = 0.15, 0.4, 0.7$, respectively. Dividing V_{head} by 2 and 4 in the worst-case conditions ($T = 50°C$, $abv = 0.7$) increases the overpressure by 17.4%. and 91%. Negative pressures (below P_{atm}) associated with important risk of collapse occurs in the presence of headspace volumes lower than 5 mL and filling temperatures 10°C above the storage temperature ($T_0 > T + 10°C$).

V.2.4. Comparison of simulated and measured water-ethanol mass transfer across bottles *M*

The capacity to simulate mass transfer across bottles *M* were tested by comparing the mass loss and *abv* variations during a large challenge test involving 425 bottles as detailed in ***Table IV-6*** and with the sealing system shown in ***Figure IV-1***d. The five-months initial test was prolonged for some bottles by adding a new packaging component (sleeve) in order to validate the capacity of the model to account for an extra mass transfer resistance. As water diffuses faster than ethanol (see ***Table IV-3***), the sleeve was thought to bring indirectly an assessment of a supplementary mass transfer resistance on its permeation.

V.2.4.1. Permeation and sorption kinetics

The methodology of measurements did not enable to separate directly the fluxes of water and ethanol as well as the fluxes crossing the walls from the amounts absorbed in the walls. Bottles filled with pure water were not subjected to typical leaks and were used as a reference baseline for comparison with hydroalcoholic solutions. The simulated results were recast to be comparable with experimental results: i) the net mass variation of the filled bottle was associated with the cumulated permeation fluxes of water and ethanol; ii) the *abv* variation combined the effects of ethanol loss (by sorption or permeation) and concentration due to water loss (by sorption or permeation). Temperature and RH variations were not accounted, and the average of recorded values in the storage chambers were applied in the simulations.

A significant total pressure difference across the lid existed for all tested storage conditions and beverages, including when the bottles were filled with pure water. For *abv* greater than 0.4, the internal pressure was estimated 86 % higher in the presence of ethanol than without and made the risk of leaking through the more likely. Leaking was detected by a rapid mass loss during the week of storage. The number of leaking bottles reached 48% at 50°C and 23% at 35°C for $abv \geq 0.4$ (see ***Table IV-6***). For low *abv* values (0.15), the number of leaking bottles dropped down to 9.4% and was reduced to zero in the case of pure water. After discarding leaking bottles, 1889 mass measurements and 286 *abv* determinations were collected on 358 bottles for all tested conditions (see **Table IV-7**).

Experimental and simulated mass losses and *abv* values are reported in **Figure V-6** with the individual fluxes of water and ethanol reconstructed by simulation detailed in **Figure V-7**. Experimental losses were also standardized to the same filling weight to remove the initial dispersion of data. To facilitate the interpretation of coupled water-ethanol mass transfer, the permeation curve of water alone is shown as reference for all tested conditions. The variations of *abv* corrected from water loss are also presented by assuming that the permeation of water was proportional to the applied driving forces.

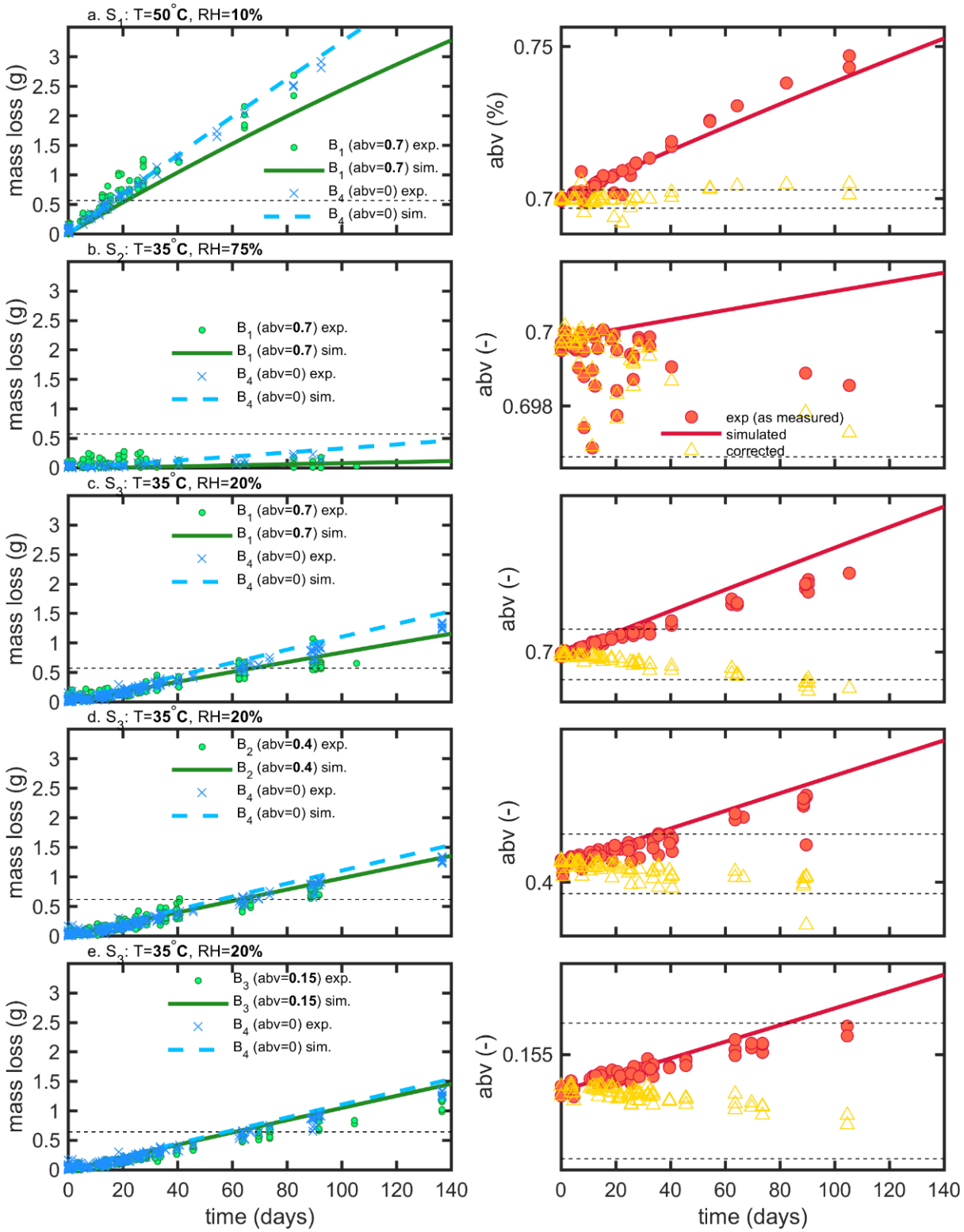

Figure V-6. *Comparison of experimental (exp) and simulated (sim) mass loss and abv variations. The dashed lines plot the thresholds used to calculate shelf-life (see text). Empty symbols (triangles) represent the theoretical variation of abv when concentration effects due to water permeation are corrected.*

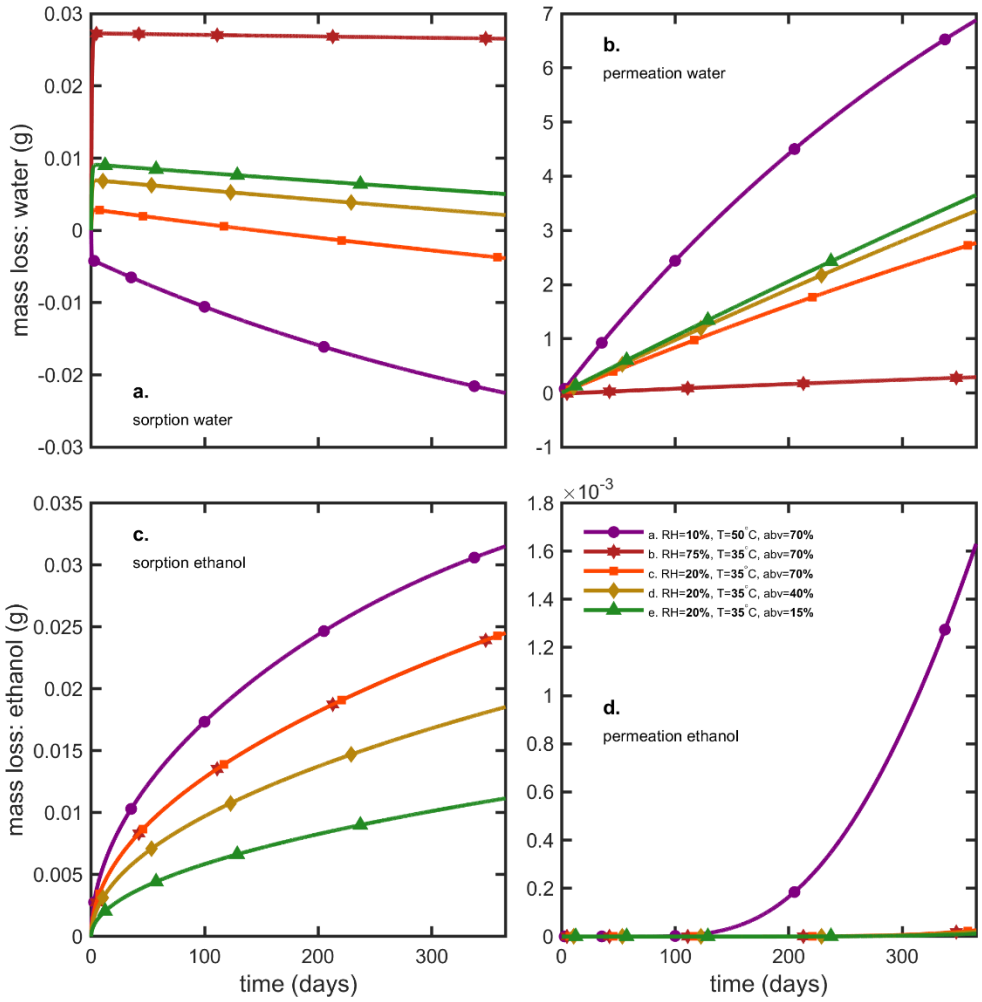

Figure V-7. *Reconstruction of mass losses by sorption and permeation for (a,b) water and (c,d) ethanol.*

Weight differences between bottles filled with water and hydroalcoholic mixtures were small and controlled by the differences in water activities, $a_w^{(abv)} - \frac{RH}{100}$, on both sides of bottle walls. Though water losses dominated in alcoholic beverages, the shelf-life was determined mainly by the variation of the *abv* criterion in hydroalcoholic mixtures. The maximum storages times fulfilling weight loss and *abv* criteria are summarized in **Table V-1** for the strictest conditions associated with containers larger than 1 L and extrapolated down to containers of 50 mL. The rapid permeation of water trough bottle walls caused a concomitant fast increase in ethanol strength (*abv*) in conditions S1 and S3 (see **Figure V-6**a,c-d). Weight losses exceed faster limits only for mixtures with low *abv* values (**Figure V-6**e) or when the difference of water activities was low. For both observed criteria (*abv* and weight loss), a steady regime was reached within three to six days. Simulations enabled to reconstruct all aspects of mass transfer for all tested conditions and provided a mechanistic interpretation of coupled mass transfer. **Figure V-7** decomposes mass losses for water and ethanol into sorption and permeation fluxes. Contact times were much longer than permeation lag-times (**Figure V-7**b)

and justified the apparent steady state of weight losses and *abv* variations. The water content in bottle walls evolved in a non-linear manner with desorption dominating in very dry conditions (condition S1). At high (S2) and intermediate (S3) relative humidities, the rapid water sorption is followed by a slow drying when the surrounding *RH* during storage is lower than the equilibration *RH* before the experimentation starts (**Figure V-7**a). Ethanol diffuses slowly through PET without reaching a steady state. Lag-times beyond which permeation of ethanol may reach a steady state are evaluated ca. 1.4 and 3.6 years, at 50°C and 35°C, respectively.

Table V-1. *Comparison of shelf-lives extrapolated from experiments and calculated from simulations.*

Storage condition	Beverage	Time to reach 1.5% m/m mass loss† (days) t_m		Time to reach ±0.3% variation of abv‡ (days) t_a		Theoretical shelf-life for 50 mL bottles* (days) $\min\left(\left\lfloor \frac{9}{1.5} t_m \right\rfloor, \lfloor t_a \rfloor\right)$	
		exp.	sim.	exp.	sim.	exp.	sim.
S1	B1	18 (16,20)[a]	21.1	8.5 (8,9)[a]	7.3	8.5	7
S1	B4	17±1.5[b]	19.2	-	-	102	115
S2	B1	>140	>730	>140	225	>140	224
S2	B4	>140	197		-	>140	1182
S3	B1	64 (63,65)[a]	67.1	31 (29,33)[a]	22.9	31	22
S3	B4	64 (63,65)[a]	58.6	-	-	384	351
S3	B2	54±5[b]	62.3	38 (36,40)[a]	33.5	38	33
S3	B4	66.5 (64,69)[a]	58.6	-	-	399	351
S3	B3	69 (64,74)[a]	60.7	105	82	105	82
S3	B4	65.5 (64,67)[a]	58.6	-	-	393	351

†see Annex 1 of EU Directive 76/211/EEC (class 'B' product with a package capacity over 1 L); ‡see Annex XII of EU regulation 1169/2011/EC (applicable for any beverage containing more than 1.2% vol); *shelf-life extrapolated for 50 mL bottles according to EU Directive 72/211/EEC.
a. shelf-life on average days (min, max); b. shelf-life in days ± 95% confidence interval.

V.2.4.2. Flux reduction brought by the addition of a sleeve

The results presented a significant variability between bottles, which could not be reduced experimentally, and which could not be reproduced by simulation. The sealing was identified as the source of major leaks and defects, but the contribution of a weak gas leak, which could be confused with permeation, could not be tested directly along with other sources of variabilities: variable plasticizing of PET and variable distribution of PET material at injection-blowing time. It is worth noticing that possible heterogeneities in hydrodynamic, temperature and humidity conditions around bottles cannot be invoked to explain variabilities, as all climatic chambers were equipped with an efficient air recirculation and renewal. Further insights were brought by adding a shrinking 60 µm biaxially oriented PET film (sleeve) around

the thinnest part of the bottle (cylindrical section of the bottle as seen in ***Figure IV-1***), which was thought to contribute the most to the overall permeation rate. The sleeve was added to bottles of B3 ($abv = 0.15$) and B4 (water only) at the end of storage S3 (see **Table IV-7**); it covered ca. 80% of the total surface area. Since ethanol could not significantly cross the ca. 800 µm thick bottle walls, the external film reduced mainly the flux of water. Mass losses before and after the addition of the sleeve are analyzed individually for twenty bottles containing ethanol (10) or not (10) in **Figure V-8**. The results were not normalized to highlight the different evolutions of the bottles. Before the addition of the sleeve, the "trajectories" followed by the bottles diverged (different permeation rates). Adding a sleeve inflected all permeation rates in a very similar way and made all permeation kinetics looking very similar with almost parallel slopes. This trend confirmed the prevalence of the body of the bottle and water permeation on overall mass transfer. Since the thickness of the sleeve was commensurable to the thickness fluctuations in the body region (see ***Figure IV-1***c), the dispersion of permeation rates between bottles was associated to the slight variations of the distribution of weight after injection-blowing (see similar analyses in Figures 3-6 and Figure 10 of Daver *et al.*, 2012;Demirel and Daver, 2012, respectively). The flux reduction followed approximately the rules of serial association of mass transfer resistances: $\left(l_{wall}^{-1} + l_{sleeve}^{-1}\right)^{-1}$, with l_{wall} and l_{sleeve} the thicknesses of the wall and the sleeve, respectively.

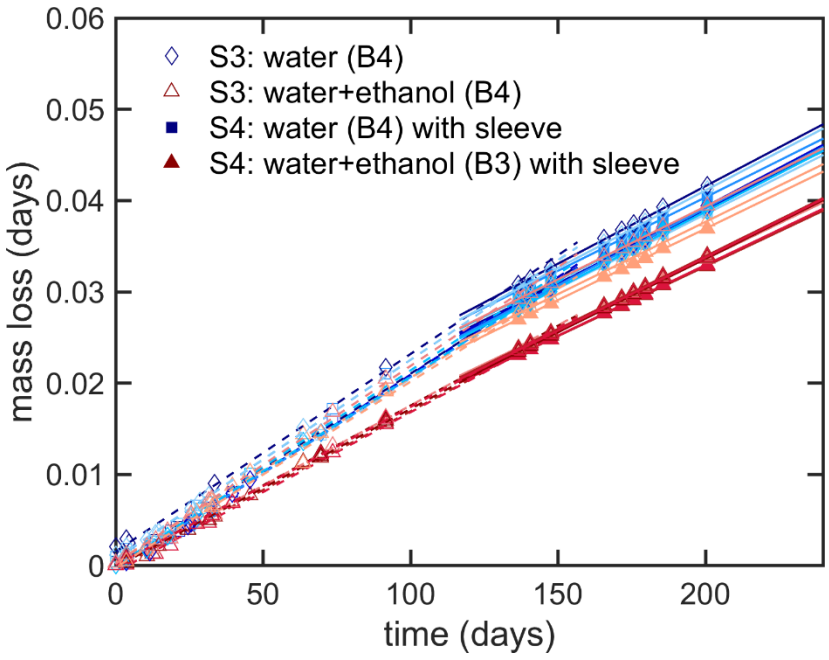

Figure V-8. *Modifications of mass transfer when a sleeve is added to the bottles containing the beverage B3 and B4 after several months of storage: mass loss during condition S3 (dash lines, one line per considered bottle) and S4 (continuous lines, one line per considered bottle).*

V.2.5. Optimal design of packaging systems for liquors: bottles X as a case study

- *Justification of the design template of bottle X*

The design of a new packaging can be seen either as a problem of a relationship between wall thickness and shelf-life or as a more global problem seeking the maximization of shelf-life while minimizing the mass of plastic material. As previously shown on bottles M, wall thickness and shelf-life are not independent parameters as soon as a steady regime is reached. Under a strict permeation control, doubling shelf-life requires twice the initial thickness and doubles the weight of plastics. Substantial gain can be achieved without damaging weight only if some non-linearities can be introduced in the original engineering problem. They appear spontaneously if the shape and, in particular, the surface-to-volume ratio is also a degree of freedom. Its contribution was investigated by analyzing the effects of parameters W and D on the weight of bottles matching the design X (see ***Figure IV-2***).

- *Optimization procedure*

For each value of W and D, the wall thickness of the main sides was optimized to grant a minimum shelf-life of 6 months for a vodka-type product stored in tempered conditions (25°C at 50% RH). The full explored domain covered a 30×30 grid describing a uniform variation of both parameters between 30 mm and 120 mm. All other properties were recovered by simulation-optimization. It is worth noticing that only l_{wall} was updated for each bottle. The other constraints were managed by mathematical constraints applied to the bottle geometry. For efficiency and robustness in particular close to edges, all bottles were modeled as cylindrical B-spline surfaces rather than swept surfaces. All integrations (masses, fluxes) were integrated accordingly. The corresponding space of explored shapes is shown in **Figure V-9** with optimized values summarized in **Figure V-10**. Shapes vary from almost symmetric cylindrical bottles, flask shapes, long tubes, flat bottles. Some shapes were exotic, but they could be examined at no extra cost by calculations.

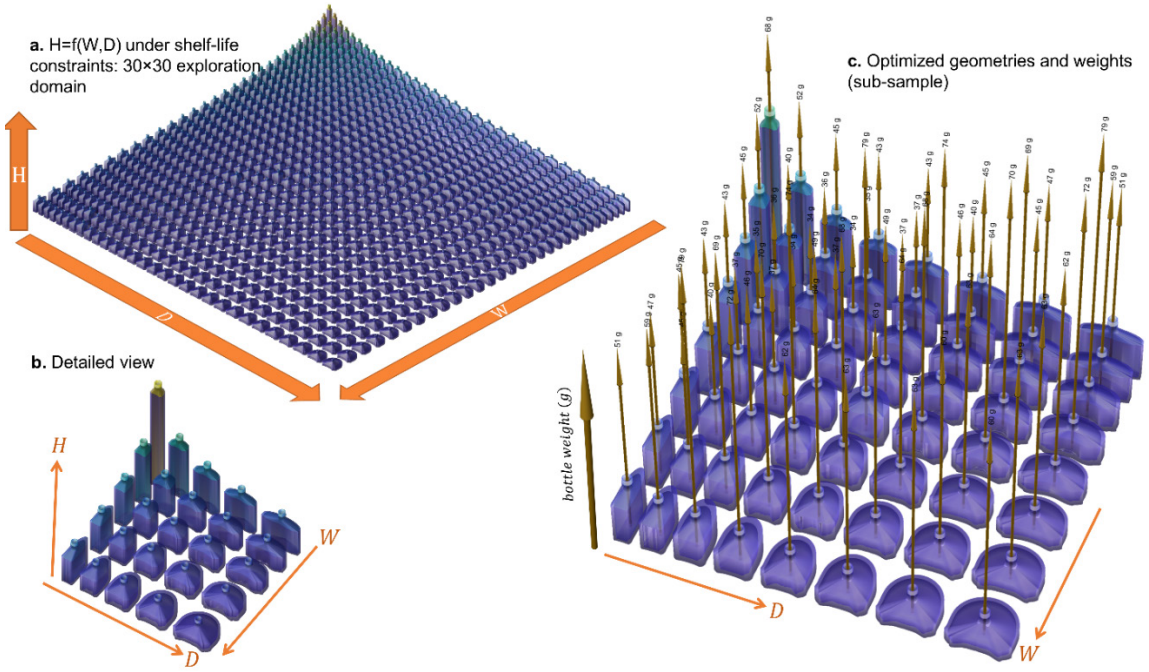

***Figure V-9**. Space of geometries explored and optimized for a 160 mL bottle (capacity 150 mL) containing a vodka-type beverage: (a) shapes corresponding to a 30×30 combination of W and D, (b) 5×5 combination, (c) weights of bottles optimized to fulfill a shelf-life of 180 days at 25°C.*

- *Generated solutions*

The optimization procedure generates two families of solutions for the same final capacity 150 mL and shelf-life but with weights varying in a ratio 1:2. Flat geometries associated with large W and D values led to heavy bottles and large weights. On the contrary square sections with intermediate W and D values led to very similar weight reductions, while keeping the same shelf-life. The transition between the two regions appears noisy with several maxima. The transition region corresponded to a shift of the shelf-life criterion controlled by abv for heavy bottles and by the mass loss for light bottles. For a given W or D value, a unique bottle minimizes the weight of the PET bottle. The continuous curve connecting all points represents the Pareto front for all the criteria considered: capacity, shelf-life, weight, shape factor. Changing W or D will at the expense of either the shape of the bottle or of its weight. A selection of bottles along the Pareto front is shown in **Figure V-10**c. The result can be seen as a shape interpolation process from one shape where the curvature is on the smallest side to a final shape where the curvature dominates the largest side. As the bottle is not symmetric, the transformation is not equivalent to a swap of sides. The optimal shape is closer to the cylinder shape and offers as expected the minimum surface-to-volume ratio.

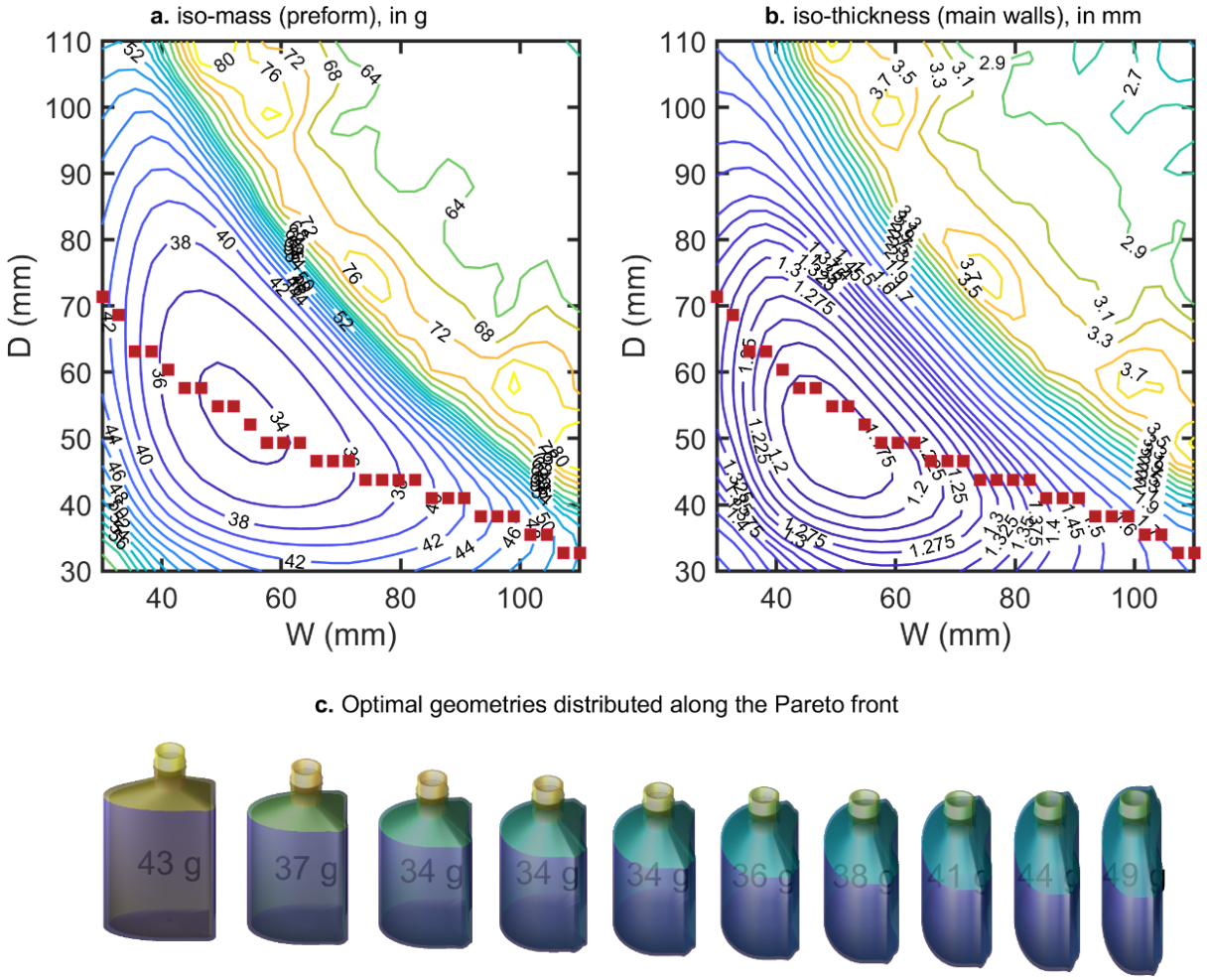

Figure V-10. *(a) iso-weight and (b) iso-thickness contours of optimized bottles (minimum shelf-life of 180 days) shown in* ***Figure V-9****. The filled symbols locate the sampled Pareto front. A selection of designs sampled along the Pareto front (from left to right) is presented in (c).*

V.2.6. Main directions and limits of the optimization of PET bottles with fixed shelf-life

- *Contribution of the [E][D][S] approach*

This section generalized the case-study presented in §III.2. to simultaneous mass transfer of water and ethanol and real bottles geometries. It provides solid grounds for more systematic methodologies to solve the problems defined in §III.2.1. :

- P2: minimizing packaging weight (S2);
- P3: optimizing shape;
- P6: optimizing food shelf-life (considered here as a minimum value).

Problem P4 "*mitigating transportation and retailing conditions, including the risk of overpressure and collapse*" was indirectly addressed in §V.2.3.2. but not optimized. Problem P5 "*updating the packaging format to the food volume consumed*" could be addressed using the last review of alcoholic beverage preference and dietary habits (Sluik *et al.*, 2016).

- *Validation of the shelf-life criterion/constraint at tiers 1,2*

The dual geometry and the thermodynamical coupling were able to provide comparable performances to experimental tests running over several months. The principles of *in-silico* determinations of mass transfer are well established. In details, the exact rates of sorption and permeation of ethanol could not be guessed from experiments. They were too noisy to offer reliable estimates. More specific measurements are required to validate the principles of the description of the cosorption of water and ethanol at various temperatures.

- *Adding other [E]valuation steps and its generalization to other polymers*

Step [E] can be extended to a broad range of mass transfer phenomena (aroma scalping, migration of plastic additives). With this respect, safe-by-design and ecodesign approaches can be treated in parallel without substantial additional cost and by adding rows to *Eq.*(IV.6) -(IV.9). The only limit is the availability of diffusion and partition coefficients for the considered solutes and polymers.

- *Directions for optimizing the design of bottles M*

The detailed case-study demonstrate that very small formats (miniatures) cannot compete with larger PET bottles for storing alcoholic beverages. Similar tolerance on mass loss and alcohol strength by combining two strategies: increasing wall thicknesses and changing their shapes. Additionally, the main stressors have been identified and are associated contrary to intuition to the difference of partial pressure of water across the walls and not the one of

ethanol. As the thickening of the wall is beneficial only for water permeation, keeping miniatures in a humid place or even immersed in water can contribute to extending shelf-life without producing additional waste.

V.3. Ternary isotherms of water and ethanol in PET at tiers 2,3

The condition of local thermodynamical equilibrium, LTE, (see definition in §II.2.3.5.) between the liquid content of the bottle and the surface of PET walls is an essential property to enable the integration of transport equations in simulations (see §.II.2.3. LTE controls the intensity of the incoming flux (sorption) on the inner side and sets the outcoming flux (desorption) on the opposite side. **At tier 1**, mass uptake was thought linear with partial pressure and without interactions between water and ethanol in PET. Water and ethanol non-ideal behaviors were accounted on the liquid side. **At tier 2**, the equivalent Henry constants or saturation concentrations were authorized to increase with *abv* (see ***Table IV-3***).

At tier 3, the effects of composition and temperature are thought to be integrated into a continuous single ternary isotherm (PET+water+ethanol) governed by the activity of water, ethanol, and temperature. Additional driving forces created by the gradient of elastic energy are assumed negligible at this level of details in thick bottle walls, but they should be considered when the ternary model is calibrated from thin films results. Replacing direct liquid contact by successive step-changes of partial pressure is a known source of artifacts in the presence of non-reversible polymer swelling.

The distinction between diffusion in a solid with an elastic behavior (coined “elastic diffusion”) or with a viscoelastic behavior (coined “viscoelastic diffusion”) is fundamental. Indeed, the linear theory of diffusion, so-called Fickian diffusion and controlled by the random walk of solutes, applies only when the reorganization of the surrounding environment is faster than the translation of the solutes or when it is much slower. When the time scales of the two processes are not separable, a coupling may exist and may complicate the definition of the equilibrium: chemical equilibrium for one single or multiple components, mechanical equilibrium, a combination of both.

The relaxation of a glassy polymer is associated with various time scales in the function of its degree of subcooling, its history, temperature, solute, and concentration ranges. According to the duration of the sorption experiment and the thickness of the sample, some relaxations are observed or not. These interactions undermine our capacity to observe true binary

equilibrium concentrations, $\{C_{i,eq}\}_{i=w,e}^{T,T_g}$ even after several months. An overview of the constraints is shown in **Figure V-11** in relationship with the experimental strategies followed in this work and in the literature. Thick materials (bottle walls) tend to show strict Fickian behavior when they are exposed to a rapid differential step-change of partial pressure. By contrast, thin materials offer the highest flexibility to sample the full spectrum of behaviors with concentration and the duration of exposure. The large rectangle showed the domain explored recently by Dubelley *et al.* (2017a) for the sorption of water in PET (280 µm thick materials) and which was used in the analysis in the complement of thinner (thickness: 12 µm) and thicker materials (thickness: ~628 µm). Changing thickness is a common strategy to accelerate the obtention of equilibrium before the polymer initiates an irreversible crystallization. Since ethanol is diffusing more slowly than water, direct immersion was preferred for ethanol.

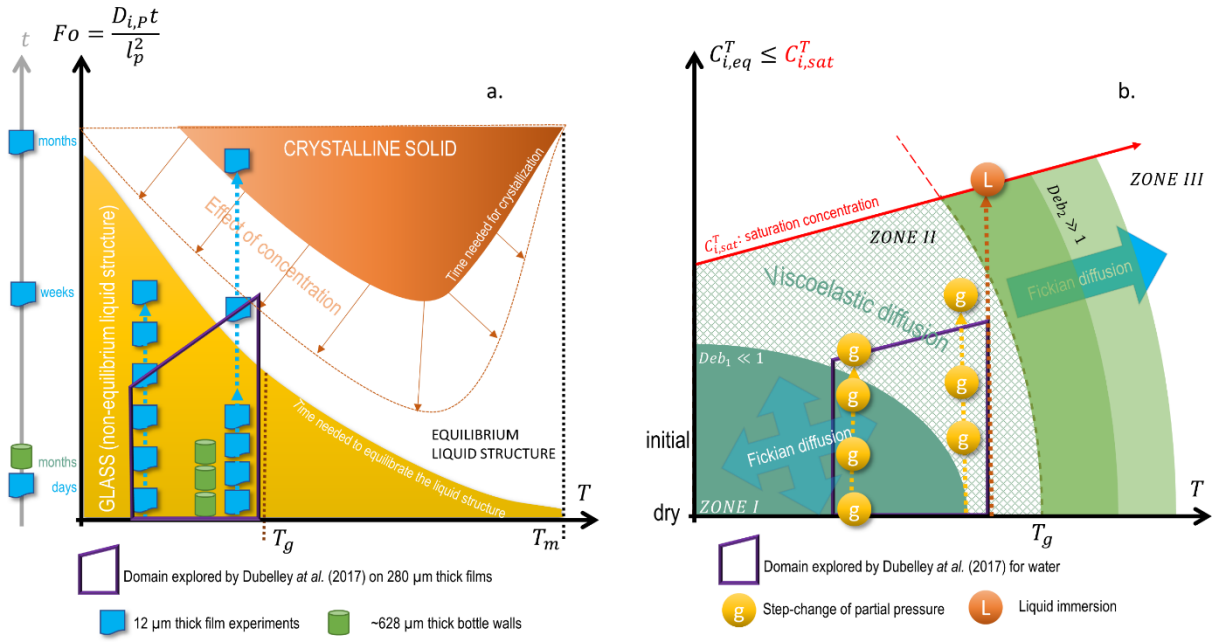

***Figure V-11**. Schematic representation (a) of the state of the polymer and (b) the corresponding mechanism of diffusion during a sorption experiment. Deb stands for the Deborah number. (modified fromVrentas et al., 1975).*

The experimental difficulties inherent to PET at glassy state are firstly illustrated for the transport of water using both a new interpretation of the results of Dubelley *et al.* (2017a) and of those obtained in this work. The basis for deriving a Flory-type ternary isotherm is subsequently justified, parameterized, and validated.

It is emphasized that due to the difficulty of validation and implementation history and non-local effects in a numerical code, their effects on mass transfer are not considered **at tier 3** (see discussion inKrüger and Sadowski, 2005;Kadam *et al.*, 2014). Free-volume effects and polymer degradation on sorption are neglected at this stage.

V.3.1. Why is it difficult to estimate $\{C_{i,eq}^{T,T_g}\}_{i=w,e}$ in PET at glassy state?

A consistent simulation model should implement the "right" $\left\{C_{i,eq}^{T,T_g}\right\}_{i=w,e}$ value at its boundaries (LTE), but experiments provide only an estimate of the macroscopic version of $\left\{C_{i,eq}^{T,T_g}\right\}_{i=w,e}$. A discrepancy between the interfacial and macroscopic value is known to occur when i) the time to reach equilibrium is not accessible or ii) the material itself is subjected to important macroscopic modifications during the sorption process. The best time window to estimate $C_{w,eq}^{T,T_g}$ depends on temperature and on the thickness of the material as shown in **Figure V-11**.

V.3.1.1. *Diffusion vs. polymer relaxation time scales*

For walls of thickness l_P, the typical diffusion time for solute i is given by $\frac{l_P^2}{D_{i,P}}$ (single-sided contact), whereas the longest relaxation time of the polymer is associated to an apparent first-order rate β, independent of the solute. Phenomenologically, the volume relaxation process causes an extra mass transfer, which can be written in a non-causal manner as:

$$\frac{\partial C_i^{(x,t)}}{\partial t} = \beta\left(C_{i,eq} - C_i^{(x,t)}\right) \text{ with } i = w,e \qquad \text{(V.1)}$$

with $C_i^{(x,t)}$ the local concentration expressed here in kg·m^{-3} along the coordinate x at time t. Eq. (V.1) written in 1D adds a source term, which is not entirely satisfactory as it does not explain how the solute is not accessing to the position x, but at least it describes how the concentration at the interface may increase with time and may subsequently provoke an acceleration of mass transfer, beyond the time scale of diffusion. As shown in Kadam *et al.* (2014), $C_{i,eq}$ is the theoretical value when the sorption is fully reversible. The dimensionless kinetic modulus $Deb_i = \frac{D_{i,P}}{\beta l_p^2}$, also known as Deborah correlation number or diffusion Deborah number, estimates the relaxation time respectively to the diffusion time to reach $C_{i,sat}$:

$$\frac{\partial\left(C_i^{(x,t)}/C_{i,e}\right)}{\partial Fo_i}=\frac{1}{Deb_i}\left(1-C_i^{(x,t)}/C_{i,e}\right) \text{ with } i=w,e \tag{V.2}$$

An interpretation of the diffusion Deborah number is shown in **Figure V-11**b. When $Deb \ll 1$ (high temperature), polymer relaxation occurs faster than diffusion and LTE is maintained all along the sorption process, $C_{i,eq}$ is a constant. When $Deb \gg 1$, polymer relaxation occurs after the chemical equilibrium is reached and $C_{i,eq}$ appears increasing slowly with time. In both cases, diffusion scales as the square root of sorption time. At intermediate Deb numbers, several time scales are intricate, and no general interpretation rule exists.

Magnitude orders of β for PET can be determined directly by measuring stress and creep relaxation. Billovits and Durning (1988) determined that the longest relaxation time of PET, denoted τ_0 , was about 10^{12} s. From time-temperature superposition principles, the authors suggested a double activation by temperature, T, and plasticizing (T_g shift) as follows:

$$\beta\left(T,T_g^{mix}\right)=\frac{1}{\tau_0}\exp\left(\frac{17.74\left(T-T_g^{i+PET}\right)}{51.6+T-T_g^{i+PET}}\right) \text{ with } i=w,e \tag{V.3}$$

where T_g^{i+PET} is the glass transition temperature of the mixture, 17.74 (-) and 51.6 K are the "universal" constants of the Williams-Landel-Ferry model.

Corresponding Deb values are reported in ***Table IV-3*** for 12 µm thin PET films and 760 µm thick PET bottle walls. Viscoelastic diffusion (relaxation times ca. 3-4 days) controls the kinetics water uptake in thin films on the long term (Deb>10^3) but is entangled with diffusional transport in thick walls (Deb~2). Due to the lower diffusion rate of ethanol, diffusion Deborah numbers are closer to unity for ethanol transport.

V.3.1.2. Sorption-induced changes in PET

- *A simple formulation of the coupling between Fickian and viscoelastic diffusion*

Equilibration times are not only particularly long in PET, but they are also coupled to the physical aging of the polymer itself. Aging includes polymer relaxation (Billovits and Durning, 1988), morphological alterations (Vieth *et al.*, 1967), densification, and finally, a cold crystallization (Ouyang and Shore, 1999). These phenomena have been frequently reported for the sorption of water in PET, but they occur during the sorption of ethanol (Chandra and Koros, 2009b) and toluene (van Lune *et al.*, 1997). Dubelley *et al.* (2017a) proposed recently a state diagram showing that the conditions of plasticizing and densification processes were

related to relative humidity and temperature. Without theoretical justification, it has been suggested that the limits between the different behaviors were controlled by the partial pressure of water, an intrinsic property of water, and not by the polymer itself. We propose a different interpretation of the extensive data collected by Dubelley *et al.* (2017a) on 280 µm thick PET materials, with an independent validation on 12 µm thin films at the temperature minimizing relaxation effects (50°C, justified hereafter). Decreasing thickness is indeed the most efficient method to evidence the asymptotic behavior of non-Fickian relaxations.

Mass uptake of samples subjected to water vapor was thought to be the linear superposition of a non-Fickian (see Eq. (V.1)) and Fickian (see Eq. (II.17)) contribution, as follows:

$$\begin{aligned}\frac{m_i^t}{m_i^e} &= \phi\left[non-Fickian\ uptake\right]+\left(1-\phi\right)\left[Fickian\ uptake\right] \\ &= \phi\left[1-\exp\left(-\frac{Fo_i}{Deb_i}\right)\right]+\left(1-\phi\right)\left\{1-\frac{8}{\pi^2}\sum_{n=0}^{\infty}\frac{1}{\left(2n+1\right)^2}\exp\left[-\left(2n+1\right)^2\frac{\pi^2}{4}Fo_i\right]\right\}\end{aligned} \quad (V.4)$$

with $Fo_i=\frac{4D_{i,P}^{T,RH}}{l_p^2}$ and $Deb_i=\frac{4D_{i,P}^{T,RH}}{\beta^{T,RH}l_p^2}$ for double-sided contact.

The likely values of $\beta(T,RH)$, $Deb(T,RH)$ and the theoretical mass uptake at equilibrium m_i^e were estimated by least-square deconvolution of high resolution sorption data obtained by microbalance.

- *A pseudo-state-diagram of sorption-induced changes inferred from Dubelley et al. (2017a) data (280 µm thick PET film)*

The values of β and Deb were inferred from the step-wise sorption of *Dubelley et al. (2017a)* data are shown as isocontours in **Figure V-12**. A good signal-to-noise ratio was obtained by estimating the isocontours from a bivariate regularized spline approximant dropping 2% of the total variance. The sign of β and of was negative (condition of polymer densification) when the uptake kinetics exhibited a maximum before decreasing slowly. In all tested conditions by authors, relaxation-times were much longer than diffusion time ($|Db| \gg 1$); relaxation times $|1/\beta|$ could be estimated with very confidence until 50 days (i.e., 20 times the duration of each kinetics) and with large uncertainty beyond. Similarly, absolute $|Db|$ values lower than 70 are judged significant. A positive contribution of relaxation on mass uptake appears when RH>50%. Temperature does not change the trend but shortens relaxation times roughly as predicted by Eq. (V.3). The contribution of relaxation on sorption is negative when the temperature approaches T_g (75°C in the tested sample) with cold crystallization identified between 60°C and 70°C. The figure shows that PET films stored in room temperature conditions (T=25°C, RH=50%) are subjected to a slow evolution (**Figure V-12**a). Minimizing $|Db|$ values

(**Figure V-12**b) requires working at 50-55°C and 40-50% RH. In the conditions more representative of liquors (RH>85%), relaxation times are commensurable to the shelf-life of beverages at room temperature and would be responsible for a slightly higher sorption than the one expected for short-time contacts. For $1/\beta$ values shorter than one month, it could be expected that the sorption of water could be doubled after six months. This scenario of doubling water uptake at high water activity has been also suggested by Burgess *et al.* (2014b) (see Table 3 herein) with a swelling up to 2.4%±0.6% in value. As the swelling was assumed isotropic, this value might be three times smaller in bottles, where swelling is enabled essentially across the walls.

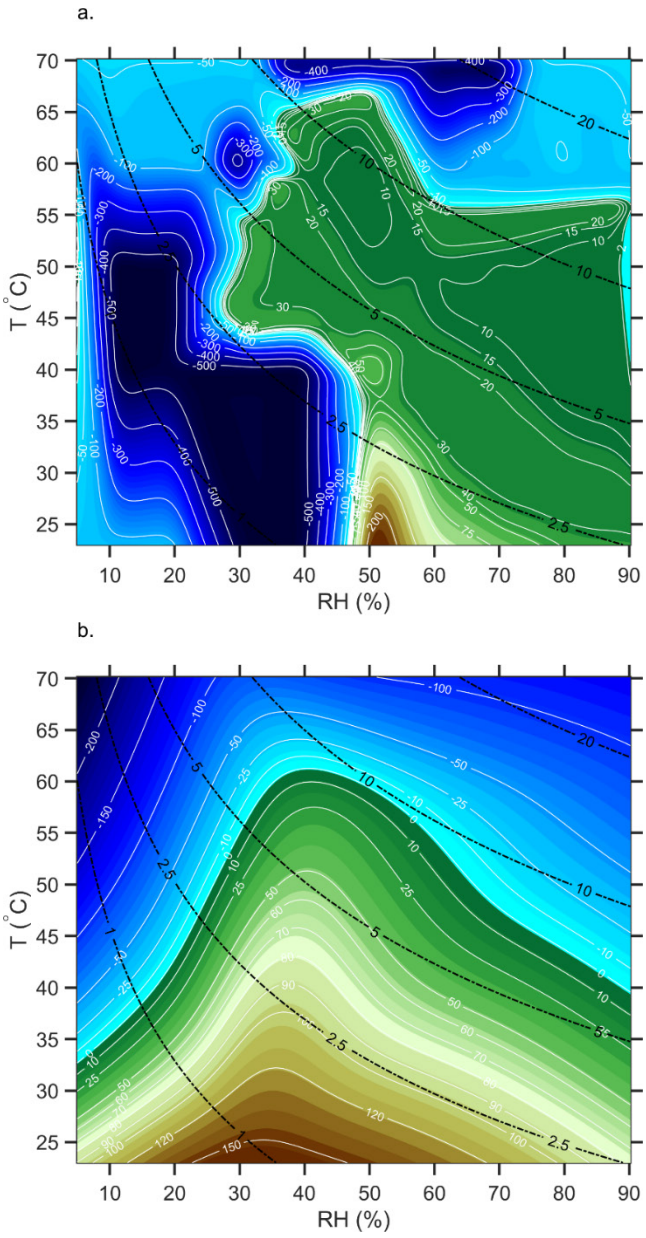

***Figure V-12**. Interpretation of water sorption kinetics in 280 µm thick PET of Dubelley et al. (2017a): (a) $1/\beta$-isocontours in days (continuous lines; $\beta>0$: positive effect of relaxation on uptake, i.e. swelling; $\beta<0$: negative effect of relaxation on uptake, i.e. densification); (b) corresponding iso-Deborah numbers (continuous lines; same sign as β). Dashed lines represent iso-p_w in kPa of the corresponding water vapor.*

V.3.1.3. Independent validation of non-Fickian relaxations in PET

Relaxation times are independent of thickness, but diffusion times are not. Independent validation of *Dubelley et al. (2017a)* behaviors was sought by analyzing the water sorption kinetics of 12 µm thick PET films and 629±33 µm.

- *Non-Fickian relaxation in 12 µm thick PET films*

Studying relaxations with a microbalance requires either short steps or a small number of steps to prevent relaxation from occurring during the first steps and not to be visible beyond. To prevent artifacts, the films were studied fresh (equilibrated at ~40% RH) without preliminary drying. The two strategies are depicted on two cycles of sorption-desorption in **Figure V-13** and **Figure V-14**, respectively. All kinetics were fitted in a satisfactory manner with Eq. (V.4) even when the absence of a visible equilibrium could question the existence of a uniform concentration profile at the end of the sorption step. In details, the Fickian contribution was clearly visible only during the first step before being overwhelmed by relaxation. Fickian diffusion represented more than half of the total flux during the first step and almost vanished during final desorption steps. Relaxation times were faster in desorption than in sorption but increased again at low RH. Drying from 10% down to 0% RH required theoretically one to three weeks with $1/\beta$ values up to 4.6 days (see step 16 in **Figure V-13**).

Non-Fickian relaxations exist undoubtfully in thin samples or samples exposed by their both sides. Corresponding time scales are ranging from several hours to days at 50°C, with magnitude orders consistent with determinations shown in **Figure V-12**a. When sorption is carried out rapidly, the relaxation process was reversible (no densification) in amount but not in time scale. Relaxations appear 30-40 times faster during desorption than during sorption. Viscoelastic and Fickian diffusions are poorly separable when they are associated with comparable time scales ($Deb \rightarrow 1$). Corollary, Eq. (V.4) is acceptable only at intermediate and large diffusion Deborah numbers. Otherwise, a full coupling at microscopic scale should be preferred.

Eq. (V.4) does not explicit the origin of the driving force (*i.e.,* the variation of free energy) controlling mass transfer. Strong temperature effects could suggest an enthalpic nature (chemical interactions), but also an entropic control governed by free-volume variations. The distinction between both alternative descriptions is required to justify a ternary formulation of the sorption isotherm.

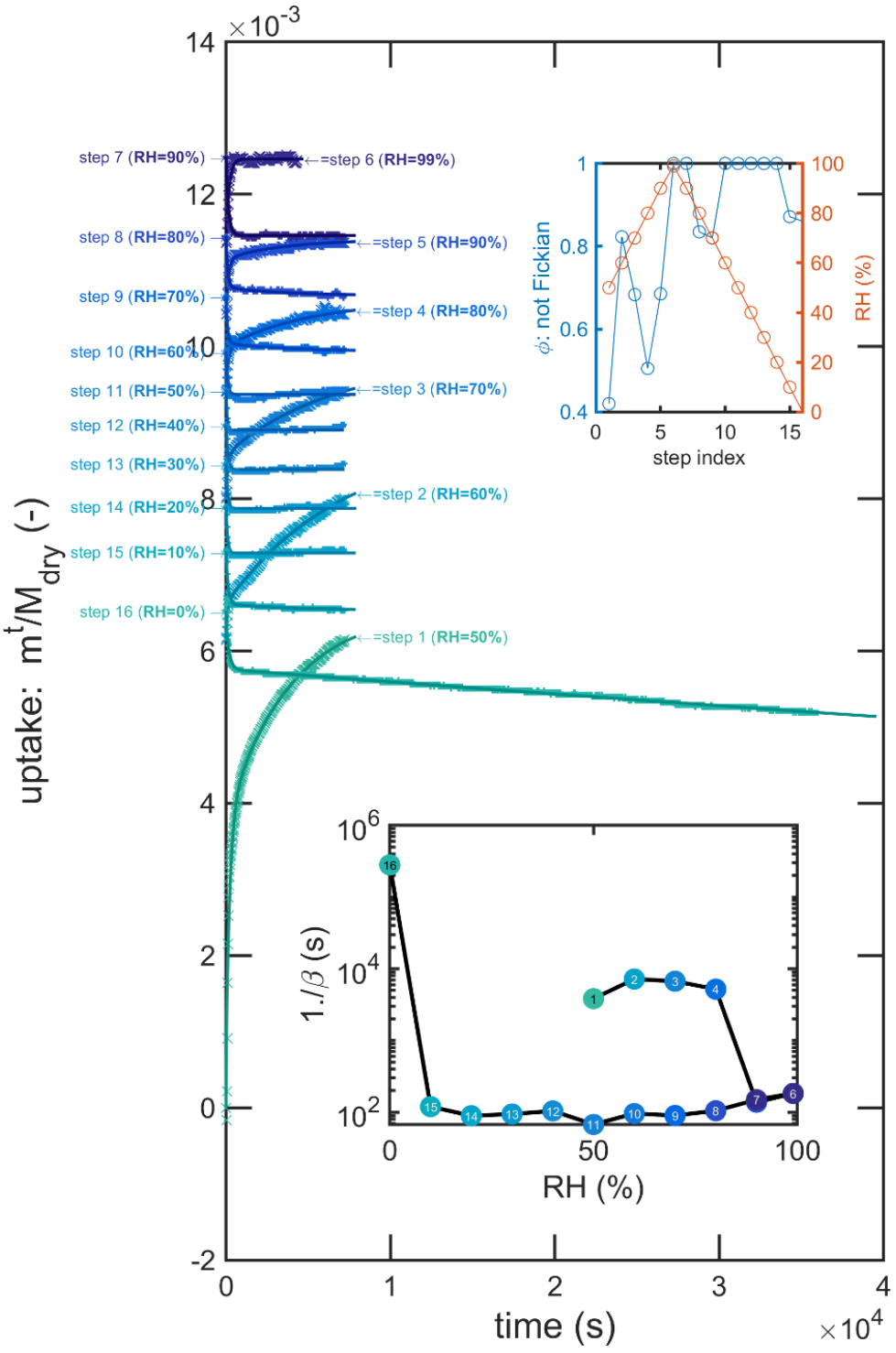

Figure V-13. *Cycle of sorption-desorption of water in 12 µm think PET films (reference F1) involving 16 steps from 50% to 99% RH (steps 1-6) and from 99% down to 0% RH (steps 7-16) at 50°C. Continuous lines are fitted models from Eq.* (V.4). *Corresponding values of* $1/\beta$ *and* ϕ *are plotted in the lower and upper insets.* M_{dry} = *sample dry mass.*

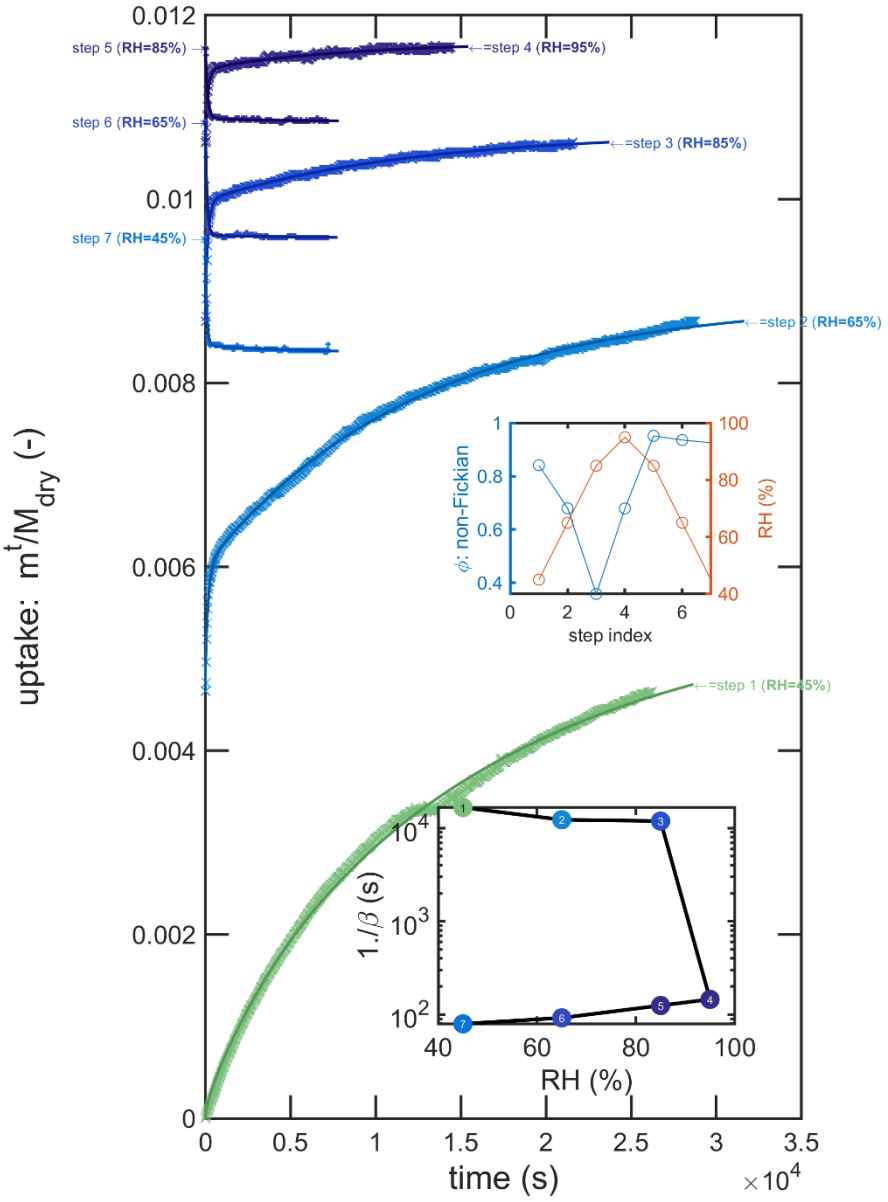

Figure V-14. *Cycle of sorption-desorption of water in 12 µm think PET films (reference F1) involving seven steps from 45% to 95% RH (steps 1-4) and from 95% down to 45% RH (steps 5-7) at 50°C. Continuous lines are fitted models from Eq.* (V.4). *Corresponding values of* $1/\beta$ *and* ϕ *are plotted in the lower and upper insets.* M_{dry} *= sample dry mass.*

- *Evidence of non-Fickian relaxations in bottle walls*

Sorption kinetics are expected to be strongly affected by the sample thickness while keeping unchanged equilibrium values in PET. Typical sorption/desorption kinetics of water at 50°C for the walls of bottles M are shown in **Figure V-15** for four different conditions. All kinetics normalized by their final values looked homothetic and independent of applied RH values. By contrast with kinetics obtained on thinner materials, they were linear with the square root of time, and Fickian fluxes contributed to more than 70% of the total sorption ($\phi \approx 70 \mp 11$). According to Eq. (V.4), relaxing times $1/\beta$ values were ranging from 3 and 3.5 hours.

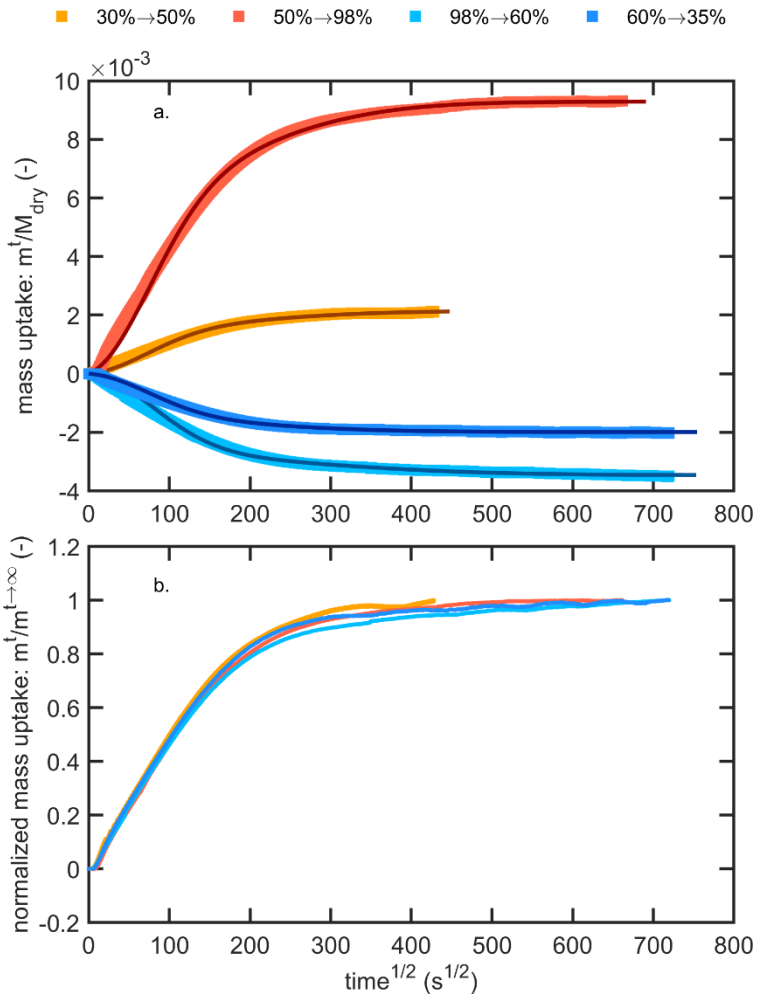

Figure V-15*. Water sorption/desorption kinetics of the PET walls (thickness 629±33 µm) at 50°C for four stepwise variations of relative humidity (RH steps are indicated in legend): (a) mass uptake relative to dry mass M_{dry}; (b) mass uptake normalized by its final value. Continuous lines are fitted models from Eq.* (V.4).

V.3.2. Interpretation of swelling in ternary isotherms of PET

In the experimental work of Dubelley *et al.* (2017a), the authors use "swelling" as a generic term without separating entropic and osmotic causes. The distinction is crucial to building a ternary isotherm with water and ethanol, which are both well-known plasticizing substances of PET. In an incompressible polymer, adding more solutes will cause entropic constraints in the polymer network, and the polymer will start swelling beyond a threshold value (see molecular dynamics simulations in (see molecular dynamics simulations in Nguyen *et al.*, 2016). Cooperative hydrogen bonding may accelerate the process by promoting clusters in the polymer.

If swelling were opposed by an external hydrostatic pressure, which acts on the polymer but not on the contacting medium, solute sorption would require an external work and

therefore a pressure change. The local dilation of the polymer looks hence caused by an apparent osmotic or mechanical pressure π, defined locally or non-locally (Edwards, 2001). By following the same arguments of Thomas and Windle (1982), Eq. (V.1) can be rewritten as a simple viscous constitutive equation involving the simultaneous sorption of two solutes. The phenomenological is not solute-specific and reads:

$$M_w\overline{V}_w\frac{\partial\phi_w^{(x,t)}}{\partial t}+M_e\overline{V}_e\frac{\partial\phi_e^{(x,t)}}{\partial t}=k\frac{\pi^{(x,t)}}{\eta\left(\phi_w^{(x,t)}+\phi_e^{(x,t)}\right)} \tag{V.5}$$

where $\phi_i=M_i\overline{V}_iC_i^{(x,t)}$ is the volume fraction in solute *i* with M_i its molecular weight and $\overline{V_i}$ its molecular volume . ϕ_P is the volume fraction in polymer with $\phi_w+\phi_e+\phi_P=1$. $\eta\left(1-\phi_p\right)$ is a composition dependent viscosity and *k* is a constant.

According to Eq. (V.5), sorption of water and ethanol due to swelling should be symmetric, and the ratio of water: ethanol saturation concentrations should be proportional to the ratio of densities $\frac{M_w\overline{V_w}}{M_e\overline{V_e}}$~1.27. Experimental binary sorption shows on opposite a ratio ca. 1:2 invalidating a swelling controlled by the volume of the solute alone. Contrarily to osmotic descriptions, non-idealities (*i.e.,* activity coefficients) would play on the dominant role. Eq. (V.1) observed experimentally should be justified by the indiscernibility of the effects of an osmotic pressure opposing to swelling from the kinetic immobility of the network. Most of the authors describe sorption of water via a dual mode sorption model (DMSM) until RH 60% (Shigetomi *et al.*, 2000;Burgess *et al.*, 2014b;Dubelley *et al.*, 2017a) and shift to Flory-Huggins model beyond.

V.3.3. Ternary Flory-Huggins model with temperature and composition effects

At tier 3, the risk of non-Fickian relaxations in the long term are acknowledged but not considered explicitly. The concept of onset between two sorption mechanisms across 50-60% RH is also not physically satisfactory. The analysis with diffusion Deborah numbers suggested that it could be interpreted more like a kinetic transition between slow and fast relaxation rather than a brusque change in the topology of accessible voids. Similar considerations of a possible deviation to a perfect mixing have been early discussed by Zimm and Lundberg (1956), as an attempt of finding a justification to the deviations of Flory-Huggins-Guggenheim theory for the sorption of water in polar polymers. The conservative hypotheses for the construction of ternary isotherm for PET+water+ethanol systems at tier 3 are discussed hereafter.

V.3.3.1. Justification of a single isotherm over the whole concentration ranges

DMSM combines a Henry and Langmuir isotherms; it is popular to describe the sorption of gases in polymers (Paul, 2016). It is usually associated with different mechanisms of sorption between the relaxed and non-relaxed volume of the glass. Despite the absence of ternary formulation for DMSM, its main limitation is a concavity which is opposed to plasticizing effects.

A ternary Flory-Huggins (FH3) formulation is preferred at tiers 2 and 3 and is tested in this section. In the perspective of consolidating the prediction of shelf-life for alcoholic beverages at tiers 2-3, the FH3 instead of alternatives could be justified as follows. FH3 model is concave up and will describe well all plasticizing effects (if any) on the inner side of bottle walls. By contrast, it may underestimate the desorption flux on the outer side in contact with dry air. At worse, the permeation flux may be overestimated and will authorize conservative estimations of shelf-life. At best, the desorption rate will be realistic at intermediate relative humidities.

V.3.3.2. FH3 formulation

General formulations of FH3 were proposed by Flory himself (Flory, 1953) and used sparingly in the literature (Mulder and Smolders, 1984;Favre *et al.*, 1996;Fornasiero *et al.*, 2002;Yang and Lue, 2013;Godbole *et al.*, 2017) for apolar and polar liquids in polymers. The cases of the simultaneous or competitive sorption of water and ethanol have been historically studied for pervaporation applications (abv~0.96). The activity coefficients $\left\{\gamma_{i,P}^{v}\right\}_{i=w,e}$ with respect to volume fractions $\left\{\phi_i\right\}_{i=e,w}$ read:

$$\begin{aligned}
\ln\gamma_{w,P}^{v}\left(\phi_w,\phi_e,T\right) &= \left(1-\phi_w\right)-\phi_e\frac{\overline{V}_w}{\overline{V}_e}-\left(1-\phi_w-\phi_e\right)\frac{\overline{V}_w}{\overline{V}_P}+\left(\chi_{w+e}^{\left(\phi_e,\phi_w\right)}\frac{\overline{V}_w}{\overline{V}_e}\phi_e+\chi_{w+P}^{T}\left(1-\phi_w-\phi_e\right)\right)\left(1-\phi_w\right)\\
&\quad-\chi_{e+P}^{T}\frac{\overline{V}_w}{\overline{V}_e}\phi_e\left(1-\phi_w-\phi_e\right)\\
\ln\gamma_{e,P}^{v}\left(\phi_w,\phi_e,T\right) &= \left(1-\phi_e\right)-\phi_w\frac{\overline{V}_e}{\overline{V}_w}-\left(1-\phi_w-\phi_e\right)\frac{\overline{V}_e}{\overline{V}_P}+\left(\chi_{w+e}^{\left(\phi_e,\phi_w\right)}\frac{\overline{V}_e}{\overline{V}_w}\phi_w+\chi_{e+P}^{T}\left(1-\phi_w-\phi_e\right)\right)\left(1-\phi_e\right)\\
&\quad-\chi_{w+P}^{T}\frac{\overline{V}_e}{\overline{V}_w}\phi_w\left(1-\phi_w-\phi_e\right)
\end{aligned}$$

(V.6)

where χ_{w+P}^{T} and χ_{e+P}^{T} are the binary Flory-Huggins interaction parameters of water-PET and ethanol-PET, respectively (see their definitions in §II.2.5.2.2.). They may depend on temperature and of the state of the polymer. By following the same approach as in Gillet *et al.* (2010), $\chi_{w+e}^{(\phi_w,\phi_e)} < 0$ is the binary Flory-Huggins parameter for water-ethanol mixtures taken at the equivalent composition of the liquid mixture $\frac{\phi_e}{\phi_w+\phi_e}$ (see **Figure II-22**).

Eq. (V.6) is derived from the lattice theory of Flory (mean-field approximation) and assumes that the ternary mixture is an incompressible model and swells as soon as water and ethanol are introduced. The effect is however very minor at low concentrations, and the solution coincides with the superposition of two Henry isotherms (approximation used at tiers 1 and 2). The absorptions of water and ethanol are cooperative and promote plasticizing by decreasing the number of contacts between polymer blobs and therefore the cohesion energy of the polymer (*nota-bene*: the variation of the chemical potential of the polymer is not shown). Free-volume effects and hence, thermal expansion is not considered.

V.3.3.3. Known limitations for interacting liquids

The application of Flory-Huggins theory to ternary systems has been seriously questioned for polar liquids in amorphous and semi-crystalline polymers (see discussions in Favre *et al.*, 1996;Fornasiero *et al.*, 2002). The discrepancies with experiments were mainly associated with the nonconstancy of interactions parameters and possible effects of the local composition (i.e., different radial distributions). Nguyen *et al.* (2017) demonstrated that the substitution of partial molar volumes by molar volumes in lattice models was responsible for the deviations observed with atomistic (compressible) models.

To avoid previous limitations, the binary coefficients χ_{w+P}^{T} and χ_{e+P}^{T} were allowed to vary with temperature not only to describe a less importance of hydrogen-bonding at higher temperatures (see the thermal averaging of Flory-Huggins coefficients in §II.2.5.3.), but also to account for kinetic effects shown in **Figure V-12**. The point of view expressed here is that the observed effect of RH on swelling is captured (with overestimation) within the Flory theory whereas the temperature effect on swelling is associated to the initial delay before polymer relaxation ceases to be the limiting factor. This strategy is an ersatz to replace the lack of ergodicity of the system; that is the solute-polymer configurations deviate from their equilibrium distributions due to the presence of residual energy barriers. Densification effects are not considered but could be incorporated a posteriori by considering that crystallites are inaccessible to solutes (see Eq. (II.48)). Effects of composition were added only to the water-ethanol binary term χ_{w+e}^{T}; it was negative as expected for exothermic mixtures (see **Figure II-22**), whereas

the calculations of Favre *et al.* (1996) led to positive values (see Figure 1 herein). Independently the theoretical choices, the authors used FH3 when the experimental sorption of water and ethanol were concave down or subjected to a risk of densification (see Figures 4 and 5 herein).

V.3.4. Parameterization of binary parameters: χ_{w+P}^{T} and χ_{e+P}^{T}

V.3.4.1. Isothermal data

Eq. (V.6) involves only binary pair interactions (3 possibilities: $w+P$, $e+P$, $w+e$) and neglect ternary pair interactions (as justified in Nguyen *et al.*, 2017). Only polymer specific parameters χ_{w+P}^{T} and χ_{e+P}^{T} required to be determined as water-ethanol interactions χ_{w+e}^{T} are well established. They were identified by fitting Eq.(II.50) (binary Flory-Huggins isotherm: FH2) to full isotherms from literature or $\{\chi_{i+P}^{T}\}_{i=w,e}$ or inferred from saturation values obtained by contacting thin films F1-F5 (***Table IV-1***) with pure water or ethanol for periods up to three months. Methanol was added as a control to validate the effects of solute polarity on the estimation of χ_{i+P}^{T}. Fitted isotherms are compared with experimental values in **Figure V-16** by assuming that considered binary mixtures were incompressible (*i.e.*, molar volumes are used instead of partial molar volumes). The direct comparison enabled to validate globally the hypotheses supporting a single FH2 isotherm for the three solutes and the whole activity range. The presence of persistent relaxation questions, however, the risk of underestimation χ_{i+P}^{T} at low and intermediate activities.

Mass uptakes were obtained by drying the samples in vacuum or dry nitrogen at the same temperature before applying a stepwise ramp of partial pressure. All kinetics exhibited non-Fickian relaxations, but as the sample thicknesses, the number of steps and their durations were different, the cumulated relaxation times were not comparable. Additionally, since relaxation times are much longer at low relative humidity, total relaxation times were longer at high activities rather at low and intermediate activities. All these phenomena justified the variabilities observed between data sources. Fitted FH2 reproduced only an averaged behavior with errors about 10% at low activities.

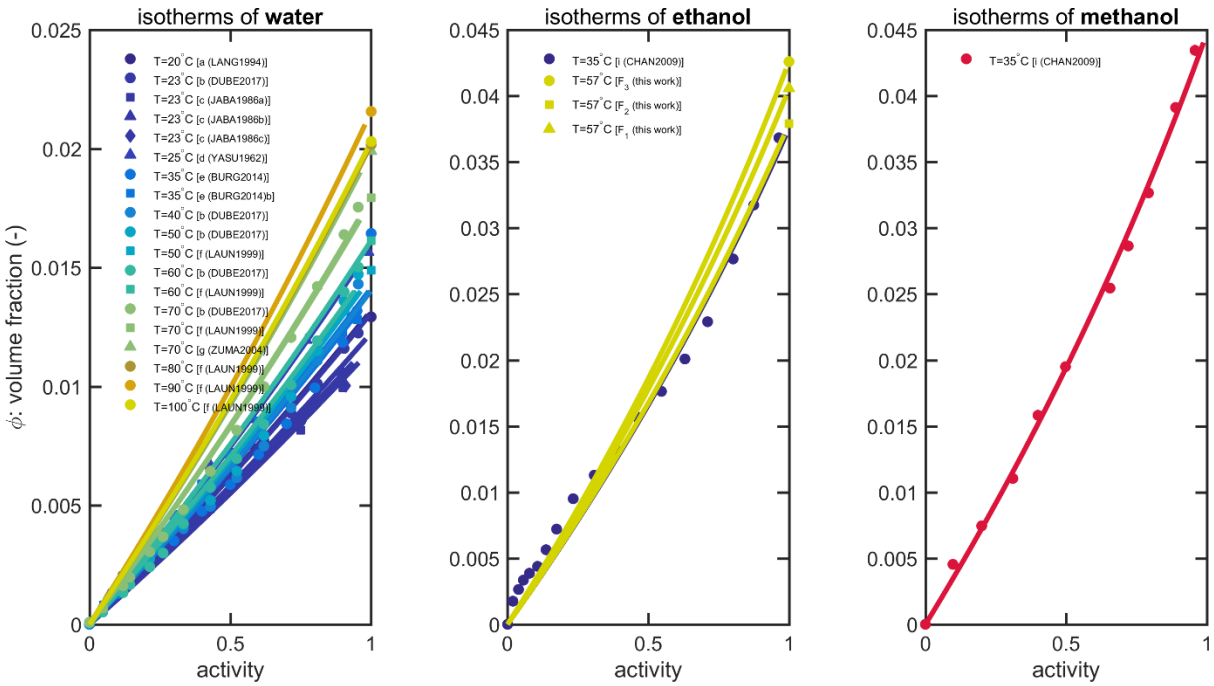

***Figure V-16**. Fitted binary Flory-Huggins isotherms for (a) water, (b) ethanol and (c) methanol at temperatures ranging from 20°C to 100°C.*

Sources: a. Langevin *et al.* (1994); b. Dubelley *et al.* (2017a); c. Jabarin and Lofgren (1986); d. Yasuda and Stannett (1962); e. Burgess *et al.* (2014b); f. Launay *et al.* (1999); g. Zumailan *et al.* (2004); h. Rueda and Varkalis (1995) cited in **Figure V-17**; i. Chandra and Koros (2009b).

V.3.4.2. Temperature dependence at glassy state

Sorption was significantly activated by temperature for water and less for ethanol. $\{\chi_{i+P}^{T}\}_{i=w,e}$ values inferred from **Figure V-16** are plotted in **Figure V-17** versus the reciprocal temperature. For water sorption at glassy state, two families of results were identified according to the sample has been put in contact with pure water or whether the temperature (upper bound) or not (lower bound). The difference was associated to the lowering of the densification temperature at high RH (see **Figure V-12**b), sorption was lower and χ_{w+P}^{T} values were higher. By contrast, automatic microbalances investigated mainly intermediate RH values, where the swelling was dominant, yielding lower χ_{w+P}^{T} values. Both curves converged close to the minimum T_g value of PET swollen by water (ca. 60°C see in Langevin *et al.*, 1994). The corresponding fork shape mirrors the variation of free volumes between equilibrated and subcooled polymers (White and Lipson, 2016). Extra-free volumes brought in subcooled polymers enable a sorption more similar to the one observed at rubber state. The trend was also observed with pure ethanol, but with a lower effect than water due to the largest steric of ethanol molecules.

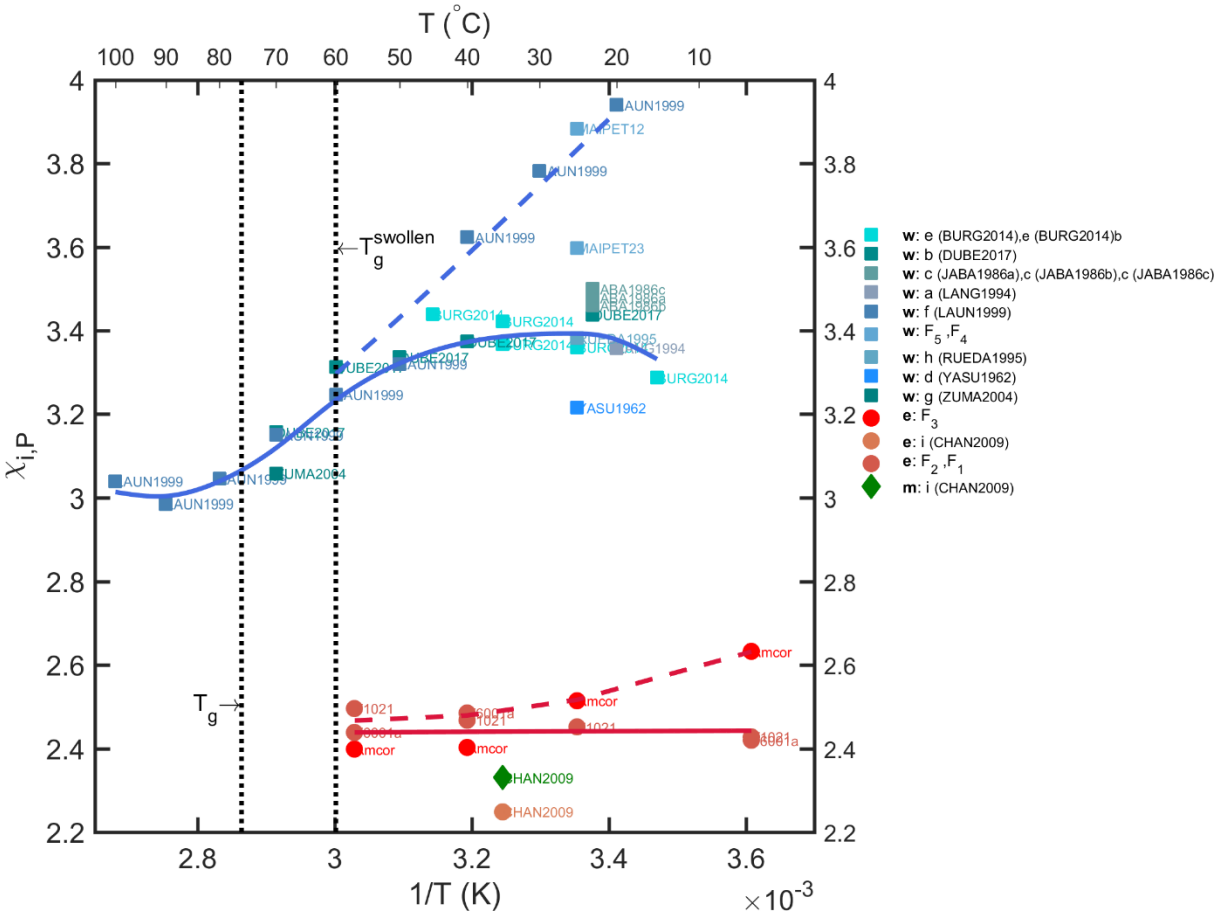

***Figure V-17**. Effect of temperature on χ^{T}_{i+P} values. Data sources are shown in **Figure V-16**. The models for subcooled PET are shown in continuous lines (smoothed cubic spline). The model for densified PET materials are shown as dashed lines (smoothed quintic spline).*

Mixing water or ethanol with PET is endothermic and requires energy. The corresponding isosteric heat of sorption $-R\left.\frac{\partial \chi^{T}_{w+P}}{1/T}\right|_{\phi_w}$ for water varies between -14±2 kJ·mol^{-1} at 20°C and -8±3°C at 60°C. For ethanol, sorption energy varied from -2±0.3 kJ·mol^{-1} at 20°C up to -0.1 kJ·mol^{-1} at 60°C. Magnitude orders for ethanol are similar to endothermic sorption heat measured by DSC with values ranging from ~0 and -2.3 kJ·mol^{-1} between undrawn and drawn PET filaments (Khanum *et al.*, 2015). Because the energy required to insert water molecules in bulk PET is significantly lower than the energy required to adsorb water molecules at the surface of PET materials and reported -38 kJ·mol^{-1} from Sancaktar *et al.* (1974), entropic forces (capacity to disperse water) are governing sorption. The lower sorption energy required to insert a larger penetrant confirmed the weakness of the interactions in PET and the existence of large free-volumes accessible to PET. Densification and cold crystallization reduce accordingly the capacity to pack water molecules and therefore, sorption.

V.3.4.3. Sensitivity analysis: long-term effects and cold crystallization

$\left\{C_{i,eq}^{T,T_g}\right\}_{i=w,e}$ values used to set $\left\{\chi_{i+P}^{T}\right\}_{i=w,e}$ ones are not perfectly defined as a chemical equilibrium is assumed without having necessarily the polymer also at mechanical equilibrium. $C_{i,eq}^{T,T_g}(t)$ estimates tend consequently to be a function of experimental time in subcooled polymers. Most of the authors choose the sorption at a prescribed time (e.g., 48 hours for Dubelley *et al.*, 2017a) as a reference value. The true equilibrium is expected to be achieve in the absence of concentration gradients when the subcooled polymer reaches a more stable crystalline form. During this very slow transition, $\left\{C_{i,eq}^{T,T_g}\right\}_{i=w,e}$ decreases and consequently $\left\{\chi_{i+P}^{T}\right\}_{i=w,e}$ increases. The maximum extent of this shift is not reported in the literature.

Water sorption in worst-case conditions accelerating densification (97% *RH* at 60°C, see **Figure V-12**a) has been studied in jars for long periods with saturated salt solutions. A similar experiment has been run by immersing the same fresh films in 99% ethanol. The results are shown in **Figure V-18**. All films reached an apparent chemical equilibrium in water and ethanol in one month (see the inset of **Figure V-18**a). The sorption of water was, however, significantly lower than the one observed at 50°C (see **Figure V-13** and **Figure V-14**). After one month, sorption of water decreases before increasing again. The corresponding time constants were 99±34 days for swelling and 19±7 days for densification. The rate constant for densification matches the values shown in **Figure V-12**a for similar conditions. Densification decreases sorption by 31±2% and Fickian diffusion represents less than 10% of the total mass uptake in this condition. Densification and swelling were not separable and occur concomitantly. The differential of swelling with and without densification could explain the two branches of χ_{w+P}^{T} shown in **Figure V-17**. Sorption of ethanol looked Fickian for all films, but long exposures were followed by an additional increase of absorbed amounts suggesting an effect of polymer relaxation beyond 30-45 days. Drawing low-oriented amorphous PET filaments in ethanol has been shown to enhance sorption and to cause crystallization as water do (Khanum *et al.*, 2015). Drawing stresses are lower in ethanol confirming that ethanol is a better plasticizer of PET than water.

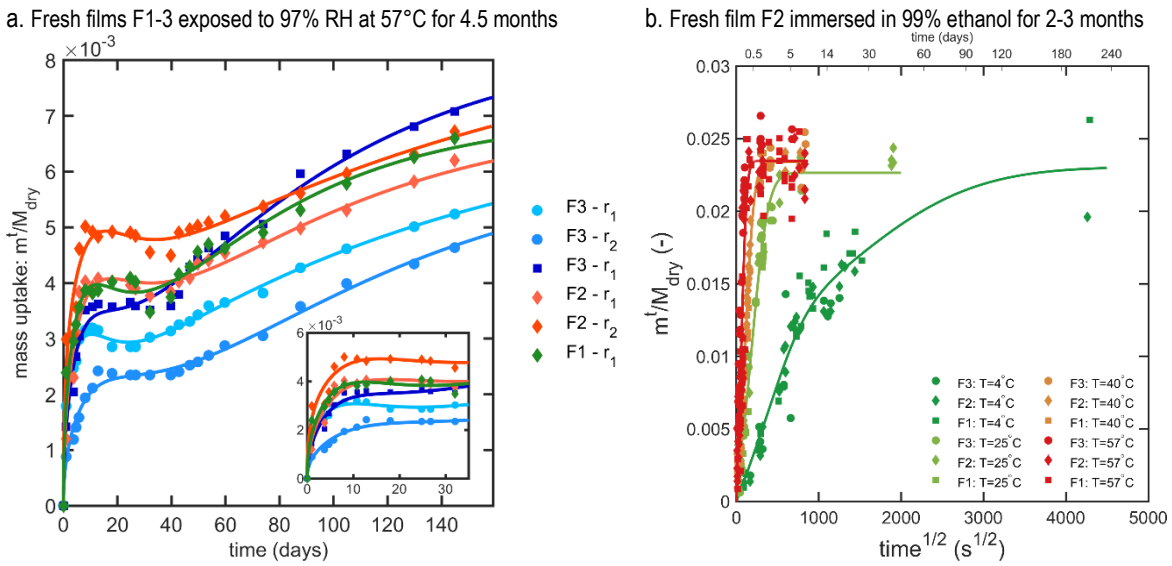

***Figure V-18**. Long-term sorption behavior of 12 µm thick PET films after exposure (a) to 97.5% RH and (b) 99% ethanol. Two repetitions are shown in (a) (denoted r_1 and r_2); five repetitions are combined in (b). The inset is showing the same kinetics during the first month. The continuous lines describe a sorption model similar to Eq* (V.4) (a) with double relaxation (one positive for swelling and one negative to describe densification) and (b) with a single relaxation.

Glassy polymers exhibit a tremendous complexity with non-linearities, memory effects and coupling between fluxes, stresses and strains. Densification and the slow cold crystallization make even the evolution of uptake not monotonic.

The typical evolution of glassy polymers during differential sorption has been summarized by Vrentas and Vrentas (2001) into a single scheme, adapted to the context of PET in **Figure V-19**. On the very long term, any glassy polymer exposed to vapors or pure liquids is subjected to two major transitions: i) from glassy to rubber state (associated with Deb_1) and ii) from rubber behavior to a viscous liquid or gel (Deb_2). In the case of PET, only the first kind of transition has been observed either in the presence of water or ethanol. The maximum sorption concentrations were approached on very thin materials for different partial pressures and used as estimates of $\left\{C_{i,eq}^{T,T_g}\right\}_{i=w,e}$. By identification with abacus plotted in **Figure V-19**, sorption of water at 57°C is associated to a Deb_1 value ranged between 5 and 10. For ethanol, contact times are not enough long to provide an accurate estimation of a Deb_1. Since relaxation effects were more detectable at low that at high temperature, Deb_1 was thought to be much greater than unity with a much faster relaxation in ethanol than water.

As a result, the binary interaction coefficients $\left\{\chi_{i+P}^{T}\right\}_{i=w,e}$ derived from experimental determinations of $\left\{C_{i,eq}^{T,T_g}\right\}_{i=w,e}$ were assumed to be representative of PET close to equilibrium state for both water and ethanol (see **Figure V-11**a). Viscoelastic diffusion is thought to be

maximized as confirmed by the Fickian diffusion behavior recovered from a two-stage sorption mechanism.

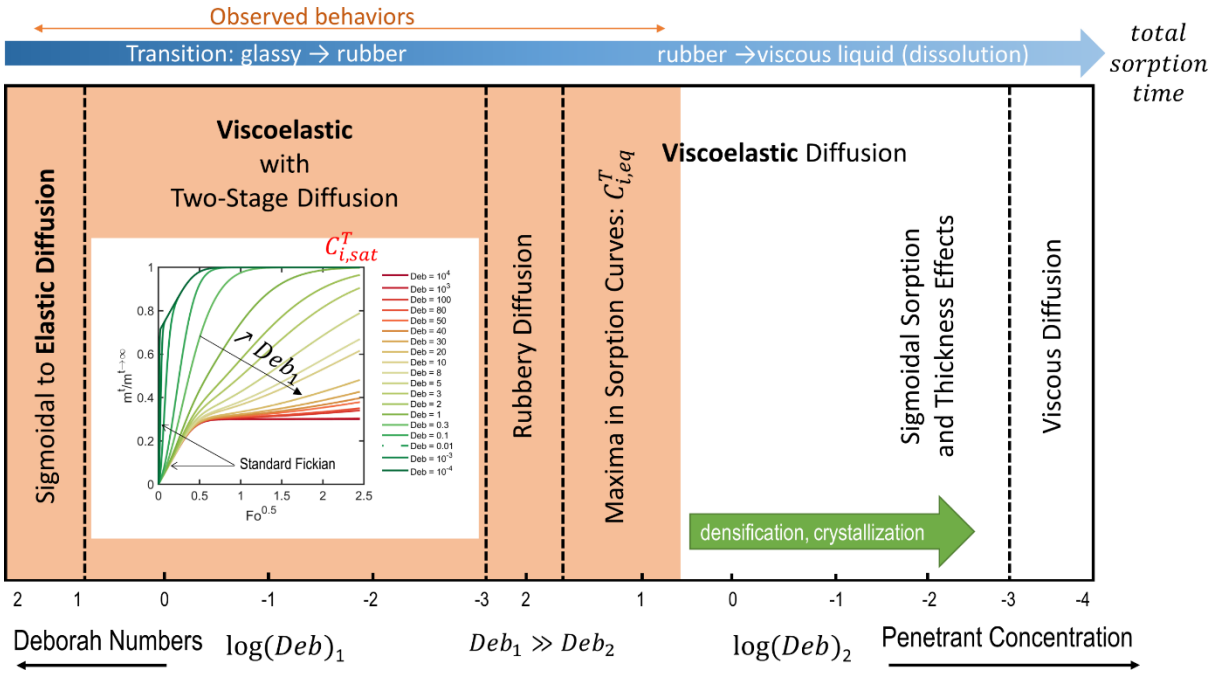

***Figure V-19**. Typical diffusion behaviors in glassy polymers with penetrant concentration and Deborah numbers for differential step-change sorption experiments. (modified from (modified from Vrentas and Vrentas, 2001), the dimensionless sorption curves are calculated from Eq.* (V.4) for $\phi = 0.7$*).*

It is worth noticing that descriptions on thin films subjected to symmetric sorption cannot be extrapolated to thick bottle walls. After bottle filling, only one side of the bottle is exposed to high *RH* whereas the other remain close to their initial conditions. Viscoelastic diffusion plays consequently a minor role in this case. Storing PET films, preforms and bottles in wet conditions and high temperature will, however, cause densification after few weeks.

V.3.5. Experimental validation of ternary isotherms

The capacity to predict the equilibrium mass uptake of PET in contact with hydroalcoholic solutions was tested at 35°C on 12 µm PET films (F1) for contacts up to five months. The films were not subjected to any initial drying to prevent any densification or change in structure. Absolute water and ethanol content were obtained by drying the samples at the end of the experiment at high temperature (85°C). A similar determination was also carried out by thermogravimetry analysis (TGA). Due to the overlapping of ethanol and water losses in TGA measurements, the separation of water and ethanol content was thought not reliable, and the results are presented as total mass uptake. The ternary isotherm offers a separation of both contributions.

V.3.5.1. Reconstruction the FH3 isotherm at 35°C

Eq. (V.6) is implicit in ϕ_w and ϕ_e. The full isotherm was reconstructed by tabulating the activities of water and ethanol for the entire domain of ϕ_w and ϕ_e values. The corresponding mass uptakes ($m_w^{(a_w,a_e)}$, $m_e^{(a_w,a_e)}$ and $m_w^{(a_w,a_e)} + m_e^{(a_w,a_e)}$) was finally analyzed as a two-dimensional manifold of a_w and a_e back-mapped onto ϕ_w and ϕ_e space. Temperature was added as a third dimension of the final manifold. Typical iso-mass uptake values calculated at 35°C on a 500×500 grid are shown in **Figure V-20**. The choice of the branch to describe the temperature dependence of $\{\chi_{i+P}^T\}_{i=w,e}$ with temperature is critical at glassy state (see **Figure V-16**). Since validation focused mainly on high activities and very long contact, the upper branch was preferred. For conservative shelf-life calculations, the lower branch would have been preferred. Due to the negative value of χ_{w+e}^T, the presence of water promotes the sorption of ethanol and reciprocally.

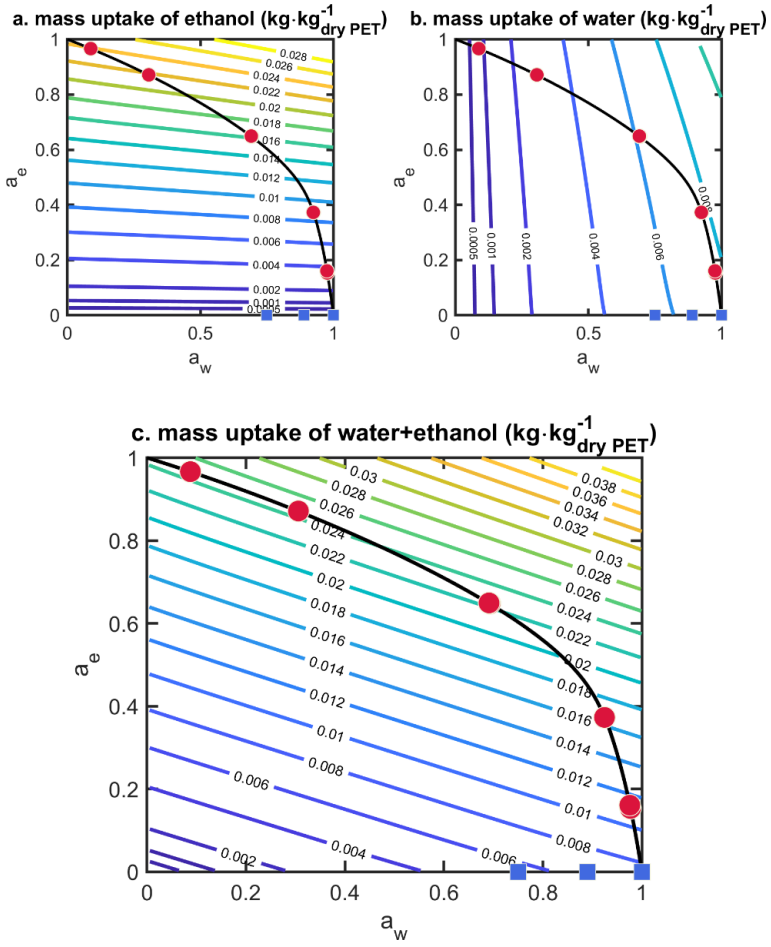

***Figure V-20**. Theoretical iso-mass uptake of water and ethanol in PET at 35°C at equilibrium with a water or ethanol gas mixture (below the liquidus curve), with a hydroalcoholic solution (on the liquidus curve) and at high pressure (above the liquidus curve): (a) $m_e^{(a_w,a_e)}$ (b) $m_w^{(a_w,a_e)}$ and (c) $m_w^{(a_w,a_e)} + m_e^{(a_w,a_e)}$). The liquidus curve calculated from **Figure V-4**a is plotted as a continuous line. The symbols depict the conditions tested experimentally.*

V.3.5.2. Comparison with experiments

The nine tested conditions for validation are depicted in **Figure V-20**c as symbols (filled circles for hydroalcoholic solutions and square ones for saturated salt solutions. Experimental values and predictions are compared in **Figure V-21**. All experiments were duplicate or triplicate. The variation between samples was lower than the variations during long-term viscoelastic sorption. Measurements during the last two months are reported for all samples. Equilibriums with hydroalcoholic solutions were interpreted along the liquidus curve and plotted either versus the activity of water or ethanol. Binary and ternary theoretical isotherms predicted in a satisfactory manner all experimental values without requiring any fitting or correction procedure. Prediction errors are smaller than experimental errors. Underestimations persisted, however, at high water activities and coincided with residual relaxations in some samples. It was, therefore, confirmed that the ternary sorption of water and ethanol were higher than their binary counterparts. The linear superposition of both binary isotherms was systematically underestimating the sorption from hydroalcoholic solutions.

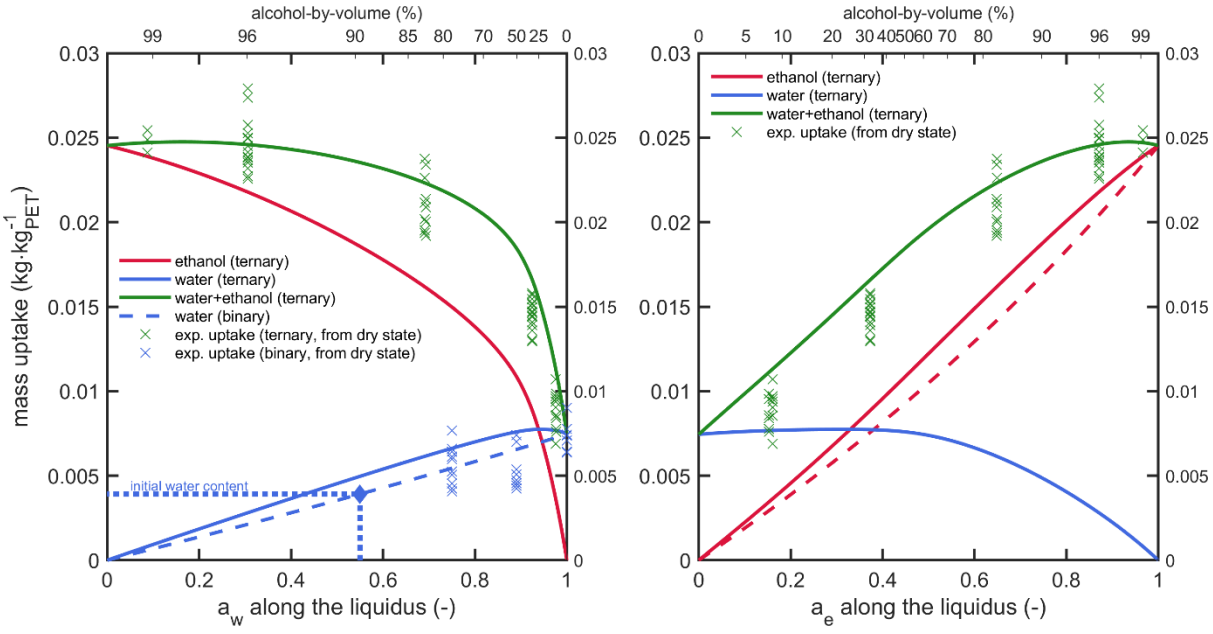

***Figure V-21**. Comparison of mass uptakes for conditions depicted in **Figure V-20** with continuous predictions from ternary isotherms (to be used for equilibriums with hydroalcoholic solutions) and ternary isotherms (to be used for equilibriums with saturated salt solutions).*

V.3.6. Ternary FH3 isotherms from 20°C to 50°C

In binary mixtures, water sorption is significantly more activated by temperature than ethanol. In ternary isotherms and despite the almost absence of dependence of χ_{i+P}^{T} with temperature, higher sorption of water at higher temperature will cause also higher sorption of ethanol. The same cooperation between water and ethanol occurs when the activity of water

increases. The theoretical FH3 isotherms at 20°C and 50°C are shown in **Figure V-22**. At high water activity corresponding to alcoholic beverages (a_w>0.85), the iso-water uptake lines are tangent to the liquidus curve from 20 to 50°C. That is the same water uptake is reached whatever the *abv* value of the mixture. As the equivalent sorption isotherm along the liquidus is Henry-like (see **Figure V-21**a), the uptake of ethanol is almost proportional to *abv*. Sorption of water and ethanol are almost equivalent ca. 0.8-0.9 w% for vodka-type products (*abv*~40 %).

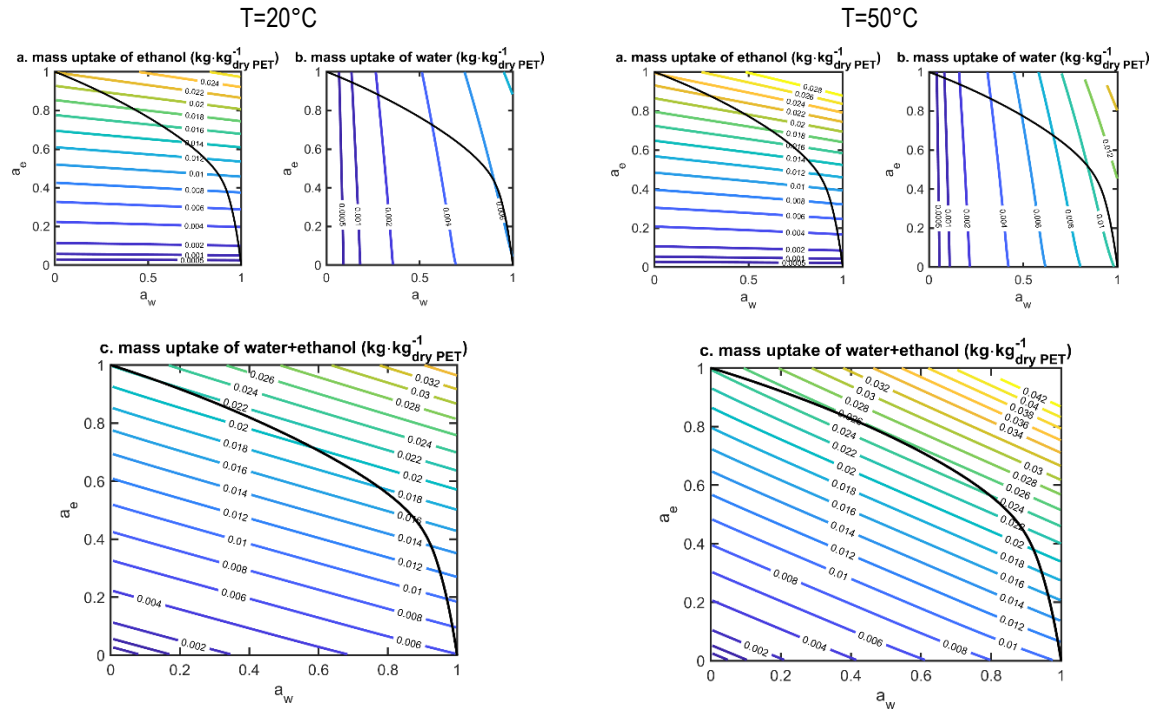

***Figure V-22**. Ternary FH3 isotherm of water and ethanol in PET at 20°C and 50°C.*

True equilibriums are verified with difficulty experimentally even on thin materials. The ternary Flory-Huggins formulation offers an efficient alternative to approximate maximum sorption and LTE conditions (internal and external) for arbitrary beverage and temperature. As the formulation is available for all polymers and can be derived easily from molecular calculations (see §II.2.5.2.). It can be postulated reasonably that sorption on a liquid equilibrated polymer (at rubber state) overestimates the real sorption for all conditions. A more realistic estimate can be achieved subsequently by extrapolating the sorption at glassy state from an isosteric heat of sorption accounting for free-volume effects.

V.4. A blob-free-volume model of solute diffusion coefficients in polymers at tiers 3-4

V.4.1. Ambition and assumptions

- *A reductionist point of view*

Section §V.3. highlighted various diffusional mechanisms ranging from elastic to viscous diffusion in glassy polymers. Viscoelastic diffusion is the diffusion behavior occurring in differential step-change of partial pressure or during periodic sorption experiments. The hereditary nature of the diffusion flux is its main characteristic, as discussed in §V.5. Another significant feature of viscoelastic effects is that they affect all solutes similarly regardless of their chemical nature. This assumption is reasonable only for thin materials. For thick materials and while solute concentrations are low, macroscopic viscoelastic effects are more suitably described within the material by the combination of elastic effects (Fickian diffusion) with a time-dependent surface concentration. During a sorption step, the origin of the mass transfer resistance at the interface originates from the local transitions (see **Figure V-19**):

$$\begin{matrix}\textit{elastic Fickian}\\ \textit{diffusion}\end{matrix} \xrightarrow{Deb_1} \begin{matrix}\textit{two}-\textit{stage viscoelastic}\\ \textit{diffusion}\end{matrix} \xrightarrow{Deb_2} \begin{matrix}\textit{rubbery Fickian}\\ \textit{diffusion}\end{matrix} \tag{V.7}$$

A similar sequence has been presented in **Figure V-19** and discussed in Chapter 16 of Vrentas and Vrentas (2013). Each transition is assumed to be controlled by the time scale of relaxation $Deb_1 \gg 1$ and $Deb_2 \ll 1$. In both cases, the dispersion of non-covalently bonded substances is controlled by their random walk in polymer even if the mechanism obeys to different diffusion coefficients, $D_{i,P}^{T,T_g}$. This section discusses the construction of a general framework to predict diffusion coefficients of arbitrary solutes in arbitrary polymers from one side to other (from glassy to rubber states or vice-versa). The chief difficulty is that no general model exists, but only attempts.

- *Generalizing free-volume theory*

Although it is incomplete and it has been questioned, the free-volume theory (FVT) of Vrentas and Duda (first formulation: (first formulation: Vrentas and Duda, 1977b) is the most advanced (see the discussion in II.2.4.). It generalizes the early mechanistic interpretation of the translation of the center-of-mass (CM) of rigid solutes in liquids due to the rearrangement of the empty voids (free-volumes, FV) around them (Cohen and Turnbull, 1959). FV in glassy and rubber polymers exist also, they include both empty spaces and partly occupied voids due to the vibration of atoms (White and Lipson, 2016) for general discussion on the nature of FV). The analogy between liquids and polymers ceases, when the ergodicity of the voids is

considered. In a liquid, the all voids can be redistributed in the whole volume at a rate equal or higher than the translation of the solute CM. In the polymer, only a particular and hypothetical type of free-volumes, coined hole-FV, could be redistributed without any energy barrier. The nature of these FV is unknown, and their parameterization is indirect and has been proposed only for a limited number of polymers and only for rigid solutes. As the theory of Flory-Huggins, it is a somewhat mean-field theory, which does not capture atomistic details. A different route is proposed here by using the scaling relationships of Fang for linear solutes to reach three purposes:

1) parameterizing undocumented polymers (e.g., polyesters including PET);
2) extending the scaling to glassy polymer;
3) bridging the original theory of rigid and flexible solutes by introducing the concept of anchored solutes.

The strategy fills mainly gaps between existing FV theories and their extensions, as shown in **Figure V-23**. The concept of subcooled polymer is shown as the extra hole free volume available in glass.

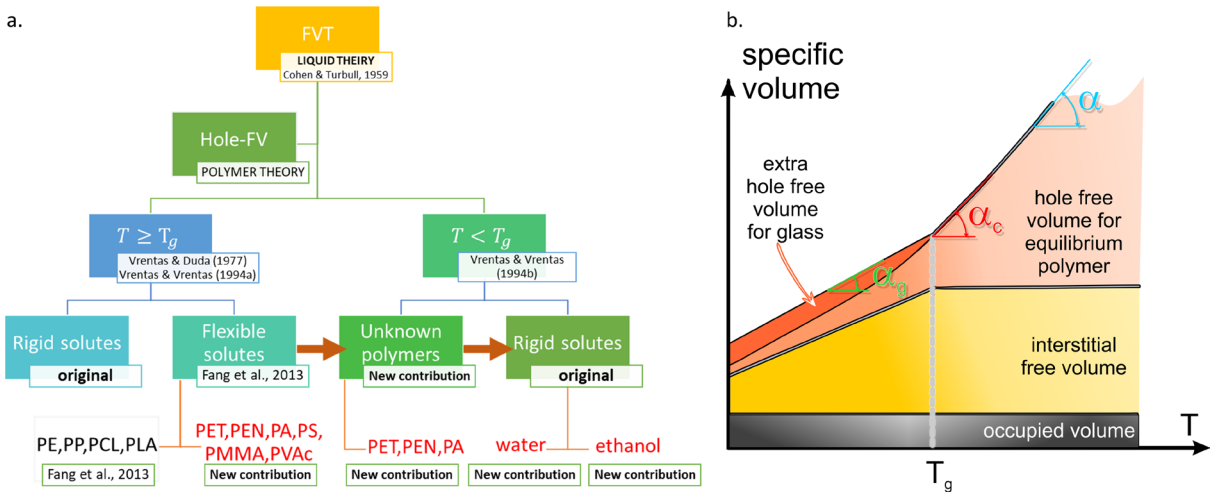

***Figure V-23**. Inheritance between FV contributions (a) and (b) definitions of free-volumes. The horizontal arrows define the direction of the extensions. α_g and α_c are the thermal expansion coefficients at glassy state and at the critical temperature.*

- *Towards a "universal" blob-free-volume model*

The proposed procedure to calculate from first principles (no adjustment) diffusion coefficients of water from the diffusion coefficients of *n*-alkanes is sketched in **Figure V-24**. The core feature is a coarse-grained model, so-called blob FV model, assuming that the translation of each blob in large solutes obeys to h-FV theory, whereas the CM of connected blobs

obey to the scaling of Fang *et al.* (2013). It has been already shown that the diffusion coefficients of solutes including N identical patterns, D_{lin} , scales as $N^{-\alpha}$ with an apparent activation energy verifying $E_a \propto K_\alpha \, lnM$. We will show that the scaling exponent can be recasted as $\alpha = 1 + \frac{K_\alpha}{r(T-T_g)+K_\alpha}$ for any polymer with $r = 1$ at rubber state and $r < 1$ at glassy state. Parameters K_α and K_β are related to conventional FV theory can be use to predict diffusion coefficients for arbitrary solutes including water.

.

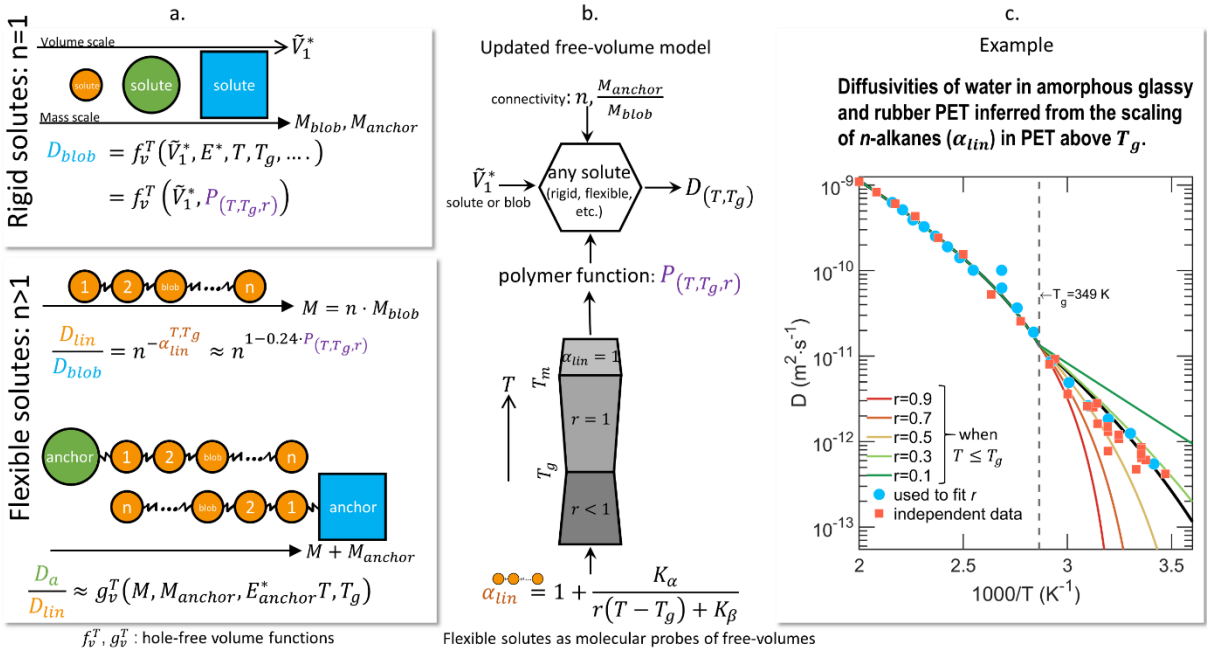

Figure V-24. *Illustration of the procedure to calculate arbitrary diffusion coefficients from the proposed blob-FV model a) solute blob model; b) free volume parameterization and D model; c) example of water diffusion prediction in PET*

V.4.2. Derivation of the blob free-volume theory

Although the concept of hFV has been widely accepted as well as its linear increase with T , its quantitative determination remains a challenge. The amount of free space, which participates effectively to the translation of organic solutes, is unknown. We address the issue in two different manners: firstly, from the perspective of Vrentas and Duda when the concentration in solutes approaches zero, and secondly, from the scaling of diffusion coefficients of linear probes, namely linear alkanes taken as generic a generic blob model probing accessible hole free volumes.

V.4.2.1. The original theory of Vrentas and Duda at infinite dilution

The theory of Vrentas and Duda has been elaborated initially for polymer solvent-mixtures. It has been tested extensively on mutual diffusion coefficients when solvent concentrations are sufficient for plasticizing or swelling the polymer. Comparatively, the theory has been far less examined at infinite dilution when only the polymer contributes to free volumes and when solute geometry effects dominate. For solute trace diffusion coefficients, the indices of the solute (1) and of the polymer (2) can be dropped in all places, where no confusion is expected. The interested reader could refer to the review (Ramesh *et al.*, 2011) and the seminal summary of the free volume methods in Vrentas and Vrentas (1998).

In the limit of trace amount, the solute diffusion coefficient reads:

$$D = D_0 \exp\left(-\frac{E^*}{RT}\right)\exp\left[-\xi\frac{\hat{V}_2^*}{\hat{V}_{FH2}\left(T,T_g\right)/\gamma}\right] \tag{V.8}$$

where $\hat{V}_2^*$ is the specific hole free volume of the polymer required for a jump; $\hat{V}_{FH2}\left(T,T_g\right)$ is the specific hole free volume of the equilibrium liquid polymer; γ is an overlap factor, which is introduced because the same free volume is available for several jumping units.

$\hat{V}_{FH2}\left(T,T_g\right)$ is strongly related to the thermal expansion of the polymer as (Vrentas and Duda, 1979;Vrentas and Vrentas, 1994b):

$$\frac{\hat{V}_{FH2}\left(T,T_g\right)}{\gamma} = \frac{K_{12}}{\gamma}\left[K_{22} + \lambda\left(T,T_g\right)\left(T-T_g\right)\right] \text{ with } \begin{cases}\lambda = 1 \text{ when } T \geq T_g \\ \lambda < 1 \text{ otherwise}\end{cases} \tag{V.9}$$

where new constants K_{12} and K_{22} can be related to the WLF constants as:

$$\frac{K_{12}}{\gamma} = \frac{\hat{V}_2^*}{2.303\left(C_{12}\right)\left(C_{22}\right)} \tag{V.10}$$

$$K_{22} = C_{22} \tag{V.11}$$

At glassy state, the parameter λ accounts for the deviation of the polymer to an equilibrated liquid. This effect can be related to the change in the thermal expansion coefficient of the polymer with temperature at rubber state, α_2 and at glassy state α_2^g. By considering that thermal expansion coefficients on both sides of T_g being constant, Vrentas and Duda (1979) proposed the following approximation:

$$\lambda = 1 - \frac{\hat{V}_2^0\left(T_g\right)\left[\alpha_2 - \alpha_2^g\right]}{K_{12}} \quad \text{for} \quad T < T_g \tag{V.12}$$

ξ , E^* and D_0 are the parameters related to the solute. $\xi = \frac{\tilde{V}_1^*}{\tilde{V}_2^*\left(T_g\right)}$ is the most cryptic parameter and is associated with the ratio of the critical (i.e., minimum) volume of the solute jumping unit to the critical (minimum) volume of the polymer jumping unit required for a jump. For small and rigid solutes, this number has values between 0.10 and 1.3 (Vrentas *et al.*, 1980;Vrentas *et al.*, 1996). Empirically, linear relationships in the form of $\tilde{V}_2^*\left(T_g\right) = u + vT_g$ have been proposed (Zielinski and Duda, 1992;Hong, 1995):

$$\tilde{V}_2^*\left(T_g\right) \text{ in } \frac{\text{cm}^3}{\text{mol}} = \begin{cases} -86.95 + 0.6224T_g & \text{for} \quad T_g \geq 295 \text{ K} \\ 69.47 + 0.0925T_g & \text{for} \quad T_g < 295 \text{ K} \end{cases} \tag{V.13}$$

As a rule of thumb, it is worthy noticing that the critical polymer jumping unit is roughly 1.5 the monomer unit (Zielinski and Duda, 1992).The choice of two branches according to T_g is justified in Figure 2 of Shapiro *et al.* (2004) and the approximation herein $\tilde{V}_2^*\left(T_g\right) = 11.018\exp\left(7.4\cdot 10^{-3}T_g\right)$. The parameter E^* is a solute-specific energy barrier, which is very often neglected near T_g, when most of temperature effects are driven by free volume effects. In this study, we will show that it is an essential quantity for polar solutes in polar polymers. In the limit of a pure solvent, the pre-exponential factor D_0 can be compared to the self-diffusion coefficient of the solute or its viscosity. In the context of trace diffusion in a polymer, the interpretation can be different and can be related to the solute entropy of translation in the polymer (see (Fang *et al.*, 2013) for details).

By referring polymer effects to T_g and solute ones to ξ, the trace diffusion coefficients between an unknown solute associated to ξ and a reference one associated to ξ_0 scales as:

$$\begin{aligned} \frac{D\left(\xi,T,T_g\right)}{D\left(\xi_0,T,T_g\right)} &= \frac{D_0\left(\xi\right)}{D_0\left(\xi_0\right)}\exp\left(-\frac{E^*\left(\xi\right)-E^*\left(\xi_0\right)}{RT}\right)\exp\left[-\left(\xi-\xi_0\right)\frac{\hat{V}_2^*\left(T_g\right)}{\hat{V}_{FH2}\left(T,T_g\right)/\gamma}\right] \\ &= \frac{D_0\left(\xi\right)}{D_0\left(\xi_0\right)}\exp\left(-\frac{E^*\left(\xi\right)-E^*\left(\xi_0\right)}{RT}\right)\exp\left(-\left[\tilde{V}_1^*\left(\xi\right)-\tilde{V}_1^*\left(\xi_0\right)\right]P\left(T,T_g\right)\right) \end{aligned} \tag{V.14}$$

where the so-called polymer function, $P\left(T,T_g\right)$ lumps all polymer parameters (see Eqs. (V.9) -(V.13)). It is defined as:

$$P\left(T,T_g\right)=\frac{1}{\tilde{V}_2^*\left(T_g\right)}\frac{\hat{V}_2^*\left(T_g\right)}{\hat{V}_{FH2}\left(T,T_g\right)/\gamma}=\frac{1}{\tilde{V}_2^*\left(T_g\right)}\frac{\hat{V}_2^*\left(T_g\right)}{\frac{K_{12}}{\gamma_2}\left(K_{22}+T-T_g\right)}$$
$$=\frac{1}{u+vT_g}\cdot\frac{2.303\left(C_{12}\right)\left(C_{22}\right)}{\left[C_{22}+\lambda\left(T,T_g\right)\left(T-T_g\right)\right]} \quad \text{(V.15)}$$

The original FVT formulation assumes that expression (V.14) assumes that $E^*\left(\xi\right)$ does not contain any substantial polymer effect. In practice, $E^*\left(\xi\right)$ is usually discarded in apolar polymers whereas a value greater than zero is suspected in the presence of hydrogen bonding between the solute and the polymer (Hall *et al.*, 1999). Tonge and Gilbert (2001a) concluded that this parameter is critical to estimate D values in new polymers. For molecules with repeated patterns, we will show later that $E^*\left(\xi\right)$ can be recast in Eq. (V.14), so that it is associated with the energy barrier of one single rigid pattern or blob rather than the total energy barrier for the entire molecule.

At this stage, the applicability of Eq. (V.14) is very limited, but it exemplifies that scaling the diffusion of solutes with their sizes may have a sound mechanistic basis. Nevertheless, the ratio of diffusivities alone does not remove polymer effects. Eq. (V.14) assumes, in particular, that small (ξ_0) and large (ξ) solutes translate as single jumping units, even when the large solute consists of repeated patterns commensurable to ξ_0. The next section will introduce the concept of scaling law between ξ and the molecular mass, M for solutes with linearly repeated patterns to justify that the diffusion coefficient associated to the center-of-mass of N connected blobs or patterns can be recovered from the diffusion behavior of one single blob or pattern. As such scaling is thought to be "universal", it can be used to estimate the function $P\left(T,T_g\right)$ for either new polymers or for polymers with undocumented FV parameters.

V.4.2.2. Scaling of the diffusion for linear probes

Fang *et al.* (2013) showed that ξ was proportional to the logarithm of M for linear solutes, including *n*-alkanes and *p*-oligophenyls regardless the considered polymer. It was shown that the diffusion of solutes with linearly repeated patterns proceeds by the independent displacements of rigid units or blobs. The jump dynamics of each blob is very slow and

controlled by the strong coupling between the displacements of the blob itself and of the surrounding atoms. In this study, we follow the same ideas and assume that the displacements of one single blob obey to FVT and that the diffusion of the entire molecule still verify Eqs. (V.14) and (V.15). As a consequence of Eq. (7) of Fang *et al.* (2013) or of any similar equation, short and long-lived contacts can be factorized so that the displacements of connected blobs can be separated from the displacements of one single blob. Besides, it is worth noticing that not only ξ scales with M (denoted ξ_M), but also the pre-exponential factor $D_0\left(\xi_M\right)$. The apparent complication can be resolved by applying once again the original FV theory, which covers "in theory" the whole solute concentration range: from infinite dilution (trace diffusion, this work) to pure solute (self-diffusion, assuming that the solute is still at liquid state). According to Vrentas and Vrentas (1993), $D_0\left(\xi_M\right)$, which appears in both expressions of trace and self-diffusion coefficients, is related to its reciprocal viscosity and should reasonably scale as a power law for linear solutes. By appending the subscript "*lin*" to diffusion coefficients associated with linear probes, one gets:

$$D_{0,lin}\left(\xi_M\right) = D_0\left(\xi_{M_{blob}}\right)\left(\frac{M}{M_{blob}}\right)^{\beta_{lin}} \tag{V.16}$$

where ξ_M and $\xi_{M_{blob}}$ are the values of ξ for the chain of length M and M_{blob}, respectively. According to the Rouse model (Ferry, 1980), β_{lin} is expected to be close to unity for solutes with linearly repeated patterns (blob model). A justification of the unique definition of $D_0\left(\xi_M\right)$, independent the of polymer, can be found in Figure 4 of Vagias *et al.* (2015).

From Figure 2 of Fang *et al.* (2013) based on data obtained on polyvinyl acetate (PVAc), $\tilde{V}_1^*\left(M\right) = \xi\left(M, T_g\right)\tilde{V}_2^*\left(T_g\right)$ scales for linear solutes as:

$$\tilde{V}_{1,lin}^*\left(M\right) = \tilde{V}_{1,lin}^*\left(M_{blob}\right) + a_{lin}\ln\left(\frac{M}{M_{blob}}\right) \tag{V.17}$$

where the approximation $a_{lin}\left(T_g\right) \approx 0.24\tilde{V}_2^*\left(T_g\right) = 0.24\left(u + vT_g\right)$ has been proposed for a broad range of solutes: linear *n*-alkanes, *n*-alkyl acetates, and aromatic solutes.

By introducing Eqs. (V.16) and (V.17) into Eq. (V.14), a general scaling law can be proposed, in particular, for *n*-alkanes:

$$\frac{D_{lin}\left(\xi_M, T, T_g\right)}{D\left(\xi_{M_{blob}}, T, T_g\right)} = \left(\frac{M}{M_{blob}}\right)^{\beta_{lin}} \exp\left(-a_{lin}\left(T_g\right)\ln\frac{M}{M_{blob}}P\left(T, T_g\right)\right) = \left(\frac{M}{M_{blob}}\right)^{\beta_{lin} - a_{lin}\left(T_g\right)\cdot P\left(T, T_g\right)} \tag{V.18}$$

The power law (V.18) can be directly compared with Eqs (1) and (8) of Fang *et al.* (2013):

$$\frac{D_{lin}\left(M,T,T_g\right)}{D\left(M_{blob},T,T_g\right)}=\left(\frac{M}{M_{blob}}\right)^{-\alpha_{lin}\left(T,T_g\right)}$$
$$\text{with } \alpha_{lin}\left(T,T_g\right)=1+\frac{K_\alpha}{T-T_g+K_\beta} \text{ for } T\geq T_g \tag{V.19}$$

where K_α and K_β were suggested to be "universal" scaling constants with values ca. 150 K and 40 K (for *n*-alkanes), respectively.

Equating Eqs. (V.18) and (V.19) leads to capture all polymer-related parameters through the scaling exponent of *n*-alkanes, α_{lin}. At rubber state ($T\geq T_g$), the corresponding polymer function reads:

$$P\left(T,T_g\right)=\frac{\alpha_{lin}\left(T,T_g\right)+\beta_{lin}}{a_{lin}\left(T_g\right)} \tag{V.20}$$

At molten state ($T>>T_g$), the behavior of $P\left(T,T_g\right)$ is guessed from the asymptotic scaling of α_{lin} by assuming that the translation of all connected blobs obeys to the Rouse dynamics ($\alpha_{lin}\to 1$). Eq. (V.20) is, however, not applicable to glassy state without a proper extension of Eq. (V.19) when $T<T_g$.

Eq. (V.19) can be prolonged to glassy state by replacing K_α and K_β by similar constants K_α^g and K_β^g, respectively. The new constants are identified by noticing that both expressions of α_{lin} on both sides of require to be continuous at $T=T_g$ and by assuming that the change in apparent activation energy across T_g must be similar to the one met in the original FVT:

$$\frac{\left.\frac{\partial \ln D}{\partial 1/T}\right|_{T\overset{<}{\to}T_g}}{\left.\frac{\partial \ln D}{\partial 1/T}\right|_{T\overset{>}{\to}T_g}}=\frac{\alpha_2^g}{\alpha_2} \tag{V.21}$$

Such reasoning leads to $K_\alpha^g=\frac{\alpha_2}{\alpha_2^g}\left(1-\frac{\alpha_2}{\alpha_2^g}\right)K_\alpha$ and $K_\beta^g=\frac{\alpha_2}{\alpha_2^g}\left(1-\frac{\alpha_2}{\alpha_2^g}\right)K_\beta$. In the general case, the scaling exponent becomes:

$$\alpha_{lin}\left(T,T_g\right)=1+\frac{K_\alpha}{r\cdot\left(T-T_g\right)+K_\beta} \text{ with } r=\begin{cases}1 \text{ when } T\geq T_g\\ \dfrac{\alpha_2^g}{\alpha_2} \text{ otherwise}\end{cases} \tag{V.22}$$

Eq. (V.22) provides a practical approximation of the polymer function $P\left(T,T_g\right)$, where free volumes are probed by the scaling law of the trace diffusion of any linear solutes:

$$P\left(T,T_g\right)\approx\frac{1}{0.24\left(u+vT_g\right)}\left[2+\frac{K_\alpha}{r\cdot\left(T-T_g\right)+K_\beta}\right] \tag{V.23}$$

At this stage, it is important to note that Eq. (V.23) is physically valid while the inequality $T\geq T_g-K_\beta/r$ (condition to get $\alpha_{lin}\geq 1$). Below this value, the model fails because it assumes a constant thermal expansion at glassy state, which is not reasonable too far below T_g. This strategy offers to probe polymer hole free volumes indirectly by studying the trace diffusion of a homologous series of linear solutes (oligomers resembling the host polymer or not).

The existence or not of a polymer function $P\left(T,T_g\right)$, universal and independent of the polymer, can be sought by equating Eqs. (V.15) and (V.23):

$$\frac{2.303\left(C_{12}\right)\left(C_{22}\right)}{\left[C_{22}+\lambda\left(T,T_g\right)\left(T-T_g\right)\right]}\approx\frac{1}{0.24}\left[2+\frac{K_\alpha}{r\cdot\left(T-T_g\right)+K_\beta}\right] \tag{V.24}$$

By identification, the following estimates of scaling parameters are obtained for $T\geq T_g$: $K_\alpha\approx\left[0.553\left(C_{12}\right)-2\right]\left(C_{22}\right)-\left(T-T_g\right)$ and $K_\beta\approx\left(C_{22}\right)$. At $T=T_g$, universal WLF constants $\left(C_{12}\right)\approx 17.44$ and $\left(C_{22}\right)=51.6$ K suggests $K_\alpha\approx 394$ K and $\alpha\approx 8.64$, whereas α values were reported to range between 5 and 6 near T_g in linear polymers(Fang *et al.*, 2013). The magnitude orders predicted by the so-called WLF constants and FV theory are realistic, but they tend to overestimate the real mass dependence for flexible solutes. White and Lipson (2016) provided, recently, an elegant justification why the WLF constants are not as universal as it could be expected. The main argument is that these values assume that the whole free volume contributes to the transport properties instead of the excess free volume or hole free volume.

In the absence of a universal polymer function, introducing realistic estimates of K_α and K_β from the trace diffusion of linear probes offer a better alternative to predict D for arbitrary solutes, irrespectively the availability of FV parameters for the considered polymer. Introducing either Eq. (V.20), or its approximation (V.23), in Eq. (V.8) gives the general formulation for an arbitrary solute in an arbitrary polymer:

$$
\begin{aligned}
D\left(\xi,T,T_g\right) &= D_0\left(\xi\right)\exp\left(-\frac{E^*\left(\xi\right)}{RT}\right)\exp\left(-\tilde{V_1^*}\left(\xi\right)P\left(T,T_g\right)\right) \\
&= D_{0,lin}\left(\xi\right)\exp\left(-\frac{E^*\left(\xi\right)}{RT}\right)\exp\left(-\tilde{V_1^*}\left(\xi\right)\frac{\alpha_{lin}\left(T,T_g\right)+\beta_{lin}}{a_{lin}\left(T_g\right)}\right) \\
&\approx D_0\left(\xi\right)\exp\left(-\frac{E^*\left(\xi\right)}{RT}\right)\exp\left[-\frac{\tilde{V_1^*}\left(\xi\right)}{0.24\left(u+vT_g\right)}\left(2+\frac{K_\alpha}{r\left(T-T_g\right)+K_\beta}\right)\right] \\
&\approx D_0\left(\xi\right)\exp\left(-\frac{E^*\left(\xi\right)}{RT}\right)\exp\left[-\frac{\xi}{0.24}\left(2+\frac{K_\alpha}{r\left(T-T_g\right)+K_\beta}\right)\right]
\end{aligned}
\tag{V.25}
$$

where is chosen equal to unity above T_g and lower than unity below . T_g

For many small solutes such as solvents, the solute parameters $D_{0,lin}$, E^* and $\tilde{V_1^*}$ or $\xi\cdot\left(u+vT_g\right)$ have been tabulated in the literature with some discussions on how to derive them in Zielinski and Duda (1992) and their shortcomings in Vrentas and Vrentas (2003). For solutes with repeated patterns, Eq. (V.18) can be used instead. The approach will be extended in §V.4.3.2. to linear solutes including an anchor.

V.4.2.3. Parameterization of hole FV parameters from linear probes

(V.26)

The new FVT formulation requires a determination of parameters from linear molecules. Diffusion data needs to be collected at solid state, but it can be at any temperature irrespectively the temperature to which Eq. (V.25) will be used. Using determinations at rubber state, when D values are faster to measure, is particularly promising for polymers, which are glassy in conditions of use. In some respect, the proposed strategy is analogous to previous attempts, where D values at zero concentration were extrapolated from mutual diffusion coefficients in plasticized polymers.

Eqs. (V.19) and (V.22) express that $D\left(M_{blob},T,T_g\right)$ and $D_{lin}\left(M,T,T_g\right)$ are differently activated by temperature due to a loss of mass dependence when temperature is increasing. In other words, diffusion of long solutes is more activated by temperature than the diffusion of short solutes. This effect is related to the coupling between the displacements of the blobs in the solute and surrounding atoms (Fang *et al.*, 2013). Indeed, increasing temperature contributes to make the release of solute-polymer constraints more likely for long solutes. This effect is controlled by FV and two constants: K_α and K_β. In this description, an additional energy barrier, E_{blob}^*, independent of the polymer, can occur due to the internal reorganization of the

degrees of freedom inside the blob. Its effect is included in the apparent activation energy of the blob itself and denoted $E_a\left(M_{blob}\right)$.

- *Constants:* K_α *and* K_β

K_α and K_β can be determined either i) by fitting $\alpha_{lin}\left(T,T_g\right)$ estimated at different temperatures for linear probes to Eq. (V.22) or more directly ii) by comparing the apparent activation energies of linear probes, $E_a\left(M_{blob}\right)$, with the corresponding average value of α_{lin}. The first method is described in Fang *et al.* (2013). The optimal parameter identification strategy consists in noticing that $\alpha_{lin}-1$ is linear with K_α, so that K_β can be guessed with the golden section search technique. The second methodology is detailed hereafter.

Due to FV effects, the activation energy is not constant over the temperature range $T_1 \le T \le T_2$ used to assess it. As a result, only an average value, denoted $\left\langle E_a\left(M\right)\right\rangle$, can be estimated. From Eqs. (V.19) and (V.22), one gets:

$$\left\langle E_a\left(M\right)\right\rangle - \left\langle E_a\left(M_{blob}\right)\right\rangle = \left\langle RT^2 \left.\frac{\partial \ln \dfrac{D\left(M,T,T_g\right)}{D\left(M_{blob},T,T_g\right)}}{\partial T}\right|_{M,M_{blob},T_g} \right\rangle_{\text{between } T_1 \text{ and } T_2} \qquad \text{(V.27)}$$

$$= RK_\alpha \ln\frac{M}{M_{blob}}\left\langle I\right\rangle$$

where $\left\langle I\right\rangle$ is a dimensionless temperature capturing the deviation to the Arrhenian behavior:

$$\left\langle I\right\rangle = \frac{1}{T_2-T_1}\int_{T_1}^{T_2} r\left(T\right)\left(\frac{T}{r\left(T\right)\left(T-T_g\right)+K_\beta}\right)^2 dT \qquad \text{(V.28)}$$

For any guess of K_β, K_α and $\left\langle E_a\left(M_{blob}\right)\right\rangle$ are determined from the linear regression of $\left\langle E_a\left(M\right)\right\rangle$ vs $\ln\frac{M}{M_{blob}}\left\langle I\right\rangle$. In practice, T_1 and T_2 can vary between solutes due to different experimental conditions and $\left\langle I\right\rangle$ may also be a function of M. $\left\langle E_a\left(M\right)\right\rangle$ and $\alpha\left(T,T_g\right)$ can be back mapped independently of the choice of K_β as:

$$\left\langle E_a\left(M\right)\right\rangle - \left\langle E_a\left(M_{blob}\right)\right\rangle = \frac{R}{K_\alpha\left(T_2-T_1\right)}\ln\frac{M}{M_{blob}}\int_{T_1}^{T_2} r\left(T\right)T^2\left[\alpha_{lin}\left(T,T_g\right)-1\right]^2 dT \qquad \text{(V.29)}$$

The choice of the strategy by fitting either $\ln D$ vs $\ln M$ data or $\left\langle E_a\left(M\right)\right\rangle$ vs $\ln M$ depends on the quality of the set of D values: high resolution in M (α_{lin} can be determined safely), high resolution in T ($\left\langle E_a\left(M\right)\right\rangle$ can be determined with high accuracy). The span of the considered temperature range is particularly important when Eq. (V.22) is used: the curvature with $T-T_g$ needs to be observable. Eq. (V.29) demonstrates that Eq. (V.27) offers a better alternative when the melting temperature of the polymer is approached, that is when FV effects vanish and $\alpha_{lin}\to 1$.

It is worthwhile to mention that the linearity of activation energies with the number of blobs, $n=\frac{M}{M_{blob}}$ (see Eq. (V.27)), has been previously reported for *n*-alkanes in Jeong and Douglas (2015) (see Figure 3a herein). The results obtained by molecular dynamics simulations also showed a transition from rod-like (our Eq. (V.19) and Eq. (3) in Jeong and Douglas (2015)) to coiled chain configuration occurring for a number n (number of carbon atoms in the original study) close to 17. However, the analogy cannot be analyzed further as the authors studied self-diffusion coefficients instead of trace diffusion coefficients at a constant bulk density (*i.e.,* in the presence of the same amount of hole FV), as we consider here in the discussion on density effects (Von Meerwall *et al.*, 1998;Durand *et al.*, 2010).

- *Estimation of the blob size or equivalently the mass of the rigid unit:* M_{blob}

In essence, the scaling model proposed for *n*-alkanes is different from the original free volume one, because the solute is envisioned as a collection of connected jumping units. The corresponding diffusion coefficients are found by combining Eqs (V.19) and (V.25):

$$D\left(M,T,T_g\right)=D_0\left(M_{blob}\right)\exp\left(-\frac{E^*\left(M_{blob}\right)}{RT}\right)\times \exp\left(-\tilde{V_1^*}\left(M_{blob}\right)P\left(T,T_g\right)\right)\left(\frac{M}{M_{blob}}\right)^{-\alpha_{lin}\left(T,T_g\right)} \quad \text{(V.30)}$$

When $M\to M_{blob}$ and temperature increases, the apparent activation energy vanishes apparently to approach the residual value of $E^*\left(M_{blob}\right)$, which is assumed to be close to 0:

$$\left\langle E_a\left(M_{blob}\right)\right\rangle=E^*\left(M_{blob}\right)+\frac{R\tilde{V_1^*}\left(M_{blob}\right)}{a_{lin}\left(T_g\right)K_\alpha\left(T_2-T_1\right)}\int_{T_1}^{T_2} r\left(T\right)T^2\left[\alpha_{lin}\left(T,T_g\right)-1\right]^2 dT \quad \text{(V.31)}$$

In other words, Eq. (V.31) demonstrates that all regression lines $\ln D$ vs $\ln M$ obtained at different temperatures are expected to converge towards a same D value when M approaches M_{blob} . This absence of temperature activation can be used to estimate

experimentally M_{blob}. For *n*-alkanes, M_{blob} should be identified to be commensurable to -CH_2-CH_2-, that is 28 g·mol^{-1}.

- *Subcooling ratio* $r\left(T,T_g\right)$ *at glassy state*

The subcooling ratio $r\left(T,T_g\right)$ is a crucial parameter to extend previous relationships to glassy state. It is formally defined as $\frac{\alpha_2^g}{\alpha_2}$ and it can be independently determined. When it is not possible or because D values from the literature are used, it must be identified from Eq. (V.22). Using apparent activation energies is not recommended as there are averaged over the temperature range, which smooth the transition when T_g is crossed. It deserves to note that $r\left(T,T_g\right)$ and $\lambda\left(T,T_g\right)$ (see Eq. (V.12)) originate from different roots. A closer definition of $\lambda\left(T,T_g\right)$is proposed in Eq (29) of Ramesh *et al.* (2011) from an integral description of the thermal expansion (see (Vrentas and Vrentas, 1994a) for details):

$$\lambda\left(T,T_g\right)=\frac{\alpha_2^g-\alpha_{c2}^g}{\alpha_2} \tag{V.32}$$

where α_{c2}^g is the thermal expansion coefficient for the sum of the occupied volume and of the specific interstitial volume. The authors invoke that the change of slope at T_g (α_2^g/α_2) is governed by the change in occupied volume and specific interstitial volume, which is not necessarily true if the hole free volume does not redistribute similarly as the interstitial one. This view is discussed by White and Lipson (2016). We do not take a position in the present study, and we prefer to identify the subcooling ratio r from the comparison of diffusion coefficients above and below T_g for one particular solute. This particular solute can be any diffusant and not necessarily *n*-alkanes. Additionally, the use of linear molecular probes at rubber state removes the difficulty of an explicit definition of hole FV and their variations with temperature. Only Eq. (V.21) would be affected by the exact nature of FV when T_g is crossed.

V.4.3. Experimental validation for linear probes

Rigorously, the relationship between FVT (see Eq. (V.8)) and scaling properties (see Eqs. (V.19) and (V.30)) has been established only for linear and regular solutes consisting in similar blobs, such as *n*-alkanes. The same equations cannot be used without an extension for

solutes presenting differences in blob size or exhibiting significant interactions with the polymer. The experimental verifications of Eqs. (V.19) and (V.30) are discussed, firstly, on *n*-alkanes, while highlighting the scaling differences observed with equivalent solutes series, but including a terminal "anchor" such as an alcohol or an acetate functional group. To avoid any confusion, diffusion coefficients of linear solutes are denoted, D_{lin} when the solutes are regular and D_a when they include a different terminal blob (anchor). With an initial intent of using indifferently regular and anchored solutes as molecular probes of free volume (FV) effects, the relationship between the scaling exponents of D_{lin} and D_a with the length of the solute alkyl chain M, denoted α_{lin} and α_a respectively, will be established. Intuitively, we could expect that a short alkyl chain attached to a heavy/rigid head (with an anchor) has a diffusivity comparable to a longer *n*-alkane (without anchor). That is, a large anchor would be equivalent to several ethyl blobs. Such equivalences are analyzed in Figures 1-3 by comparing successively the scaling associated to *n*-alkanes (denoted n-A), 1-alcohols (denoted 1-O) and alkyl-alkanes (a-A) in various polymers near T_g, when FV effects dominate. Results far from T_g have been reported elsewhere in Fang *et al.* (2013). In all cases, the selection of diffusion data was particularly important. The conditions of measurements are detailed in Table 1. Scaling exponents and apparent activation energies were extracted exclusively from diffusion coefficients estimated using the same experimental methodology and polymer. Measurements at infinite dilution were preferable. When it was impossible (e.g. PS data in Bernardo, 2012, 2013) obtained by immersing the polymer directly in the solute solution), it was verified that no plasticization effect affected diffusion determinations.

V.4.3.1. n-alkanes as homogeneous blob models

N-alkanes starting from ethane and beyond are the most natural homologous solute series to probe FV. The pattern CH_2CH_2 also represents the largest available rigid blob. In this study, the slight difference in size between terminal CH_3 and CH_2 is assumed to be insignificant. The scaling of diffusion coefficients of *n*-alkanes, D_{lin}, with molecular mass, M, are plotted for PET (-11 K ≤ $T-T_g$ ≤ +39 K), polyamide 6 (+11 K ≤ $T-T_g$ ≤ +31 K), polystyrene (-25 K ≤ $T-T_g$ ≤ +45 K) and, poly(vinyl acetate) (+58 K ≤ $T-T_g$ ≤ +78K), in Figures 1a, 1b, 1c and 1d, respectively. As data on PVAc were collected from Figures 8-9 in Arnould and Laurence (1992)at slightly different temperatures, they were subsequently interpolated to the same temperatures. The interpolation was carried out by assuming a linear relationship between $\ln D_{lin}$ and $1/\left(1-T_{g_2}-K_{22}\right)$, in agreement with FVT (see Eq.(12) in Vrentas and Duda,

1977c). In all series, data were sensitive to inherent methodological limitations: diffusion coefficients too large or too slow could not be inferred with the same approach. Values collected by desorption/sorption (PET and PS datasets) were scarce (fewer data in the studied series) near or below T_g due to very slow diffusion. Data obtained in permeation experiments (PET and PA6 sets) were, conversely, less reliable at high temperatures due to too short lag-times. All studied series exhibit good linearity of $\ln D_{lin}$ with $\ln M$ and with a slope increasing sharply when temperature decreases. Mass dependence loss at high temperatures looked stronger in PET (**Figure V-25**a), but it relied only on two determinations at each temperature and on two highly volatile solutes (*n*-propane and *n*-butane). For the three data sets collected near T_g (PET, PA6 and PS), trend lines associated with different measurement temperatures converge to one common diffusion coefficient, which is almost invariant with temperature and whose value is interpreted via Eq. (V.33) as the diffusion coefficient of a single rigid blob. Averaging of all pair intersections yields a theoretical molecular mass of the blob, M_{blob}, ranging from 21 g·mol^{-1} to 35 g·mol^{-1}, in good agreement with an assumption of a blob commensurable to an ethyl group. In PVAc (tested far above T_g), the intersection is poorly defined and the found value *ca.* 8.5 g·mol^{-1} underestimates the real blob size. If significant, it could be interpreted by the higher difficulty for the polymer to trap a rigid pattern far from T_g for long periods as justified in Fang *et al.* (2013).

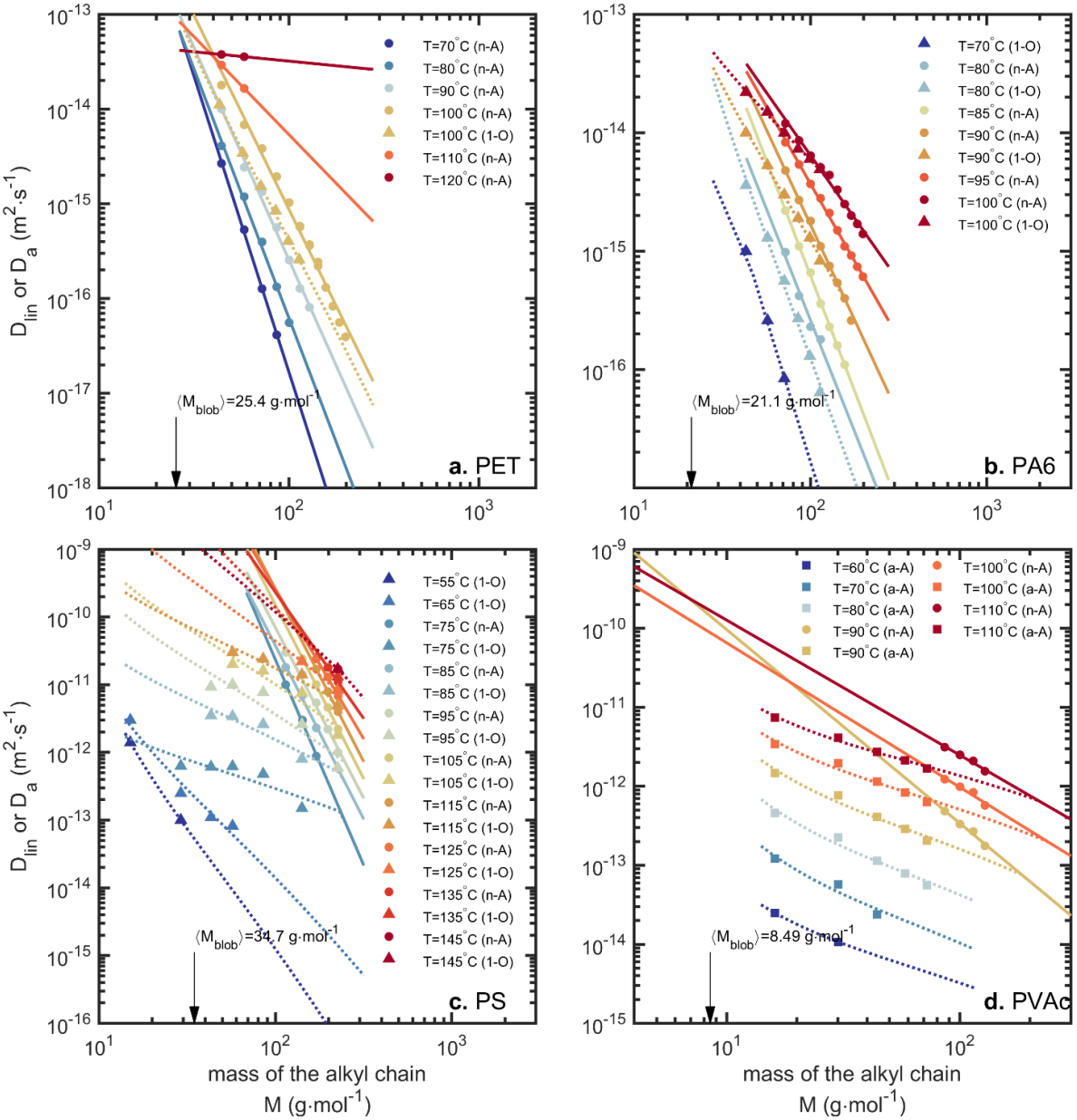

Figure V-25. *Scaling of diffusion coefficients, D_{lin} or D_a, of n-alkanes (n-A), 1-alcohols (1-O) and alkyl-acetates (a-A) with the molecular mass of the alkyl chain, M in: (a) PET, (b) PA6, (c) PS and (d) PVAc. Continuous and dotted lines correspond to the regression lines for regular solutes (n-alkanes) and their generalization to anchored ones (1-alcohols and alkyl acetates) via Eq.* (V.39)*, respectively. $\langle M_{blob} \rangle$ was estimated the common intersection of all regression lines of $\ln D_{lin}$ vs $\ln M$ (see its interpretation in Eqs.*(V.19) *and* (V.30)*).*

V.4.3.2. Anchored probes as heterogeneous solutes: 1-alcohols and n-alkyl acetates

Diffusion coefficients, D_a, of linear solutes including an anchor of mass M_{anchor} and an alkyl chain of mass M scales also as a power law with the total molecular mass: $M + M_{anchor}$. The corresponding scaling exponent, $\alpha_a(T) = -\left.\frac{\partial \ln D_a(M,T)}{\partial \ln(M+M_{anchor})}\right|_T$, differs, however, from $\alpha_{lin}(T)$; but it can be guessed that $-\left.\frac{\partial \ln D_a}{\partial \ln M}\right|_T$ could approximate α_{lin} in for sufficiently large M. Indeed, the relationship between α_a and α_{lin} reads:

$$\begin{aligned}\alpha_a(T) &= -\left.\frac{\partial \ln D_a(M,T)}{\partial \ln(M+M_{anchor})}\right|_T == -\left.\frac{\partial \ln D_a(M,T)}{\frac{\partial M}{M}\frac{M}{M+M_{anchor}}}\right|_T \\ &= -\left(1+\frac{M_{anchor}}{M}\right)\left.\frac{\partial \ln D_a(M,T)}{\partial \ln M}\right|_T \approx \left(1+\frac{M_{anchor}}{M}\right)\alpha_{lin}(T)\end{aligned} \quad \text{(V.34)}$$

When the length of the alkyl chain is varied from M_1 to M_2, the apparent slope of D_a vs. $M + M_{anchor}$ gives only an average estimate of $\alpha_{lin}(T)$, which can be approached as:

$$\left\langle \alpha_{lin}(T) \right\rangle = \frac{\alpha_a(T)}{M_2 - M_1}\int_{M_1}^{M_2}\frac{dM}{1+\frac{M_{anchor}}{M}} = \alpha_a(T)\left(1 - \frac{M_{anchor}}{M_2 - M_1}\ln\frac{M_2 + M_{anchor}}{M_1 + M_{anchor}}\right) \quad \text{(V.35)}$$

The convergence of the estimator (V.35) is fast as soon as $M_2 - M_1 >> M_{anchor}$. Similar behavior is expected for diffusion coefficients $D_a(M)$. They are expected to approach D_{lin} values, but with a positive mass shift, ΔM_{eq}^a, representing the equivalent alkyl chain leading to the same effect of the anchor, that is $D_a(M,T) \approx D\left(M + \Delta M_{eq}^a, T\right)$. For PET, the comparison between *n*-alkanes and 1-alcohols for $M \approx$ 100 g·mol^{-1} gives a shift ΔM_{eq}^a ranging between 1.4 M_{blob} and 1.8 M_{blob} (46 ± 4 g·mol^{-1}) at 100°C (**Figure V-25**a). As a result, the convergence of diffusion coefficients appeared comparable to experimental errors above M =250 g·mol^{-1}. Similar shifts were observed in other polymers above T_g: *ca.* 24 ± 3 g·mol^{-1} in PA6 (for $T - T_g \approx$ 31 K, **Figure V-25**b) and *ca.* 9 ± 7 g·mol^{-1} in PS ($T - T_g \approx$ 45 K, **Figure V-25**c). Below T_g, the shift increases dramatically from 140 ± 22 g·mol^{-1} near T_g with values above 250 g·mol^{-1} in PS when $T - T_g \approx$ -35 K. The comparison between hydroxy and acetate functional groups confirmed the complex influence of the anchor on the reduction of diffusion coefficients. In PVAc

($T - T_g \approx$ 68 K, **Figure V-25**d), ΔM_{eq}^{a} was found *ca.* 43 ± 8 g·mol^{-1} for *n*-alkyl acetates when $M \approx$100 g·mol^{-1}.

By assuming that the same constraint release mechanism acts on main blobs and anchors, the contribution of M_{anchor} on $D_a\left(M,T\right)$ is expected to fade rapidly with M. According to Eqs (V.30) and (V.34), the ratio of diffusion coefficients between an anchored probe and its non-anchored equivalent scales as:

$$\frac{D_a\left(M,T\right)}{D_{lin}\left(M,T\right)} \approx \frac{D_a\left(M_{blob},T\right)}{D_{lin}\left(M_{blob},T\right)}\left(\frac{M_{blob}}{M}\right)^{-\alpha_{lin}(T)}\left(\frac{M_{anchor}+M}{M_{anchor}+M_{blob}}\right)^{-\alpha_{lin}(T)\left(1+\frac{M_{anchor}}{M}\right)} \quad \text{(V.36)}$$

$$\xrightarrow{M>>M_{anchor}} \frac{D_a\left(M_{blob},T\right)}{D_{lin}\left(M_{blob},T\right)}\left(\frac{M_{blob}}{M_{anchor}+M_{blob}}\right)^{-\alpha_{lin}(T)} M^{-\alpha_{lin}(T)\frac{M_{anchor}}{M}} \xrightarrow{M>>M_{anchor}} 1$$

For the particular case $M = M_{blob}$, Eq. (V.36) offers an approximation of $D_a\left(M_{blob},T\right)$ as:

$$D_a\left(M_{blob},T\right) \approx \left(\frac{M_{anchor}}{M_{blob}}+1\right)^{-\alpha_{lin}(T)} D_{lin}\left(M_{blob},T\right) \quad \text{(V.37)}$$

Combining Eqs. (V.36) and (V.37) yields a practical estimator of $D_a\left(M,T\right)$ for any type of anchor:

$$D_a\left(M,T\right) \approx \left(\left(\frac{M_{anchor}}{M}+1\right)\left(\frac{M_{anchor}+M}{M_{anchor}+M_{blob}}\right)^{\frac{M_{anchor}}{M}}\right)^{-\alpha_{lin}(T)} D_{lin}\left(M,T\right) \quad \text{(V.38)}$$

Eq. (V.38) and its generalization in Eq. (V.39) fit successfully all diffusion coefficients of solute series with anchors depicted in **Figure V-25**. The supporting information of Zhu *et al.* (2019c) discusses the details of the relevance of Eqs (V.38) and (V.39) in more general cases, in particular, when the mass of the anchor is larger than the alkyl chain ($M < M_{blob}$) or when the anchor creates specific interactions (π- π electrostatic and H-bonding ones) with the polymer. It is shown that the blob concept is very flexible and can be reduced either to ethyl or methyl groups (see section 2 of the Supporting Information of Zhu *et al.*, 2019c). At first sight and by neglecting excluded volume considerations, the specific activation energy of large anchors (e.g. benzyl group), denoted $E_a^{anchor}\left(T\right)$, could be guessed from the apparent activation energy of the diffusion of the anchor alone (e.g. benzene). Both energy barriers are, however, not equivalent as the latter applies to the center-of-mass of the anchor and not to the center-of-mass of the whole solute, denoted CM. If the displacements of the anchor and of the blobs

are assumed independent on short time scales, the translation of CM is likely to follow a compound Poisson process associated to the combination of trapping times of all blobs and of the anchor. As a result, $E_a^{anchor}(T)$ introduces an additional waiting time before entering in the hydrodynamic regime, which decreases with M. When all trapping times are independent and Poisson distributed, Eq. (V.38) becomes:

$$D_a(M,T) \approx \exp\left(-\frac{M_{anchor}}{M_{anchor}+M}\frac{E_a^{anchor}(T)}{RT}\right)\times \left(\left(\frac{M_{anchor}}{M}+1\right)\left(\frac{M_{anchor}+M}{M_{anchor}+M_{blob}}\right)^{\frac{M_{anchor}}{M}}\right)^{-\alpha_{lin}(T)} D_{lin}(M,T) \quad \text{(V.39)}$$

By analogy, the term $\exp\left(-\frac{M_{anchor}}{M_{anchor}+M}\frac{E_a^{anchor}(T)}{RT}\right)$ represents the dimensionless frequency of a translational event of CM respectively to the frequency translation of an isolated alkyl chain. In practice, E_a^{anchor} was found to be essentially enthalpic and not related to the size of the anchor. As an example, the value for a benzyl group is negligible in a semi-aromatic polymer such as PET (see §2.1.1 of the Supporting Information of Zhu *et al.*, 2019c), but it is large in an aromatic polymer such as PS (see §2.1.2 of the Supporting Information of Zhu *et al.*, 2019c). For polar solutes in polar homopolymers, it also depends on the number of possible hydrogen-bonds with each monomer. The specific contribution of the hydroxy functional group in 1-alcohols depicted in **Figure V-25** was estimated lower than 15 kJ·mol^{-1} and rapidly negligible with increasing M. By contrast, they were found significant and persistent with M for *n*-alkyl acetates in PVAc, with E_a^{anchor} values above 30 kJ·mol^{-1}. It was, consequently, hinted that 1-alcohols were better molecular probes than *n*-alkyl acetates. The presence of large E_a^{anchor} values reduces not only the sensitivity of D to M (see **Figure V-25**d), but also complicates the interpretation of activation energies to extract reliable estimates of K_α and K_β.

The complications raised by a significant contribution of E_a^{anchor} are summarized as follows. Eq. (V.34) suggests that any anchor would cause $\alpha_a(T) \geq \alpha_{lin}(T)$ and that anchored probes would, consequently, overestimate FV effects; but, strong interactions between the anchor and the polymer would have antagonist effects. Indeed, Eq. (V.39) shows that $-\partial \ln D_a(M,T)/\partial \ln M\big|_T$ might underestimate α_{lin} when the effects of E_a^{anchor} are not dissipated by a large connected alkyl chain; the negative deviation reads:

$$-\left.\frac{\partial \ln D_a(M,T)}{\partial \ln M}\right|_{T,E_a^{anchor}>>0} - \alpha_{lin}(T-T_g) \approx -\left\langle \frac{M_{anchor}M}{(M_{anchor}+M)^2} \right\rangle \frac{\left\langle E_a^{anchor}(T) \right\rangle}{RT} \leq 0 \quad \text{(V.40)}$$

The same effect reduces the dependence of the apparent activation energy of anchored solutes $\left\langle E_{a,a}(M,T) \right\rangle = \left\langle RT^2 \left.\frac{\partial \ln D_a(M,T)}{\partial T}\right|_M \right\rangle$ with $\ln M$. The corresponding slope decrease is given by $-\left\langle \frac{M_{anchor}M}{(M_{anchor}+M)^2} \right\rangle E_a^{anchor}$. Relatedly, the slowdown of the diffusion due to the presence of any pattern larger the considered blob (entropic effect) and due a specific interaction with the polymer (enthalpic effect) is predicted regardless its position along the linear chain. This mechanism has been already observed in model simulations with beads of different sizes (Budzien *et al.*, 2004). It is emphasized that the additional barrier brought by E_a^{anchor} is expected to be higher in dense and glassy polymers. Because the effects of E_a^{anchor} dissipates rapidly when $M >> M_{anchor}$ and when $E_a^{anchor} \to 0$, the new concepts of energy barriers (either E_a^{anchor} or E^*) are different from their counterparts in the original FV theory (Hall *et al.*, 1999). All experimental results on anchored series were fitted acceptably with Eq. (V.39). It confirmed the consistency of the whole scaling approach for both regular and irregular solutes including various chemical groups acting as anchors in representative polymers: aliphatic, semi-aromatic, aromatic, polar/apolar ones. Because the independence of blob trapping/release kinetics is a sufficient condition for the proposed description, the linear connectivity of the blobs is not required, and the description could also be valid for branched solutes. Practically, each anchored solute series should verify the inequality $M > 2M_{anchor}$ to offer FV probing capabilities similar to regular ones. Such a condition was not fulfilled with *n*-alkyl acetates in PVAc but was partly verified for 1-alcohols in PS (see ***Table IV-5***).

V.4.3.3. Apparent activation energies of linear probes

Eq. (V.29) captures that the variation of scaling exponents with temperature has an enthalpic origin, but not Arrhenian in nature. The dependence of apparent activation energies, $\left\langle E_a^{(M)} \right\rangle$, with alkyl chain length, M, offers, consequently, a possible alternative to parameterize FV effects. $\left\langle E_a^{(M)} \right\rangle$ values calculated from **Figure V-25** are plotted against $\ln M$ in **Figure V-26**. Reliable estimates were derived by considering only probes, whose diffusion coefficients have been measured at three temperatures at least. It is, however, important noticing that temperature ranges varied between solutes belonging to the same series, so that the

correlations between $\left\langle E_a^{(M)} \right\rangle$ and $\ln M$ are not plotted for the temperature range $[T_1, T_2]$. In particular, temperature ranges were strongly disconnected between the smallest and the largest probes in PS (***Table IV-5***). As a whole, good correlations with $\ln M$ were observed for all polymers except for PS, where slopes looked randomly positive or negative.

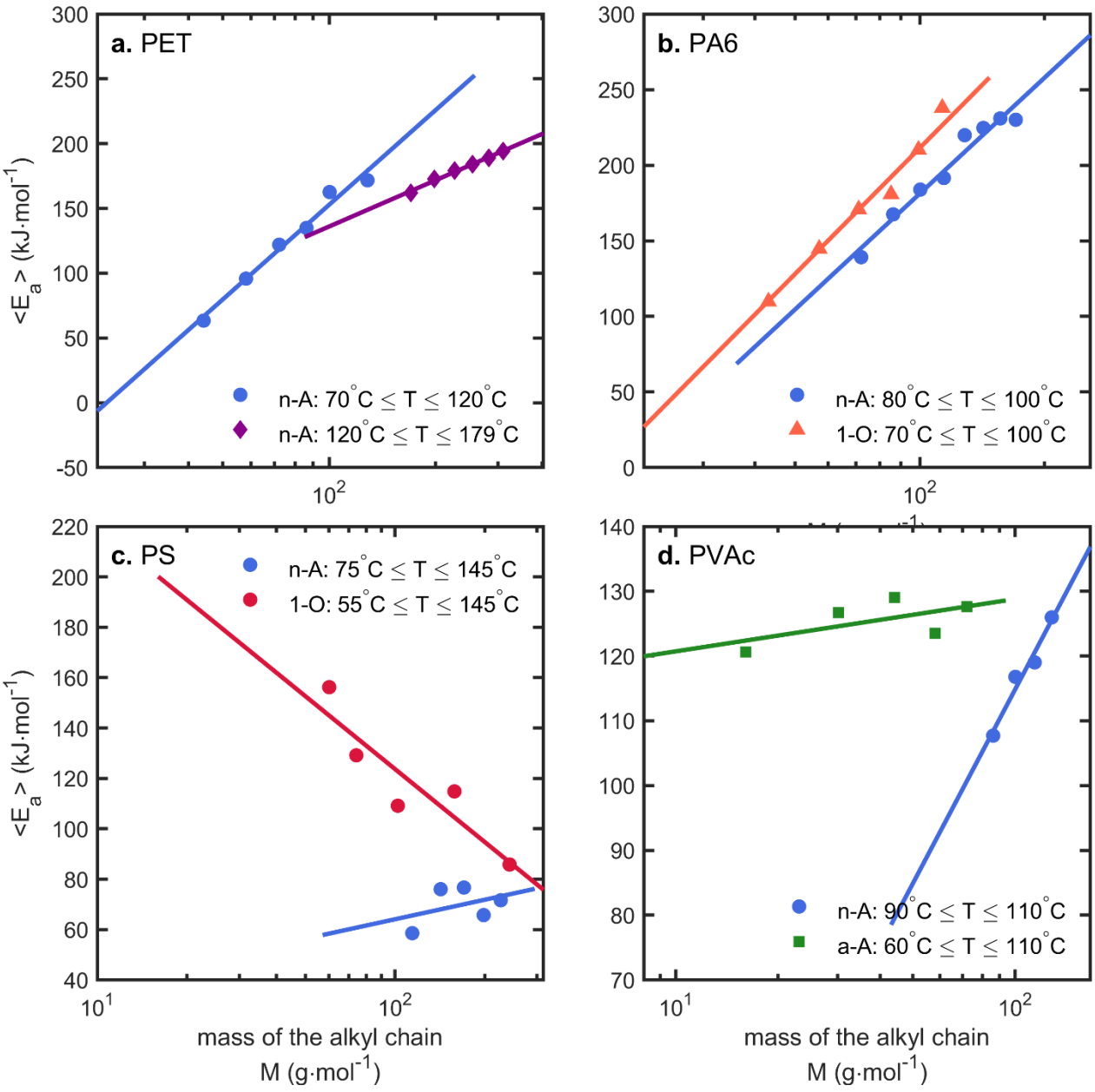

Figure V-26. *Apparent activation energies* $\langle E_a \rangle$ *of linear solutes in function of the alkyl chain mass,* M *, in: (a) PET, (b) PA6, (c) PS and (d) PVAc. Data sets were split according to the considered families of molecular probes (n-A: n-alkanes, 1-O: 1-alchols and a-A: alkyl acetates) and according to the temperature ranges used for the determination of* $\langle E_a \rangle$*. The linear regressions* $\langle E_a \rangle$ *vs* $\ln M$ *are plotted as continuous lines (see Eqs.* (V.29) *and* (V.31)*).*

Consistent interpretations were inferred by normalizing the non-Arrhenian contribution (free volume) with the dimensionless temperature $\langle I \rangle$ (defined in Eq. (V.28)) and proper estimation of K_β. The best fit of Eq. (V.27) yielded a value for K_β of 56±3 K, which was close to the "universal" WLF constant C_{22} =51.6 K. The normalized variations of $\langle E_a \rangle$ with M are expressed in **Figure V-27** respectively to an alkyl chain commensurable to $CH_3(C_5H_{10})$ (M_{ref} =85.2 g·mol^{-1}). The values are $\langle E_a(M) \rangle / \langle I \rangle$ plotted against $\ln M$ are distributed against two straight lines: one with a slope of 4.55 kJ·mol^{-1} ± 0.42 kJ·mol^{-1} and another one with a slope near zero: 0.036 kJ·mol^{-1} ± 0.318 kJ·mol^{-1}. They bounded the two extreme diffusive behaviors whether the activation of diffusion increases with the length of the alkyl chain or not.

The linearity of $\langle E_a(M) \rangle / \langle I \rangle$ with $\ln M$ was predicted for regular solutes (no anchor) in rubber polymers by Eq. (V.27), with a slope equals to RK_α. The estimated K_α value of 547 K ± 50 K was found close to the one reported in §2.2 of Zhu *et al.* (2019c) by direct comparison with the original FVT. The method cannot, however, be considered accurate, since data with very variable qualities and originating from different polymers were mixed. For PET alone, a similar crude approach gave K_α values ranging from 345 K to 420 K, depending on the value of the cooling ratio r chosen for the summation of $\langle I \rangle$ (see Eq. (V.28)). For PA6, the likely value of K_α lied between 158 K and 169 K, and was very close to the value found for PVAc: 160 ± 2 K. The data of PS were not exploitable by this method. Additionally, an empirical correlation was found between all estimates of K_α and K_β : $K_\alpha \approx -42 + 11.46 K_\beta$, demonstrating that both quantities could not be determined independently (for justification, see Eq. **(V.41)**). The apparent activation energy associated to a single blob, $\langle E_a(M_{blob}) \rangle$, was estimated between 12 and 26 kJ·mol^{-1} in PET, between 9 and 12 kJ·mol^{-1} in PA6 and finally between 8 and 12 kJ·mol^{-1} in PVAc.

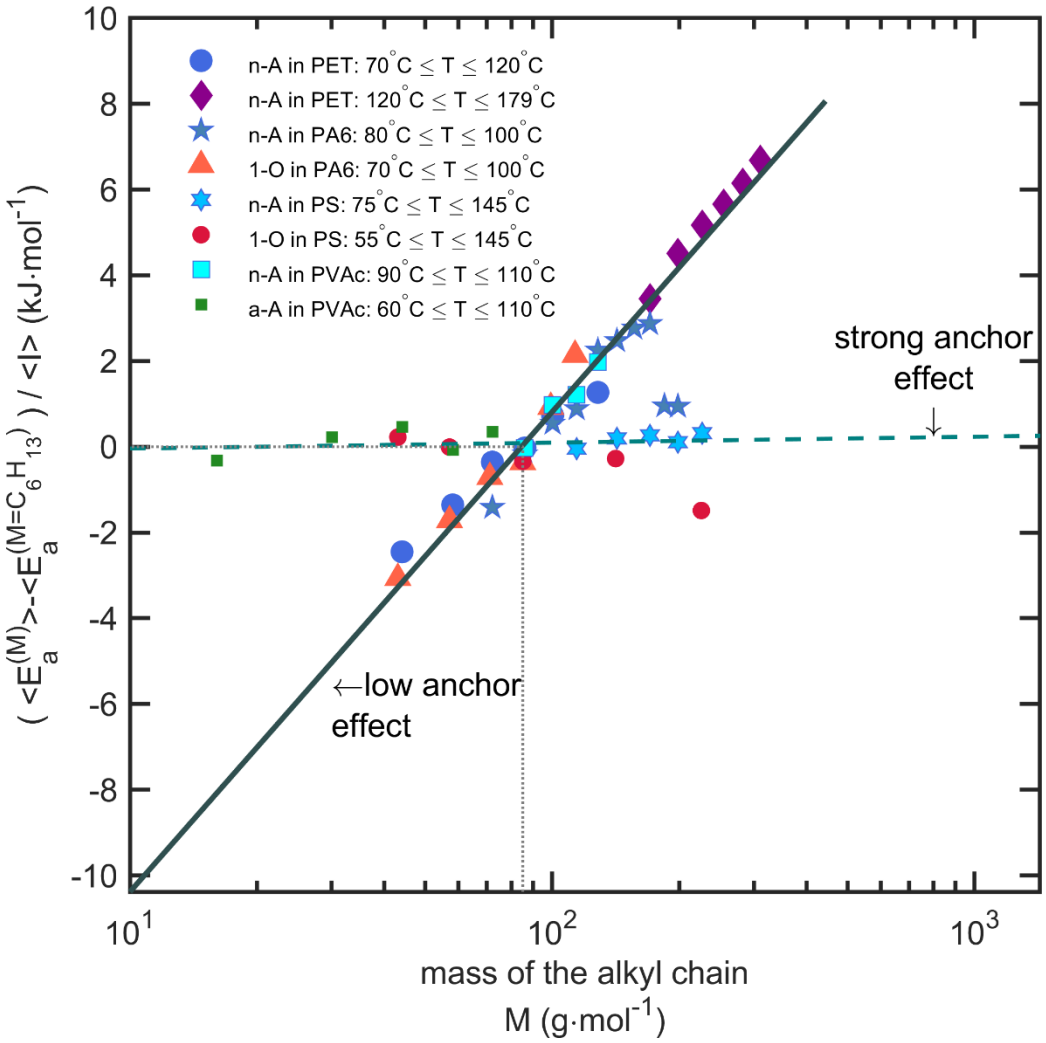

Figure V-27. *Normalized activation energies (see Eq.* (V.29)*) when free volume effects are normalized by the dimensionless temperature* $\langle I \rangle$ *defined in Eq.*(V.28)*. All values are expressed in excess to a theoretical hexyl chain (*C_6H_{13}*). Regression lines with* $\ln M$ *are plotted as continuous and dashed lines, for probes with low and high anchor effects, respectively.*

The apparent activation energies of anchored solutes near or below T_g tended to be, conversely, independent of the alkyl chain length. In other words, the activation energy of individual blobs $\langle E_a(M_{blob}) \rangle$ was overcome by the energy barrier associated with the translation of the anchor itself, E_a^{anchor}. The dominating role of E_a^{anchor} over main chain effects was shown have mainly an enthalpic nature, that is independent of $T - T_g$ and of the value of r at glassy state. The substantial barrier brought by the anchor in aromatic polymers at glassy state was interpreted as specific anchor-polymer interactions involving weak hydrogen-bonding or π - π interactions (see: **Figure V-25** and Figures S1 and S2 in the Supporting Information in (see: Figure V.25 and Figures S1 and S2 in the Supporting Information in Zhu *et al.*, 2019c).

V.4.3.4. Scaling exponents for linear probes

For sufficiently large linear probes and sufficiently close to T_g , FV effects are thought to dominate over all enthalpic contributions and scaling exponents respectively to M are expected to follow Eq. (V.22). **Figure V-28** compares the estimates of α_{lin} vs. $T - T_g$, when their values are inferred from either regular solutes or anchored ones. Fang *et al.* (2013) have suggested that the temperature dependence of α_{lin} could be polymer independent and would be affected only by the size of the repeated blob. The new values of α_{lin} cover a broader spectrum of polymers and are estimated for both regular (aliphatic) and irregular (anchored) solutes. Values from regular solutes were identified from two strategies: i) regression of $\ln D_{lin}$ vs. $\ln M$ at constant temperature (denoted method 1; see **Figure V-25** and Eq. (V.19)) and ii) regression of $\langle E_a \rangle$ vs. $\ln M$ (denoted method 2; see **Figure V-26** and Eq. (V.29)). Method 1 gives the proper scaling exponents directly, whereas method 2 proceeds reversely and requires a prior determination of K_α and K_β with the help of Eqs (V.27) and (V.28). Since α_{lin} values are finally estimated from Eq. (V.22), method 2 provides smoother results with temperature. Method 1 is, nevertheless, thought to be globally more robust and accurate, because it applies to isothermal diffusivities. For irregular solutes, only method 1 was applicable ($\ln D_a$ vs $\ln\left(M + M_{anchor}\right)$) along with Eq. (V.34) to correct the effect of the anchor on the displacement of CM. With an assumption of universal temperature dependence of scaling exponents, Eq. (V.22) was fitted to scaling exponents irrespectively the considered polymers, but independently for regular and irregular solutes. At glassy state, an indicative r value could be extracted. It was used to extrapolate the continuous models of α_{lin} below T_g.

All estimates were noisy, but they were highly consistent when *n*-alkanes were used as molecular probes. Methods 1 and 2 gave similar results. Noticeable differences were observed only when the number of data in the regression was too low. In PET, the datasets at the highest temperatures – including only two solutes (*n*-propane and *n*-butane) – each underestimated the real mass dependence (see **Figure V-25**a). Only α_{lin} values based on a minimum of three values were considered in the global fitting procedure. The following global parameters were obtained for aliphatic probes: $K_\alpha = 199 \pm 11\,\mathrm{K}$ and $K_\beta = 49 \pm 3\,\mathrm{K}$ with $r = 0.39 \pm 0.02$ at glassy state. They were in excellent agreement with the values already identified in linear polymers with linear probes (Fang *et al.*, 2013) : $K_\alpha = 144\,\mathrm{K}$ and $K_\beta = 40\,\mathrm{K}$. As a result, the new values are proposed as a reasonable refinement for aromatic and semi-aromatic polymers probed by *n*-alkanes. The loss of mass dependence with temperature and plasticizing (T_g shift)

is universal in homopolymers (Fang and Vitrac, 2017) and it has been recently shown to be also true in block copolymers (Janes *et al.*, 2017).

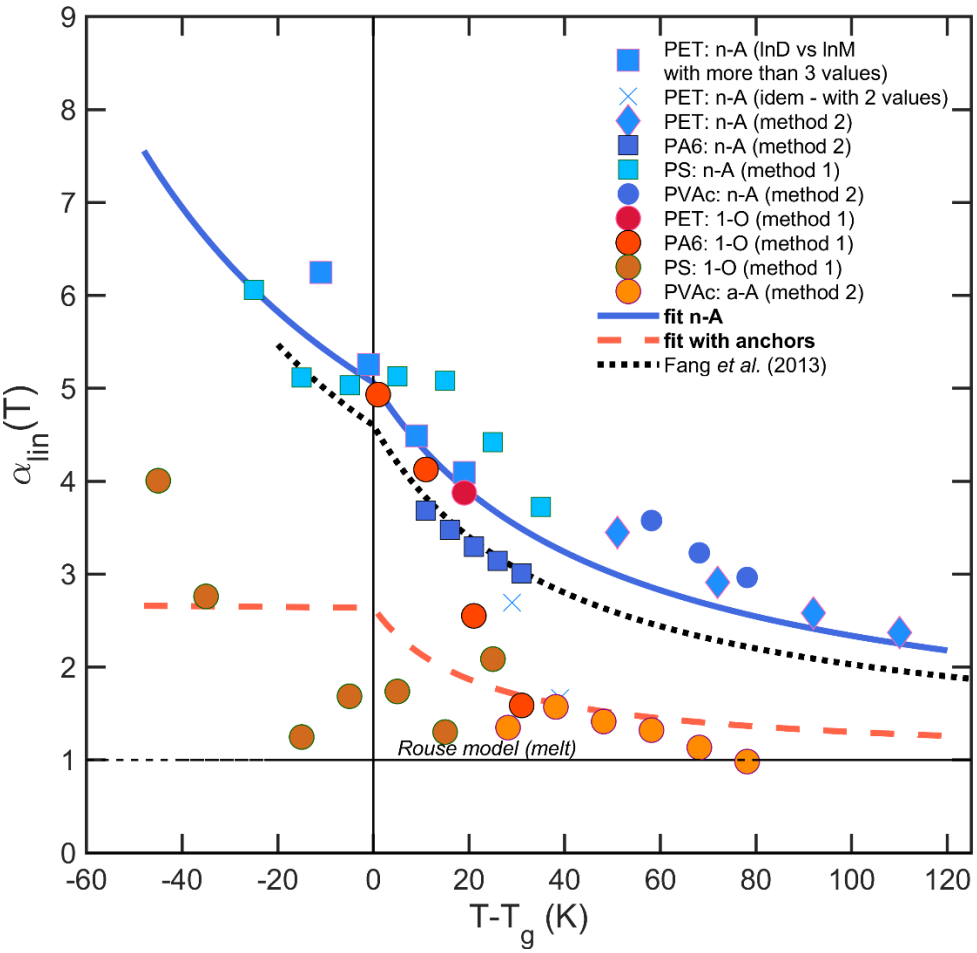

Figure V-28. *Variation of $\alpha_{lin}(T)$ with $T-T_g$ when it is estimated from regular linear probes (blob model) and equivalent anchored solutes. Symbols correspond to determinations according to method 1 (scaling of D_{lin} or D_a with M ; see* ***Figure V-25*** *and Eq.*(V.19)*) or according to method 2 (regression of $\langle E_a \rangle$ with $\ln M$; see* ***Figure V-26*** *and Eq.*(V.29)*). The continuous model (*(V.22)*) is plotted as continuous lines for different estimates of K_α, K_β and r for both regular solutes and anchored ones (see text for values).*

Apart from of 1-alcohols close to T_g (PA6 data), scaling exponents of anchored series appeared significantly below the master curve of regular solutes and was even closer to unity. The global fit for anchored solutes underestimated both K_α and K_β values consequently, with rough guesses of 37 ± 6 K and 22 ± 8 K, respectively. The ratio r was estimated close to 0 at glassy state as a significant increase of scaling exponents could be detected below T_g. The lack of sensitivity to the mass of the alkyl chain (M) offered by anchored probes is captured by Eq. (V.40) and is consistent with the review of apparent activation energies presented in **Figure**

V-27. In details, *n*-alkyl acetates with mass ratios M/M_{anchor} ranging from 0.25 and 2.5 were thought to be too short to dissipate electrostatic interactions in PVAc. By contrast, longer 1-alcohols ($2.5 \leq M / M_{anchor} \leq 6.6$) exhibited a more complex behavior, which was interpreted as a variable strength of OH-π hydrogen bonds in PS between rubber and glassy states. Values of $\left\langle E_a^{anchor} \right\rangle$ were estimated roughly from the difference between the behavior of regular and irregular solutes in the same polymer via Eq. (V.40). The estimates at rubber state are ranging between 20 and 70 kJ·mol^{-1} in PS, and between 15 and 30 kJ·mol^{-1} in PVAc. Such interactions less weak than usually thought have been discussed in (Gierszal *et al.*, 2011;Sasaki *et al.*, 2013;Feng *et al.*, 2016). For comparison, the extrapolation of data of Figure 1 in Meyer *et al.* (1980) to an equivalent number of five carbons gives a magnitude order of 35 kJ·mol^{-1}, which is also comparable to the rough estimate of $\left\langle E_a^{anchor} \right\rangle$.

V.4.4. $P(T,T_g)$ and reliable estimates of K_α and K_β

Figure V-28 and Eq. (V.23) suggest that a single relationship $P(T,T_g)$ could exist, since a single scaling law $\alpha_{lin}\left(T,T_g\right)$ could relate approximately all scaling exponents of regular solutes in homopolymers, regardless of their chemical structure (aliphatic, aromatic or semi-aromatic). However, conversely to $\alpha_{lin}\left(T,T_g\right)$, $P(T,T_g)$ cannot be considered invariant with $T-T_g$, because $\tilde{V}_2^*\left(T_g\right)=u+vT_g$ is not. Additionally, the identification of K_α and K_β values respectively to different polymers and their global comparison are particularly challenging. Complications arise both from the interpretation of measurements and from the impalpable nature of hole free volumes controlling diffusion. On the one hand, apparent activation energies and averaged scaling might hide tenuous non-linear effects and might fade detailed mechanisms of translation (see Eqs. (V.29), (V.35) and (V.38)). On the other hand, the proposed mean-field approach is only indirect as it studies the consequences of free volumes (FV) and not FV themselves.

In this study, the real nature of the holes used for solute translation is assessed macroscopically via the scaling exponents $\alpha_{lin}\left(T,T_g\right)$ and their dependence on temperature. Comparatively to alternative theories centered on the polymer, hole FV are probed on the release dynamics of blobs. As shown in Fang *et al.* (2013), near T_g one blob (rigid unit) or more is trapped at any time, due to an insufficient renewal of hole free volumes commensurable to rigid units. The value of the scaling exponent characterizes the strength of the covariances

between all blob displacements. It can be demonstrated that the diffusion of a collection of N identical blobs, associated to an isolated blob diffusion coefficient, D_{blob} , scales as $\frac{D_{blob}}{N}$ ($\alpha_{lin}=1$), only if the displacements of all blobs are independent (*i.e.* blobs are chosen randomly with replacement). On the opposite, when the blobs along the main chain are blocked successively after their translations (no replacement), their displacements are dependent and are associated with a negative covariance $-\frac{D_{blob}}{N-1}$. When the translation of CM involves $1 \le n \le N$ constrained blobs (no replacement) and $N-n$ blobs, which can displace freely (replacement), the composition of variances yields a diffusion coefficient scaling as: $\frac{1}{N^2}\left(N-\frac{n(n-1)}{N-1}\right)D_{blob}$. When n is approaching N in a dense medium, diffusion coefficients tend to 0 and α_{lin} diverges rapidly. This behavior dominates in regular solutes because all blobs are equivalent. Leaving one single blob moving freely ($n=N-1$) gives $\alpha_{lin}=2$. The transition from $\alpha_{lin}=1$ up to $\alpha_{lin}=2$ is roughly observed with anchored solutes when the temperature is decreased below T_g (see **Figure V-28**). It would correspond to the transition from independent blob displacements respectively to the anchor (n=0) to a mechanism where all blobs appear frozen except the one connected to the anchor. As the proposed interpretation takes the point of view of the alkyl chain connected to the anchor, this particular blob triggers the translation of CM in the hydrodynamic regime.

The choice of solute dynamics to probe hole free volume (hFV) contrasts with other alternatives such as polymer cell theories, which considers the whole hole fraction (Simha and Somcynsky, 1969) and its dependence with temperature (Tseng, 1946). We propose, instead, to capture hFV effects through constants K_α and K_β specifically adjusted to the diffusion behavior of linear homologous solutes in each considered polymer at equilibrium. Scaling exponents and apparent activation energies used to infer K_α and K_β cannot, however, be considered as error-free regressors. As a result, the uncertainties in K_α and K_β estimates are strongly dependent upon the quality of D values. For example, narrowing the range of α_{lin} values induces significant correlations between K_α and K_β estimates. From data collected at rubber state, the correlation reads:

$$\begin{aligned} K_\alpha &= K_\alpha^0 + \left(\left\langle \alpha_{lin}^{(T,T_g)} \right\rangle - 1 \right) \Delta k \\ K_\beta &= K_\beta^0 + \Delta k \end{aligned} \tag{V.41}$$

where $\left\langle \alpha_{lin}^{(T,T_g)} \right\rangle$ is the averaged scaling exponent, $\left(K_\alpha^0, K_\beta^0 \right)$ is an acceptable couple of values (e.g. solution with minimum norm) and Δk is an arbitrary real number. Data at glassy state complicate the identification by adding a aturedegree of freedom, r. As a rule of thumb, better estimates are inferred from isothermal scaling exponents as they are independent of enthalpic contributions, E_a^{anchor} and E^*. Despite the various limitations, it is thought that the polymer function $P(T,T_g)$ remains identifiable as it is directly related to the scaling exponent $\alpha_{lin}\left(T,T_g\right)$ via Eq. (V.20).

The identified values of K_α and K_β as well as their uncertainties are reported in **Table V-2** for all tested polymers. The corresponding values of $P(T,T_g)$ calculated from Eq. (V.20) are plotted in **Figure V-29** and compared with those estimated from Eq. (V.15) with specific WLF constants when they have been reported in the literature and universal ones otherwise. Values at glassy state are reported only for three typical subcooling ratios r =0.1, 0.25 and 0.5. The possibility to derive a unique polymer function $P(T,T_g)$ for the same polymer family (e.g. for aromatic and semi-aromatic polyesters) is tested by comparing the values of PET with those of PEN. Estimates from linear aliphatic probes were in good agreement with WLF predictions only in aliphatic polymers (PVAc and PA6). Deviations were strongly negative in aromatic polymers and all the higher than T_g was higher. The two behaviors would suggest different definitions of free volumes according to the polymer jumping units are larger or not than the ethyl group (blob) used to probe free volumes.

***Table V-2**. Main parameters used to predict diffusion coefficients, and free volume effects plotted in Figures 5-7.*

	PET	PA6	PS	PVAc	PEN
T_g (K)	354	342	373	305	397
T range (K)	343-452	343-373	328-418	333-393	373-413
r when $T < T_g$ (-)	0.32±0.03[a]	0.32±0.03[a]	1[b]	n.d.	0.32±0.03[a]
K_α (K)	181	77 (*n*-alkanes) 171 (1-alcohols)	112	142	117
K_β (K)	47	8 (*n*-alkanes) 41 (1-alcohols)	90	20 (*n*-alkanes) 15 (alkyl acetates)	44
(C_{12}) (-)	n.d.	17.4[c]	13.78[d]	15.59[d]	n.d.
(C_{22}) (K)	n.d	51.6 [c]	46[d]	46.8[d]	n.d
M_{blob} (g·mol^{-1})	28[e]				
$\tilde{V}_1^*(M_{blob})$ (cm^3·g^{-1})	39[f]				
$D_0(M_{blob})$ (m^2·s^{-1})	1.55·10^{-8} [g]				
β_{lin}	1				
u	-86.5				
v	0.6224				
$E^*(M_{blob})$ (kJ·mol^{-1})	17	15 (n-alkanes) 13 (1-alcohols)	0	0	28
M_{anchor} (g·mol^{-1})	17 for 1-alcohols [h] 59 for alkyl-acetates [i]				
E_a^{anchor} when $T \geq T_g$ (kJ·mol^{-1})	36 ± 3 (1-alcohols)	0	<1 (1-alcohols)	~0 (alkyl acetates)	27 ± 4 (1-alcohols)
E_a^{anchor} when $T < T_g$ (kJ·mol^{-1})	n.d.	0	37 ± 5 (1-alcohols)	n.d.	0

n.d. not determined

[a] likely guess for the considered polymers (similar results when the parameter is fit globally or independently).

[b] value assigned by default (data at glassy state are particularly noisy)

[c] Broudin *et al.* (2015)

[d] Table 3 in Zielinski and Duda (1992)

[e] by assuming that the blob matches -CH_2-CH_2-

[f] from the linear regression of $\tilde{V}_1^*(M)$ with *M* for *n*-alkanes as reported in Table 4 of Hong (1995)

[g] from the linear regression of $lnD_{01}$with *M* for *n*-alkanes as reported in Table 4 of Hong (1995)

[h] by assuming that the anchor corresponds to a hydroxy functional group HO-

[i] by assuming that the pattern matches the acetate functional group CH3COO-

According to Eq. (V.25), a rigid solute with a bulky jumping unit of volume would require larger hole free volumes than smaller solutes and would have, consequently, a higher probability of translation in aromatic polymers, with also large jumping units, than in aliphatic ones with a similar T_g. Substituting *n*-alkanes as molecular probes by anchored solutes did not change the trend, but provided poorer estimates of $P(T,T_g)$ due to the additional uncertainty brought by E_a^{anchor} in PS and PVAc. The deviation between linear and aromatic polymers is not linear with $T-T_g$. It reaches about -115 K, -85 K and -45 K for PS, PEN, and PET, respectively. A similar deviation, but in the opposite direction, was observed in Fang *et al.* (2013) when linear aromatic solutes in aliphatic polymers were compared with linear aliphatic solutes in aliphatic polymers; the shift in K_β value reached +91 K. Since scaling exponents larger than unity are associated to a random blocking of rigid blobs, aromatic polymer segments fail to trap solutes as efficiently as small blobs for the same value of $T-T_g$. On the opposite, large blobs are hindered more efficiently by small blob segments. When solute and polymer blobs are perfectly exchangeable (polymer and solutes considered as pure random coils), no blocking can occur whatever the applied density and the scaling exponent remains unitary, as shown in coarse-grained simulations (Durand *et al.*, 2010). WLF constants (universal or specific) capture only the situation, where the role of solute and polymer blobs are symmetric. In this case, the same kind of hole free volumes participates to the translation of all blobs. It is not the case when the blobs are dissimilar; holes controlling polymer relaxation and T_g are different from those enabling solute blob displacements. At this stage, the consistency of free volume definitions to predict diffusion coefficients needs to be challenged according to predictions are required for solutes similar or not to the ones used to probe them.

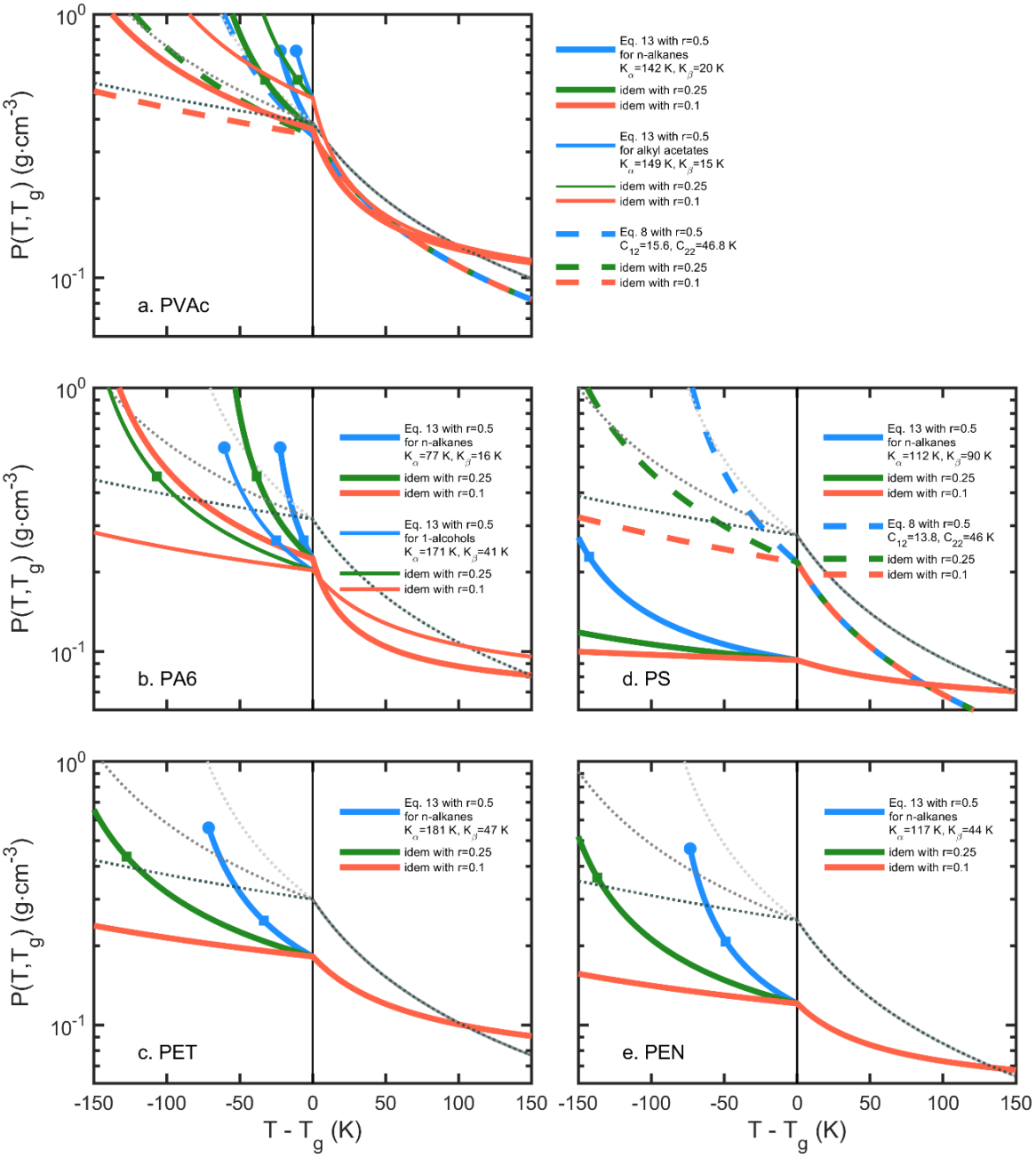

Figure V-29. *Polymer function* $P\left(T,T_g\right)$ *versus* $T-T_g$ *predicted by Eq.* (V.20)*(continuous lines) and by Eq.*(V.15) *using either specific (dashed lines) or generic (dotted lines) WLF constants. The corresponding FV parameters are listed in* ***Table V-2****. All models are plotted for three typical* r *values at glassy state (0.5, 0.25 and 0.1) leading to three branches when* $T-T_g$ *<0. As constant thermal expansion is assumed at rubber and glassy states, the diagrams are limited by the inequalities:* $T-T_g>\frac{1}{r}\left(\frac{K_\alpha}{\alpha\left(T,T_g\right)-1}-K_\beta\right)$ *and* $\alpha_{lin}\left(T,T_g\right)\geq 1$ *. The square and round symbols depict the* $P\left(T,T_g\right)$ *values corresponding to* $\alpha_{lin}=4$ *and* $\alpha_{lin}=9$*, respectively.*

V.4.5. Prediction of diffusion coefficients

V.4.5.1. Flexible and linear solutes in various polymers

Scaling relationship introduced in FVT enables the direct estimation of diffusion coefficients for any linear solutes from Eq. (V.30) in homopolymers either they resemble polymer segments (oligomers) or not (e.g. mineral oils in aromatic polymers). Eq. (V.39) generalizes it for anchored solutes. For alkyl chains, the necessary solute constants $\tilde{V}_1^*\left(M_{blob}\right)$ and $D_0\left(M_{blob}\right)$ are reported in **Table V-2** along with polymer constants K_α and K_β. $D_0\left(M_{blob}\right)$ was estimated from the scaling of *n*-alkanes in Table 4 of Hong (1995). K_α and K_β were inferred from experimental $\alpha_{lin}\left(T,T_g\right)$ values.

Predicted values for *n*-alkanes are shown in **Figure V-30** and values 1-alcohols, and 1-alkyl acetates are analyzed separately in **Figure V-31**. Continuous predictions and experimental diffusivities are plotted on a semi-log scale versus the FV term: $\left[r(T)\left(T-T_g\right)+K_\beta\right]^{-1}$ for a likely value $r=0.32$ (applied to all polymers) when $T<T_g$ and $r=1$ otherwise. Only energy barriers E^* and E_a^{anchor} were adjusted directly to experimental diffusivities. Due to inherent collinearities between FV and barrier effects, the following parsimony principle was introduced: an energy barrier was introduced only if a strong temperature dependence was noticeable far above T_g, when FV effects dissipate. Additionally, the values E^*, K_α and K_β were expected to be constant between regular and their irregular (anchored) counterparts. All identified parameters are reported in **Table V-2** with energy barriers ranged between 0 and 36 kJ·mol^{-1}. Only the estimations from PA6 data could not fulfill all rules. Significantly different K_α and K_β values were obtained between regular and irregular solutes. The situation was particular and was associated with a possible underestimation of K_α in correlation with an overestimation of E^* (see Eq. (V.30)).

All trends were reproduced without additional fitting for all polymers and chain lengths. The slopes are controlled by the values of K_α with all lines converging approximately to a same preexponential factor at high temperatures. The energy barriers of the alkyl blob, E^*, and of the anchor, E_a^{anchor} controlled the deviation to linearity. The effects were maximal for *n*-alkanes in PA6 and alcohols in polyesters (PET or PEN). The results confirmed that energy barriers are not entirely independent of the polymer. They are higher for polar solutes in polar polymers and lower diffusion coefficients for similar $T-T_g$ value. The current theory is,

however, too coarse to explicit the relationship between the interactions and the mechanism of translation, but it demonstrates that energy barriers apply independently on each blob and the anchor, and not on the entire molecule as previously stated in the original FVT.

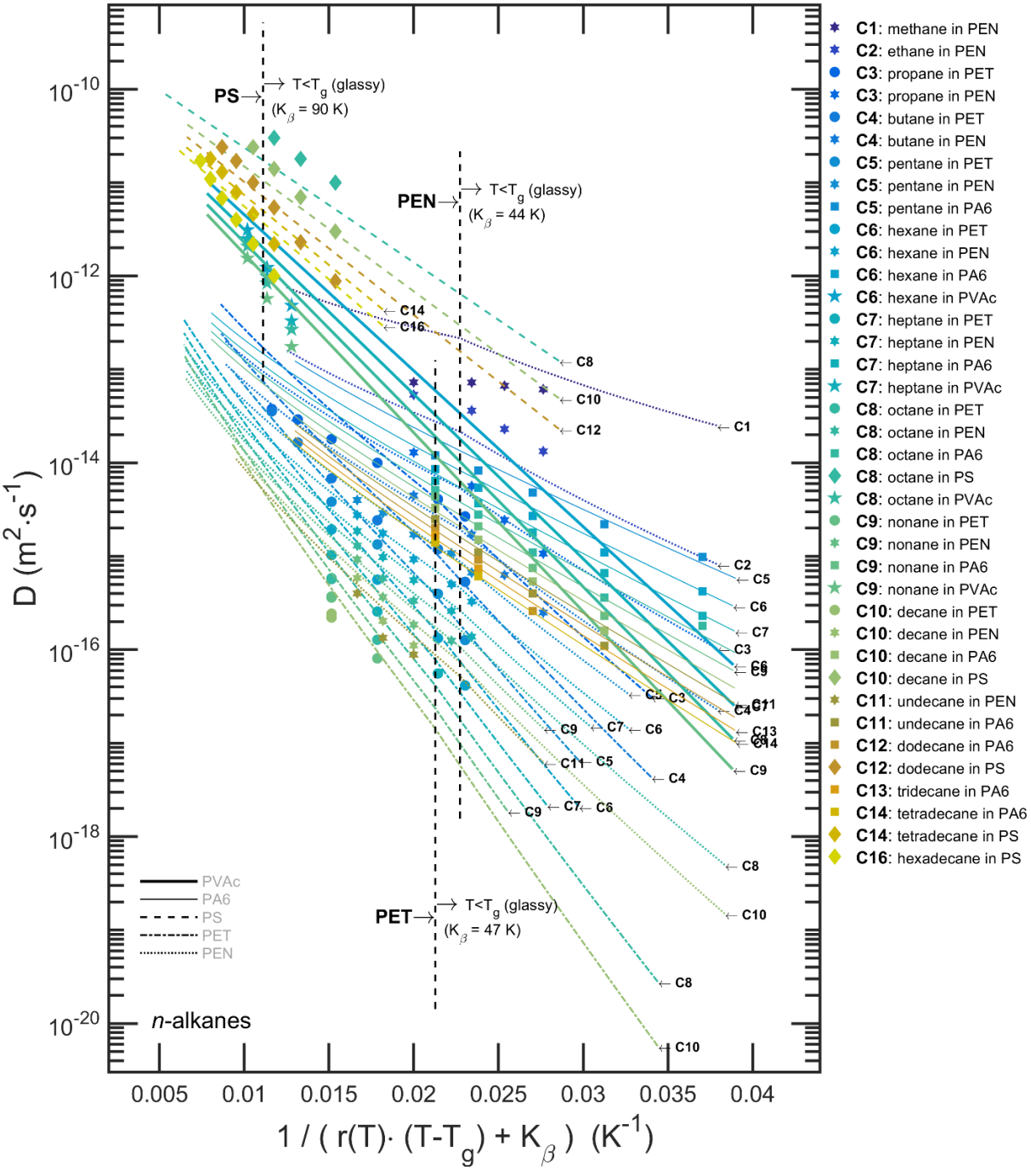

Figure V-30. *Experimental (symbols) and predicted (lines) diffusion coefficients via Eq.* (V.30)*and parameters listed in* ***Table V-2*** *for n-alkanes in PVAc (bold continuous lines), PA6 (continuous lines), PET (dashed-dotted lines), PS (dashed lines) and PEN (dotted lines). The dashed vertical line represents the* T_g *value of the polymer for the corresponding set of data. The predictions assume the inequality:* $T - T_g > \frac{1}{r}\left(\frac{K_\alpha}{\alpha_{(T,T_g)}^{-1}} - K_\beta\right)$. T_g *values of PVAc and PA6 are out of bounds.*

All rigid blobs are blocked independently with a strength depending on blob size and the type of interactions with the polymer. Steric and enthalpic effects can combine in a non-trivial manner as shown in the Supporting Information in Zhu *et al.* (2019c) (see Eq. (S2)) with apparent activation energies up to 140 kJ·mol^{-1} for alkylbenzene (see Fig. S2). In the same vein, weak hydrogen bonding between 1-alcohols and PS appears to slow down diffusion only at glassy state: E_a^{anchor} is non-zero only at glassy state and almost zero at rubber state.

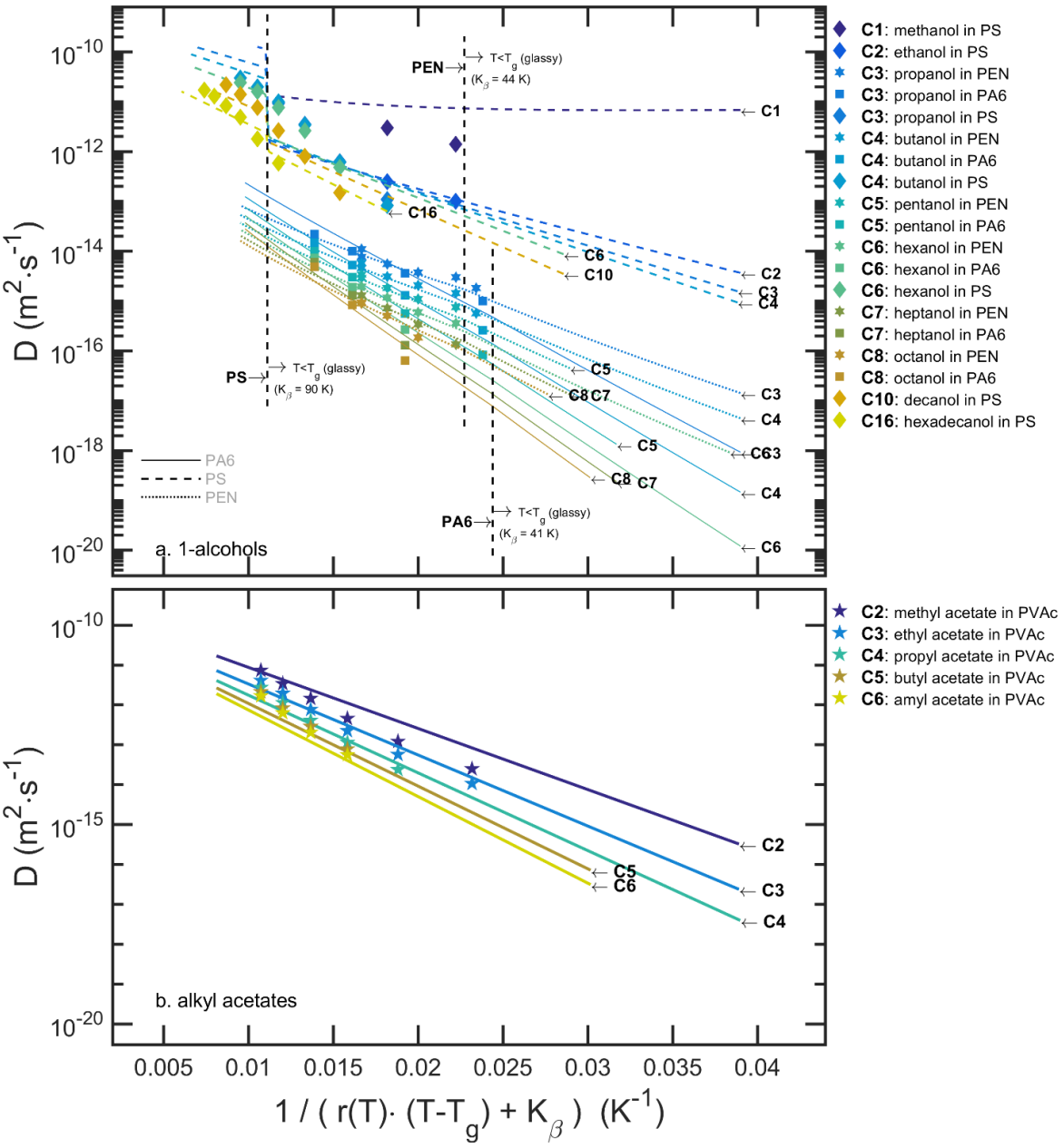

Figure V-31. *Experimental (symbols) and predicted (lines) diffusion coefficients via Eqs.*(V.30) *and* (V.39) *along with parameters in* ***Table* IV-5** *for (a) 1-alcohols and (b) alkyl acetates in PVAc (bold*

continuous lines), PA6 (continuous lines), PS (dashed lines) and PEN (dotted lines). The dashed vertical line represents the T_g value of the polymer for the corresponding set of data; the corresponding. T_g values of PVAc and PA6 are out of bounds.

V.4.5.2. Water and toluene at infinite dilution in PET

Eq. (V.25) connects scaling laws (Vrentas *et al.*, 1989;Griffiths *et al.*, 1998;Fang *et al.*, 2013) of linear and regular probes back to conventional FVT. Because all polymer-related FV parameters are lumped within a simpler function $P\left(T,T_g\right)$, the revised FVT formulation can be applied to polymers irrespectively the availability of FV parameters. Though the current formulation targets solute trace diffusion coefficients (*i.e.* without significant concentration gradient and -at infinite dilution) and analyses only the effects of hFV brought by the polymer alone, it can be prolonged to add the concentration dependence of D and generalized to mutual diffusion coefficients. Such extensions have been already discussed elsewhere (Vrentas and Duda, 1977b, a, c;Duda *et al.*, 1979).

Nevertheless, the ability of FVT to predict diffusion of small penetrants in new polymers has been strongly questioned in both rubbery (Tonge and Gilbert, 2001a) and glassy polymers (Tonge and Gilbert, 2001b). When tested by independent groups, diffusion coefficients were shown to be significantly overestimated and their corresponding activation energies underestimated. Vrentas and Vrentas (2003) argued that the practicality of FVT on new solute-polymer systems depends on the availability of acceptable values for the polymer dependent parameter $\tilde{V}_2^*$ and for the solute dependent ones, E^* and D_0. Linear relationships of $\tilde{V}_2^*$ with T_g (see coefficients u and v in Eq. (V.13)) received the most cogent criticism as they rely on experimental determinations of $\xi = \dfrac{\tilde{V}_1^*}{\tilde{V}_2^*\left(T_g\right)}$ only for small rigid solutes (e.g., carbon dioxide, methane and benzene) and in a minimal set of polymers. The linear correlation initially depicted in Figure 3 of Zielinski and Duda (1992) and updated Hong (1996) (see Figure 5 herein) contains only three polymers with T_g above 295 K. The formulation proposed in this study for arbitrary rigid solutes removes indirectly the influence of poor estimations u and v as their values are used twice: firstly, for the estimation $P(T,T_g)$ for the "unknown" polymer and, secondly, for the estimation of $\tilde{V}_1^*$ based on the value of ξ tabulated in a "well documented" polymer. When the same values of u and v are used for both polymers, their contribution is canceled (see the last approximation in Eq. (V.25)). In this regard, the proposed extension of FVT offers an elegant formulation to remove the most elusive elements of

FVT, while keeping the core concept of hole FV. Lattice FV formulations (see Eq.(23) and Eq.(12) of Costa and Storti, 2010 ;Noorjahan and Choi, 2015b,respectively) and more global correlative approaches (Thornton *et al.*, 2009) do not resolve the issue and still require specific regressions.

We illustrate the capabilities of Eq. (V.25) to estimate D values of two rigid solutes, water, and toluene, in amorphous PET over a broad range of temperatures (from 5 to 180°C) in **Figure V-32**. The two external validation tests are particularly challenging. Water must be regarded as a single jumping unit with specific interactions with PET. In this section and due to the limitations of Eq. (V.25), toluene is also envisioned as a rigid solute, although it is also described as a limit case of a short-anchored solute in the Supplementary Information. The estimated $P\left(T,T_g\right)$ function depicted in **Figure V-29** is used in both cases with a subcooling factor, r , which was set independently in both validation tests. Solute dependent properties, E^* and D_0, were extracted either from the literature or fitted from reference D values. The applied strategy is summarized in **Table V-3**. For toluene, several estimates of D_0 have been proposed in the literature consistently along with an assumption $E^* \approx 0$. We chose the value of D_0 = 1.87·10^{-8} m^2·s^{-1} proposed in Table 4 of Hong (1995) as a test value, but the set E^* = 0 and D_0 = 8.55·10^{-8} m^2·s^{-1}, also reported in the same reference, was considered unacceptable for water in a polyester. D_0 , E^* and r value at glassy state were, therefore, considered as free parameters for water in amorphous PET. They were fitted on the diffusivities reported by Launay *et al.* (1999) over a broad range of temperature crossing T_g . The corresponding continuous model is labeled "*fit*" in **Figure V-32**a and is associated with a value r of 0.34 similar to one reported in Table 2 for PET. External validation was sought by comparing the predictions with independent D values obtained in carefully controlled conditions. Data from the literature were introduced for validation. They were chosen to originate from strictly reversible Fickian sorption kinetics without noticeable swelling or densification. The contribution of polymer relaxation on water diffusion in PET is, indeed, known to be particularly severe, as discussed by Burgess *et al.* (2014a) at glassy state and by Dubelley *et al.* (2017a) over a broader temperature range, from 23°C to 70°C (see Figure 5 herein for a discussion of the combined effects of temperature and relative humidity).

Table V-3. *Main parameters used to predict diffusion coefficients of water and toluene in Figures 8 and 9.*

Parameter / solute	water	toluene
D_0 ($m^2 \cdot s^{-1}$)	[a] $2.94 \cdot 10^{-6}$	[c] $1.87 \cdot 10^{-8}$ [d] $3.03 \cdot 10^{-8}$ [e] 8.09^{-8} [f] $1.04 \cdot 10^{-8}$
E^* ($kJ \cdot mol^{-1}$)	[a] 26.5	0
$\tilde{V_1^*}$ ($cm^3 \cdot g^{-1}$)	[b] 19.3	[b] 84.48
r (-) when $T \leq T_g$	[a] 0.32±0.03	[g] 0.70 (dry PET) [g] 0.28 (swollen PET)

[a] D_0, E^* and r values of water are fitted from D values reported in Launay *et al.* (1999) (see Figure 8a); [b] value from Table 2 in Shapiro *et al.* (2004); [c] value from Hong (1995); [d-f] fitted from diffusivities of [d]PS, [e]mixed polymers (PMMA, PS, PVAc, LDPE) and [f]PET (see **Figure V-33** caption for details), [g]values fitted from diffusivities in dry and swollen PET (see Figure 8b).

The predictions for water were compared successfully with diffusion data from seven independent various sources (see details in **Figure V-32**a caption) collected on PET with crystallinities lower than 6 % (**Figure V-32**a) and a prescribed T_g of 76°C. In this work, the values of $2.94 \cdot 10^{-6}$ $m^2 \cdot s^{-1}$ and of 26.5 $kJ \cdot mol^{-1}$, for D_0 and E^*, respectively, enable to predict the diffusion coefficients of water at all temperatures with a reasonable guess for a subcooling ratio r of 0.34. It is worth noticing that the value $\tilde{V_1^*}$ for water was from Kontogeorgis and Gani (2004) and was not adjusted. The estimated value of E^* is comparable with the sorption energies of water, ca. about 27 $kJ \cdot mol^{-1}$, as reported from sorption experiments (Schmalz and Grundke, 1969;Launay *et al.*, 1999;Eslami and Müller-Plathe, 2009) and grand-canonical molecular dynamics simulations (Eslami and Müller-Plathe, 2009). As the specific energy barrier to diffusion is identical with the one required for water to translate from an absorbed state in the polymer to the gas phase, it is hinted that each water molecule would require the break of all hydrogen bonds created with the polymer before translating to a new sorption site. After the translation, a new set of hydrogen bonds would be created. The infrequent hoping mechanism from one void to the next was captured and confirmed by the molecular dynamic simulations of Eslami and Müller-Plathe (2009) (see Figure 7 herein). The deviation to an Arrhenian behavior is not significant at glassy state and gives an apparent activation energy of 51 ±6 $kJ \cdot mol^{-1}$ (uncertainty is associated to the strength of FV effects considered temperature range), which is close to the value of 47 $kJ \cdot mol^{-1}$ reported in Burgess *et al.* (2014a) As a result, the dominance of electrostatic interactions over FV effects is confirmed at glassy state and a fortiori at rubber state. We attract the attention of the reader to the fact that the proposed FV description assumes that all hole FV are distributed uniformly in PET and equally accessible

to water, which is not necessarily the case when PET swells or in strongly semi-crystalline PET (Billovits and Durning, 1988).

D values of toluene in PET are scarcer in the literature and often biased: water content not equilibrated with the ambiance or possible plasticization by the toluene solution. To enable a direct comparison, two extreme states, so-called "dry" and "swollen" PET are presented. The "dry" state was defined in Eq. (V.25) by using a T_g value of 76°C, whereas the "swollen" state was associated with the lowest T_g value of 60°C reported in Langevin *et al.* (1994). Corresponding subcooling ratios r were adjusted independently on each dataset ("dry" or "swollen"). The details are reported in **Table V-3**. Conventional FV parameters predict diffusivities of toluene at both rubber and glassy states in a satisfactory manner with E^* = 0 (**Figure V-32**b). It is shown, in particular, that D_0 values estimated generically on other polymers hold without impacting predictions whatever the polymer is plasticized or not. The determination of the subcooling ratio r remains critical and cannot be guessed from first principles. Because D is invariant with the product $r \cdot \left(T - T_g\right)$, overestimating T_g leads to a systematic underestimation of r at glassy state. As their errors were strongly correlated, the loss of barrier properties to toluene from dry to swollen PET was connected to a significant decrease of r at glassy state. The estimated r value may be uncertain but not the trend.

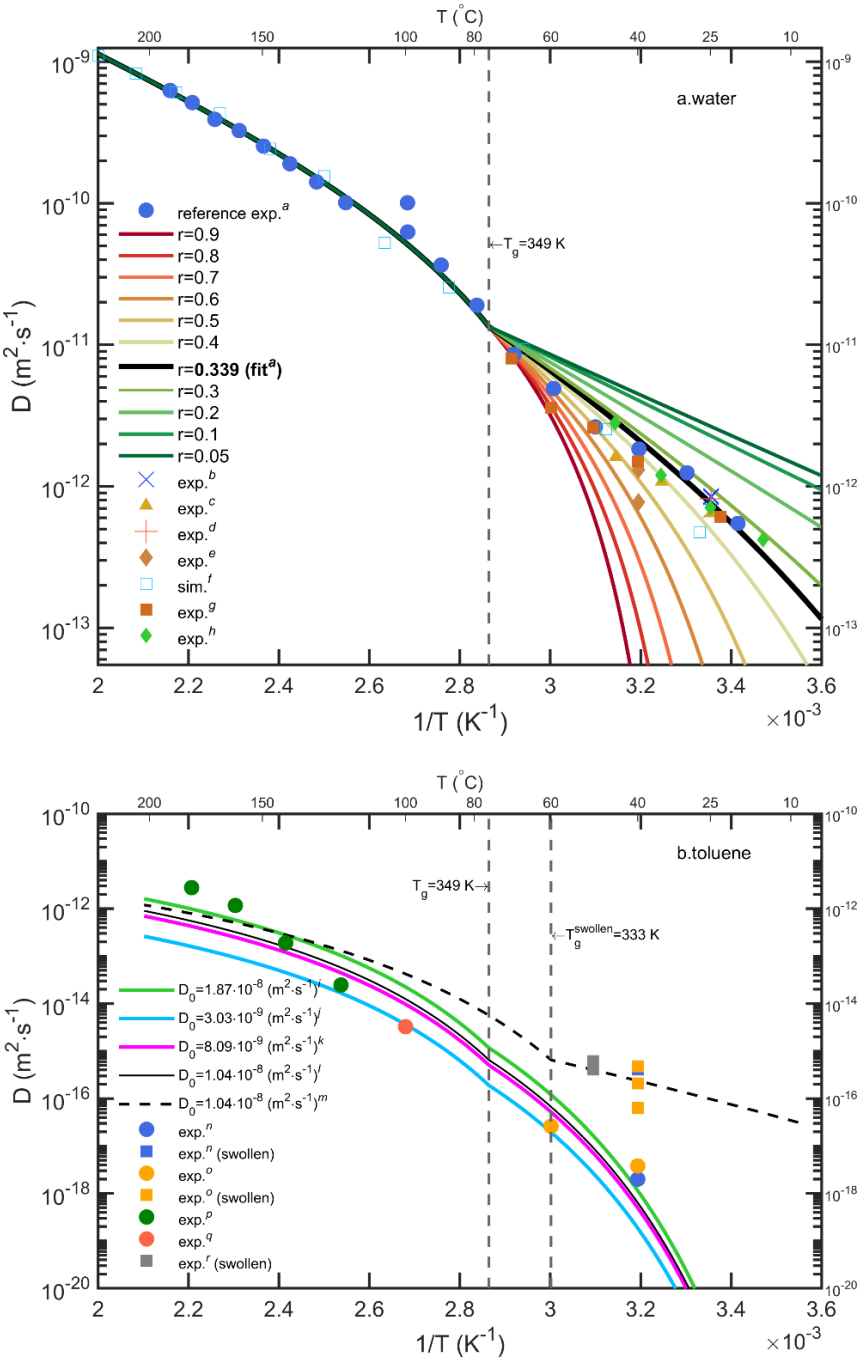

Figure V-32. *Comparison of experimental diffusion coefficients, ("exp", filled symbols), and simulated ones by molecular dynamics ("sim", open symbols) with values predicted from Eq. (V.25) and parameters reported in* ***Table V-3*** *for (a) water and (b) toluene in amorphous PET at infinite dilution of not mentioned otherwise. All calculations are performed with a theoretical* T_g *of 349 K (continuous lines). Swollen PET due to a contact with a liquid or measurements at high solute activities is identified as "swollen" and is associated to an indicative* T_g *of 333 K, value from Langevin et al. (1994) for PET fully swollen with water; corresponding values are plotted as dashed lines.*

[a]reference experimental values of water from Launay *et al.* (1999) (including also the data of (including also the data of Schmalz and Grundke, 1969) and used to estimate D_o, E^*, and r (the identified value of r is noted "*fit*"); [b]Sammon *et al.* (2000); [c]Shigetomi *et al.* (2000); [d]Rueda and Varkalis (1995); [e]Kloppers *et al.* (1993); [f] molecular simulation data from Eslami and Müller-Plathe (2009); [g]Dubelley *et al.* (2017a); [h]Burgess *et al.* (2014b).
D_o value of toluene [i] from Table 4 in Hong (1995); value fitted from diffusion coefficients in [j]PS at rubber state (see **Figure V-33**[b-d]), in [k]mixed polymers at rubber state (see **Figure V-33**[a-d,j,k]), [l,m] from plotted diffusion coefficients in non-swollen PET. Continuous models are plotted for [i-l]r=0.7 (continuous lines) and [m]r=0.28 (dashed lines).

[n]Franz and Welle (2008); [o]Pennarun *et al.* (2004); [p]Ewender and Welle (2013, 2018a); [q]this work measured from lag-times during permeation experiments; [r]this work measured by gravimetric sorption with activity close to unity.

Substantial complications deserve additionally to be noticed in polymers far from equilibrium: i) gravimetric measurements on swollen PET at glassy state (Pennarun *et al.*, 2004;Franz and Welle, 2008) demonstrated that polymer relaxation could overcome concentration gradients effects on sorption kinetics, as described in Chandra and Koros (2009a, 2009b); ii) diffusion coefficients obtained in sorption and desorption experiments may differ significantly (Burgess *et al.*, 2014a). A FV extension has been proposed by Wang *et al.* (2000) to overcome some of the previous complications, but its integration in the presented FVT for flexible and rigid solutes would require a special treatment beyond of the initial scope of this study.

The conclusions drawn in this study from the comparison of the diffusion behaviors of water (with specific intermolecular interactions) and toluene (without intermolecular interactions) in a polar polymer (PET) are very similar to those reached by comparing the mechanisms of diffusion of water and benzene in poly(vinyl alcohol) in molecular dynamics simulations (Noorjahan and Choi, 2015a). Additional blind validations of Eq. (V.25) and its parameterization from **Table V-2** and **Table V-3** are proposed in **Figure V-33** by comparing the D predictions for toluene in all tested polymers with a neutral subcooling ratio of 0.5. Reference D values at infinite dilution were extracted from various sources (Zielinski and Duda, 1992;Vrentas and Vrentas, 1994b;Lutzow *et al.*, 1999;Pennarun *et al.*, 2004;Franz and Welle, 2008;Ewender and Welle, 2013, 2018a) and were extrapolated from higher solute concentrations down to 0 when necessary. Without fitting, the predictions were commensurable to experimental errors in the whole range of tested values from $2{\cdot}10^{-18}$ to $3{\cdot}10^{-11}$ $m^2{\cdot}s^{-1}$. It is remarkable that the polymer function $P\left(T,T_g\right)$ probed with *n*-alkanes applies to the diffusion of aromatic solutes irrespectively to the considered polymer and temperature range. The same conclusion was also achieved with water and confirms the reliability of Eq. (V.25) regardless the chosen values for u and v.

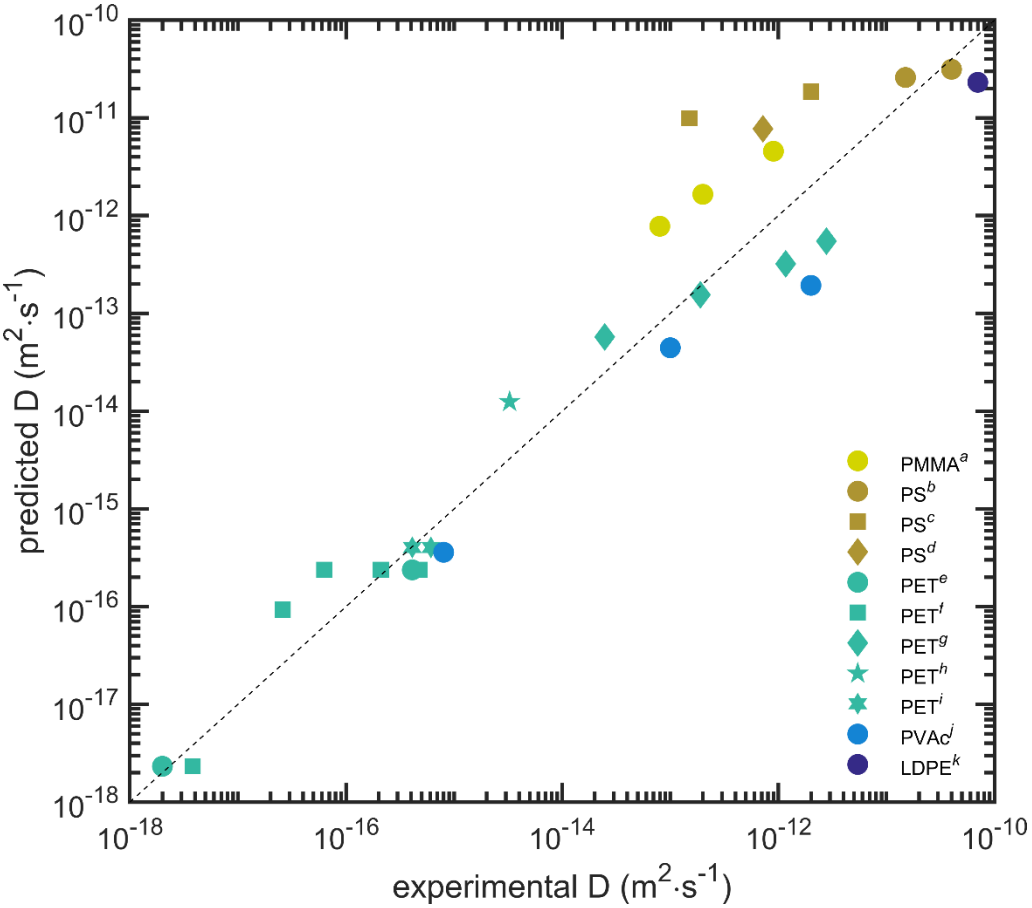

Figure V-33. *Comparison of predicted and experimental diffusion coefficients of toluene at infinite dilution in various polymers.*

[a]*D* values in PMMA at rubber state from Figure 13 of Zielinski and Duda (1992); [b-d]*D* values in PS at rubber state from [b]Figure 7 in Vrentas and Vrentas (1994b), [c]Figure 5 in Zielinski and Duda (1992) and [d]Figure 4 in Pickup and Blum (1989); [e-i]*D* values in PET corresponding to *exp.*[n-r] in **Figure V-32**b; [j]*D* values in PVAc at rubber state from Figure 6 of Zielinski and Duda (1992); [k]*D* value in LDPE from Figure 4 of Lutzow *et al.* (1999).

V.4.6. Main findings

The proposed blob free-volume theory bridges the original theory of Vrentas and Duda and the extension proposed by Fang *et al.* (2013) for flexible solutes in rubber polymers. The evasive concept of hole free volume has been replaced by more a robust concept associated to direct experimental evidences: the scaling exponents of linear probes, $\alpha_{lin}\left(T,T_g\right)$. Hole free-volumes effects are encoded in a polymer function $P\left(T,T_g\right)$, which parameterizes the rate of trapping and release of a collection of connected blobs. The early concept introduced by Fang *et al.* (2013) is extended to glassy polymers and to blobs with different sizes and shapes, and possibly interacting with the polymer. The reformulation has been tested successfully on homologous solutes: *n*-alkanes, 1-alcohols, *n*-alkyl acetates and alkyl phenyls in six polymers above and below the glass transition temperature. By considering the series already tested in

Fang *et al.* (2013), the whole theory has been assessed over ten different polymers covering five commodity polymer families: polyolefins, polyvinyls, polyesters, polyamides, polyacrylics.

Extended and conventional free volume theories can be now applied to polymers with non-documented hole free volume parameters, including polyethylene terephthalate (PET) and polyethylene naphthalate (PEN). Polymer-related parameters are lumped into two constants K_α and K_β, involved in the expression of $P\left(T,T_g\right)$, which can be related to WLF constants only when solute blobs resemble polymer blobs. In the general case and for accurate predictions, the constants K_α and K_β have to be explicitly determined for each polymer.

By construction, the prediction framework applies to large and small solutes including water, ethanol, oligomers, polymer residues and degradation products, non-intentionally added substances. Though it has not been fully verified, concentration and mutual diffusion effects can be added to the expression of $P\left(T,T_g\right)$ as in the original FVT. All tiers up to level 4 can be covered with the current theory, including for polymers not shown here (e.g. polylactide or PLA).

The derived extensions for anchored solutes and solutes with blobs of various size open the way to a more general theory for plastic additives and residues, but it also suggests a strategy to design substances with reduced diffusion coefficients or with controlled behavior with temperature. With this respect, it is worth noticing that the expressions are commutative and do not require the anchor to be connected to any of the solute ends.

V.5. General discussion on tiered packaging design

Integrating tiers above 2 (§V.1.) into the approach presented in §V.2. is the best way to evaluate the safety margins (see **Figure II-23**) of the proposed estimates at low tiers. Both possibilities, "the safety margins are either too high or too low", have negative impacts. They should be minimized while keeping the risks of having a defective quality as minimal as possible. The concept of risk should be here envisioned through two scenarios:

- a dramatic loss of mechanical resistance of the bottle due to premature aging of the polymer;
- an uncertain shelf-life value due to variable conditions of storage and transportation.

The first scenario or acute risk of mechanical rupture was examined experimentally by examining the consequences of a cumulated exposure to water, ethanol, and aromatic solutes in PET. The second scenario was considered mathematically by replacing likely estimates by probabilistic ones in a similar fashion as it used in migration modeling.

Why uncertainty and safety margins cannot be introduced in multicriteria optimization. The scientific community accepted that the safety of food contact materials could be determined by algebraic equations. In other words, the causation is accepted due to the presence of safety margins and an exhaustive list of conditions restraining the domain of validity of the approach. A very similar agreement is expected for shelf-life (no leak from the closure, no external chock, no exposure light, etc.). However, as for safety assessment, the lack of shelf-life cannot be proved alternatively by calculations (many causes not included in the model can also affect shelf-life). The lack of bijectivity justifies a monotonic sophistication of the approach as initially shown in **Figure II-7**. One practical consequence is that minimizing the overestimation of shelf-life cannot be introduced as an additional goal at the step [S]olving. It is the responsibility of the end-user to bring external knowledge initially ignored by the algorithm.

V.5.1. Critical interactions between PET and solutes

Specific interactions between PET and solutes relevant of liquors (water or ethanol) can be readily evidenced by observing the cross-sections of thin films exposed to prolonged contact with pure water and ethanol. Typical observations are shown in **Figure V-34**. Biaxially oriented PET film exhibit a layered structure in phase-contrast microscopy due to the alignment of the rigid crystalline structure with the plane of the film. After exposure to water

or ethanol, some oblique cracks can be observed, as already reported for many solutes by Billovits and Durning (1988). They are always disconnected from the outside and do not constitute preferential penetration routes in the film. They evidence the effects of the constraint release in the material either during sorption stage or during cutting.

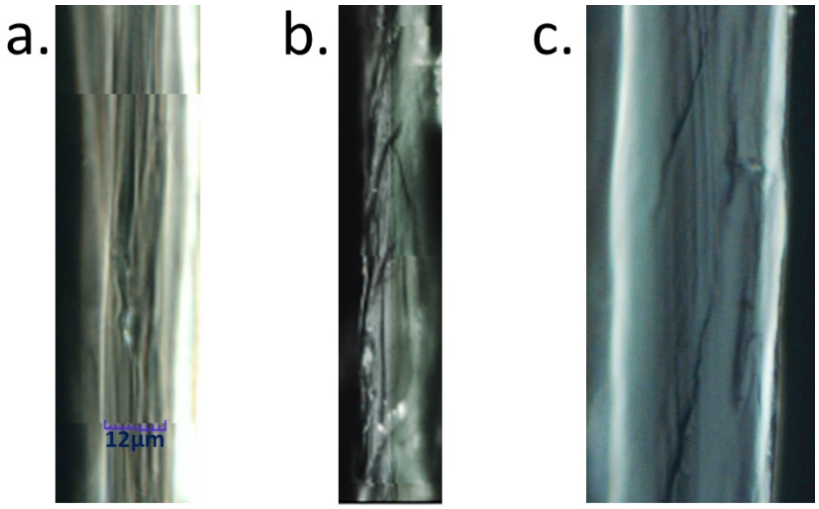

Figure V-34. *Microscopic observations in phase contrast of the cross sections of 12µm-thick PET film F1. (a) neat film; (b) film immersed in water at 50°C for 10 hours; (c) film immersed in ethanol at 50°C for 10 hours.*

Thin biaxially PET films exposed to severe conditions of ethanol content 99% and temperature close to T_g of plasticized PET (~60°C) starts to behave differently with poorly defined diffusion coefficients, as reported in the Arrhenius plots of **Figure V-38**. The behavior is globally Arrhenian with a possible change of slope at the lowest temperatures. The large differences between apparent activation energies up to 25 kJ·mol^{-1} is mainly associated with different activation of the relaxation between the three studied films.

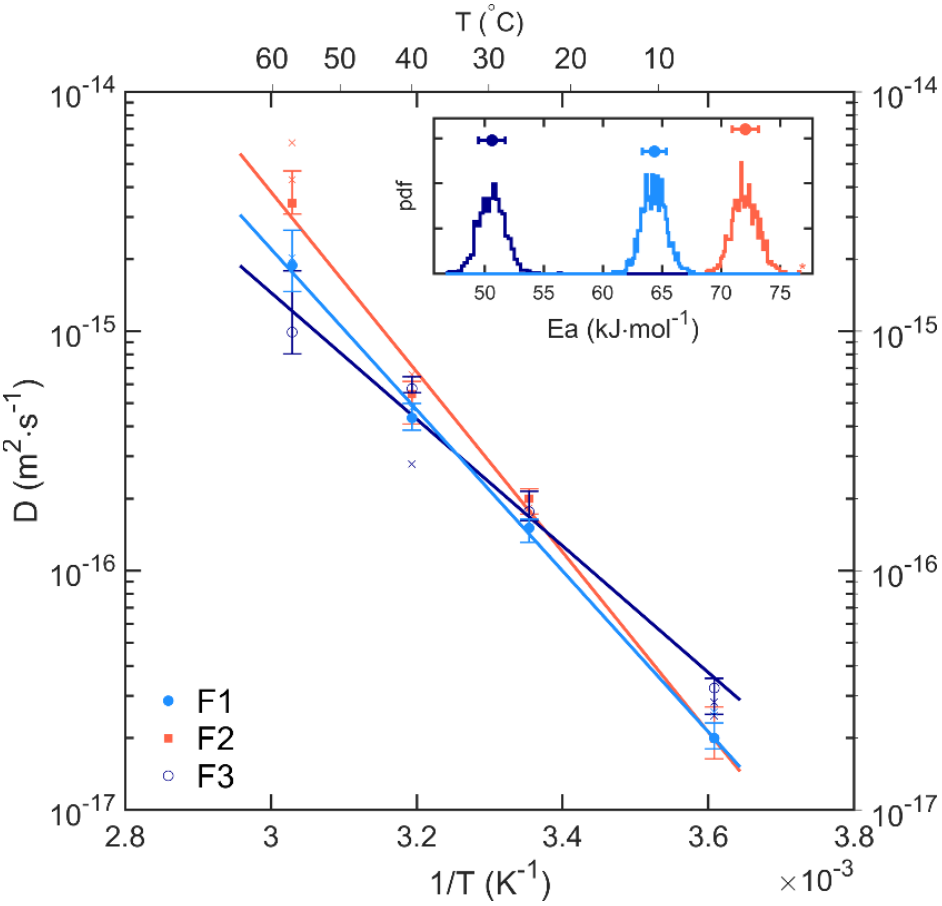

***Figure V-35**. Comparison of the apparent activation energies of diffusion of ethanol (gravimetric measurement after liquid contact with 99% ethanol, five repetitions for each condition). The inset shows the distribution of apparent activation energies based on 1000 bootstrap samples.*

Determining low diffusivities of solutes larger than water in plasticized thin films PET is hampered by the dominant contribution of relaxation at high temperatures and activities. As shown in theoretical kinetics of **Figure V-19**, the dynamics of swelling and diffusion are overlapping at intermediate diffusion Deborah numbers. Experimental sorption kinetics of ethanol and toluene at 50°C in 12 µm thick PET films are reported in **Figure V-36**. In the case of toluene, double relaxation is identified. The shapes of the kinetics are very sensitive to initial conditions and demonstrate a beginning of chaotic behavior due to heterogeneous mechanisms of constraint release (**Figure V-34**).

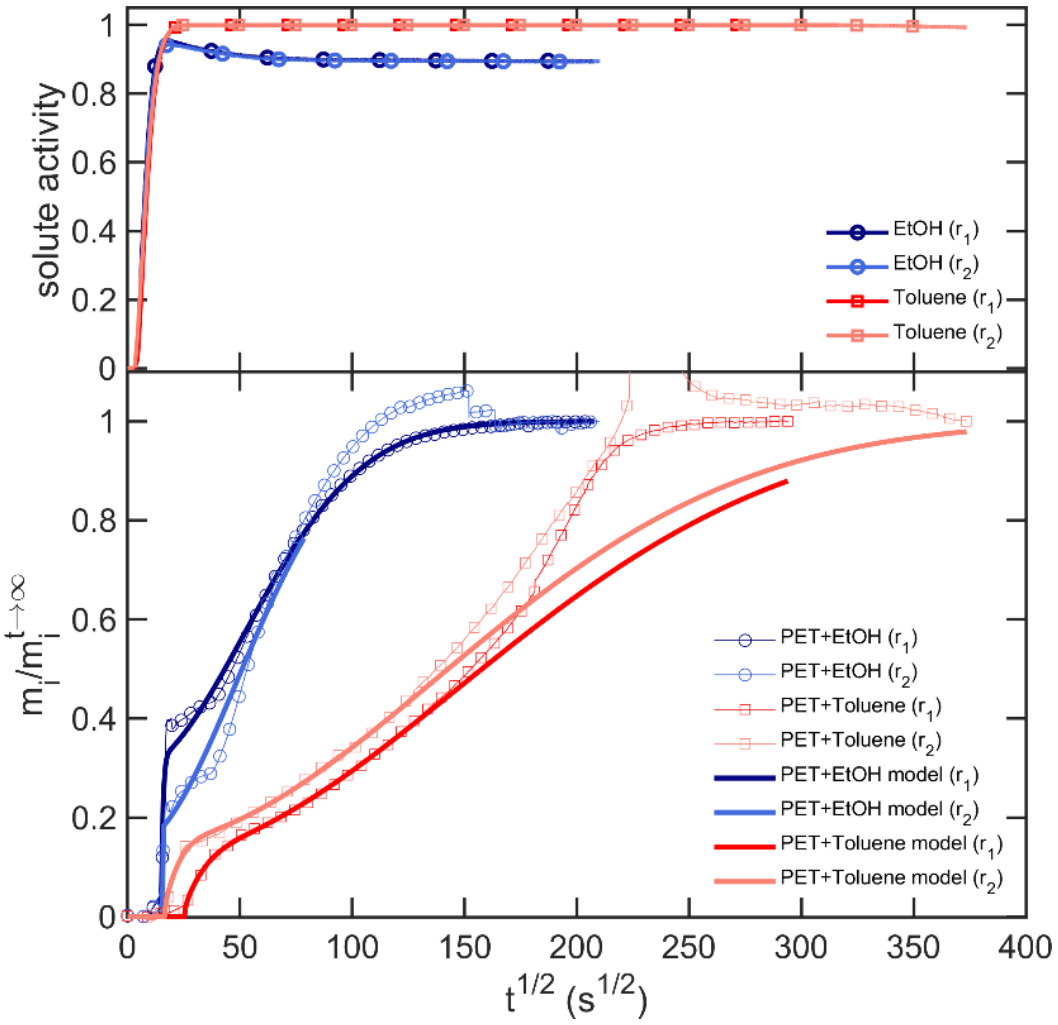

***Figure V-36**. Sorption kinetics of ethanol and toluene in 12 µm thick PET films (F_1) at 50°C at high activities. The fitted model is a delayed version of Eq.* (V.4).

V.5.2. The rule of the maximum driving force

Any glassy polymer used for producing bottles is initially in thermodynamical equilibrium with the storage conditions or production conditions, typically at low relative humidity: 30% or 50%. Exposing it to liquor triggers sorption and permeation of water, ethanol and any solute. Water is the smallest substances and therefore diffusing the fastest, activating the transfer of ethanol (see §V.3.5.1.). Polymer relaxation is an additional complication. It has been shown by transmission infrared linear dichroism that the thickness of the sample from 30 to 500 µm does not affect the relaxation kinetics of the *gauche* and *tans* conformers (Pellerin *et al.*, 2002). The same results were verified on samples M, F1, and F2 using attenuated total reflectance and front-surface reflectance at synchrotron Soleil (beamline SMIS, results not shown). As relaxation times are much longer than mass transfer (diffusion Deborah numbers greater than unity), PET exhibits:

- a strict Fickian behavior when it is subjected mass transfer replacing one solute by another one;
- a stress-dependent mass transfer when the polymer is subjected to a differential step of partial pressure;
- strong memory effects when the polymer is dried before sorption.

The persistence of relaxations prevents considering rapid variable humidity conditions (diurnal) as a stationary random process (invariant with a shift in time) as assumed for temperature variations (see V.5.4.2.). Only seasonal variations of relative humidities longer than polymer relaxation can be introduced through time-dependent boundary conditions or sequential simulations. To minimize the risk of underestimation of real sorption, permeation rates and finally shelf-life, the "*rule of the maximum driving force*" must be applied in the boundary condition: the lowest relative humidity during storage and transportation should be enforced. The linear and the deviations to the linear behavior are reported through three independent experiments.

V.5.2.1. Mutual diffusion and sorption

Ternary FH3 isotherms (see §V.3.5. and V.3.6.) demonstrate that the local composition in water and ethanol affects non-linearly the activity coefficients of each solute. This condition is sufficient to justify that the transport of water and ethanol are interacting together and should obey to mutual diffusion coefficients concepts as stated in Eq. (II.41). The effects of concentrations can be antagonist according to plasticizing or swelling effects dominate on local mobility. In the presence of strong plasticizing effects, the drop of friction coefficients causes an increase of diffusivities. In the presence of strong swelling effects, local composition effects decrease activity coefficients and finally lower diffusivities.

The effects of mutual diffusion were evidenced by studying the simultaneous desorption of water and ethanol on the side of the PET walls in contact with the beverage. Controlled conditions were reproduced experimentally by equilibrating 12 µm thick PET with a hydroalcoholic solution (*abv*=0.6; a_w=0.86 and a_e=0.49) at 50°C. The films were subsequently exposed to two different routes of differential partial pressures, as shown in **Figure V-37**. The strategies mimicked the transfer from the contact surface with the beverage towards to the internal regions. One single step of partial pressure was changed at once in order to separate the contribution of water and ethanol on mass losses. The route eliminating ethanol before removing water (ABEDF) followed well the theoretical FH3 formulation. The route eliminating alternatively water and ethanol (ABCDF) was contrarily delayed, leading to non-symmetric sorption amounts between the states E and C. The observed hysteresis would be related to a lower shrinkage of PET when ethanol was present.

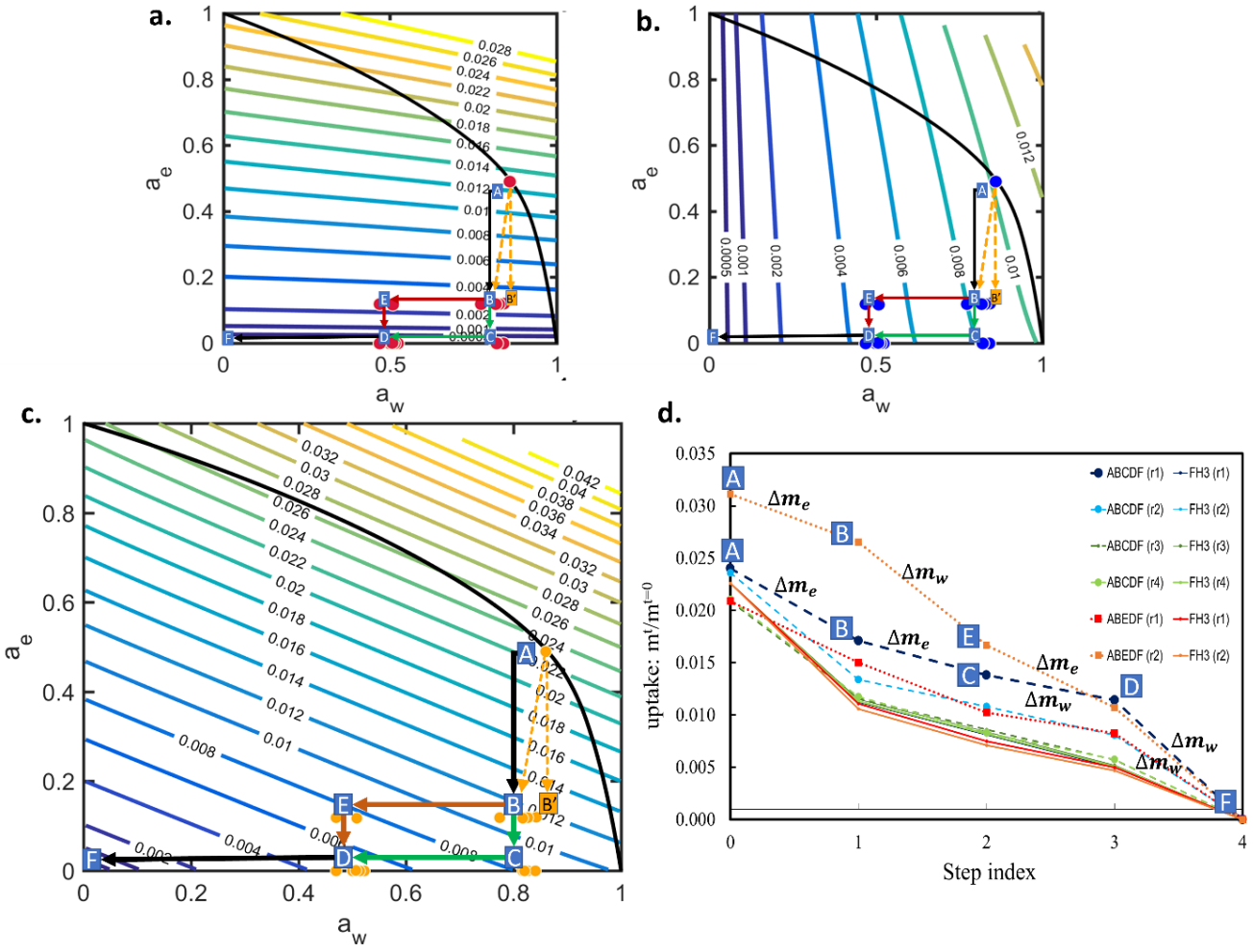

Figure V-37. *Theoretical and experimental mass losses (water and ethanol) in 12 µm thick PET film (F1) at 50°C: (a) theoretical residual ethanol content; (b) theoretical residual water content; (c) cumulated amount of water and ethanol; (d) comparison between experimental and theoretical value along the routes ABEDF and ABCDF.*

V.5.2.2. Linear behavior when ethanol can replace water in bottle walls

When the mutual diffusion is linear and reversible, the fluxes of each species are additive and independent of the order in which they occur. This assumption has been tested during a typical challenge test of bottles walls *M* equilibrated at 50°C at 50% RH and subsequently submitted to a gas mixture of water with activities of water and ethanol of 0.512 and 0.385, respectively. The transfer of each solute, simulated independently (using parameters listed in **Table V-4**), is shown in **Figure V-38** with the cumulated mass uptake compared with the experiment in **Figure V-39**.

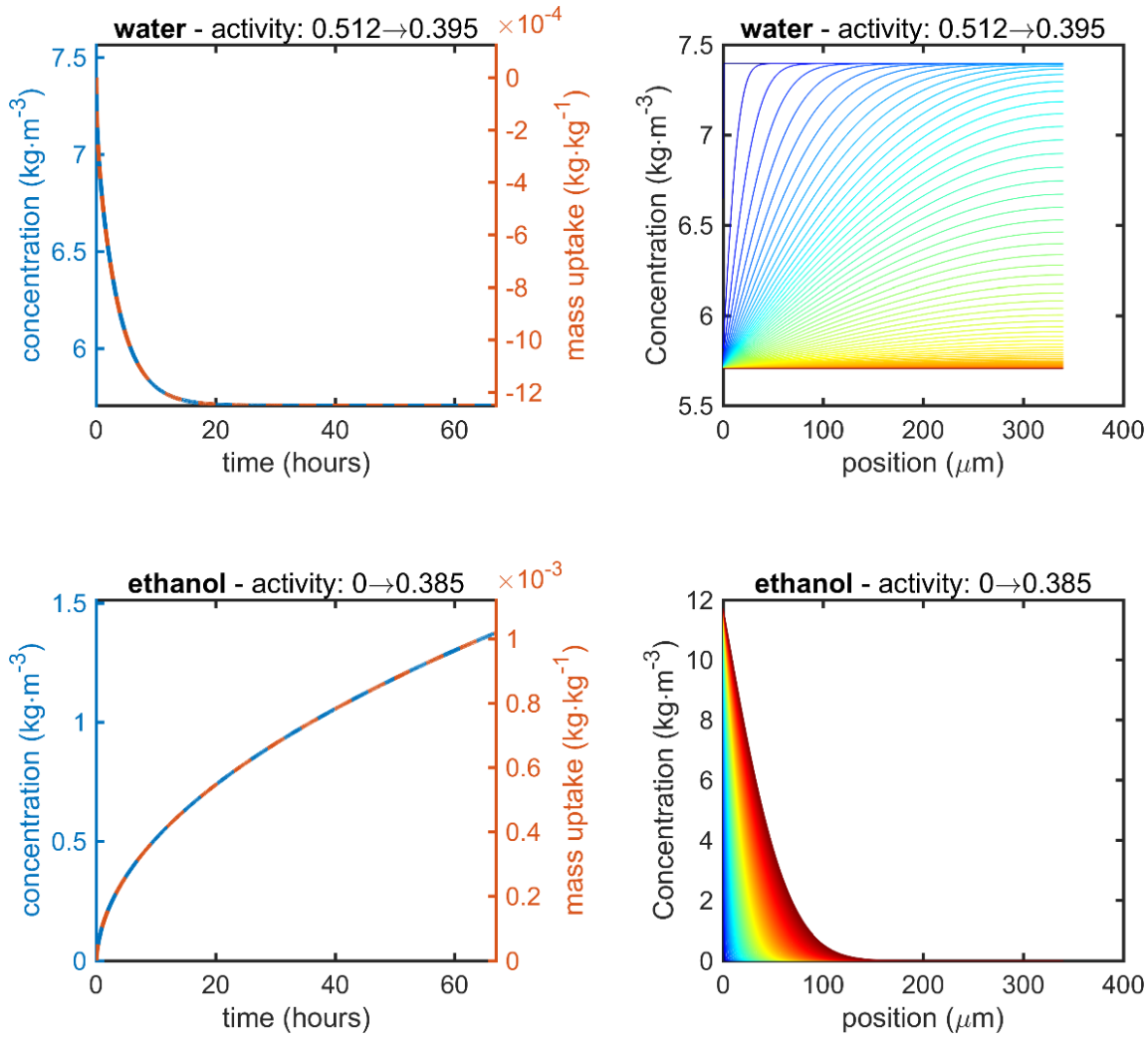

***Figure V-38**. Independent simulation of the mass transfer of water and ethanol associated with a negative step of water activity of 0.51 down to 0.40 and a positive step of ethanol activity to 0.38 at 50°C. Concentration profiles (100 times) are shown for the whole period and are distributed as the square root of time.*

No difference can be detected between experiment and simulation if the diffusivity of ethanol is substantially overestimated comparatively to the value reported in ***Table IV-3***. The asymmetry between the decreasing and increasing branches is associated with the differential rates of mass transfer between water and ethanol. In this particular experiment, greater asymmetry would have been expected, but ethanol is thought to replace water whereas drying would have cause shrinkage and a partial collapse of voids. The departure of water facilitates the sorption of ethanol by one magnitude order. The competition between the driving fluxes appear more outstanding when the value of the diffusivity of ethanol in this ternary configuration is compared with other binary estimates or determinations in **Table V-4**.

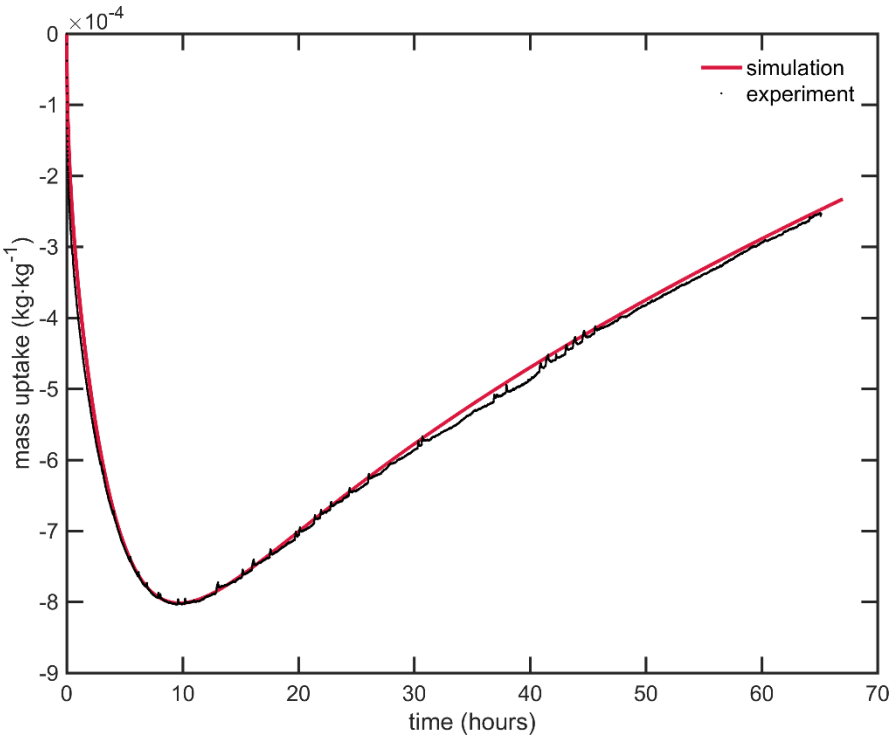

Figure V-39. *Comparison between simulated mass uptake and experimental determinations for 680 µm thick bottle walls at 50°C using the cosorption microbalance (experimental conditions and simulated results are shown in* ***Figure V-38*** *with fitted values for water and ethanol listed in* ***Table V-4****).*

V.5.2.3. A resistance to mass transfer induced by stress gradients

The existence of non-chemical driving force in sorption experiments was revealed by applying a differential step humidity followed by periodic variations as shown in **Figure V-40**a: from 7 to 47% during the first step and from 43 to 54% during the second step. The low-frequency mass uptake was removed by subtracting the signal averaged over a period 10 times greater than oscillations (period 240 s). The derivative of the residual mass variation was compared with the fluctuations of the partial pressure in **Figure V-40**b. To enable an interpretation as mass flux versus the variation of partial pressure as driving force, the average lag determined by cross-correlation was removed in the comparison. The sorption and desorption consequently looked almost reversible.

The final curve is close to the first Fick law (the flux is proportional and of the same sign of the pressure variation) with noticeable differences. Sorption is faster than desorption for both steps. The flux is not zero when the partial pressure difference is zero; a residual mass transfer (desorption) is evidenced and associated with a constant rate of 247+10 days. A significant sorption occurs when the difference in partial pressure is greater than 2-4 kPa. This threshold corresponds to the intensity of osmotic pressure opposing to sorption in the polymer.

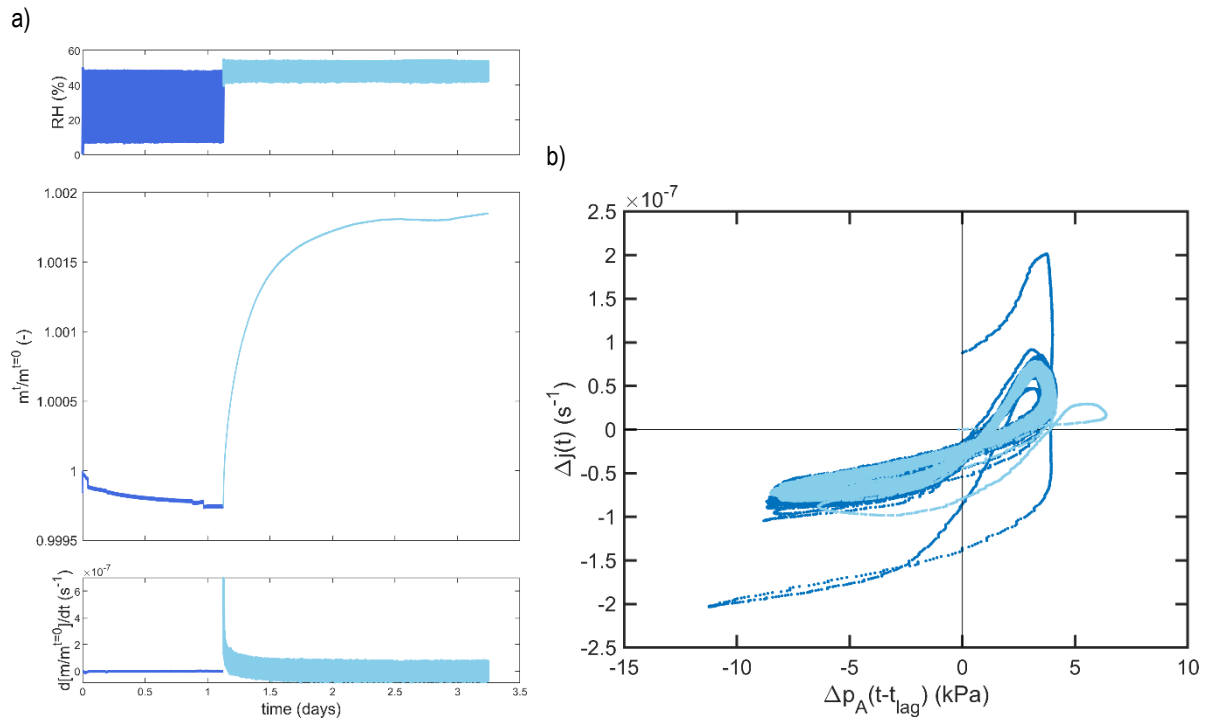

***Figure V-40**. Analysis of the fluctuations of mass uptake vs the fluctuations of relative humidity (period 240 s) in 12 µm thick PET bottle (M) at 50°C: (a) raw results, (b) correlation between fluctuations when the average delay between has been removed.*

V.5.2.4. Memory effects: shrinkage/densification opposing to swelling

The results shown in **Figure V-40**b are not different from **Figure V-12** (desorption after reaching an apparent equilibrium), but their interpretation is different. The densification process is irreversible, whereas the relaxation shown here is elastic (penetration depth of ~1 µm during the cycle). It is associated with residual elastic energy opposed to mass transfer. Viscosity effects were studied by analyzing the same behavior on longer time scales by comparing the effects of a sorption sequence was the film sample was previously dried or not. During the first step, all samples initially equilibrated ~50% RH followed the evolution imposed by the change in relative humidity (drying or sorption). After the second and third steps, almost all samples ceased to follow the evolution imposed by the external RH and continued to last one or several days of their initiated behavior during the first step. The remanence was all the higher than the samples were brought far from their initial equilibrium state. These results generalize the trends shown in **Figure V-40**b: i) a threshold oppose to sorption from dry state not only at the surface but also in the bulk, ii) desorption is much slower than sorption. After successive steps and in the presence of non-uniform concentration profiles, the different regions of the polymer are not in the state, and the whole same can exhibit chaotic behavior (i.e., sensitive to initial conditions).

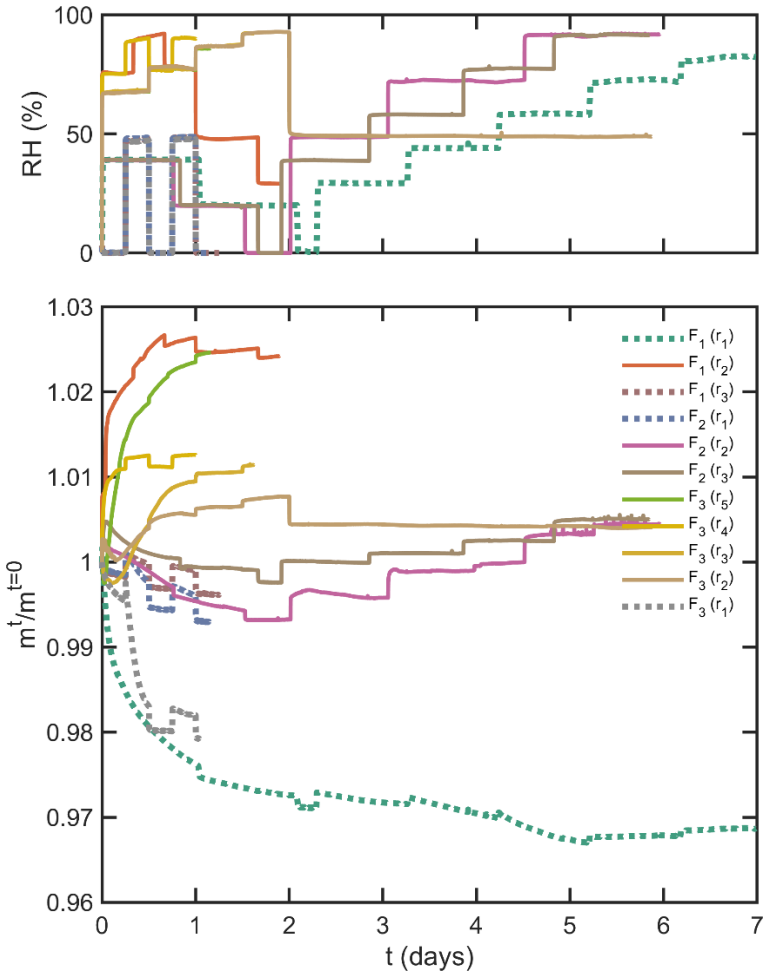

***Figure V-41**. Sorption/desorption cycles of 12 µm thick PET films at 25°C from an initial state at 50±10% RH. Cases leading to significant desorption are plotted in dashed lines.*

Memory effects and the effects of constraint release are exacerbated on microsamples and less visible on thicker materials due to slower mass transfer (see **Figure V-39**).

V.5.3. Estimation of the uncertainty in diffusivities

Apparent diffusion coefficients in glassy polymers at a given temperature can be variable for several reasons:

- a different subcooling ratio providing a different amount of extra hole free volume (see **Figure V-23**);
- a shift of T_g due to plasticizing
- extra free volumes brought by the solute itself (concentration effects);
- a contribution of polymer relaxation on apparent diffusion coefficients
- mechanical ruptures.

The developed free-volume theory (FVT) can cover the three first points, but only the first was detailed and analyzed in the manuscript. The case $r = 0$ and T_g=60°C was the worst case for the applied FVT. All other aspects can be studied by performing differential sorption experiments at different temperatures and on samples with different thicknesses. Diffusivities at low intermediate and high Deborah numbers are expected to offer the broader variability. An illustration of the dispersion is shown in **Table V-4**. Experimental diffusivities of water and toluene were remarkably bounded by the predictions of FVT. The values for ethanol are typically much higher than the FV worst case. The activation by temperature at glassy state is much higher than the one for water (see. **Figure V-35**), it is strongly affected by the concentration of both water and ethanol.

Table V-4. *Comparison of diffusion coefficients determined at different tiers and using different methods*

Level of details	D_w (m²·s⁻¹)	D_e (m²·s⁻¹)	D_T (m²·s⁻¹)
Tiers 1-2: derived or extrapolated from literature (section V.2.)			
• at 50°C	2.6×10^{-12}	2.4×10^{-15}	n.d.
• at 35°C	1.5×10^{-12}	1.91×10^{-16}	2.0×10^{-18}†
Tier 3 (ternary system): from **Figure V-39** at 50°C	3.48×10^{-12}	5.3×10^{-15}	
Tier 3-4: derived from FVT in dry PET (section V.4.) – r=0.3394, T_g=76°C			
• at 50°C	2.7×10^{-12}	3.0×10^{-16}	1.0×10^{-16}
• at 40°C	1.1×10^{-13}	1.1×10^{-16}	2.8×10^{-17}
• at 35°C	6.7×10^{-13}	6.0×10^{-17}	1.3×10^{-17}
Tier 3-4: derived from FVT in plasticized PET (section V.4.) – infinite dilution – r=0, T_g=60°C			
• at 50°C	3.7×10^{-12}	7.8×10^{-16}	1.3×10^{-15}
• at 40°C	1.8×10^{-12}	6.4×10^{-16}	1.3×10^{-15}
• at 35°C	1.2×10^{-12}	5.8×10^{-16}	1.3×10^{-15}
Tier 3-4: derived from **Figure V-36** in plasticized and swollen PET at 50°C	n.d.	$>6.8 \times 10^{-13}$	$2.8\pm3 \times 10^{-14}$
Tier 3-4: measured in PET in contact with a solution of toluene in 95% ethanol at 40°C†	n.d.	n.d.	4.1×10^{-16}

†value at 40°C (Franz and Welle, 2008). For chlorobenzene, a surrogate larger than toluene,the authors report a value of 3.8×10^{-18} at infinite dilution.

V.5.4. Probabilistic estimation of shelf-life

V.5.4.1. Problem description

Shelf-life is uniquely defined only in the absence of variability and uncertainty. Both exist, and they should be considered explicitly. Uncertainty was managed in the previous sections either by minimizing $\left\{\chi_{i+P}^{T,T_g}\right\}_{i=w,e}$ (see the lower branch in **Figure V-17**) or by maximizing $D_{i,P}^{T,T_g}$ (see the upper branch in **Figure V-32**b). For glassy polymers, the common rule consists in assuming that the considered material is closer to its rubber state, that is by maximizing the extra free volumes brought by subcooling (see **Figure V-23**b). They are mathematically equivalent to a shift of T_g (plasticizing effect) or to an underestimation of r (system frozen close to its rubbery state). Variability is related to industrial, commercial and consumer practices. They cannot be reduced in a mechanistic description and their linked consequences need to be considered.

In section §II.2.3.6. , it was suggested that the combination of two steps (e.g., transportation and long-term storage) could be handled via simple cumulants (see Eqs.(II.28), (II.34) and (II.35)). Adding variability on the terms of the sum can be managed by considering the sum of the upper bounds at the expense of large overestimations. A more robust description is required to handle variability while reducing packaging weight. Shelf-life, t_{shelf}, is mathematically defined as an acceptable duration a reference temperature T_{ref} even when the temperature conditions are known to be variable. By denoting ϵ the risk to have the criteria weight variation (m_{loss}) and alcohol-by-volume (abv) exceeding their tolerances (respectively $\%\Delta m$, $\%\Delta abv$), one probabilistic definition of t_{shelf} could be:

$$\max\left[\, pr\left(\left|abv\left(t_{shelf},T_{ref}\right)-abv\left(t=0,T_{ref}\right)\right|\geq \%\Delta abv\right), pr\left(m_{loss}\left(t_{shelf},T_{ref}\right)\geq \%\Delta m\right)\right]=\epsilon \tag{V.42}$$

No tier assumption is needed on the models of $abv(t,T)$ and of $m_{loss}(t,T)$ except that their variations can be extrapolated conservatively from any temperature to T_{ref}:

$$\begin{aligned} &activation\left(T,T_{ref}\right)\cdot\left|abv\left(t,T\right)-abv\left(t=0,T\right)\right|\geq\left|abv\left(t,T_{ref}\right)-abv\left(t=0,T_{ref}\right)\right| \\ &activation\left(T,T_{ref}\right)\cdot m_{loss}\left(t,T\right)\geq m_{loss}\left(t,T_{ref}\right) \end{aligned} \tag{V.43}$$

When temperature acts mainly on diffusion, the activation term is estimated as:

$$activation\left(T,T_{ref}\right)=\max\left(\frac{D_{w,p}^{\left(T,T_g\right)}}{D_{w,p}^{\left(T_{ref},T_g\right)}},\frac{D_{e,p}^{\left(T,T_g\right)}}{D_{e,p}^{\left(T_{ref},T_g\right)}}\right) \tag{V.44}$$

Without requiring time-consuming Monte-Carlo calculations, the methodology described in §II.2.3.6. can be used to estimate shelf-life from Eq.(V.42) with the same computational cost as a deterministic case. The principles are illustrated hereafter in a simplified but realistic case study.

V.5.4.2. An illustrative case-study

The principles of calculations of t_{shelf} are shown for a vodka-type beverage ($abv = 0.4$) stored in a PET bottle of 650 mL and subjected to two steps: a transportation step in severe conditions and a storage step in more moderated conditions. The relative humidity in the storage room is assumed to be maintained at 30% (rule of the maximum driving force). The calculations for a given bottle geometry and wall thickness are plotted in **Figure V-42**. The probability density functions (pdf) of transportation and storage temperatures were assumed independent, so that the distribution of the equivalent time at T_{ref} = 25°C, $t_{eq}^{25} = t_{storage}^{25} + t_{transportation}^{25}$ is given by the convolution product of the equivalent distributions of residence times at 25°C , denoted $pr_{storage}^{25}\left(t_{storage}^{25}\right)$ and $pr_{transportation}^{25}\left(t_{transportation}^{25}\right)$:

$$pr\left(t = t_{storage}^{25} + t_{transportation}^{25}\right) = \int_0^{+\infty} pr_{storage}^{25}\left(t - t_{transportation}^{25}\right) pr_{transportation}^{25}\left(t_{transportation}^{25}\right) dt_{transportation} \tag{V.45}$$

with the distribution of temperatures transformed into the distribution of residence times at 25°C via:

$$\begin{aligned} pr_{storage}^{25}\left(t_{storage}^{25}\right) &= \frac{pr_{strage}\left(t_{storage}^{T}\right) \cdot activation\left(T(t_{storage}^{T}), 25\right)}{\int_0^{+\infty} pr_{storage}(t) \cdot activation\left(T(t), 25\right) dt} \\ pr_{transportation}^{25}\left(t_{transportation}^{25}\right) &= \frac{pr_{transportation}\left(t_{transportation}^{T}\right) \cdot activation\left(T(t_{transportation}^{T}), 25\right)}{\int_0^{+\infty} pr_{transportation}(t) \cdot activation\left(T(t), 25\right) dt} \end{aligned} \tag{V.46}$$

The depicted example corresponds to an average transportation time of one months and a storage time of four months. Due to the variation of temperatures, the total time at 25°C is of 7.25 months, with 95% of cases varying between 4.28 and 12.9 months. In these conditions, there is 8.4 % to exceed a weight loss of 3% and a probability of 50.6% to exceed a variation of *abv* of 0.003. In the context of optimization, the current design guarantees the compliance only in 50% of cases under combined storage and transportation conditions, and above 97% for the sole transportation conditions. The same approach can be used iteratively to optimize the design, the shelf-life or the conditions of transportations and storage.

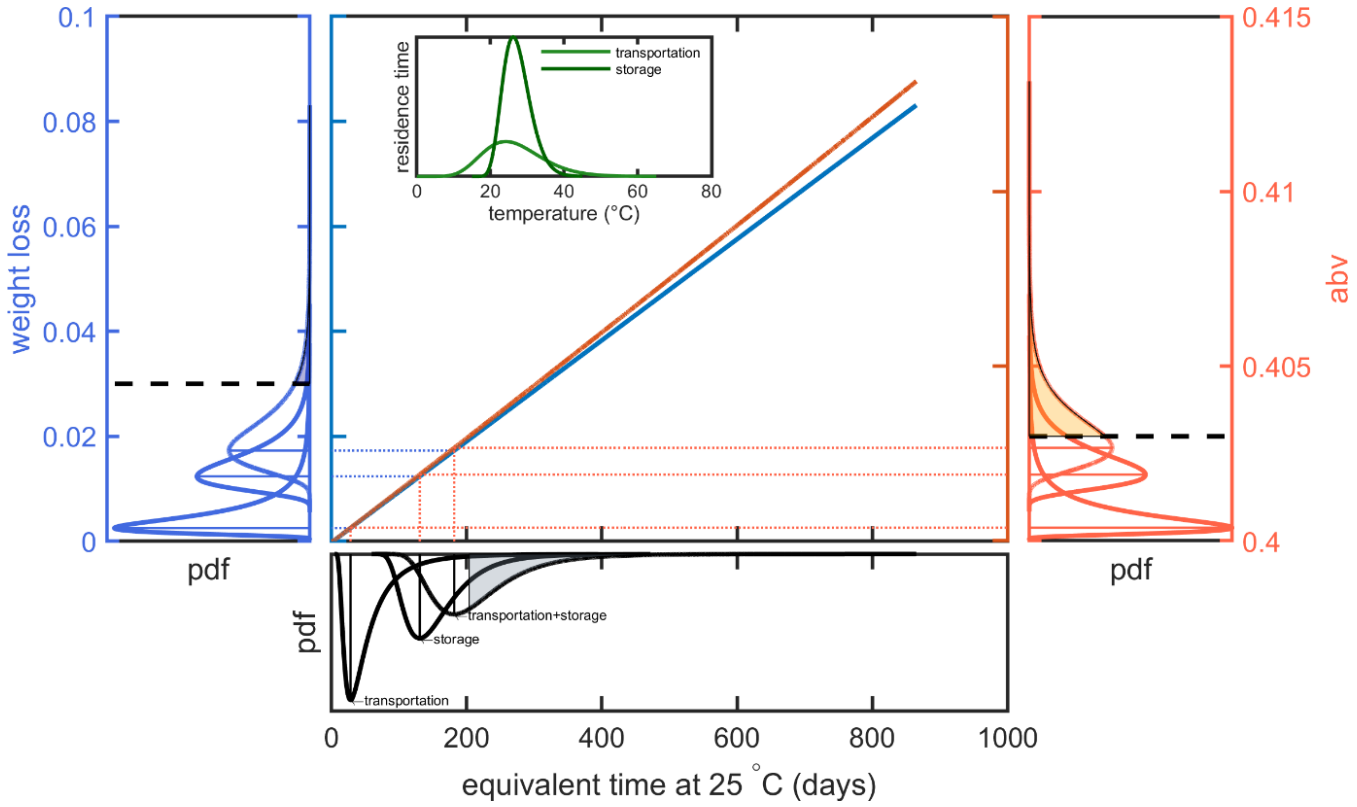

***Figure V-42**. Principles of the probabilistic determination of shelf-life based on a double criterion on weight loss and abv variation. The input temperature distributions are shown in upper inset. The corresponding transportation, storage and combined distributions are shown horizontally. The distribution of weight loss and abv variations on the left and right, respectively. The tolerances are shown as dashed lines. The filled areas represent the probability to exceed tolerances.*

this page is left blank intentionally

Chapter VI. Conclusions and Perspectives

Chapter VI. Conclusions and Perspectives

VI.1. Conclusions

The research work was devoted to the construction of a global computational framework where important contributions of food packaging design could be evaluated and optimized. The three targeted contributions shelf-life, environmental impacts, and the chemical food safety were chosen for their substantial impacts on the food and the environment, but they were paradoxically the less studied and explored through numerical calculations. The work was therefore initiated from an almost white page. The backbone was a large and ambitious software project, which could benefit the numerical approaches and modeling assumptions already used in migration modeling. The motto was "imperfect models can be used for decision making if they are built in a conservative way for that". As migration models are built rationally, they are accepted both by law and scientists, which contrast dramatically with the more subjective concepts of ecodesign and life cycle assessment. Polyethylene terephthalate (PET) bottles for alcoholic beverages were chosen as a template to build the concept, to write a specific computational code (more than 65 Klines of Matlab/Octave), to validate and extend the different refinements. Despite inherent mathematical and physical simplifications at intermediate steps, the input and final outputs of the numerical project were designed to be compatible with industrial standards of product design, engineering and rapid prototyping (augmented reality, 3D printing).

- *The 3D simulation engine for the rational design of beverage bottles*

The first cornerstone was to use tier modeling, which offers the double capability of progressive enrichment and multiscale modeling. A limit was, however, rapidly reached. Existing previous opensource projects focused only on the one-dimensional description of mass transfer. They could manage non-linear behaviors, but they not describe the differential of sorption and permeation across the different parts of the packaging. This kind of numerical problems is quite well-known for the calculation of the mechanical resistance of thin walls and packaging. They require 3D modeling and a very refined and expensive meshing across the walls. This solution was definitively not applicable to optimize thousands or more different kind of packaging. The difficulty was circumvented by using a dual geometry model: one for design and another one to calculate mass transfer. In the dual space, calculations were simpli-

fied and dramatically accelerated by the use of curvilinear coordinates and contour integrations. In more technical terms, the food representation is implicit, and mass transfer may be inaccurate in regions with low gyration radii. Other details, such as the distribution of the mass and the total surface area are well preserved. This technical choice was our vehicle or simulation engine, where the physics of mass transfer, physical chemistry and thermodynamics can be installed and configured. By choosing a multicomponent formulation, the number of simultaneous mass transfers is not limited, and the approach could be extended to situations with chemical or biochemical reactions. Dynamic storage conditions of temperature and relative humidity are applicable if needed.

- *The tier [E][D][S] approach for packaging design optimization*

The description of alcoholic beverages as hydroalcoholic solutions was crude, but remained realistic for liquors such as vodka, with low aromatic content. The considered environmental impacts were also simplistic: the mass of the packaging for a given consumption unit or given intake, chosen as a functional unit. The adding value was, however, elsewhere. Can we put all mass transfer problems (with arbitrary complexity) related to food shelf-life, environmental and safety issues within a single mathematical formalism, that standards algorithms and methodologies can optimize efficiently. An iterative process involving thee steps: a first [E]valuation step based on our simulation engine; a [D]ecision step where the expertise on the food and consumption is introduced; and finally, a last [S]olving step exploring the tradeoff between contradictory criteria. The framework is very not specific and modular; it can accommodate any bioproduct and packaging and follow the future demands of the industry and authorities. It was tested successfully at the very first tiers for the optimization of PET bottle miniatures used in airplanes. The loss of ethanol is minimum, and most of the weight loss is related to water permeation. Due to legal requirements, the shelf-life is determined by the concentration of ethanol in the bottle. Alternative shapes and formats were optimized, which much greater performances: longer shelf-life or minimum waste.

- *Multiscale extensions to the main engine*

The capacity to extend the computational framework to new criteria (e.g., amount of recycled material), to new mass transfer (migration, aroma scalping) and to reduce the safety margins for optimized designs depends heavily on the quality of the [E]valuation step. Glassy polymers, such as PET, are chosen for their excellent barrier properties, but like any material far from their equilibrium state, they evolve rapidly in the presence of small molecules. Polymer relaxation hampers dramatically our capacity to access to intrinsic properties: final equilibrium state (sorption and mutual sorption), diffusion properties (trace or mutual, activation by temperature). Two complementary were followed directions: i) removing the difficulty by

measuring the properties of glassy polymers above their glass transition temperature (T_g) and by using a molecular theory to extrapolate them below T_g, where they are used; ii) addressing frontally the complexity by a depth analysis of literature data and acquiring cosorption kinetics for water and ethanol at temperature representing a worst-case for bottle storage. Two theories have been implemented in the engine: a generalized version of the free volume theory (FVT) of Vrentas and Duda for diffusivities, and a temperature-dependent ternary free-Flory-Huggins (FH) formulation. The latter contribution is more a suitable parameterization for water and ethanol in PET rather than a real formulation. The modification of the FVT is more profound and with broader applications behind the scope of this work. Based on the initial formalism of Fang *et al.* (2013), organic solutes are described as connected blobs, each one obeying to FVT. The scaling exponent α_{lin}^{T,T_g} of the diffusivities of the center-of-mass with the number of blobs carries the information of the rate of the renewal of voids accessible to each blob. α_{lin} was used to setup a generic polymer function P^{T,T_g} enabling to extend existing and modified FVT to any polymer at glassy or rubber state including PET. Additional sophistications of the new blob-FVT enable to manage solutes with similar or dissimilar blobs. Though the FVT theory equipped with its extensions is still not fully complete, it covers all major polymer families (polyolefins, polyesters, polyvinlys, polyamides, polyacrylics), their oligomers, water, ethanol, any combination of rigid and flexible solutes.

- *The non-linear behaviors of PET*

PET is the preference thermoplastic material for one-third of all food packaging applications. It can be partly biosourced and is fully recyclable. The diffusion and sorption properties or many important molecules (water, ethanol and noble alcohols, aroma, oligomers and residues, non-initially added substances including post-consumer contaminants) can be derived from quantitative structure relationships. Polymer relaxations can, however, modify profoundly the nominal performances of PET (biaxially oriented or not) especially at high temperature, high relative humidity or in the presence of high organic content such as ethanol or aromatic solutes. They were not directly studied, but their consequences on mass transfer were considered for the interpretation of stepwise sorption. Additional results, not shown, were obtained on the synchrotron SOLEIL using the beamline DISCO (intrinsic fluorescence microspectroscopy) and SMIS (FTIR-ATR microspectroscopy and imaging, Raman microspectroscopy). They show that the interactions between mass transfer, structural changes and chemical interactions (e.g., π-π interactions between terephthalic groups, between them and organic solutes) are driven by local gradients (non-local interactions not evidenced), but were very heterogeneous due to the spatial organization of crystallites.

The interactions between non-linear behaviors of PET and mass transfer were understood and tabulated by the dimensionless diffusion Deborah number. For solutes diffusing fast (water) or in thick materials, initial sorption and permeation rates obey well to FV and FH theories. On the very long term, polymer relaxations generate an additional driving force promoting or opposing mass transfer according to the history of the material. The magnitude order of the induced driving force is equivalent to several kPa. It cannot be ignored, but its effect can be managed by overestimating the value of the diffusion coefficients at low tiers. This approach was shown to be viable for thick bottle walls with asymmetric contact even after several months. With symmetric contacts, a high diffusion coefficient would be necessary. As the uncertainty in diffusion coefficients is ranged between a factor 1 and 4 according to the considered conditions (temperature, relative humidity: RH, thickness), the [E][D][S] approach cannot be used without safety margins by assuming that the benefit of packaging weight reduction is linearly correlated with shelf-life. For critical applications, probabilistic modeling to manage the effects of temperature conservatively and with overestimations the effects of RH.

VI.2. Perspectives

- *Beverages in PET bottles*

This work finds direct application for alcoholic beverages and the optimization of the design PET bottles. The capacity to calculate shelf-life and the risk of collapse in variable storage and transport conditions is important feature. The optimization of the full design of a real bottle requires more considerations than those presented: marketing, mechanical resistance during stacking, consumer convenience, etc. The optimization framework [E][D][S] found already its application for recommending an amount of recycled PET, which may the risk of migration of NIAS acceptable according to the rules set by the European Food Safety Authority. It is thought that the same approaches are readily available for any beverage stored in PET bottles, including mineral water. Aroma scalping (i.e., sorption of aroma) is the mass transfer phenomena symmetric to migration issues, it is available for evaluation and optimization if the partition coefficients between the beverage and the polymer have been previously tabulated. In the case of PET, it is preferable to use a free-volume formulation including concentration effects (not considered explicitly in this work) to account for the cumulate plasticizing effects brought by multiple solutes.

- *How to integrate other mass transfer and reactions affecting shelf-life*

The current developments do not enable the estimation of the shelf-life of products sensitive to oxidation (e.g., vegetable oil, sensitive fruit juice, mayonnaise). The whole

[E][D][S] framework remains, however, fully applicable. Adding an evaluation of the risk of oxidation and related collapse requires a small number of extensions. The oxygen permeability of PET is well known, and predictive oxidation models have been already developed by the group (Patsioura *et al.*, 2017;Touffet *et al.*, 2018). Simulation with an implicit food model is not acceptable for semi-solid and solid food products, but the approach could be used as pre-optimizer of a more detailed optimization step (at a high tier) considering mass transfer and reactions in structured foods. Other phenomena such as leaks in sealing and closure systems should be integrated also.

- *The global challenge posed by the interactions between PET containers and its content*

Plasticizing, swelling, and polymer relaxation effects bring large uncertainty not only in the values of diffusivities and solubilities but also in the driving forces controlling mass transfer. Bottle walls are consequently not at the same mechanical state according to their thickness. Important safety margins need to be preserved to keep the determination of shelf-life robust and not to damage the whole mechanical resistance of the bottle. These effects are highly non-linear, the consequences associated to a too large thinning of walls can be studied with a finite element technique. We propose, however, a better solution by exploring a broader "*safe harbor region*" integrating both shelf-life, packaging weight, packaging format, packaging shape, storage, and transport conditions as goals to optimize rather than strict requirements to reach. It is preferable to use PET at its nominal performance rather than in extreme conditions. Too high sorption of food constituents in disposed bottles can preclude the capability of recycling mechanically PET, that is decontamination by washing with solvents.

- *Hydrolysis of PET and its consequences in severe conditions*

Physical and chemical aging of PET is a global issue, in particular, in the context, where more recycled PET will be used with time. The industry reported difficulties in processing recycled PET in the same way as virgin PET. PET sorption and mechanical properties are known to be affected by hydrolysis (Hosseini *et al.*, 2007). Hydrolysis occurs in the time frame of a few months and can lead to variation in local crystallinity from ~30% to ~40% in a few weeks. Recycling recycled PET will accelerate degradation and related issues. It has been tested that the whole approach was extendable to other polymers including PEN and PLA, offering additional alternatives for some specific applications. It is highly desirable to integrate the [E][D][S] in a broader perspective integrating polymer alternatives and the pro and con associated with recycling loops and collection circuits. By diverting the concepts of multiscale modeling (VITRac and Touffet, 2019) and by reusing massive numerical strategies used for the evaluation of consumer exposure (Vitrac *et al.*, 2007a;Vitrac and Leblanc, 2007), it could be possible to integrate the [E][D][S] approach in a context of multiple sourcing and food. The

global goal could be to optimize the design of many packaging at once to facilitate their collection and promote their sustainable recycling and to minimize food waste.

- *Towards integrated engineering*

This work exemplifies the need of integrated engineering and expertise to address global challenges. Chemical engineering can bridge many domains that no specific science and related technology can solve alone (polymer, material, mechanical or food science and technology). Global engineering will contribute to reduce human impacts only if the methodologies and principles are stated and taught. More effort is needed in education and training to initiate and support large collaborative projects on the long term with reusable pieces of software and databases. The robustness of computational tools and approaches is essential when human decisions are transferred to automatic algorithms subjected to various sources of uncertainty. Some standardization and reporting should be invented in the future to facilitate interoperability, maintenance and reuse.

Finally, there is a solution to the Zeno paradox: more human, more food, more packaging, more waste, more impact. We do not have the solution but have the tool to find it. (see **Figure V-41**)

- More personally,

I acquired not only scientific knowledge, but also learnt and enabled to build and manage a general EDS approach with multiobjectives and multidisciplinary. I would like to transfer these knowledge, methodologies and approaches with complexities into reasonable, understandable and applicable numerical tools and make them more robust and sophisticated through further study and collaborative works.

this page is left blank intentionally

Chapter VII. Résumé du travail de thèse en français

Chapter VII. Résumé du travail de thèse en français

VII.1. Contexte du projet de thèse

- *Les défis de l'emballage alimentaire*

Au cours de la dernière décennie, deux points de vue se sont opposés sur les avantages des emballages alimentaires. La population mondiale devrait atteindre 9,8 milliards en 2050, contre 7,6 aujourd'hui (UN, 2017), dont 68% dans des zones urbaines (UN, 2018).

Selon le point de vue dominant, les emballages alimentaires offriraient une solution à la distribution des denrées alimentaires aux populations urbaines et vieillissantes. Ces populations, qui vivent loin des zones de production, privilégient la commodité de préparation et l'expérience de consommation. Dans cette logique, les emballages alimentaires permettraient une réduction des déchets alimentaires (Williams and Wikström, 2011;Williams *et al.*, 2012). Tous les choix devraient donc être durables et efficaces : premier sur le marché, à des coûts compétitifs, avec une expérience de consommation améliorée, minimisation les impacts environnementaux (Coles and Kirwan, 2011). La sécurité alimentaire serait introduite comme un compromis entre la protection des aliments, l'hygiène apportée par l'emballage et le risque de contamination associé à leur utilisation.

Des avis alternatifs significativement négatifs sur les emballages alimentaires sont progressivement apparus (Hamaide *et al.*, 2014). Ils ont été associés successivement à des sources potentielles de substances toxiques, de déchets, de gaz à effet de serre, etc. Lors du dernier forum du Food Packaging Forum (Stieger, 2018), les experts ont conclu que les matériaux en contact avec les aliments (plastiques, élastomères, vernis, adhésifs, encres d'impression, papier et carton) représentaient la principale source de contaminants chimiques dans les aliments. Parmi eux, les matériaux plastiques occupent la plus grande part du marché des applications au contact des aliments (Geueke *et al.*, 2018). Ils sont responsables de 80 à 85% du total des déchets marins sur la planète (Bergmann *et al.*, 2017;Pierdomenico *et al.*, 2019) et d'une partie des microplastiques qui contaminent l'environnement (EFSA, 2016;Lusher *et al.*, 2017;Silberbauer and Schmid, 2017;Pierdomenico *et al.*, 2019).

- *L'objectif général des travaux : conception raisonnée des emballages pour les boissons alcoolisées*

L'innovation continue dans les matériaux et la conception des emballages peut contribuer à relever les défis mondiaux que posent l'emballage, la transformation et la distribution

d'aliments. La virtualisation des étapes fastidieuses de la conception des emballages telles que la conceptualisation, le prototypage, l'optimisation des emballages et la validation de la durée de conservation peut accélérer l'exploration de solutions alternatives. Une méthode d'ingénierie concurrente a été développée pour concevoir des emballages sûrs (Nguyen *et al.*, 2013). L'approche est en deux étapes. La première consiste à [E]valuer les transferts de toutes les substances qui peuvent être désorbées par les composants de l'emballage. La seconde réutilise les concepts de l'Analyse des Modes de Défaillance, de leurs Effets et de leur Criticité (AMDEC) pour prendre classer les combinaisons (substances, composants, designs) et ainsi prendre une [D]écision sur l'acceptabilité des risques. Si la criticité cible n'est pas obtenue, la méthode ne permet toutefois pas d'explorer de solutions alternatives. Les travaux visent à généraliser l'approche pour les boissons alcoolisées en introduisant i) une étape de ré[S]olution sous contraintes (ex. durée de vie, géométrie), ii) les impacts environnements, iii) une géométrie 3D paramétrable compatible avec les logiciels de conception assistée par ordinateur.

- *Une illustration de l"étape de résolution*

L'analyse de cycle de vie, définis dans les normes ISO 14040 (2006a) and ISO 14044(2006b), est une technique bien établie, mais elle reste rétrospective et encourage principalement l'utilisation de matériaux biosourcés, recyclables ou biodégradables. Des éléments d'ingénierie sont introduits dans la démarche d'écoconception (Brezet and Van Hemel, 1997;Crul *et al.*, 2009). Comme l'a souligné Dufrene *et al.* (2013), la démarche d'écoconception tend à être idiographique, cas dépendant, sans généralisation ni standard. La thèse propose d'introduire une étape d'optimisation multicritère (étape [S]), qui pallie les défauts des deux méthodes précédentes pour résoudre les objectifs contradictoires suivants : augmenter la durée de vie des boissons alcoolisées sans augmenter les impacts environnementaux et les risques de contamination. Le principe général de l'optimisation convexe est illustré sur un exemple de conception mettant en jeu quatre géométries simplifiées de bouteilles (numérotées $D_1..D_4$) représentées sur la **Figure III-1**. La question générale est qu'elle est la(les) géométrie(s) de bouteille (de capacité variable $V_F^{t=0}$) parmi les quatre représentées ou issues de leurs généralisations qui permettent d'obtenir le meilleur compromis ?

Le raisonnement repose sur liqueur (ex. vodka) pour laquelle la durée de vie est limitée essentiellement par la perte en eau vers l'ambiance de stockage. On suppose que la perméation d'eau au travers des parois (épaisseur uniforme : l_p ; surface exposée à la boisson et à sa vapeur : A) est unidirectionnelle et à l'état stationnaire. Ces hypothèses conduisent à une relation linéaire entre la masse de la bouteille à vide, m_P, et la durée de vie de la boisson, t_{shelf} :

$$m_P = A\rho_p l_p = \frac{\rho_p}{\rho_F}\frac{D_p}{k_p}\frac{A}{V_F^{t=0}}\cdot A\frac{M\Delta p}{\%\Delta m_F}t_{shelf} \qquad \text{(VII.1)}$$

où $\{\rho_k\}_{k=P,F}$ est la masse volumique des parois de l'emballage ($k = P$) et de la boisson ($k = F$) ; Δp est la différence de pression partielle de part et d'autre de la paroi ; D_p et k_p sont respectivement les coefficients de diffusion et de Henry de la paroi.

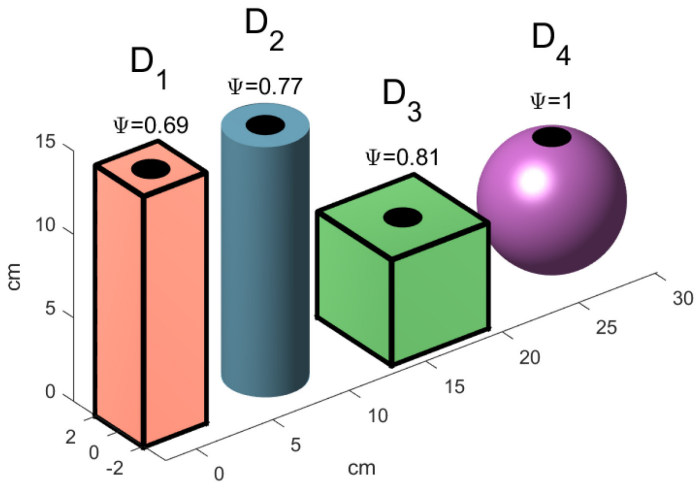

***Figure VII-1**. Designs simplifiés de bouteilles (D_1..D_4) utilisés pour illustrer la démarche d'optimisation géométrique sous contraintes du matériau et du produit emballé. La hauteur b of D_1 and D_2 est fixée à 15 cm. Le disque noir (∅ 2 cm) représente l'ouverture de la bouteille (le bouchon n'est pas visible).*

L'impact environnemental peut être évalué en considérant la bouteille comme unité fonctionnelle (m_p : masse de déchets), si $V_F^{t=0}$ est imposé, ou, de manière plus générale, la masse cumulée totale des bouteilles correspondant à un profil de consommation donné (p. ex. quantité moyenne bue annuellement par un individu $\langle V_{consumption} \rangle$) :

$$M_P\left(V_F^{t=0}\right) = \max\left(\frac{\left\langle V_{consumption}\right\rangle}{V_F^{t=0}}, \frac{t_{consumption}}{t_{shelf}}\right) m_P \qquad \text{(VII.2)}$$

où $t_{consumption}$ est le temps de consommation de la bouteille. Dans le cas où un facteur de sphéricité $\Psi = \frac{\pi^{\frac{1}{3}}\left(6V_F^{t=0}\right)^{\frac{2}{3}}}{A} \leq 1$ est introduit pour extrapoler continûment les géométries, il est trivial de démontrer que l'impact est réduit quand la sphéricité de la bouteille est plus grande ($\Psi = 1$ pour une sphère) et quand sa capacité est maximisée :

$$M_P = \frac{\left\langle V_{consumption}\right\rangle}{V_F^{t=0}} m_P = \left(\frac{36\pi}{V_F^{t=0}}\right)^{\frac{2}{3}} \frac{\rho_p}{\rho_F} \frac{D_p}{k_p} \frac{1}{\Psi^2} \frac{M\Delta p}{\%\Delta m_F} t_{shelf} \left\langle V_{consumption}\right\rangle \qquad \text{(VII.3)}$$

En l'absence de contraintes, les Eqs. (VII.1) et (VII.3) admettent un seul minimum global correspondant à $t_{shelf} = 0$. Le problème d'optimisation multicritère est mieux posé mathématiquement en introduisant des contraintes sur la capacité des bouteilles, les durées de vie minimales et maximales ainsi que sur les performances des bouteilles :

$$
\begin{aligned}
&(a)\ t_{\text{chain}}^{\text{supply}} + t_{\text{consumption}}^{\text{low-profile}} \le t_{shelf} \le 2 \text{ years} \\
&(b)\ m_p^{sphere} \le m_p \le m_p^{D_1, V_F^{t=0}} \\
&(c)\ 0.25 \text{ L} \le V_F^{t=0} \le 0.75 \text{ L}
\end{aligned}
\tag{VII.4}
$$

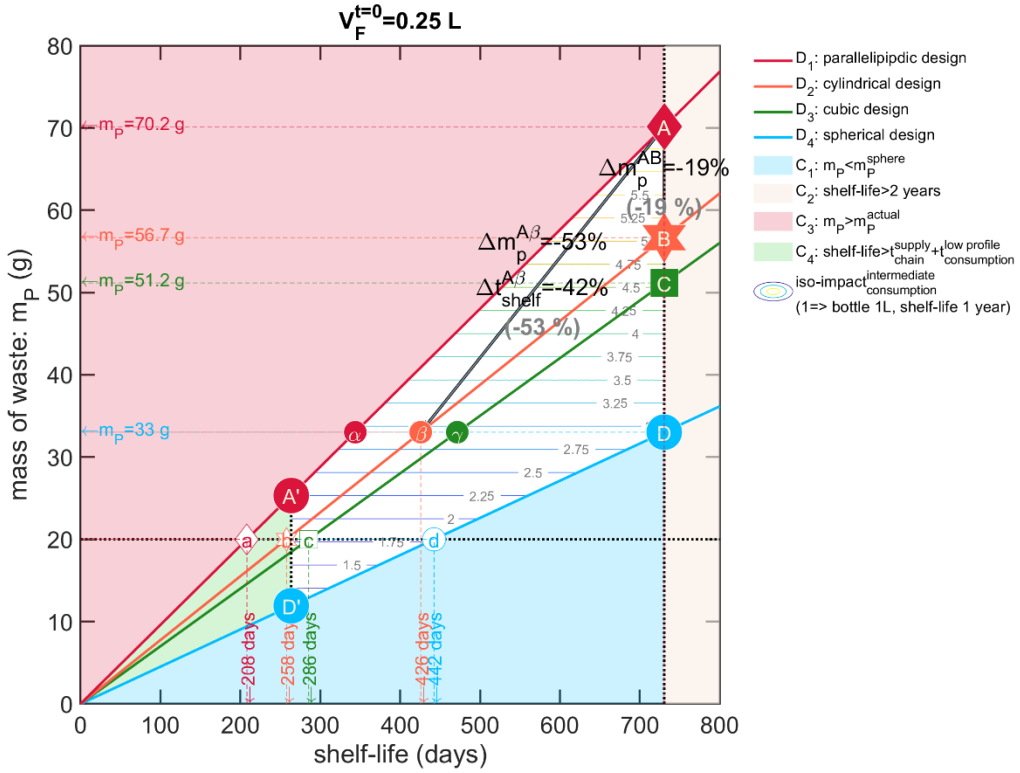

***Figure VII-2**. Représentation géométrique des équations (VII.1) et (VII.3)-(VII.4) pour une bouteille de 0.25 L. Les isocontours représentent les valeurs du rapport* $\frac{M_P\left(V_F^{t=0}=0.25\ L\right)}{M_P\left(V_F^{t=0}=1\ L\right)}$.

Le problème complet associé aux Eqs. (VII.1) et (VII.3)-(VII.4) est représenté géométriquement sur la **Figure VII-2** en prenant en compte un temps de distribution $t_{chain}^{supply} = 3$ mois et en considérant une consommation minimale d'un verre par mois. Pour un volume donné $V_F^{t=0} = 0.25$ L, l'optimum de Pareto, tel que m_P soit minimisé et t_{shelf} soit maximisé, est nécessairement un sommet du polygone convexe $AA'D'D$; il s'agit du point D correspondant à la sphère D4. Tout point intérieur est moins performant, ainsi le point β représente le gain associé au remplacement du design D1 par D2. La substitution permet d'obtenir un impact équivalent au point D (réduction de poids de -53%), mais au prix d'une réduction de la durée de vie de -42%. L'analyse des impacts en prenant M_P comme unité fonctionnelle donne une image plus nuancée, réduire la durée de vie quand celle-ci est supérieure à la durée de consommation n'a aucune conséquence sur la l'impact puisque le consommateur achètera de toute façon une autre bouteille. Ainsi, il est démontré que l'introduction de contraintes d'inégalités ou d'égalité permet de construire une optimisation itérative prenant en compte l'ensemble des paramètres

géométriques, de la boisson, du profil de consommation et des propriétés physicochimiques du matériau retenu.

- *L'approche [E][D][S] et la démarche poursuivie pour sa paramétrisation et validation*

L'étude de cas présentée précédemment est très simplifiée. La durée de vie des boissons alcoolisées dépend du transfert mutuel de l'eau et de l'éthanol dans des bouteilles présentant des profils d'épaisseur variables. Ni les propriétés du polymère ni celles de la boisson ne sont linéaires avec la composition de la boisson et la température. Une approche générique à trois étapes a été développée en prenant le polyéthylène téréphtalate et les mélanges hydroalcooliques comme prototype.

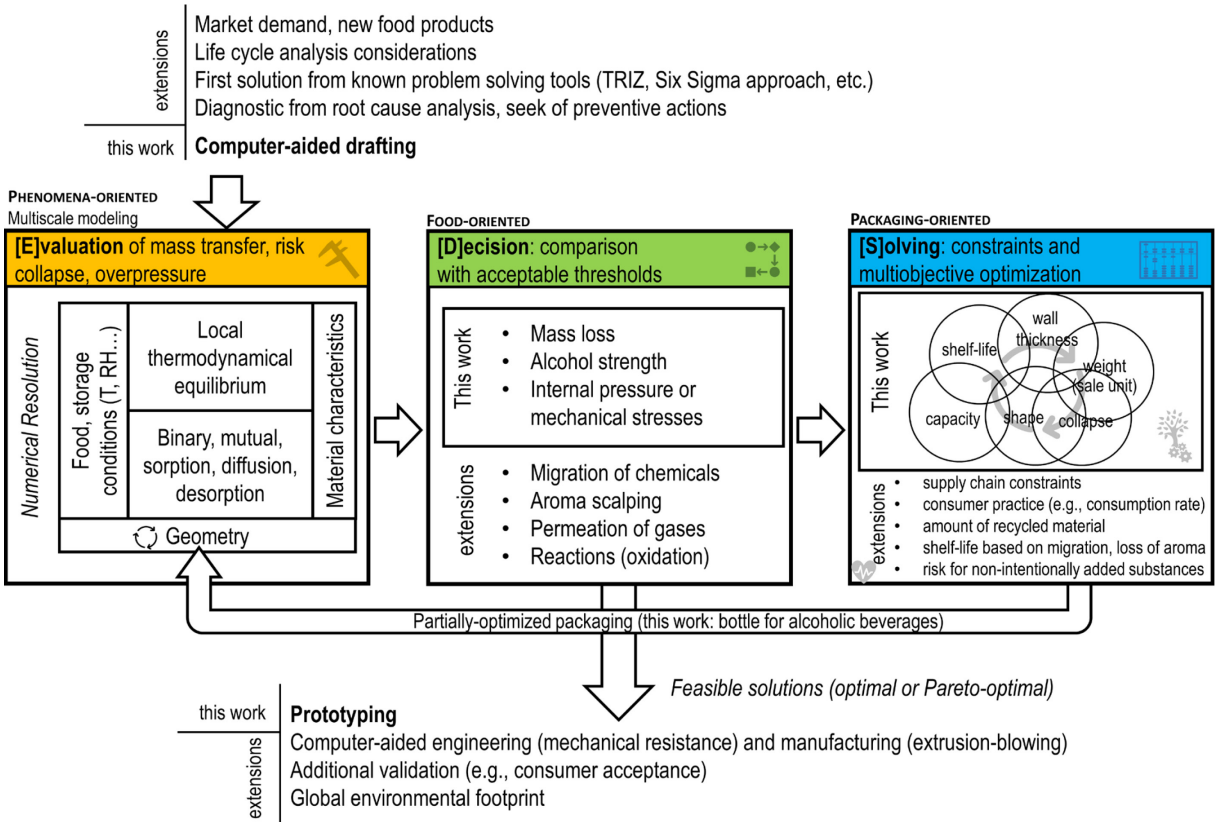

***Figure VII-3**. Principe du prototypage rapide de bouteilles pour les boissons alcoolisées via l'approche itérative à trois Etapes [E]valuation, [D]écision et ré[S]olution proposée.*

En remarquant que la conception d'emballages écoresponsables et sûrs doit tenir également compte de critères d'alimentarité de plus en plus stricts (ex. risques associés aux substances non intentionnellement ajoutées) ainsi que possibles, mais aussi des interactions contenant-contenu, plusieurs niveaux de sophistication ont été introduits. Il s'agissait notamment de prédire les coefficients de diffusion de l'eau, de l'éthanol et des solutés organiques dans des matrices polymères arbitraires à partir de la théorie des volumes libres. Le schéma

[E][D][S] avec ses modules développés et ses extensions possibles est présenté sur la Figure VII-3.

VII.2. Principaux résultats

L'approche [E][D][S] requiert beaucoup d'hypothèses et de données. L'étude de cas présentée précédemment a montré qu'un même modèle fruste pouvait permettre une formalisation objective et robuste. Parce que les principes de l'optimisation convexe sont bien établis, les travaux se sont focalisés sur les différents raffinements nécessaires de l'étape de d'[E]valuation. Une modélisation par paliers a été proposée. Aux paliers 1 et 2, la géométrie réelle de la bouteille est introduite sans simplification, mais les données physicochimiques de la littérature sont utilisées. Seul un couplage non linéaire est considéré au niveau de la condition limite matière entre la boisson et le polymère. Ce niveau de détail est retenu pour l'optimisation non supervisée du design. Aux paliers 3 et 4, les propriétés de diffusion et/ou de sorption mesurées pendant la thèse sont utilisées. Il s'agit notamment d'obtenir une analyse de sensibilité aux hypothèses retenues et permettre l'extension des résultats à des scénarios plus complexes.

VII.2.1. Exemple d'optimisation non supervisée aux paliers 1 et 2

Les transferts couplés d'eau et d'éthanol sont résolus numériquement sur la géométrie réelle en coordonnées curvilignes. L'utilisation d'un modèle implicite de boissons permet de réduire considérablement l'effort de calcul pour des durées de vie très longues tout en conservant les profils d'épaisseur réels et les surfaces d'échange (plane ou courbe, avec ou sans symétrie). Les géométries de bouteille sont optimisées itérativement afin de vérifier plusieurs niveaux de contraintes incluant la consistance du modèle tridimensionnel, la capacité de la bouteille et d'autres facteurs de forme (ex. col, fond). Pour chaque géométrie de bouteille testée, l'épaisseur des parois est optimisée de manière à satisfaire le critère de durée de vie de la boisson en fonction de ses conditions de stockage et de sa composition. Un exemple d'optimisation pour des mignonnettes destinées à la consommation en avion est présenté sur la **Figure VII-4**. Le critère de durée de vie s'appuie sur une double condition : variation du titre alcoolique inférieure à 0.3 %v et à une variation de masse inférieure à 1.5 %. La méthode permet d'obtenir une réduction de poids de plus de 50% par rapport à un modèle de bouteille grossier et non optimisé (**Figure VII-4**e). L'approche permet en outre d'identifier automatiquement toutes les géométries qui présentent des performances équivalentes, ici en fonction de l'épaisseur W et de la profondeur D (**Figure VII-4**g).

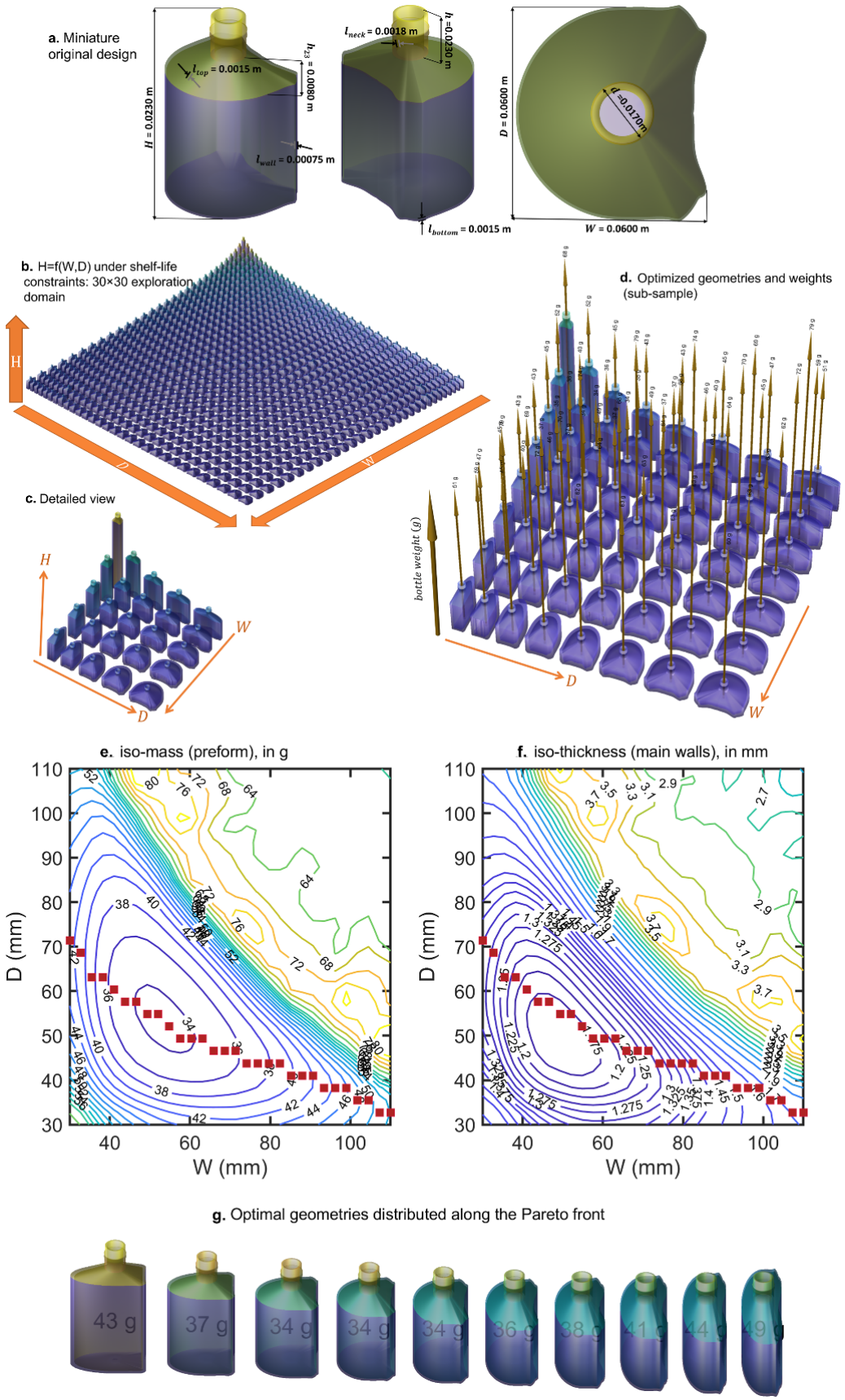

***Figure VII-4**. Optimisation de la géométrie d'une mignonnette (capacité 150 mL et un volume d'espace de tête de 10 mL) utilisée pour le transport aérien avec une durée de vie de 180 jours à 25°C pour une boisson de type vodka.*

VII.2.2. Cosorption non linéaire dans le polyéthylène téréphtalate (PET)

Les polymères vitreux sont des liquides sous-refroidis (solides amorphes) hors équilibre. Ils évoluent donc au cours du temps et présentent un fort effet mémoire. Dans ses conditions d'utilisation inférieure à la température de transition vitreuse T_g, le PET présente donc un comportement en sorption fortement non linéaire résumé sur la **Figure VII-5**a,b (les effets d'hystérésis ne sont pas représentés).

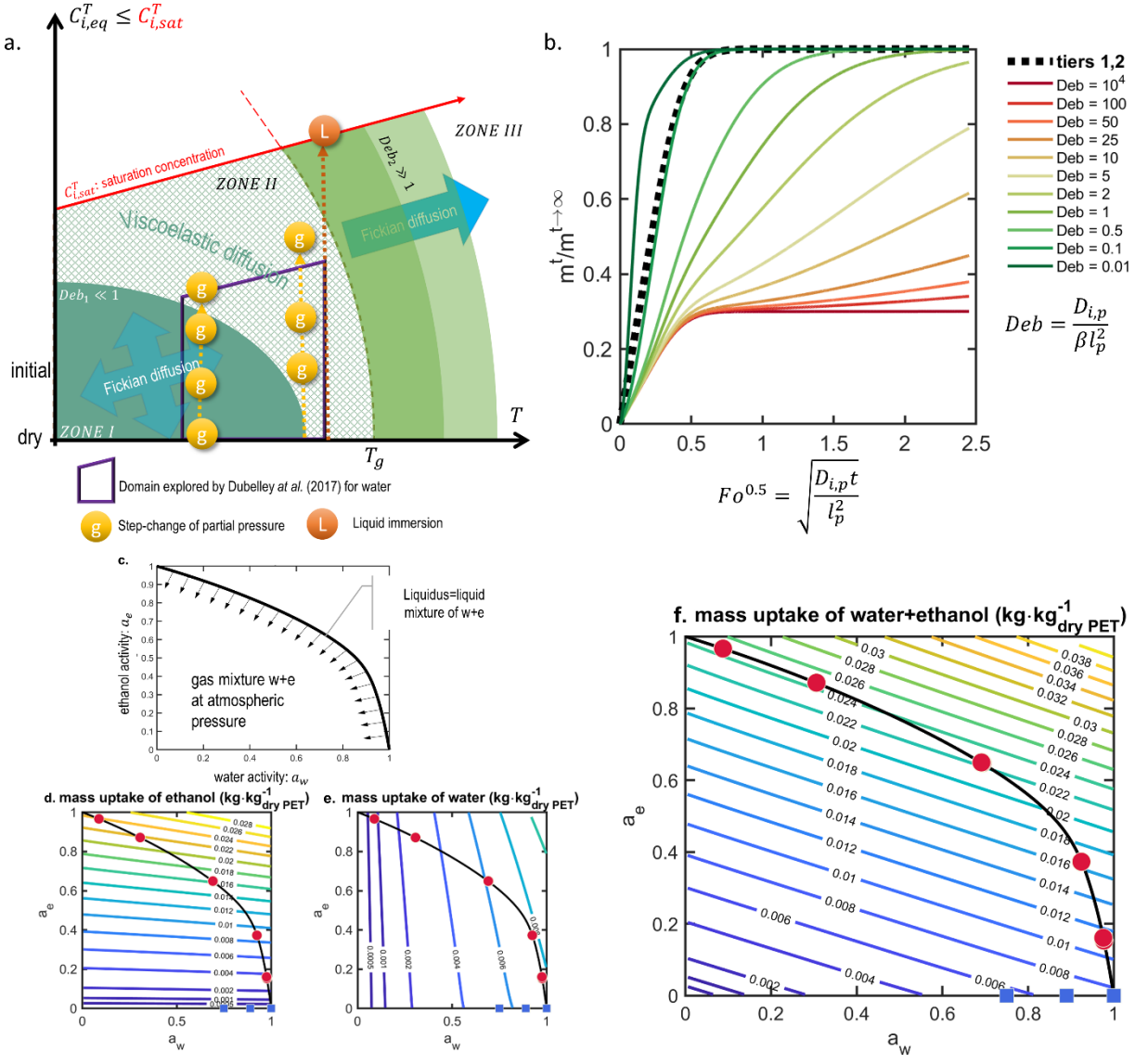

Figure VII-5**. Principe de l'étude des propriétés de sorption dans le PET (a-b) et isotherme ternaire eau-éthanol déterminée à 50°C (c-f).* La courbe en gras représente le « liquidus » et les symboles les conditions utilisées pour la validation présentée dans la ***Figure V-21.

Un comportement Fickien soumis aux seuls effets du gradient de concentration existe soit à l'état caoutchoutique ($T > T_g$), soit loin de la température de transition vitreuse ($T \ll T_g$). Aux températures intermédiaires inférieures à T_g, deux forces motrices se combinent aux mêmes échelles de temps : le gradient de concentration et la relaxation viscoélastique. Leurs

effets sur les cinétiques de transfert dépendent de de la valeur du coefficient de diffusion $D_{i,p}$ du soluté i considéré (unité en $m^2 \cdot s^{-1}$) et de la vitesse de la relaxation du polymère β (unité en s^{-1}). Le nombre de Deborah $Deb = \frac{D_{i,p}}{\beta l_p^2}$ caractérise le rapport entre le temps de relaxation du polymère et le temps caractéristique de diffusion du soluté i. Les coefficients de diffusion ne peuvent être déterminés expérimentalement par sorption avec confiance que pour $Deb \to \infty$ et $Deb \to 1$. A contrario, les propriétés d'équilibre à l'état vitreux ne sont déterminables à l'état vitreux que pour des temps de diffusion suffisamment longs ($Fo \gg Deb$), tels que la relaxation du polymère soit complètement établie. Dans une logique de surestimation des transferts (estimation conservatrice de la durée de vie des boissons), l'utilisation dans un modèle de transfert négligeant la relaxation, mais prenant en compte les vraies valeurs des coefficients de diffusion et de sorption, surestime toujours la sorption réelle tant que $Deb > 1$. La démonstration est fournie par la courbe en pointillés sur la **Figure VII-5**b. Cette propriété justifie les estimations des transferts aux paliers 1 et 2 ainsi que l'utilisation de la théorie de Flory-Huggins pour estimer la cosorption de l'eau et de l'éthanol dans le PET.

Un modèle d'isotherme ternaire, donnant la sorption maximale de l'eau et de l'éthanol dans le polymère P=PET en fonction des activités de l'eau a_w, de l'éthanol a_e et de la température T, a été paramétré à partir des coefficients de Flory-Huggins binaires dans le PET, $\{\chi_{i+P}^T\}_{i=w,e}$ et du coefficient binaire non-idéal eau-éthanol $\chi_{w+e}^T < 0$. Il s'exprime en fonction des fractions volumiques $\{\phi_i\}_{i=w,e}$:

$$\begin{aligned}
\ln a_{w,P}\left(\phi_w,\phi_e,T\right) &= \ln\left(\phi_w\right)+\left(1-\phi_w\right)-\phi_e\frac{\overline{V}_w}{\overline{V}_e}-\left(1-\phi_w-\phi_e\right)\frac{\overline{V}_w}{\overline{V}_P} \\
&\quad+\left(\chi_{w+e}^{(\phi_e,\phi_w)}\frac{\overline{V}_w}{\overline{V}_e}\phi_e+\chi_{w+P}^T\left(1-\phi_w-\phi_e\right)\right)\left(1-\phi_w\right)-\chi_{e+P}^T\frac{\overline{V}_w}{\overline{V}_e}\phi_e\left(1-\phi_w-\phi_e\right) \\
\ln a_{e,P}\left(\phi_w,\phi_e,T\right) &= \ln\left(\phi_e\right)+\left(1-\phi_e\right)-\phi_w\frac{\overline{V}_e}{\overline{V}_w}-\left(1-\phi_w-\phi_e\right)\frac{\overline{V}_e}{\overline{V}_P} \\
&\quad+\left(\chi_{w+e}^{(\phi_e,\phi_w)}\frac{\overline{V}_e}{\overline{V}_w}\phi_w+\chi_{e+P}^T\left(1-\phi_w-\phi_e\right)\right)\left(1-\phi_e\right)-\chi_{w+P}^T\frac{\overline{V}_e}{\overline{V}_w}\phi_w\left(1-\phi_w-\phi_e\right)
\end{aligned} \tag{VII.5}$$

où $\{\overline{V}_i\}_{i=e,w,P}$ sont les volumes molaires.

Les isothermes de sorption ternaires à 35°C ainsi que leur interprétation pour des boissons alcoolisées sont reproduites sur la **Figure VII-5**c,f. Dans une boisson alcoolisée, les activités de l'eau et de l'éthanol sont mathématiquement dépendantes. La relation est appelée « liquidus » (c-a-d : mélange en phase condensée) et tracée en trait gras. L'espace sous la courbe représente un mélange gazeux d'eau et d'éthanol à pression atmosphérique explorable avec la

microbalance de sorption mise en œuvre dans ce travail. Les résultats de validation aveugle de l'isotherme ternaire sont présentés sur la **Figure V-21**. Les mesures ont été obtenues ont été réalisées par immersion à l'aide de la méthode des sels saturés (plusieurs répétitions). La déviation résiduelle a été associée par une relaxation incomplète du PET aux fortes activités en eau.

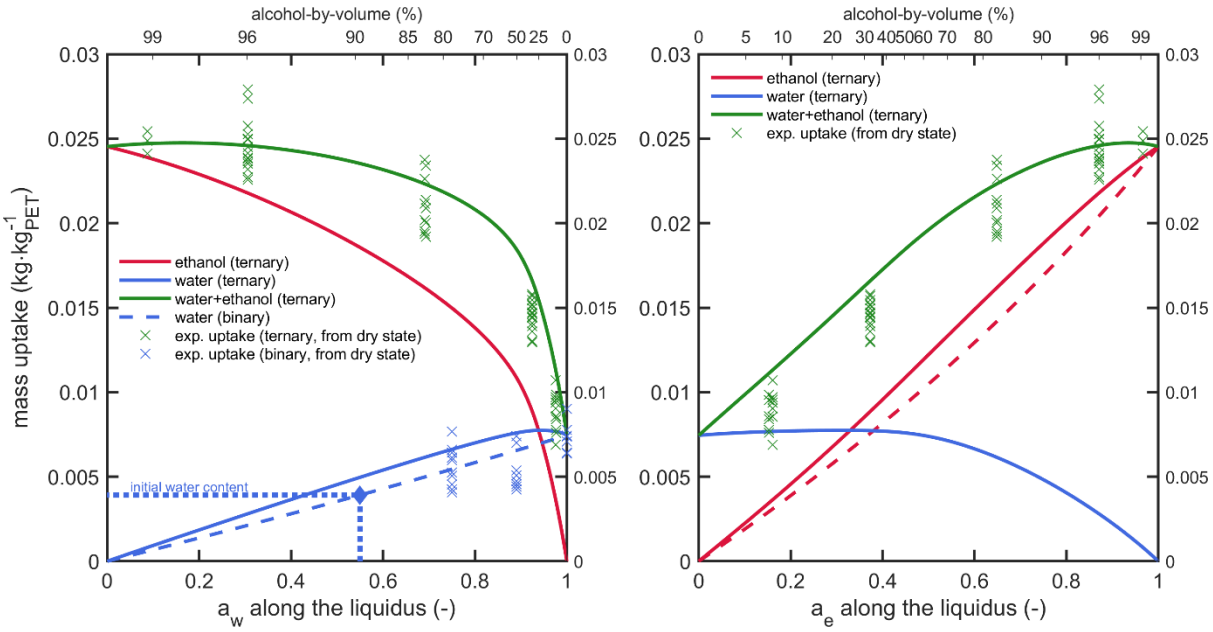

***Figure VII-6**. Comparaison entre les prédictions de l'isotherme ternaire eau-éthanol dans le PET à 35°C avec les sorptions expérimentales.*

VII.2.3. Prédiction des coefficients de diffusion à partir d'une généralisation de la théorie des volumes libres

Les coefficients de diffusion sont indispensables à la généralisation de l'approche [E]valuation, [D]écision, ré[S]olution à des solutés autres que l'eau et l'éthanol et à des polymères autres que le PET. Il a été proposé de reformuler la théorie des volumes à partir du comportement de solutés linéaires à l'état caoutchoutiques, où ils sont aisés de les mesurer, et de réutiliser les nombreux résultats de la théorie des volumes pour les généraliser à l'état vitreux et à des solutés de géométrie variable et présentant éventuellement des interactions spécifiques avec la matrice polymère. Les principes et la filiation avec les théories existantes sont résumés sur la **Figure VII-7**. L'élément central de la nouvelle théorie est de remarquer qu'il existe une relation d'invariance entre les coefficients de diffusion et le nombre de motifs répétés dans le soluté. En d'autres termes, la théorie classique des volumes libres permet de prédire l'effet du volume d'un soluté rigide alors que les lois d'échelle permettent de généraliser le comportement à plusieurs unités. Parce que des déplacements concertés des unités rigides

sont requis, les lois d'échelle permettent également d'accéder aux paramètres spécifiques au polymère hôte à l'état caoutchoutique. La généralisation à l'état vitreux repose sur la même hypothèse que la théorie de Vrentas et Duda originale, les énergies d'activation de la diffusion sont de part et d'autre de la T_g dans le même rapport que les coefficients d'expansion thermique. Ces travaux théoriques réalisés en collaboration avec l'Institut Fraunhofer IVV (Freising, Allemagne) a conduit à de nombreux résultats originaux, qui sont détaillés dans les chapitres précédents.

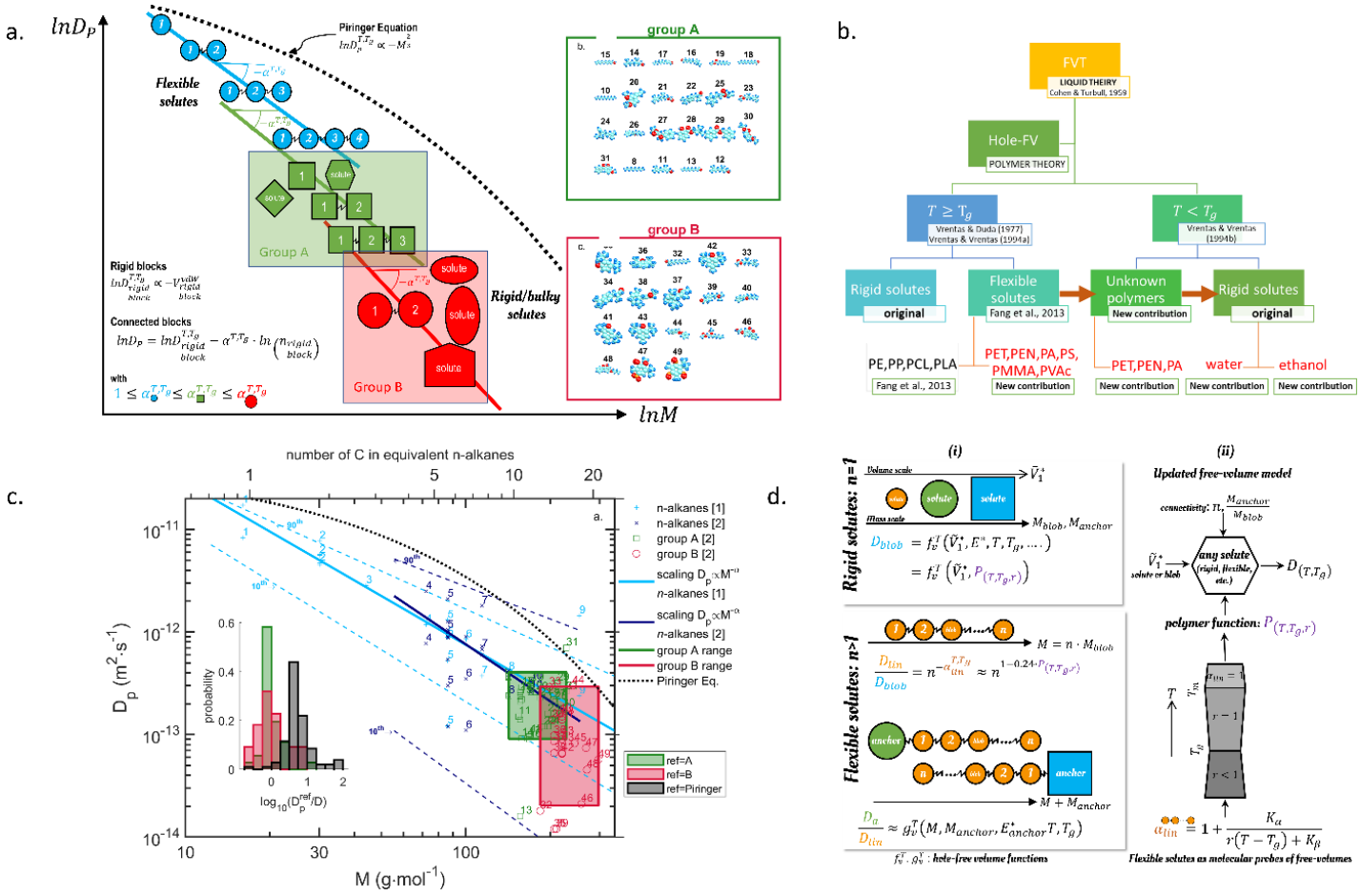

***Figure VII-7**. Relations en lois d'échelle, théorie des volumes libres et coefficients de diffusion : (a) comparaison des lois d'échelle avec la masse moléculaire pour des solutés linéaires et encombrés ; (b) filiation de la théorie des volumes libres ; (c) lois d'échelle dans le polyéthylène basse densité à 23°C ; (d) principe du paramétrage de la théorie des volumes libres à partir des coefficients de diffusion de molécules sondes linéaires. L'équation de Piringer utilisée pour démontrer la conformité des matériaux d'emballages alimentaires est représentée en pointillés sur la figure (a) ; elle correspond à un surestimateur empirique qui sous-estime la dépendance réelle à la masse moléculaire M.*

Données des coefficients de diffusion : [1] Flynn (1982), [2] Hinrichs and Piringer (2002);NIST (2019).

Les expressions pratiques pour prédire les coefficients de diffusion dans des polymères arbitraires pour des solutés rigides ou flexibles sont présentées dans la **Figure VII-8**a,b. Elles apportent une avancée majeure pour les polymères, dont les volumes libres participant à la

diffusion ne sont pas renseignés, notamment pour les polyesters comme le PET. Le seul prérequis est de disposer du comportement de molécules sondes de type *n*-alcanes à l'état caoutchoutique. La capacité à prédire les coefficients de diffusion de deux solutés indépendants, l'eau et l'éthanol, à l'état vitreux à partir des coefficients de diffusion des *n*-alcanes à l'état caoutchoutique est illustré sur la **Figure VII-8**c-e.

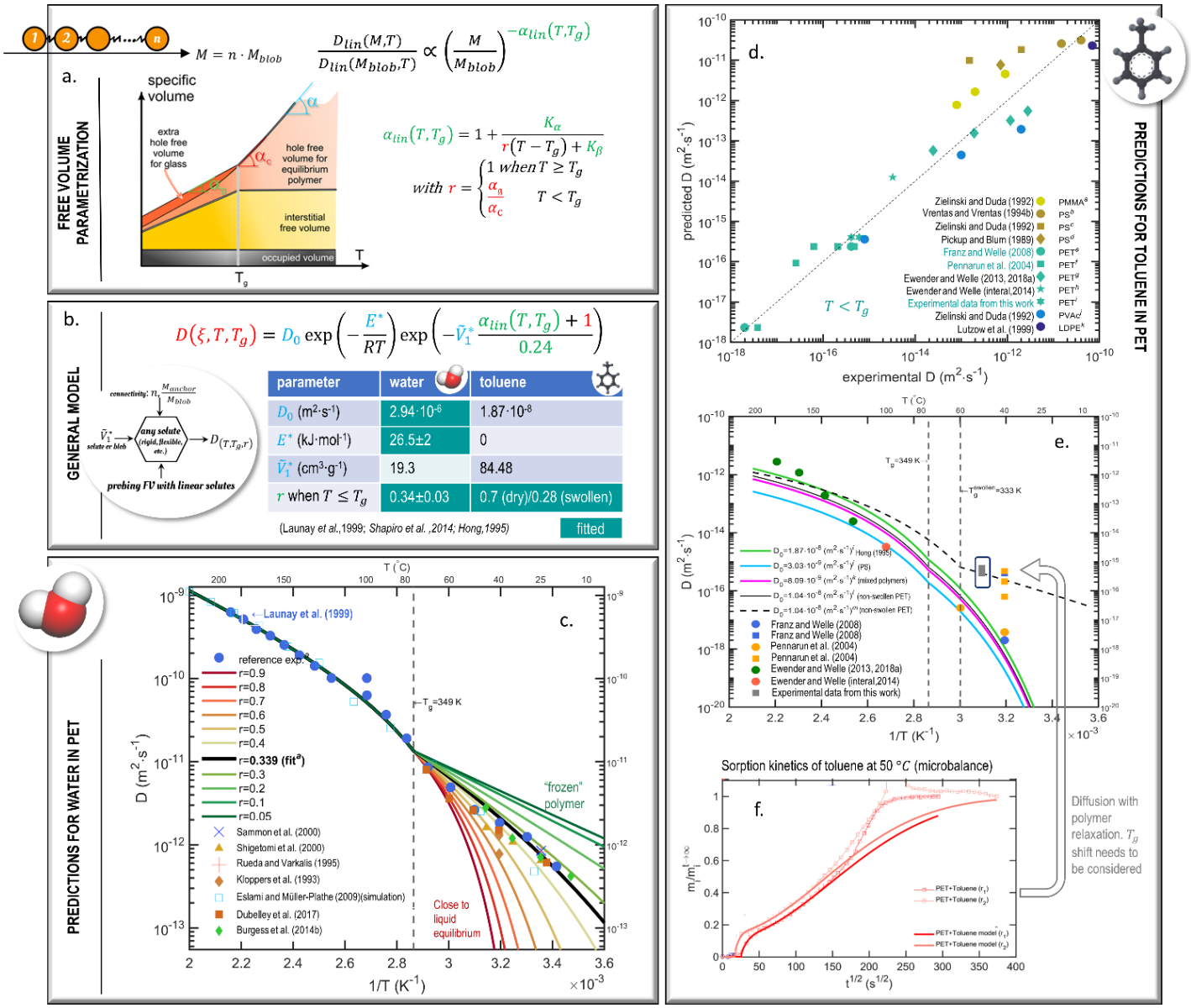

***Figure VII-8**. Paramétrisation et prédictions des coefficients de diffusion de l'eau et de l'éthanol dans le PET à l'état caoutchoutique et vitreux : (a) lois d'échelle à l'état caoutchoutique et vitreux pour des molécules sondes linéaires ; (b) modèle générique de coefficients de diffusion et paramétrage du modèle pour l'eau et le toluène ; (c) validation pour l'eau sur la base d'une identification de r à partir des données de Launay et al. (1999) ; (d) validation pour le toluène dans cinq polymères ; (e) dépendance des coefficients de diffusion du toluène à la température ; (f) cinétiques de sorption à 50°C mettant en évidence la relaxation du polymère.*

Pour l'eau, il faut tenir compte d'une interaction spécifique entre l'eau et le PET. La valeur retenue de l'énergie d'interaction spécifique E^*est proche de sa chaleur isostérique de sorption. Pour le toluène, cette énergie est nulle et les valeurs du facteur préexponentiel D_0 publiées dans la littérature sont directement utilisables. Seul de facteur de sous-refroidissement r et la T_g doivent être identifiés ou mesurés expérimentalement. Parce que toutes les propriétés peuvent être obtenues indépendamment des coefficients de diffusion du soluté d'intérêt, la théorie étendue des volumes libres reste une théorie générique basée sur des principes premiers. Il est important de remarquer que la formulation proposée, à la différence de la formulation initialement proposée par Vrentas et Duda, ne requiert pas une définition explicite de la nature des volumes libres dans le polymère qui participent à la translation des blocs rigides. Leurs effets sont compris dans la valeur de l'exposant α_{lin}^{T,T_g} qui englobe tous les effets de couplage entre les relaxations du polymère et la capacité à translater des segments rigides du soluté (Fang *et al.*, 2013). Les constantes K_α et K_β acceptent des constantes génériques pour neuf polymères (polyoléfines, polystyrènes, polyvinyles, polyesters), respectivement 65±11 K et 252±22 K, respectivement.

VII.3. Discussion, conclusions et perspectives

- *La relaxation comme principale source d'incertitude*

L'évaluation de la durée de vie d'une boisson alcoolisée est très simplifiée parce qu'elle considère que l'eau et l'éthanol, les fuites par le bouchage ne sont pas considérées, les pertes d'arômes et le risque de migration ne sont pas directement considérés. Il n'y a toutefois pas de biais particulier dans l'approche [E][D][S] développée et, a priori, l'ensemble des phénomènes peut être intégré via des modules et des critères supplémentaires. La non-prise en compte de la relaxation du polymère est en revanche plus problématique, mais qu'elle entraîne nécessairement une estimation par défaut de la durée de vie du polymère. Il serait trompeur de considérer que la relaxation est un phénomène lent et que la diffusion est un phénomène rapide. Les deux mécanismes se produisent simultanément et sans délai. Aux temps courts, l'intensité de la diffusion tend à masquer le transfert de matière induit par la relaxation. Les deux phénomènes peuvent être mis en évidence en temps réel en étudiant la prise de masse suivie de la perte de poids d'un échantillon épais de parois de bouteille en PET soumis à une fluctuation périodique de l'humidité relative. La réponse typique d'une paroi de 630 µm d'épaisseur est présentée sur la **Figure VII-9** en réponse à une fluctuation sinusoïdale de ±20% de période 640 s. Les fluctuations du flux de matière et de la pression partielle sont comparées après avoir retiré le retard du signal de la masse sur celui de la pression partielle. La courbe obtenue présente un signal qui reboucle sur lui-même avec une forte hystérèse et déviant d'un modèle

linéaire passant par zéro : condition de de flux nul en l'absence de gradient de potentiel chimique. Le flux est plus fort en sorption qu'en désorption. Cela démontre l'existence de deux forces motrices lors de la sorption (diffusion Fickienne et relaxation), alors qu'une seule subsiste lors de la désorption (diffusion Fickienne). Le point A correspond au seuil de pression partielle requis pour observer un gain de masse. Le point B correspond à la perte de masse sans différence de pression partielle. Il n'y a pas de théorie triviale pour intégrer ses effets dans l'étape d'[E]valuation. La perméation met en jeu à la fois une sorption sur la face interne (avec théoriquement deux forces motrices) et une désorption sur la face externe (avec théoriquement une force motrice). Il ne peut toutefois y avoir qu'une seule relaxation soumise à des éventuels effets mémoires. A ce stade, il existe une différence notable entre le comportement d'un échantillon isolé (contact symétrique, pas de rigidité de structure) et une bouteille. Pour cette dernière, les conditions de contact sont asymétriques avec des vitesses de relaxation possiblement différentes sur les deux faces, la rigidité de structure est importante et seul le gonflement transverse paraît possible. Ces phénomènes ne sont pas pris en compte et c'est le cas conservatif en pointillés de la **Figure VII-5**b qui est retenu pour plus de robustesse.

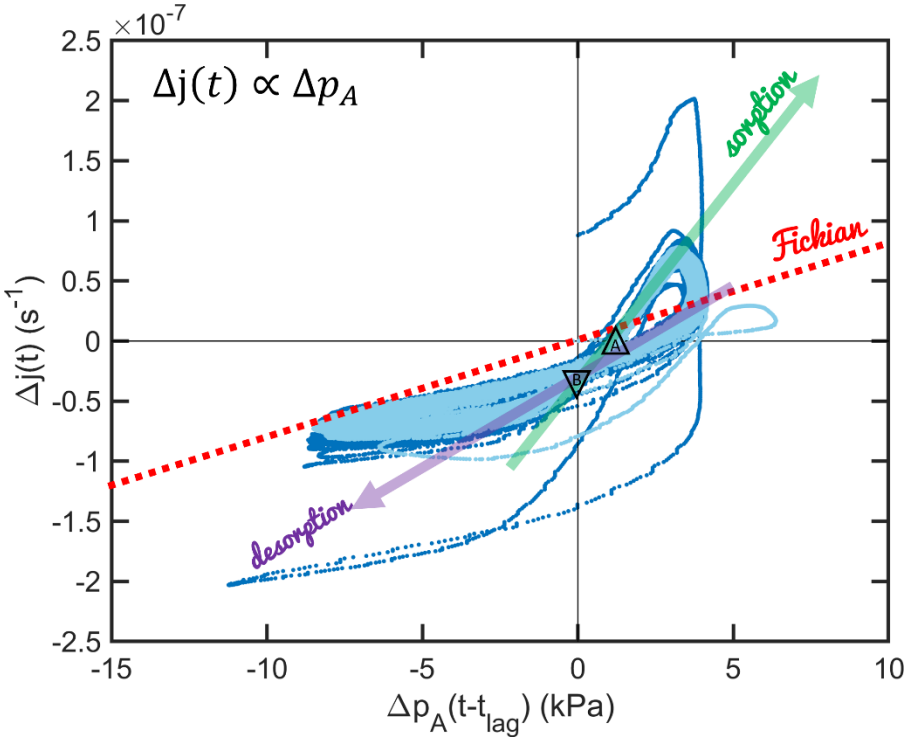

***Figure VII-9**. Analyse des fluctuations du flux de matière en fonction de la fluctuation périodique (période de 240 s) de la pression partielle en vapeur d'eau à 50°C pour un échantillon de 630 µm d'épaisseur.*

- *Description probabiliste de la durée de vie d'une boisson conditionnée en bouteilles*

Dans la pratique les conditions de stockage (durée, température) sont extrêmement variables. Les résultats présentés pour des conditions contrôlées peuvent être généralisés pour

des variations de température arbitraire en introduisant une représentation probabiliste comme celle déjà utilisée pour évaluer le risque de contamination par un matériau Vitrac and Hayert (2005). Sa généralisation aux courbes de perméation de deux solutés est présentée sur la **Figure VII-10**. La distribution des temps de séjours combinés est obtenue par convolution en supposant que les temps de transport et de stockage à une température équivalente de 25°C sont deux variables aléatoires indépendantes.

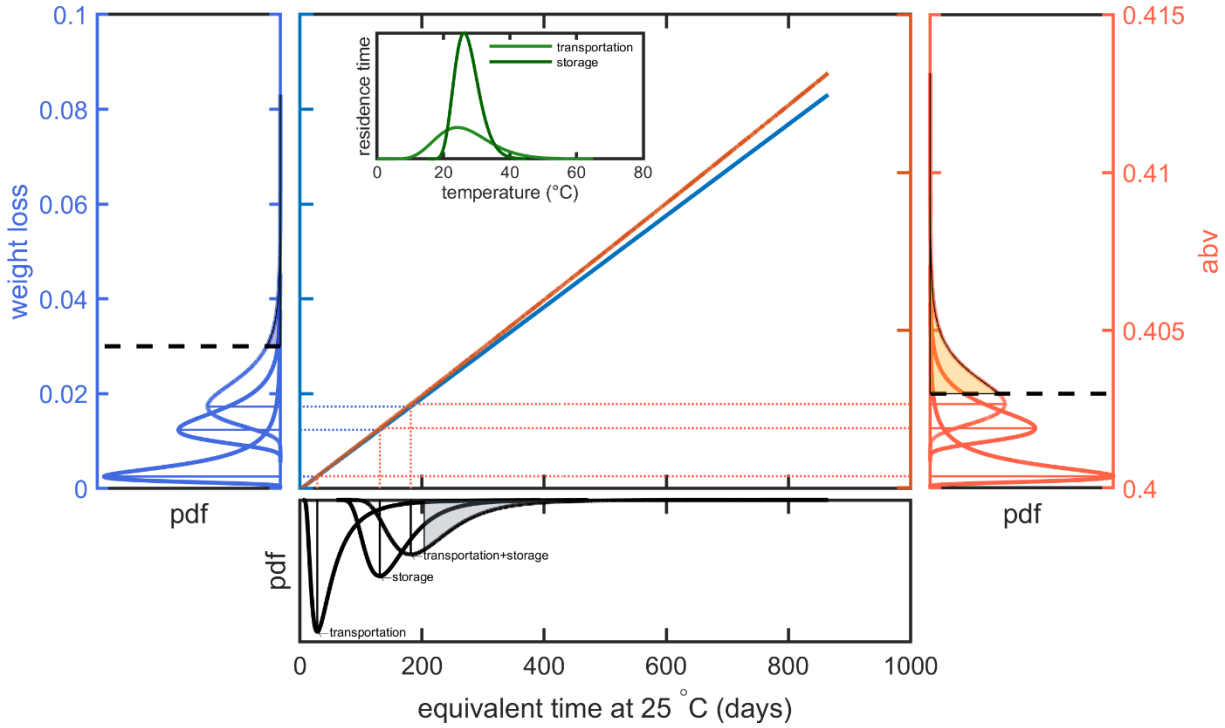

***Figure VII-10**. Distribution de la perte de poids (droite) et de la variation du titre alcoolique (gauche) en fonction des distributions combinées des températures au cours du transport et du stockage (encart). La figure centrale montre la variation déterministe de la perte de poids et du titre alcoolique (abv) en avec un temps de séjour équivalent à 25°C.*

- *Principales conclusions*

Les travaux de recherche ont permis de construire un cadre de calcul dans lequel la conception des emballages alimentaires peut être envisagée comme un problème d'optimisation global. Trois critères ont été ciblés : la durée de conservation, les impacts environnementaux et la sécurité sanitaire des aliments. Ces critères sont généralement étudiés à partir d'essais et d'expériences, et sont donc moins explorés au moyen de calculs numériques. Le travail a donc été initié à partir d'une page presque blanche. La colonne vertébrale de ce projet ambitieux est un logiciel de grande ampleur, qui réutilise de nombreuses briques et concepts de modélisation déjà utilisés pour la modélisation du risque de migration. La devise est «même les modèles imparfaits peuvent être utilisés pour la prise de décision s'ils sont construits de manière conservatrice pour cela». Les modèles de migration, dont le projet s'inspire fortement,

sont construits de manière rationnelle, ils ont une valeur légale et scientifique. Ils diffèrent sans s'y opposer des modèles plus subjectifs d'écoconception et d'évaluation du cycle de vie. Les bouteilles en polyéthylène téréphtalate (PET) pour boissons alcoolisées ont été choisies comme modèle pour élaborer les concepts, écrire un code de calcul spécifique (plus de 65 Klignes de Matlab / Octave), valider et étendre les différentes améliorations. Malgré des simplifications mathématiques et physiques inhérentes aux étapes intermédiaires, les entrées et sorties du projet numérique ont été conçues pour être compatibles avec les standards industriels de conception de produits, d'ingénierie et de prototypage rapide (réalité augmentée, impression 3D).

- *Principales perspectives*

Ces travaux illustrent le besoin d'ingénierie intégrée et de pluridisciplinarité pour faire face aux défis mondiaux. Le génie chimique peut couvrir de nombreux domaines qu'aucune science spécifique ni aucune technologie associée ne peuvent résoudre seules (sciences et technologies des polymères, des matériaux, de la mécanique ou de l'alimentation). L'ingénierie globale ne contribuera à réduire les impacts humains que si les méthodologies et les principes sont énoncés et enseignés. Des efforts supplémentaires sont nécessaires dans le domaine de l'éducation et de la formation pour lancer et soutenir de grands projets de collaboration à long terme avec des logiciels et des bases de données réutilisables. La robustesse des approches et des outils informatiques est essentielle lorsque les décisions humaines sont transférées à des algorithmes peu ou pas supervises et soumis à diverses sources d'incertitude. La modélisation mutltiéchelle couplée à la prise de décision et l'optimisation multicritère sont proposées comme approche commune. Une certaine standardisation et formulation des raisonnements issus des calculs doivent encore être inventée pour faciliter l'interopérabilité, la maintenance et la réutilisation.

Enfin, il existe une solution au paradoxe de Zénon : plus d'êtres humains, plus de besoins d'aliments, plus de transformations et de conditionnements, plus de déchets et finalement plus d'impacts. Nous n'avons pas la solution, mais nous avons l'outil pour la trouver.

this page is left blank intentionally

Chapter VIII. Reference

Chapter VIII. References

Accorsi, R., Versari, L., and Manzini, R. (2015). Glass vs. Plastic: Life Cycle Assessment of Extra-Virgin Olive Oil Bottles across Global Supply Chains. *Sustainability* 7 (3), 2818-2840.

Akeel, U.U., and Bell, S.J. (2013). Discourses of systems engineering. *Engineering Studies* 5 (2), 160-173.

Alexiou, K., Johnson, J., and Zamenopoulos, T. (2010). *Embracing Complexity in Design*. New York, USA: Taylor & Francis.

Almeida, C.M.V.B., Rodrigues, A.J.M., Agostinho, F., and Giannetti, B.F. (2017). Material selection for environmental responsibility: the case of soft drinks packaging in Brazil. *Journal of Cleaner Production* 142, 173-179.

Almeida, C.M.V.B., Rodrigues, A.J.M., Bonilla, S.H., and Giannetti, B.F. (2010). Emergy as a tool for Ecodesign: evaluating materials selection for beverage packages in Brazil. *Journal of Cleaner Production* 18 (1), 32-43.

Amaran, S., Sahinidis, N.V., Sharda, B., and Bury, S.J. (2014). Simulation optimization: a review of algorithms and applications. *4OR* 12 (4), 301-333.

Amienyo, D. (2012). *Life Cycle Sustainability Assessment in the UK Beverage Sector* Thesis, School Of Chemical Engineering And Analytical Science, University of Manchester,UK.

Amienyo, D., Gujba, H., Stichnothe, H., and Azapagic, A. (2013). Life cycle environmental impacts of carbonated soft drinks. *The International Journal of Life Cycle Assessment* 18 (1), 77-92.

Anastas, P.T., and Warner, J.C. (2000). *Green Chemistry: Theory and Practice*. Oxford University Press.

Arnould, D., and Laurence, R.L. (1992). Size effects on solvent diffusion in polymers. *Industrial & Engineering Chemistry Research* 31 (1), 218-228.

Ashurst, P., Hargitt, R., and Palmer, F. (2017). *Packaging, storage and distribution of soft drinks and fruit juice*. Elsevier Science.

Ashurst, P.R. (2016). "Carbonated Beverages," in *Reference Module in Food Science*. Elsevier).

Azzi, A., Battini, D., Persona, A., and Sgarbossa, F. (2012). Packaging Design: General Framework and Research Agenda. *Packaging Technology and Science* 25 (8), 435-456.

Bansal, J.C., Das, K.N., Nagar, A., Deep, K., and Ojha, A.K. (2018). *Soft Computing for Problem Solving: SocProS 2017, Volume. 2*. Springer.

Baumann, H., Boons, F., and Bragd, A. (2002). Mapping the green product development field: engineering, policy and business perspectives. *Journal of Cleaner Production* 10 (5), 409-425.

Becker, L., Van Rompay, T.J.L., Schifferstein, H.N.J., and Galetzka, M. (2011). Tough package, strong taste: The influence of packaging design on taste impressions and product evaluations. *Food Quality and Preference* 22 (1), 17-23.

Belay, Z.A., Caleb, O.J., and Opara, U.L. (2016). Modelling approaches for designing and evaluating the performance of modified atmosphere packaging (MAP) systems for fresh produce: A review. *Food Packaging and Shelf Life* 10, 1-15.

Belley, C. (2011). "Comparative Life Cycle Assessment Report of Food Packaging Products". (Montreal, Quebec: Chemical Engineering Department École Polytechnique de Montréal).

Belnap, N. (2007). Propensities and probabilities. *Studies in History and Philosophy of Science Part B: Studies in History and Philosophy of Modern Physics* 38 (3), 593-625.

Bergmann, M., Tekman, M.B., and Gutow, L. (2017). Sea change for plastic pollution. *Nature* 544, 297.

Bernardo, G. (2012). Diffusivity of alkanes in polystyrene. *Journal of Polymer Research* 19 (3).

Bernardo, G. (2013). Diffusivity of alcohols in amorphous polystyrene. *Journal of Applied Polymer Science* 127 (3), 1803-1811.
Bettin, H., and Spieweck, F. (1990). A Revised Formula for the Calculation of Alcoholometric Tables. *PTB - Mitteilungen. Forschen und Prüfen* 100(6), 457-463.
Billovits, G.F., and Durning, C.J. (1988). Penetrant transport in semicrystalline poly(ethylene terephthalate). *Polymer* 29 (8), 1468-1484.
Boesen, S., Bey, N., and Niero, M. (2019). Environmental sustainability of liquid food packaging: Is there a gap between Danish consumers' perception and learnings from life cycle assessment? *Journal of Cleaner Production* 210, 1193-1206.
Bomgardner, M.M. (2017). Building a better plastic bottle-DuPont, Corbion, and Synvina pilot furan-based polymers made from sugar but must confront PET's dominance. *Chemical & Engineerig News* 95 (43), 17-19.
Bovea, M.D., and Pérez-Belis, V. (2012). A taxonomy of ecodesign tools for integrating environmental requirements into the product design process. *Journal of Cleaner Production* 20 (1), 61-71.
Boyd, S., Boyd, S.P., Vandenberghe, L., and Press, C.U. (2004). *Convex Optimization*. Cambridge University Press.
Boyne, J.A., and Williamson, A.G. (1967). Enthalpies of mixture of ethanol and water at 25.degree.C. *Journal of Chemical & Engineering Data* 12 (3), 318.
Brezet, J.C., and Van Hemel, C.G. (1997). *Ecodesign: A promising approach to sustainable production and consumption*. United Nations Environment Programme.
Brones, F.A., Carvalho, M.M.D., and Zancul, E.D.S. (2017). Reviews, action and learning on change management for ecodesign transition. *Journal of Cleaner Production* 142, 8-22.
Broudin, M., Le Gac, P.Y., Le Saux, V., Champy, C., Robert, G., Charrier, P., and Marco, Y. (2015). Water diffusivity in PA66: Experimental characterization and modeling based on free volume theory. *European Polymer Journal* 67, 326-334.
Brower, M., and Leon, W. (2009). *The Consumer's Guide to Effective Environmental Choices: Practical Advice from The Union of Concerned Scientists*. Potter/Ten Speed/Harmony/Rodale.
Buchert, T., Halstenberg, F.A., Bonvoisin, J., Lindow, K., and Stark, R. (2017). Target-driven selection and scheduling of methods for sustainable product development. *Journal of Cleaner Production* 161, 403-421.
Budzien, J., Mccoy, J.D., Rottach, D., and Curro, J.G. (2004). Effects of chain stiffness and penetrant size on penetrant diffusion in simple polymers: deduced relations from simulation and PRISM theory. *Polymer* 45 (11), 3923-3932.
Buglass, A.J., Mckay, M., and Lee, C.G. (2011). *Handbook of Alcoholic Beverages: Technical, Analytical and Nutritional Aspects*. Malaysia: John Wiley and Sons.
Burgess, S.K., Mikkilineni, D.S., Yu, D.B., Kim, D.J., Mubarak, C.R., Kriegel, R.M., and Koros, W.J. (2014a). Water sorption in poly(ethylene furanoate) compared to poly(ethylene terephthalate). Part 2: Kinetic sorption. *Polymer* 55 (26), 6870-6882.
Burgess, S.K., Mikkilineni, D.S., Yu, D.B., Kim, D.J., Mubarak, C.R., Kriegel, R.M., and Koros, W.J. (2014b). Water sorption in poly(ethylene furanoate) compared to poly(ethylene terephthalate). Part 1: Equilibrium sorption. *Polymer* 55 (26), 6861-6869.
Cappelli, F., Delogu, M., Pierini, M., and Schiavone, F. (2007). Design for disassembly: a methodology for identifying the optimal disassembly sequence. *Journal of Engineering Design* 18 (6), 563-575.
Cappuccio, R., Full, G., Lonzarich, V., and Savonitti, O. (2001). "Staling of roasted and ground coffee at different temperatures: combining sensory and GC analysis", in: *19eme Colloque Scientifique International sur le Cafe*), 1-11.
Carrieri, G., De Bonis, M.V., and Ruocco, G. (2012). Modeling and experimental validation of mass transfer from carbonated beverages in polyethylene terephthalate bottles. *Journal of Food Engineering* 108 (4), 570-578.
Carson, R., Lear, L., Wilson, E.O., and Darling, L. (2002). *Silent Spring*. Houghton Mifflin.

Cavallucci, D. (2017). *TRIZ – The Theory of Inventive Problem Solving: Current Research and Trends in French Academic Institutions*. Springer International Publishing.
Cfr (2006). "§§30.66-Gauging manual ", in: *Title 27-Alcohol,Tobacco Products and Firearms*. (U.S. Government Publishing Office).
Chandra, P., and Koros, W.J. (2009a). Sorption and transport of methanol in poly(ethylene terephthalate). *Polymer* 50 (1), 236-244.
Chandra, P., and Koros, W.J. (2009b). Sorption of lower alcohols in poly(ethylene terephthalate). *Polymer* 50 (17), 4241-4249.
Chanson, E. (2015). Traceability and computerization of alcoholometric tables. *OIML Bulletin* LVI, 3, 1-44.
Chen, L., Pelton, R.E.O., and Smith, T.M. (2016). Comparative life cycle assessment of fossil and bio-based polyethylene terephthalate (PET) bottles. *Journal of Cleaner Production* 137, 667-676.
Chilton, T., Burnley, S., and Nesaratnam, S. (2010). A life cycle assessment of the closed-loop recycling and thermal recovery of post-consumer PET. *Resources, Conservation and Recycling* 54 (12), 1241-1249.
Cohen, M.H., and Turnbull, D. (1959). Molecular Transport in Liquids and Glasses. *The Journal of Chemical Physics* 31 (5), 1164-1169.
Coles, R., and Kirwan, M.J. (2011). *Food and Beverage Packaging Technology*. Wiley.
Costa, L.I., and Storti, G. (2010). Self-diffusion of small molecules into rubbery polymers: A lattice free-volume theory. *Journal of Polymer Science Part B: Polymer Physics* 48 (5), 529-540.
Courgneau, C., Vitrac, O., Ducruet, V., and Riquet, A.-M. (2013). Local demixion in plasticized polylactide probed by electron spin resonance. *Journal of Magnetic Resonance* 233, 37-48.
Crank, J. (1975). *The Mathematics of Diffusion* Bristol, UK: Oxford University Press.
Crul, M.R.M., and Diehl, J.C. (2006). *Design for Sustainability: A Practical Approach for Developing Economies*. UNEP, Division of Technology, Industry, and Economics.
Crul, M.R.M., Diehl, J.C., and Ryan, C. (2009). *Design for Sustainability a step-by-step approach*. Paris, France: United Nations Environment Programme, Delft University of Technology, Sustainable Consumption and production Branch.
Csiszar, S.A., Meyer, D.E., Dionisio, K.L., Egeghy, P., Isaacs, K.K., Price, P.S., Scanlon, K.A., Tan, Y.-M., Thomas, K., Vallero, D., and Bare, J.C. (2016). Conceptual Framework To Extend Life Cycle Assessment Using Near-Field Human Exposure Modeling and High-Throughput Tools for Chemicals. *Environmental Science & Technology* 50 (21), 11922-11934.
Daniel, S.E., Tsoulfas, G.T., Pappis, C.P., and Rachaniotis, N.P. (2004). Aggregating and evaluating the results of different Environmental Impact Assessment methods. *Ecological Indicators* 4 (2), 125-138.
Dantzig, G.B. (1998). *Linear Programming and Extensions*. Princeton University Press.
Dattorro, J. (2005). *Convex Optimization & Euclidean Distance Geometry*. Meboo Publishing.
Daver, F., Demirel, B., Sutanto, J., and Pang, C.W. (2012). An integrative simulation approach to weight reduction in poly(ethylene terephthalate) bottles. *Journal of Applied Polymer Science* 126 (S2), E433-E439.
Ddbst (2018). *Saturated Vapor Pressure Calculation by Antoine Equation* [Online]. DDBST GmbH. Available: http://ddbonline.ddbst.de/AntoineCalculation/AntoineCalculationCGI.exe?component=Ethanol [Accessed Nov,18 2018].
Delft, and Ce (2004). "Recycling versus refilling of PET bottles: an environmental comparison. "Recycling for all' milieukundig vergeleken met hervullen voor enkelen". (Delft, Netherlands).
Demirel, B., and Daver, F. (2009). The effects on the properties of PET bottles of changes to bottle-base geometry. *Journal of Applied Polymer Science* 114 (6), 3811-3818.

Demirel, B., and Daver, F. (2012). Effects of preform deformation behavior on the properties of the poly(ethylene terephthalate) bottles. *Journal of Applied Polymer Science* 126 (4), 1300-1306.
Dogan, S.K. (2008). *Life cycle assessment of PET bottle (Master Thesis)*. Dokuz Eylül University, İzmir, Turkey. .
Dombre, C., Rigou, P., and Chalier, P. (2015). The use of active PET to package rosé wine: Changes of aromatic profile by chemical evolution and by transfers. *Food Research International* 74, 63-71.
Dong, C., Zhang, C., and Wang, B. (2003). Integration of Green Quality Function Deployment and Fuzzy Multi-Attribute Utility Theory-Based Cost Estimation for Environmentally Conscious Product Development. *International Journal of Environmentally Conscious Design & Manufacturing* 11 (1), 12-28.
Dubelley, F., Planes, E., Bas, C., Pons, E., Yrieix, B., and Flandin, L. (2017a). Water Vapor Sorption Properties of Polyethylene Terephthalate over a Wide Range of Humidity and Temperature. *Journal of Physical Chemistry B* 121 (8), 1953-1962.
Dubelley, F., Planes, E., Bas, C., Pons, E., Yrieix, B., and Flandin, L. (2017b). Water Vapor Sorption Properties of Polyethylene Terephthalate over a Wide Range of Humidity and Temperature. *The Journal of Physical Chemistry B* 121 (8), 1953-1962.
Ducruet, V., Vitrac, O., Saillard, P., Guichard, E., Feigenbaum, A., and Fournier, N. (2007). Sorption of aroma compounds in PET and PVC during the storage of a strawberry syrup. *Food Additives and Contaminants Part a-Chemistry Analysis Control Exposure & Risk Assessment* 24 (11), 1306-1317.
Duda, J.L., Ni, Y.C., and Vrentas, J.S. (1979). An Equation Relating Self-Diffusion and Mutual Diffusion Coefficients in Polymer-Solvent Systems. *Macromolecules* 12 (3), 459-462.
Dufrene, M., Zwolinski, P., and Brissaud, D. (2013). An engineering platform to support a practical integrated eco-design methodology. *CIRP Annals* 62 (1), 131-134.
Durand, M., Meyer, H., Benzerara, O., Baschnagel, J., and Vitrac, O. (2010). Molecular dynamics simulations of the chain dynamics in monodisperse oligomer melts and of the oligomer tracer diffusion in an entangled polymer matrix. *Journal of Chemical Physics* 132 (19), 194902.
Earnhart, D.H., and Glicksman, R.L. (2015). Coercive vs. cooperative enforcement: Effect of enforcement approach on environmental management. *International Review of Law and Economics* 42, 135-146.
EC (1999). *White Paper on Food Safety* [Online]. Brussels: Commission of the European Communities. Available: https://eur-lex.europa.eu/legal-content/EN/TXT/PDF/?uri=CELEX:51999DC0719&from=EN [Accessed May 03, 2019].
EC (2002). "Commission Directive 2002/72/EC of 6 August 2002 relating to plastic materials and articles intended to come into contact with foodstuffs", in: *Official Journal of the European Union*.).
EC (2004a). Commission Directive 2004/1/EC of 6 January 2004 amending Directive 2002/72/EC as regards the suspension of the use of azodicarbonamide as blowing agent (Text with EEA relevance). *Official Journal of the European Union* C007, 45-46.
EC (2004b). DIRECTIVE 2004/35/CE OF THE EUROPEAN PARLIAMENT AND OF THE COUNCIL of 21 April 2004 on environmental liability with regard to the prevention and remedying of environmental damage. *Official Journal of the European Union* L143, 56-75.
EC (2004c). REGULATION (EC) No 1935/2004 OF THE EUROPEAN PARLIAMENT AND OF THE COUNCIL of 27 October 2004 on materials and articles intended to come into contact with food and repealing Directives 80/590/EEC and 89/109/EEC. *Official Journal of the European Union* L338, 4-17.
EC (2005). DIRECTIVE 2005/20/EC OF THE EUROPEAN PARLIAMENT AND OF THE COUNCIL of 9 March 2005 amending Directive 94/62/EC on packaging and packaging waste. *Official Journal of the European Union* L70, 17-18.

EC (2006). COMMISSION REGULATION (EC) No 2023/2006 of 22 December 2006 on good manufacturing practice for materials and articles intended to come into contact with food (Text with EEA relevance). *Official Journal of the European Union* L384, 75-78.
EC (2008a). COMMISSION REGULATION (EC) No 282/2008 of 27 March 2008 on recycled plastic materials and articles intended to come into contact with foods and amending Regulation (EC) No 2023/2006 (Text with EEA relevance). *Official Journal of the European Union* L86, 9-18.
EC (2008b). DIRECTIVE 2008/98/EC OF THE EUROPEAN PARLIAMENT AND OF THE COUNCIL of 19 November 2008 on waste and repealing certain Directives (Text with EEA relevance). *Official Journal of the European Union* 312, 3-30.
EC (2008c). Regulation (EC) No 110/2008 of the European Parliament and of the Council of 15 January 2008 on the definition, description, presentation, labelling and the protection of geographical indications of spirit drinks and repealing Council Regulation (EEC) No 1576/89. *Official Journal of the European Union* L39, 16-54.
EC (2009). DIRECTIVE 2009/125/EC OF THE EUROPEAN PARLIAMENT AND OF THE COUNCIL of 21 October 2009 establishing a framework for the setting of ecodesign requirements for energy-related products (recast) (Text with EEA relevance). *Official Journal of the European Union* L285, 10-34.
EC (2011a). Commission Regulation (EU) No 10/2011 of 14 January 2011 on plastic materials and articles intended to come into contact with food Text with EEA relevance. *Official Journal of the European Union* L12, 1-89.
EC (2011b). Regulation (EU) No 1169/2011 of the European Parliament and of the Council. *Official Journal of the European Union* L304, 69.
EC (2015). DIRECTIVE (EU) 2015/720 OF THE EUROPEAN PARLIAMENT AND OF THE COUNCIL of 29 April 2015 amending Directive 94/62/EC as regards reducing the consumption of lightweight plastic carrier bags (Text with EEA relevance). *Official Journal of the European Union* L115, 11-15.
EC (2018). *Proposal for A Directive of the European Parliament and of the Council on the reduction of the impact of certain plastic products on the environment*. Brussels: European Commission.
Eco Paper Loop (2015). "WP5-LCA of selected packaging products". Central Europe and Europe Union).
Ecoinvent (2019). *Life Cycle Inventory ecoinvent database* [Online]. Available: https://www.ecoinvent.org/ [Accessed April 30, 2019].
Edwards, D.A. (2001). A spatially nonlocal model for polymer-penetrant diffusion. *Zeitschrift für angewandte Mathematik und Physik ZAMP* 52 (2), 254-288.
EEC (1976). COUNCIL DIRECTIVE of 20 January 1976 on the approximation of the laws of the Member States relating to the making-up by weight or by volume of certain prepackaged products. *Official Journal of the European Communities* L46, 1-11.
EEC (1994). EUROPEAN PARLIAMENT AND COUNCIL DIRECTIVE 94/62/EC of 20 December 1994 on packaging and packaging waste. *Official Journal of the European Communities* L365, 10-23.
Eerhart, A.J.J.E., Faaij, A.P.C., and Patel, M.K. (2012). Replacing fossil based PET with biobased PEF; process analysis, energy and GHG balance. *Energy & Environmental Science* 5 (4), 6407-6422.
EFSA (2016). Presence of microplastics and nanoplastics in food, with particular focus on seafood. *EFSA Journal* 14 (6), 4501.
Engel, A. (2013). *Problem-Solving Strategies*. Springer New York.
Ernstoff, A.S., Fantke, P., Huang, L., and Jolliet, O. (2017). High-throughput migration modelling for estimating exposure to chemicals in food packaging in screening and prioritization tools. *Food and Chemical Toxicology* 109, 428-438.
Eslami, H., and Müller-Plathe, F. (2009). Water permeability of poly(ethylene terephthalate): A grand canonical ensemble molecular dynamics simulation study. *The Journal of Chemical Physics* 131 (23), 234904.

Eu (2008). Consolidated version of the Treaty on the Functioning of the European Union - PART THREE: UNION POLICIES AND INTERNAL ACTIONS - TITLE XX: ENVIRONMENT - Article 191 (ex Article 174 TEC) *Official Journal 115*, 132-133.
Eur-Lex (2019a). *EuroVoc Classification* [Online]. Available: https://eur-lex.europa.eu/browse/eurovoc.html [Accessed April 21, 2019].
Eur-Lex (2019b). *Food plastic environment searching results from EUR-Lex* [Online]. Available: https://eur-lex.europa.eu/search.html?qid=1555858682344&text=food%20plastic%20environment&scope=EURLEX&type=quick&lang=en [Accessed April 21, 2019].
Ewender, J., and Welle, F. (2013). Determination of the activation energies of diffusion of organic molecules in poly(ethylene terephthalate). *Journal of Applied Polymer Science* 128 (6), 3885-3892.
Ewender, J., and Welle, F. (2014). Determination and Prediction of the Lag Times of Hydrocarbons through a Polyethylene Terephthalate Film. *Packaging Technology and Science* 27 (12), 963-974.
Ewender, J., and Welle, F. (2016). Functional Barrier Performance of a Polyamide-6 Membrane Towards n-Alkanes and 1-Alcohols. *Packaging Technology and Science* 29 (6), 277-287.
Ewender, J., and Welle, F. (2018a). Determination of the activation energies of diffusion of organic molecules in poly(ethylene terephthalate). *Journal of Applied Polymer Science*, 1097-4628.
Ewender, J., and Welle, F. (2018b). Determination of the activation energies of diffusion of organic molecules in poly(ethylene terephthalate). *Journal of Applied Polymer Science*.
Fang, X., Domenek, S., Ducruet, V., Refregiers, M., and Vitrac, O. (2013). Diffusion of Aromatic Solutes in Aliphatic Polymers above Glass Transition Temperature. *Macromolecules* 46 (3), 874-888.
Fang, X., and Vitrac, O. (2017). Predicting diffusion coefficients of chemicals in and through packaging materials. *Critical Reviews in Food Science and Nutrition* 57 (2), 275-312.
Favre, E., Nguyen, Q.T., Clement, R., and Neel, J. (1996). Application of Flory-Huggins theory to ternary polymer-solvents equilibria: A case study. *European Polymer Journal* 32 (3), 303-309.
Feigenbaum, A., Dole, P., Aucejo, S., Dainelli, D., Garcia, C.D.L.C., Hankemeier, T., N'gono, Y., Papaspyrides, C.D., Paseiro, P., Pastorelli, S., Pavlidou, S., Pennarun, P.Y., Saillard, P., Vidal, L., Vitrac, O., and Voulzatis, Y. (2005). Functional barriers: Properties and evaluation AU - Feigenbaum, A. *Food Additives & Contaminants* 22 (10), 956-967.
Feng, Y.J., Huang, T., Wang, C., Liu, Y.R., Jiang, S., Miao, S.K., Chen, J., and Huang, W. (2016). π-Hydrogen Bonding of Aromatics on the Surface of Aerosols: Insights from Ab Initio and Molecular Dynamics Simulation. *The Journal of Physical Chemistry B* 120 (27), 6667-6673.
Ferry, J.D. (1980). *Viscoelastic Properties of Polymers*. Wiley.
Finkbeiner, M., Schau, E.M., Lehmann, A., and Traverso, M. (2010). Towards Life Cycle Sustainability Assessment. *Sustainability* 2 (10).
Flanagan, W.P., Dhaliwal, H., and Browne, M. (2015). "Glass or Plastic: An Environmental Life Cycle Assessment (LCA) and Related Economic Impact of Contrast Media Packaging", in: *ERC2015*.).
Flanigan, L., Rolf, F., and Montalbo, T. (2013). "An Analysis of Life Cycle Assessment in Packaging for Food & Beverage Applications". UNEP/SETAC Life Cycle Initiative).
Flory, P.J. (1953). *Principles of Polymer Chemistry*. Iathaca, NY, USA: Cornell University Press.
Flynn, J.H. (1982). A collection of kinetic data for the diffusion of organic compounds in polyolefins. *Polymer* 23 (9), 1325-1344.
Foolmaun, R.K., and Ramjeawon, T. (2008). Life Cycle Assessment (LCA) of PET bottles and comparative LCA of three disposal options in Mauritius. *International Journal of Environment and Waste Management* 2 (1-2), 125-138.

Fornasiero, F., Olaya, M.M., Wagner, I., Brüderle, F., and Prausnitz, J.M. (2002). Solubilities of nonvolatile solutes in polymers from molecular thermodynamics. *AIChE Journal* 48 (6), 1284-1291.
Franklin Associates (2007). "LCI Summary for PLA and PET 12-Ounce Water Bottles". (Prairie Village, Kansas).
Franklin Associates (2009a). "Life Cycle Assessment of Drinking Water Systems: Bottle Water, Tap Water, and Home/Office Delivery Water ". (Oregon State).
Franklin Associates (2009b). "Life Cycle Inventory of Three Single-Serving Soft Drink Containers". (Prairie Village, Kansas).
Franklin Associates (2011). "Life Cycle Inventory of 100% Postconsumer HDPE and PET Recycled Resin from Post-consumer Containers and Packaging. ". (Prairie Village, Kansas).
Franz, R., and Welle, F. (2008). Migration measurement and modelling from poly(ethylene terephthalate) (PET) into soft drinks and fruit juices in comparison with food simulants. *Food Additives & Contaminants: Part A* 25 (8), 1033-1046.
Fry, J.M., Hartlin, B., Wallén, E., and Aumônier, S. (2010). "Life Cycle Assessment of Example Packaging Systems for Milk". Waste & Resources Action Programme(WRAP) and Environmental Resources Management Limited(ERM)).
Garfí, M., Cadena, E., Sanchez-Ramos, D., and Ferrer, I. (2016). Life cycle assessment of drinking water: Comparing conventional water treatment, reverse osmosis and mineral water in glass and plastic bottles. *Journal of Cleaner Production* 137, 997-1003.
Gb (2008). GB/T 16288-2008 : Marking of Plastics Products. *NATIONAL STANDARD OF THE PEOPLE'S REPUBLIC OF CHINA* (ICS 83. 140, Y 28), 1-17.
Geueke, B., Groh, K., and Muncke, J. (2018). Food packaging in the circular economy: Overview of chemical safety aspects for commonly used materials. *Journal of Cleaner Production* 193, 491-505.
Giannoulis, A., Mistriotis, A., and Briassoulis, D. (2017). 3D numerical simulations as optimization tool for the design of novel EMAP systems. *Computers and Electronics in Agriculture* 143, 119-129.
Gierszal, K.P., Davis, J.G., Hands, M.D., Wilcox, D.S., Slipchenko, L.V., and Ben-Amotz, D. (2011). π-Hydrogen Bonding in Liquid Water. *The Journal of Physical Chemistry Letters* 2 (22), 2930-2933.
Gillet, G., Vitrac, O., and Desobry, S. (2009). Prediction of Solute Partition Coefficients between Polyolefins and Alcohols Using a Generalized Flory–Huggins Approach. *Industrial & Engineering Chemistry Research* 48 (11), 5285-5301.
Gillet, G., Vitrac, O., and Desobry, S. (2010). Prediction of Partition Coefficients of Plastic Additives between Packaging Materials and Food Simulants. *Industrial & Engineering Chemistry Research* 49 (16), 7263-7280.
Gironi, F., and Piemonte, V. (2011). Life cycle assessment of polylactic acid and polyethylene terephthalate bottles for drinking water. *Environmental Progress & Sustainable Energy* 30 (3), 459-468.
Godbole, R.V., Khabaz, F., Khare, R., and Hedden, R.C. (2017). Swelling of Random Copolymer Networks in Pure and Mixed Solvents: Multi-Component Flory–Rehner Theory. *The Journal of Physical Chemistry B* 121 (33), 7963-7977.
Goff, J.A. (1957). Saturation pressure of water on the new Kelvin temperature scale. *Trans. ASHVE* 63, 347–354.
Goff, J.A., And Gratch, S. (1946). "Low-pressure properties of water from –160 to 212 °F, in Transactions of the American Society of Heating and Ventilating Engineers, pp 95-122", in: *52nd annual meeting of the American Society of Heating and Ventilating Engineers*. (New York).
Goldenberg, J., Lehmann, D.R., and Mazursky, D. (2001). The Idea Itself and the Circumstances of Its Emergence as Predictors of New Product Success. *Management Science* 47 (1), 69-84.

Gomes, T.S., Visconte, L.L.Y., and Pacheco, E.B.a.V. (2019). Life Cycle Assessment of Polyethylene Terephthalate Packaging: An Overview. *Journal of Polymers and the Environment* 27 (3), 533-548.
Gouissem, L., Douibi, A., and Benachour, D. (2014). The evolution of properties of recycled poly(ethylene terephthalate) as function of chain extenders, the extrusion cycle and heat treatment. *Polymer Science Series A* 56 (6), 844-855.
Goujot, D., and Vitrac, O. (2013). Extension to nonlinear adsorption isotherms of exact analytical solutions to mass diffusion problems. *Chemical Engineering Science* 99, 2-22.
Greendelta (2019). *LCA software openLCA* [Online]. Available: http://www.openlca.org/ [Accessed April 30, 2019].
Griffin, A.S., and Guez, D. (2014). Innovation and problem solving: A review of common mechanisms. *Behavioural Processes* 109, 121-134.
Griffiths, M.C., Strauch, J., Monteiro, M.J., and Gilbert, R.G. (1998). Measurement of Diffusion Coefficients of Oligomeric Penetrants in Rubbery Polymer Matrixes. *Macromolecules* 31 (22), 7835-7844.
Grönman, K., Soukka, R., Järvi-Kääriäinen, T., Katajajuuri, J.-M., Kuisma, M., Koivupuro, H.-K., Ollila, M., Pitkänen, M., Miettinen, O., Silvenius, F., Thun, R., Wessman, H., and Linnanen, L. (2013). Framework for Sustainable Food Packaging Design. *Packaging Technology and Science* 26 (4), 187-200.
Gunningham, N. (2011). Enforcing Environmental Regulation. *Journal of Environmental Law* 23 (2), 169-201.
Hall, D.B., Hamilton, K.E., Miller, R.D., and Torkelson, J.M. (1999). Translational and Rotational Diffusion of Probe Molecules in Polymer Films near Tg: Effect of Hydrogen Bonding. *Macromolecules* 32 (24), 8052-8058.
Hamaide, T., Deterre, R., and Feller, J.F. (2014). *Environmental Impact of Polymers*. Wiley.
Han, J.H. (2014). *Innovations in Food Packaging*. Plano, TX, USA: Elsevier Science.
Hanke, G. (2016). "Marine Beach Litter in Europe – Top Items". (Ispra, Italy: European Commission, Joint Research Centre (JRC)).
Hansen, C.M. (2007). *Hansen Solubility Parameters: A User's Handbook, Second Edition*. Boca-Raton, FL, USA: CRC Press.
Harrington, H.J. (2017). *Lean TRIZ: How to Dramatically Reduce Product-Development Costs with This Innovative Problem-Solving Tool*. Taylor & Francis.
Hatcher, G.D., Ijomah, W.L., and Windmill, J.F.C. (2011). Design for remanufacture: a literature review and future research needs. *Journal of Cleaner Production* 19 (17), 2004-2014.
Héder, M. (2017). From NASA to EU: the evolution of the TRL scale in Public Sector Innovation. *The Innovation Journal: The Public Sector Innovation Journal* 22 (2).
Hermann, B.G., Kroeze, C., and Jawjit, W. (2007). Assessing environmental performance by combining life cycle assessment, multi-criteria analysis and environmental performance indicators. *Journal of Cleaner Production* 15 (18), 1787-1796.
Herstein, K.M., and Gregory, T.C. (1935). *Chemistry and Technology of Wines & Liquors*. New York, USA: D. VAN NOSTRAND COMPANY, INC. .
Hinrichs, K., and Piringer, O. (2002). Evaluation of Migration Models to Be Used Under Directive 90/128/EEC; Final repot Contract SMT4-CT9867513. EUR 20604 EN. *European Commission, Directorate General for Research*.
Hiriart-Urruty, J.B., and Lemaréchal, C. (2004). *Fundamentals of Convex Analysis*. Springer Berlin Heidelberg.
Hoekstra, E., Brandsch, R., Dequatre, C., Mercea, P., Milana, M.R., Stoermer, A., Trier, X., Vitrac, O., Schaefer, A., and Simoneau, C. (2015). "Practical guidelines on the application of migration modelling for the estimation of specific migration - EUR 27529 EN - https://ec.europa.eu/jrc/en/publication/practical-guidelines-application-migration-modelling-estimation-specific-migration".).
Hoffmann, E. (2007). Consumer integration in sustainable product development. *Business Strategy and the Environment* 16 (5), 322-338.

Hong, S.-U. (1995). Prediction of Polymer/Solvent Diffusion Behavior Using Free-Volume Theory. *Industrial & Engineering Chemistry Research* 34 (7), 2536-2544.
Hong, S.-U. (1996). Predicting ability of free-volume theory for solvent self-diffusion coefficients in rubbers. *Journal of Applied Polymer Science* 61 (5), 833-841.
Horowitz, N., Frago, J., and Mu, D. (2018). Life cycle assessment of bottled water: A case study of Green2O products. *Waste Management* 76, 734-743.
Horváth, I.T. (2018). Introduction: Sustainable Chemistry. *Chemical Reviews* 118 (2), 369-371.
Hosseini, S.S., Taheri, S., Zadhoush, A., and Mehrabani-Zeinabad, A. (2007). Hydrolytic degradation of poly(ethylene terephthalate). *Journal of Applied Polymer Science* 103 (4), 2304-2309.
Hu, Q.C., Sha, W.J., Li, Y.H., and Wang, Y.S. (2012). Structural Optimization and Lightweight Design of PET Bottle Based on ABAQUS. *Advanced Materials Research* 346, 558-563.
Huang, H.-H., Chen, L.-W., Lu, W.-H., Lin, W.-C., and Chen, Y.-C. (2018a). Design and Simulation Analysis of Lightweight HDPE Milk Bottle. *Polymers and Polymer Composites* 26 (1), 91-98.
Huang, L., Anastas, N., Egeghy, P., Vallero, D., Jolliet, O., and Bare, J. (2018b). *Integrating exposure to chemicals in building materials during use stage*.
Iec (2009). International Standard IEC 62430:2009-Environmentally conscious design for electrical and electronic products. *International Electrotechnical Commission*.
ISO (1993). *ISO/TC 207/SC 1 on Environmental management systems* [Online]. International Organization for Standardization. Available: https://committee.iso.org/home/tc207sc1 [Accessed May 2, 2019].
ISO (2002). *Environmental management -- Integrating environmental aspects into product design and development*. Geneva, Switzerland: International Organization for Standardization.
ISO (2006a). *International Standard ISO 14040:2006 - Environmental management-life cycle assessment-principles and framework*. Geneva, Switzerland: International Organization for Standardization.
ISO (2006b). *International Standard ISO 14044:2006 - Environmental management — Life cycle assessment — Requirements and guidelines*. Geneva, Switzerland: International Organization for Standardization.
ISO (2011). *International Standard ISO 14006:2011- Environmental management systems-guidelines for incorporating ecodesign*. Geneva, Switzerland: International Organization for Standardization.
ISO (2015a). *International Standard ISO 9001:2015- Quality management systems — Requirements*. Geneva, Switzerland International Organization for Standardization.
ISO (2015b). "International Standard ISO 14001:2015 Environmental management systems -- Requirements with guidance for use". (Geneva, Switzerland,: International Organization for Standardization).
ISO (2016). International Standard ISO/TS 9002:2016 Quality management systems -- Guidelines for the application of ISO 9001:2015. *International Organization for Standardization*.
Jabarin, S.A., and Lofgren, E.A. (1986). Effects of water absorption on physical properties and degree of molecular orientation of poly (ethylene terephthalate). *Polymer Engineering & Science* 26 (9), 620-625.
Jacxsens, L., Devlieghere, F., and Debevere, J. (2002). Predictive modelling for packaging design: equilibrium modified atmosphere packages of fresh-cut vegetables subjected to a simulated distribution chain. *International Journal of Food Microbiology* 73 (2), 331-341.
Jain, H. (2016). *Problem Solving in Data Structures & Algorithms Using Python: Programming Interview Guide*. CreateSpace Independent Publishing Platform.
Jalali, A., Seiiedlou, S., Linke, M., and Mahajan, P. (2017). A comprehensive simulation program for modified atmosphere and humidity packaging (MAHP) of fresh fruits and vegetables. *Journal of Food Engineering* 206, 88-97.

Janes, D.W., Chandrasekar, V., Woolford, S.E., and Ludwig, K.B. (2017). Predicting the Effects of Composition, Molecular Size and Shape, Plasticization, and Swelling on the Diffusion of Aromatic Additives in Block Copolymers. *Macromolecules* 50 (16), 6137-6148.

Jeong, C., and Douglas, J.F. (2015). Mass dependence of the activation enthalpy and entropy of unentangled linear alkane chains. *The Journal of Chemical Physics* 143 (14), 144905.

Jorgensen, S.E., and Johnsen, I. (1989). *Principles of Environmental Science and Technology*. Elsevier Science.

Kadam, A., Karbowiak, T., Voilley, A., Bellat, J.-P., Vitrac, O., and Debeaufort, F. (2014). Sorption of n-hexane in amorphous polystyrene. *Journal of Polymer Science Part B: Polymer Physics* 52 (19), 1252-1258.

Kahneman, D., and Tversky, A. (1979). Prospect Theory: An Analysis of Decision under Risk. *Econometrica* 47 (2), 263-291.

Kang, D. (2015). "Environmental Evaluation of Non-Alcoholic Single-Serve PET Beverage Bottles in the State of California Using Life Cycle Assessment and System Dynamics". Michigan State University).

Kang, D., Auras, R., and Singh, J. (2017). Life cycle assessment of non-alcoholic single-serve polyethylene terephthalate beverage bottles in the state of California. *Resources, Conservation and Recycling* 116, 45-52.

Karlsson, R., and Luttropp, C. (2006). EcoDesign: what's happening? An overview of the subject area of EcoDesign and of the papers in this special issue. *Journal of Cleaner Production* 14 (15), 1291-1298.

Keeney, R.L., and Raiffa, H. (1993). *Decisions with Multiple Objectives: Preferences and Value Trade-Offs*. Cambridge University Press.

Khan, F.I., Sadiq, R., and Veitch, B. (2004). Life cycle iNdeX (LInX): a new indexing procedure for process and product design and decision-making. *Journal of Cleaner Production* 12 (1), 59-76.

Khanum, R., Takarada, W., Aneja, A., and Kikutani, T. (2015). Crystallization of poly(ethylene terephthalate) filaments by infusion of ethanol upon cold drawing. *Polymer* 59, 26-34.

Khosravani, M.R., Nasiri, S., Anders, D., and Weinberg, K. (2019). Prediction of dynamic properties of ultra-high performance concrete by an artificial intelligence approach. *Advances in Engineering Software* 127, 51-58.

Kleingeld M. (2010). *Simplification in engineering : contributing real value* [Online]. Potchefstroom Campus, South Africa. Available: http://hdl.handle.net/10394/8564 [Accessed access on April 21, 2019].

Kloppers, M.J., Bellucci, F., Latanision, R.M., and Brennan, J.E. (1993). Transport and dielectric properties of poly(ethylene terephthalate) as determined via electrochemical techniques. *Journal of Applied Polymer Science* 48 (12), 2197-2205.

Kobayashi, H. (2006). A systematic approach to eco-innovative product design based on life cycle planning. *Advanced Engineering Informatics* 20 (2), 113-125.

Kolsch, D., Saling, P., Kicherer, A., Grosse-Sommer, A., and Schmidt, I. (2008). How to measure social impacts? A socio-eco-efficiency analysis by the SEEBALANCE® method. *International Journal of Sustainable Development* 11 (1), 1-23.

Komly, C.-E., Azzaro-Pantel, C., Hubert, A., Pibouleau, L., and Archambault, V. (2012). Multiobjective waste management optimization strategy coupling life cycle assessment and genetic algorithms: Application to PET bottles. *Resources, Conservation and Recycling* 69, 66-81.

Kontogeorgis, G.M., and Gani, R. (2004). *Computer Aided Property Estimation for Process and Product Design: Computers Aided Chemical Engineering*. Elsevier Science.

Kowalski, R. (1979). *Logic for Problem Solving*. Elsevier North Holland.

Krüger, K.-M., and Sadowski, G. (2005). Fickian and Non-Fickian Sorption Kinetics of Toluene in Glassy Polystyrene. *Macromolecules* 38 (20), 8408-8417.

Kuczenski, B., and Geyer, R. (2011). "Life Cycle Assessment of Polyethylene Terephthalate (PET) Beverage Bottles Consumed in the State of California". (California: California Department of Resources Recycling and Recovery).

Kutsche, I., Gildehaus, G., Schuller, D., and Schumpe, A. (1984). Oxygen solubilities in aqueous alcohol solutions. *Journal of Chemical & Engineering Data* 29 (3), 286-287.
Langevin, D., Grenet, J., and Saiter, J.M. (1994). Moisture sorption in pet influence on the thermokinetic parameters. *European Polymer Journal* 30 (3), 339-345.
Launay, A., Thominette, F., and Verdu, J. (1999). Water sorption in amorphous poly(ethylene terephthalate). *Journal of Applied Polymer Science* 73 (7), 1131-1137.
Leejarkpai, T., Mungcharoen, T., and Suwanmanee, U. (2016). Comparative assessment of global warming impact and eco-efficiency of PS (polystyrene), PET (polyethylene terephthalate) and PLA (polylactic acid) boxes. *Journal of Cleaner Production* 125, 95-107.
Leibrecht, S. (2005). Fundamental Principles for CAD-based Ecological Assessments (9 pp). *The International Journal of Life Cycle Assessment* 10 (6), 436-444.
Lewis, H., Gertsakis, J., Grant, T., Morelli, N., and Sweatman, A. (2001). *Design + Environment: A Global Guide to Designing Greener Goods*. Greenleaf Pub.
Liu, J., Jin, X.L., and Tsui, K.C. (2006). *Autonomy Oriented Computing: From Problem Solving to Complex Systems Modeling*. Springer US.
Liu, J., and Ma, Y. (2016). A survey of manufacturing oriented topology optimization methods. *Advances in Engineering Software* 100, 161-175.
Lockwood, T. (2009). *Design Thinking: Integrating Innovation, Customer Experience and Brand Value*. New York, US: Allworth Press.
Lorite, G.S., Rocha, J.M., Miilumäki, N., Saavalainen, P., Selkälä, T., Morales-Cid, G., Gonçalves, M.P., Pongrácz, E., Rocha, C.M.R., and Toth, G. (2017). Evaluation of physicochemical/microbial properties and life cycle assessment (LCA) of PLA-based nanocomposite active packaging. *LWT* 75, 305-315.
Luenberger, D.G., and Ye, Y. (2008). *Linear and Nonlinear Programming*. Springer US.
Luger, G.F., and Stubblefield, W.A. (1998). *Artificial Intelligence: Structures and Strategies for Complex Problem Solving*. Addison-Wesley.
Lusher, A.L., Hollman, P.C.H., and Mendoza-Hill, J.J. (2017). Microplastics in fisheries and aquaculture: status of knowledge on their occurrence and im-plications for aquatic organisms and food safety. *FAO Fisheries and Aquaculture Technical Paper*. No. 615.
Lutzow, N., Tihminlioglu, A., Danner, R.P., Duda, J.L., De Haan, A., Warnier, G., and Zielinski, J.M. (1999). Diffusion of toluene and n-heptane in polyethylenes of different crystallinity. *Polymer* 40 (10), 2797-2803.
Madival, S., Auras, R., Singh, S.P., and Narayan, R. (2009). Assessment of the environmental profile of PLA, PET and PS clamshell containers using LCA methodology. *Journal of Cleaner Production* 17 (13), 1183-1194.
Mahbub, M.S., De Souza, P., and Williams, R. (2017). Describing environmental phenomena variation using entropy theory. *International Journal of Data Science and Analytics* 3 (1), 49-60.
Mair, C., Martincova, M., and Shepperd, M.J. (Year). "A Literature Review of Expert Problem Solving using Analogy", in: *Evaluation And Assessment In Software Engineering (EASE)*).
Mangaraj, S., Yadav, A., Bal, L.M., Dash, S.K., and Mahanti, N.K. (2019). Application of Biodegradable Polymers in Food Packaging Industry: A Comprehensive Review. *Journal of Packaging Technology and Research* 3 (1), 77-96.
Mansour, A.M.H., and Ali, S.A. (2015). Reusing waste plastic bottles as an alternative sustainable building material. *Energy for Sustainable Development* 24, 79-85.
Marathe, K.V., Chavan, K.R., and Nakhate, P. (2019). "8 - Life Cycle Assessment (LCA) of PET Bottles," in *Recycling of Polyethylene Terephthalate Bottles,* eds. S. Thomas, A. Rane, K. Kanny, A. V.K & M.G. Thomas. William Andrew Publishing), 149-168.
Marsh, K., and Bugusu, B. (2007). Food Packaging—Roles, Materials, and Environmental Issues. *Journal of Food Science* 72 (3), R39-R55.
Masood, S.H., and Keshavamurthy, V. (2005). Development of collapsible PET water fountain bottles. *Journal of Materials Processing Technology* 162-163, 83-89.

Masys, A.J. (2015). *Applications of Systems Thinking and Soft Operations Research in Managing Complexity: From Problem Framing to Problem Solving*. Springer International Publishing.
Matamoros, C.A. (2019). *How is food waste regulated in Europe?* [Online]. Available: https://www.euronews.com/2019/02/06/how-is-food-waste-regulated-in-europe [Accessed June 1, 2019].
Matlack, A.S., and Dicks, A.P. (2015). *Problem-Solving Exercises in Green and Sustainable Chemistry*. CRC Press.
Meyer, E.F., Awe, M.J., and Wagner, R.E. (1980). Cohesive energies in polar organic liquids. 4. n-Alkyl acetates. *Journal of Chemical & Engineering Data* 25 (4), 371-374.
Molina-Besch, K., Wikström, F., and Williams, H. (2019). The environmental impact of packaging in food supply chains—does life cycle assessment of food provide the full picture? *The International Journal of Life Cycle Assessment* 24 (1), 37-50.
Morrison, J.R., Azhar, M., Lee, T., and Suh, H. (2013). Axiomatic Design for eco-design: eAD+. *Journal of Engineering Design* 24 (10), 711-737.
Mudgil, D., and Barak, S. (2018). *Beverages : Processing and Technology*. Scientific Publishers.
Mulder, M.H.V., and Smolders, C.A. (1984). On the mechanism of separation of ethanol/water mixtures by pervaporation I. Calculations of concentration profiles. *Journal of Membrane Science* 17 (3), 289-307.
Muthu, S.S. (2015). *Environmental Footprints of Packaging*. Springer Singapore.
Nasa (2018). *Outgassing Data for Selecting Spacecraft Materials* [Online]. Available: https://outgassing.nasa.gov/ [Accessed accessed on March 29, 2019 2019].
Nessi, S., Rigamonti, L., and Grosso, M. (2012). LCA of waste prevention activities: A case study for drinking water in Italy. *Journal of Environmental Management* 108, 73-83.
Nfpa (1994). *NFPA 325 Guide to fire hazard properties of flammable liquids, gases, and volatile solids*. Massachusetts, US: National Fire Protection Association.
Nguyen, P.-M., Goujon, A., Sauvegrain, P., and Vitrac, O. (2013). A Computer-Aided Methodology to Design Safe Food Packaging and Related Systems. *Aiche Journal* 59 (4), 1183-1212.
Nguyen, P.-M., Guiga, W., Dkhissi, A., and Vitrac, O. (2017). Off-lattice Flory-Huggins approximations for the tailored calculation of activity coefficients of organic solutes in random and block copolymers. *Industrial & Engineering Chemistry Research* 56 (3), 774–787.
Nguyen, P.-M., Guiga, W., and Vitrac, O. (2016). Molecular thermodynamics for food science and engineering. *Food Research International* 88,Part A, 91-104.
Nguyen, P.-M., Lyathaud, C., and Vitrac, O. (2015). A two-scale pursuit method for the tailored identification and quantification of unknown polymer additives and contaminants by 1H NMR. *Industrial & Engineering Chemistry Research* 54 (10), 2667-2681.
Nicoli, M.C. (2012). *Shelf Life Assessment of Food*. CRC Press.
Nicoli, M.C., and Calligaris, S. (2018). Secondary Shelf Life: an Underestimated Issue. *Food Engineering Reviews* 10 (2), 57-65.
Nielsen, S., and Bastianoni, S. (2007). *A Common Framework for Emergy and Exergy based LCA in accordance with Environ Theory*.
Nilsson, N.J. (1971). *Problem-solving methods in artificial intelligence*. McGraw-Hill.
Nist (2019). *NIST Chemistry WebBook* [Online]. National Institute of Standards and Technology. Available: https://webbook.nist.gov/chemistry/ [Accessed accessed on March 31, 2019].
Nogueda, D.I. (2013). *Life cycle assessment of pet bottle recycling: a case study for Mexico* Thesis.
Noorjahan, A., and Choi, P. (2015a). Effect of free volume redistribution on the diffusivity of water and benzene in poly(vinyl alcohol). *Chemical Engineering Science* 121, 258-267.
Noorjahan, A., and Choi, P. (2015b). Prediction of self diffusion coefficients of selected solvents in poly(vinyl alcohol) using lattice-free volume theory. *Polymer* 58, 53-59.

Nrc (1983). "Risk Assessment in the Federal Government: Managing the Process. ". (Washington (DC): National Academies Press (US)).
Odum, H.T. (1996). *Environmental Accounting: Emergy and Environmental Decision Making*. Wiley.
Oecd (2017). "Economic Features of Chemical Leasing", in: *Series on Risk Management No. 37*. Environment, Health and Safety, Environment Directorate,OECD).
Ofitserov, D.V., and German, O.V. (1995). *Problem Solving: Methods, Programming, and Future Concepts*. Elsevier Science Limited.
Oiml (1975). "International Alcoholometric Tables". (Paris, France: International Organization of Legal Metrology).
Osborne, N.S., Mckelvy, E.C., and Bearce, H.W. (1913). Density and thermal expansion of ethyl alcohol and of its mixtures with water. *Bulletin of the Bureau of Standards* 9, 327-474.
Ouyang, H., and Shore, S.H. (1999). The mass transport in poly(ethylene terephthalate) and related induced-crystallization. *Polymer* 40 (19), 5401-5406.
Ozdemir, M., and Floros, J.D. (2004). Active Food Packaging Technologies. *Critical Reviews in Food Science and Nutrition* 44 (3), 185-193.
Papong, S., Malakul, P., Trungkavashirakun, R., Wenunun, P., Chom-In, T., Nithitanakul, M., and Sarobol, E. (2014). Comparative assessment of the environmental profile of PLA and PET drinking water bottles from a life cycle perspective. *Journal of Cleaner Production* 65, 539-550.
Patsioura, A., Ziaiifar, A.M., Smith, P., Menzel, A., and Vitrac, O. (2017). Effects of oxygenation and process conditions on thermo-oxidation of oil during deep-frying. *Food and Bioproducts Processing* 101, 84-99.
Paul, D.R. (2016). "Dual Mode Sorption Model," in *Encyclopedia of Membranes,* eds. E. Drioli & L. Giorno. (Berlin, Heidelberg: Springer Berlin Heidelberg), 601-602.
Pawlisch, C.A., Bric, J.R., and Laurence, R.L. (1988). Solute diffusion in polymers. 2. Fourier estimation of capillary column inverse gas chromatography data. *Macromolecules* 21 (6), 1685-1698.
Pe-Americas, and Five International. (2010). "Corrugated Packaging Life-cycle Assessment Summary Report". Corrugated Packaging Alliance).
Pe International Inc. (2012). "Life Cycle Assessment of Polymers in an Automotive Assist Step". (Boston, USA: PE INTERNATIONAL, Inc.).
Pearl, J. (1984). *Heuristics: Intelligent Search Strategies for Computer Problem Solving*. Addison-Wesley.
Pellerin, C., Rousseau, M.-E., Prud'homme, R.E., and Pézolet, M. (2002). Orientation and Relaxation in Thick Poly(ethylene terephthalate) Films by Transmission Infrared Linear Dichroism. *Applied Spectroscopy* 56 (1), 17-23.
Pennarun, P.Y., Dole, P., and Feigenbaum, A. (2004). Functional barriers in PET recycled bottles. Part I. Determination of diffusion coefficients in bioriented PET with and without contact with food simulants. *Journal of Applied Polymer Science* 92 (5), 2845-2858.
Pernod Ricard (2015). *[Innovation] Discover the Gutenberg Project* [Online]. Available: https://www.youtube.com/watch?v=4KmR7sqpHhg [Accessed May 31, 2019].
Petcore Europe. (2017). *PET Collection and Recycling Rates in Europe Significantly Increased in 2016* [Online]. Available: https://petcore-europe.org/news-events/110-pet-collection-recycling-rates-europe-significantly-2016.html [Accessed Access on May 1, 2019].
Pickup, S., and Blum, F.D. (1989). Self-diffusion of toluene in polystyrene solutions. *Macromolecules* 22 (10), 3961-3968.
Pierdomenico, M., Casalbore, D., and Chiocci, F.L. (2019). Massive benthic litter funnelled to deep sea by flash-flood generated hyperpycnal flows. *Scientific Reports* 9 (1), 5330.
Pira, S. (2016). *The Future of PET Packaging to 2021* [Online]. Smithers Pira. Available: https://www.smitherspira.com/industry-market-reports/packaging/pet-packaging-to-2021 [Accessed May 01, 2019].

Piringer, O.G., and Baner, A.L. (2008). *Plastic Packaging Interactions with Food and Pharmaceuticals*. Weinheim, Germany: Wiley-VCH Verlag.
Plasticseurope (2018). "Annual Review 2017-2018". (Belgium).
Press, W.H. (1992). *Numerical Recipes in C: The Art of Scientific Computing*. Cambridge University Press.
Pressman, A. (2018). *Design Thinking: A Guide to Creative Problem Solving for Everyone.* Taylor & Francis.
Pritchard, M.S. (2001). Responsible engineering: The importance of character and imagination. *Science and Engineering Ethics* 7 (3), 391-402.
Rahman, M.S. (2007). *Handbook of Food Preservation*. CRC Press.
Ramani, K., Ramanujan, D., Bernstein, W.Z., Zhao, F., Sutherland, J., Handwerker, C., Choi, J.K., Kim, H., and Thurston, D. (2010). Integrated Sustainable Life Cycle Design: A Review. *Journal of Mechanical DESIGN* 132 (9).
Ramesh, N., Davis, P.K., Zielinski, J.M., Danner, R.P., and Duda, J.L. (2011). Application of Free-Volume Theory to Self Diffusion of Solvents in Polymers Below the Glass Transition Temperature: A Review. *Journal of Polymer Science Part B-Polymer Physics* 49 (23), 1629-1644.
Ramos, M., Valdés, A., Mellinas, C.A., and Garrigós, C.M. (2015). New Trends in Beverage Packaging Systems: A Review. *Beverages* 1 (4).
Rangaiah, G.P. (2009). *Multi-Objective Optimization: Techniques and Applications in Chemical Engineering*. World Scientific.
Remmen, A., Jensen, A.A., Programme, U.N.E., Frydendal, J., and Setac (2007). *Life Cycle Management: A Business Guide to Sustainability*. United Nations Environment Programme.
Rezaei, J., Papakonstantinou, A., Tavasszy, L., Pesch, U., and Kana, A. (2019). Sustainable product-package design in a food supply chain: A multi-criteria life cycle approach. *Packaging Technology and Science* 32 (2), 85-101.
Rijk, R., and Veraart, R. (eds.). (2010). *Global Legislation for Food Packaging Materials.* Weinheim, Germany: WILEY-VCH Verlag GmbH & Co. KGaA.
Robertson, G.L. (2009a). *Food Packaging and Shelf Life: A Practical Guide*. CRC Press.
Robertson, G.L. (2009b). "Sustainable food packaging " in *Handbook of Waste Management and Co-Product Recovery in Food Processing Volume 2,* ed. K.W. Waldron. Elsevier Science), 221-254.
Robertson, G.L. (2016a). *Food Packaging: Principles and Practice, Third Edition*. Boca-Raton, USA: CRC Press.
Robertson, S.I. (2016b). *Problem Solving: Perspectives from Cognition and Neuroscience.* Taylor & Francis.
Rogers, E.M. (2003). *Diffusion of Innovations, 5th Edition*. Free Press.
Romero-Hernández, O., Romero Hernández, S., Muñoz, D., Detta-Silveira, E., Palacios-Brun, A., and Laguna, A. (2009). Environmental implications and market analysis of soft drink packaging systems in Mexico. A waste management approach. *The International Journal of Life Cycle Assessment* 14 (2), 107-113.
Romli, A., Prickett, P., Setchi, R., and Soe, S. (2015). Integrated eco-design decision-making for sustainable product development. *International Journal of Production Research* 53 (2), 549-571.
Rosenboom, J.-G., Hohl, D.K., Fleckenstein, P., Storti, G., and Morbidelli, M. (2018). Bottle-grade polyethylene furanoate from ring-opening polymerisation of cyclic oligomers. *Nature Communications* 9 (1), 2701.
Rossi, M., Germani, M., and Zamagni, A. (2016). Review of ecodesign methods and tools. Barriers and strategies for an effective implementation in industrial companies. *Journal of Cleaner Production* 129, 361-373.
Roy, R. (1994). The evolution of ecodesign. *Technovation* 14 (6), 363-380.
Rueda, D.R., and Varkalis, A. (1995). Water sorption/desorption kinetics in poly(ethylene naphthalene-2,6-dicarboxylate) and poly(ethylene terephthalate). *Journal of Polymer Science Part B: Polymer Physics* 33 (16), 2263-2268.

Runde, J. (1996). On Popper, Probabilities, and Propensities. *Review of Social Economy* 54 (4), 465-485.
Sagiv, A. (2001). Exact solution of mass diffusion into a finite volume. *Journal of Membrane Science* 186 (2), 231-237.
Sagiv, A. (2002). Theoretical formulation of the diffusion through a slab—theory validation. *Journal of Membrane Science* 199 (1), 125-134.
Saic (2006). "Life Cycle Assessment: Principles And Practice". (Reston, USA: National Risk Management Research Laboratory, Office Of Research And Development,Environmental Protection Agency).
Sakao, T. (2007). A QFD-centred design methodology for environmentally conscious product design. *International Journal of Production Research* 45 (18-19), 4143-4162.
Saleh, Y. (2016). Comparative life cycle assessment of beverages packages in Palestine. *Journal of Cleaner Production* 131, 28-42.
Salhi, S. (2017). *Heuristic Search: The Emerging Science of Problem Solving*. Springer International Publishing.
Sammon, C., Yarwood, J., and Everall, N. (2000). A FTIR-ATR study of liquid diffusion processes in PET films: comparison of water with simple alcohols. *Polymer* 41 (7), 2521-2534.
Sancaktar, E.A., Takeno, H., and Wightman, J.P. (1974). Adsorption—desorption of water on poly(ethylene terephthalate). *Journal of Colloid and Interface Science* 47 (3), 682-686.
Sasaki, H., Daicho, S., Yamada, Y., and Nibu, Y. (2013). Comparable Strength of OH−O versus OH−π Hydrogen Bonds in Hydrogen-Bonded 2,3-Benzofuran Clusters with Water and Methanol. *The Journal of Physical Chemistry A* 117 (15), 3183-3189.
Savransky, S.D. (2000). *Engineering of Creativity: Introduction to TRIZ Methodology of Inventive Problem Solving*. CRC Press.
Schmalz, E.O., and Grundke, H. (1969). *Faserforsch. Textil- tech* 20 (8), 377.
Schweitzer, J.-P., and Janssens, C. (2018). *Overpackaging. Briefing for the report: Unwrapped: How throwaway plastic is failing to solve Europe's food waste problem (and what we need to do instead).* [Online]. Brussels: Institute for European Environment Policy (IEEP), A study by Zero Waste Europe and Friends of the Earth Europe for the Rethink Plastic Alliance. Available: https://ieep.eu/publications/plastic-packaging-and-food-waste-new-perspectives-on-a-dual-sustainability-crisis [Accessed May 31, 2019].
Schwope, A.D., Goydan, R., and Reid, R. (1990). "Methodology for Estimating the Migration of Additives and Impurities from Polymeric Materials - EPA 560/5-85-015", in: *Methods for assessing exposure to chemical substances.* (ed.) U.S.E.P.a.E. Office of Pesticides and Toxic Substances. (Washington DC, USA - https://nepis.epa.gov/Exe/ZyPURL.cgi?Dockey=P100BCMB.TXT: Office of Pesticides and Toxic Substances, U.S. Environmental Protection Agency (EPA)).
Shapiro, A.A., Davis, P.K., and Duda, J.L. (2004). "Part II. Models for Properties. Chapter 9. Diffusion in muulticompenent mixtures.," in *Computer aided property estimation for process and product design,* eds. G.M. Kontogeorgis & R. Gani. (Amsterdam, The Netherlands: Elsevier B. V.), 205-227.
Shen, L., Worrell, E., and Patel, M.K. (2010). Open-loop recycling: A LCA case study of PET bottle-to-fibre recycling. *Resources, Conservation and Recycling* 55 (1), 34-52.
Shen, L., Worrell, E., and Patel, M.K. (2012). Comparing life cycle energy and GHG emissions of bio-based PET, recycled PET, PLA, and man-made cellulosics. *Biofuels, Bioproducts and Biorefining* 6 (6), 625-639.
Shigetomi, T., Tsuzumi, H., Toi, K., and Ito, T. (2000). Sorption and diffusion of water vapor in poly(ethylene terephthalate) film. *Journal of Applied Polymer Science* 76 (1), 67-74.
Shuaib, M., Seevers, D., Zhang, X., Badurdeen, F., Rouch, K.E., and Jawahir, I.S. (2014). Product Sustainability Index (ProdSI). *Journal of Industrial Ecology* 18 (4), 491-507.
Silberbauer, A., and Schmid, M. (2017). Packaging Concepts for Ready-to-Eat Food: Recent Progress. *Journal of Packaging Technology and Research* 1 (3), 113-126.

Simapro (2019). *LCA Software SIMAPRO* [Online]. Available: https://www.simapro.co.uk/ [Accessed April 30, 2019].
Simha, R., and Somcynsky, T. (1969). On the Statistical Thermodynamics of Spherical and Chain Molecule Fluids. *Macromolecules* 2 (4), 342-350.
Simon, B., Amor, M.B., and Földényi, R. (2016). Life cycle impact assessment of beverage packaging systems: focus on the collection of post-consumer bottles. *Journal of Cleaner Production* 112, 238-248.
Singh, P., Wani, A.A., and Langowski, H.C. (2017). *Food Packaging Materials: Testing & Quality Assurance*. CRC Press.
Singh, R.K., and Singh, N. (2013). "Quality of pack-aged foods," in *Innovations in Food Packaging,* ed. J.H. Han. Elsevier Science).
Sluik, D., Bezemer, R., Sierksma, A., and Feskens, E. (2016). Alcoholic Beverage Preference and Dietary Habits: A Systematic Literature Review. *Critical Reviews in Food Science and Nutrition* 56 (14), 2370-2382.
Song, H.-S., Moon, K.-S., and Hyun, J.C. (1999). A Life-Cycle Assessment (LCA) study on the various recycle routes of pet bottles. *Korean Journal of Chemical Engineering* 16 (2), 202-207.
Spiegelman, M.W. (2019). *Myths and Methods in Modeling* [Online]. Lamont -Doherty Earth Observatory, The Trustees of Columbia University. Available: https://www.ldeo.columbia.edu/~mspieg/mmm/ [Accessed May 4, 2019].
Stieger, G. (2018). *Predicting the safety of food contact articles: New science and digital opportunities* [Online]. Zurich, Switzerland: Food Packaging Forum. Available: https://www.foodpackagingforum.org/events/predicting-the-safety-of-food-contact-articles-new-science-and-digital-opportunities [Accessed June 5, 2019].
Tawarmalani, M., and Sahinidis, N.V. (2013). *Convexification and Global Optimization in Continuous and Mixed-Integer Nonlinear Programming: Theory, Algorithms, Software, and Applications*. Springer US.
The Coca-Cola Company (2019). *Why don't you get rid of plastic bottles altogether?* [Online]. Available: https://www.coca-cola.co.uk/faq/why-dont-you-get-rid-of-plastic-bottles-altogether [Accessed May 1, 2019].
Thinkstep (2019). *LCA Software GaBi* [Online]. Available: http://www.gabi-software.com/france/index/ [Accessed April 30,2019].
Thomas, N.L., and Windle, A.H. (1982). A theory of case II diffusion. *Polymer* 23 (4), 529-542.
Thomas, S., Rane, A.V., Kanny, K., Vk, A., and Thomas, M.G. (2019). *Recycling of Polyethylene Terephthalate Bottles*. Elsevier Science.
Thornton, A.W., Nairn, K.M., Hill, A.J., Hill, J.M., and Huang, Y. (2009). New relation between diffusion and free volume: II. Predicting vacancy diffusion. *Journal of Membrane Science* 338 (1), 38-42.
Thurston, D.L., and Srinivasan, S. (2003). Constrained Optimization for Green Engineering Decision-Making. *Environmental Science & Technology* 37 (23), 5389-5397.
Till, D., Schwope, A.D., Ehntholt, D.J., Sidman, K.R., Whelan, R.H., Schwartz, P.S., Reid, R.C., and Rainey, M.L. (1987). Indirect Food Additive Migration from Polymeric Food Packaging Materials. *CRC Critical Reviews in Toxicology* 18 (3), 215-243.
Tonge, M.P., and Gilbert, R.G. (2001a). Testing free volume theory for penetrant diffusion in rubbery polymers. *Polymer* 42 (4), 1393-1405.
Tonge, M.P., and Gilbert, R.G. (2001b). Testing models for penetrant diffusion in glassy polymers. *Polymer* 42 (2), 501-513.
Toniolo, S., Mazzi, A., Niero, M., Zuliani, F., and Scipioni, A. (2013). Comparative LCA to evaluate how much recycling is environmentally favourable for food packaging. *Resources, Conservation and Recycling* 77, 61-68.
Touffet, M., Patsioura, A., Ziaiifar, A.M., Eveleigh, L., and Vitrac, O. (2018). Online reconstruction of oil oxidation kinetics and reaction schemes during deep-frying by deconvolution of ATR-FTIR spectra. *Journal of Food Engineering* 224, 1-16.
Truesdale, G.A., and Downing, A.L. (1954). Solubility of Oxygen in Water. *Nature* 173 (4417), 1236-1236.

Tseng, T.-P. (1946). Hole Theory of the Liquid State. *Nature* 157 (4000), 873-874.
Tuy, H. (2016). *Convex Analysis and Global Optimization*. Springer International Publishing.
Uehara, T., and Ynacay-Nye, A. (2018). How Water Bottle Refill Stations Contribute to Campus Sustainability: A Case Study in Japan. *Sustainability* 10 (9).
Un (2015). "United Nations General Assembly Draft outcome document of the United Nations summit for the adoption of the post-2015 development agenda", in: *United Nations Sustainable Development Summit*. (New York).
Un (2017). *World Population Prospects: The 2017 Revision* [Online]. United Nations. Available: https://www.un.org/development/desa/publications/world-population-prospects-the-2017-revision.html [Accessed May 5, 2019].
Un (2018). *2018 Revision of World Urbanization Prospects* [Online]. United Nations. Available: https://www.un.org/development/desa/publications/2018-revision-of-world-urbanization-prospects.html [Accessed May 5, 2019].
Vagias, A., Schultze, J., Doroshenko, M., Koynov, K., Butt, H.-J., Gauthier, M., Fytas, G., and Vlassopoulos, D. (2015). Molecular Tracer Diffusion in Nondilute Polymer Solutions: Universal Master Curve and Glass Transition Effects. *Macromolecules* 48 (24), 8907-8912.
Valentina, B., Federica, A.P., Fruergaard, A., T., and Anders, D. (2018). *Life Cycle Assessment of management options for beverage packaging waste*. København, Denmark: Ministry of Environment and Food of Denmark, Environmental Protection Agency.
Vallero, D.A., and Brasier, C. (2008). *Sustainable Design: The Science of Sustainability and Green Engineering*. Wiley.
Vallet, F., Eynard, B., Millet, D., Mahut, S.G., Tyl, B., and Bertoluci, G. (2013). Using eco-design tools: An overview of experts' practices. *Design Studies* 34 (3), 345-377.
Valsaraj, K.T., and Melvin, E.M. (2018). *Principles of Environmental Thermodynamics and Kinetics, Fourth Edition*. CRC Press.
Van Krevelen, D.W., and Te Nijenhuis, K. (2009). *Properties of Polymers: Their Correlation with Chemical Structure; their Numerical Estimation and Prediction from Additive Group Contributions*. Amsterdam, NL: Elsevier Science.
Van Lune, F.S., Nijssen, L.M., and Linssen, J.P.H. (1997). Absorption of methanol and toluene by polyester-based bottles. *Packaging Technology and Science* 10 (4), 221-227.
Velasco, C., Salgado-Montejo, A., Marmolejo-Ramos, F., and Spence, C. (2014). Predictive packaging design: Tasting shapes, typefaces, names, and sounds. *Food Quality and Preference* 34, 88-95.
Verghese, K., Lewis, H., Lockrey, S., and Williams, H. (2013). "The role of packaging in minimising food waste in the supply chain of the future". (Melbourne: Centre for Design, RMIT University).
Vieth, W.R., Matulevicius, E.S., and Mitchell, S.R. (1967). Detection of stress-induced morphological alterations of polyethylene terephthalate by gas permeation. *Kolloid-Zeitschrift und Zeitschrift für Polymere* 220 (1), 49-55.
Vignali, G. (2016). "Life-Cycle Assessment of Food-Packaging Systems," in *Environmental footprints of packaging,* ed. S.S. Muthu.), 1-22.
Vitrac, O. (2018). *FMECAengine: FMECA software developed in the framework of the project SafeFoodPack Design* [Online]. Available: https://github.com/ovitrac/FMECAengine [Accessed accessed on Nov 22, 2018 2018].
Vitrac, O., Challe, B., Leblanc, J.C., and Feigenbaum, A. (2007a). Contamination of packaged food by substances migrating from a direct-contact plastic layer: Assessment using a generic quantitative household scale methodology. *Food Additives & Contaminants* 24 (1), 75-94.
Vitrac, O., and Gillet, G. (2010). An Off-Lattice Flory-Huggins Approach of the Partitioning of Bulky Solutes between Polymers and Interacting Liquids. *International Journal of Chemical Reactor Engineering*. Vol.8, A6.
Vitrac, O., and Hayert, M. (2005). Risk assessment of migration from packaging materials into foodstuffs. *Aiche Journal* 51 (4), 1080-1095.

Vitrac, O., and Hayert, M. (2006). Identification of Diffusion Transport Properties from Desorption/Sorption Kinetics: An Analysis Based on a New Approximation of Fick Equation during Solid–Liquid Contact. *Industrial & Engineering Chemistry Research* 45 (23), 7941-7956.

Vitrac, O., and Hayert, M. (2007a). "Design of safe packaging materials under uncertainty," in *Chemical Engineering Research Trends,* ed. L.P. Berton. (New-York, USA: Nova Science Publishers), 251-292.

Vitrac, O., and Hayert, M. (2007b). Effect of the distribution of sorption sites on transport diffusivities: A contribution to the transport of medium-weight-molecules in polymeric materials. *Chemical Engineering Science* 62 (9), 2503-2521.

Vitrac, O., and Leblanc, J.-C. (2007). Consumer exposure to substances in plastic packaging. I. Assessment of the contribution of styrene from yogurt pots. *Food Additives and Contaminants* 24(2) (2), 194–215.

Vitrac, O., Lézervant, J., and Feigenbaum, A. (2006). Decision trees as applied to the robust estimation of diffusion coefficients in polyolefins. *Journal of Applied Polymer Science* 101 (4), 2167-2186.

Vitrac, O., Mougharbel, A., and Feigenbaum, A. (2007b). Interfacial mass transport properties which control the migration of packaging constituents into foodstuffs. *Journal of Food Engineering* 79 (3), 1048-1064.

Vitrac , O., and Touffet, M. (2019). "Food Process Modeling," in *Encyclopedia of Food Security and Sustainability-General and Global Situation,* eds. P. Ferranti, E.M. Berry & J.R. Anderson. (Amsterdam, Netherlands: Elsevier Inc.).

Von Falkenstein, E., Wellenreuther, F., and Detzel, A. (2010). LCA Studies Comparing Beverage Cartons And Alternative Packaging: can overall conclusions be drawn? *The International Journal of Life Cycle Assessment* 15 (9), 938-945.

Von Meerwall, E., Beckman, S., Jang, J., and Mattice, W.L. (1998). Diffusion of liquid n-alkanes: Free-volume and density effects. *The Journal of Chemical Physics* 108 (10), 4299-4304.

Vrentas, J.S., Chu, C.H., Drake, M.C., and Von Meerwall, E. (1989). Predictive capabilities of a free-volume theory for solvent self-diffusion coefficients. *Journal of Polymer Science Part B: Polymer Physics* 27 (5), 1179-1184.

Vrentas, J.S., and Duda, J.L. (1977a). Diffusion in polymer–solvent systems. II. A predictive theory for the dependence of diffusion coefficients on temperature, concentration, and molecular weight. *Journal of Polymer Science: Polymer Physics Edition* 15 (3), 417-439.

Vrentas, J.S., and Duda, J.L. (1977b). Diffusion in polymer—solvent systems. I. Reexamination of the free-volume theory. *Journal of Polymer Science: Polymer Physics Edition* 15 (3), 403-416.

Vrentas, J.S., and Duda, J.L. (1977c). Solvent and temperature effects on diffusion in polymer–solvent systems. *Journal of Applied Polymer Science* 21 (6), 1715-1728.

Vrentas, J.S., and Duda, J.L. (1979). Diffusion of large penetrant molecules in amorphous polymers. *Journal of Polymer Science: Polymer Physics Edition* 17 (6), 1085-1096.

Vrentas, J.S., Jarzebski, C.M., and Duda, J.L. (1975). A Deborah number for diffusion in polymer-solvent systems. *AIChE Journal* 21 (5), 894-901.

Vrentas, J.S., Liu, H.T., and Duda, J.L. (1980). Effect of solvent size on diffusion in polymer–solvent systems. *Journal of Applied Polymer Science* 25 (8), 1793-1797.

Vrentas, J.S., and Vrentas, C.M. (1993). A new equation relating self-diffusion and mutual diffusion coefficients in polymer-solvent systems. *Macromolecules* 26 (22), 6129-6131.

Vrentas, J.S., and Vrentas, C.M. (1994a). Solvent Self-Diffusion in Glassy Polymer-Solvent Systems. *Macromolecules* 27 (20), 5570-5576.

Vrentas, J.S., and Vrentas, C.M. (1994b). Solvent Self-Diffusion in Rubbery Polymer-Solvent Systems. *Macromolecules* 27 (17), 4684-4690.

Vrentas, J.S., and Vrentas, C.M. (1998). Predictive methods for self-diffusion and mutual diffusion coefficients in polymer–solvent systems. *European Polymer Journal* 34 (5–6), 797-803.

Vrentas, J.S., and Vrentas, C.M. (2001). Viscoelastic diffusion. *Journal of Polymer Science Part B: Polymer Physics* 39 (13), 1529-1547.
Vrentas, J.S., and Vrentas, C.M. (2003). Evaluation of the free-volume theory of diffusion. *Journal of Polymer Science Part B: Polymer Physics* 41 (5), 501-507.
Vrentas, J.S., and Vrentas, C.M. (2013). *Diffusion and Mass Transfer*. Boca-Raton, FL, USA: CRC Press.
Vrentas, J.S., Vrentas, C.M., and Faridi, N. (1996). Effect of Solvent Size on Solvent Self-Diffusion in Polymer–Solvent Systems. *Macromolecules* 29 (9), 3272-3276.
Wadell, H. (1935). Volume, Shape, and Roundness of Quartz Particles. *The Journal of Geology* 43 (3), 250-280.
Wang, B.G., Yamaguchi, T., and Nakao, S.I. (2000). Solvent diffusion in amorphous glassy polymers. *Journal of Polymer Science Part B: Polymer Physics* 38 (6), 846-856.
Wang, Y., and Chiew, V. (2010). On the cognitive process of human problem solving. *Cognitive Systems Research* 11 (1), 81-92.
Welle, F. (2011). Twenty years of PET bottle to bottle recycling—An overview. *Resources, Conservation and Recycling* 55 (11), 865-875.
Welle, F. (2013). A new method for the prediction of diffusion coefficients in poly(ethylene terephthalate). *Journal of Applied Polymer Science* 129 (4), 1845-1851.
Welle, F. (2015). *The Facts about PET*. European Federation of Bottled Waters.
Welle, F. (2016). "12 µm PET correlations at 100°C". (Freising, Germany: Fraunhofer Institut für Verfahrenstechnik und Verpackung (IVV)).
White, R.P., and Lipson, J.E.G. (2016). Polymer Free Volume and Its Connection to the Glass Transition. *Macromolecules* 49 (11), 3987-4007.
Williams, H., and Wikström, F. (2011). Environmental impact of packaging and food losses in a life cycle perspective: a comparative analysis of five food items. *Journal of Cleaner Production* 19 (1), 43-48.
Williams, H., Wikström, F., Otterbring, T., Löfgren, M., and Gustafsson, A. (2012). Reasons for household food waste with special attention to packaging. *Journal of Cleaner Production* 24, 141-148.
Wittig, R., Lohmann, J., and Gmehling, J. (2003). Vapor–Liquid Equilibria by UNIFAC Group Contribution. 6. Revision and Extension. *Industrial & Engineering Chemistry Research* 42 (1), 183-188.
WOS (2019). *Web of Science* [Online]. Available: https://apps.webofknowledge.com [Accessed May 2, 2019].
Wunderlich, B. (2005). *Thermal Analysis of Polymeric Materials*. Berlin, Germany: Springer-Verlag.
Yang, T.-H., and Lue, S.J. (2013). Modeling Sorption Behavior for Ethanol/Water Mixtures in a Cross-linked Polydimethylsiloxane Membrane Using the Flory-Huggins Equation. *Journal of Macromolecular Science, Part B* 52 (7), 1009-1029.
Yasuda, H., and Stannett, V. (1962). Permeation, solution, and diffusion of water in some high polymers. *Journal of Polymer Science* 57 (165), 907-923.
Yirka, B. (2015). *LiquiGlide poised to market superhydrophobic coating for wide range of products* [Online]. Phys.org. Available: https://phys.org/news/2015-03-liquiglide-poised-superhydrophobic-coating-wide.html [Accessed June 1, 2019].
Yu, X., Zhang, H., Shu, H., Zhao, W., Yan, T., Liu, Y., and Wang, X. (2017). A Robust Eco-Design Approach Based on New Sensitivity Coefficients by Considering the Uncertainty of LCI. *Journal of Advanced Manufacturing Systems* 16 (03), 185-203.
Zhang, M., Meng, X., Bhandari, B., and Fang, Z. (2016). Recent Developments in Film and Gas Research in Modified Atmosphere Packaging of Fresh Foods. *Critical Reviews in Food Science and Nutrition* 56 (13), 2174-2182.
Zhao, Y.H., Abraham, M.H., and Zissimos, A.M. (2003). Fast Calculation of van der Waals Volume as a Sum of Atomic and Bond Contributions and Its Application to Drug Compounds. *The Journal of Organic Chemistry* 68 (19), 7368-7373.
Zhu, Y., Guillemat, B., and Vitrac, O. (2019a). Rational Design of Packaging: Toward Safer and Ecodesigned Food Packaging Systems. *Frontiers in Chemistry* Vol. 7. Article 349.

Zhu, Y., Nguyen, P.M., and Vitrac, O. (2019b). "Risk assessment of migration from packaging materials into food," in *Reference Module in Food Science,* ed. G. Robertson. (Amsterdam: Elsevier), 64.
Zhu, Y., Welle, F., and Vitrac, O. (2019c). A blob model to parameterize polymer hole free volumes and solute diffusion. *Manuscript to be submitted in Soft-Matter*.
Zielinski, J.M., and Duda, J.L. (1992). Predicting polymer/solvent diffusion coefficients using free-volume theory. *AIChE Journal* 38 (3), 405-415.
Zimm, B.H., and Lundberg, J.L. (1956). Sorption of Vapors by High Polymers. *The Journal of Physical Chemistry* 60 (4), 425-428.
Zou, Q., and Feng, H.-Y. (2019). Push-pull direct modeling of solid CAD models. *Advances in Engineering Software* 127, 59-69.
Zumailan, A., Dargent, E., and Saiter, J.M. (2004). Characterization of polyethylene terephthalate films drawn in hot water. *Polymer Engineering & Science* 44 (2), 223-230.
Zuo, Z.H., and Xie, Y.M. (2015). A simple and compact Python code for complex 3D topology optimization. *Advances in Engineering Software* 85, 1-11.

this page is left blank intentionally

université PARIS-SACLAY
ÉCOLE DOCTORALE
Agriculture, alimentation, biologie, environnement, santé (ABIES)

Titre : Conception raisonnée d'emballages en plastique pour les boissons alcoolisées

Mots clés : écoconception d'emballage alimentaire, transferts de matières couplés, modélisation multiéchelle et optimisation multicritères, thermodynamique moléculaire, polymères, théories des volumes libres et Flory-Huggins

Résumé : La perception des emballages alimentaires est passée d'utile à source majeure de contaminants dans les aliments et menace pour l'environnement. La substitution du verre par des contenants en plastiques recyclés ou biosourcés réduit l'impact environnemental des boissons embouteillées. La thèse a développé de nouveaux outils de simulation 3D et d'optimisation pour accélérer le prototypage des emballages éco-efficaces pour les boissons alcoolisées. La durée de conservation des boissons, la sécurité sanitaire des matériaux plastiques recyclés, les contraintes mécaniques, et la quantité de déchets sont considérées comme un seul problème d'optimisation multicritères. Les nouvelles bouteilles sont générées virtuellement et itérativement en trois étapes comprenant : i) une évaluation multi échelle des transferts de masse couplés ; ii) une étape de décision validant les contraintes techniques (forme, capacité, poids) et réglementaires (durée de conservation, migrations) ; iii) une étape globale de résolution recherchant des solutions de Pareto acceptables. La capacité de prédire la durée de vie des liqueurs dans des conditions réelles a été testée avec succès sur environ 500 miniatures en PET (polyéthylène téréphtalate) sur plusieurs mois. L'ensemble de l'approche a été conçu pour gérer tout transfert de matière couplé (perméation, sorption, migration). La sorption mutuelle est prise en compte via une formulation polynaire de Flory-Huggins. Une formulation gros grain de la théorie des volumes libres de Vrentas et Duda a été développée pour prédire les propriétés de diffusion dans les polymères vitreux de l'eau et des solutés organiques dans des polymères arbitraires (polyesters, polyamides, polyvinyles, polyoléfines). 409 diffusivités issues de la littérature ou mesurées ont été utilisée pour validation. La contribution de la relaxation du PET vitreux a été analysée par sorption différentielle (binaire et ternaire) de 25 à 50 °C. Une partie du code source sera partagé afin d'encourager l'intégration de davantage de paramètres affectant la durée de conservation des boissons et des produits alimentaires (cinétique d'oxydation, piégeage d'arômes).

Title: Rational design of plastic packaging for alcoholic beverages

Keywords: ecodesign of food packaging, coupled mass transfer, multiscale modeling and multicriteria optimization, molecular thermodynamics, polymers, free-volume theory and Flory-Huggins theory

Abstract: The view of plastic food packaging turned from useful to a major source of contaminants in food and an environmental threat. Substituting glass by recycled or biosourced plastic containers reduces environmental impacts for bottled beverages. The thesis developed a 3D computational and optimization framework to accelerate the prototyping of eco-efficient packaging for alcoholic beverages. Shelf-life, food safety, mechanical constraints, and packaging wastes are considered into a single multicriteria optimization problem. New bottles are virtually generated within an iterative three steps process involving: i) a multiresolution evaluation of coupled mass transfer; ii) a decision step validating technical (shape, capacity, weight) and regulatory (shelf-life, migrations) constraints; iii) a global solving step seeking acceptable Pareto solutions. The capacity to predict shelf-life of liquors in real conditions was tested successfully on ca. 500 hundred bottle miniatures in PET (polyethylene terephthalate) over several months. The entire approach has been designed to manage any coupled mass transfer (permeation, sorption, migration). Mutual sorption is considered via polynary Flory-Huggins formulation. A blob formulation of the free-volume theory of Vrentas and Duda was developed to predict the diffusion properties in glassy polymers of water and organic solutes in arbitrary polymers (polyesters, polyamides, polyvinyls, polyolefins). The validation set included 433 experimental diffusivities from literature and measured in this work. The contribution of polymer relaxation in glassy PET was analyzed in binary and ternary differential sorption using a cosorption microbalance from 25 to 50°C. Part of the framework will be released as an open-source project to encourage the integration of more factors affecting the shelf-life of beverages and food products (oxidation kinetics, aroma scalping).

Université Paris-Saclay
Espace Technologique / Immeuble Discovery
Route de l'Orme aux Merisiers RD 128 / 91190 Saint-Aubin, France